Open Source Malaria: Potent Triazolopyrazine-Based Antiplasmodium Agents that Probe an Important Mechanism of Action

Edwin Gar-On Tse

A thesis submitted in fulfilment of the requirements for the degree of Doctor of Philosophy

The University of Sydney
School of Chemistry, Faculty of Science

2019

Abstract

Malaria is one of the most prevalent causes of death in low income countries and considerable effort has been made to combat this disease. Current frontline treatments involve the use of artemisinin combination therapies, but there are increasing reports of the development of resistance to these drugs. Since 2011, the Todd group has applied the principles of open science to the discovery of new antimalarial medicines in the Open Source Malaria consortium. All aspects of the work are publicly available with experimental results and biological data shared in real-time.

This thesis describes the design and synthesis of novel triazolopyrazine-based compounds for the fourth series of OSM. The *in vitro* biological evaluation of these compounds against *P. falciparum* is presented, along with key studies on the mechanism of action and hERG activity.

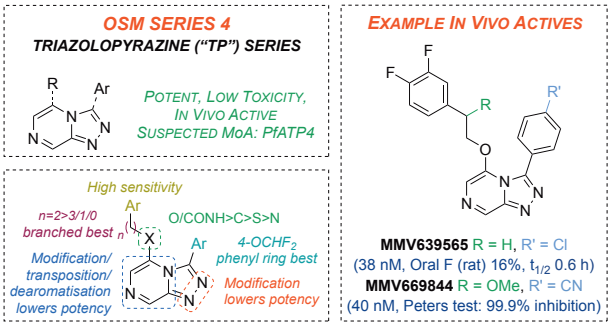

Chapter 1 provides a general background on malaria and outlines those antimalarial medicines that have been used in the past, those that are currently being used and those being developed for the future. The concept of conducting open science is discussed with respect to open data screens and OSM.

Investigation into a set of compounds determined by the OSM consortium to be high value targets for further development, named the Frontrunners, is described in Chapter 2. These targets were resynthesised in order to obtain a more complete dataset including measurements on *in vitro P. falciparum* potency, solubility, metabolic stability and mechanism of action. The results indicated beneficial structure activity relationships for the series including a 4-$OCHF_2$ substituted phenyl ring in the northeast position, a fluorinated phenyl ring in the northwest position and benzylic substitution with alcohol or amine moieties.

Chapter 3 describes the design, synthesis and *in vitro* biological evaluation of several novel Series 4 compounds that probe unexplored areas of SAR. Substitution at the northwest position with a thiol led to the isolation of an unexpected *tele*-substitution product. This phenomenon is currently under investigation but it has been seen to occur among amines, alcohols and diols as well. Replacement of the ether linker (with sulfoxide, sulfone or triazoles) was poorly tolerated

while benzylic substitution (with alkylamines, ketones or alcohols) was generally beneficial.

The replacement of the phenyl rings in the Series 4 compounds was conducted in Chapter 4 *via* the use of phenyl bioisosteres as a means to improve series solubility and metabolic stability. The northwest position was highly tolerant to non-aromatic and non-planar replacements such as cubane and adamantane. Conversely, saturated heterocycles were poorly tolerated suggesting a degree of rigidity must be present. Surprisingly, the use of carborane as a phenyl bioisostere led to significantly improved *in vitro* potency. While the cubane and carborane analogues were found to possess poorer physicochemical and metabolic properties when compared to the parent phenyl compound, the BCP analogue showed significantly improved metabolic properties.

Chapter 5 outlines the validation of the Series 4 mechanism of action. A range of compounds synthesised throughout this thesis was evaluated for activity against *Pf*ATP4 in the Kirk lab at the Australian National University. Based on the results, there is a high level of confidence that the Series 4 triazolopyrazines act *via* the inhibition of the malaria parasites ability to regulate its intracellular sodium concentration. This target has been implicated for a number of structurally diverse compounds currently in development. A predictive modelling competition was run to help design future compounds for the series as well as novel compounds which target *Pf*ATP4.

A key safety parameter, hERG activity, was investigated after some sub-optimal values had been observed for the series, as described in Chapter 6. The design and synthesis of a key compound possessing a carboxylic acid moiety was conducted as a means of reducing unwanted hERG activity. The desired reduction in hERG binding and improvements to solubility and metabolic stability were seen upon incorporation of the carboxylic acid, however this resulted in reduction to *in vitro* activity. In an attempt to improve upon the *in vitro* potency, a series of phenyl substituted analogues were synthesised. Unfortunately, these compounds were found to be less active.

Finally, in Chapter 7 is discussed the idea of crowdsourcing chemical synthesis and the incorporation of OSM into an undergraduate laboratory class at The University of Sydney run by Dr. Alice Motion. To act as a demonstrator for the class from 2016 to 2018 required a number of roles to be taken. These included the design of synthetic targets for the students, supervision and mentoring throughout the course and assessment of the students performance and reports from the class.

Overall, these studies contribute to the progression of a Series 4 compound as the first "born open" molecule to progress towards a late lead and, hopefully, as the first such molecule to move into a Phase I trial in the near future.

Declaration and Authorship Attribution

The work presented in this thesis was carried out by the author at The University of Sydney School of Chemistry between January 2016 and September 2018 and at the University College London (UCL) School of Pharmacy between October 2018 and August 2019, under the supervision of Prof. Matthew Todd and Prof. Peter Rutledge. This thesis contains no material which has been accepted for the award of any other degree.

Mass spectrometry measurements were acquired by Dr. Nicholas Proschogo and his staff at The University of Sydney School of Chemistry or by Mr. Emmanuel Samuel at the UCL School of Pharmacy. A small number of NMR spectra were acquired by Dr. Ian Luck and his staff at The University of Sydney School of Chemistry.

The *in vitro P. falciparum* assay was performed by the University of Dundee Drug Discovery Unit. Physicochemcial and metabolic evaluation of compounds was performed by the Charman group at Monash University. Mechanism of action studies were performed with the Kirk group at the Australian National University. The hERG assay was performed by Dr. Matthew Perry and Dr. Adam Hill at the Victor Chang Cardiac Research Institute.

As this project was conducted in a completely open manner, all data and ideas were publicly available throughout the project and the community was able to contribute at any point. Any instances where this occurred has been acknowledged in the body of the thesis.

Sections of this thesis have been proof-read by Prof. Matthew Todd, Prof. Peter Rutledge and Dr. Alice Motion.

Portions of this thesis have been published as:

E. G. Tse, M. Korsik, M. H. Todd. The Past, Present and Future of Anti-Malarial Medicines. *Malar. J.* **2019**, *18*. DOI: 10.1186/s12936-019-2724-z.

I certify that this document contains work carried out by myself except where otherwise acknowledged.

Edwin G. Tse

.....

Date: 2020

Acknowledgements

These acknowledgements could not begin without first thanking Prof. Matthew Todd. I am forever grateful to have been a part of such an amazing project and will be excited to see what's in store for OSM in the future. I will never forget the countless opportunities you have given me to explore the science, not just with the chemistry, but with the biology as well. A big thank you for allowing me to come to London and spend time in your labs at UCL. Additional thanks to Prof. Peter Rutledge for your ongoing guidance and support, especially in these final few months.

A special thanks to all the postdocs that I've had the pleasure of working alongside over the years; you have all been pillars of support for the group, always prepared to answer questions and share your wisdom. To Dr. Alice Motion, you have been there from the beginning and have always been ready to lend a helping hand. Working with you on the SSP course has been one of the definite highlights of these last few years. To Dr. Malcolm Spain, it was definitely nice to have someone else to do Biotage troubleshooting with. It was great hearing about all your travels around Australia. To Dr. David Smith, the case of the OHOH compound has been an interesting one to say the least. Thanks for all the thoughtful discussions in the lab and in the office. To Dr. Fahima Idiris and Dr. Dana Klug, the amount of work and effort that you have both put into keeping G25 running cannot be understated. It is safe to say that, in a short amount of time, everyone in G25 has benefited from your combined knowledge and experience.

To the past and present members of the Cornforth and Robinson labs, and the Todd and Rutledge groups; the music and conversations have made working in the lab a much more enjoyable experience. Particular thanks go to Paul King, Jamie Batten, Tha Bhebhe, Marat Korsik, Nicole Chapman and Elva Shi.

Thank you to the professional staff at the School of Chemistry for keeping the labs and instruments up and running: Dr. Nick Proschogo (mass spectrometry), Dr. Ian Luck (NMR spectroscopy), Dr. Shane Wilkinson and Mr. Carlo Piscicelli (Service room). Thank you to the collaborators that have helped on the wide range of areas covered in this thesis. To Ms. Irene Hallyburton for being our point of contact at Dundee and for fielding all my questions about the potency assay. To Prof. Louis Rendina for sharing your precious carboranes with me. To Prof. Kiaran Kirk, Dr. Adele Lehane and Dr. Adelaide Dennis for welcoming me to your labs and teaching me about the ins and outs of *Pf*ATP4. To Dr. Matthew Perry and Dr. Adam Hill for all your help with the hERG assay and for allowing me to come visit your labs. To all the members of the OSM community for your helpful comments and suggestions on GitHub throughout my time working

on this project: A/Prof. Chase Smith (MedChemProf), Dr. Christopher Southan (cdsouthan), Dr. Chris Swain (drc007), Dr. Mark Coster (mcoster) and Mandrake Fernflower (MFernflower). I would like to thank the Medicines for Malaria Venture for their financial and in-kind support of this project, and Tim Wells, Jeremy Burrows and Paul Willis for their ongoing support and insights.

Finally, to my family; I can't thank you enough for your never ending support. I don't think I could have made it through all these years without it.

Table of Contents

List of Abbreviations

3D7	sensitive strain of *Plasmodium falciparum*
7GB	multi-drug resistant strain of *Plasmodium falciparum*
Å	Ångstrom
AcOH	acetic acid
ACTs	artemisinin combination therapies
ADME	absorption, distribution, metabolism or excretion
ANU	Australian National University
APCI	atmospheric-pressure chemical ionisation
aq.	aqueous
BCECF	2',7'-bis(2-carboxyethyl)-5(6)-carboxyfluorescein
BCP	bicyclo[1.1.1]pentane
CCDC	Cambridge Crystallographic Data Centre
CDC	Centers for Disease Control and Prevention
CG	cycloguanil
CL_{int}	*in vitro* intrinsic clearance
cLogD	calculated logarithm of the 1-octanol:H_2O distribution coefficient
cLogP	calculated logarithm of the 1-octanol:H_2O partition coefficient
COX	cyclooxygenase
CQ	chloroquine
CRO	contract research organisation
CTP	Compound Transfer Program
CuAAC	copper(I)-catalysed alkyne-azide cycloaddition
D3	Distributed Drug Discovery
D6	sensitive strain of *Plasmodium falciparum*
DALYs	disability-adjusted life years
Dd2	multi-drug resistant strain of *Plasmodium falciparum*
DDU	Drug Discovery Unit
DHO	dihydroorotate
DIAD	diisopropyl azodicarboxylate
DIBAL-H	diisobutylaluminium hydride
DIPEA	*N,N*-diisopropylethylamine
DMAP	4-dimethylaminopyridine

DMF	*N,N*-dimethylformamide
DMSO	dimethyl sulfoxide
DND*i*	Drugs for Neglected Diseases *initiative*
EC_{50}	half maximal effective concentration
ECG	electrocardiogram
ED_{90}	90% effective dose
EDGs	electron donating groups
E_H	hepatic extraction ratio
ELN	electronic laboratory notebook
equiv.	equivalent(s)
ESI	electrospray ionisation
EWGs	electron withdrawing groups
F	oral bioavailability
FDA	food and drug administration
g	gram(s)
GSK	GlaxoSmithKline
h	hour(s)
hERG	human ether-à-go-go related gene
HLM	human liver microsomes
HRMS	high resolution mass spectrometry
IC_{50}	half maximal inhibitory concentration
I_K	rapid delayed rectified potassium current
i.p.	intraperitoneal injection
IPA	isopropylalcohol
i.v.	intravenous injection
IVIEWGA	*in vitro* evolution and whole genome analysis
IVIVC	*in vitro-in vivo* correlation
J	coupling constant
K1	multi-drug resistant strain of *Plasmodium falciparum*
kg	kilogram(s)
LCMS	liquid chromatography-mass spectrometry
LQTS	long QT syndrome
M	molar
m-CPBA	*meta*-chloroperoxybenzoic acid

MeCN	acetonitrile
mg	milligram(s)
MHz	megahertz
min	minute(s)
mL	millilitre(s)
MLEM	Model List of Essential Medicines
MLM	mouse liver microsomes
mM	millimolar
mmol	millimole
MMV	Medicines for Malaria Venture
MoA	mode/mechanism of action
m.p.	melting point
MS	malaria saline
MTX	methotrexate
m/z	mass-to-charge ratio
NADPH	reduced nicotinamide adenine dinucleotide phosphate
Nampt	nicotinamide phosphoribosyltransferase
NBS	*N*-bromosuccinimide
nm	nanometre
nM	nanomolar
NMR	nuclear magnetic resonance
NF54	sensitive strain of *Plasmodium falciparum*
OSM	Open Source Malaria
OSN	Open Synthesis Network
P. berghei/*Pb*	*Plasmodium berghei*
P. chabaudi	*Plasmodium chabaudi*
P. cynomolgi/*Pc*	*Plasmodium cynomolgi*
P. falciparum/*Pf*	*Plasmodium falciparum*
*Pf*ATP4	*Plasmodium falciparum* P-type Na^+–ATPase 4
*Pf*ATP6	*Plasmodium falciparum* P-type Ca^{2+}–ATPase 6
*Pf*CARL	*Plasmodium falciparum* cyclic amine resistance locus
*Pf*CPSF3	*Plasmodium falciparum* cleavage & polyadenylation specificity factor 3
*Pf*CRT	*Plasmodium falciparum* chloroquine resistance transporter
*Pf*CYTbc_1	*Plasmodium falciparum* cytochrome bc_1

*Pf*cPheRS	*Plasmodium falciparum* cytosolic phenylalanyl-tRNA synthetase
*Pf*DHFR	*Plasmodium falciparum* dihydrofolate reductase
*Pf*DHODH	*Plasmodium falciparum* dihydroorotate dehydrogenase
*Pf*eEF2	*Plasmodium falciparum* translation elongation factor 2
*Pf*MDR2	*Plasmodium falciparum* multi-drug resistance transporter 2
*Pf*PI(3)K	*Plasmodium falciparum* phosphatidylinositol-3-kinase
*Pf*PI(4)K	*Plasmodium falciparum* phosphatidylinositol-4-OH kinase
*Pf*PNP	*Plasmodium falciparum* purine nucleoside phosphorylase
pIC_{50}	negative log of the IC_{50} value in molar
PK	pharmacokinetic
pK_a	negative log of the acid dissociation constant
PKC-β	protein kinase C-β
P. knowlesi	*Plasmodium knowlesi*
Ph	phenyl
PhMe	toluene
P. malariae	*Plasmodium malariae*
p.o.	(*per os*) orally
P. ovale	*Plasmodium ovale*
ppm	parts per million
PPTS	pyridinium *p*-toluenesulfonate
P. vinckei	*Plasmodium vinckei*
P. vivax	*Plasmodium vivax*
P. yoelii/*Py*	*Plasmodium yoelii*
PYR	pyrimethamine
q.d.	(*quaque die*) one a day
RBCs	red blood cells
RCH	rat cryopreserved hepatocytes
RCQ(s)	reversed chloroquine(s)
RLM	rat liver microsomes
rt	room temperature
SAR	structure activity relationship
SBFI	Na^+-binding benzofuran isophthalate
SCID	severe combined immunodeficiency
SGC	Structural Genomics Consortium

SHArK	Solar Hydrogen Activity Research Kit
Sol.	solubility
SSP	Special Studies Program
STPHI	Swiss Tropical and Public Health Institute
$T_{1/2}$	half-life
T3P	propylphosphic anhydride
TAP	triaminopyrimidine
TEMPO	(2,2,6,6-tetramethylpiperidin-1-yl)oxyl
TFA	trifluoroacetic acid
THF	tetrahydrofuran
THP	tetrahydropyran
TLC	thin layer chromatography
TM90C2A	multi-drug resistant strain of *Plasmodium falciparum*
TMS	trimethylsilyl/tetramethylsilane
TP	triazolopyrazine
TQ	tafenoquine
UPR	unfolded protein response
USS	Unit of Study Surveys
V1/S	multi-drug resistant strain of *Plasmodium falciparum*
V_{ss}	apparent volume of distribution at steady state
VEGFR-2	vascular endothelial growth factor receptor 2
W2	multi-drug resistant strain of *Plasmodium falciparum*
WHO	World Health Organisation
°C	degree(s) Celsius
μL	microlitre
μM	micromolar
μmol	micromole

1. Introduction

1.1 Malaria

Malaria is among the top ten leading causes of death in low income countries, and has been said to affect nearly half of the world's population (Figure 1.1).[1] The most recent report from the World Health Organization (WHO) in 2017 estimates that there are 219 million cases of malaria in 90 countries, with patients in Africa making up the majority of these (∼90%).[2] This level of infection resulted in 435,000 deaths that year, or 1190 per day, mostly young children. Encouragingly, between 2000 and 2015, the global incidence rate of malaria has decreased by about 37% and the mortality rate has decreased by about 60%. In terms of disability-adjusted life years (DALYs), which gives an indication of the overall burden of a disease, between 2006 and 2016 malaria has shown a decrease of ∼27% in the number of DALYs, going from the 7th to the 13th leading cause of all DALYs.[3] While these numbers demonstrate the success of efforts worldwide to combat malaria, there is always the danger of becoming complacent with current treatments. Indeed, there have been a number of reports in the last few years showing that these improvements are slowly plateauing, with resistance emerging to our best treatments and medications.[4,5]

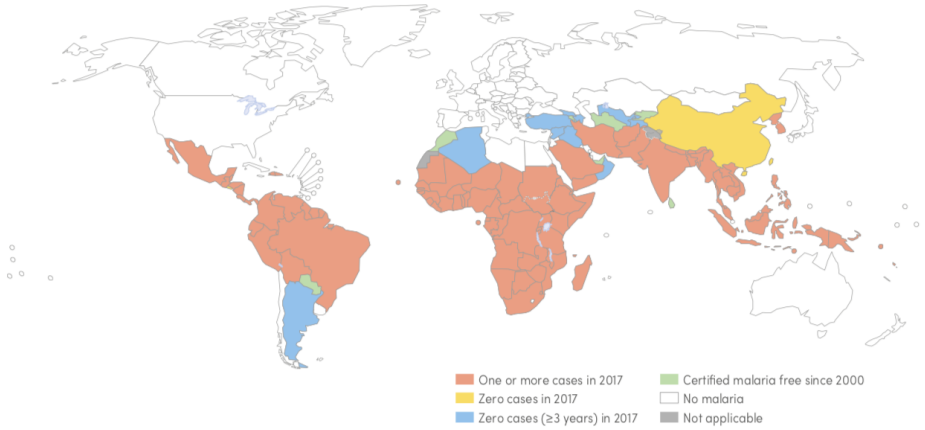

Figure 1.1: Geographical distribution of malaria in 2017. Adapted from the WHO World Malaria Report 2018.[2]

There are over 250 species of the *Plasmodium* parasite that have been found to infect a large range of hosts including mammals, reptiles and birds. Human malaria can be classified into three categories and is known to be caused by five species of the parasite.[6] Asymptomatic malaria can be caused by all five species and refers to when a patient has been infected but shows no symptoms. Uncomplicated malaria may also be caused by all species with non-specific symptoms (fever, chills, headache, nausea, etc.) showing 7–10 days after infection. Severe malaria is typically caused by *P. falciparum*, but may be caused by *P. vivax* or *P. knowlesi*, with more serious symptoms including

severe anaemia, pulmonary complications and hypoglycaemia. This type of malaria is associated with hyperparasitemia and carries an increased mortality rate.

The most widespread species is *P. falciparum* which mostly affects tropical and subtropical regions in Africa and can also cause severe malaria. The next most widespread, *P. vivax*, is predominantly found in Asia and Latin America, but can also be found in parts of Africa and is the most common cause of recurring malaria. *P. ovale* is mostly found in West Africa and the western Pacific islands. It is much less widespread than the former two species and much less dangerous. *P. malariae* can be found worldwide and may cause long-lasting, chronic infections but this species is also less dangerous. *P. knowlesi* was originally only found to infect long-tailed and pig-tailed macaque monkeys, but was reported in 1965 to have infected humans.[7] It is now known to be a significant cause of zoonotic malaria which infects humans in southeast Asia.

With *P. falciparum* being so prevalent, a large number of drugs (in use and in development) have been made to target this species. The current frontline treatments for *P. falciparum* malaria are artemisinin-based combination therapies (ACTs), however, as previously mentioned, reports of resistance are slowly emerging and these highlight the need for the discovery and development of new antimalarial drugs. A priority in combating the rapid generation of resistance is the exploitation of newly-discovered mechanisms of action (see Chapter 5).

1.2 Life Cycle of the *Plasmodium* Parasite

The life cycle of the malaria parasite is long and complicated, existing across both mosquito and human hosts (Figure 1.2). It can, most broadly, be divided into two stages; the asexual stage and the sexual stage. The asexual stage takes place within the human host and can be further subdivided into two cycles; the exo-erythrocytic cycle A which occurs in the liver, and the erythrocytic cycle B which occurs in the blood. The sexual stage takes place in the *Anopheles* mosquito and is known as the sporogonic cycle C.

The cycle begins when an infected female *Anopheles* mosquito bites a human and transmits the *Plasmodium* parasite ❶. Sporozoites are injected and make their way towards the liver. What follows are two cycles of asexual reproduction. The exo-erythrocytic cycle begins once the parasite infects the liver cells ❷, where the sporozoites begin to multiply and divide into schizonts ❸. The schizonts then erupt, releasing thousands of merozoites ❹, which concludes the liver stage.

The erythrocytic cycle begins when these merozoites make their way into the blood stream ❺ and proceed to infect red blood cells (RBCs). Following this, the merozoites develop into trophozoites (commonly known as the ring stage of the parasite). These further mature, and form erythrocytic

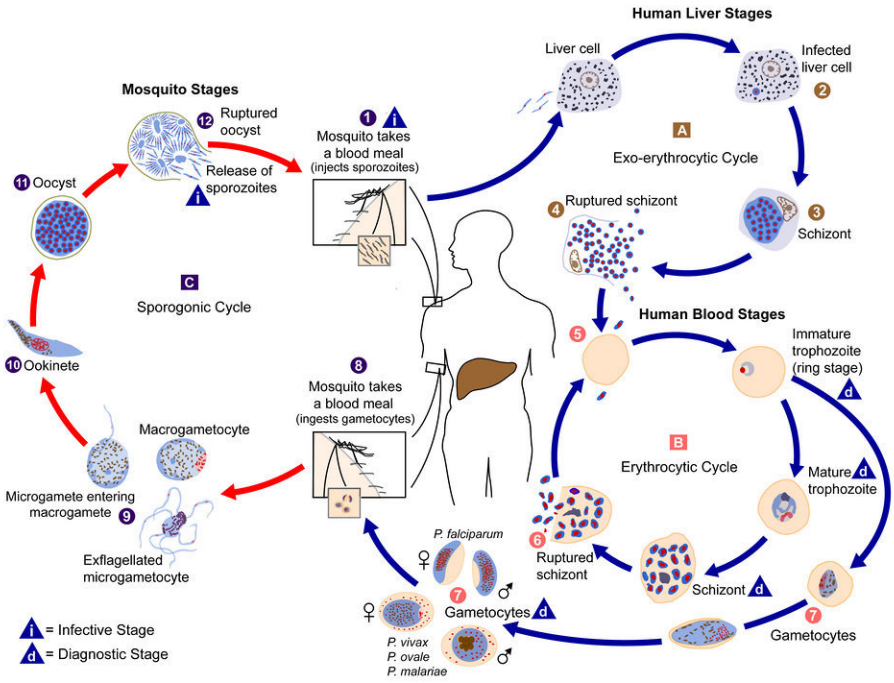

Figure 1.2: Life cycle of the *Plasmodium* parasite. This complex life cycle occurs across both human (blue pathway) and mosquito (red pathway) hosts. Adapted from the Centers for Disease Control and Prevention (CDC).[8]

schizonts which lead to new merozoites in the same manner as in the liver stage. At this point, the RBCs erupt and further RBCs are infected with the newly formed merozoites, repeating this cycle ❻. Typical symptoms of malaria begin to appear during this phase including fever, chills, headache, muscle aches and tiredness.

This stage also forms the divergence point from which new sporozoites are eventually created and more humans are infected. Following the introduction of merozoites into the blood stream and the formation of ring stage trophozoites, the parasites may diverge to a path of sexual reproduction. These trophozoites develop into male and female gametocytes ❼. While the male and female gametocytes are non-pathogenic, it is these that are ingested when a new female *Anopheles* mosquitoes takes a blood meal from the infected human ❽. Once inside the mosquito, the sporogonic cycle begins. The microgametes (male) enter the macrogametes (female) ❾ allowing for the division and fertilisation of the gamete nuclei which form zygotes. These zygotes develop into elongated ookinetes ❿ which penetrate the midgut wall of the mosquito and become oocysts ⓫. Thousands of new sporozoites are released when the growing oocyst bursts ⓬, allowing them to make their way to the salivary glands of the mosquito. The infected mosquito will then inject the parasite into another human during a blood meal to begin the cycle anew ❶.

It is notable that for *P. vivax* and *P. ovale*, the sporozoites may stay dormant in the liver stage (known as hypnozoites) anywhere from weeks to years. Relapses may occur when the hypnozoites

reactivate, releasing merozoites and beginning the cycle again.

1.3 Antimalarial Medicines

Even though the malaria parasite has been in existence for thousands of years, effective antimalarial medicines have only been around since the 1800s. The majority of these past and present drugs fall into four main structural classes of compounds: artemisinin derivatives, 4-aminoquinolines, 8-aminoquinolines and amino alcohols (Figure 1.3). Additionally, other drugs such as antifolates and antibiotics have been repurposed from their original use after having been shown to be efficacious as antimalarials.

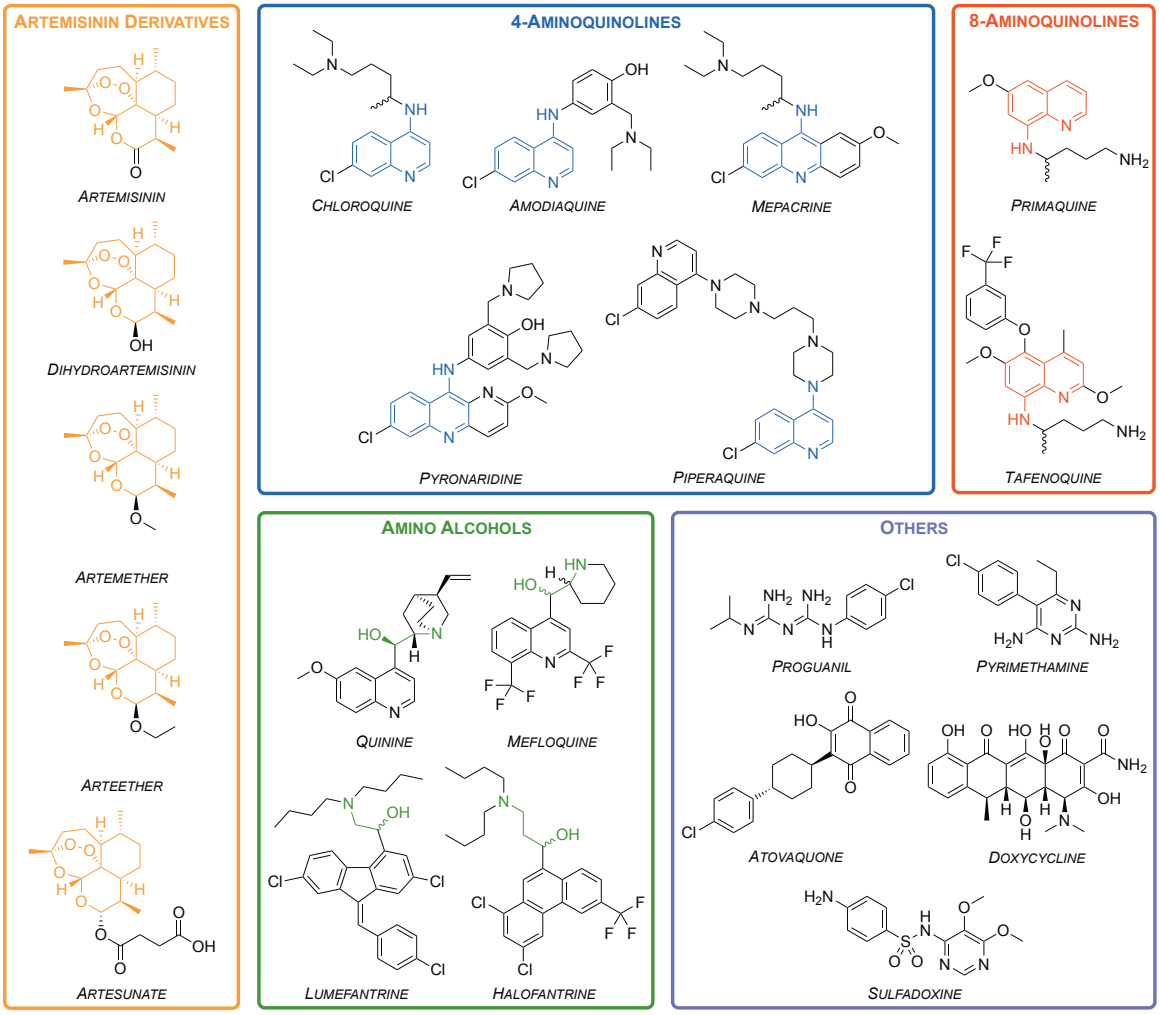

Figure 1.3: Main classes of the common antimalarial drugs used in the past and present. These broadly fit into artemisinin derivatives, 4-aminoquinolines, 8-aminoquinolines and amino alcohols.

Many new antimalarial medicines currently in development (*vide infra*) show structural classes unlike those above. This is typically a consequence of their being targeted towards new mechanisms of action.

1.3.1 Past Antimalarial Drugs

Since the isolation and first use of purified quinine in 1820, a number of other natural and synthetic compounds have been developed. However, as time has passed, strains of the parasite have begun to show signs of resistance towards these drugs, rendering them less effective. Accordingly, their use has ceased or is restricted to particular situations. The following table summaries a number of these historic antimalarial compounds (Table 1.1).

Table 1.1: List of past antimalarial drugs. Summary of well known antimalarials discovered between 1820 and the 1980s.

Compound	Description
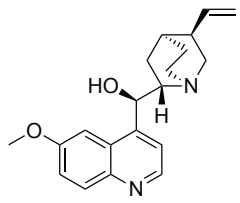 **Quinine**	First isolated from the bark of the cinchona tree in 1820, quinine has been one of the most effective treatments for malaria to date.[9] Resistance was first reported in the 1980s[10] and as of 2006 quinine is no longer used as a frontline treatment.
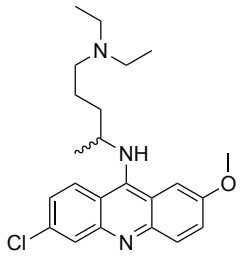 **Mepacrine**	Mepacrine (a.k.a quinacrine) was predominantly used throughout the Second World War as a prophylactic, sold under the trade name Atabrine.[11] It is no longer used due to the high chance of undesirable side effects such as toxic psychosis.[12]
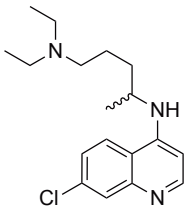 **Chloroquine**	During the 1940s, chloroquine (CQ) was used to treat all forms of malaria with few side effects.[13] Resistance to CQ was first reported in the 1950s and over the years many strains of malaria have developed resistance. Indeed, CQ-resistant strains (e.g. K1, 7GB, W2 and Dd2) of the malaria parasite are now used in potency evaluation assays as a way of showing desirable efficacy.[14]
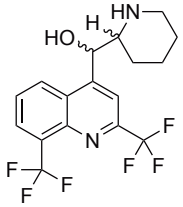 **Mefloquine**	Mefloquine was developed in the 1970s by the United States Army[15] and is still used today. Originally introduced for the treatment of chloroquine-resistant malaria, it has been used as both a curative and a prophylactic drug. Resistance was first reported in 1986.[16] It is thought that the structurally related quinoline drugs (such as quinine, mepacrine, chloroquine and mefloquine) act through the disruption of

	haemoglobin digestion in the blood stage of the parasite.[17]. These drugs are commonly used in combination with a complementary drug (e.g. mefloquine and artesunate, sold as Artequin™) to reduce the chance of resistance development to the quinoline family of compounds. Mefloquine is commonly sold in its racemic form under the brand name Lariam®, however it is no longer widely used due to the central nervous system toxicity that has been suggested to affect a large number of its users.[18]
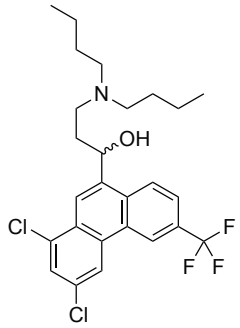 **Halofantrine**	Developed between the 1960s and 1970s by the Walter Reed Army Institute of Research,[19] halofantrine was initially used for treatment against all forms of the *Plasmodium* parasite. Its use has diminished over time due to a number of undesirable side effects, such as the potential for high levels of cardiotoxicity. It is only used as a curative drug and not for prophylaxis due to the high toxicity risks and its unreliable pharmacological properties. Halofantrine is still used today, under the brand name Halfan™, but only in cases where patients are known to be free of heart disease and where infection is due to severe and resistant forms of malaria.[20]

1.3.2 Current Antimalarial Drugs

Since 1977, the WHO has published a list of medications that have been deemed to be essential for basic health care systems.[21] This so-called Model List of Essential Medicines (MLEM), contains the most safe, efficacious and cost-effective medicines for a large range of conditions. In terms of antimalarials, there are currently listed 14 medicines for curative (10) and prophylactic (4) treatment, with formulations as either single compounds or as combinations (Figure 1.4). As described previously, quinine, chloroquine and mefloquine are still used today and are all on the MLEM. Specifically, quinine is used for the treatment of severe malaria in cases where artemisinins are not available, chloroquine is used for the treatment of *P. vivax* in regions where resistance has not developed and mefloquine is only used in combination with artesunate. Of all these medicines, perhaps the most effective are the artemisinin-based combination therapies (ACTs) which use an artemisinin derivative (short-acting) in combination with one or more complementary compounds (long-acting and possessing different mechanisms of action).

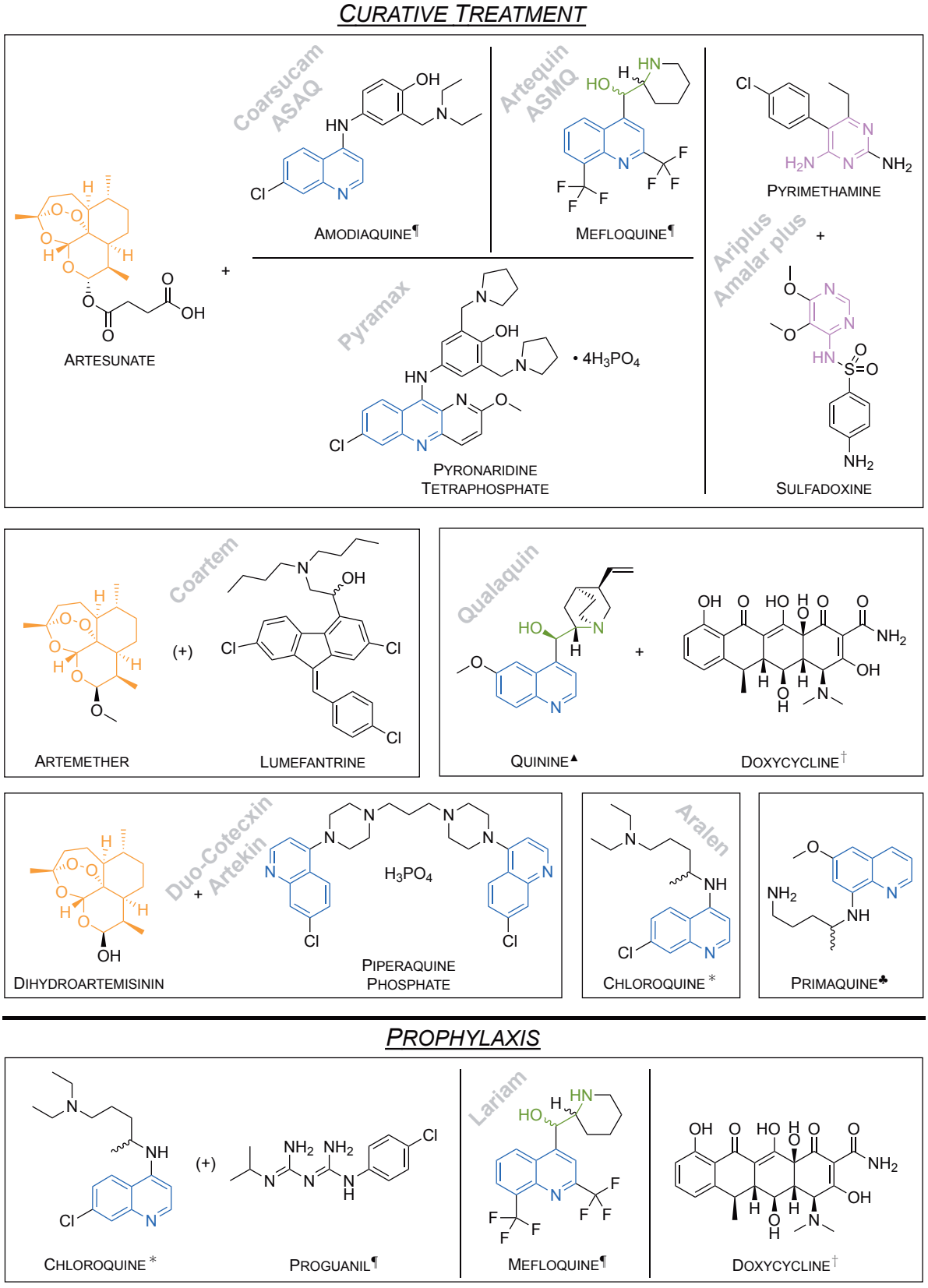

Figure 1.4: Entries in the WHO Model List of Essential Medicines for the treatment and prophylaxis of malaria. (+) indicates the drug on the left may either be used by itself OR in combination with the drug on the right. Formulated as salts: *phosphate or sulfate; †hydrochloride or hyclate; ¶hydrochloride; ▲ hydrochloride or sulfate or bisulfate; ♣diphosphate.

The following table summaries the antimalarial compounds that are widely used today (Table 1.2). Information regarding their discovery, mechanism of action (MoA) and use are provided.

Table 1.2: List of current antimalarial drugs. Summary of the antimalarials widely used today.

Compound	Description
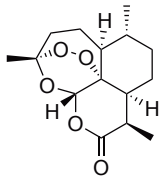 **Artemisinin & its derivatives**	Artemisinin was first isolated in 1971 by Tu Youyou from the plant *Artemisia annua*, a herb that has commonly been used in Chinese traditional medicine.[22] Due to the great positive impact of artemisinin in combating malaria, Youyou was jointly awarded the Nobel Prize in Physiology or Medicine in 2015 for "*her discoveries concerning a novel therapy against malaria*".[23] Artemisinin has been shown to be efficacious against all multi-drug resistant forms of *P. falciparum*. The most common derivatives of artemisinin are artemether, artesunate and arteether. These semi-synthetic derivatives are prodrugs which are transformed to the active metabolite, dihydroartemisinin. The use of artemisinins has been integral in the fight against malaria with ACTs making up the majority of modern day treatments.[24] Although slow to develop, the first report of resistance to artemisinin was in western Cambodia in 2008.[25] Ten years later, in February of 2018, a report was published identifying more than 30 independent cases of artemisinin resistance in southeast Asia, specifically with resistance to the dihydroartemisinin–piperaquine combination therapy.[26]
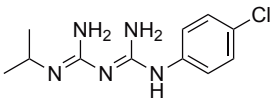 **Proguanil** 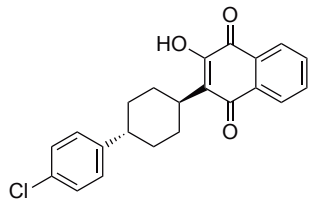 **Atovaquone**	Proguanil was first reported in 1945 as one of the first antifolate antimalarial drugs,[27] while atovaquone was first reported in 1991 for the treatment of protozoan infections.[28] The combination of these, commonly sold as Malarone^{TM}, has been marketed by GlaxoSmithKline (GSK) since the early 2000s, and has proven to be a very effective antimalarial due to the synergistic effect of the two components. This is, in large part, due to the compounds' different MoAs. Atovaquone acts as a cytochrome bc_1 complex inhibitor which blocks mitochondrial electron transport.[29] Proguanil (when used alone) acts as a dihydrofolate reductase (DHFR) inhibitor through its metabolite, cycloguanil (CG) which

	disrupts deoxythymidylate synthesis. When used in combination with atovaquone, however, proguanil does not act as a DHFR inhibitor but has instead been shown to reduce the concentration of atovaquone required for treatment.[30] Generic atovaquone/proguanil is still available for the treatment of chloroquine-resistant malaria.
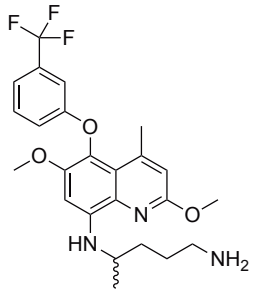 **Tafenoquine**	First discovered in 1978 at the Walter Reed Army Institute of Research, tafenoquine (TQ) was recently approved by the United States Food and Drug Administration for use as the first new single-dose treatment of *P. vivax* malaria in over 60 years.[31] TQ is thought to be a prodrug which is metabolised to the active TQ-quinone, however the MoA is not well understood.[32] It is currently sold under the brand name Krintafel^{TM}.
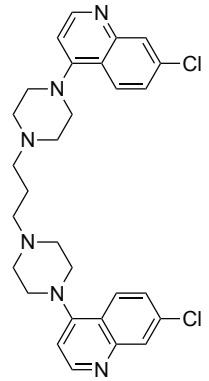 **Piperaquine**	Piperaquine was developed in the 1960s as part of the Chinese National Malaria Elimination Programme.[33] Initially used throughout China as a replacement for chloroquine, resistance led to its diminished use as a monotherapy. While the MoA of piperaquine is not completely understood, studies have suggested that it acts by accumulating in the digestive vacuole and inhibiting haem detoxification through the binding of haem-containing species.[24,34] These days, piperaquine is used as a partner drug with dihydroartemisinin (commonly sold under the trade name Eurartesim®).
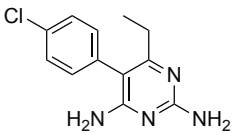 **Pyrimethamine** 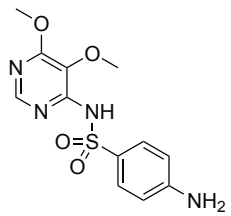 **Sulfadoxine**	Pyrimethamine (PYR) was developed in the early 1950s by Gertrude Elion and George Hitchings and is now sold under the trade name Daraprim^{TM}.[35] The development of pyrimethamine was a part of the efforts that won Elion, Hitchings and Black the joint Nobel Prize in Physiology or Medicine in 1988 for "*their discoveries of important principles for drug treatment*".[36] Sulfadoxine was developed in the early 1960s.[37] It is no longer used as a preventative drug due to high levels of resistance. The combination of pyrimethamine and sulfadoxine was approved for use for the treatment of malaria in 1981 and is now commonly sold under the trade name Fansidar®. Both drugs are known to

	target the parasite folate biosynthesis pathway.[38] Pyrimethamine inhibits dihydrofolate reductase, while sulfadoxine inhibits dihydropteroate synthetase.
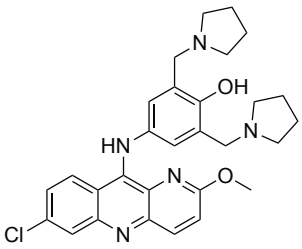 **Pyronaridine**	Pyronaridine was first synthesised in the 1970s at the Institute of Chinese Parasitic Disease.[39,40] It has been found to be efficacious against chloroquine-resistant strains and has been in use for over 40 years, sold under the trade name Pyramax® (in combination with artesunate). Like lumefantrine, pyronaridine has been found to act through the inhibition of β-haematin formation.[41]
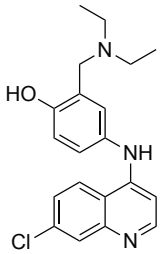 **Amodiaquine**	Amodiaquine was first synthesised in 1948.[42] It is mainly used for the treatment of uncomplicated *P. falciparum* malaria when used in combination with artesunate and is commonly sold under the trade name Camoquine® or Coarsucam™.[43] Similar to chloroquine, amodiaquine's MoA is thought to involve complexation with haem and inhibition of haemozoin formation.[44]
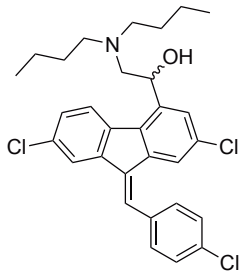 **Lumefantrine**	Lumefantrine (a.k.a. benflumetol) was first synthesised in 1976 as part of the Chinese antimalarial research effort "Project 523" which also resulted in the discovery of artemisinin.[45] It is currently sold under the trade name Coartem®. The exact MoA of lumefantrine is unknown, however studies suggest that it inhibits nucleic acid and protein synthesis through the inhibition of β-haematin formation by complexation with haemin.[44] Lumefantrine is currently used only in combination with artemether.

1.3.3 Future Antimalarial Drugs

At the forefront of antimalarial research and development is the Medicines for Malaria Venture (MMV). Founded in 1999, MMV has been supporting a large number of projects from universities and pharmaceutical companies with the goal of discovering and implementing new medicines to combat the ever increasing drug-resistant strains of the *Plasmodium* parasite. Collaborations with MMV occur at multiple stages of the antimalarial pipeline (Figure 1.5), ranging from the beginnings of drug discovery and development to the various preclinincal and clinical stages, and

finally through to the commercialisation of new antimalarial drugs.

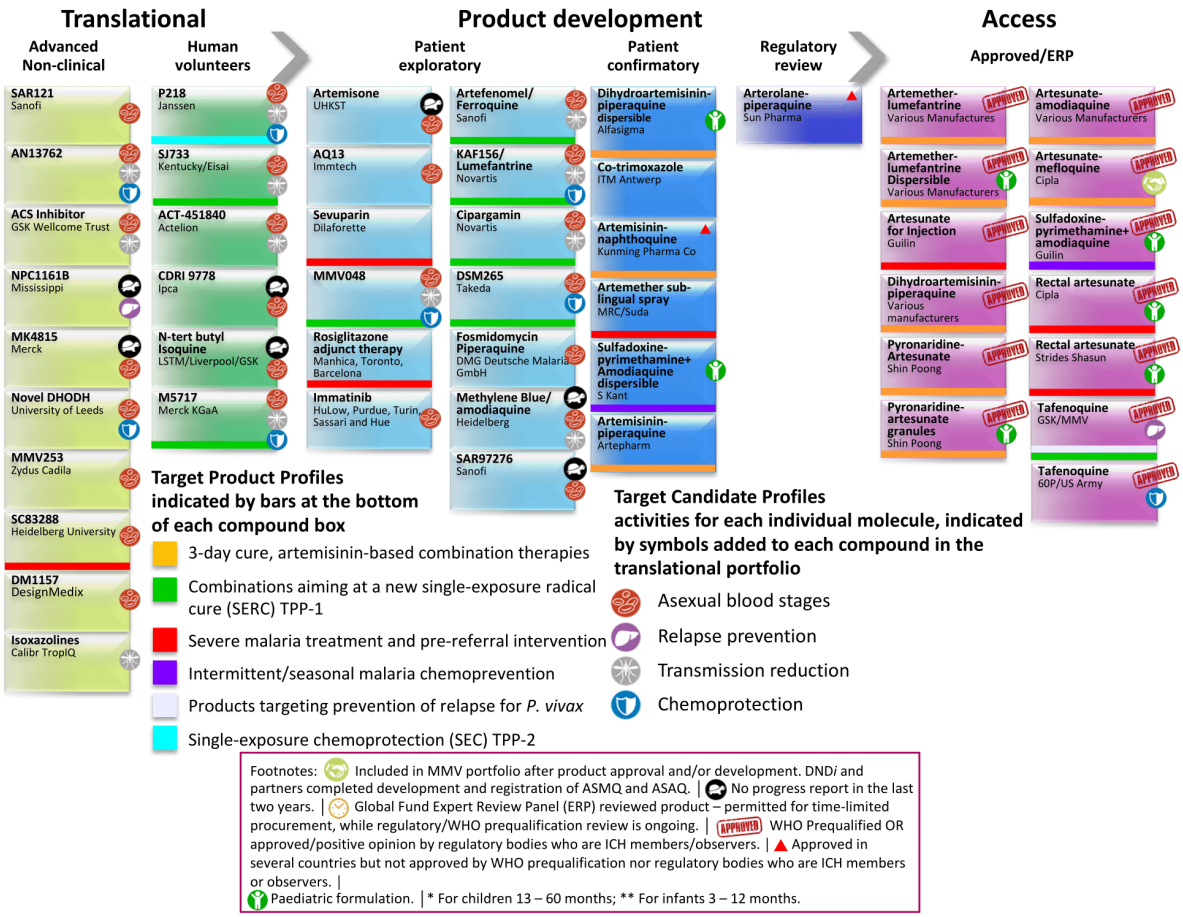

Figure 1.5: Snapshot of the projects supported by MMV at the later stages of the drug discovery pipeline. Adapted from the MMV-supported projects webpage.[46]

The potential for these compounds to act as new antimalarials is judged by a number of requirements: novel modes of action with no cross-resistance to current drugs; single-dose cures (artesunate and chloroquine are unable to do this); activity against both the asexual blood stages that cause disease and the gametocytes responsible for transmission; compounds that prevent infection (chemoprotective agents); and compounds that clear *Plasmodium vivax* hypnozoites from the liver (anti-relapse agents).[47,48]

Over the past few years, a number of reviews have been published evaluating the potential future of antimalarial drugs. Of note: triple-antimalarial drug combinations were examined in 2014;[49] a review on the numerous strategies currently used in antimalarial drug discovery was published in early 2017;[50] and an in-depth primer on all aspects of malaria was published in late 2017.[51] In early 2018, two reviews were published highlighting the discovery and development of a number of new antimalarial drug candidates.[52,53]

New antimalarial compounds can be discovered not only through traditional methods (e.g. high-throughput screening followed by lead optimisation) but also by exploiting existing drugs. For instance, a new treatment may be found through the exploration of new combinations and formulations of current antimalarials. This may help overcome issues with resistance to a particular component or may assist in the delivery of the drug allowing it to be more effective. Alternatively, existing drugs used for other purposes may be found efficacious against malaria and subsequently be repurposed as a new antimalarial treatment. This can be advantageous since these compounds may have already shown good biological properties (e.g. an acceptable safety profile) and may also reveal novel MoAs. Examples include those shown in the left panel of Figure 1.6.

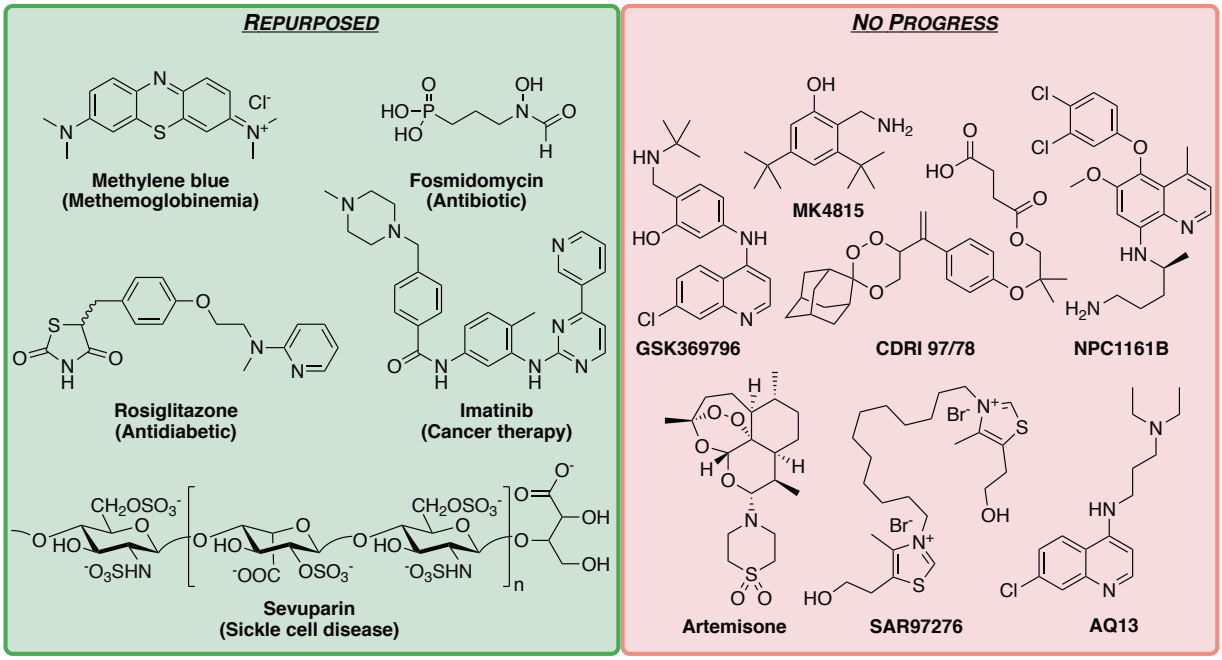

Figure 1.6: New antimalarial compounds in development as a result of drug repurposing and candidates that have reported no significant progress in the last two years. Original indications for the drugs are shown in parentheses. Many of these repurposed drugs are already in Phase II trials as new potential antimalarials. Those compounds showing no recent progress may have encountered issues during preclinical or early clinical studies.

- **Methylene blue**, a drug traditionally used for the treatment of methemoglobinemia. Last completed Phase II trials in 2017 (NCT02851108) as a combination with primaquine.
- **Fosmidomycin**, an antibiotic. Most recently in Phase II trials in 2015 (NCT02198807) as a combination with piperaquine.
- **Rosiglitazone**, an antidiabetic drug. Currently in clinical trials as an adjunctive therapy for severe malaria (NCT02694874).
- **Imatinib**, a cancer therapy drug. Currently in Phase II trials (NCT03697668) as a triple combination with dihydroartemisinin-piperaquine.

- **Sevuparin**, a drug for the treatment of sickle cell disease. Last in Phase I/II trials in 2014 (NCT01442168) as a combination with atovaquone-proguanil.

The seven compounds in the right panel of Figure 1.6 were discovered and developed with the hope of progressing into clinical trials as potential new antimalarial candidates. However, over the past two years, progress in the development of these compounds has slowed, making the fate of these drug candidates less clear.

- Developed at the Liverpool School of Tropical Medicine in 2009, **GSK369796** (a.k.a *N-tert* butyl isoquine) was designed as an alternative to amodiaquine.[54,55] It completed preclinical studies,[56] and was last in Phase I trials in 2008 (NCT00675064).
- **MK4815** was developed in 2012 at Merck but is still in preclinical studies due to safety issues.[57]
- **CDRI 97/78** is a fast-acting novel trioxane antimalarial first synthesised in 2001 by a team at the Council of Scientific and Industrial Research in India.[58] Having passed all preclinical studies, it was last seen to have completed first-in-human Phase I trials in 2014.[59]
- The chiral 8-aminoquinoline derivative, **NPC1161B** was developed at the University of Mississippi and was still in preclinical studies in 2014.[60–63]
- **Artemisone** is a second-generation semi-synthetic artemisinin derivative developed at the Hong Kong University of Science and Technology, that has previously been shown to be as efficacious as artesunate, with minimal neuro- and cytotoxicity and a comparably low cost of production.[64–68] It was withdrawn from Phase II/III trials in 2010 (NCT00936767).
- The bisthiazolium salt, **SAR97276**, was discovered and developed by Sanofi in 2005,[69] however further investigation was terminated in 2012 after Phase II trials (NCT01445938).
- **AQ-13** is a chloroquine derivative that was first described in 1946.[70] While only differing to CQ in the amine side-chain, this difference has been linked to its increased efficacy against CQ-resistant strains.[71] It has a MoA and pharmacokinetic properties similar to that of CQ.[72,73] **AQ-13** last completed Phase II trials at the end of 2017 (NCT01614964),[74] however there has been no mention of any following active trials so the ongoing status of this compound is unclear.

The compounds in the remainder of this section are currently still actively being pursued. Key biological data for each compound will be shown in a graphical summary, along with a description of the key physical and biological properties identified during the hit to lead campaigns.

1.3.3.1 Preclinical

Once a lead compound has been identified, optimisation of the structure can begin. This largely involves investigation into the structure activity relationship (SAR) of the drug, optimising for properties such as potency (both *in vitro* and *in vivo*), solubility and metabolic stability. The candidate must also be assessed for any possible toxicity (e.g. dosing, cytotoxicity/genotoxicity levels, etc.).

– **M5717**

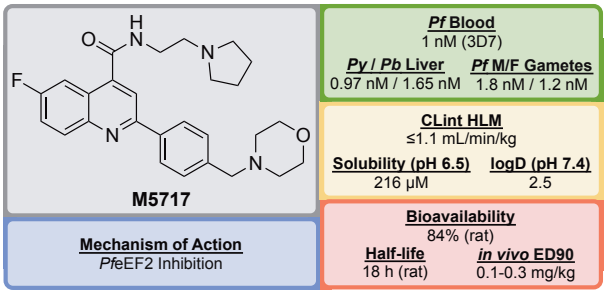

M5717 was developed in 2015 by a team led by the Drug Discovery Unit (DDU) in Dundee and was shown to have potent activity against multiple stages of the *Plasmodium* parasite *via* a novel mechanism of action.[75,76]

Initial phenotypic screening of the Dundee protein kinase scaffold library against the 3D7 multi-drug-resistant *P. falciparum* strain identified a compound (**M1**, Figure 1.7) that possessed high potency against the parasite, albeit with poor physicochemical properties. Optimisation of this structure (*via* **M2** and **M3**) led to improvements across the board (**M5717**).

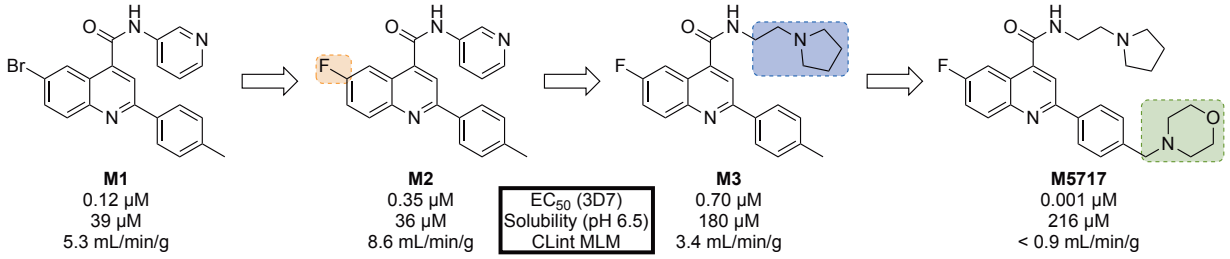

Figure 1.7: Key stages in the hit to lead pathway of M5717. Initial replacement of Br for F, replacement of pyridine with ethylpyrrolidine, and addition of a morpholine fragment led to the optimised compound **M5717**.

In addition to the nanomolar activity against the 3D7 strain, **M5717** has shown almost equal potency against a number of other drug-resistant strains (K1, W2, 7G8, TM90C2A, D6 and V1/S) as well as similar potencies across multiple life cycle stages (liver schizonts, gametocytes and ookinetes). **M5717** was found to be as effective as current antimalarial drugs (chloroquine, mefloquine, artemether, dihydroartemisinin and artesunate) when evaluated in the *in vivo P. berghei* mouse model for single-dose efficacy showing >99% reduction in parasitemia at doses of 4 × 30 mg/kg *p.o. q.d.* and an ED_{90} of 0.1-0.3 mg/kg. Due to its novel MoA (*Pf*eEF2 inhibition, see Chapter 5) and its ability to clear blood stage parasites completely, **M5717** satisfies the

requirements to be a long duration partner and could be used as part of a combination therapy with a fast-acting compound.[77] Additionally, it has shown the ability to act as a transmission-blocking drug (stage IV–V) and also to be effective for chemoprotection. In late 2017, **M5717** was cleared for progression from development to Phase I clinical trials for volunteers in Australia (NCT03261401).

– MMV253

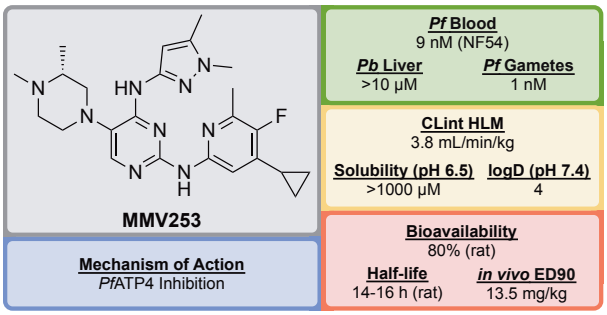

Identified by AstraZeneca in 2015, **MMV253** is a novel triaminopyrimidine (TAP) that has shown good *in vitro* potency and *in vivo* efficacy, and acts through another novel MoA.[78]

High-throughput screening of 500,000 compounds from AstraZeneca's library against blood stage *P. falciparum* resulted in the identification of a promising series of TAPs. The initial hit (Figure 1.8) suffered from hERG inhibition and poor solubility which, through lead optimisation, was improved upon to give a compound that possessed high potency and desirable pharmacokinetic properties (**MMV253**).

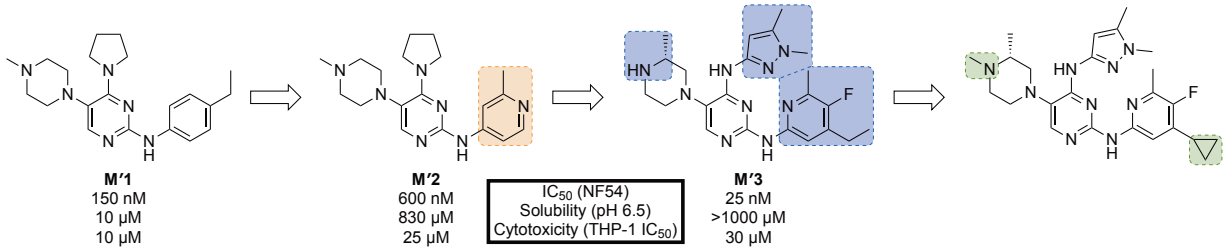

Figure 1.8: Key stages in the hit to lead pathway of MMV253. Initial replacement of ethylbenzene on **M′1** with 2-methylpyridine resulted in lower hERG affinity and improved solubility. Substitution of the pyrrolidine in **M′2** with an imidazole containing an amine spacer further improved solubility and greatly improved the potency. Addition of an *N*-methyl group and a cyclopropane moiety led to the optimised compound **MMV253**.

When screened against numerous mutant resistant strains with various mechanisms of resistance, **MMV253** showed no spontaneous reduction in potency, which can be attributed to its novel MoA of P-type Na^+–ATPase transporter (*Pf*ATP4) inhibition (see Chapter 5). Good *in vitro-in vivo* correlation (IVIVC) was shown with a predicted human half-life of ∼36 hours (which is long compared to another fast-killing drug, artemisinin, which has a human half-life of 1 hour). As of late 2016, the pharmaceutical company Cadila Healthcare owns the license for the compound series and is now doing further lead development in order to progress the drug through preclinical trials.[79]

– UCT943

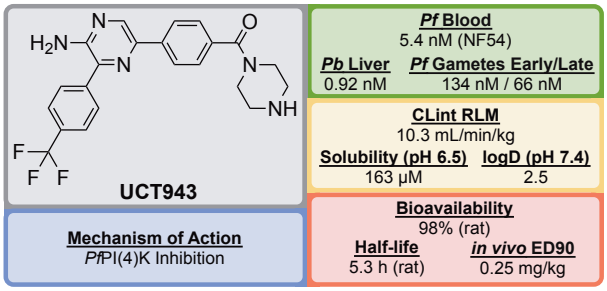

Discovered in 2016 by a team at the University of Cape Town, South Africa, **UCT943** is a key compound in a novel class of 2-aminopyrazine antimalarials that has shown single dose curative ability *in vivo* and the potential to be a clinical candidate.[80]

The original 3,5-diaryl-2-aminopyridine series was identified from a high-throughput screen of ~36,600 compounds from the commercially available SoftFocus kinase library.[81] The initial hit (**U1**, Figure 1.9) showed good *in vitro* potency against the drug-sensitive NF54 strain (IC_{50} = 49 nM) but suffered from poor solubility and high metabolic clearance. The issues with poor *in vivo* stability were addressed by replacing the labile hydroxy and methoxy groups with a single trifluoromethyl group (**U2**). While this change did result in an improvement in metabolic clearance, the solubility of the compound was significantly reduced. Replacement of the mesyl group with a piperazine carboxamide group (**U3**) and introduction of another nitrogen atom into the pyridine ring led to the lead compound (**UCT943**).[82,83]

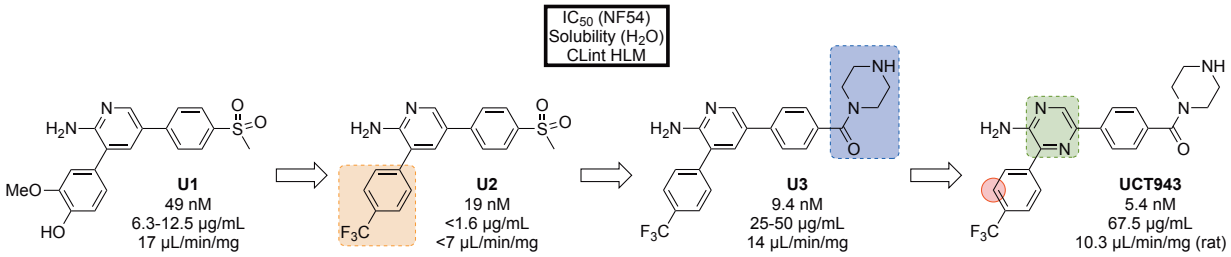

Figure 1.9: Key stages in the hit to lead pathway of UCT943. Initial change of the phenyl substituents with a single trifluoromethyl group led to greater *in vivo* stability. Introduction of piperazine amide instead of methylsulfonyl and a pyrazine instead of a pyridine led to the improved solubility and potency of the optimised compound. Interestingly, introduction of a nitrogen atom in the red circle resulted in complete inactivity *in vivo*.

UCT943 has shown curative ability at doses of 4 × 10 mg/kg and has an ED_{90} of 1 mg/kg in the *P. berghei* mouse model. Interestingly, another closely related molecule (with a nitrogen atom instead of a carbon atom in the red circle of **UCT943**) was evaluated during the SAR study and displayed similar *in vitro* activity (IC_{50} = 9.1 nM) and solubility (198 μM) however, it showed a complete lack of *in vivo* activity with a <40% reduction in parasitemia using a comparable dosage. **UCT943** is potent across multiple parasite life stages of both *P. falciparum* and *P. vivax*. Its target is the *P. falciparum* phosphatidylinositol-4-OH kinase (*Pf*PI(4)K), which has also been implicated as the target for MMV048 (*vide infra*).[84] **UCT943** was originally in development to be a back-up to **MMV048**, however, due to preclinical toxicity, **UCT943** has since been

withdrawn.

– **AN13762**

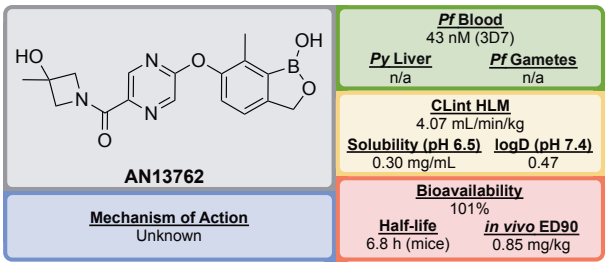

From a drug discovery campaign run at Anacor Pharmaceuticals, beginning in 2010 with a novel class of benzoxaborole antimalarial compounds,[85] lead compound **AN13762** was identified in 2017. Key properties include excellent *in vitro* and *in vivo* activity, efficacy against multiple strains of the parasite and the ability to perform as a fast-acting drug.[86]

The initial hit compound, **AN3661** (**A1**, Figure 1.10), which possessed 26 nM *in vitro* potency against the 3D7 strain, was identified by screening a library of boron-containing compounds (previously shown to have selective activity against fungi, bacteria, parasites and inflammation) in a *P. falciparum* whole cell assay. Further SAR studies resulted in compound **A2**, in which the alkylcarboxylic acid chain was transposed and replaced by a substituted pyrazine ether moiety. While the potency was improved from the hit compound, it suffered from high metabolic clearance.[87] This was addressed by replacing the ester with an amide (**A3**), improving the metabolic stability and bioavailability, but this time reducing the potency. The lead compound **AN13762** was identified by modification of the primary amide to a cyclic tertiary amide, and by introduction of a methyl group on the benzoxaborole, resulting in improved potency and metabolic stability.[86]

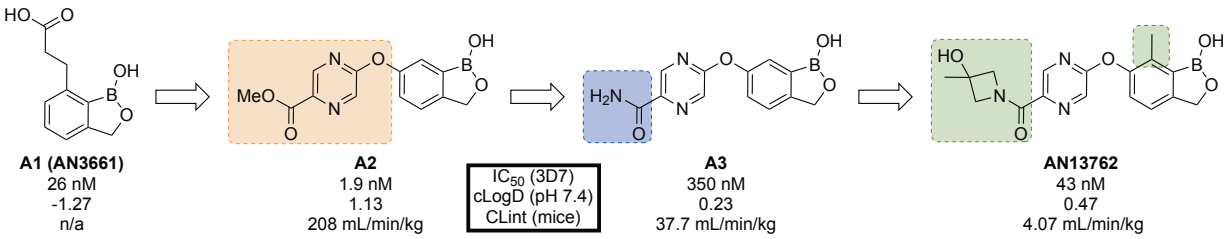

Figure 1.10: Key stages in the hit to lead pathway of AN13762. Initial replacement of the carboxylic acid chain with a pyrazine, and subsequent switch of the ester to a substituted amide helped to improve *in vivo* stability and bioavailability leading to the optimised compound.

AN13762 has been shown to be equipotent across a wide range of drug resistant strains and has displayed *in vivo* clearance rates similar to artesunate. There is no inherent genotoxicity (as shown in Ames assays and *in vivo* rat micronucleus studies) or cytotoxicity (at concentrations up to 100 μM in human cell lines).[86] The precise mechanism of action for **AN13762** is currently unknown, however initial MoA studies on **AN3661** have identified the *P. falciparum* cleavage and polyadenylation specificity factor 3 (*Pf*CPSF3) as a potential target.[88] **AN13762** has proceeded into the preclinical phase, with first-in-human studies planned for 2019.

– SC83288

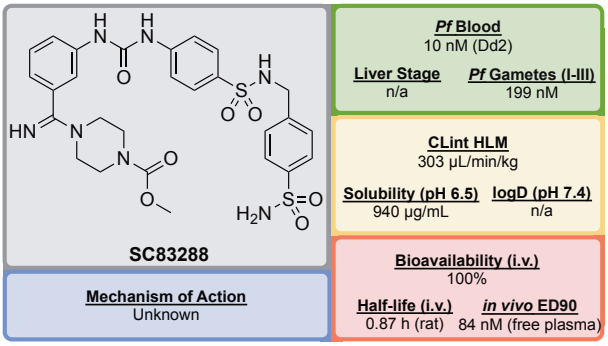

Developed in 2017 by a team at Heidelberg University, **SC83288** is an amicarbalide derivative that possesses a novel chemotype for current antimalarials, may have a potentially new MoA and has shown the ability to be a fast-acting drug for the intravenous treatment of severe malaria.[89]

An *in silico* screen of a library of small molecule compounds for their ability to dock into *P. falciparum* lactate dehydrogenase led to the identification of amicarbalide (**S1**, Figure 1.11), which was found to be highly potent (IC_{50} = 10 nM) against the Dd2 strain.[90] In order to overcome a potential DNA binding effect, an amidine group was replaced with a sulfonamide linker leading to **S2**, which possessed better solubility and improved metabolic stability. Further modification of the other amidine group with a substituted piperazine ring (**S3**) led to improved potency and aqueous solubility, but the compound suffered from poor permeability. Ultimately, replacement of the butyl chain with an acetyl group led to the highly potent lead compound **SC83288**.

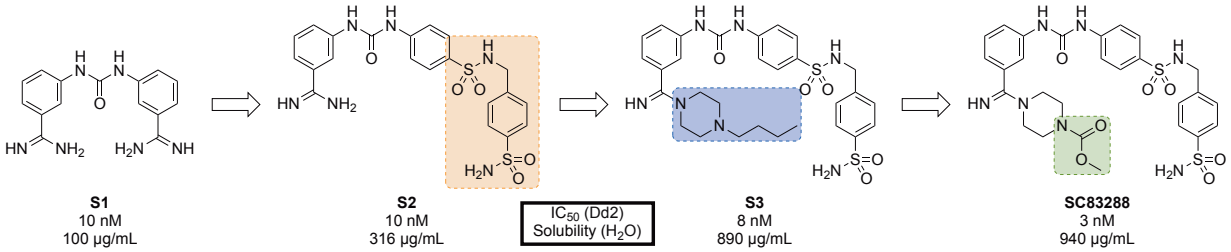

Figure 1.11: Key compounds in the discovery of SC83288. Initial modification of one amidino group with a sulfonamide linker (**S2**) resulted in improved solubility. Further modification of the remaining amidine group with substituted piperazine moieties ultimately led to the optimised compound with good solubility, permeability and high potency.

SC83288 has been shown to be potent against a number of drug-resistant strains at IC_{50} values <20 nM and is also efficacious against early stage (I-III) gametocytes (IC_{50} = 199 nM) but not against late stage (IV and V) gametocytes. It has an excellent safety profile, with no cytotoxicity, genotoxicity or hERG binding. In the *P. vinckei* rodent malaria model, **SC83288** was able to fully cure the infection at a dose of 4 × 20 mg/kg i.p. *q.d.* with no resurgence of infection. It is however, completely inactive against *P. berghei*. While the exact MoA of **SC83288** is unknown, the generation of resistant clones has identified *Pf*ATP6 as a possibly relevant target. However, it has been shown that **SC83288** does not directly inhibit this target suggesting *Pf*ATP6 may have a less direct role in the mechanism of action. Additionally, the *P. falciparum* multi-drug resistance transporter 2 (*Pf*MDR2) has been identified as a possible mechanism of resistance for

SC83288, which would facilitate the clearance of the drug from the parasite. **SC83288** has been evaluated alongside artemisinins, showing no cross-resistance and highlighting its potential as an alternative to artesunate for the treatment of severe malaria when combined with a slow-acting partner drug.[91]

– **DM1157**

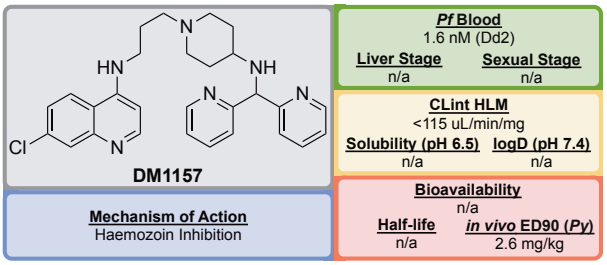

Discovered in 2010 by a team at Portland State University and further developed by DesignMedix, **DM1157** is part of a class of compounds known as "reversed chloroquines" (RCQs), designed to overcome chloroquine-resistant and chloroquine-sensitive strains of the malaria parasite. The compound has been shown to be efficacious *in vitro* and *in vivo*.[92]

CQ resistance is known to be linked to the *P. falciparum* chloroquine resistance transporter (*Pf*CRT): mutations to this target facilitate the expulsion of CQ from the parasite. A class of molecules has been identified, so-called "reversal agents", that can inhibit *Pf*CRT, thus slowing the export of CQ from the parasite. By combining the chloroquinoline core of CQ (**D1**, Figure 1.12) with the known reversal agent, imipramine, the first RCQ (**D2**) was designed, but this molecule suffered from poor bioavailability and metabolic stability.[93] Subsequent SAR studies resulted in the substitution of the imipramine motif with a 1-(2,2-diphenylethyl)piperazine moiety which led to a compound (**D3**) that was more stable to metabolic cleavage, but suffered from a high cLogP. In order to overcome this, the two phenyl groups were replaced with pyridines and the piperazine replaced with an aminopiperadine resulting in the lead compound, **DM1157** that possessed a lower cLogP value (3.6) while still maintaining high potency against both CQ-resistant (Dd2 = 1.6 nM) and CQ-sensitive strains (D6 = 0.9 nM) when compared to CQ (cLogP = 5.1, Dd2 = 102 nM, D6 = 6.9 nM).

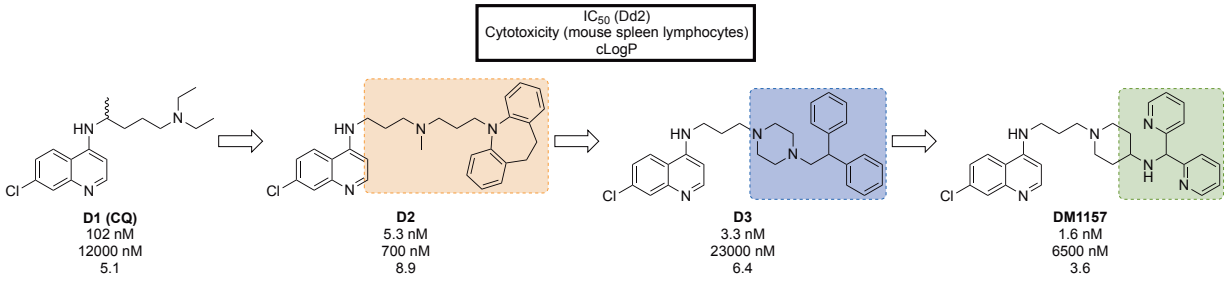

Figure 1.12: Key compounds in the discovery of DM1157. Initial combination of the reversal agent, imipramine, with the CQ core resulted in the potent RCQ compound **D2**. Subsequent replacement of the reversal agent with 1-(2,2-diphenylethyl)piperazine (**D3**), and further modification with pyridine rings led to improved potency and cLogP values for the optimised compound.

In a *P. berghei* rodent model, **DM1157** showed good efficacy both orally and subcutaneously. Most notably, a >99.9% reduction in parasitemia was seen at an oral dose of 4 × 30 mg/kg with 2 of 3 mice cured 30 days postinfection. **DM1157** has also been evaluated against *P. falciparum* and *P. vivax* multi-drug resistant field isolates in Indonesia and was found to be 3-fold more potent than CQ in both species.[94] CQ is known to bind to haem and inhibit β-haemozoin formation. **DM1157** (and other RCQ compounds) have been shown also to act in this manner, but with much higher levels of inhibition of β-haemozoin both *in vitro* and *in vivo*. **DM1157** is currently in Phase I trials to evaluate its safety and pharmacokinetics in humans (NCT03490162).

1.3.3.2 Translational

Upon the completion of preclinical trials, the drug will have either passed or failed the required safety standards and pharmacokinetic profiling. For a compound that has passed these requirements, trials may then be conducted in human volunteers in order to show its efficacy as a potential treatment.

– **P218**

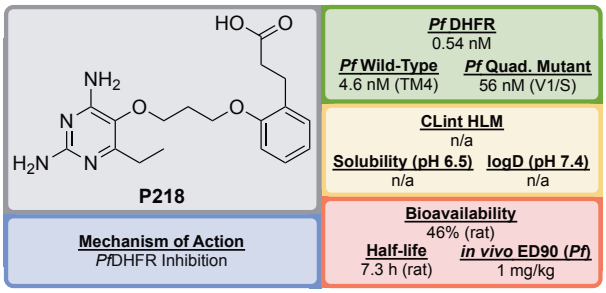

P218, discovered by BIOTEC Thailand in 2012, is an antifolate antimalarial drug bearing resemblance to the 2,4-diaminopyrimidine core structure of PYR, and is highly selective for the *P. falciparum* dihydrofolate reductase (*Pf*DHFR).[95]

Unlike the typical high-throughput screening that is used for the identification of hit compounds in medicinal chemistry, **P218** was identified through careful examination of the cocrystal structures of known *Pf*DHFR inhibitors and their protein targets. It was initially observed that 2,4-diaminopyrimidines acted as antagonists to folic acid, leading to the discovery and development of methotrexate (**MTX**) as an antitumor drug (Figure 1.13). By examining the binding interactions with DHFR, the structure of **P65** was identified. Over 200 compounds (not described in the original report) were designed and synthesised after further examination of potential interactions with amino acid residues, with the optimised structure of **P218** being identified as the best compound.

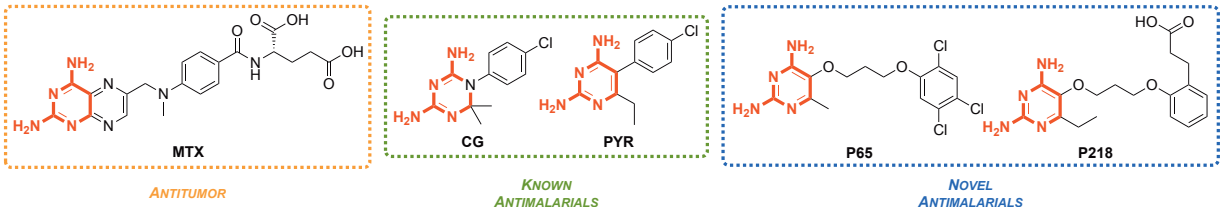

Figure 1.13: Key compounds in the discovery of P218. The key 2,4-diaminopyrimidine core highlighted in red can be found in a number of DHFR inhibitors.

The 2,4-diaminopyrimidine scaffold of **P218** has been found to bind deep in the active site of *Pf*DHFR in both wild-type and mutant strains. This, along with the hydrogen bonding interaction of the carboxylate group with an Arg residue at the opposite end of the active site results in tighter binding and a longer residence time when compared to **PYR**. Since **P218** is contained almost entirely within the dihydrofolate binding site, the strength of the binding should be strong enough to overcome any amino acid mutations, thus minimising the chance of drug-resistant mutations to arise. The novel two-step mechanism of action for binding to *Pf*DHFR (see Chapter 5) allows **P218** to overcome resistance that has emerged from the use of pyrimethamine. **P218** has also shown high selectivity to the binding of malarial over human DHFR, which translates into reduced toxicity. *In vivo* studies have shown **P218** to be highly efficacious against *P. falciparum* and *P. chabaudi* in mice with ED_{90} values of 1 mg/kg and 0.75 mg/kg respectively. In the *in vitro* and *in vivo* potency assays that were run, **P218** was found to be more potent than **PYR** in all cases. Along with its high potency and good safety profile, **P218** has the potential to be a replacement for **PYR** combination with **CG** in areas where *Pf*DHFR resistance has emerged. **P218** has currently completed Phase I trials (NCT02885506).

– (+)-SJ733

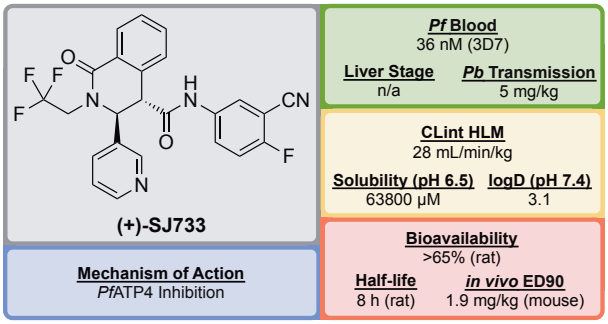

In a campaign originating from a partnership between St Jude Children's Research Hospital and Rutgers University in 2010, **(+)-SJ733** was identified as a novel tetrahydroisoquinolone carboxanilide that possessed excellent *in vivo* antimalarial activity.[96]

A high-throughput phenotypic screen of >300,000 compounds against the *P. falciparum* 3D7 strain revealed a number of bioactive scaffold types, one of which was the tetrahydroisoquinolone carboxanilide compound (**S′1**, Figure 1.14) possessing an *in vitro* EC_{50} of 53 nM. Further metabolic studies using mouse liver microsomes (MLM) revealed the susceptibility of the methoxy group to metabolism by demethylation. This was overcome by replacing the aniline substituents with

fluoro and cyano groups (**S′2**), with an added effect of twofold increase in potency. Another suspected metabolic hotspot, the thiophene group, was replaced with a pyridyl group (**S′3**) leading to improved solubility and maintenance of the potency. A further increase in solubility was seen when the last metabolically vulnerable isobutyl group was replaced with a trifluoromethyl moiety giving the lead compound **(+)-SJ733**. It was notable that the (+)-(3*S*,4*S*) enantiomer was found to be significantly more potent (EC_{50} = 36 nM) than the corresponding (–)-(3*R*,4*R*) enantiomer (EC_{50} = 587 nM).[97]

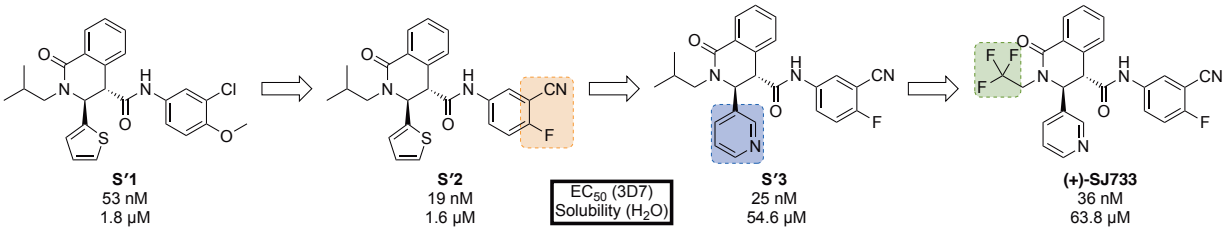

Figure 1.14: Key stages in the hit to lead pathway of (+)-SJ733. Poor metabolic stability of the hit compound was addressed by replacement of the chloro and methoxy groups with cyano and fluoro groups respectively. Further *in vivo* stability and solubility improvements were made by changing the thiophene to a pyridine. Finally, the *gem*-dimethyl group was substituted with a trifluoromethyl group to eliminate possible metabolic oxidation.

(+)-SJ733 was found able to cure malaria at doses of 4 × 100 mg/kg in the *P. berghei* mouse model with an ED_{90} of 1.9 mg/kg. Its transmission blocking potential was shown in infected mice with an ED_{50} of 5 mg/kg. There is no cytotoxicity and, when compared to the currently used antimalarials such as artesunate, chloroquine, and pyrimethamine, it has been found to be more potent *in vivo*.[98] The mechanism of action of **(+)-SJ733** has been shown to be through the inhibition of *Pf*ATP4 (see Chapter 5). This target has been implicated as the MoA for a number of other structurally diverse compounds.[99] The compound is currently in the recruiting stage of first-in-human study trials (NCT02661373).

– ACT-451840

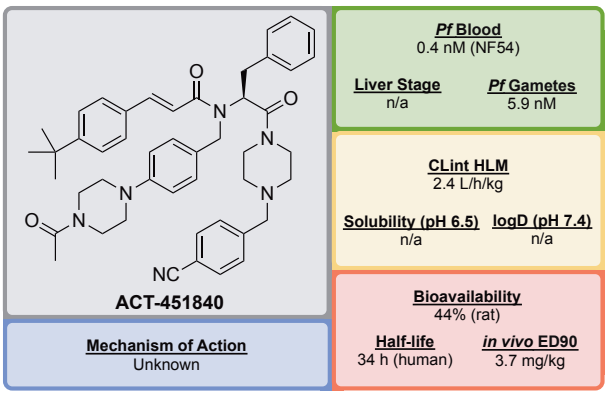

Developed in 2016 through a collaboration between Actelion Pharmaceuticals and the Swiss Tropical and Public Health Institute (STPHI), **ACT-451840** is an *N*-substituted phenylalanine-based compound that has shown potential to be a fast-acting drug with a long half-life and efficacy against multiple stages of the *P. falciparum* parasite.[100]

The hit compound (**A′1**, Figure 1.15) was identified in an erythrocyte-based phenotypic screen of ∼5,000 compounds and showed an IC_{50} of 3.8 nM against the K1 strain (chloroquine-resistant) of *P. falciparum*. The methods used in this project for the development of the hit compound were unique as two different media (10% bovine serum albumin and 50% human serum) were used in parallel to optimise the potency. Experiments using the latter media allowed for the early identification of potential problems with protein binding. The stereogenic centre of the amino acid residue was found to be critical for its antimalarial activity, with the (*S*)-isomer showing more than 10-fold higher activity compared to the non-natural (*R*)-isomer. Replacement of the *n*-pentyl chain with an acylpiperazine group (**A′2**) led to an improvement in the physicochemical properties of the compound. The trifluoromethyl group was replaced with a *tert*-butyl group (**A′3**) to give a more potent compound, particularly in the presence of human serum proteins. Finally, a 4-cyano moiety was installed on the southern pendant phenyl ring giving the highly potent (IC_{50} = 0.4 nM) lead candidate **ACT-451840**.

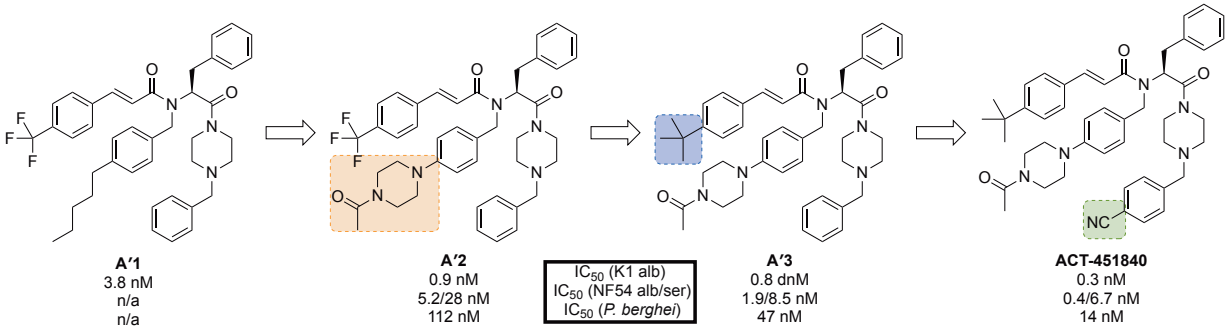

Figure 1.15: Key stages in the hit to lead pathway of ACT-451840. Initial change of the *n*-pentyl group to an acylpiperazine (**A′2**) helped to improve the physicochemical properties. Subsequent introduction of a *tert*-butyl in place of the trifluoromethyl (**A′3**) and a cyano group on the southern phenyl ring resulted in the optimised compound.

Interestingly, all of the compounds that were made during this campaign were found to be significantly less active against *P. berghei* than the human parasite, which is notable since many of the antimalarial drugs currently in development show similar potencies in both rodent and human parasites. Because of this, it was crucial to use a humanised *P. falciparum* severe combined immunodeficiency (SCID) mouse model for *in vivo* studies. **ACT-451840** showed the ability to cure malaria at doses of 3 × 300 mg/kg in the *P. berghei* mouse model, with an ED_{90} of 13 mg/kg and an ED_{90} of 3.7 mg/kg in the *P. falciparum* SCID mouse model. Experiments *in vivo* revealed the importance of the delivery media for **ACT-451840** with a 60 mg dose in corn oil proving as effective as a 100 mg dose in a mixture of Tween-EtOH/water = 10:90. **ACT-451840** has shown efficacy against multiple life cycle stages of both *P. falciparum* and *P. vivax*.[101] While the MoA is suspected to be novel, it is currently unknown. **ACT-451840** last completed first-in-human studies in 2014 (NCT02223871)[102] and is currently awaiting a decision to proceed further.

1.3.3.3 Product Development – OZ439

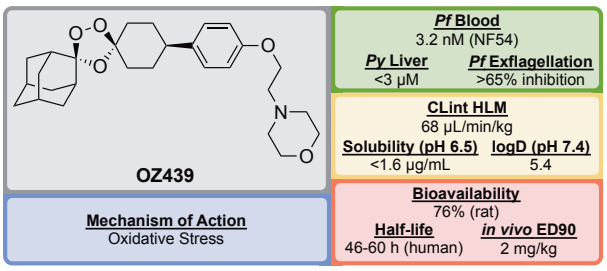

A 2011 partnership between Monash University, the University of Nebraska and the STPHI led to the discovery of **OZ439**, a synthetic trioxolane that possessed fast-acting curative and transmission-blocking ability, and was active against artemisinin-resistant parasites.[103]

OZ439 (a.k.a. Artefenomel) emerged from the lead optimisation campaign of the pre-existing trioxolane **OZ277** (**O1**, Figure 1.16, a.k.a. Arterolane), which was discovered in 2004.[104,105] In these previous studies, it was shown that the adamantane-peroxide moiety was essential for antimalarial activity, so the studies towards **OZ439** were focused on the eastern portion of the molecule.[106–108] Analogues resulting from variation to this area were found to have largely similar *in vitro* potencies. The curative ability of the original lead compound **OZ277** (mean survival 11 days, 0 of 5 mice cured) was improved upon by replacing the amide linker with a phenyl ether linker (**O2**), resulting in an improvement to exposure and single-dose curative efficacy (mean survival >30 days, 5 of 5 mice cured with a single dose of 30 mg/kg 1 day after infection). Further improvement to the exposure was attempted by replacing the alkylamine chain with a terminal piperazine moiety (**O3**), however this led to a significant reduction in the curative efficacy (mean survival 17 days, 0 of 5 mice cured). This was recovered by using a morpholine moiety instead (mean survival of >30 days, with 5 of 5 mice cured), giving the new lead compound **OZ439**.[109] It is notable that, as no clear correlations were found between *in vitro* and *in vivo* activity or physiochemical properties and exposure, this lead compound possessed a significantly lower solubility and slightly lower potency than **OZ277**.

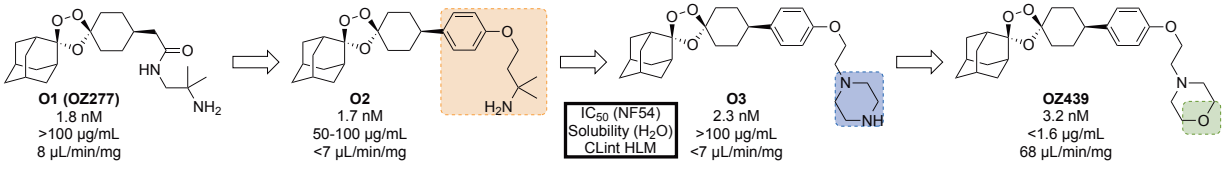

Figure 1.16: Key stages in the hit to lead pathway of OZ439. Initial replacement of the amide linker with a phenyl ether linker resulted in improved exposure while maintaining potency (**O2**). The exposure was further improved by changing the alkylamine chain to a piperazine ring (**O3**). Final replacement of the piperazine ring with a morpholine unit led to the optimised compound **OZ439**, which possessed better curative efficacy *in vivo*.

Unlike other peroxide-containing antimalarials, like artemisinin, **OZ439** was found to be curative at a single dose of 20 mg/kg in the *P. berghei* mouse model and possessed prophylactic activity superior to mefloquine when applied as a 30 mg/kg dose 24 hours prior to malaria infection. When

administered at a dose of 100 mg/kg 96 hours before infection, **OZ439** showed full chemoprotection. Minor signs of toxicity were seen when administered in a rat model in 5 × 300 mg/kg doses with 3 days interval. In comparison, the same dosage of **O2** resulted in the death of 9 of 12 animals.[109] **OZ439** shows a significantly longer half-life in humans (∼46-62 hours) than **OZ277** (3 hours).[110–112] Similar to other peroxide-containing antimalarials, the precise MoA for **OZ439** has yet to be discovered but it is believed that oxidative stress plays a major role.[113,114] First-in-human study results for **OZ439** were published in 2013[115] and the molecule has since progressed into Phase IIb clinical trials with planned completion in 2019 (NCT02497612).[116]

– KAF156

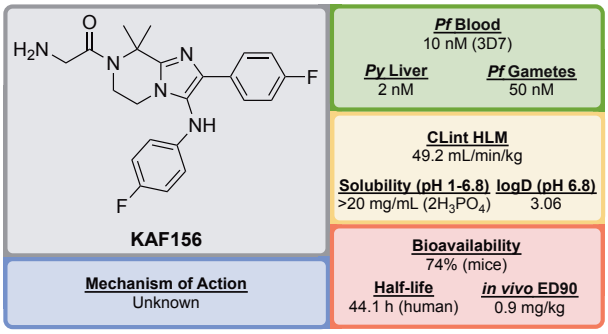

Identified in 2008 by Novartis and The Scripps Research Institute, **KAF156** is a second-generation imidazolopiperazine antimalarial that potentially possesses a novel MoA and performs as a fast-acting drug.[117]

The hit compound (**K1**, Figure 1.17) was identified in from a high-throughput screen of 1.7 million compounds in a *P. falciparum* proliferation assay. The metabolically labile positions were addressed by replacing the benzodioxole and phenyl fragments with 4-fluorobenzene groups (**K2**). Introduction of a *gem*-dimethyl group on the piperazine ring gave the lead compound **KAF156**, which had a twofold improvement in potency.[118,119] Interestingly, an increase in *in vitro* potency (EC_{50} = 5 nM) was seen with the removal of the glycine residue on the piperazine ring, however this came with an associated lowering of parasitemia reduction, indicating the importance of this amino acid residue for *in vivo* efficacy.[118]

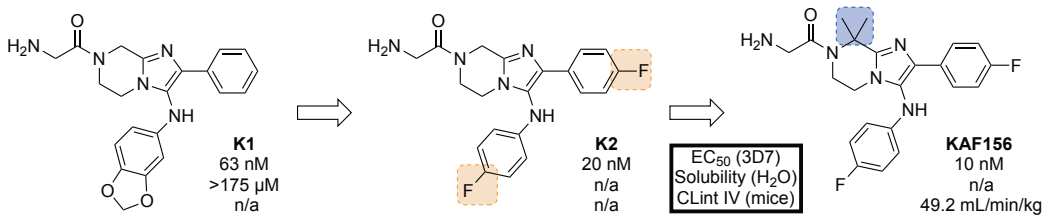

Figure 1.17: Key stages in the hit to lead pathway of KAF156. Potential metabolic stability issues were addressed through fluorine bioisosteres giving **K2**. Introduction of a dimethyl group on the piperazine ring resulted in increased potency and led to the optimised compound.

A single 10 mg/kg oral dose of **KAF156** administered 2 hours before intravenous infection with *P. berghei* sporozoites resulted in full protection in the causal prophylactic rodent malaria model. It has also shown transmission blocking ability in the *P. berghei* mouse model. The MoA for

KAF156 is currently unknown but through the culturing of resistant strains mutations have been identified in three genes: *P. falciparum* Cyclic Amine Resistance Locus (*Pf*CARL) and the UDP-galactose and Acetyl-CoA transporters.[120]. **KAF156** is currently in Phase IIb clinical trials, administered in combination with Lumefantrine (NCT03167242).

– KAE609

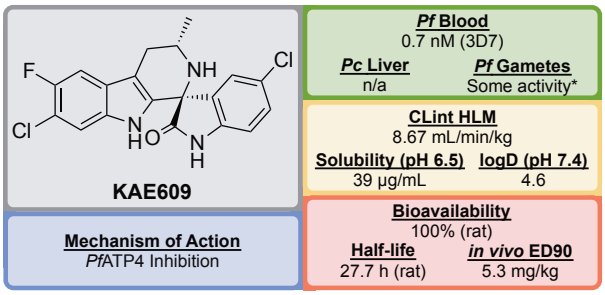

KAE609/Cipargamin/NITD609 was discovered by a partnership between Novartis, the STPHI and the Wellcome Trust.[121,122]

A high-throughput *P. falciparum* proliferation assay identified a racemic spiroazepineindole compound (**K′1**, Figure 1.18) which possessed moderate potency against K1 and NF54 strains, as well as potent *in vivo* efficacy. Confirmation of the hit result by resynthesis of **K′1** resulted in the isolation of a ∼9:1 diastereomeric ratio favouring the (1*R*,3*S*) and (1*S*,3*R*) pair of enantiomers. Chiral separation of this major pair identified the (1*R*,3*S*) enantiomer **K′2** as being >250-fold more potent than the (1*S*,3*R*) enantiomer. Reduction of the ring size (**K′3**) facilitated a diastereoselective Pictet–Spengler reaction, which ultimately led to the production of highly potent spiroindolone **KAE609**.

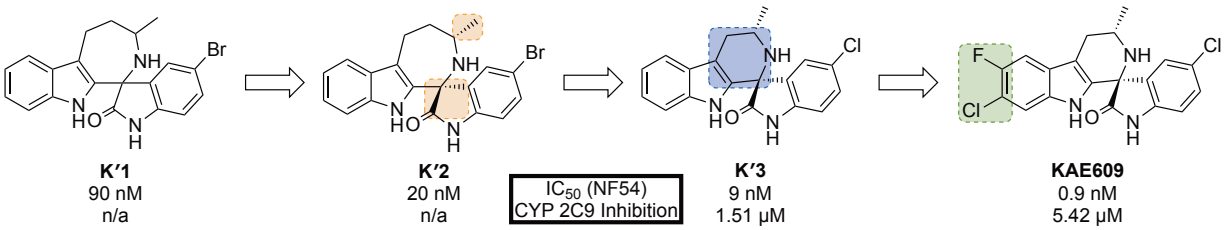

Figure 1.18: Key stages in the hit to lead pathway of KAE609. Resolution of the initial racemic hit (**K′1**) gave the significantly more potent stereoisomer (**K′2**). Reducing the ring size further increased the potency and final halogenation of the indole ring led to the optimised compound **KAE609**.

KAE609 is equipotent against drug-resistant strains and was found to be as effective as artesunate against *P. falciparum* and *P. vivax* isolates.[123] It shows a good safety profile, with low cytotoxicity, cardiotoxicity and mutagenic activity, and is able to clear parasitemia rapidly in adults with uncomplicated *P. falciparum* or *P. vivax* malaria at a dose of 30 mg/day for 3 days. **KAE609** displays low clearance from the body, has a long half-life and excellent bioavailability. **KAE609** is one of the key novel compounds that has been found to act through inhibition of *Pf*ATP4 (see Chapter 5). Along with a number of other structurally distinct compounds that are also thought to inhibit *Pf*ATP4 as their MoA, **KAE609** has shown great promise as an new antimalarial candidate and is currently in Phase IIb trials (NCT03334747).

– DSM265

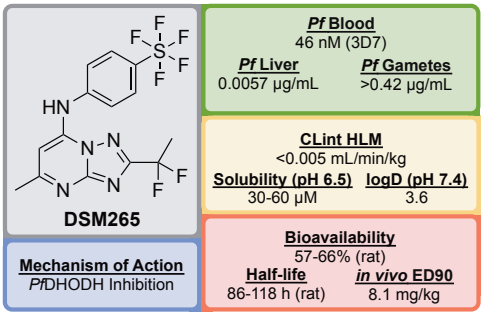

DSM265 was discovered through a collaboration between the University of Texas Southwestern, the University of Washington and Monash University.[124]

Identified in a high-throughput screen of *P. falciparum* dihydroorotate dehydrogenase (*Pf*DHODH)-based enzyme activity, the selective inhibitor **D′1** was found (Figure 1.19). The compound showed high potency but was rapidly metabolised and was inactive *in vivo*. Substitution of the naphthyl ring with a trifluoromethylphenyl group led to a metabolically stable analogue (**D′2**). Examination of the bound crystal structures of **D′1** and **D′2** with *Pf*DHODH identified key residue interactions which eventually led to the installation of a difluoroethyl group (**D′3**) which significantly improved the potency and solubility. Final replacement of the trifluoromethyl group with a pentafluorosulfur group led to the optimised compound **DSM265**.

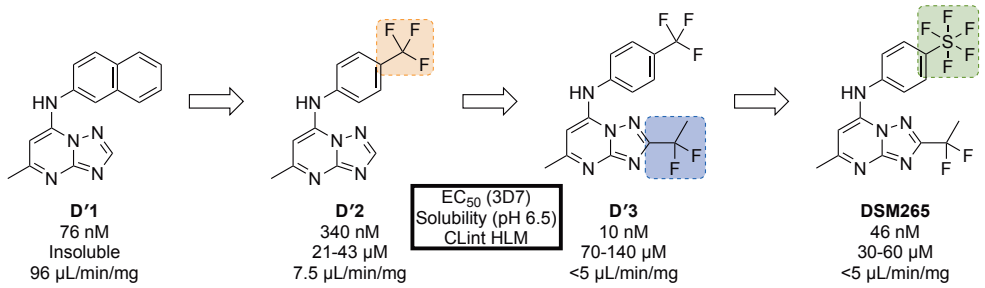

Figure 1.19: Key stages in the hit to lead pathway of DSM265. Replacement of the second phenyl ring in the naphthyl group with a trifluoromethyl group improved solubility. Addition of a 1,1-difluoroethyl group significantly increased the potency and final replacement of the trifluoromethyl group in **D′2** with a pentafluorosulfur moiety led to the optimised compound **DSM265**.

DSM265 has been shown to be a highly selective inhibitor of malarial DHODH and is potent against both blood and liver stages of *P. falciparum* and also drug-resistant parasite isolates. It has an excellent safety profile (provides therapeutic concentrations after 8 days of a single oral dose, tolerated in repeat-doses, non-mutagenic, inactive against human enzymes/receptors) and has a very low clearance rate and a long half-life in humans.[125] **DSM265** has completed Phase IIa trials in Peru in patients with *P. falciparum* or *P. vivax* (NCT02123290) and also completed a controlled human malaria infection study in combination with OZ439 (NCT02389348).

– MMV048

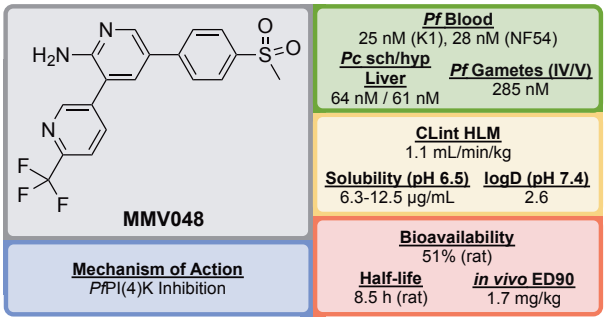

Identified in 2012 by the same team at the University of Cape Town, South Africa in the campaign that resulted in UCT943 (*vide supra*), **MMV048** emerged as another 3,5-diaryl-2-aminopyridine compound that possessed good prophylactic activity against *P. cynomolgi in vivo* with the potential to act as a transmission-blocking drug.[81]

While the initial hit (**M″1**, Figure 1.20) showed potent *in vitro* activity against the drug-sensitive NF54 strain of *P. falciparum* (IC_{50} = 49 nM), it suffered from poor solubility and high metabolic clearance. The poor stability was addressed by replacing the metabolically labile 3-methoxy-4-hydroxyphenyl moiety with a methoxypyridyl ring giving the more stable compound **M″2**. Further improvement to the potency and metabolic stability was seen when the methoxy group was replaced by a trifluoromethyl group, giving the lead compound **MMV048**.

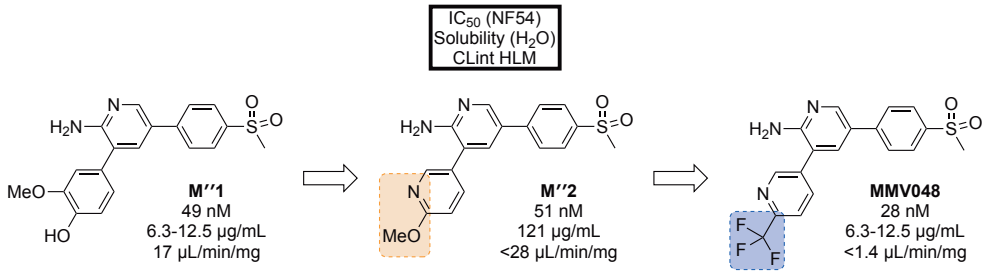

Figure 1.20: Key stages in the hit to lead pathway of MMV048. Initial replacement of the 3-methoxy-4-hydroxyphenyl moiety helped to improve *in vivo* stability and solubility. Further replacement of the methoxy group with a trifluoromethyl group improved potency and metabolic stability leading to the optimised compound.

A 99.3% reduction in parasitemia was seen in the *P. berghei* mouse model at a single dose of 30 mg/kg and an ED_{90} of 1.7 mg/kg with no signs of parasites after 30 days, highlighting the potential of **MMV048** to act as a single dose treatment. The target of **MMV048** is *Pf*PI(4)K, which was recently revealed as a new MoA for antimalarial drugs (see Chapter 5).[84] **MMV048** is currently in Phase IIa clinical trials in Ethiopia.

As can be seen from these examples of antimalarial medicines currently in development, the pipeline for malaria is well represented, something that is not the case for many other tropical diseases. Nevertheless, the continual threat of developing resistance to frontline treatments and the high levels of attrition in drug development mean that there can be no complacency, and a focus on the discovery of promising candidates must be maintained.

1.4 Open Science

While not a new concept, open science has recently seen considerable growth, and also been the topic of debate amongst scientists around the world. The idea that research conducted in university laboratories and big pharmaceutical companies should be available for everyone to see goes against the more traditional model of research. As we move to a more digital world, it is becoming easier and easier to share our research online.

Open science has been sub-classified into six categories:[126,127]

1. **Open Educational Resources**: The use of free and open materials for education and university teaching.
2. **Open Access**: Publishing of data in a way that makes it accessible to everyone.
3. **Open Peer Review**: Peer review carried out in a transparent and traceable manner.
4. **Open Methodology**: Documenting methods and procedures openly.
5. **Open Source Technologies**: The use of open source software and hardware to conduct research.
6. **Open Data**: Making all research data publicly available.

A number of benefits can come from working in an open manner. Of the categories above, numbers 4, 5 and 6 are most applicable to research. By applying open methodology, not only are the successful experiments documented, but the unsuccessful ones are as well. This more easily allows for the replication of experiments and eliminates unnecessary duplication. By using open source technologies, the outputs are no longer restricted to academic institutions, making it easier for anyone to take part. Finally, by making all research data publicly available, more meaningful discussions can be had with input from people that would otherwise not have contributed and it becomes easier for others to re-use data to address their own scientific questions.

A 2014 article in *Research Policy* gave an excellent overview of the use of open science across a range of different fields.[128] A prominent example of this in the field of biochemistry is that of Foldit, a game developed and released in 2008 at the University of Washington in a collaboration between the Center for Game Science and the Department of Biochemistry. This program was designed to extend the functionality of the protein structure prediction program Rosetta@home by allowing non-scientist users to interact with the protein structure solving process, complementing the computational methods. Since the release of this program, over 240,000 players have registered. The utility of Foldit was demonstrated in 2010 when players used the program to predict protein structures that were able to match or even improve upon computed solutions.[129]

A major breakthrough came in 2011 when Foldit players were able to solve the crystal structure of the Mason-Pfizer monkey virus retroviral protease in under two weeks. This had been an unsolved scientific problem for 15 years.[130] Most recently, in 2012, players successfully redesigned an enzyme used to catalyse the Diels-Alder reaction by remodelling the active site amino acid loops to increase ligand contact and stabilising this new transition state. A number of these new proteins were then synthesised, with the leading enzyme showing an increase in activity of over eighteen times the original.[131]

While the application of open science principles has been prevalent in fields such as biology, astronomy and mathematics for some time, its application to the field of chemistry has been limited.[132] One notable exception is the Structural Genomics Consortium (SGC) Open Science Probe Project.[133,134] This initiative is conducted in collaboration with a number of pharmaceutical companies including Pfizer and Bayer, and makes, not only a large range of chemical probes available for researchers to use, but also all the probe-associated data and control compounds as well. The combined list of SGC[135] and donated[136] chemical probes currently tallies over 100 compounds.

1.5 Open Data Screens

The discovery of novel classes of compounds that are biologically relevant is one of the most important stages in any drug discovery project. This typically consists of a phenotypic screen of a library (usually in-house) of thousands of compounds to achieve the desired phenotype (usually the killing of a pathogen). The resulting hits are then analysed for the most promising compounds that can be further developed.

The classical method for phenotypic screening involves the identification of potent, non-target-specific compounds, with determination of potential targets done thereafter. This is known as phenotypic drug discovery.[137] Alternatively, compounds may first be screened against a particular biological target with any compounds found to be active against this target evaluated for potency. This is known as target-based drug discovery.[138]

One of the first big-name pharmaceutical companies to establish an open data screen was GSK. In 2010, they released into the public domain structures of 13,500 compounds with antiplasmodium activity against *P. falciparum*.[139] This was done in an effort to encourage researchers to further develop new treatments for malaria by giving them the starting points for lead discovery. In this same year, St. Jude Children's Research Hospital[96] (∼1,500 compounds) and Novartis[140] (∼5,700 compounds) released their own lists of potential antimalarial drug leads.

Between 2011 and 2015, MMV assembled and distributed a set of compounds, named the Malaria Box, containing 400 samples that had confirmed antiplasmodium activity, free of charge to researchers around the world.[141] The aim was to give researchers an incentive to develop the compounds as new potential antimalarial candidates, with the condition that any research data resulting from these compounds be placed in the public domain.[142,143] In 2015, MMV followed up with a new box of 400 compounds named the Pathogen Box[144] targeting a range of tropical diseases such as tuberculosis, malaria and toxoplasmosis. Again, researchers have taken this box of compounds and found starting points for new drugs.[145,146] Most recently in 2019, MMV have released their latest box of compounds, called the Pandemic Response Box.[147] This time, the 400 compounds contained in the box were chosen as potential candidates with confirmed activity as antibacterial, antiviral or antifungal compounds.

The latest open data screen to be released to the public was in late 2018, when a list of 631 compounds with activity against the liver stage of the parasite was put into the public domain.[148] With all these examples demonstrating the power of putting research data into the public domain and the results that can follow, it is hoped that this trend will continue with even more public and private sector groups taking part in releasing data for wider benefit.

1.6 Open Source Malaria

The Open Source Malaria (OSM) project was founded in 2011 (originally named Open Source Drug Discovery for Malaria) by Matthew Todd at The University of Sydney, with the idea of applying the open science principles described above to the discovery of new medicines for the treatment of malaria.[149,150] By working on a drug discovery project in this manner, the secrecy that is traditionally associated with drug discovery is intentionally circumvented. It was envisaged that this would translate to a more efficient route to the identification of lead compounds, as a result of more potential collaborations and wider input from the scientific community. Most importantly, the unnecessary duplication and competition of different laboratories to publish the same experimental data (something that occurs regularly in academic research) can be avoided with the sharing of data in real-time.

At the inception of OSM, six rules were created that underlined the project as a whole. As such, anyone wanting to be a part of the OSM consortium must adhere to the following:

1. All data are open and all ideas are shared
2. Anyone can take part at any level
3. There will be no patents

4. Suggestions are the best form of criticism
5. Public discussion is much more valuable than private email
6. An open project is bigger than, and is not owned by, any given lab

This, in essence, boils down to the use of four key platforms which underpin the project (Figure 1.21). The Open Source Malaria website aggregates information and activity for the project (**A**). GitHub is a place where collaborators can ask and discuss questions relating to recent activity in the project ranging from chemical synthesis to biology (**B**). Social media such as Twitter allows for a much broader audience to engage and be involved with the project (**C**). Finally, experiments and results are available publicly online and updated in real-time in an electronic laboratory notebook (**D**).

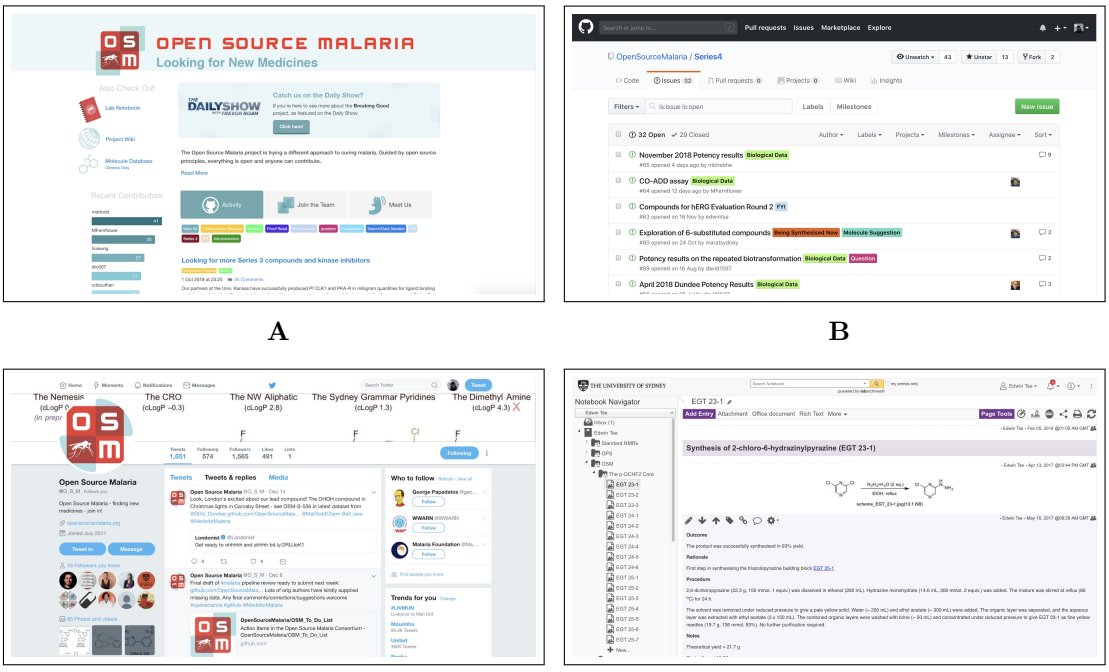

Figure 1.21: Four key platforms for the OSM project. (A) The OSM website aggregates project information;[150] (B) OSM GitHub for discussion of project aspects;[151] (C) OSM Twitter for sharing with and reaching out to collaborators around the world;[152] (D) Electronic Laboratory Notebooks for all experimental information.[153]

To date, OSM has investigated four series of compounds based around the structures shown in Figure 1.22. Work done on **Series 1** was published in 2016.[154] Work on **Series 2** began in 2012, but as it transpired that another research group was working on the same series,[155] this was no longer pursued so as to not duplicate this work. Progress on **Series 3** was recently restarted in 2017 after a brief hiatus, and **Series 4** has been the most active series and is the focus of this thesis.

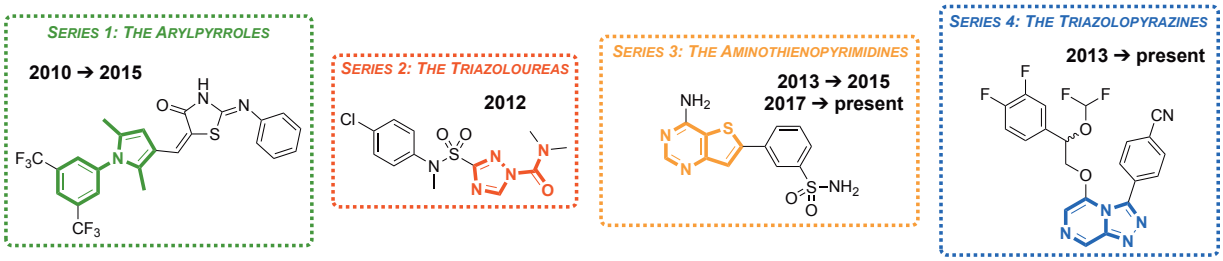

Figure 1.22: The Open Source Malaria compound series and their active years. While work on Series 1 and 2 have concluded, Series 3 and 4 are currently active.

1.7 The Series 4 Triazolopyrazines

Research on Series 4 first began in late 2013 when the Medicines for Malaria Venture announced that a new class of potential antimalarials would be released to the public to allow researchers from around the world to further optimise and develop the series.[156] A team led by Matthew Todd at The University of Sydney took on this challenge to try to explore and improve upon the data as the fourth series of the OSM consortium.

1.7.1 Surrounding Chemical Space

The triazolopyrazine motif is part of a larger family of fused 5,6-nitrogen heterocycles. Other members of this family include bicyclic systems in which there are fewer, or transposed, nitrogen atoms. Some of these related structures have even been shown to possess antimalarial activity (Figure 1.23).

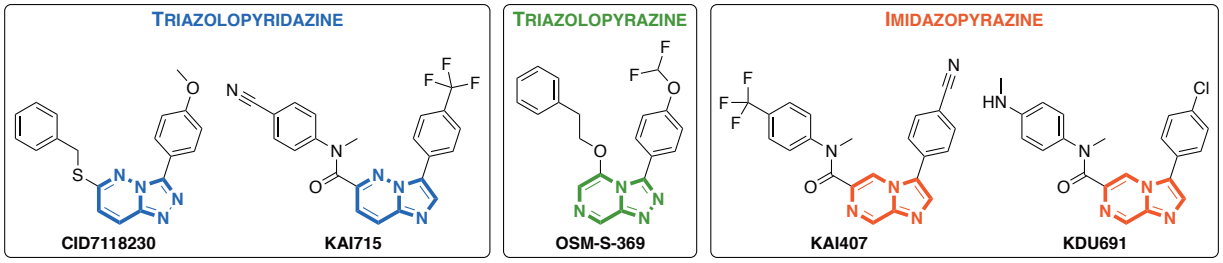

Figure 1.23: Structurally related bicyclic systems with antimalarial activity. Compounds with triazolopyridazine and imidazopyrazine cores have high potency against malaria. Compounds from both classes have been shown to act through phosphatidylinositol 4-kinase inhibition.

The triazolopyridazine compound **CID7118230** was reported to have a potency of 2.9 nM as an inhibitor for *P. falciparum* apicoplast development in a study conducted by the National Clinical Guideline Centre.[157] Additionally, a number of structurally related compounds, including the ones below, have been shown to act though the inhibition of *Pf*PI(4)K.[84] **KAI715** is one such compound that is highly potent against the *P. falciparum* blood stage (3.9 nM) and *P. yoelii* liver schizonts (9 nM).[84,158] The imidazopyrazine **KAI407** was developed at Novartis and has

been shown to be efficacious against *P. cynomolgi* hypnozoites (0.69 μM) and developing liver stages (0.64 μM), and possesses an activity profile similar to primaquine.[159] The prophylactic ability of this compound has been demonstrated with a single dose of 100 mg/kg able to prevent blood stage parasitemia in mice. Furthermore, it is potent against the *P. falciparum* blood stage (34.6 nM) and *P. yoelii* liver schizonts (156 nM).[84] The related compound, **KDU691**, shows *P. falciparum* blood stage activity (29.9 nM), prophylactic activity (protection at doses of 7.5 mg/kg or greater), gametocyte activity (220 nM) and oocyst activity (316 nM).[84] In addition, it shows potency against *P. yoelii* liver schizonts and *P. cynomolgi* liver hypnozoites (36 nM and 196 nM respectively). While not active against the regular ring stage of the parasite, KDU691 has been shown to be highly potent against dihydroartemisinin-pretreated ring stage parasites.[160]

It is noted that the MoA of the Series 4 triazolopyrazines appears to differ from that of the structurally similar traizolopyridazines and imidazopyrazines mentioned above. This was validated *via* experiments with a known *Pf*ATP4 inhibitor (a spiroindolone analogous to KAE609) which was evaluated against PI(4)K mutants, and showed no cross-resistance. This strongly suggests different MoAs between these structural classes of compounds.[84,161]

1.7.2 Inheriting the Data

Originating from a high-throughput screen of 160,000 compounds performed at Pfizer in collaboration with MMV, the triazolopyrazine series emerged as a class of compounds showing potential for further development. The series was then passed on to the contract research organisation (CRO) TGS Lifesciences for further optimisation. Compounds in this series were shown to possess good potency (down to 16 nM) and had no significant toxicity concerns. One compound, **MMV639565**, was shown to possess high potency (38 nM) and no cross-resistance with the K1 (multidrug-resistant) strain of the parasite (Figure 1.24). Additionally, this compound was evaluated *in vivo* showing rapid parasite clearance (ED_{90} = 6.3 mg/kg).

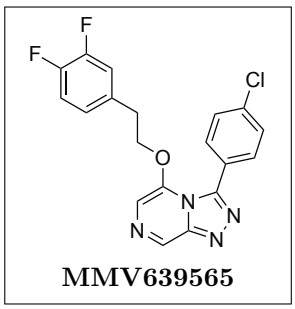

MMV639565

***in vitro* data**
– EC_{50} (*Pf* 3D7) = 38 nM
– No cross-resistance with K1 strain
– HLM CLint = 16 μM/min/mg
– RLM CLint = 70 μM/min/mg
– IC_{50} (Dofetilide binding) = 23.8 μM

***in vivo* data**
– Rat PK (*i.v.*) = 0.5 mg/kg
– Rat PK (*p.o.*) = 3 mg/kg
– CL = 44 mL/min/kg
– V_{ss} = 0.9 L/kg
– $T_{1/2}$ = 0.6 h
– Oral F = 16%

Figure 1.24: Key biological data for MMV639565. Both *in vitro* and *in vivo* data were obtained for this compound.

While this series showed promise, there were still concerns with high clearance/low metabolic stability, particularly in rat liver microsomes (RLM). In an attempt to address the issues with poor metabolic stability, a total of 118 compounds were made by the CRO to probe all aspects of the triazolopyrazine core, however, none of these compounds achieved the desired clearance parameters.

Among the documents from MMV for the series was a list of experimental procedures, and ^{1}H NMR data for select intermediates, used for the synthesis of a model triazolopyrazine compound **MMV670652** (Figure 1.25).[162] Beginning with 2,6-dichloropyrazine **1**, displacement with hydrazine monohydrate gave the hydrazine **2**. Acid catalysed condensation with an aldehyde gave the hydrazone **3**, which was cyclised with $PhI(OAc)_2$ to give the triazolopyrazine core **4**. The northwest side chain was prepared from 3,4-difluorobenzaldehyde **5**, first by reaction with TMSCN and TBACN to give the nitrile **6**. Hydrolysis with 50% H_2SO_4 gave the acid **7**, which was esterified in MeOH to give **8**. The benzylic difluoromethoxy substituent was installed using Freon gas to give intermediate **9**, which was then reduced with $LiAlH_4$ giving the alcohol **10**. Finally, NaH mediated nucleophilic displacement of the chlorine atom from the TP core with **10** led to the desired **MMV670652**. Many of these steps are still used by the OSM project to synthesise new triazolopyrazine compounds.

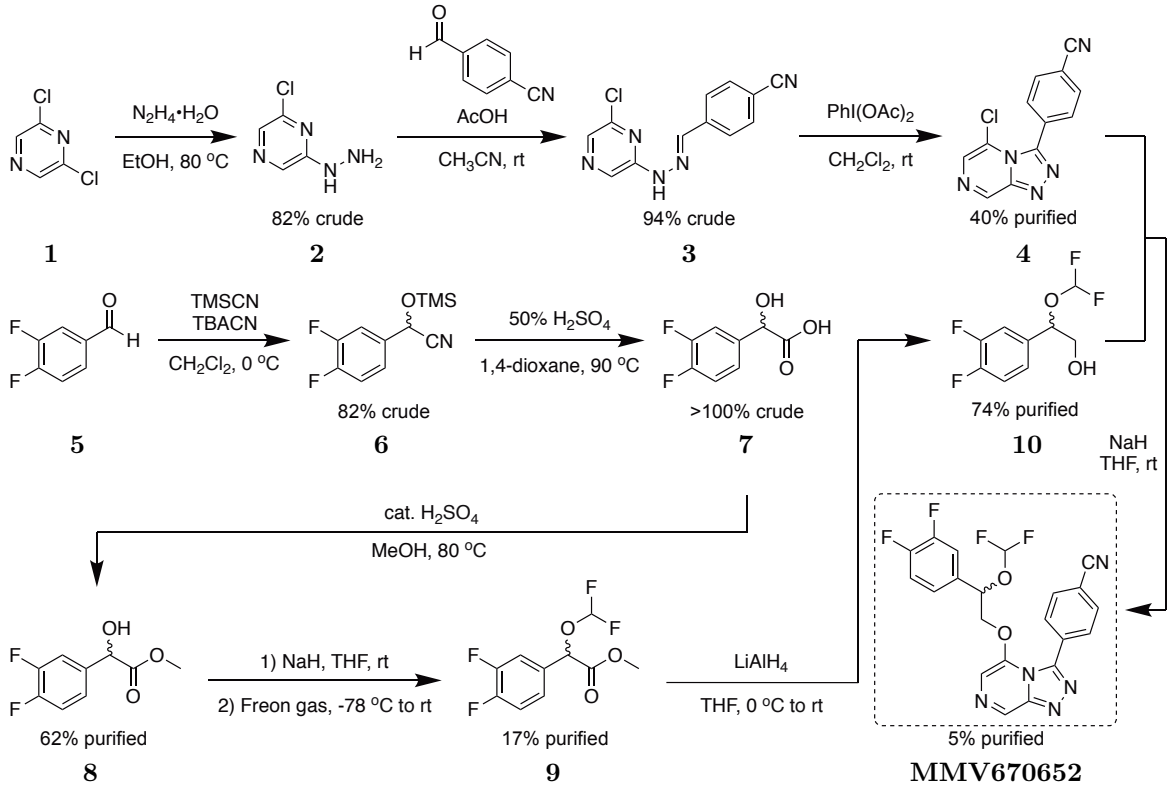

Figure 1.25: Original report from the CRO documenting the synthesis of MMV670652. Synthesis of the core **4** was achieved in three steps from the commercially available 2,6-dichloropyrazine **1**. The alcohol nucleophile **10** was accessed in five steps.

Another key piece of inherited data was information regarding the possible mechanism of action for the triazolopyrazines. This came in the form of five compounds which had been evaluated in an ion regulation assay run by Kiaran Kirk and co-workers at the Australian National University (ANU). This assay tested for the inhibition of the *P. falciparum* P-type ATPase transporter, which modulates the intracellular Na^+ of the parasite.[99,163] The data showed good correlation, revealing that compounds that were active *in vitro* also showed inhibition of *Pf*ATP4 and *vice versa* (Figure 1.26). Further work on this MoA has since been performed and is discussed in Chapter 5.

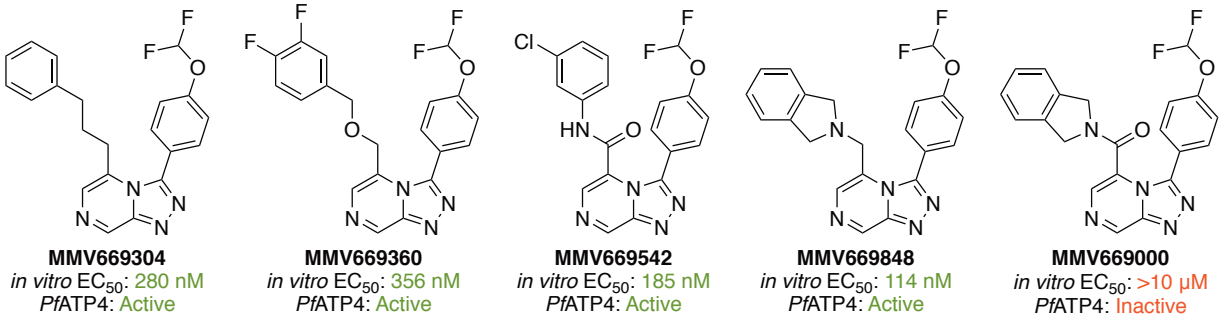

Figure 1.26: Five inherited compounds evaluated for mechanism of action. Though the study was on a limited number of compounds, good correlation between *in vitro* activity and *Pf*ATP4 inhibition was seen.

1.7.3 OSM and Onwards

After inheriting the triazolopyrazine series, the OSM consortium began to synthesise more compounds in an attempt to optimise the series. The combined Series 4 dataset has been summarised in a structure activity relationship (SAR) diagram (Figure 1.27). It was found that modification of the pyrazine and triazole rings by removal or transposition of the nitrogens led to reduced potency, as did dearomatisation of the core. The use of an ether linker on the pyrazine ring gave the best potencies, and the pendant aromatic ring itself was seen to be quite sensitive to modification, with a chain length of two methylene units found to be ideal. Attempts to block the α-carbon on the pyrazine ring as a means to prevent aldehyde oxidase metabolism led to reduced potency. Finally, transposition of the pyrazine substituent to the adjacent carbon lowered the potency as well. While a number of potent compounds have been made, none have possessed the desired RLM stability (example data shown in Figure 1.24). Such optimisation in liver microsomes is important since drugs can be prone to elimination *via* metabolism in the liver. Multiple species are often used for this process to better understand the inter-species differences. For example rats are often used as the species for pharmacokinetics measurements.

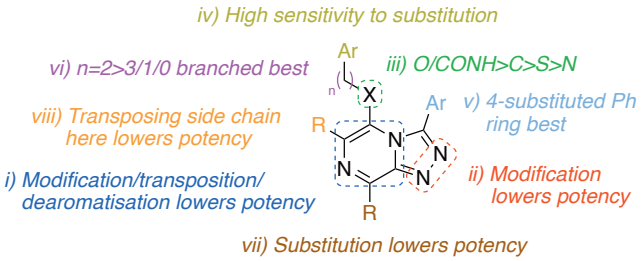

Figure 1.27: Summary of the SAR of the Series 4 triazolopyrazines. The combined data show a many areas of the core structure that are sensitive to modification.

Most broadly, Series 4 can be divided into two sub-classes of compounds: those with an ether linker as the northwest pyrazine substituent, and those with an amide linker. The synthetic routes to access the core triazolopyrazine structures have been well established (as described above) and subsequently optimised by past contributors to the OSM project.[164,165] In particular, the reaction conditions for two key steps have been modified from the route originally developed by the CRO (Figure 1.28). Rather than performing the condensation step using catalytic AcOH in CH_3CN, this transformation could effectively be performed by simply stirring the reactants in EtOH. The final nucleophilic displacement step was also altered to be performed using an excess of KOH and catalytic 18-crown-6. While the typical yields between the different reaction conditions for the condensation step are essentially equivalent, the large increase in yield with the final displacement step (from 5% to 50–70%) demonstrates the amount of optimisation that was achieved.

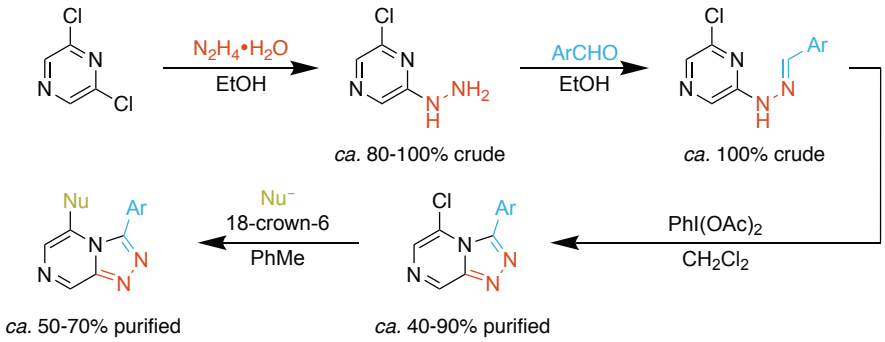

Figure 1.28: General synthetic scheme for the ether triazolopyrazines. The process involves displacement of a chlorine atom from 2,6-dichloropyrazine with hydrazine, condensation with an aromatic aldehyde, oxidative cyclisation using phenyliodine diacetate and subsequent displacement of the remaining chlorine atom with an appropriate nucleophile. Selected intermediates may be carried through without further purification.

The route towards the amide-linked compounds was established by Mr Thomas MacDonald during an undergraduate Honours project at The University of Sydney and is performed in a similar manner.[166] Initial amide coupling mediated by propylphosphonic anhydride (T3P) and *N,N*-diisopropylethylamine (DIPEA) afforded the precursor which could then be taken through the same steps as the ether analogues to give the final amide compounds (Figure 1.29).

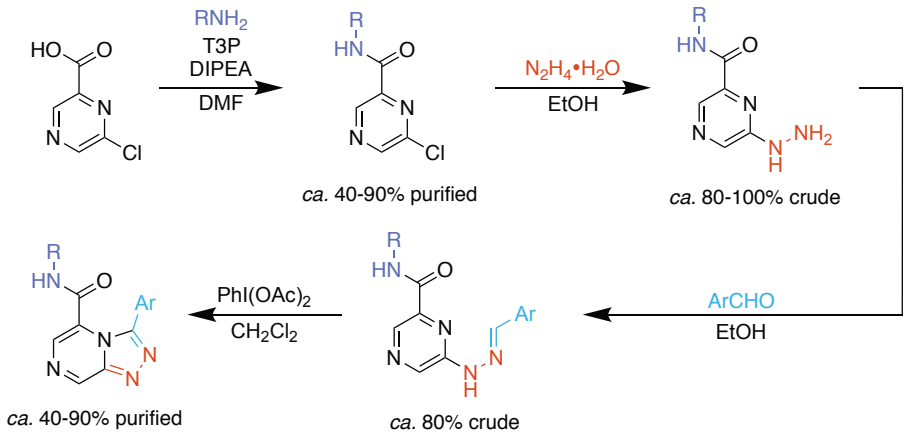

Figure 1.29: General synthetic scheme for the amide triazolopyrazines. The process involves propylphosphonic anhydride (T3P) mediated amide formation through coupling of 6-chloropyrazine-2-carboxylic acid and a desired amine, displacement of the chlorine atom with hydrazine, condensation with an aromatic aldehyde and subsequent oxidative cyclisation using $PhI(OAc)_2$. Select intermediates may be carried through without further purification.

To reduce repetition of the steps above in the schemes throughout the remainder of this thesis, unless otherwise described, the full synthetic route towards the cyclised cores for the Series 4 ether-linked compounds will be abbreviated by showing only the corresponding final core analogues. The cLogP values for the compounds in this thesis were calculated using DataWarrior.[167]

1.8 Project Aims

With the Series 1 project having successfully demonstrated what can be achieved by working on an open science model,[154] the approach was applied to the much larger Series 4 triazolopyrazines. While the inherited set of compounds from Pfizer provided solid groundwork for the project, the associated data given were not enough to substantiate the inherited findings. As a result, it was necessary to resynthesise key compounds in order to validate the conclusions about this series. In addition, optimisation of the solubility and metabolic stability of the compounds must be done in order to identify a so-called late lead compound that satisfies the MMV criteria.[168] For example an *in vitro* potency of $<$10 nM against and an aqueous solubility of $\geq$100 μM.

The first aim of the project was to synthesise a range of compounds to explore key areas of SAR (Figure 1.30). Variation of the ether linker would probe of the tolerance of this area of the SAR. Functionalisation of the benzylic position with amines and alcohols will be explored, in the hope that it would aid in modulating the potency and solubility of the compounds as well as blocking this potential metabolic hotspot. Finally, further to the standard methods of improving solubility (e.g. installation of alcohol or amine groups), solubility improvements for the series will be pursued *via* the replacement of the northwest and northeast phenyl rings, specifically

through the use of non-planar and non-aromatic derivatives to impart increased deplanarisation and reduced aromaticity.

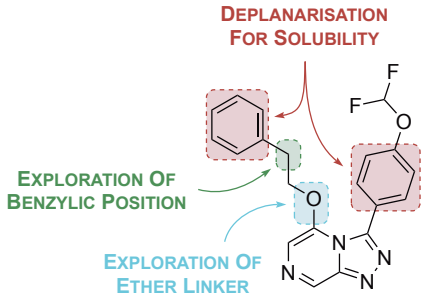

Figure 1.30: SAR investigation for Series 4. Modification of the ether linker, functionalisation of the benzylic position and replacement of the northwest and northeast phenyl rings will be carried out to establish more SAR for the series.

The second aim for the project involved investigating key biological aspects of the series (Figure 1.31). Validation of the MoA will be attempted through the synthesis of a number of important compounds (the Frontrunners), as well as a number of novel Series 4 compounds. Additionally, improvement of a key safety parameter, hERG binding (an ion channel responsible for regulating the electrical activity of the heart), will be investigated for the series by synthesising a number of compounds designed to minimise such binding.

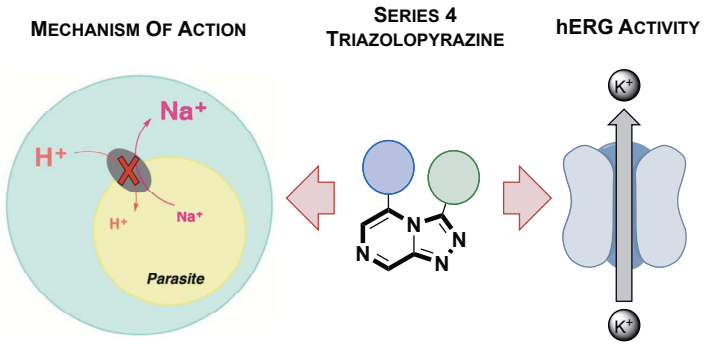

Figure 1.31: Biological investigations for Series 4. Compounds will be designed and synthesised to probe the MoA and potential hERG activity for the series.

The final aim was to increase the crowdsourced synthesis aspect of the OSM project by developing a medicinal chemistry research module for a first year undergraduate laboratory course, the Special Studies Program (SSP) at The University of Sydney (Figure 1.32). This would involve the design and selection of target compounds for previously unexplored areas of SAR, guiding and supervising undergraduate students as they complete the synthesis of these targets, and the purification and characterisation of the final compounds. The challenges associated with educating and assessing undergraduate research work performed in the open will be discussed.

Figure 1.32: Development of OSM as an open source project through crowdsourced synthesis. Students in the first year undergraduate chemistry laboratory at The University of Sydney will assist in synthesising new compounds for the series.

All of these aims are underpinned by the over-arching goal of identifying a lead compound with enhanced efficacy against malaria, and progressing it through to preclinical trials. Realising this goal would not only mean a new potential antimalarial drug, but also be the first molecule to reach the preclinical stage through a completely open source approach. A summary of the overall screening cascade appears in Figure 1.33.

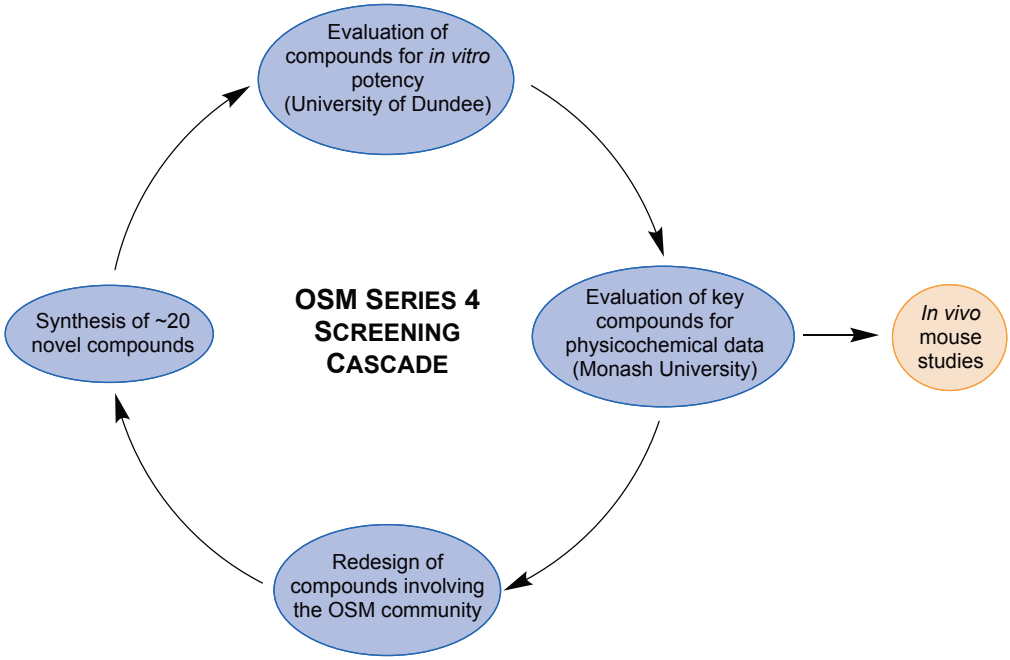

Figure 1.33: Screening cascade for the development of novel OSM Series 4 compounds. This process involves the design, synthesis and evaluation of novel Series 4 compounds with the goal of identifying a lead candidate that satisfies the MMV late lead criteria and progression into *in vivo* studies.

2. The Frontrunners Campaign

This chapter covers the (re)synthesis and further evaluation of a set of compounds that has been identified by the OSM consortium as containing the most promising targets for further exploration. Some aspects of chemistry will be discussed in more detail in subsequent chapters. The *in vitro* biological evaluation of these compounds is discussed, as well as the evaluation of the compounds' metabolic and physicochemical properties. All data relevant to the mechanism of action will be presented in Chapter 5.

2.1 Background

In 2016, with the series having been active for three years and with many potent compounds identified, a directed effort was made to obtain a range of missing biological data for a number of the most promising compounds. This set, named "the Frontrunners", originally consisted of twelve compounds **11**–**22** all with *in vitro* potency data (predominantly active), but with varying levels of other biological data, such as solubility and metabolic stability (Figure 2.1).[169] Two of these Frontrunners were inherited along with their *in vivo* potency data and had been shown to be efficacious at killing the malaria parasite in a mouse model of malaria, though had yet to be evaluated for mechanism of action. Other compounds had been shown to have high potency but were lacking any metabolic or physicochemical information. An additional six compounds were included in the Frontrunners list for other reasons. The inherited compound **23** was found to be very potent *in vitro* (24 nM) so this compound and the regular phenyl derivative **24** were included for further evaluation. Four weakly active compounds (**25**–**28**) were chosen to act as negative controls in subsequent biological evaluations. With so many promising compounds, it was necessary to obtain this missing information to narrow down the list of potential lead candidates and also to generate a unified set of data for eventual publication, allowing for an accurate comparison between molecules. However, many of these compounds were not available and needed to be synthesised first. Of these compounds, just under two thirds were inherited and had not been synthesised by the OSM project, therefore it was important to remake these compounds to validate the original results. The remaining compounds were synthesised by previous students and were remade to replenish the exhausted stocks.

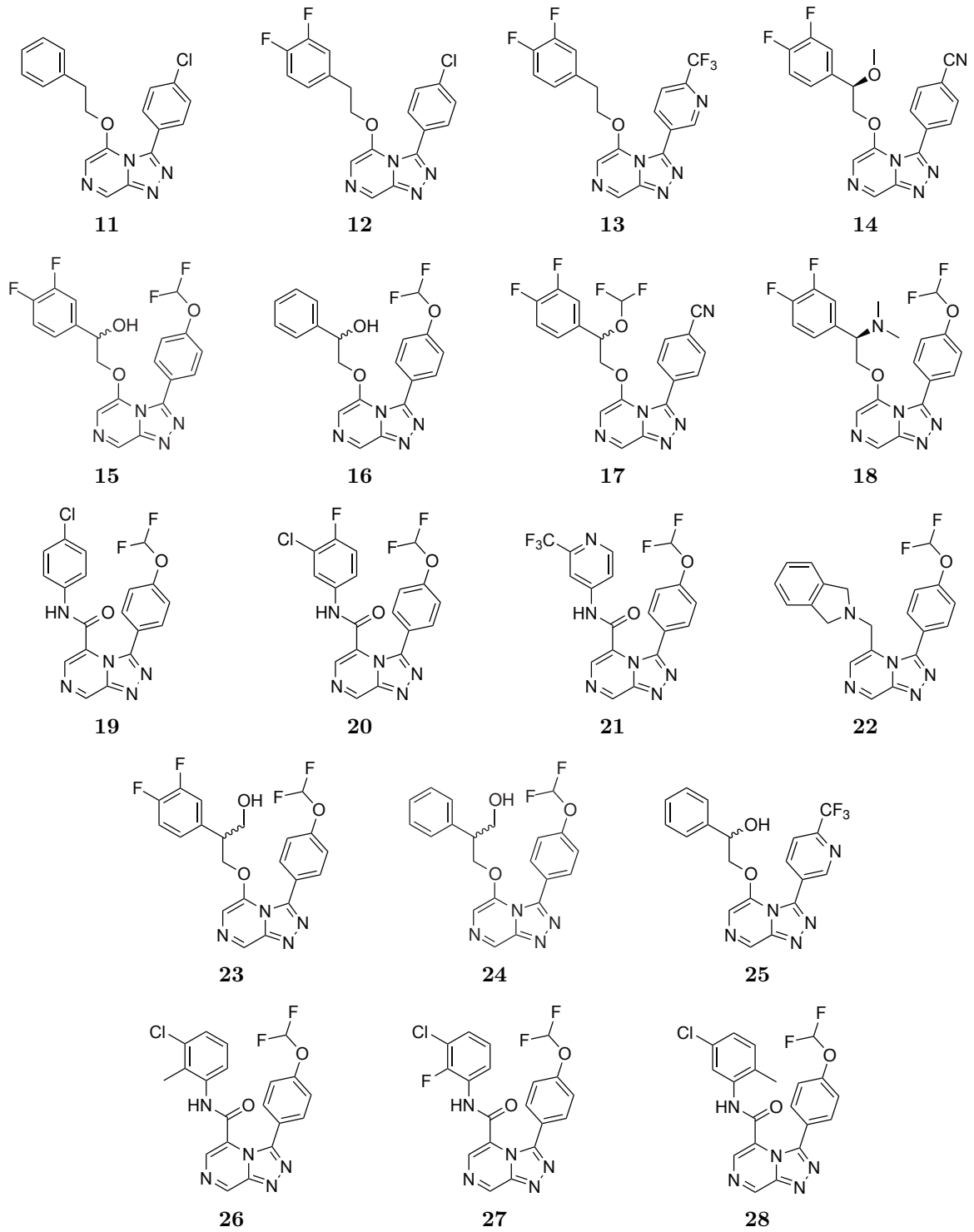

11 **12** **13** **14**

15 **16** **17** **18**

19 **20** **21** **22**

23 **24** **25**

26 **27** **28**

in vitro activity	*in vivo* activity	metabolic	solubility	ion regulation
11–22	**12**, **14**	**12**, **13**, **14**, **19**, **21**	**19**, **21**	**19**, **22**

Figure 2.1: The original set of eighteen Frontrunner compounds chosen for resynthesis and further biological evaluation. All compounds possessed *in vitro* potencies, but only a handful of compounds had been evaluated in other assays for data such as solubility, metabolic stability and influence on ion regulation (with potential relevance to mechanism of action).

When assessing the synthetic requirements needed to obtain these compounds, a number of observations were made which led to changes to the Frontrunners list.

- Compounds **14** and **18** contain a stereogenic centre at the benzylic position. The synthesis of these two compounds could be achieved through enantioselective methods or by resolution of the racemates, however the additional effort required to make these derivatives as single enantiomers at this stage was thought to be large versus the benefit to be gained from data specifically on the enantioenriched compounds. Therefore, the racemic versions (**29** and **30** respectively) of both compounds were made instead. While the change from enantiopure to racemic could have an associated decrease in potency, the differences in solubility and metabolic stability between the enantiomers and the racemic compounds should not be significant. If however, these physicochemical properties associated with the compounds were found to be optimal for the series, then further efforts could be made toward the synthesis of the enantiopure derivatives.

- Another inherited compound, **17**, possessed a benzylic difluoromethoxy substituent and was one of the most potent (17 nM) compounds for Series 4. The original synthetic route used by the CRO prior to the inheritance of the series by the OSM project involved installing the difluoromethoxy substituent on the benzylic position by reaction of the benzylic hydroxy group with NaH and Freon gas. However, due to restrictions on the use of this reagent in Australia an alternate route would be needed. As a result, a number of attempts were made by Dr. Alice Motion to synthesise this compound with alternative methods based on a literature reaction for the difluoromethylation of phenols using trimethylsilyl 2,2-difluoro-2-(fluorosulfonyl)acetate or 2,2-difluoro-2-(fluorosulfonyl)acetic acid, NaH and CsF.[170] An initial reaction indicated consumption of the methyl ester starting material and a possible trace of product, however increasing reaction times led to a recovery of only starting material. A suggestion was made by Joie Garfunkle (Merck) for the use of CuI instead of CsF but this resulted in no reaction proceeding to give the desired product and again, recovery of starting material.[170] Based on these known synthetic difficulties, this compound was ultimately removed from the Frontrunners list in favour of the synthesis of the other benzyl-substituted compounds.

- Another compound that was eventually replaced was the isoindoline **22**. Several different routes were used when attempting to make this compound (*vide infra*) but all of them were unsuccessful. While this compound was not made, the amide version **31** (known to be inactive) was made *en route* and evaluated in its place.

- Finally, when comparing the benzylic primary alcohol compounds **23** and **24**, it was decided that only the latter phenyl version was to be pursued. This was due to the greater availability of the required phenyl-based starting materials versus the difluorophenyl reagents.

With all these considerations in mind, the Frontrunners list was revised to include a total of sixteen compounds (Figure 2.2).

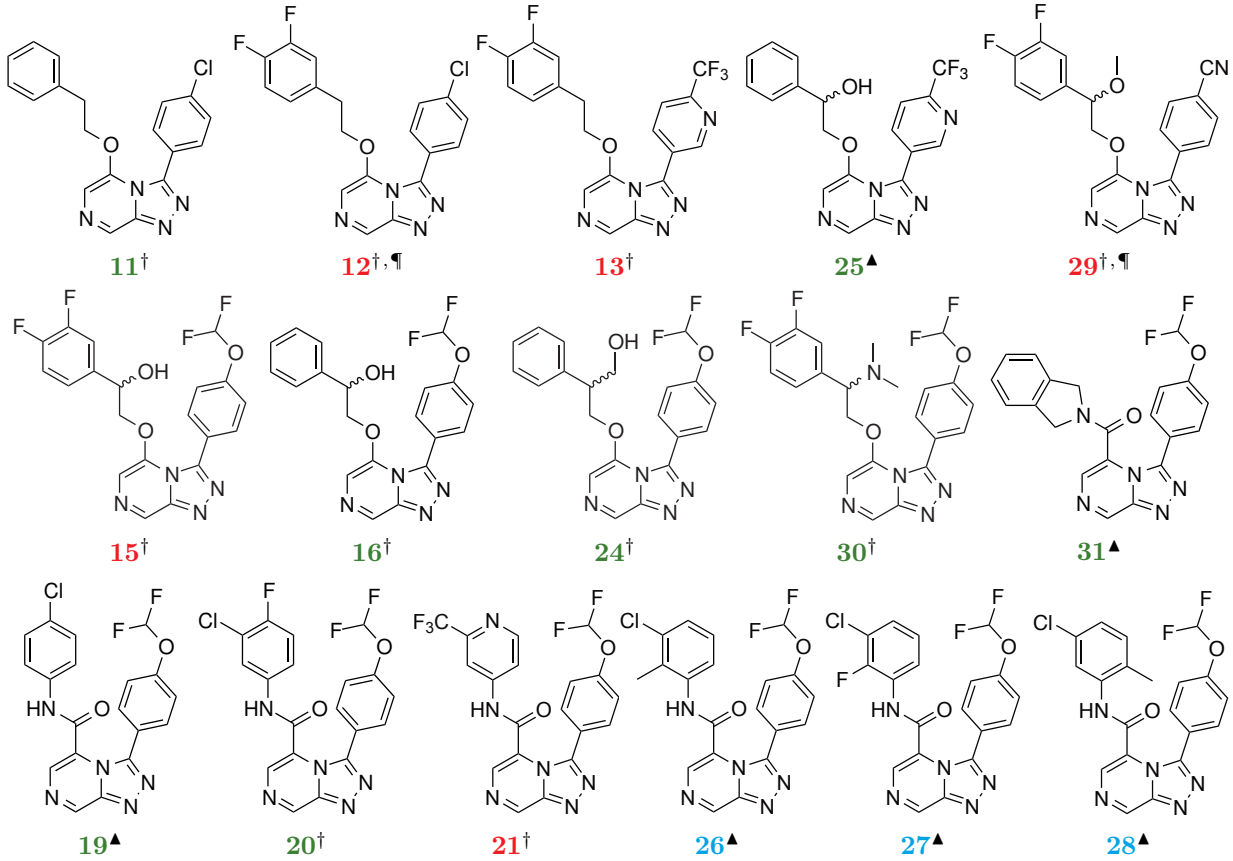

Figure 2.2: The final set of 16 Frontrunner compounds chosen for resynthesis and further biological evaluation. †good activity; ¶*in vivo* active; ▲negative control. Compounds with numbers in **green** were synthesised by the author. Compounds with numbers in **red** were synthesised by Dr. Alice Motion. Compounds with numbers in **blue** were previously synthesised by Thomas MacDonald.[166]

To make these synthesis efforts as streamlined and efficient as possible, they were conducted as a joint effort between the author and Dr. Alice Motion (postdoctoral researcher for the group during the time of this campaign). For completeness, the synthesis of all Frontrunner compounds will be described, however, as this was a combined effort, the colour of the compound numbers will indicate the person who did the majority of the synthesis towards the said compound and there will be a greater focus on the work carried out by the author.

2.2 Synthesis

Details regarding the synthesis of the Frontrunners will be outlined below. In certain cases, more detailed information will be provided in subsequent chapters.

2.2.1 Simple Ethers and Amides

The synthesis of the simple ether- (no benzylic substitution) and amide-linked Frontrunners was easily achieved by following the now-standard triazolopyrazine synthesis protocols outlined in Chapter 1 (Figure 2.3). Briefly, the TP cores for the simple ether compounds were made using the standard three steps (hydrazine displacement, condensation, cyclisation), with the appropriate commercially available aldehyde used in the condensation step. Final coupling with either 2-phenylethanol or 2-(3,4-difluorophenyl)ethanol gave compounds **11**–**13**. Such coupling reactions generally gave yields between 40 and 80% and were typically performed on a 250 mg scale. Similarly, the amide-linked compounds were prepared following the standard reaction conditions (amide coupling, hydrazine displacement, condensation, cyclisation) to give compounds **19**–**21** and **31**. The amides **26**–**28** were previously synthesised in this way by Thomas MacDonald; since enough samples of these compounds remained in storage, they were not resynthesised but their identity and purity were confirmed prior to sending them for further biological evaluations.[166]

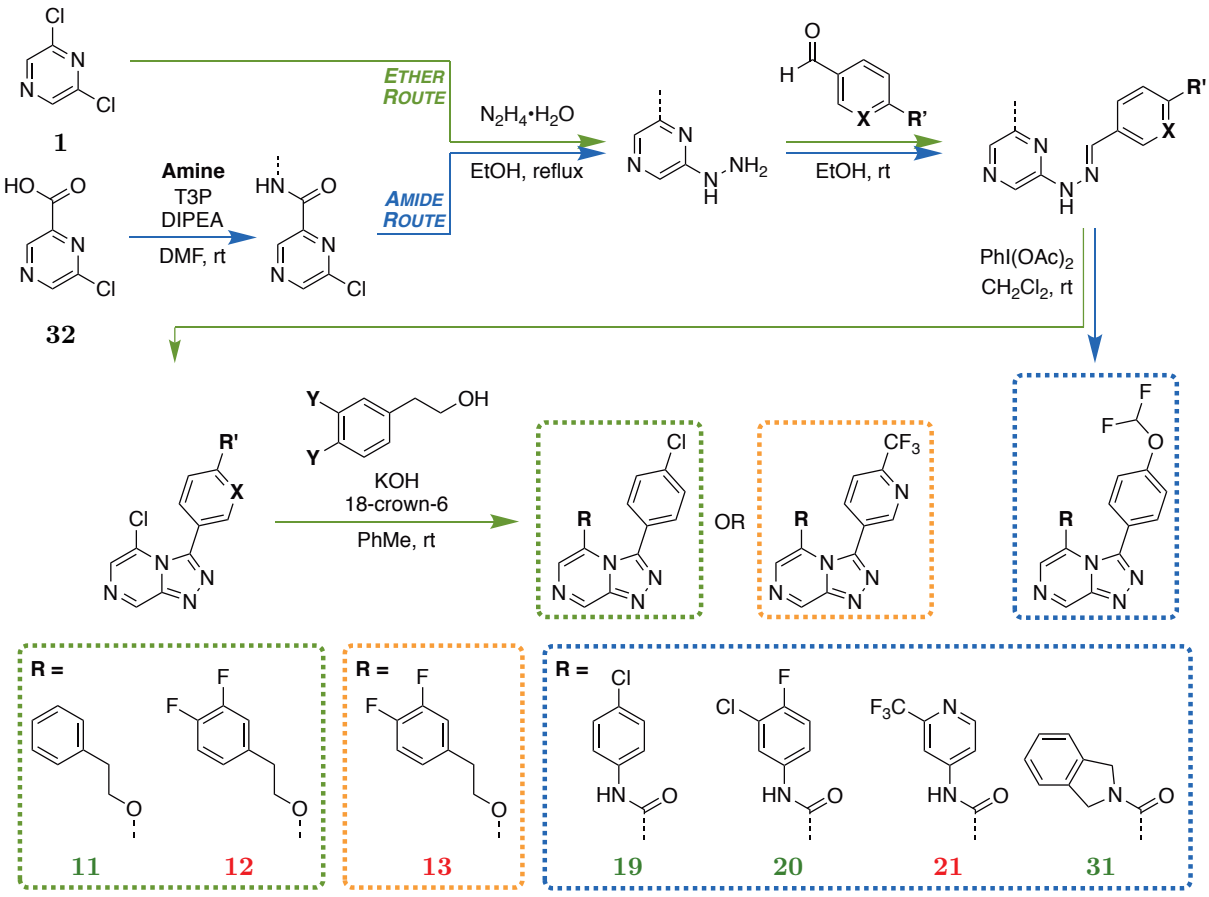

Figure 2.3: General route for the synthesis of the simple ether and amide Frontrunners. Compounds with numbers in green were synthesised by the author. Compounds with numbers in red were synthesised by Dr. Alice Motion. Amide compounds **26**, **27** and **28** were already available and were not resynthesised.

2.2.2 The Isoindoline

The inherited isoindoline compound **22** came with a reported potency of 0.11 μM while the corresponding amide derivative **31** had been found to be inactive at >10 μM. It was initially thought that the amine-linked compound could be accessible through a simple reduction of the amide as synthesised above (Figure 2.4). When this was attempted for the first time, standard reduction conditions using $LiAlH_4$ in Et_2O failed to provide the desired product even at elevated temperatures with no reaction taking place. Switching the solvent to THF had no effect on improving the reaction. An alternate procedure for the reduction of amides to amines involving activation by Tf_2O and reduction using $NaBH_4$ was also tried,[171] and while there was apparent consumption of the starting material according to analysis of the crude mixture by TLC, attempted purification of this mixture led to no desired product being isolated. Analysis of the crude product from these reduction reactions by mass spectrometry indicated a major peak at 434.13 *m/z*. The peak corresponds to the sodium adduct of the amide starting material **31** with four additional hydrogen atoms present, possibly suggesting that the pyrazine ring of the core is more susceptible to reduction than the amide group.

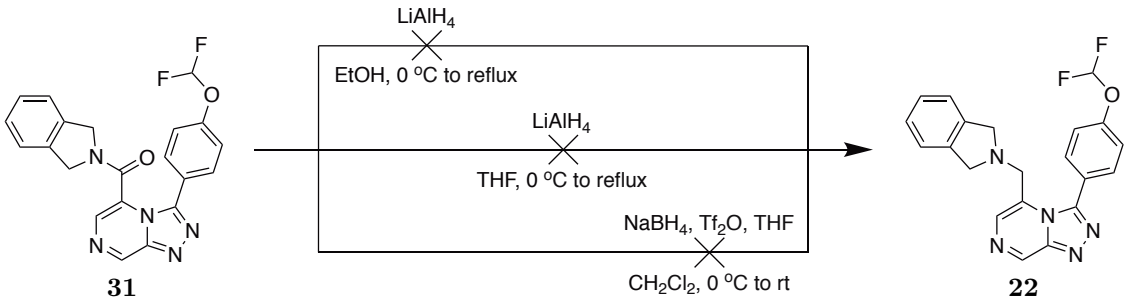

Figure 2.4: Attempted direct reduction of the isoindoline amide. None of the reduction conditions appeared to give the desired amine product; rather it is suspected that the reduction occurred on the pyrazine ring itself.

Having had no luck with direct reduction of the amide, a lengthier approach was taken with the aim of installing the isoindoline chain prior to constructing the complete TP core (Figure 2.5). This could in theory be accomplished by mesylation of an appropriate pyrazine alcohol, with subsequent displacement of the mesylate with isoindoline. Following this, the core could then be constructed using standard conditions. The required pyrazine alcohol **33** could be accessed from the commercially available 6-chloropyrazine-2-carboxylic acid **32**, which is also the starting material used for the synthesis of the Series 4 amide compounds. Unfortunately, reduction of this carboxylic acid with $LiAlH_4$ to give **33** was again unsuccessful. It was thought possible that the reduction would proceed more readily on the ester analogue of the starting material, and so esterification of the carboxylic acid with 32% HCl in MeOH was carried out to give the methyl ester **34** in good yield. Subsequent reduction using $NaBH_4$ in H_2O gave the desired

alcohol precursor **33** in 35% yield. Mesylation of the alcohol with MsCl in the presence of Et_3N to give **35**, and immediate displacement of the mesylate with isoindoline gave the product **36**. This material was subjected to the hydrazine displacement conditions, however no reaction took place. An alternative route was attempted involving reduction of the amide precursor **37** (from the first step in the synthesis of **31**) using $LiAlH_4$. Analysis by TLC indicated consumption of the starting material, but again no hydrazine reaction occurred and the starting material was recovered. This result is contrary to the reduction reaction on the final amide compound **31**, which did not proceed, suggesting that the electronics of the TP core allow for the reduction of the aromatic system in a way that does not happen with the isolated pyrazine ring. Due to these synthetic difficulties and the time constraints to have the Frontrunners evaluated together, the isoindoline compound **22** was not pursued further.

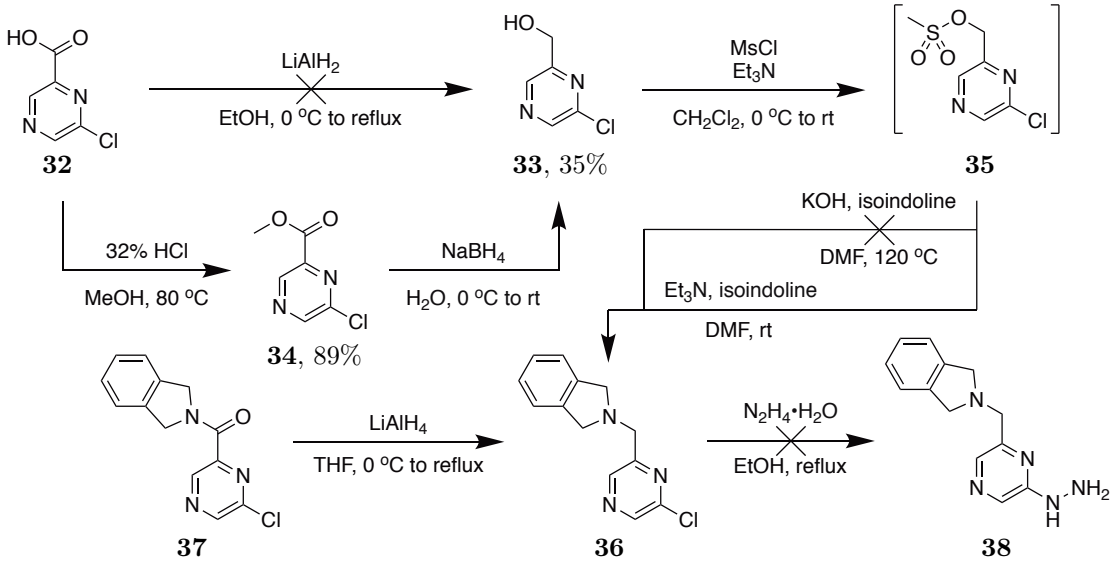

Figure 2.5: Attempted alternative synthesis of the inherited isoindoline compound. Reduction of the starting material used in the standard amide coupling reaction, followed by mesylation and displacement with isoindoline gave the desired intermediate, as did reduction of the isoindoline amide precursor **37**. Unfortunately, neither of these proceeded to give any hydrazine displacement product.

2.2.3 Benzylic Alcohol Substitution

The ether compounds containing benzylic substituents could be synthesised using the standard approach of nucleophilic displacement from the chlorinated TP core, but several of the required nucleophiles needed additional synthesis from commercially available materials. Compounds **15** and **29**, bearing the 3,4-difluorophenyl ring, were accessed through the same pathway, diverging at a key intermediate. Compounds **16**, **24** and **25**, bearing a regular phenyl ring, were accessed through an alternative route based on availability of starting materials. The synthesis of **24** will be described in Chapter 6 and approaches to **16** and **25** will be described in Chapter 3.

The route towards compound **29**, the methyl ether, was adapted from the route used by the CRO to obtain the nucleophile coupling partner for **17**, described above, and performed by Dr. Alice Motion. Starting from 3,4-difluorobenzaldehyde **5**, a $ZnCl_2$-promoted cyanation using TMSCN gave the TMS-protected α-hydroxy nitrile derivative **6** (Figure 2.6). Hydrolysis of the nitrile and concurrent deprotection of the TMS group using 50% H_2SO_4 led to the α-hydroxy carboxylic acid **7**, which was then esterified in MeOH to give the methyl ester **8**. The benzylic methoxy group was then installed by methylation of the hydroxy moiety using MeI and Ag_2O (**39**), and the ester reduced with $LiAlH_4$ to furnish the desired nucleophile **40**. Using this same route, the coupling partner for **15** could also be made. Diverging the synthesis at compound **8**, THP protection of the hydroxy group (to give **41**) and reduction of the ester gave the corresponding nucleophile **42**. Coupling of both nucleophiles with the appropriate TP cores, and THP deprotection (using the method described in Chapter 3) in the case of **43**, led to the desired Frontrunners **29** and **15** respectively.

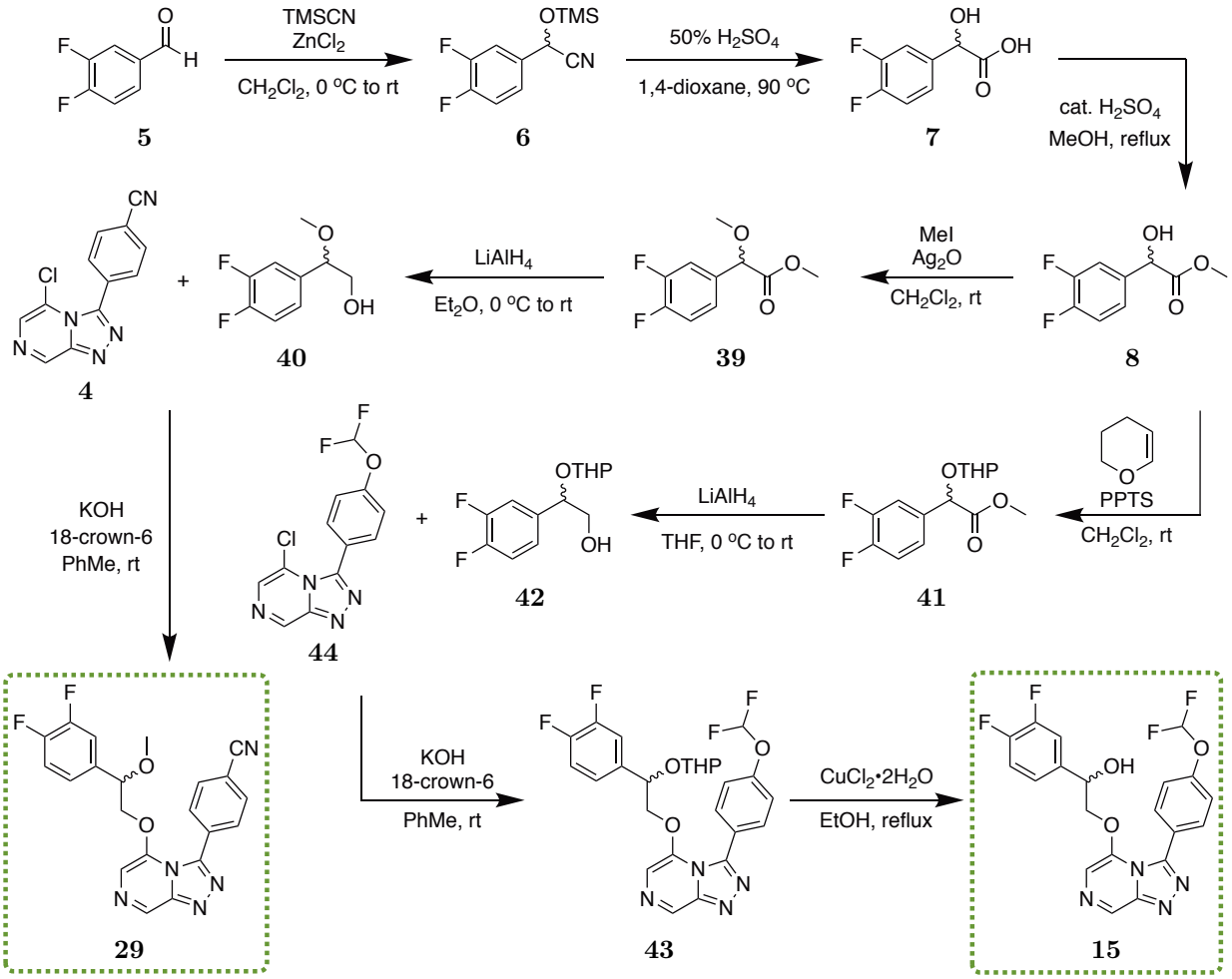

Figure 2.6: Synthetic route towards Frontrunner compounds 29 and 15 as performed by Dr. Alice Motion. Cyanation of **5**, hydrolysis of the nitrile and esterification gave the common intermediate **8**. Diverging from this, methylation or protection of the hydroxy group and ester reduction gave the desired nucleophiles. Coupling to the TP cores (and deprotection for **43**) gave the final compounds.

2.2.4 Benzylic Amine Substitution

Having synthesised building block **8** *en route* to the previous benzylic hydroxy compounds, it was thought that this key intermediate could again act as a point of divergence for the synthesis of the benzylic dimethylamine compound **30**.

In a similar manner to that used for the attempted synthesis of the isoindoline compound (*vide supra*), mesylation of the hydroxy group in **8** and subsequent displacement with dimethylamine was thought be an efficient route towards the desired benzylic amine coupling partner (Figure 2.7). In practice, the mesylation proceeded smoothly when analysed by TLC to give **45**, which was immediately subjected to displacement with dimethylamine, however the crude reaction mixture only showed signs of the starting material and not of the desired product **46**. While this method was unsuccessful, another possibility for converting the benzylic hydroxy group to an amine would be through a Mitsunobu reaction, using DIAD and PPh_3. When this was attempted, the alcohol starting material was consumed as indicated by TLC, however, no reaction took place when subjecting this material to the following reduction reaction using $LiAlH_4$ in Et_2O. Replacing the solvent with THF and heating the reaction to reflux also gave no reduced product **47** and only the starting material remained.

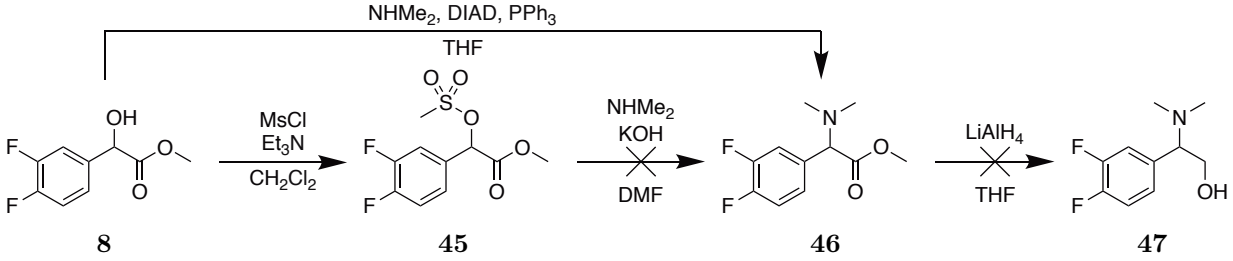

Figure 2.7: Initial attempts to synthesise the nucleophile required for Frontrunner compound 30. Mesylation of **8** proceeded to give the corresponding mesylate, however no amine displacement took place. A Mitsunobu reaction consumed the alcohol starting material, however no reduction occurred in the subsequent reaction.

Encouraged by the success of the Mitsunobu reaction on the benzylic alcohol intermediate, it was hoped that this could be applied on the already synthesised Frontrunner compound **15** to access the benzylic amine directly (Figure 2.8). After several days under the reaction conditions, analysis of the reaction mixture by TLC indicated the presence of a new spot, but the reaction had not proceeded to completion. Additional amine and Mitsunobu reagents were added and the reaction was stopped after five days. Multiple issues were encountered during purification due the presence of the Mitsunobu reaction by-product, Ph_3PO. Initial purification by column chromatography carried through significant amounts of Ph_3PO with the desired product. Eluting at a slower gradient resulted in an improvement in the separation between Ph_3PO and **15** but this was not enough to isolate the product pure. One common way of removing this phosphine

oxide by-product is by recrystallisation in Et_2O. While this worked to an extent, there were still amounts remaining even after multiple recrystallisations. A final attempt to purify this material using preparative TLC managed to separate the majority of the Ph_3PO, however at this stage, only small amounts of the desired product remained which still contained trace amounts of Ph_3PO.

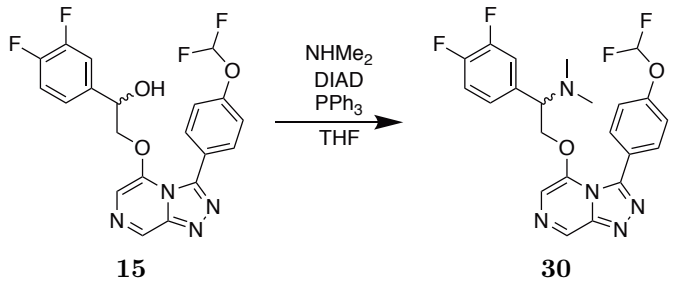

15 **30**

Figure 2.8: Attempted Mitsunobu reaction from Frontrunner 15. While this method worked, isolation proved difficult due to the presence of the Ph_3PO by-product.

Another route that was attempted employed the Strecker reaction. While this reaction still makes use of the highly toxic TMSCN reagent, it would provide a much more efficient route to the intermediate should it work. Beginning with the same 3,4-difluorobenzaldehyde starting material **5** as for the benzylic methoxy and hydroxy compounds above, Strecker reaction with $NHMe_2$ and TMSCN in MeOH gave the α-aminonitrile **48** in 96% yield (Figure 2.9). Unfortunately, a number of difficulties were encountered when trying to obtain the amino acid. Hydrolysis of the nitrile with 32% HCl in MeOH did not lead to the methyl ester **46** and only the starting material was recovered. Instead, only when using a 6 M HCl solution, was the amino acid **49** successfully synthesised, in 67% yield. Surprisingly, when this acid was subjected to reduction conditions using $LiAlH_4$ only a trace amount of possible product was seen by ^{1}H NMR spectroscopy. As a last attempt to use the nitrile intermediate, it was thought that reduction of the nitrile in **48** to the corresponding aldehyde **50** would allow the following reduction to the alcohol to proceed more readily. A typical reaction of this type uses DIBAL-H to convert the nitrile to the imine, which is then hydrolysed *in situ* to give the desired aldehyde. Performing this reaction on **48** led to consumption of the starting material but nothing resembling the product was able to be identified by ^{1}H NMR spectroscopy of the crude material.

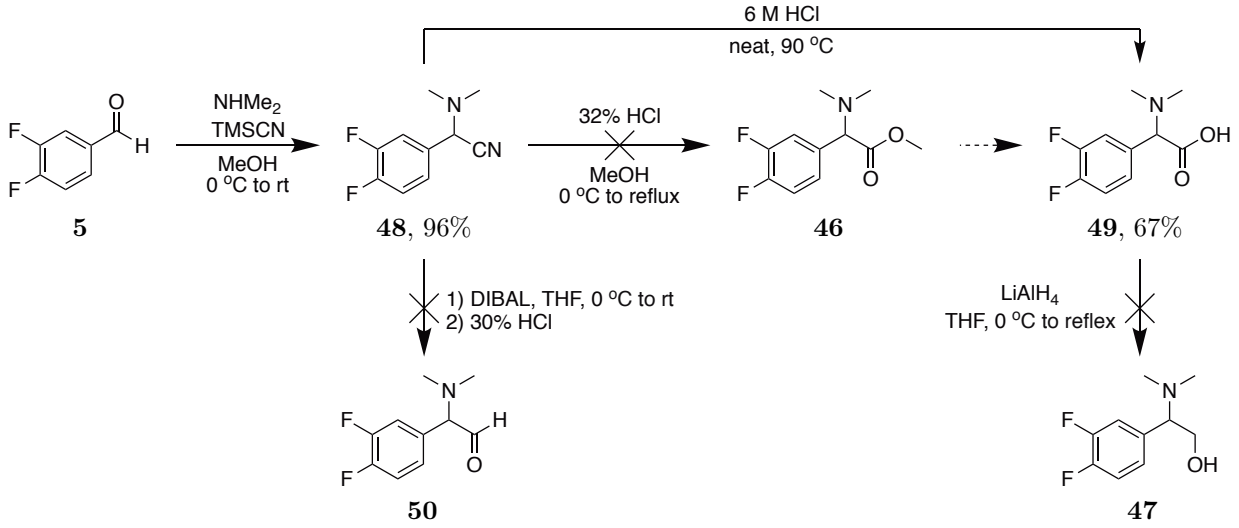

Figure 2.9: Attempted synthesis of the dimethylamine building block through a Strecker reaction. Synthesis of the α-aminonitrile and the corresponding amino acid were successful, but the respective hydrolysis and reduction reactions on these compounds failed.

Having no success in synthesising the dimethylamine compound, it was thought appropriate to reach out to the members of the OSM consortium for advice. A quick literature search provided one method for the double nucleophilic *N*-alkylation of α-oxime-esters with Grignard reagents, but this method was surprisingly reported not to proceed when using MeMgBr (A, Figure 2.10).[172] So, upon presenting these synthetic difficulties to the OSM community, a number of suggestions were returned for possible alternative routes to access this intermediate.[173] The oxime could be accessed from the corresponding carbonyl compound (*via* oxidation of **8** with MnO_2[174]), which could potentially be used for a reductive amination reaction using $NaBH(OAc)_3$.[175] One suggestion was based upon a method for the direct coupling of α-carbonyls with amines using catalytic $CuBr_2$ (B).[176] Another suggestion was based on a Hartwig-α-arylation reaction using $[Pd(PtBu_3)_2]$ and K_3PO_4 (C).[177] But perhaps the most attractive suggestion was from A/Prof. Chase Smith from the Massachusetts College of Pharmacy and Health Sciences. This route, starting from ethyl 2-(3,4-difluorophenyl)acetate, involved bromination of the benzylic position, displacement by an amine, then reduction to the alcohol either directly or *via* the acid (D). The major benefit to all three of these routes is the elimination of the need to use the highly toxic reagent, TMSCN. In addition, these routes would provide a much more step efficient way to reach the desired nucleophile. Based on the potential versatility of the benzylic bromine intermediate in route D, this was the route chosen for further investigation.

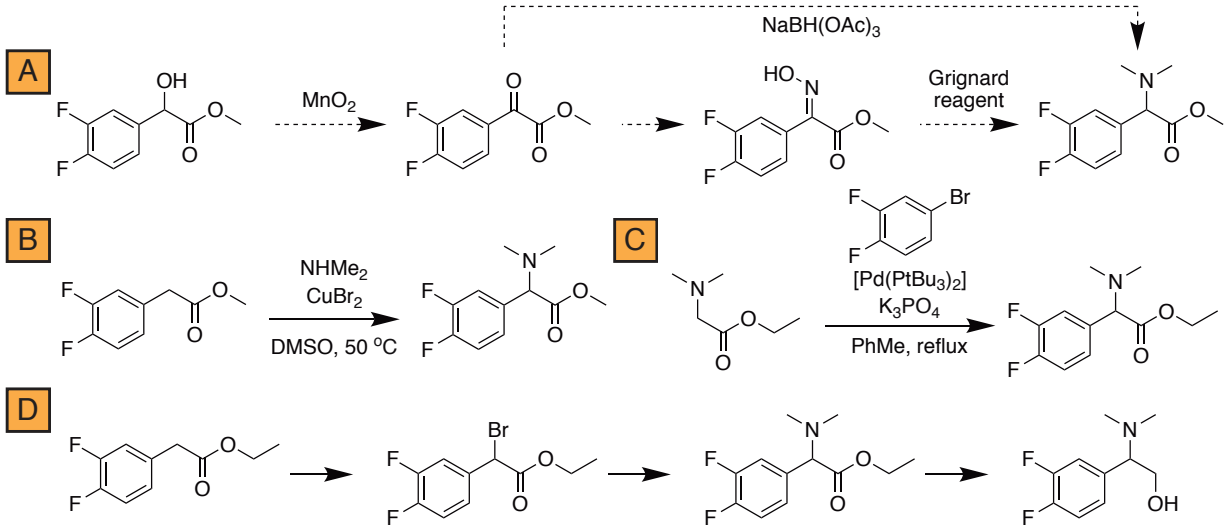

Figure 2.10: Suggestions for an improved route towards the benzylic amine coupling partner. A number of routes were proposed by the OSM community to overcome the previous synthetic difficulties.

While the ethyl 2-(3,4-difluorophenyl)acetate starting material for the bromination was not readily attainable, the corresponding 2-(3,4-difluorophenyl)acetic acid **51** was commercially available and inexpensive. The ethyl ester was easily accessed by esterification with *p*-TsOH in EtOH to give **52** (Figure 2.11). Benzylic bromination was achieved through the use of NBS and catalytic HBr solution affording the benzylic bromine intermediate **53**. This bromination was carried out in CCl_4, however due to the environmental concerns with this solvent it was eventually replaced with α, α, α-trifluorotoluene, giving the brominated product in only slightly lower yields. Displacement of the bromine under basic conditions proceeded smoothly to give the benzylic dimethylamine intermediate **54**. Finally, reduction to **47** and coupling to the TP core **44** led to the desired benzylic dimethylamine Frontrunner **30**.

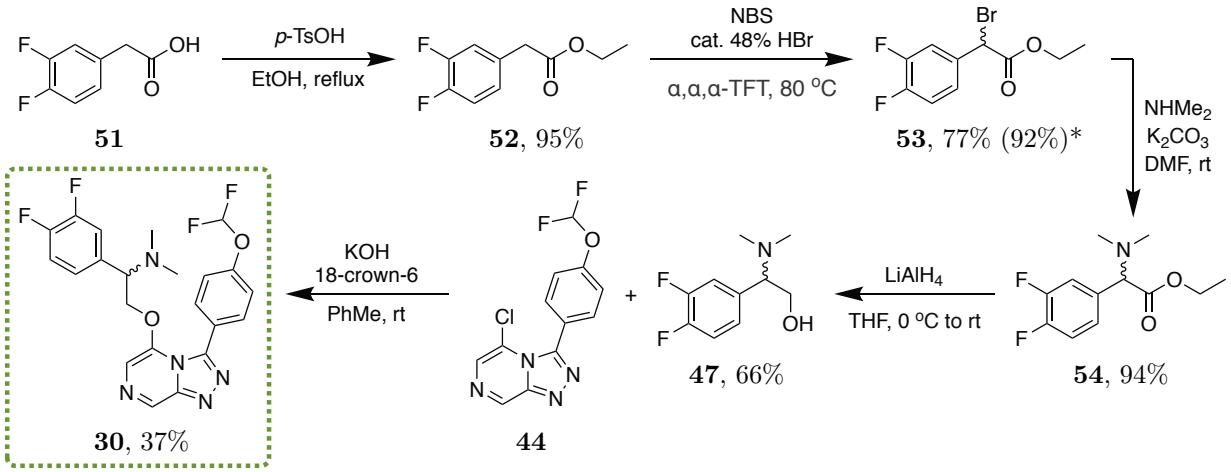

Figure 2.11: Revised route for the synthesis of the benzylic dimethylamine Frontrunner compound. A more reliable synthesis of the coupling partner involved esterification of the commercially available acid, bromination of the benzylic position, bromine displacement with dimethylamine and reduction of the ester. *Yield in brackets when performed in CCl_4.

2.3 Biological Evaluation: *in vitro* Potency

With all the Frontrunners successfully synthesised, they were sent to the University of Dundee Drug Discovery Unit (DDU) for re-evaluation of their activity against *P. falciparum* (Table 2.1). It should be noted that the NF54 strain was used for obtaining the potency values for the inherited compounds and those evaluated in the assay at Syngene. The Frontrunners, on the other hand, were all evaluated at Dundee against the 3D7 strain of the malaria parasite. The results may be compared. Both strains are commonly used for *in vitro* evaluations and are very similar, however the original NF54 strain is sensitive to all known drugs, while the 3D7 strain is a clone of the NF54 strain and is known to produce fewer gametocytes in *in vitro* cultures.[178]

Table 2.1: *in vitro* potency values of the Frontrunner compounds against *P. falciparum*. [a]NF54 strain. [b]3D7 strain. [c]Potency values are an average of ≥2 repeats. [d]Potency of enantiopure compound **14**. [e]Potency of enantiopure compound **18**.

Entry	Compound	Inherited EC_{50} (μM)[a]	Syngene IC_{50} (μM)[a]	Dundee IC_{50} (μM)[b,c]
1	**11**	–	0.06	0.17
2	**12**	0.04	–	0.14
3	**13**	0.26	–	0.52
4	**25**	–	3.57	4.87
5	**29**	0.04[d]	–	0.15
6	**15**	0.12	–	0.07
7	**16**	–	0.26	0.36
8	**24**	–	0.07	0.13
9	**30**	0.04[e]	–	0.19
10	**31**	>10	–	>10
11	**19**	5	–	9.79
12	**20**	0.19	–	0.40
13	**21**	0.14	–	0.45
14	**26**	>5	–	4.19
15	**27**	–	0.70	1.00
16	**28**	–	0.39	0.97

The previously obtained *in vitro* potency data was seen to correlate fairly well with the results from the re-evaluation, indicating that the active compounds were indeed active, and *vice versa*. Most cases showed a slight decrease in activity, with the sole exception of **15** which showed an almost doubling of its potency (Entry 6).

2.4 Biological Evaluation: Metabolic & Physicochemical Properties

While the Frontrunner compounds were being re-evaluated for their *in vitro* potencies they were also sent to the Charman lab at Monash University for evaluation of their metabolic and physicochemical properties (Table 2.2). The physicochemical properties that were measured were the

kinetic solubilities at pH 6.5 and the distribution coefficient (LogD) at pH 7.4. In contrast to thermodynamic solubility, which may aid in determining *in vivo* formulations and is typically done in the later stages of drug development, kinetic solubility measurements are high-throughput, use relatively small amounts of compound and typically done in the earlier stages of drug discovery. The metabolic stability data included *in vitro* clearance and half-life measurements in both human and mouse liver microsomes (HLM and MLM respectively). It is noted that mouse microsomal clearance is perhaps less relevant to eventual progression of these compounds as a rat model is typically employed for *in vivo* PK studies. This is due to a number of factors including greater ease of handling, higher tolerance to blood volume loss, larger sample size and genetic characteristics that closely resemble humans.[179] In order to be consistent with inherited data, and for publication purposes, MLM was measured for these compounds. In addition to this, the hepatic extraction ratio (E_H) was calculated for both humans and mice, which allowed for the clearance of each compound to be classified as either low (<0.3), intermediate (0.3–0.7) or high (0.7–0.95).

Table 2.2: Metabolic and physicochemical properties of the Frontrunner compounds. HLM: human liver microsomes. MLM: mouse liver microsomes. Sol.: aqueous solubility (μg/mL). CL_{int}: *in vitro* intrinsic clearance (mL/min/kg). $T_{1/2}$: half-life (min). E_H: hepatic extraction ratio. Data acquired by the Charman Laboratory at the Centre for Drug Candidate Optimisation, Monash University.

Entry	Compound	cLogP	LogD (pH 7.4)	Sol. (pH 6.5)	HLM ($CL_{int}/T_{1/2}$)	MLM ($CL_{int}/T_{1/2}$)	E_H (H/M)
1	**11**	3.6	3.8	6.3 - 12.5	94/18	319/5	0.79/0.87
2	**12**	3.8	3.8	3.1 - 6.3	33/53	193/9	0.57/0.81
3	**13**	3.1	3.4	3.1 - 6.3	71/24	132/13	0.74/0.74
4	**25**	1.8	2.5	50 - 100	25/50	117/15	0.58/0.72
5	**29**	2.4	3.4	12.5 - 25	47/37	159/11	0.65/0.77
6	**15**	2.3	3.1	12.5 - 25	38/45	170/10	0.60/0.79
7	**16**	2.1	2.9	25 - 50	7/246	278/6	0.22/0.86
8	**24**	2.7	2.8	12.5 - 25	49/35	361/5	0.66/0.89
9	**30**	2.5	3.5	6.3 - 12.5	264/7	478/4	0.91/0.91
10	**31**	1.6	2.8	12.5 - 25	89/19	417/4	0.78/0.90
11	**19**	2.8	3.1	1.6 - 3.1	11/164	15/115	0.30/0.24
12	**20**	2.9	3.1	3.1 - 6.3	47/37	91/19	0.65/0.66
13	**21**	2.1	2.7	6.3 - 12.5	18/95	24/73	0.42/0.34
14	**26**	3.2	3.1	12.5 - 25	114/15	166/10	0.82/0.78
15	**27**	2.9	3.1	3.1 - 6.3	90/19	160/11	0.78/0.77
16	**28**	3.2	3.1	3.1 - 6.3	201/9	360/5	0.89/0.89

For the most part, the calculated cLogP values were a good estimate for the experimental LogD which assists with future compound design. In terms of metabolic stability and solubility, the simple ether compounds **11**, **12** and **13** generally had high clearance in both human and mouse liver microsomes, as well as relatively low solubilities (Entries 1–3).

The introduction of benzylic alcohol groups generally led to significant improvements in the solubility of the compounds. The best solubilities among the Frontrunners were seen with the benzylic hydroxy compounds **16** and **25** (Entries 7 and 10), both of which exhibited improvements to clearance in HLM compared to the unsubstituted derivatives, though whether this arises from benzylic blocking or improved solubility is not clear from these data. The 3,4-difluorophenyl derivative **15** performed slightly worse for solubility and metabolic stability (Entry 6). The benzylic methoxy and benzylic primary alcohol compounds **24** and **29** respectively, both performed slightly worse with lower solubility and moderate clearance (Entries 4 and 9). While the benzylic dimethylamine compound **30** had moderate solubility, its clearance was very high and its half-life correspondingly short (Entry 8).

The amide compound **19** showed excellent clearance properties with a long half-life and low clearance in both humans and mice, but the solubility was very poor (Entry 11). As one of the compounds which already possessed inherited human microsomal data, it could be seen that these new values ($CL_{int}/T_{1/2}$ = 11/164) were in accordance with the previous data ($CL_{int}/T_{1/2}$ = 8.6/115). All other amide compounds **20**, **21**, **26**, **27**, **28** and **31** had relatively high clearance profiles and low solubilities (Entries 5 and 12–16).

From this information, a number of general trends can be seen:

- Solubility for the 3,4-difluorophenyl analogues is poorer than for the regular phenyl analogues, but they are typically more potent *in vitro*.
- Excellent solubility is seen with benzylic hydroxy substitution
- The lowest clearance was also seen with the benzylic hydroxy substitution
- Amide compounds are generally worse than the ether compounds with lower solubilities and higher clearances
- Clearance in MLM are generally high throughout, although this parameter is not as crucial as HLM clearance.

2.5 Concluding Remarks

The synthesis of all the Frontrunner compounds was successfully completed through various routes. The compounds were all re-evaluated for *in vitro* potency, and showed results consistent with the inherited and previously obtained data. Evaluation of the metabolic and physicochemical properties of the Frontrunners revealed varying levels of stability and solubility. These results provide an excellent framework for the future of the Series 4 triazolopyrazines. By identifying a

number of desirable and undesirable aspects that contribute to the key biological properties, a more concerted effort can be made for development and identification of a lead Series 4 compound with these aspects in mind.

For examples where a direct comparison could be made, compounds possessing a northwest pendant 3,4-difluorophenyl ring were more potent than the corresponding pendant phenyl ring compounds. While there is an associated reduction in solubility and increase in metabolic clearance with the fluorinated compounds, in future Series 4 compounds (where possible) the 3,4-difluorophenyl ring should be used.

Compounds containing the trifluoromethylpyridine group as the northeast triazole substituent were less potent than the related compounds containing a 4-Cl or 4-$OCHF_2$ substituted phenyl ring. As a result, in favour of the latter TP cores, the trifluoromethylpyridine TP core was no longer to used for future Series 4 compounds.

The introduction of benzylic substitution to the ether-linked compounds had a very positive effect. The potency of these compounds was maintained or improved compared to those with no benzylic substitution. More importantly, the solubility was greatly increased and the metabolic clearance lowered. These results suggest that designing future Series 4 compounds with the aim of improving solubility may be an effective way to improve metabolic clearance as well.

The further development of amide-linked compounds as Series 4 leads will be minimised in favour of the ether-linked compounds, not only due to the lower potency of the amides but also the lower solubility and higher metabolic clearance that is generally seen. Additionally, amide compounds have also exhibited poor hERG properties (discussed in Chapter 6).

Overall, the benzylic hydroxy compound **16** was seen to possess the best properties with good potency, excellent solubility and low metabolic clearance. These results warranted further exploration into benzylic substitutions for future Series 4 compounds, as will be discussed as part of the following chapter.

3. Novel Series 4 Compounds

This chapter covers the design and synthesis of a range of compounds with the aim of probing areas of SAR that have yet to be explored or remain incomplete. The *in vitro* biological evaluation of each series of novel compounds against *P. falciparum* is discussed at the end of each section.

3.1 Ether Chain Length

Even with an inherited dataset consisting of over 100 compounds, there were still obvious gaps in the SAR that needed addressing. For instance, it was stated in the inherited summary document that an ether chain length of two methylene groups was optimal between the heterocyclic core and the northwest pendant phenyl ring (Figure 3.1). While this may have been the case, the compounds required to prove this statement were, surprisingly, absent. Since this part of the molecule is such an integral aspect of the series, it was important to validate this conclusion with the appropriate compounds.

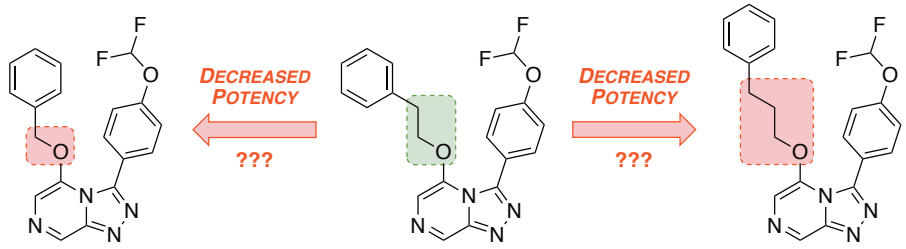

Figure 3.1: The inherited summary document stated that an ether chain length of two methylene units was ideal. Surprisingly, the compounds required to prove this were absent from this document.

3.1.1 Synthesis of the Ether-Linked Triazolopyrazines with Varying Chain Length

Before varying the ether linker length, it was essential to decide on a fixed structure for the rest of the analogues to be synthesised. Based on the existing SAR around the northeast triazole substituent, *para*-substituted phenyl rings were ideal for the best activity. The two most common of these were the 4-CN and 4-$OCHF_2$ substituents. While a number of potent compounds possessed the 4-CN, it had been seen that the solubility of these compounds was comparatively poor. As such, for all investigations into the variation of the northwest position, the 4-$OCHF_2$ substituent was used on the northeast phenyl ring. With a robust, three step synthesis of the TP core already established, multi-gram amounts of this core could be made (Figure 3.2), allowing more time to be focused on the synthesis of the more complicated northwest building blocks. The first hydrazine displacement step could be done with as much as 42 g of the 2,6-dichloropyrazine

starting material **1**, giving high yields of **2** between 80 and 95%. The subsequent condensation step was performed with up to 9.25 g of the hydrazine **2** in yields of around 80%. The final cyclisation step was successfully completed with up to 17 g of the hydrazone **55** giving the core **44** in yields also around 80%. With a large amount of the core in hand, the appropriate commercially available phenyl alcohols bearing ether chain lengths from zero to three methylene groups were attached to the northwest position using the standard nucleophilic displacement method, affording the desired compounds **56**, **57**, **58** and **59** in yields between 38 and 83%. In addition to these four compounds, a side chain bearing an extra ether oxygen was made using commercially available 2-phenoxyethanol to give **60** in 47% yield.

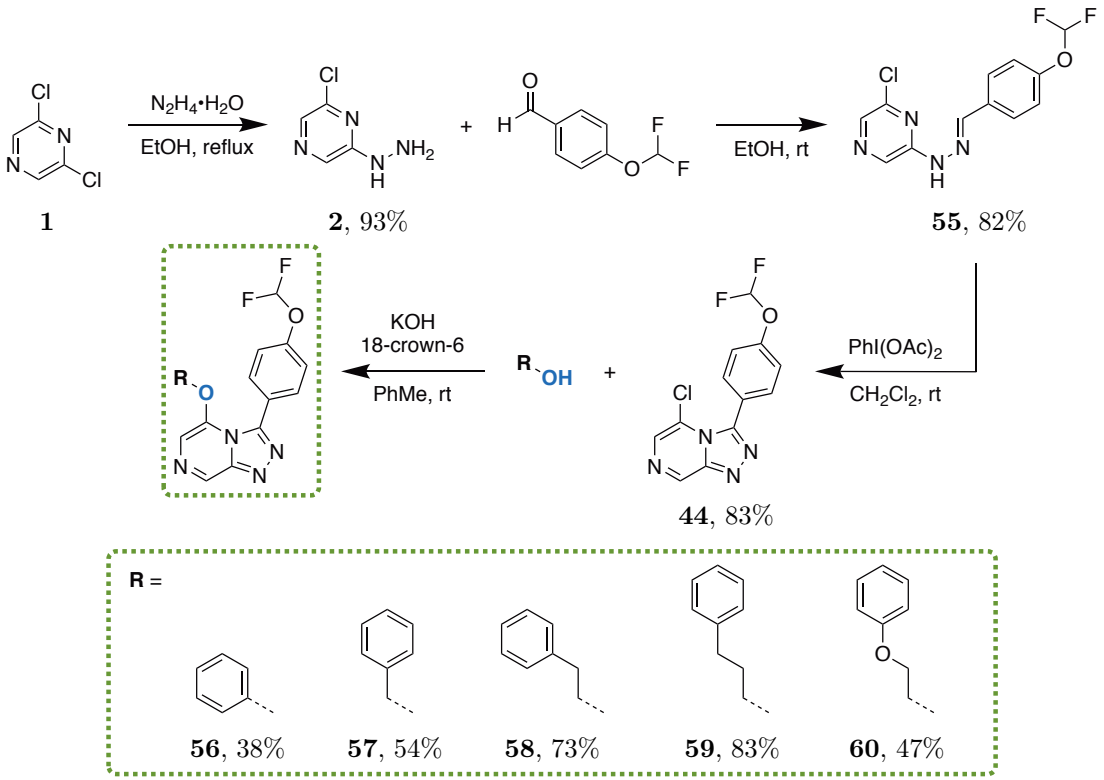

Figure 3.2: Synthesis of varied ether chain length compounds. Multi-gram synthesis of the core **44**, followed by coupling with the appropriate phenyl alcohol gave the desired compounds in moderate yields.

3.1.2 Biological Evaluation

Upon evaluation of these compounds for antiplasmodium activity, it was clear that the separation of the phenyl ring from the TP core was indeed important for maintaining potency (Table 3.1). Ether chain lengths of more than or less than two methylene units led to a decrease in activity, with no activity seen with the compound containing the phenol side chain (Entries 1–4). Attempts to bridge the longer carbon chain of **59** with an additional ether group (**60**) also resulted in reduction in potency (Entry 5). With the validation of this essential piece of SAR complete, the development

of more varied linkers of this length could be targeted.

Table 3.1: IC_{50} potency values of varied ether chain length compounds against *P. falciparum*. An ether chain length of two methylene units was found to be ideal.

Entry	Compound	cLogP	IC_{50} (μM)
1	**56**	2.8	>25
2	**57**	2.7	2.24
3	**58**	3.2	0.25
4	**59**	3.6	1.32
5	**60**	2.7	1.21

3.2 The Thioether Series

Another aspect of the inherited dataset that appeared to be missing was whether or not a thioether linker was tolerated. In order to fill in this missing information, during Joanna Ubels' 2014 Honours year at The University of Sydney,[165] a Series 4 compound was synthesised in which the ether linker was replaced by a thioether linker (**61**, Figure 3.3). This compound was subsequently evaluated for its efficacy by GSK in a rapid "single shot" (rather than a dose-response) assay, returning a 22% inhibition in their *P. falciparum* whole cell assay conducted at 2 μM. Compounds with inhibition less than 50% were classified as inactive and no IC_{50} value was obtained. By comparison, the corresponding ether-linked compound **62** was found to be quite potent at 0.534 μM.

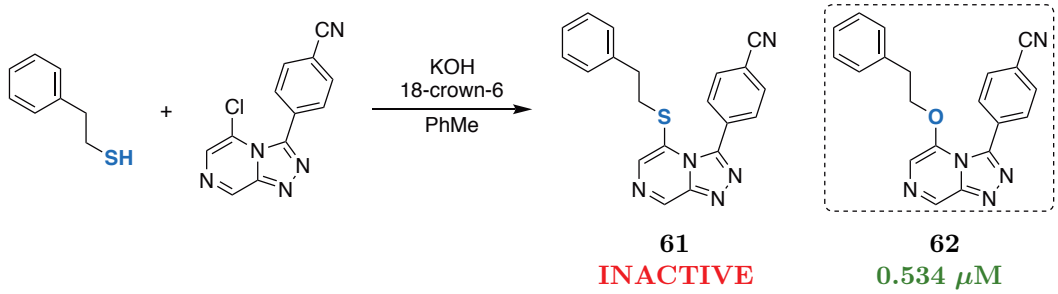

Figure 3.3: Series 4 thioether compound synthesised by Joanna Ubels. This thioether was found to be inactive against *P. falciparum* when compared to the corresponding ether compound.

With only one data point showing the thioether linker was detrimental to potency, it was felt necessary to validate this with another compound. In favour of improved solubility, and for better comparison with other data obtained for the series, the nitrile group in **61** was replaced with the 4-$OCHF_2$ group as previously synthesised (*vide supra*). The thioether series was further expanded upon with oxidised derivatives, specifically the sulfoxide and sulfone variants, with the hope of gaining further SAR data.

3.2.1 Synthesis of the Thioether-Based Triazolopyrazines

Thioether compounds with one and two methylene unit chain lengths were easily synthesised using the commercially available phenyl mercaptans and the TP core **44** to give **63** and **64** in moderate to low yields respectively (Figure 3.4). With these compounds in hand, it was thought that direct oxidation would allow quick access to the sulfoxide and sulfone derivatives. Oxidations to sulfones are typically carried out using reagents such as *m*-CPBA, 30% H_2O_2 and $KMnO_4$, while sulfoxides usually require milder oxidants like $NaIO_4$ which allow for only partial oxidation of the sulfide.[180] Initial attempts to oxidise **63** and **64** to the sulfoxide or sulfone using $KMnO_4$ or 30% H_2O_2 were unsuccessful with no reaction proceeding and only starting material being recovered. Reaction attempts involving increased time and/or equivalents of oxidant were also ineffective at producing the desired oxidation products.

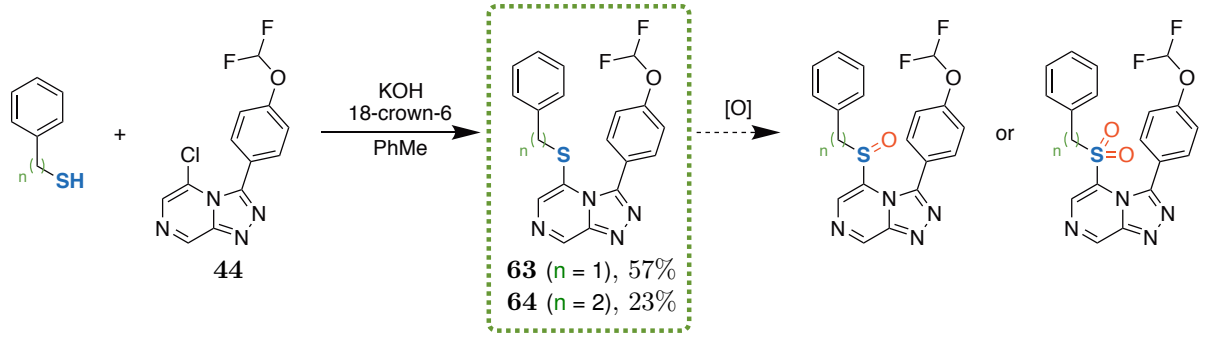

Figure 3.4: Synthesis of thioether compounds and unsuccessful direct oxidation to the sulfoxide and sulfone. Synthesis of the initial thioether compounds was successfully carried out. Attempts at direction oxidation to the sulfoxide and sulfone were unsuccessful using common oxidants such as $KMnO_4$ and H_2O_2.

It was suspected that the electronics of the fully formed triazolopyrazine core was not suitable for the oxidation to proceed so an alternative approach was pursued, by which the sulfoxide or sulfone would be appended to the pyrazine at an earlier stage of the synthesis. A survey of the literature highlighted a number of examples of the oxidation of thio-substituted pyrazine compounds. Of note, as part of a 1971 paper by Cheeseman and Godwin, they discussed displacements using sodium benzyl sulfide on 2,6-dichloropyrazine to give either the mono- or di-substituted benzylthiopyrazines, of which the characterisation of these compounds involved oxidation to the corresponding sulfones (to avoid the pungent smell of the thioether compounds).[181] A high-yielding method for obtaining the sulfoxide precursor was reported by Golchoubian and Hosseinpoor that used a combination of 30% hydrogen peroxide and glacial acetic acid.[182] This method was demonstrated with a number of phenyl- and alkyl-based symmetric and asymmetric sulfides providing the corresponding sulfoxides with complete conversion and excellent yields (90–99%).

While the original paper performed this initial thiol coupling step using benzene as the solvent,

this was replaced with the similar but non-carcinogenic solvent, toluene. Indeed, a large scale displacement reaction using 2,6-dichloropyrazine and phenylmethanethiol in the presence of NaH was performed to afford the thioether intermediate **65** (Figure 3.5); using 2-phenylethanethiol allowed access to intermediate **66**. Due to the pungent odour of these intermediates, their handling was kept to a minimum, with half the material going into the oxidation to the sulfoxide and the remainder into the oxidation to the sulfone. Encouragingly, the oxidation of **65** and **66** proceeded to give the corresponding sulfoxides (**67** and **68** respectively) using the literature method, albeit in low yields. In comparison with the high yields seen in the paper when using substrates predominantly bearing phenyl rings, it is possible that in this case, the electron deficient pyrazine ring contributed to the reduced yields. The remaining amounts of thioether intermediates were oxidised to the sulfones using $KMnO_4$ and glacial acetic acid to give the corresponding one- and two-carbon sulfones (**69** and **70** respectively), again in low yields. In this case, the reduced yields were likely due to exclusion of the decolourisation step which involved the use of sulfur dioxide gas. All four precursors were subjected to the standard core forming conditions to give the desired final compounds **71**, **72**, **73** and **74** in moderate yields over the three steps.

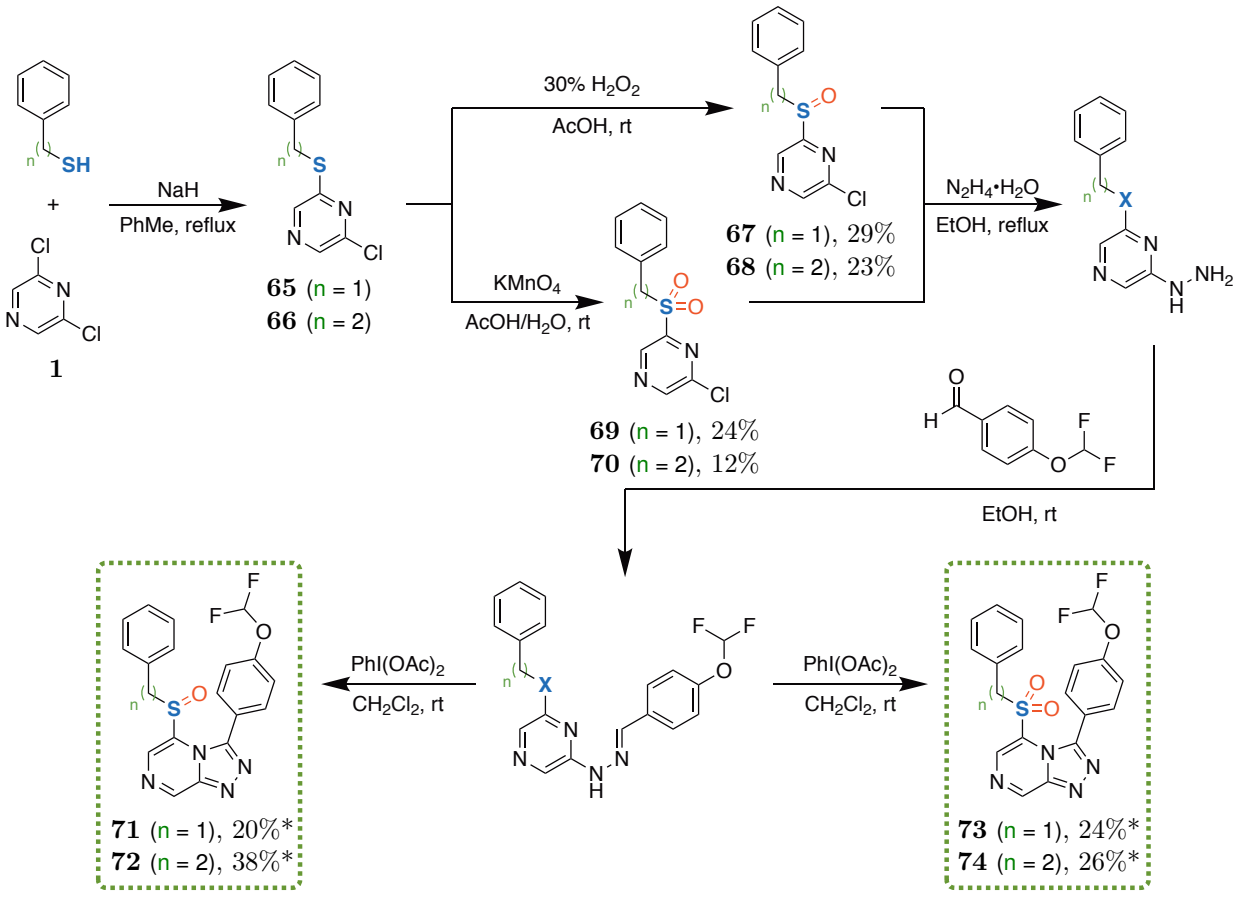

Figure 3.5: Synthesis of the oxidised thioether analogues. The common benzylthio-pyrazine intermediates **65** and **66** enabled oxidation to the sulfoxide and sulfone derivatives, which were then subjected to the standard core forming reactions to give the desired final products. *Yields of the final products are over three steps from **67**–**70**.

3.2.2 Biological Evaluation: Part 1

Following the synthesis of the thioether series of compounds, they were sent to Syngene for screening in the whole cell assay against *P. falciparum* (Table 3.2). The thioether compounds **63** and **64** were both inactive which validated the previously obtained result (Entries 1 and 2). Unfortunately, oxidation of the thioether linker had no effect on improving potency with all oxidised compounds showing inactivity (Entries 3–6).

Table 3.2: IC_{50} potency values of the thioether series of compounds against *P. falciparum*. All regular and oxidised thioether compounds were found to be inactive.

Entry	Compound	cLogP	IC_{50} (μM)
1	**63**	3.1	>10
2	**64**	3.5	>10
3	**71**	2.1	>2.5
4	**72**	2.6	>10
5	**73**	1.6	>10
6	**74**	2.1	>10

While these results indeed validated the original data, it still remained surprising that **64** was found to be completely inactive when the corresponding ether compound **58** was potent. The small differences in the properties between oxygen and sulfur were not expected to have made such a drastic impact on the potency.

Upon further investigation, inconsistencies were noticed between the ^{1}H NMR spectra of the three thioether compounds **61**, **63** and **64** (Figure 3.6). While the number of peaks and the integration ratios were correct for all three compounds, a key distinction in the spectra for **61** (blue trace) and **64** (green trace) was the apparent absence of a characteristic pyrazine signal, typically seen in Series 4 compounds at ~9.25 ppm. It is known that this signal corresponds to the proton H_b on the pyrazine ring, and the absence of this signal would suggest that the thioether side chain had in fact been installed in this position rather than the desired one. Interestingly, out of these thioethers, only one compound, **63** (red trace) showed this expected signal at this position, suggesting this particular compound was the correct 5-substituted product.

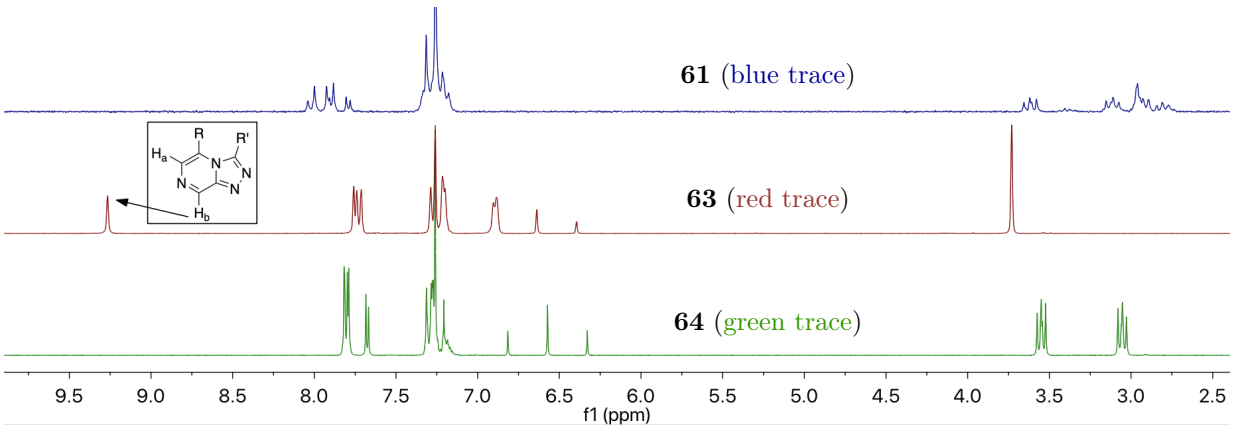

Figure 3.6: Differences in the NMR spectra of thioether compounds 61, 63 and 64. The absence of the characteristic pyrazine proton at ~9.25 ppm in the top and bottom spectra suggest different substitution products than expected.

3.2.3 Abnormal Substitution Products

Delving into the literature provided a possible answer to the identity of compounds **61** and **64**. While nucleophilic aromatic substitution (*ipso*-substitution) is a process in which a nucleophile displaces a leaving group on an aromatic system, resulting in the nucleophile being bonded to that carbon, alternative substitution patterns may also be possible. For example, in aryne chemistry it is possible for the nucleophile to end up bonded to the carbon adjacent to the leaving group, so-called *cine*-substitution. In less common cases, the nucleophile may even be situated more than one atom away from the leaving group, so-called *tele*-substitution (A, Figure 3.7). In our case, the thioether linker appears to be situated three atoms away from the leaving group, constituting a case of *tele*-substitution.

Since the inception of this term in 1977,[183] there have only been a few reviews specifically addressing *cine*- and *tele*-substitution reactions,[184–186] and of the latter *tele*-substitution, a relatively small number have been observed or directly investigated on triazolopyrazine systems. The first mention of this occurring in such a system was in 1974 by Verček and co-workers (B, Figure 3.7).[187] In an effort to investigate the reactivity patterns of the s-triazolo[1,5-*a*]pyrazine system, 5-bromination and subsequent displacement of the halide with a variety of nucleophiles was found to lead to unexpected products. In particular, the use of certain nucleophiles resulted in the isolation of 8-substituted products instead of the expected 5-substituted products. Further reactivity experiments indicated that isomerisation (Dimroth rearrangement) of the bicyclic system was not the mechanism for the formation of these abnormal substitution products. A few years later, as part of an investigation into new transformations for imidazo[1,2-*a*]- and s-triazolo[4,3-*a*]pyrazine systems, these cores were similarly brominated and the products of nucleophilic displacement analysed.[183] Much like before, the 5-halo triazolopyrazine systems were

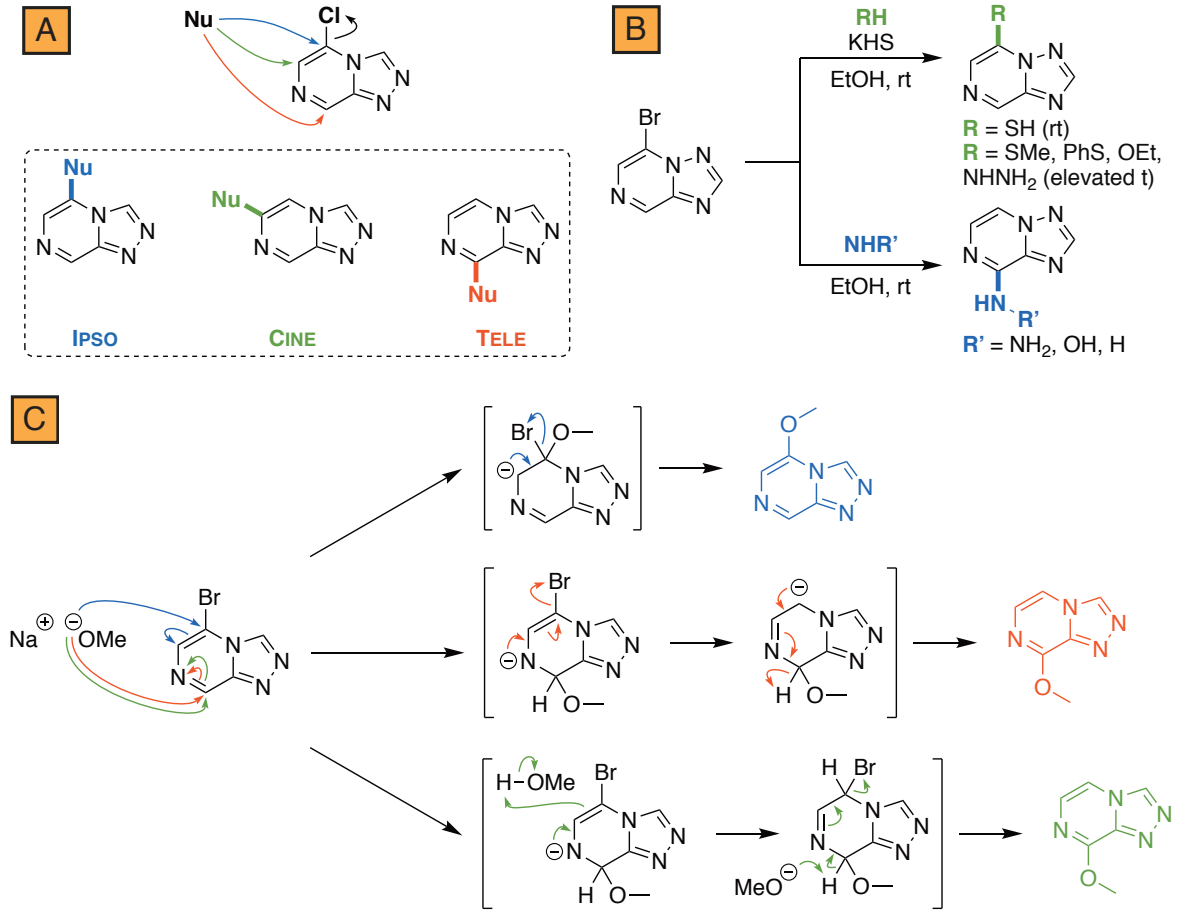

Figure 3.7: Possible substitution patterns on the Series 4 core. (A) *Ipso*-, *cine*- and *tele*-substitution products from nucleophilic displacement of the chlorine. (B) Examples of 5- and 8-substituted products isolated from the analogous s-triazolo[1,5-*a*]pyrazine system by Verček and co-workers. (C) Proposed mechanisms for *ipso*- (blue pathway) and *tele*-substitutions (red pathway) as reported by Bradač and co-workers. An alternative proposed mechanism taking into account the balancing of charges (green pathway).

observed to give not only the expected 5-substituted displacement product, but in some cases products of 8-substitution too. A mechanism for the *tele*-substitution was proposed by Bradač and co-workers (C, Figure 3.7) involving nucleophilic attack at the 8-position of the heterocyclic core (red pathway), a process that takes place competitively to the normal addition-elimination pathway (blue pathway).[183] It is noted that this proposed *tele*-substitution mechanism is not correct, as elimination of the bromine should leave the triazolopyrazine ring uncharged, which is not the case. A more reasonable mechanism is suggested, where the bromine elimination occurs in a subsequent step on the neutral triazolopyrazine core (green pathway).

Isolation of these supposed *tele*-substitution products from our thiol coupling reactions would therefore explain the discrepancies between the associated ^{1}H NMR spectra. If this is in fact correct, then the distinguishing feature in the ^{1}H NMR spectrum of an 8-substitution product would be the disappearance of the pyrazine 8-H signal at ~9.25 ppm. Additionally, the two

pyrazine protons at the 5- and 6-positions would appear as doublets due to adjacent coupling. Based on these hypotheses it could be deduced that, while **63** was in fact the correct 5-substituted product, **61** and **64** were actually the 8-substituted products.

3.2.4 Synthesis of the *tele*-Substituted Thioether Triazolopyrazines

In light of this information, the thiol coupling experiments in Figure 3.4 were repeated with extra care taken to isolate all reaction products (A, Figure 3.8). Indeed, when monitoring both reactions, it was clear by TLC that there were two apparent reaction products (B, Figure 3.8). The 5-substituted products typically appear below (more polar) the spot for the TP core in the regular alcohol coupling reactions (first lane of the TLC plate). It is clear that another product, the 8-substituted compound, appears much higher up the plate (less polar). Interestingly, at first glance, in the reaction with phenylmethanethiol (third lane of the plate), there appears to be more of the 5-substituted product **63** than the 8-substituted product **75**, however in the reaction with 2-phenylethanethiol (fourth lane of the plate), there appears to be more of the 8-substituted product **76** than the 5-substituted product **64**. Upon completion of the reactions, both were purified by automated flash chromatography and encouragingly, both substituted products from the two reactions were successfully isolated (C, Figure 3.8). Again, comparison of the ^{1}H NMR spectra for all four compounds confirmed that **61** and **64** were originally misassigned as the 5-substituted products (D, Figure 3.8).

While the combined yield from each reaction was around 92–93%, the ratio of the 5- and 8-substitution products was seen to vary depending on the alkyl chain length of the thiol nucleophile. Interestingly, when phenylmethylthiol was used, formation of the 5-substituted product was favoured fivefold. Conversely, when 2-phenylethanethiol was used, the ratios were more even but there was still a preference for the formation of the 8-substituted product. It is possible that nucleophilicity has an influence on whether or not *tele*-substitution occurs, with it more likely to happen with stronger nucleophiles such as sulfides and amines.

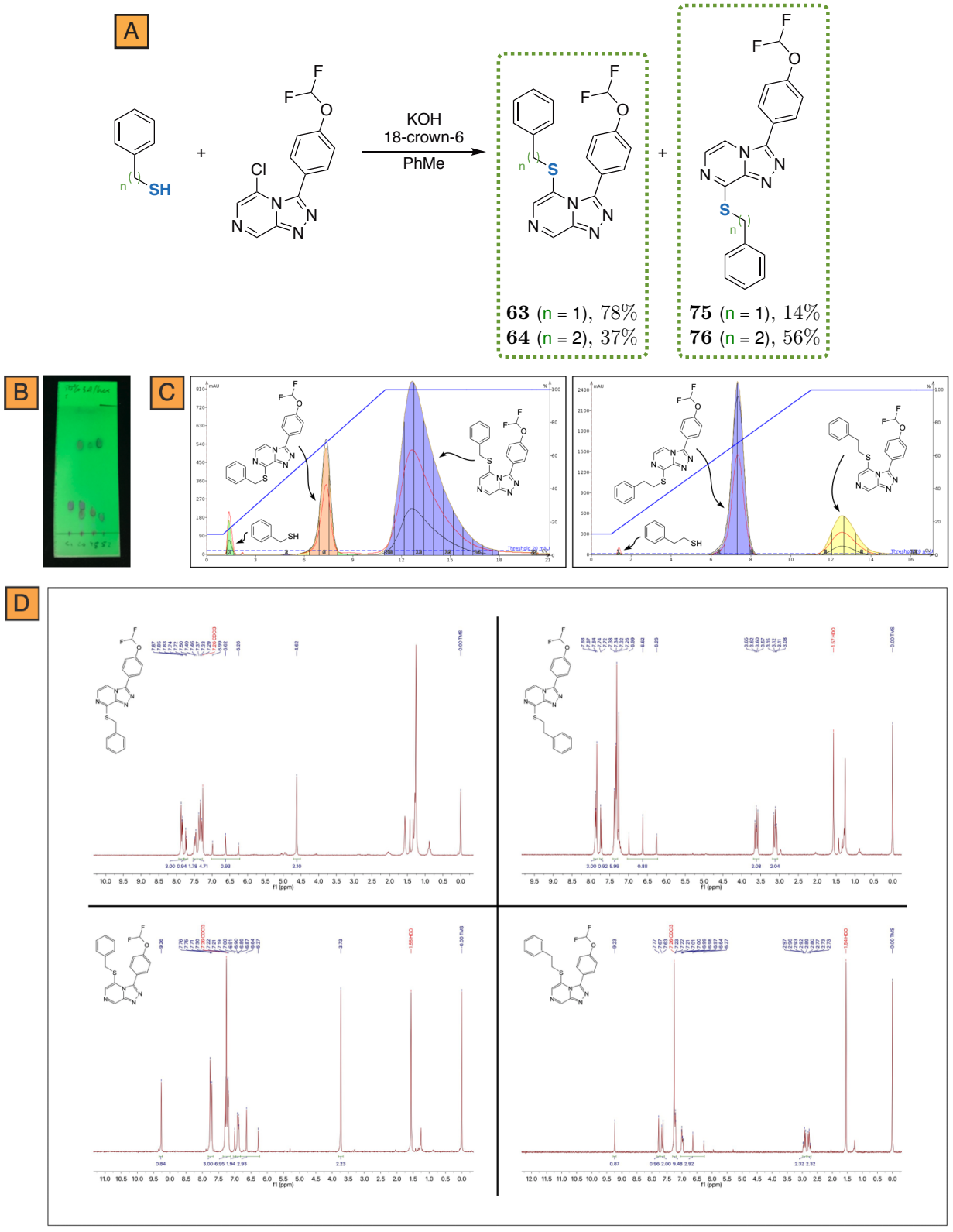

Figure 3.8: Repeat thioether experiments with TLC monitoring, purification traces and NMR spectra. (A) Both 5- and 8-substituted product were isolated from the repeat experiment. (B) TLC in 50% EtOAc in hexanes. Lane 1: TP core **44**, Lane 2: co-spot, Lane 3: reaction giving **63**, Lane 4: reaction giving **64**. (C) Biotage Isolera purification traces for both reactions. (D) ^{1}H NMR spectra of the four isolated substitution products from both reactions.

3.2.5 Biological Evaluation: Part 2

All four newly synthesised thioether compounds were subsequently sent for potency evaluation (Table 3.3). The now correctly identified, 5-substituted thioether compound **64**, returned a potency value of 1.05 μM (Entry 3). Even though this compound was still less potent that its ether counterpart **58** (IC_{50} = 0.25 μM), this result was much more in line with what was expected in terms of activity difference between an oxygen and sulfur replacement. The other 5-substituted thioether **63** (correctly identified previously) was confirmed to be non-potent (Entry 1). Interestingly, the 8-substituted thioether **75** was found to be weakly active while the longer chain variant **76** was completely inactive (Entries 2 and 4).

Table 3.3: IC_{50} potency values of the thioether isomers against *P. falciparum*. The now correctly identified 5-substituted thioether **64** was shown to be moderately active, while the other isomer was not. The shorter chain thioethers were much less active.

Entry	Compound	cLogP	IC_{50} (μM)
1	**63**	3.1	>25
2	**75**	3.1	5.62
3	**64**	3.5	1.05
4	**76**	3.5	>25

These results not only confirmed the suspicions about the original thioether compound, but also served as a way of cross-checking previous data from the series. Had these compounds not been made, it is possible that these discoveries would have gone unnoticed, leaving incorrect information in the Series 4 SAR. It should be noted that *tele*-substitution products have also been identified for a set of previously synthesised amine-linked compounds. Having been originally classified as the 5-substituted products, closer inspection of the ^{1}H NMR spectra again reveal the absence of the pyrazine signal at ~9.25 ppm. In addition, TLC images show product spots higher than that of the core, again suggesting an 8-substituted product instead. Other members of the Series 4 consortium are now working towards the synthesis of the actual 5-substituted amine products.

3.3 The Triazole Linker Series

When looking at the types of northwest linkers in the existing SAR, it was noticed that three analogous compounds with an amide, alkyl and ether linker between the pyrazine and phenyl ring all had very similar potencies (Figure 3.9). Based on this observation, it was thought that the type of linker may not be an important determinant of potency. Upon posing the question of possible alternative linkers to the OSM community, a number of suggestions were made including a ketone, reversed amide, sulfone and sulfoxide linkers (*vide supra*).[188] A triazole linker was suggested; it is known in medicinal chemistry that triazoles can act as suitable substitutes for amide groups.

The triazole linker was selected as the next synthetic target.

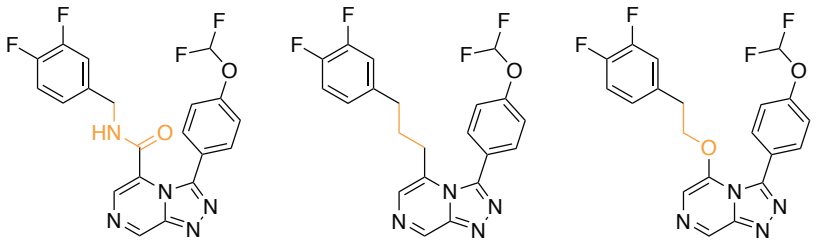

Figure 3.9: Three Series 4 compounds with different linkers showing similar biological activities. This would suggest that the type of linker group is not important for activity.

Triazoles are well known motifs in medicinal chemistry appearing in all manner of biologically relevant compounds.[189] Interestingly, of the two possible triazole isomers, the 1,2,4-triazole motif is much more common than the 1,2,3-triazole among the list of U.S. FDA approved drugs.[190] The synthesis of both isomers has been well studied over the years, with a range of methods allowing access to a variety of substituted triazoles. There are many methods for the formation of 1,2,4-triazoles, but perhaps the most common involve the cyclisation of hydrazones, hydrazides and hydrazines.[191] On the other hand, 1,2,3-triazoles are, more often than not, prepared by the copper(I)-catalysed alkyne-azide cycloaddition (CuAAC) reaction, or as it is more commonly known, the "click" reaction.[192] In keeping with the orientation of the amide group, a *C*-linked triazole (i.e. a triazole carbon attached to the pyrazine ring) was targeted and for ease of synthesis, the 1,2,3-triazole isomer was chosen.

3.3.1 Synthesis of the Triazole-Linked Triazolopyrazine

In order to append the triazole group as the northwest linker, an alkyne would have to be installed at the 5-position of the TP core. This would then facilitate a simple click reaction with phenyl azide. The most convenient way to access the desired alkyne precursor would be through direct transformation of the chlorine in the TP core **44** to an alkyne. A substructure reaction search of a simpler transformation, 2-ethynylpyrazine from 2-chloropyrazine revealed a number of conditions to effect this transformation. In particular, Bosch and co-workers reported the synthesis of 2-ethynylpyrazine *via* palladium catalysed coupling of 2-chloropyrazine with TMS acetylene, followed by base deprotection of the TMS group (Figure 3.10).[193]

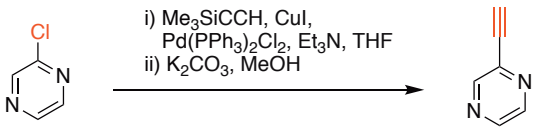

Figure 3.10: Synthesis of alkynylpyrazine through Pd catalysed TMS addition followed by deprotection with K_2CO_3 as reported by Bosch and co-workers. Displacement of the chlorine from the pyrazine ring to give the TMS protected alkyne, followed by deprotection would lead to the desired alkyne substituted pyrazine.

Initial attempts at this reaction using **44** were unsuccessful, with no reaction seen and only starting material recovered (Figure 3.11). Increasing the reaction temperature and/or the amounts of copper and palladium catalysts also provided no conversion to the desired product. It was thought that the triazolopyrazine core was negatively impacting the reaction, perhaps by poisoning of the palladium catalyst. Since the literature reported the use of 2-chloropyrazine as the reactant, the closest relevant analogue 2,6-dichloropyrazine **1** was thought to be more suitable for the reaction conditions. The only potential issue with this reactant would be the possibility of reaction with both chlorines, leading to a bis-alkyne substituted pyrazine. Nevertheless, when subjecting this to the reaction conditions the desired product was again not formed, with the ^{1}H NMR spectra indicating only starting materials present.

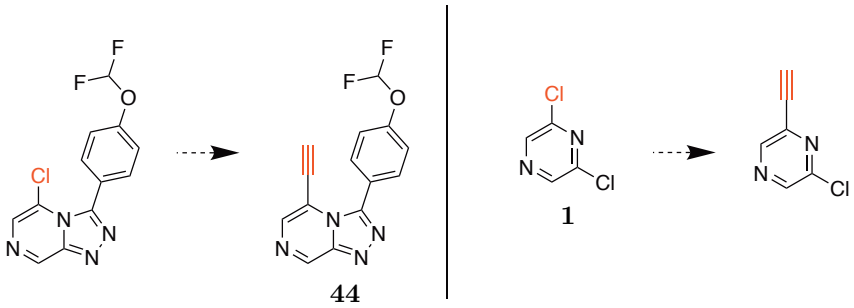

Figure 3.11: Attempts at the displacement of the chlorine with an alkyne using the literature methods were unsuccessful. Reactions with both the completed TP core **44** and the 2,6-dichloropyrazine starting material **1** were tried.

With no success in synthesising the alkyne core, efforts were then made towards the alternative *N*-linked triazole (i.e. a triazole nitrogen attached to the pyrazine ring). While the connectivity of this triazole would more closely resemble a reversed amide linker, the dimensions of the linker would remain the same. The *N*-linked compound would require an azide group at the 5-position of the TP core. This transformation was easily accomplished on **44** by displacement of the chlorine atom with NaN_3 in DMF to give the corresponding azido-TP core **77** in good yield (Figure 3.12). The subsequent click reaction was then attempted using 10 mol% sodium ascorbate and 1 mol% $CuSO_4$ catalyst in a mixture of CH_2Cl_2:H_2O with phenyl acetylene, but no conversion was seen when the crude mixture was analysed by TLC and ^{1}H NMR spectroscopy. Switching the reaction

solvent to a mixture of THF:H_2O and increasing the copper and ascorbate loadings (first to 5 mol% copper/10 mol% ascorbate, then to 40 mol% copper/80 mol% ascorbate) also did not improve the reaction. Upon increasing the loadings to 140 mol% copper/280 mol% ascorbate however, a small amount of the desired click product **78** was successfully isolated. While optimisation of this reaction could be done to obtain higher yields of the product, the amount isolated was enough for evaluation of its biological activity, which if found potent, the optimisation could then be undertaken.

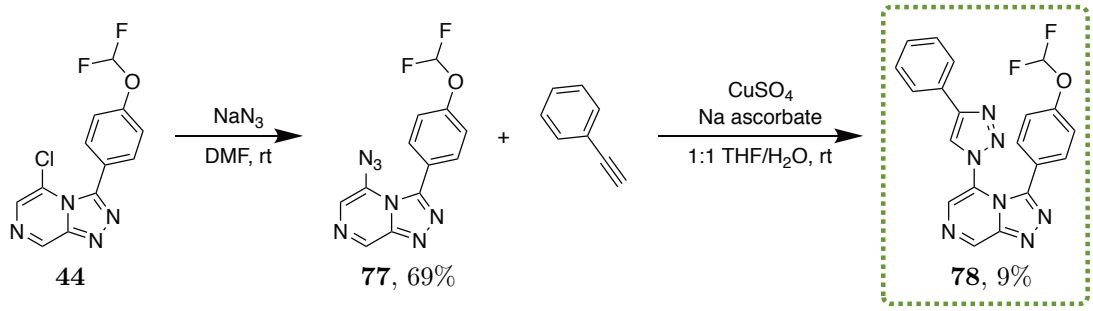

Figure 3.12: Synthesis of the *N*-linked triazole compound. Displacement of the chlorine atom with an azide, and subsequent click reaction led to the desired compound.

3.3.2 Biological Evaluation: Part 1

Interestingly, when the *N*-linked triazole **78** was evaluated for antiplasmodium activity, it was found to have an IC_{50} of >10 μM (Figure 3.13). This seemed surprising as the analogous amide compound **MMV669543** was found to be potent. It is possible that the flexibility of the northwest side chain is important for maintaining potency, and that by installing a rigid triazole linker, this flexibility is greatly reduced, translating to the loss in activity. With this in mind, it was thought that the activity could be regained by reincorporating an ether linker between the pyrazine ring and the triazole group, which would in turn bring back some associated flexibility.

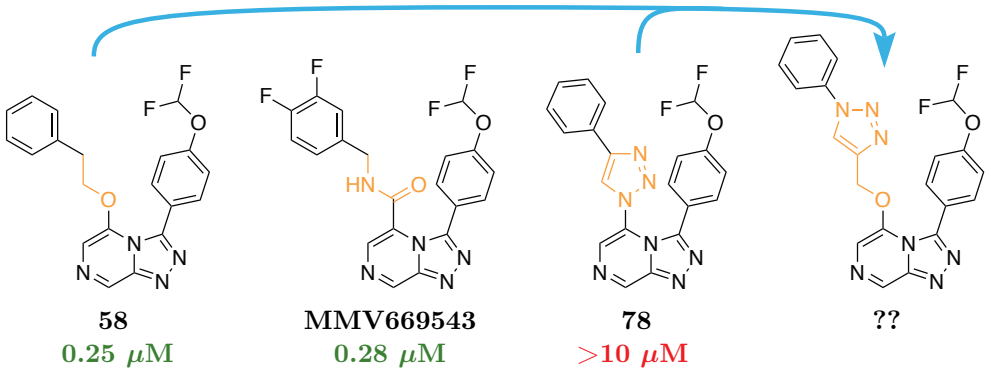

Figure 3.13: The triazole-linked compound had an IC_{50} of >10 μM. While the triazole linker was inactive, it was thought a combination of an ether and the triazole could regain potency.

3.3.3 Synthesis of the Ether-Triazole-Linked Triazolopyrazines

In order to reincorporate the ether linker into the side chain, the appropriate nucleophile containing an aromatic substituent on one side of the triazole and an alcohol substituent on the other, was required. Once again, this opened up the question for the orientation of the triazole group. Synthesis of the *C*-linked triazole (i.e. a triazole carbon connected to the ether linker) would require an azido alcohol coupling partner, the simplest being azidomethanol which would be synthesised *in situ* from acidic formaldehyde and NaN_3. Alternatively, the *N*-linked triazole (i.e. a triazole nitrogen connected to the ether linker) would require an alkyne alcohol coupling partner, the simplest and most readily available being propargyl alcohol. Based on this, the latter *N*-linked triazole was chosen for simplicity of reagents and methods. The other coupling partner for this click reaction would be an aryl azide derivative. Such aryl azides may be easily synthesised with a number of methods, for instance by halide displacement or by transformation of an amine. In terms of target compounds, the phenyl and benzyl derivatives were synthesised (Figure 3.14).

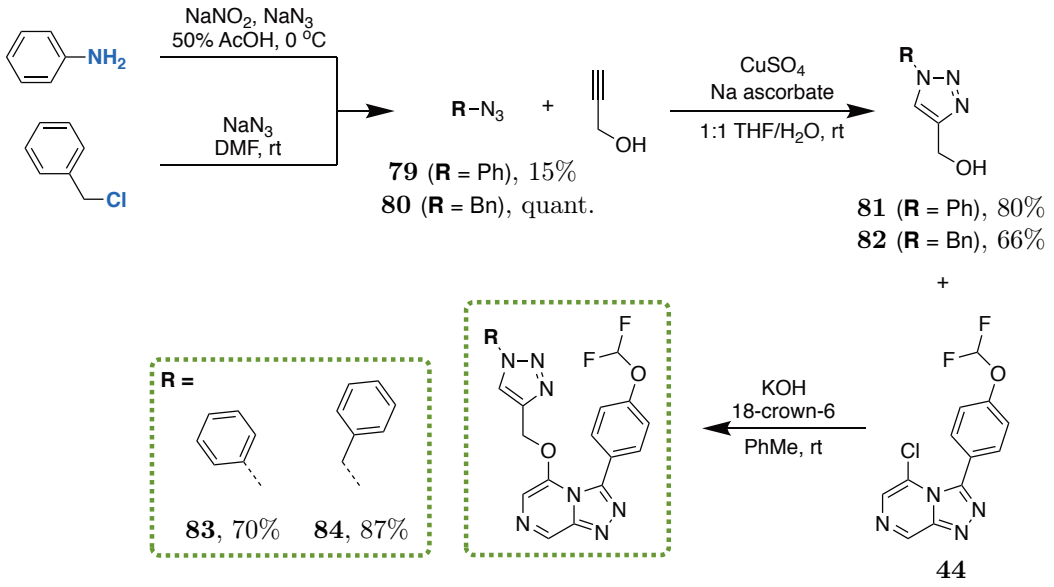

Figure 3.14: Synthesis of ether-triazole linker compounds. Click reaction with an aryl azide and propargyl alcohol gave the corresponding ether-triazole nucleophiles, which could then be coupled to the TP core.

The phenyl derivative was synthesised from aniline as the starting reagent. This was transformed to the corresponding azide **79** using $NaNO_2$ and NaN_3 in 50% aqueous acetic acid. Following work-up of the reaction mixture, the crude product was used in the subsequent click reaction with propargyl alcohol to give the corresponding triazole coupling partner **81**. The benzyl derivative was synthesised from benzyl chloride as the starting reagent. Displacement of the chlorine with NaN_3 in DMF afforded the corresponding azide **80** which, again, was used without further purification in the following click reaction to give the triazole coupling partner **82**. With both triazole alcohols in hand, they were readily coupled to the TP core **44** to give compounds **83** and **84** in

good yields.

While the above compounds were successfully synthesised, attempts to synthesise the pyridine variant were overall unsuccessful (Figure 3.15). Initially, it was unclear whether formation of the azide from 2-chloropyridine using NaN_3 in DMF had occurred, however, when subjecting this crude material to the following click reaction, no desired product was formed suggesting the initial reaction was unsuccessful. By subjecting 2-chloropyridine to the first step in forming the Series 4 core, the corresponding hydrazine compound could be made. Then using the conditions described above, the azide could be accessed. Indeed, formation of 2-hydrazinylpyridine and 2-azidopyridne proceeded smoothly, however, when subjecting this azide to click reaction conditions, no formation of the desired product was observed. This derivative was not pursued further as it was deemed no longer desirable.

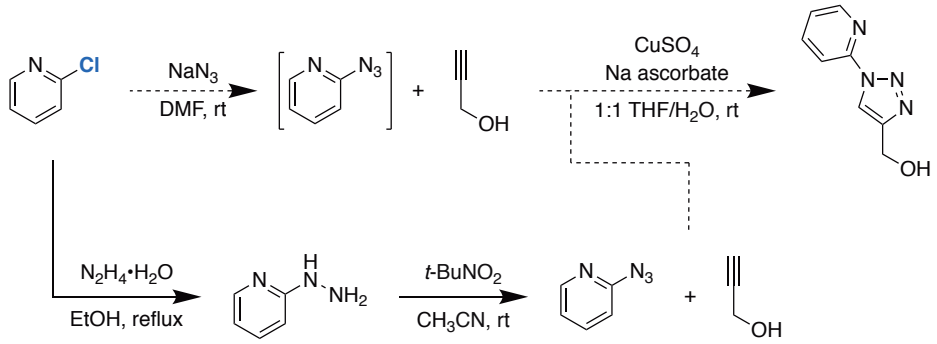

Figure 3.15: Attempted synthesis of the pyridine variant of the ether-triazole-linked compound. Pyridine azides accessed through different methods did not give the desired click product.

3.3.4 Biological Evaluation: Part 2

Much like the initial triazole compound **78**, the two ether-triazole compounds were also found to be inactive (Table 3.4). Even though a degree of flexibility was reintroduced into the compound, this did not appear to help. It may be the case that the combined triazole and aromatic ring moieties are too bulky for binding in the active site of the enzyme. Nevertheless, it appears that triazoles are not well tolerated within the Series 4 triazolopyrazines and the extra chain length is probably detrimental to the potency (as seen with the less potent compound **59** possessing a three methylene unit ether chain).

Table 3.4: IC_{50} potency values of the ether-triazole-linked compounds against *P. falciparum*. All three compounds were found to be inactive.

Entry	Compound	cLogP	IC_{50} (μM)
1	**83**	1.6	>10
2	**84**	1.8	>10

3.4 Benzylic Substitution

Drug metabolism is an important aspect of biologically relevant compounds, having direct impact on the efficacy of a drug and influencing factors such as half-life. A number of functional groups are well known to be particularly vulnerable to metabolic change,[194] including benzylic, allylic and phenyl ring positions vulnerable to oxidation, nitrogen-containing heterocycles vulnerable to *N*-oxidation or *N*-demethylation and ester or amide hydrolysis. Such processes typically translate to the reduced efficacy of a drug, with it being cleared from the system too quickly for it to have the desired effect. A common way to reduce the impact of these metabolically labile positions is to install additional functionality so as to inhibit these enzymatic reactions. For example, benzylic oxidation can often be prevented by installing an additional functional group such as a halogen at this position and phenyl oxidation can be slowed by substituting a hydrogen atom for a fluorine atom which results in a more stable molecule *via* a stronger bond strength and electron withdrawing effects.

With high rates of metabolism already posing an issue for Series 4 compounds, it was important to explore methods to block these metabolic hotspots, in particular the benzylic position. The inherited dataset already contained a number of compounds with substitutions at this position (Table 3.5). These ranged from primary, secondary and tertiary amines **85**–**89**, fluorines **90**–**91** and alcohols **23**–**93**. Perhaps the most interesting trend seen within this set of compounds was that within the benzylic amines. While all primary and tertiary amines were active, secondary amines were completely inactive. In order to investigate further this trend and to expand the SAR surrounding the benzylic position, a number of new compounds were designed and synthesised.

Table 3.5: Compounds from the inherited dataset containing benzylic substitutions. †Entries shown as single enantiomers in the inherited data, however there is no evidence of whether the samples were enantioenriched.

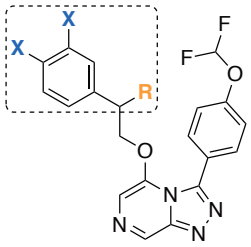

Entry	Compound	X	R	MMV Number	EC_{50} (μM)
1	**85**	H		MMV688899	2.00

2	**86**	H		MMV688898	>10
3†	**87**	F		MMV671651	0.28
4†	**88**	F		MMV670763	>10
5†	**18**	F		MMV670437	0.04
6	**89**	F	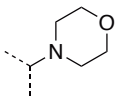	MMV671647	0.61
7	**90**	F		MMV672936	0.07
8	**91**	F		MMV672727	0.12
9	**23**	F		MMV670947	0.02
10	**92**	F		MMV672723	0.10
11	**93**	F		MMV670438	0.48

3.4.1 Synthesis of the Benzylic Ketone-Based Triazolopyrazines

As a means to access the benzylic amines readily, it was thought that a Series 4 compound with a benzylic ketone would enable a highly efficient and direct route *via* a simple reductive amination reaction. This would eliminate the need to synthesise the individual precursors required for each benzylic amine, effectively providing a late-stage functionalisation approach. To access this ketone intermediate, the appropriate northwest building block would need to be synthesised. A patent was identified describing the required transformation.[195] An additional attractiveness of this report was the use of a 3,4-difluorophenyl derivative as the starting material: the desired precursor could be accessed from the corresponding acetophenone **94**, *via* the dimethyl acetal **95** giving the 2-hydroxyacetophenone **96** in 66% yield over the two steps (Figure 3.16).

The initial precursor **94** was not readily available, so it was first synthesised by the oxidation of 1-(3,4-difluorophenyl)ethan-1-ol with iodic acid in the presence of catalytic TEMPO to give 3',4'-difluoroacetophenone **94** in good yield following literature procedures (A, Figure 3.18).[196] Subsequently, the α-position was oxidised using $PhI(OAc)_2$ affording the α-hydroxy dimethyl

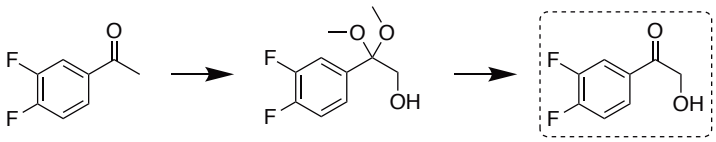

Figure 3.16: Potential synthetic route towards the benzylic ketone coupling partner. Two step method from 3,4-difluoroacetophenone involving α-oxidation and hydrolysis to the desired precursor.

acetal **95**, which after conversion of the ketal to the ketone gave the desired α-hydroxy ketone precursor **96** in moderate yield. Unfortunately, upon reaction of **96** with the TP core **44**, no coupling product **97** was produced. Interestingly, the only isolated material (10%) was identified to be the TP core **44** in which the chlorine had been replaced by a hydrogen atom (B, Figure 3.18, blue trace). The origins of this surprising product, arising from a formal reduction of the TP core, were not pursued further. The majority of the material was likely to have been decomposition products as evident by baseline material on TLC. It was also suspected that, to some extent, **96** could intermolecularly react with itself, potentially consuming the nucleophile faster than it would be able to react with the TP core. The suspicion that having the benzylic ketone already present in the nucleophile coupling partner was detrimental to the reaction led to the diemethyl acetal **95** being used as the coupling partner instead. Encouragingly, this reaction did lead to the corresponding coupled product **98** in good yield. Subjecting **98** to the same ketone deprotection conditions successfully gave the benzylic ketone compound **97** in 27% yield or an overall yield of 13%.

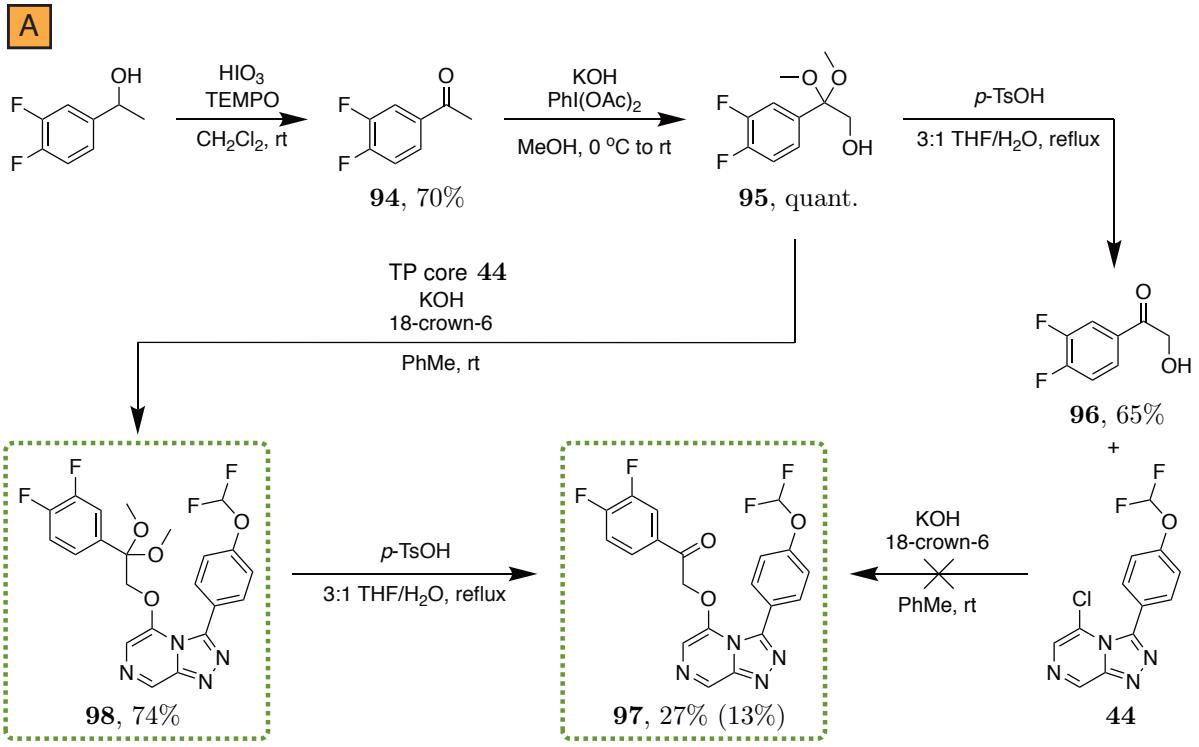

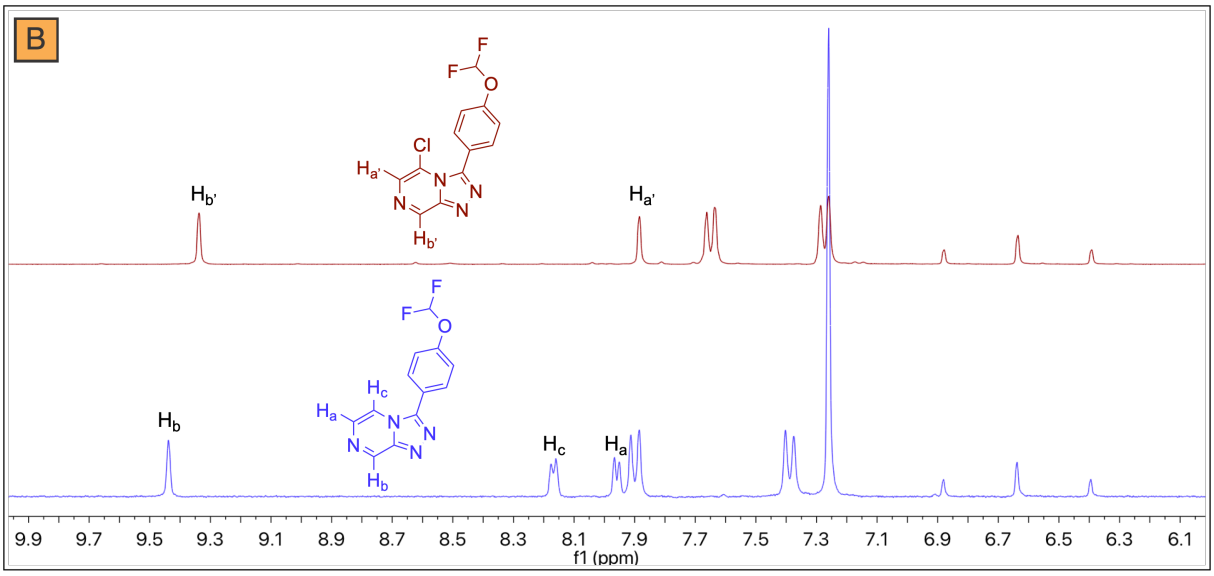

Figure 3.18: Synthesis of the benzylic dimethyl acetal and benzylic ketone compounds. (A) The benzylic ketone coupling partner was accessed in three steps from 1-(3,4-difluorophenyl)ethanol, however the coupling was unsuccessful. Coupling of the protected precursor and subsequent deprotection to the ketone was, however, successful. Final yield in brackets is the overall yield of the longest linear sequence starting from the core synthesis. (B) Reduced TP core (blue trace) isolated from the attempted coupling of **96** with **44** (red trace).

With both the benzylic ketone and the dimethyl acetal compounds successfully made, it was appropriate to complete this set through the synthesis of a cyclic acetal, namely the benzylic 1,3-dioxolane **100** (Figure 3.19). This was accomplished by protection of the ketone in **96** using ethylene glycol in refluxing PhMe with an acid catalyst giving the 1,3-dioxolane nucleophile **99** in excellent yield. Coupling of this with the TP core **44** gave the final benzylic 1,3-dioxolane product **100** in 7% yield. The relatively low yield was due to in part to the reaction not proceeding to completion, as well as to the multiple purifications required to isolated the pure compound.

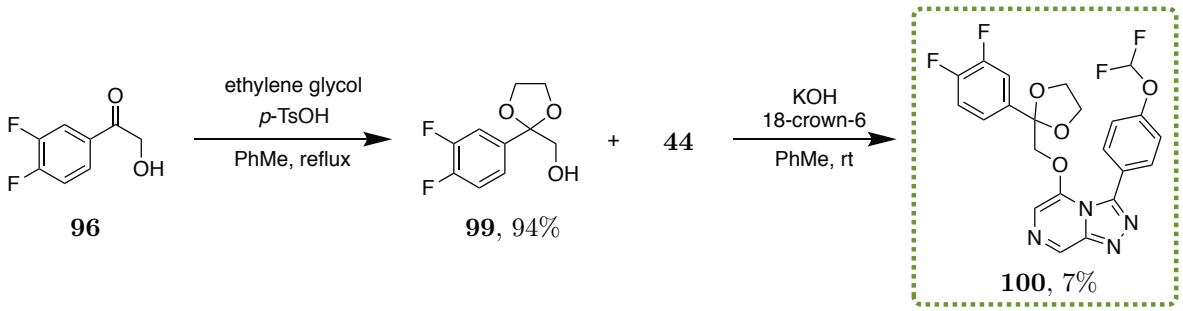

Figure 3.19: Synthesis of the benzylic 1,3-dioxolane compound. Protection of the ketone in **96** using ethylene glycol, and subsequent coupling with the TP core led to the benzylic cyclic acetal derivative.

There is an obvious alternative route to the benzylic ketone compound, *via* direct oxidation of the corresponding benzylic hydroxy compound **16** (a Frontrunner compound previously described in Chapter 2). The route requires the initial synthesis of the benzylic hydroxy compound, and as the requisite nucleophile precursor would contain two hydroxy groups, the benzylic alcohol would

need protection to prevent unwanted side reactions. Various options exist for the protection of alcohols including through the use of esters, ethers (methyl/benzyl/silyl) and acetals. Performing a structure search of the desired nucleophile with the different protecting groups showed a number of possible routes. Beginning with styrene oxide, epoxide ring opening can be achieved with a number of reagents leading to the methyl, benzyl, TMS and acetyl protected alcohols (A, Figure 3.20). The downside to this method is the possibility of the epoxide being opened from both positions, giving a mixture of regioisomers. Silyl and acetyl protection can be achieved by starting from 1-phenylethane-1,2-diol (B). Again there is the possibility of unwanted protection of both hydroxy groups. While these protecting groups may be effective in other cases, the sensitivity of the acetyl and silyl protecting groups to basic conditions, such as the ones required for coupling with the TP core, favoured other possibilities. Another potential protecting group is that derived from tetrahydropyran (THP). This strategy could be pursued starting from 2-hydroxyacetophenone, but would first require protection of the primary alcohol with another protecting group, reduction of the ketone, protection of the resulting secondary alcohol group and finally deprotection of the primary alcohol (C). The downside to this route is the number of steps required to obtain the desired nucleophile. An alternative route to this intermediate begins from mandelic acid and involves esterification, protection of the alcohol and reduction of the ester to give the desired alcohol (D). After consideration of all the methods, route D was seen as the most attractive and straightforward option and the one that was ultimately pursued. Due to the availability of the corresponding starting materials, the plain des-fluoro phenyl variant was used as the basis for the following synthesis.

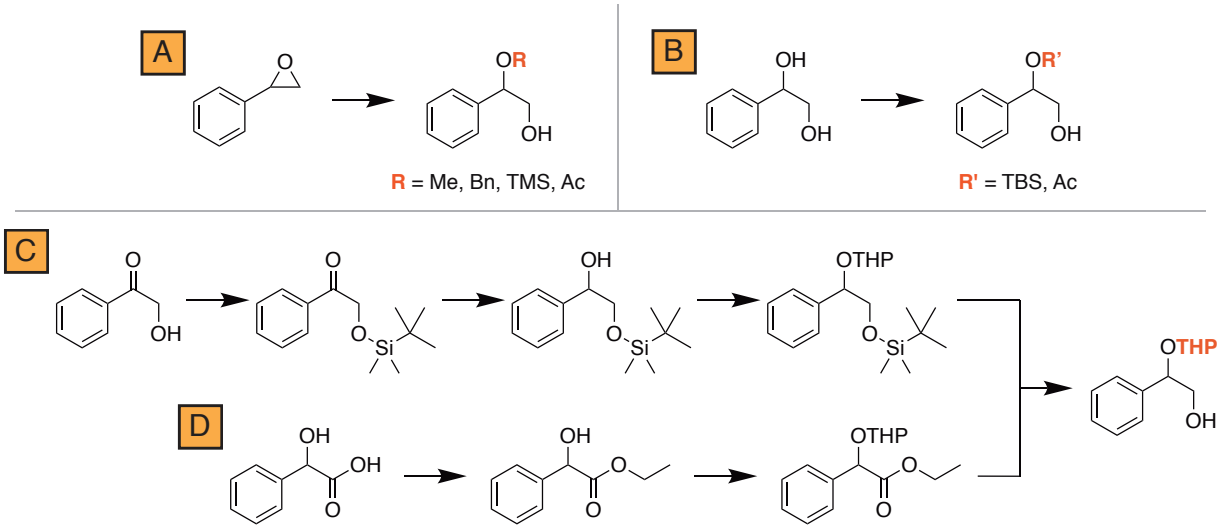

Figure 3.20: Possible methods for the synthesis of the protected nucleophile coupling partner. (A) Ether, silyl and ester protection from styrene oxide. (B) Silyl and ester protection from 1-phenylethane-1,2-diol. (C) Acetal protection from 2-hydroxyacetophenone. (D) Acetal protection from mandelic acid.

Starting from racemic mandelic acid, esterification using EtOH and catalytic *p*-TsOH gave the corresponding ethyl ester **101** in excellent yield (Figure 3.21). THP protection of the hydroxy group was achieved using 3,4-dihydro-2*H*-pyran and *p*-TsOH in CH_2Cl_2 to give the protected alcohol **102** in moderate yield. Reduction of the ester group using $LiAlH_4$ in THF led to the desired alcohol nucleophile **103** in good yield. This was then coupled with the TP core **44** to give the protected benzylic alcohol intermediate **104**, which was immediately deprotected without further purification. Initial attempts at deprotection using a 4 M HCl solution in dioxane were ultimately unsuccessful. While there was apparent disappearance of starting material by TLC, the crude product contained too many unidentified products to isolate any desired product **16**. Searching for alternative deprotection conditions identified a procedure for the deprotection of THP ethers and 1-ethoxyethyl ethers using copper(II) chloride dihydrate.[197] Encouragingly, when subjecting **104** to this reaction conditions, clear conversion to the deprotected product was seen by TLC and the desired product could be isolated in good yield. Oxidation of the benzylic alcohol was then achieved using manganese(IV) oxide giving the highest yield of the benzlic ketone product **105** as 37%, even with upwards of fifty equivalents of MnO_2. Although this demonstrated that the benzylic ketone could be accessed through other methods, the initial route shown in Figure 3.18 was more favourable in terms of the number of synthetic steps required and overall yield of the final compounds.

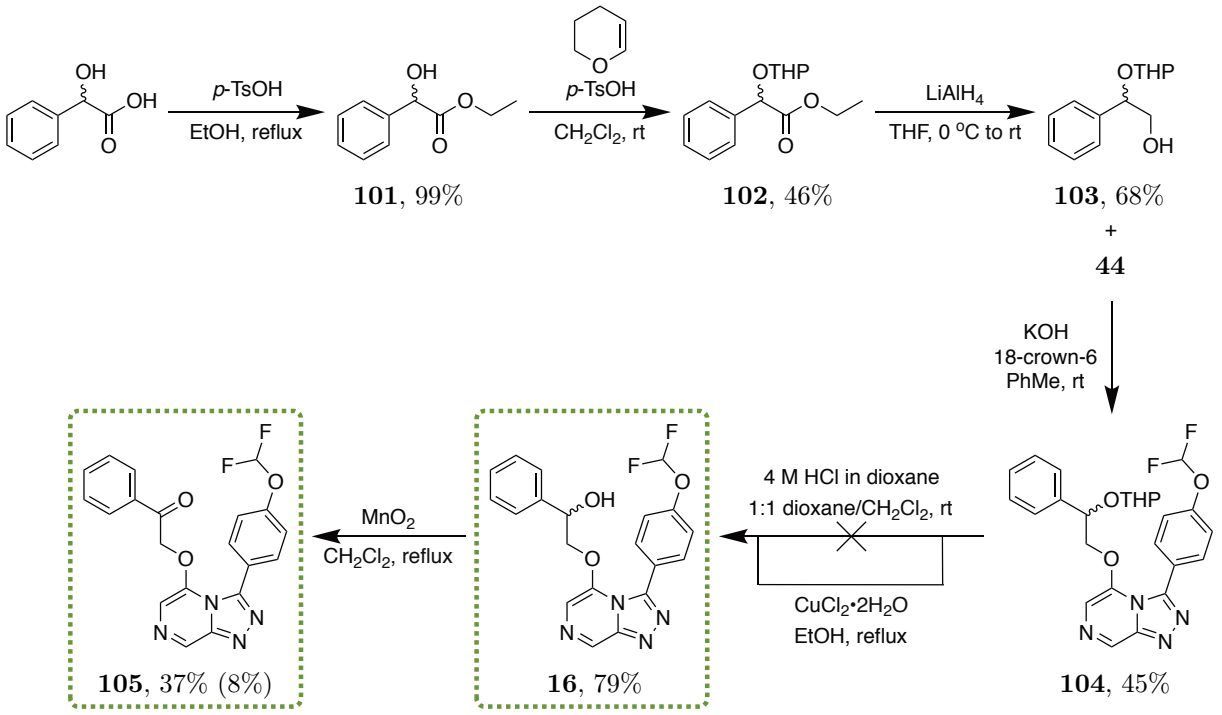

Figure 3.21: Alternative synthesis of the benzylic ketone compound. This alternative route first involves the synthesis of the benzylic hydroxy compound, with subsequent oxidation. Final yield in brackets is the overall yield of the longest linear sequence starting from the core synthesis.

In addition to obtaining Frontrunner compound **16** *via* this route, the THP-protected alcohol **103** was also used for the synthesis of Frontrunner compound **25** (Figure 3.22). Nucleophilic displacement with TP core **106** (synthesised by Dr. Alice Motion) gave the coupled product in 55% yield. This was then deprotected to give the desired Frontrunner **25** in 88% yield.

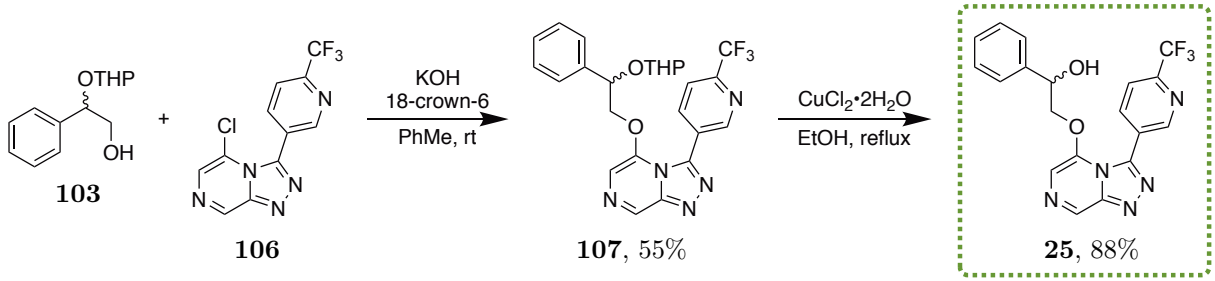

Figure 3.22: Synthesis of Frontrunner compound 25. The THP-protected alcohol **103** used for the benzylic ketone compound was also used to access another Frontrunner compound.

3.4.2 Biological Evaluation: Part 1

Before the synthesis of the benzylic amine derivatives, the above benzylic ketone-based compounds were first evaluated for potential antiplasmodium activity (Table 3.6). Both benzylic ketone compounds **97** and **105** were found to be quite potent, and much like in other examples, the latter 3,4-difluorophenyl derivative was more potent than the phenyl counterpart, in this case around 1.6 times more potent (Entries 1 and 5). Interestingly, both protected ketone compounds **98** and **100** were more potent than the benzylic ketone compound itself, with the most notable being the former dimethyl acetal, which was more than 5 times more potent than the unprotected ketone **97** (Entries 2 and 3). The similar activities seen across the benzylic ketone-based compounds are likely due to the ketones being, to some extent, in equilibrium with the acetal forms in the target environment.

Table 3.6: IC_{50} potency values of the benzylic ketone derivatives against *P. falciparum*. All benzylic ketone and benzylic acetal derivatives showed good activity.

Entry	Compound	cLogP	IC_{50} (μM)
1	**97**	2.5	0.83
2	**98**	3.0	0.16
3	**100**	2.7	0.67
4	**16**	2.1	0.36
5	**105**	2.3	1.37

3.4.3 Synthesis of the Benzylic Amine-Based Triazolopyrazines

After having successfully synthesised the benzylic ketone compounds, attempts were made to access the benzylic amines through reductive amination. To investigate the potency trends seen

among the various amine derivatives, analogues containing longer alkyl amines were made. Based on the inherited data in Table 3.5, a trend appeared to be consistent across both racemic and (reportedly) enantiopure benzylic amines, with the primary and tertiary amines showing good potency and the secondary amines being completely inactive. To simplify the synthetic efforts, the racemic versions of all analogues were pursued.

As a larger amount of the benzylic ketone compound **105** was available from the previous syntheses (compared to the 3,4-difluorophenyl derivative **97**), this was used for the subsequent reductive amination reactions. Attempts were made with dimethylamine, diethylamine and morpholine using $NaBH(OAc)_3$, however no benzylic amine products were detected (Figure 3.23). Rather, only reduction of the ketone to the alcohol was seen (i.e. **105** to **16**). Increasing the reaction time to allow for imine formation prior to the addition of the borohydride was ineffective, as was increasing the amount of acid to compensate for possible protonation of the triazolopyrazine ring.

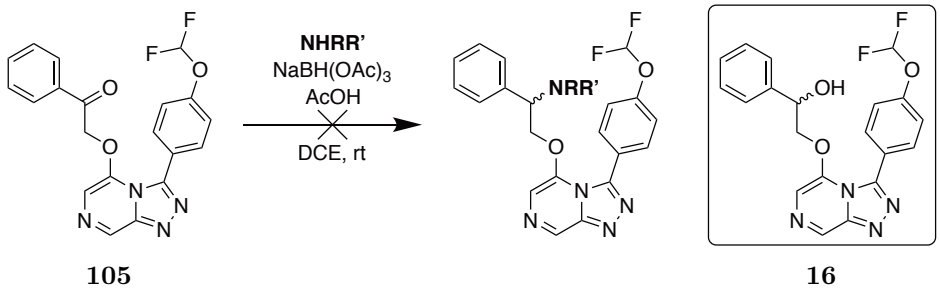

Figure 3.23: Attempted reductive amination on the benzylic ketone compound 105. Reductive amination using dimethylamine, diethylamine and morpholine were unsuccessful, with only reduction to the alcohol **16** observed.

To scope out alternatives to the direct reductive amination, routes involving the synthesis of the benzylic amine intermediate prior to nucleophilic coupling with the core were investigated. In searching for another possible method to access these amine precursors, one was found that used $Mg(ClO_4)_2$ as a catalyst for the ring opening of epoxides with amines.[198] As mentioned for the analogous epoxide ring opening for protected alcohols, an obvious drawback to this method is the likely generation of a mixture of regioisomers, however it was thought that following the coupling step with the TP core, the desired product could be easily separated. Indeed, the ring opening of styrene oxide with diethylamine and morpholine under these conditions led to a mixture of ring-opened products, which were then coupled to the TP core **44** as crude mixtures (Figure 3.24). Unfortunately, in the case of the diethylamine derivative, while the reaction proceeded to give the desired product, isolation of this product proved troublesome, even after multiple attempts at purification. Fortunately, while the morpholine derivative also gave a mixture of products, the desired compound **108** was successfully isolated, with none of the other possible coupling product

detected or isolated.

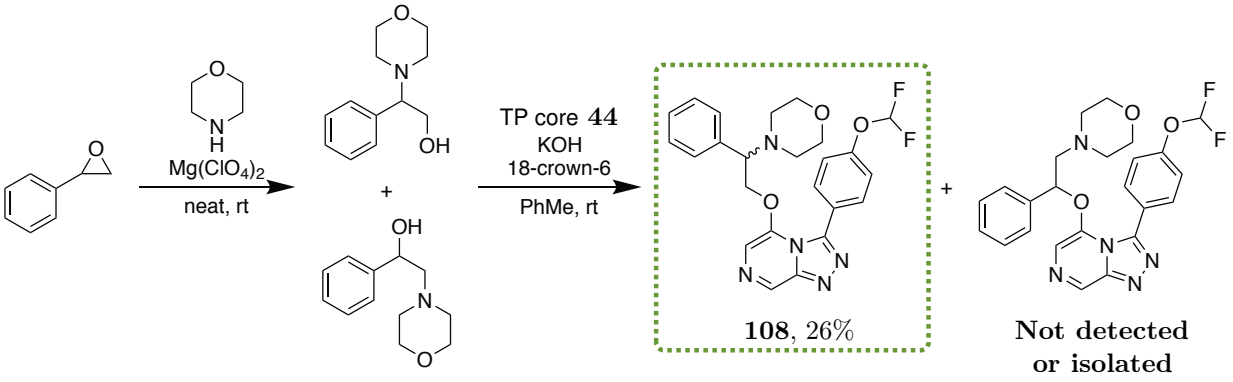

Figure 3.24: Synthesis of the benzylic morpholine compound. Epoxide ring opening gave a mixture of products, which when coupled to the TP core **44** allowed for the desired product to be isolated.

Concurrently, efforts were being made towards the synthesis of the Frontrunner compounds, in particular the benzylic dimethylamine Frontrunner compound **30**. Difficulties in making this compound led to consultation with the OSM community, and a revised route was found (see Chapter 2) which was ultimately applied to the synthesis of the remaining benzylic amine derivatives (Figure 3.25). Using the α-bromo ester **53**, NHEtMe and $NHEt_2$ were used to give the corresponding amines **109** and **110** respectively in good yields. These were then reduced to the required alcohol nucleophiles (**111** and **112**), and coupled to the TP core **44** to give the final compounds **113** and **114** respectively in moderate yields.

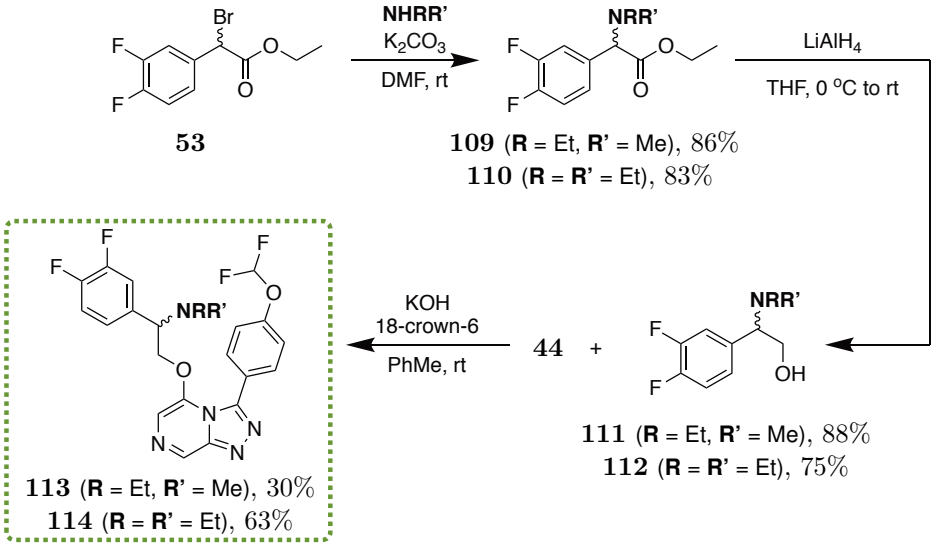

Figure 3.25: Synthesis of the longer alkyl chain benzylic amine derivatives. Using the route established during the Frontrunners campaign, the ethylmethylamine and diethylamine derivatives were made.

3.4.4 Biological Evaluation: Part 2

A number of interesting trends were seen upon the evaluation of these benzylic amine compounds for antiplasmodium activity (Table 3.7). Similar to other cases of phenyl versus 3,4-difluorophenyl, the morpholine compound **108** (Entry 1) was slightly less potent (~2.5 times) than the previously inherited analogue **89** bearing the 3,4-difluorophenyl ring (Entry 6, Table 3.5).

Given the strong influence of the amine substitution pattern on the potency previously seen, it was expected that the ethylmethylamine derivative **113** would be inactive and that potency would be regained with the diethylamine derivative **114**. Instead, weak activity was seen with the ethylmethylamine **113** and complete inactivity was seen with the diethylamine **114** (Entries 3 and 4). Perhaps even more surprising, was the drastic loss in potency when going from the dimethylamine **30** to the ethylmethylamine substituent (Entries 2 and 3). Such a change in potency seemed surprising considering other larger benzylic substitutions such as morpholine and 1,3-dioxolane were quite well tolerated.

Table 3.7: IC_{50} potency values of the benzylic amine compounds against *P. falciparum*. The increased alkyl chain length of the benzylic amines led to a large reduction in activity.

Entry	Compound	cLogP	IC_{50} (μM)
1	**108**	2.3	1.58
2	**30**	2.5	0.19
3	**113**	2.9	8.85
4	**114**	3.3	>10

It is clear that the benzylic position is sensitive to the nature of the substituent. While bulkier cyclic substituents are tolerated, alkyl chains longer than one methyl group are not. Considering the compounds synthesised here, along with the Frontrunners containing benzylic groups, there is still a clear preference for benzylic alcohol substitution over other functionality.

3.5 The Phenylalaninol Ether

Prior to the completion of her Honours year in 2014, Joanna Ubels began work on the synthesis of a Series 4 compound bearing a phenylalaninol ether side chain. The compound was originally proposed in order to investigate further the influence of ether chain length on bioactivity. Her attempted synthesis involved the coupling of (*R*)-2-amino-3-phenylpropan-1-ol with the 4-Cl TP core (Figure 3.26).[199] While this reaction appeared to have gone to completion by TLC analysis, upon purification and isolation of the major fractions, neither the starting material nor product were seen. It is possible that in this case, substitution by the amino alcohol is outcompeted by substitution with KOH. Unfortunately, due to time constrains, no further attempts were made to synthesise this compound.

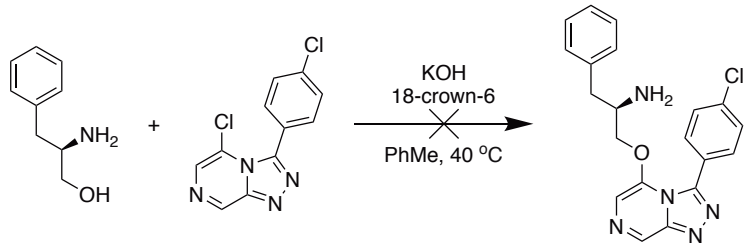

Figure 3.26: Previously attempted synthesis of the phenylalaninol ether compound. Direct coupling of phenylalaninol was unsuccessful.

Following this, in mid-2017, Griffith University joined the OSM consortium.[200] In an undergraduate class led by Dr. Mark Coster, the students were tasked with synthesising new Series 4 compounds for the project, including previously-attempted, but also novel, compounds. One student was assigned the synthesis of the aforementioned phenylalaninol compound.[201] The plan to tackle this synthesis was to use the Boc protected phenylalaninol in the coupling step to prevent any unwanted reactions. At the conclusion of the semester, the student had synthesised the 4-$OCHF_2$ TP core, and had attempted a model coupling reaction with 2-phenylethanol. However, not enough time remained to purify or characterise the reaction products, or to perform this coupling with the Boc protected phenylalaninol.

3.5.1 Synthesis of the Phenylalaninol Ether-Linked Triazolopyrazines

With a clear route to the desired compound having been laid out by the previous attempts, it remained only to complete this relatively straightforward synthesis (Figure 3.27). Both the (*R*)- and (*S*)-enantiomers of phenylalaninol are readily available and were mono-Boc protected under standard conditions with Boc_2O in CH_2Cl_2 to give the corresponding compounds **115** and **116** in good to excellent yields. The coupling of these Boc-protected nucleophiles with the TP core **44** proceeded smoothly to give coupled products **117** and **118** in moderate yields. Final deprotection of the Boc groups under acidic conditions gave the desired (*R*)- and (*S*)-enantiomers **119** and **120** respectively.

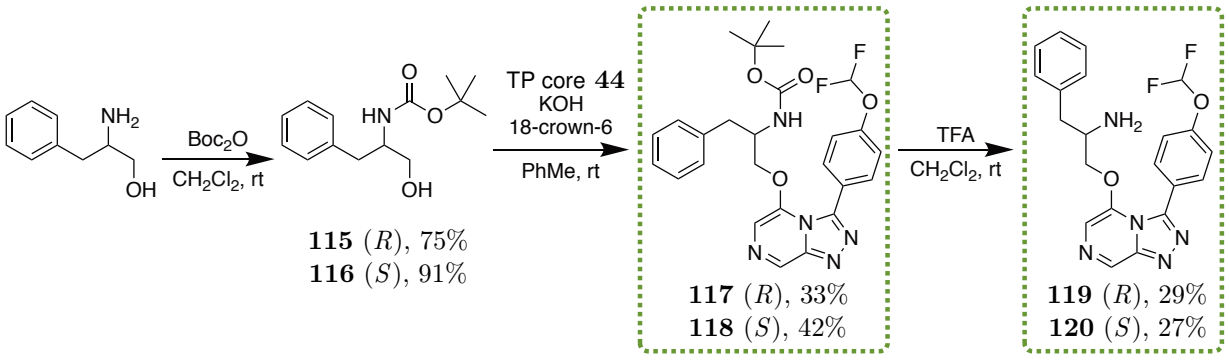

Figure 3.27: Synthesis of the (*R*)- and (*S*)-phenylalaninol compounds. Boc protection of the phenylalaninol prior to coupling allowed the reaction to proceed smoothly giving the desired products.

Since these reactions were performed using enantiopure starting materials, attempts were made to determine the *e.e.* of the final products using chiral HPLC. In a sample containing a mixture of the two enantiomeric products **119** and **120**, two closely eluting peaks were seen when running a gradient of 0–1% IPA in hexanes for 30 minutes, however attempts at further resolution were unsuccessful. Surprisingly, performing the same gradient on each of the products separately resulted in the same peak shape being seen revealing the compounds had racemised. To determine the extent of this, the intermediates **117** and **118** and the Boc protected amino alcohols **115** and **116** were examined by chiral HPLC as well. Two closely eluting peaks were seen with all four samples indicating that they had all racemised. These results suggest that the racemisation occurred during the initial Boc protection step. Due to time constraints, this was not pursued further.

3.5.2 Biological Evaluation

The evaluation of these compounds was performed prior to the chiral HPLC experiments described above. Interestingly, these amine-containing compounds showed far less potency than the regular three methylene unit ether compound **59**, which had a potency of 1.32 μM (Table 3.8). The two enantiomers showed differences in potency. While they were all essentially inactive, in the case of the (*R*)-enantiomer, the Boc-protected analogue **117** was more potent than the free amine **119** (Entries 1 and 3). The opposite was true for the (*S*)-enantiomer, with the Boc-protected compound **118** being less potent than the weakly active free amine **120**. These results highlight the importance of the stereogenic centre on the potency of the final compound. Should a lead Series 4 compound be identified that contains a stereogenic centre, it will be important to either resolve, or separately synthesise, the enantiomers to discover whether there is a eutomer.

Table 3.8: IC_{50} potency values of the phenylalaninol enantiomers against *P. falciparum*. The (*S*)-enantiomer was more active than the corresponding (*R*)-enantiomer, but all compounds were relatively non-potent.

Entry	Compound	cLogP	IC_{50} (μM)
Reference	**59**	3.6	1.32
1	**117**	3.9	8.6
2	**118**	3.9	10
3	**119**	2.2	17
4	**120**	2.2	2.3

3.6 Miscellaneous Compounds

An additional small set of novel compounds was synthesised, mainly as a result of inputs from the OSM community.

3.6.1 Northeast Phenyl Ring Substitution

The inherited data suggested that a 4-substituted (either CN, Cl or $OCHF_2$) phenyl ring as the northeast substituent was ideal for activity, however the compounds confirming this conclusion were absent from the dataset. The obvious missing compounds included one with no northeast substituent and one with a plain phenyl substituent. Synthesis of the core without any northeast substituent required an alternative method to the standard core forming reactions (Figure 3.28). Cyclisation of the hydrazine intermediate **2** with $HC(OEt)_3$ led to the desired core **121** in 44% yield. Nucleophilic displacement of the chlorine atom with 2-(3,4-difluorophenyl)ethanol gave the final compound **122** in moderate yield. The northeast phenyl substituted core was synthesised using benzaldehyde during the condensation step to give **123**, which was then cyclised to **124** and finally coupled with 2-(3,4-difluorophenyl)ethanol to give **125** in low yield. Another compound suggested by the OSM community was the 4-SF_5 core. This moiety is known to be an effective replacement for CF_3 and OCF_3 groups.[202] This was again synthesised by using 4-(pentafluorosulfanyl)benzaldehyde in the condensation step to give **126**, cyclised to **127** and coupled with 2-phenylethanol to give the final compound **128** in 83% yield.

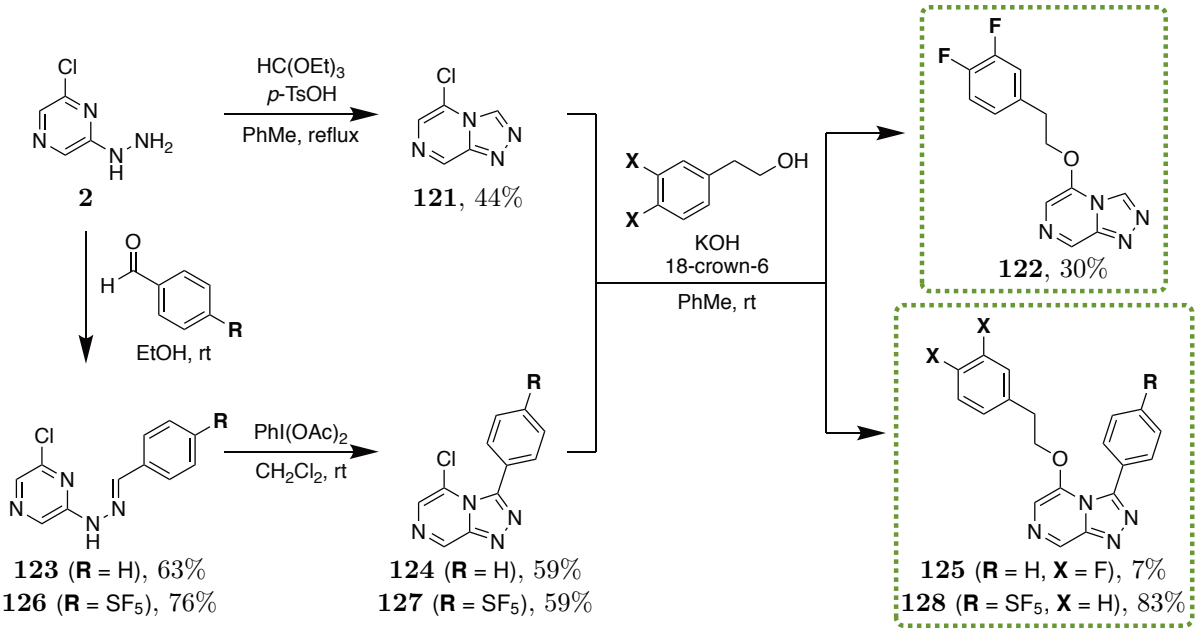

Figure 3.28: Synthesis of Series 4 compounds with varying northeast substitutions. Compounds with no triazole substitution, phenyl substitution and 4-SF_5 phenyl substitution were synthesised to confirm the importance of this substituent.

Indeed, the northeast phenyl ring was important for maintaining potency (Table 3.9). With no substituent in this position, complete inactivity was seen (Entry 1). Installing a bare phenyl ring led to a recovery of potency (Entry 2), but the best activity was seen with the 4-substituted phenyl rings. A 4-SF_5 substitution led to a large increase in potency (Entry 3). While the cLogP of this compound is quite high, it is noted that the same calculation performed by ChemDraw Professional 17.1 returns a cLogP of 3.7 showing the SF_5 group is not well tolerated in these calculations. By comparison, the model Series 4 compound **58** possessing a 4-$OCHF_2$ substituent still showed the best activity. These results validate the use of a 4-substituted phenyl rings in the northeast position, in particular the 4-$OCHF_2$ core.

Table 3.9: IC_{50} potency values of the northeast substituted compounds against *P. falciparum*. The northeast phenyl ring is important for potency, with 4-substitution being ideal.

Entry	Compound	cLogP	IC_{50} (μM)
Reference	**58**	3.2	0.25
1	**122**	1.5	>10
2	**125**	3.2	2.15
3	**128**	8.1	0.48

3.6.2 Northwest Methoxyphenyl Substitution

Another suggestion by the OSM community was for the evaluation of a Series 4 compound with an electron donating group on the northwest phenyl ring. Such a compound was surprisingly absent from the SAR. A methoxy substituted ring would be ideal for this purpose, and luckily the 3- and 4-substituted methoxyphenethyl alcohols were readily available for coupling. The nucleophilic substitution of these alcohols with the TP core **44** gave the respective final compounds **129** and **130** in moderate yields (Figure 3.29).

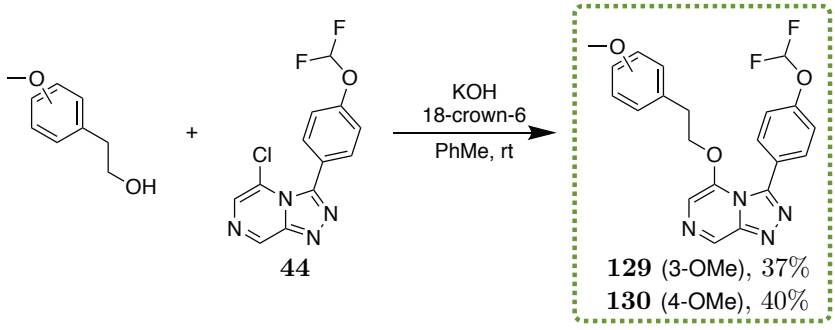

Figure 3.29: Synthesis of the methoxy substituted compounds. These two compounds were easily synthesised by coupling of the commercially available alcohols with the TP core **44**.

Interestingly, the 3-OMe isomer **129** was highly potent, even more than the bare phenyl compound **58**. The 4-OMe isomer **130** was less potent but still showed good activity. While both compounds

were potent, methoxyphenyl moieties are not always the best functionality to have in a drug as the methoxy group is prone to metabolism by *O*-demethylation leading to undesired clearance of the drug.[203]

Table 3.10: IC_{50} potency values of the northwest methoxyphenyl compounds against *P. falciparum*. Both isomers were potent but were not pursued further due to the metabolic lability of the methoxyphenyl moiety.

Entry	Compound	cLogP	IC_{50} (μM)
Reference	**58**	3.2	0.25
1	**129**	3.1	0.14
2	**130**	3.1	0.93

3.6.3 Northwest Hydroxy Transposition

With the highly potent benzylic hydroxy compound **16** synthesised as part of the Frontrunners, it was thought possible that transposition of this benzylic carbon and hydroxy group onto the phenyl ring might be beneficial for activity and solubility. Such a transposition would require a symmetric diol nucleophile, which could potentially be coupled with the TP core without the protection of one alcohol group. Should the coupling of this unprotected diol proceed smoothly to give desired product (and not the doubly coupled product), future coupling reactions involving diol nucleophiles may be conducted without the requirement of alcohol protection.

The required diol could be synthesised following literature procedures through the reduction of terephthaldehyde with $NaBH_4$ giving 1,4-phenylenedimethanol **131** in 33% yield (Figure 3.30).[204] Direct coupling of this unprotected diol to the TP core **44** using coupling conditions slightly different from the standard conditions led to the desired product in 15% yield after two successive purifications. Even though a low yield was seen with this reaction, the coupling of the unprotected diol did proceed and no doubly coupled product was observed.

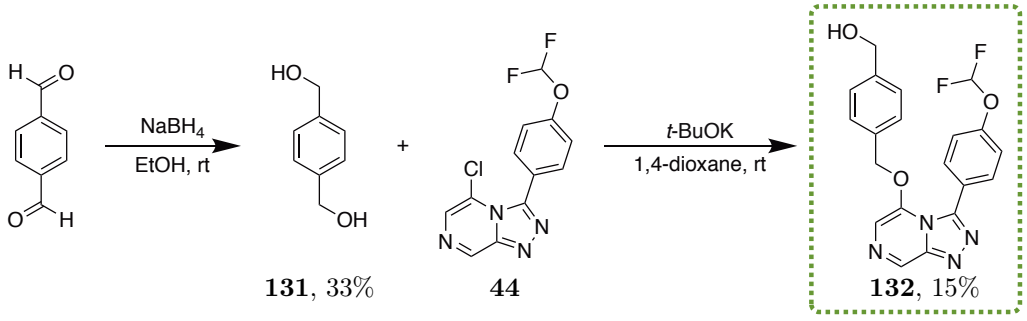

Figure 3.30: Synthesis of the transposed hydroxy compound. The coupling of the unprotected diol proceeded to give the desired product, albeit in low yield.

Unfortunately, the transposition of the alcohol to the phenyl ring led to a complete loss in potency when compared to the untransposed compound **16** (Figure 3.31). Additionally, this transposition was seen to negatively impact the potency when compared to the corresponding bare phenyl compound **57**.

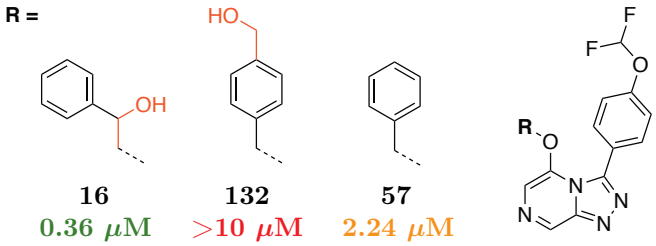

Figure 3.31: The transposed alcohol compound had an IC_{50} of >10 μM. There was a complete loss in potency when compared to the untransposed compound.

3.7 Concluding Remarks

A wide range of novel compounds was successfully synthesised and evaluated for their *in vitro* potencies, contributing to the larger set of existing SAR data for the Series 4 triazolopyrazines (Figure 3.32).

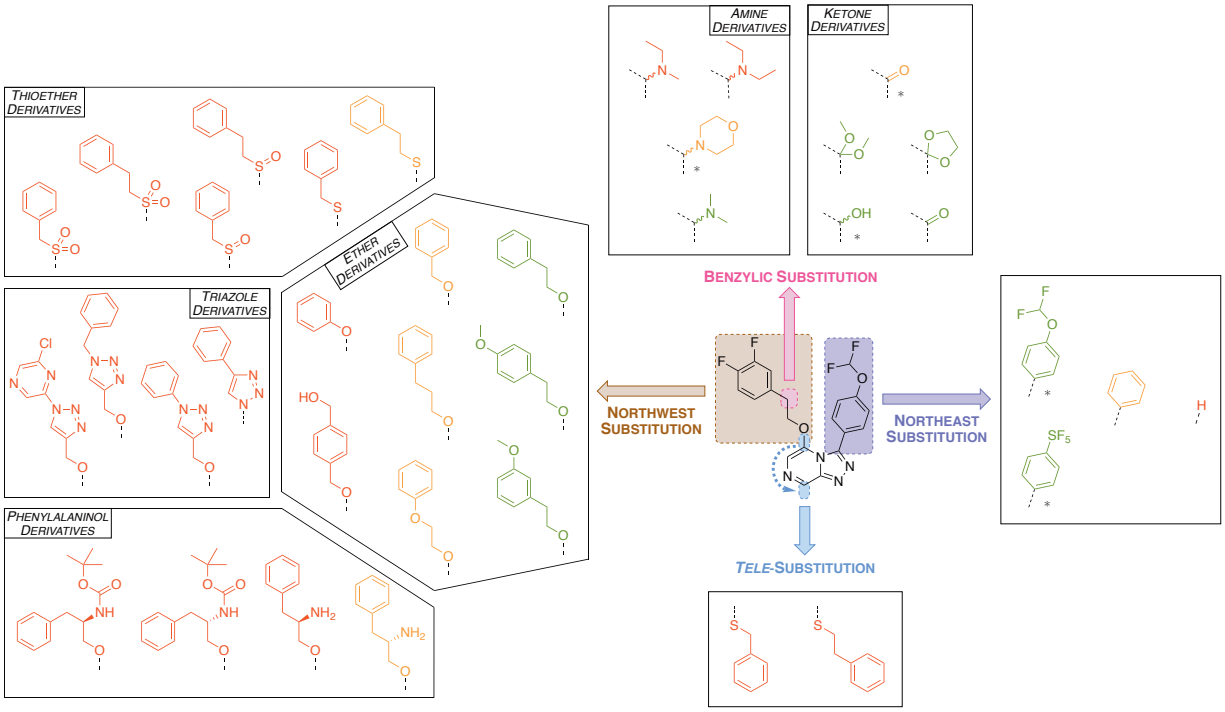

Figure 3.32: Summary of the SAR for compounds in this chapter. Colour coding: <1.0 μM = green, 1.0–2.5 μM = orange, >2.5 μM = red. *Compound has northwest phenyl ring instead.

While the inherited dataset for this series suggested an ether chain length of two methylene groups was optimal between the heterocyclic core and the northwest pendant phenyl ring, the specific

compounds to prove this relationship were absent from the dataset. This was confirmed through the synthesis of the relevant compounds, showing that this separation of the phenyl from the core was indeed important to maintain potency. The importance of the 4-substituted northeast phenyl ring was confirmed in a similar manner.

A series of thioether-based compounds was made, revealing a misassignment in a previously synthesised analogue. As a result, two substitution products were isolated and characterised, thereby correcting the original data but also revealing the possibility of unexpected side products in the standard nucleophilic displacement reaction.

Attempts to substitute or incorporate a triazole moiety in the northwest side chain led to a complete loss in potency. While triazoles have been know to be effective mimics for amide groups, in our case this was not seen to help. It is possible the reduced freedom of movement of the side chain (in the case of **78**) and increased bulkiness (in the case of **83** and **84**) led to this inactivity.

A series of compounds with benzylic ketone, acetal and amine substitutions were made through various routes, revealing a number of potent Series 4 compounds. The benzylic ketone compounds (including the acetals) were relatively well tolerated, with the majority of potencies below 1 μM. The longer alkyl amines were poorly tolerated, the best being the benzylic dimethylamine.

A select number of compounds from this chapter were further evaluated for mechanism of action, and will be discussed in Chapter 5. The following chapter will cover the synthesis and evaluation of further novel compounds based specifically around the replacement of the northwest pendant phenyl and northeast phenyl rings with non-aromatic moieties.

4. Series 4 Phenyl Bioisosteres

This chapter covers further investigations into the SAR of Series 4, focusing on the design and synthesis of a range of compounds based around replacements of the pendant phenyl rings. The *in vitro* biological evaluation of these compounds against *P. falciparum* is discussed at the end of each section. Select compounds were used to generate late-stage biofunctionalised products using liver microsomes, which were also evaluated for *in vitro* activity.

4.1 Background

Phenyl rings are ubiquitous in medicinal chemistry, appearing in all manner of biologically relevant molecules. Yet phenyl groups may not always be the optimal motif to use. They are relatively non-polar and are involved in π-π stacking interactions that can contribute to low aqueous solubility. Luckily, in medicinal chemistry, there are several well known strategies for addressing these concerns.[205,206] Perhaps the most common is to append charged or polar groups such as alcohol or amine moieties. Such changes will typically reduce the hydrophobicity of the compound, but may often dramatically impact the potency of the compound and therefore may not always be desired. Similar effects may be seen by using heterocyclic ring replacements (e.g. pyridyl in place of phenyl), but this again may alter the potency of the desired compound.[207] Alternatively, modifications can be made to alter the crystalline stability of the compound by either removing aromaticity or changing the geometry or topology of the compound. For example, replacement of a phenyl ring by an aliphatic group (linear, cyclic or caged) will eliminate π-π stacking interactions and may help improve aqueous solubility. These latter replacements have the added advantage of introducing further options for chemical derivatisation that may not be accessible with a phenyl ring. Again, however, there is the caveat that these changes can heavily influence the binding interactions between a drug and its target. Some of these strategies for improving solubility have already been applied to the Series 4 compounds, mainly focused around the introduction of alcohol and amine functional groups. One area that has not been extensively investigated is reducing the extent of the aromaticity of the series. Replacing the phenyl rings with moieties that are not aromatic will result in decreased aromaticity and π-π stacking, which should translate to improved solubility and, it is hoped, better metabolic clearance properties. Before incorporating these changes, the types of suitable phenyl ring replacements (known commonly as phenyl bioisosteres) must be considered.

The concept of an isostere was originally formulated by Irving Langmuir in 1919, stating that if compounds having the same number of atoms have also the same total number of electrons, the electrons may arrange themselves in the same manner.[208] Harris Friedman then introduced the term "bioisostere" in 1950, which redefined the original term as "compounds or groups that possess near-equal molecular shapes and volumes, approximately the same distribution of electrons, and which exhibit similar physical properties".[209] By making a bioisosteric change in a compound, a number of properties may be altered including toxicity, solubility, metabolic stability or potency. As such, these changes can constitute an extremely useful strategy in medicinal chemistry programs for optimising certain physical and biological properties in a compound.[210–214]

Bioisosteres may be grouped into two categories: classical and non-classical (Figure 4.1). A classical bioisostere follows the previously mentioned definition in which the change made results in a structurally similar compound. Common examples include the exchange of hydrogen with deuterium, carbon with silicon or phenyl with pyridine. Perhaps the most useful of these for medicinal chemists is the exchange of hydrogen with fluorine. This substitution is most effective for blocking metabolically labile sites due the the higher strength of the C–F bond versus the C–H bond. It is often easy to purchase the required fluorinated starting materials and the synthetic chemistry remains largely unchanged. Perhaps as a result, it is estimated that ∼20–25% of drugs on the market contain a fluorine atom.[215] The second category, non-classical bioisosteres, differ in that the resulting compounds may contain a group that is structurally distinct from the original compound (typically containing different atoms or more substantial steric/electronic changes). In many cases, the use of a non-classical bioisostere results from hypotheses derived from target binding studies. Examples include the exchange of a halogen with a CF_3/CN group or a carboxylic acid with a tetrazole.

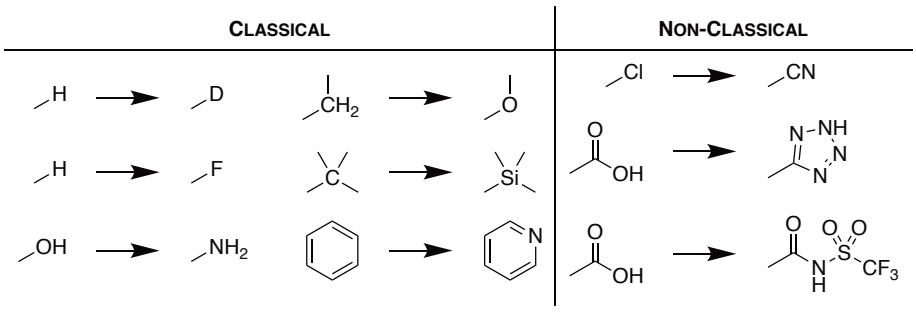

Figure 4.1: Examples of classical and non-classical bioisosteric changes. All are commonly used strategies in medicinal chemistry for optimising certain biological properties.

While classical phenyl ring bioisosteres focus on the introduction of heteroatoms, this change does not significantly affect the overall aromaticity of the compound. The focus in the present work therefore was on the use of non-classical bioisosteres, with motifs ranging from simple changes

involving saturated heterocycles, to less common changes involving cubanes and carboranes. In a typical planning context, performing cLogP calculations on a molecule is a good way to approximate the potential solubility of a compound. As will be seen, performing these calculations on the phenyl bioisosteric motifs discussed below resulted in inconsistencies across different software platforms, limiting the usefulness of this calculated parameter.

4.2 Simple Non-Planar Derivatives

Saturated heterocyclic rings can be found in a large number of the small molecule drugs approved by the FDA. The most common of these systems are nitrogen containing heterocycles such as piperidine and piperazine.[216,217] With so many successful drugs already exploiting these heterocycles, it was felt appropriate to incorporate them into the Series 4 compounds as replacements for either the northwest or northeast phenyl rings as a deplanarisation strategy (Figure 4.2).

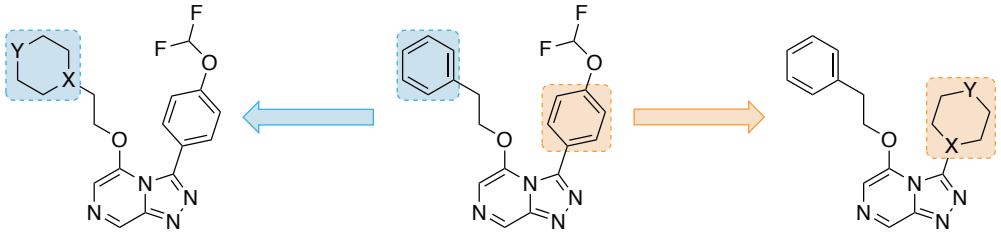

58

IC_{50} = 0.25 μM

Figure 4.2: Replacement of the northwest or northeast aromatic rings with a saturated heterocycle (X,Y = N/C/O). This should improve the aqueous solubility through increased H-bonding capabilities and deplanarisation.

4.2.1 Synthesis of the Northwest Saturated Heterocycle Series 4 Bioisosteres

A variety of alcohols (2-cyclopropylethanol, 2-[2-oxa-6-azaspiro[3.3]heptan-6-yl]ethan-1-ol, 1-(2-hydroxyethyl)pyrrolidine, 1-(2-hydroxyethyl)piperidine and 4-(2-hydroxyethyl)morpholine) were proposed as coupling partners with TP core **44** and gave the corresponding final compounds **133**–**138** in moderate yields (Figure 4.3). A majority of the required saturated heterocycle alcohol precursors were readily available with no further modification of the material required. In the case of the oxetane compound **134**, the required nucleophile was obtained from the lithium salt of 2-(oxetan-3-yl)acetic acid. This was first converted to the free acid by treatment with 32% HCl and extraction with EtOAc, then reduced to give the alcohol nucleophile which was finally coupled to **44** to give the desired Series 4 compound.

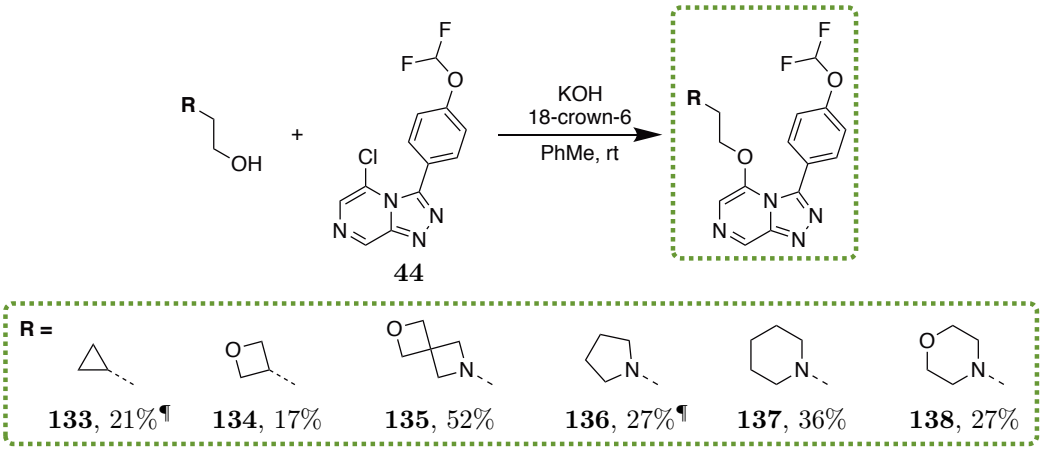

Figure 4.3: Deplanarisation of the northwest phenyl ring using simple saturated heterocyclic alcohols. Varying the alcohol nucleophile for nucleophilic displacement with TP core **44** gave the desired compounds in moderate yields. ¶Alternative reaction conditions were used: *t*-BuOK (1.2 equiv.), 1,4-dioxane (55 mM), rt, overnight.

The synthesis of a piperazine containing analogue (**141**) was attempted, however, while direct coupling of 1-(2-hydroxyethyl)piperazine led to consumption of the TP core **44** as indicated by TLC, no desired product was identified or isolated (Figure 4.4). It is possible that the presence of the free amine resulted in unwanted side-reactions which consumed the TP core. To overcome this, the free amine was protected using Boc_2O to give the *N*-Boc protected compound **139** in moderate yield. This was coupled to the TP core **44** to give **140** which, following acidic deprotection of the amine, gave the desired compound **141** in excellent yield.

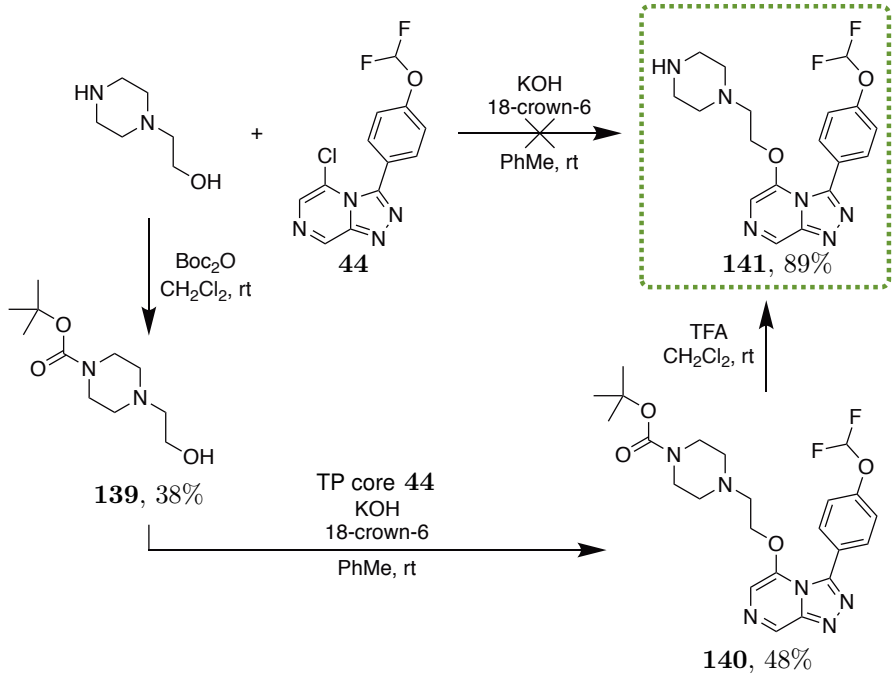

Figure 4.4: Synthesis of the northwest piperazine analogue. Direct coupling with the piperazine alcohol was unsuccessful. When the free amine was *N*-Boc protected before coupling the desired product could be formed.

4.2.2 Synthesis of "the Nemesis"

The Series 4 compound named "the Nemesis" was originally proposed as a means to investigate deplanarisation of the northeast phenyl ring.[188] Dr. Alice Motion first attempted its synthesis, however difficulties were encountered with purifications at multiple steps during the synthesis resulting in the compound not being isolated (and giving rise to the compound's nickname). A year later, a class led by Robert Broadrup at Haverford College in Pennsylvania joined the OSM project and were tasked with synthesising Series 4 compounds, one of which was the Nemesis.[218] While it appeared from mass spectrometry analysis that the students were able to synthesise the Nemesis, there was not a sufficient amount of the product for further analysis and, due to time constraints, no more attempts were made to obtain the compound.[219,220]

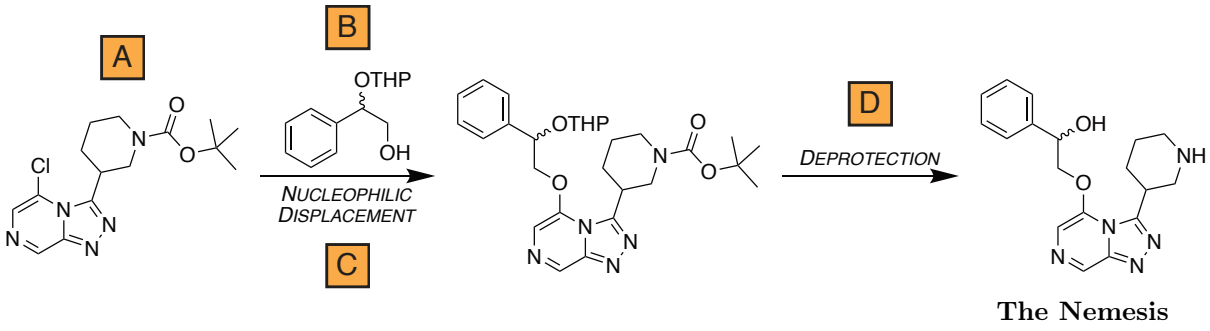

Figure 4.5: Key steps in the synthesis of the Nemesis. (A) Synthesis of the Nemesis TP core. (B) Synthesis of the alcohol side chain. (C) Nucleophilic displacement. (D) THP/Boc deprotection.

Ultimately, the Nemesis was synthesised as part of the phenyl bioisosteres investigation (Figure 4.6). Condensation reaction with 1-Boc-3-piperidinecarboxaldehyde and hydrazine **2** gave the hydrazone **142** in 66% yield. Cyclisation led to TP core **143**, on which nucleophilic displacement was performed with alcohol **103** (synthesised in Chapter 3) to give the protected Nemesis compound **144** in 32% yield. Rather than performing the deprotection step using THP deprotection conditions (HCl in dioxane), since this reaction had provided mixtures with analogous compounds, it was thought that Boc deprotection conditions (TFA in CH_2Cl_2) would be cleaner and suitable to deprotect both groups at the same time. When the deprotection was performed in this latter way the Nemesis **145** was obtained in 66% yield. Having some of the Nemesis TP core **143** remaining, it was also coupled with 2-(3,4-difluorophenyl)ethanol to give the protected compound **146**. Deprotection afforded the difluorophenyl derivative of the Nemesis (**147**) in excellent yield.

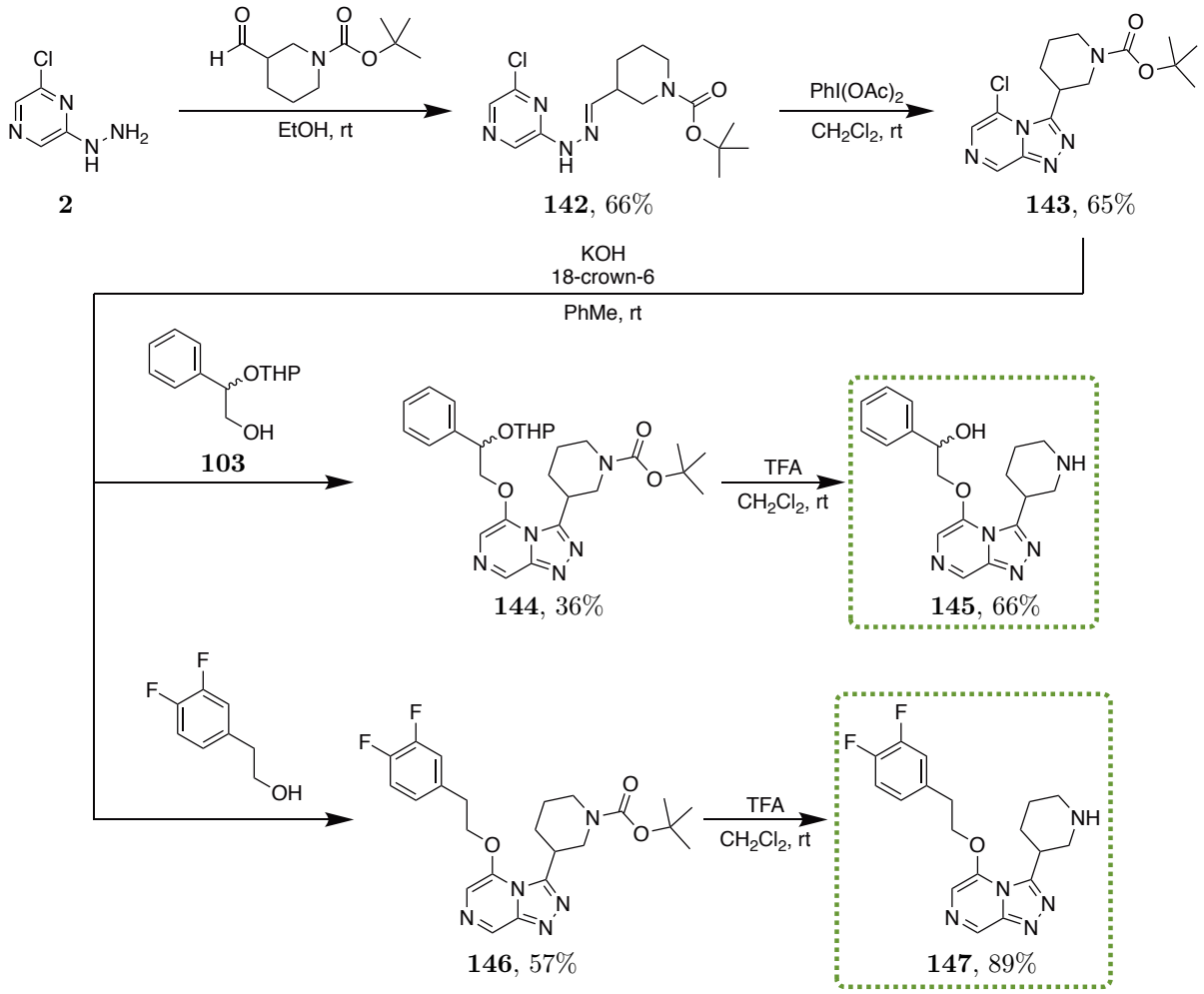

Figure 4.6: Synthesis of the Nemesis. Synthesis of the *N*-Boc protected TP core followed by coupling with the alcohol nucleophile synthesised for the benzylic ketone compound in Chapter 3 led to the Nemesis. A difluorophenyl derivative was also synthesised with leftover TP core.

4.2.3 Synthesis of the Northeast Saturated Heterocycle Series 4 Bioisosteres

The same process as above was used for the incorporation of the remaining saturated heterocycles as a replacement of the northeast phenyl ring (Figure 4.7). The following compounds were intended for synthesis by the undergraduate Special Studies Program (SSP) lab course, however due to complications with their synthesised products (discussed in Chapter 7), the compounds were synthesised here separately. Condensation reactions were performed with hydrazine **2** and the commercially available aldehydes with oxygen heterocycles (tetrahydrofuran and tetrahydropyran) and *N*-Boc protected nitrogen heterocycles (pyrrolidine and piperidine) giving the corresponding hydrazones. These were then cyclised to give the respective TP cores, which after coupling with 2-phenylethanol gave the final compounds **148**, **149**, **150** and **151** in good yields. Compounds **150** and **151** were deprotected under acidic conditions to give the free amine products **152** and **153** respectively.

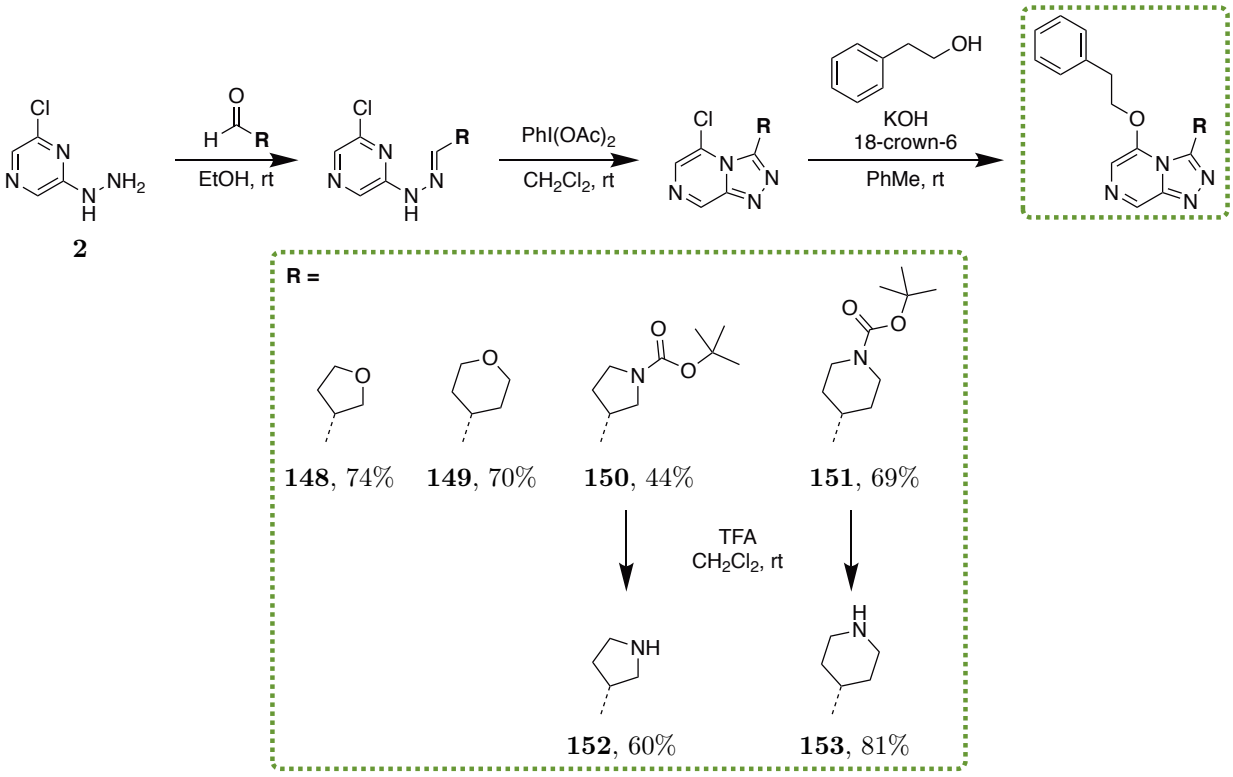

Figure 4.7: Deplanarisation of the northeast phenyl ring using simple saturated heterocyclic aldehydes. Varying the aldehyde in the initial condensation step, followed by cyclisation and nucleophilic displacement with 2-phenylethanol gave the desired compounds.

4.2.4 Biological Evaluation

By comparison with the northwest phenyl compound **58** (IC_{50} = 0.25 μM), it could be seen that replacement of this phenyl ring with saturated heterocycles led to a significant loss in activity (Table 4.1). The only notable compound was the cyclopropyl analogue **133** which was found to be very weakly active (Entry 1).

Table 4.1: IC_{50} potency values of northwest saturated heterocycle analogues against *P. falciparum*. All northwest replacements were found to result in inactive compounds.

Entry	Compound	cLogP	IC_{50} (μM)
Reference	**58**	3.2	0.25
1	**133**	2.5	3.03
2	**134**	1.7	>10
3	**135**	0.9	>10
4	**136**	1.8	>10
5	**137**	2.1	>10
6	**138**	1.0	>10
7	**140**	2.5	>10
8	**141**	0.8	>10

Similarly, all northeast saturated heterocycle analogues were found to be inactive *in vitro* (Table 4.2).

Table 4.2: IC_{50} potency values of northeast saturated heterocycle analogues against *P. falciparum*. All northeast replacements were found to result in inactive compounds.

Entry	Compound	cLogP	IC_{50} (μM)
Reference	**58**	3.2	0.25
1	**148**	1.9	>25
2	**149**	2.2	>25
3	**150**	3.4	>25
4	**151**	3.7	14.5
5	**152**	1.7	>25
6	**153**	2.1	>25

The inactivity seen with all saturated heterocyclic replacements could suggest that the rigidity of the phenyl ring is important to maintaining biological activity. With this in mind, a more closely related phenyl bioisostere, cubane, was investigated. Such a structure would keep the desired deplanarisation but reintroduce a degree of rigidity to the side-chain that would, it was hoped, lead to a more active compound.

4.3 Cubanes

First synthesised in 1964 by Eaton and Cole,[221] cubane is a synthetic hydrocarbon compound belonging to the class of prismanes. The original synthesis began with 2-cyclopentenone and required 12 steps to obtain the unfunctionalised cubane framework, in low yield (A, Figure 4.8). Six years later, Chapman and co-workers improved upon this with a lower yielding, but much shorter, 5 step synthesis providing the more versatile, dimethyl 1,4-cubanedicarboxylate (B).[222] Most recently in 2013, Tsanaktsidis and co-workers developed a multigram synthesis, yielding the dimethyl dicarboxylate in *ca.* 20% overall yield over 8 steps (C).[223] Nowadays, although expensive, the methyl dicarboxylate is commercially available from many suppliers. The pre-installed ester functionality allows for a large range of chemical transformations, providing cubane building blocks that can be incorporated into compounds used in areas such as medicinal and polymer chemistry.[224,225]

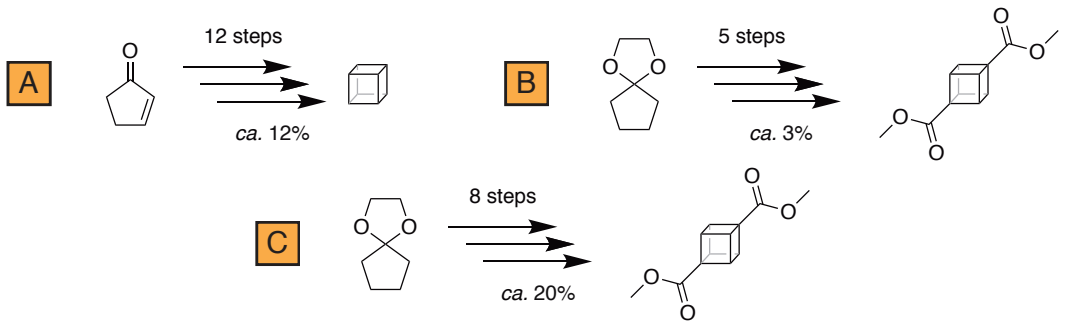

Figure 4.8: The synthesis of cubane and its dimethyl dicarboxylate derivative have been improved upon over the years resulting in a shorter and higher yielding synthesis. (A) Eaton and Cole; *1964*. (B) Chapman and co-workers; *1970*. (C) Tsanaktsidis and co-workers; *2013*.

The size and volume of cubane is said to mimic the size and rotation volume of a phenyl ring (102 Å^3), and therefore may act as a suitable phenyl bioisostere.[226] Accordingly, several biologically active molecules were studied for their ability to tolerate a cubane replacement, examining changes in activity, solubility, metabolism, stability and tractability.[227] Five compounds were evaluated including those with chemotherapeutic (Vorinostat), anaesthetic (Benzocaine) and neotropic (Leteprinim) applications (Figure 4.9). It was found that four of the five showed equivalent or improved potency when the phenyl ring was replaced with a cubane. In these four cases, the slight increase in measured logP with the cubane replacements (largest difference of ∼0.5) did not have a significant impact on compound solubility. However, in the one case that led to decreased potency, a much larger increase in measured logP (∼1.4) was seen for the cubane analogues that translated to a large reduction in solubility. This was attributed to the unsubstituted nature of the cubane in the relevant analogues (of benzyl benzoate).

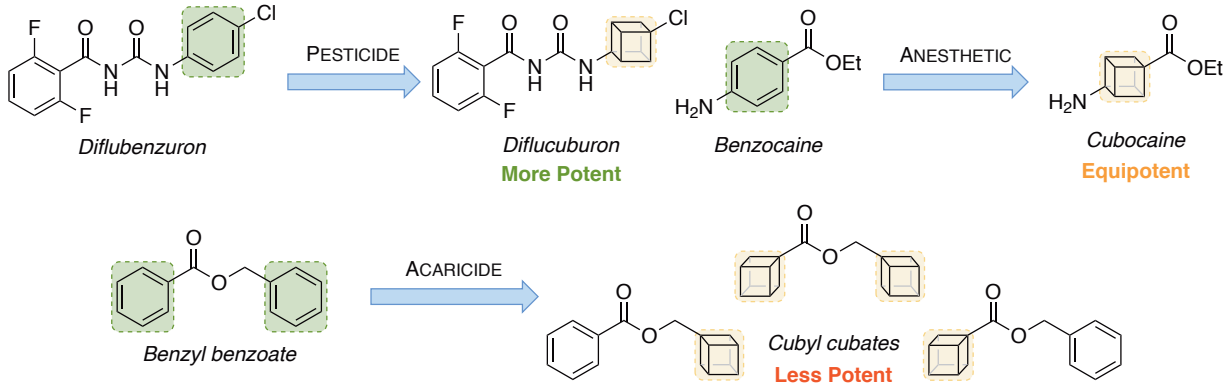

Figure 4.9: Validation of cubane as a bioisostere for phenyl. Bioisosteric replacement of phenyl rings in known bioactive compounds with cubanes generally gave similar or higher potencies when compared to their phenyl counterparts.

4.3.1 Synthesis of the Northwest Cubane Series 4 Bioisosteres

With solubility and metabolic stability being known issues throughout Series 4, based on the report above, it was thought that replacing the phenyl rings in the Series 4 compounds with cubane could lead to improvements in these areas through deplanarisation and dearomatisation.[228] The Williams group at the University of Queensland generously synthesised and sent samples of cubane building blocks (2-cubylpropan-1-ol, 3-cubylethan-1-ol and 4-iodocubane-1-carboxylic acid) for incorporation as the northwest and northeast substituents (Figure 4.10).

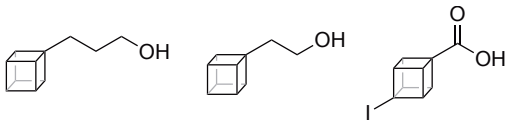

Figure 4.10: Cubanes donated by Professor Craig Williams. The cubane building blocks 2-cubylpropan-1-ol, 3-cubylethan-1-ol and 4-iodocubane-1-carboxylic acid were kindly provided by the Williams group for incorporation in new Series 4 compounds.

Accordingly, both cubane alcohols were readily reacted with TP core **44** under the standard nucleophilic displacement conditions to give the final compounds **154** and **155** in moderate yields (Figure 4.11).

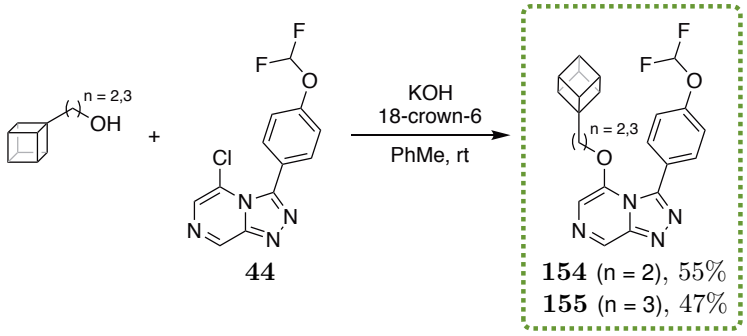

Figure 4.11: Synthesis of the northwest cubane analogues. Nucleophilic displacement using the two cubane alcohols of different chain lengths gave the corresponding final products **154** and **155**.

4.3.2 Synthesis of the Northeast Cubane Series 4 Bioisosteres

In order to incorporate the cubane into the northeast position of a Series 4 compound, the provided carboxylic acid had to first be converted into an aldehyde. The Priefer group previously reported the synthesis of various iodocubane derivatives, detailing the desired conversion of iodocubane carboxylic acid into iodocubane aldehyde.[229] By following these methods, the carboxylic acid was reduced to the corresponding primary alcohol **156** using borane dimethylsulfide complex. Subsequent Swern oxidation afforded the aldehyde **157** in good yield (Figure 4.12).

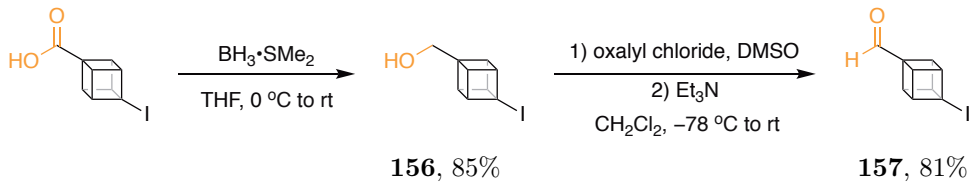

Figure 4.12: Conversion of the provided cubane carboxylic acid to the desired cubane aldehyde. Following literature methods, the carboxylic acid was first reduced to the primary alcohol, then oxidised to the aldehyde to give the desired precursor for the following condensation reaction.

The aldehyde **157** was then used to obtain the ether- and amide-linked analogues (Figure 4.13). The ether-linked compound was obtained through condensation of **157** with hydrazine **2** giving the hydrazone **158**, which was then cyclised to **159** in good yield. Final nucleophilic displacement with 2-(3,4-difluorophenyl)ethan-1-ol led to the desired ether-linked compound **160** in moderate yield. The amide-linked compound was obtained using the amide intermediate for **21** synthesised by Dr. Alice Motion during the Frontrunners campaign (see Chapter 2). Condensation of **157** with this hydrazine gave intermediate **161**, which was cyclised to give the final amide-linked compound **162** in moderate yield.

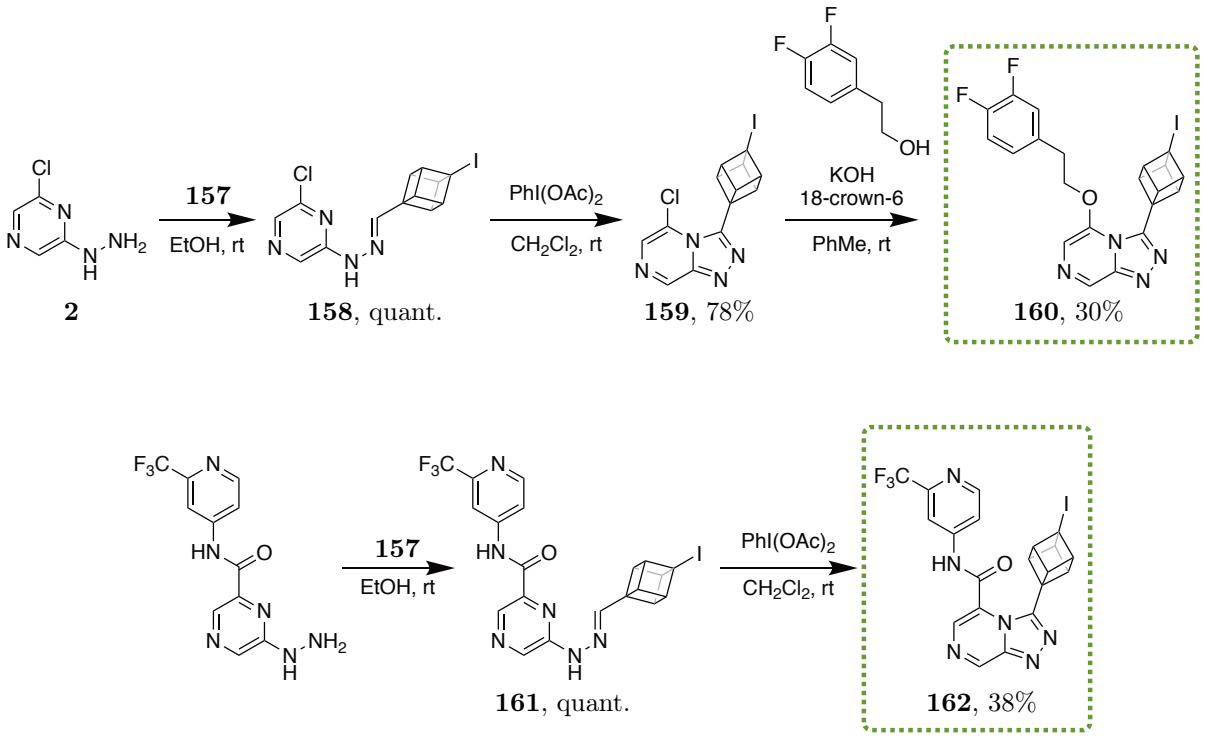

Figure 4.13: Routes used to synthesise the ether- and amide-linked northeast cubane compounds. Synthesis of the cubane aldehyde **157** allowed access to the ether- and amide-linked compounds.

The cubane precursor had been provided with a 4-iodo substituent, so before any valid comparisons could be made the corresponding northeast 4-iodo substituted phenyl analogue needed to be synthesised. It was decided that, of the two northeast cubane compounds synthesised above,

only the phenyl analogue of the ether-linked compound would be made (Figure 4.14). Following literature procedures, 4-bromobenzaldehyde was converted to 4-iodobenzaldehyde **163** under Finkelstein reaction conditions in 21% yield.[230] The aldehyde **163** was condensed with hydrazine **2** and cyclised to give the iodophenyl TP core **164** in 79% yield. Nucleophilic displacement with 2-(3,4-difluorophenyl)ethan-1-ol gave the final compound **165** in 61% yield.

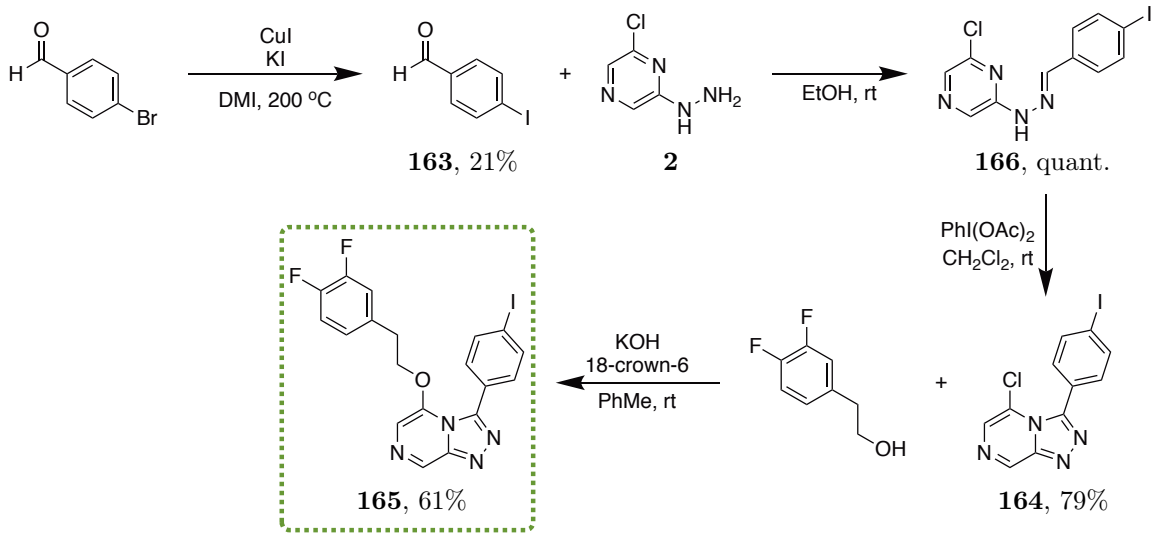

Figure 4.14: Synthesis of the northeast iodophenyl compound. Finkelstein reaction of 4-bromobenzaldehyde gave 4-iodobenzaldehyde **163** which was then condensed with hydrazine **2**, cyclised and coupled with 2-(3,4-difluorophenyl)ethan-1-ol to give the northeast 4-iodo substituted phenyl compound **165**.

4.3.3 Biological Evaluation

Evaluation of the Series 4 cubane bioisostere compounds revealed a number of interesting results (Table 4.3). Unlike the saturated hetereocycle replacements above (which were all inactive), replacement of the northwest phenyl ring with a cubane possessing a two (**154**) or three (**155**) methylene unit ether chain (Entries 1 and 2 respectively) led to only a slight decrease in activity when compared to the corresponding two (**58**) and three (**59**) methylene unit ether chain phenyl analogues. Conversely, replacement of the northeast phenyl ring with cubane resulted in a complete loss in activity in both the ether- (**160**) and amide-linked (**162**) compounds (Entries 3 and 4 respectively). By comparison, the related northeast 4-iodo substituted phenyl compound **165** was active (Entry 5).

Table 4.3: IC_{50} potency values of northeast and northwest cubane analogues against *P. falciparum*. Replacement of the northwest phenyl ring with cubane was well tolerated, while replacement of the northeast phenyl ring was not.

Entry	Compound	cLogP	IC_{50} (μM)
Reference	**58**	3.2	0.25
	59	3.6	1.32
1	**154**	2.5	0.37
2	**155**	3.0	2.00
3	**160**	3.0	>10
4	**162**	1.7	>10
5	**165**	3.6	0.35

These results, along with those for the saturated heterocycle replacements, demonstrated the low tolerability for deplanarisation of the northeast phenyl ring. Conversely, it appears that deplanarisation is tolerated in the northwest position provided that a degree of rigidity is maintained. The remaining bioisosteres explored were therefore other hydrocarbon cage replacements in the northwest position.

4.4 Adamantanes

Pre-dating the first synthesis of cubane by just over 20 years, adamantane was first made in 1941 by Vladimir Prelog in 5 steps starting from Meerwein's ester, giving a yield of *ca.* 0.16% (A, Figure 4.15).[231] The synthesis was refined a number of times, with each refinement reducing the step count and improving the yield,[232] ultimately resulting in a near-quantitative synthesis of adamantane by Olah and co-workers which utilised sonication and a superacid catalyst (C).[233] These days, adamantane is widely available from commercial suppliers costing as little as \$1/g, with many simple derivatives at similar prices.

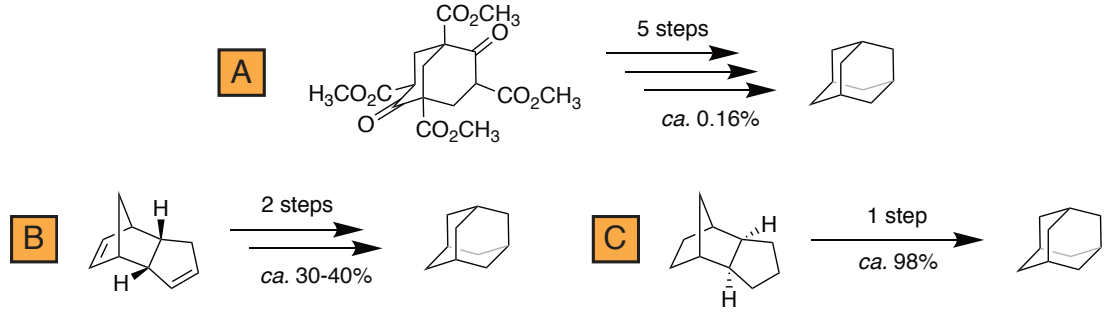

Figure 4.15: The synthesis of adamantane has been improved upon over the years resulting in a significantly shorter and near-quantitative synthesis. (A) Prelog and Seiwerth; *1941.* (B) von R. Schleyer; *1957.* (C) Olah and co-workers; *1986.*

Due to the unique structural, chemical and physical properties of adamantane, the incorporation of the motif into biologically relevant compounds may result in a number of changes to the absorption, distribution, metabolism or excretion (ADME) properties of the molecule. For example, in specific cases, the high hydrophobicity of the resulting compound may allow for favourable binding to an enzyme hydrophobic site allowing the compound to act as an inhibitor. Additionally, due to the high rigidity and cage size (6.36 Å H–H distance) of the adamantane scaffold, it may be used as a framework to organise the conformation of other functional groups.[234] As a result, adamantane has seen use in a wide range of biologically relevant molecules. For instance, originally developed by researchers at Pfizer as a phenyl based β_2-adrenoreceptor agonist,[235] the adamantyl-derived analogue was found to perform as well as the phenyl based lead compound (A, Figure 4.16).[236] In another case, several adamantane containing *N*-hydroxypropenamides were identified to have activity against histone deacetylase and be able to reverse the resistance of cisplatin in non-small cell lung cancer cell lines (B).[237] Importantly, the adamantyl derivative showed improved inhibitory activity and a lower resistance index (ratio of the IC_{50} in resistant cells to the IC_{50} in parental cells) when compared to belinostat and cisplatin. Adamantane has even found its way into antimalarials with OZ439 (described in Chapter 1) currently in development as a potential new medicine (C).[103]

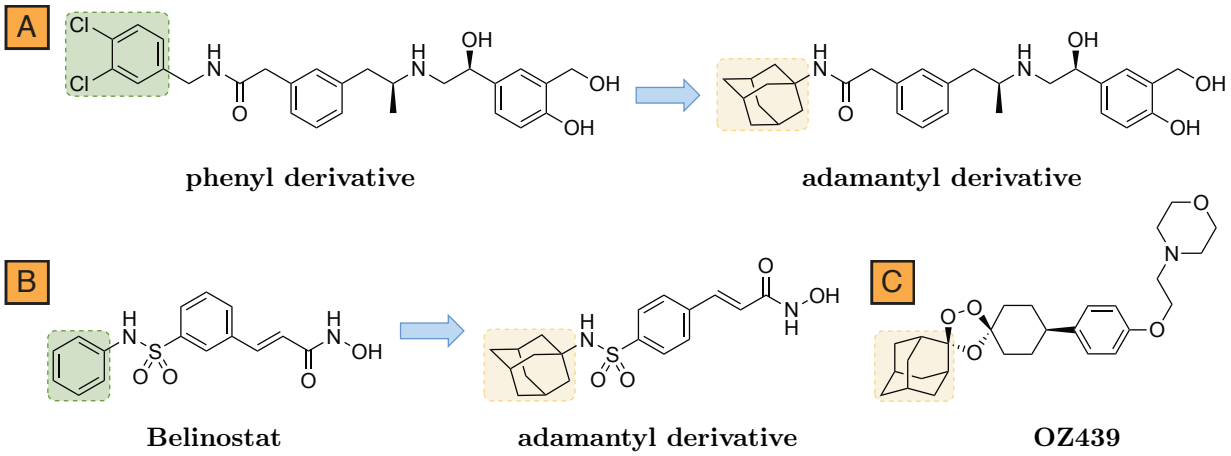

Figure 4.16: Examples of the use of adamantane as a phenyl bioisostere. Adamantane has also been incorporated into a potential antimalarial drug, OZ439.

4.4.1 Synthesis of the Northwest Adamantane Series 4 Bioisosteres

Due to the ease of accessibility of prefunctionalised adamantane precursors, incorporating it as a northwest phenyl bioisostere was a matter of finding the desired adamantane alcohol nucleophile. For this purpose, adamantane alcohols with one and two methylene unit chains were used for the nucleophilic displacement. Both alcohols were readily reacted with TP core **44** to give the corresponding adamantane bioisostere compounds **167** and **168** in good yields (Figure 4.17).

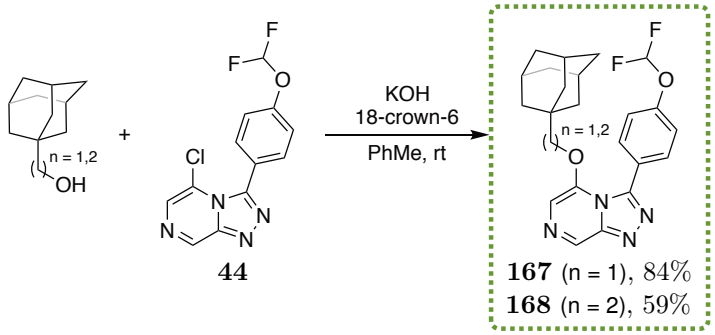

Figure 4.17: Synthesis of the Series 4 northwest adamantane compounds. Direct nucleophilic displacement with the commercially available adamantane alcohols with TP core **44** gave the desired final compounds.

4.4.2 Biological Evaluation

When compared to the phenyl compounds with one (**57**) and two (**58**) methylene unit ether chains, the adamantane analogues (**167** and **168**) were less potent but still showed weak activity (Entries 1 and 2) Table 4.4.

Table 4.4: IC_{50} potency values of northwest adamantane analogues against *P. falciparum*. The adamantane replacements were less well tolerated than the cubane derivatives.

Entry	Compound	cLogP	IC_{50} (μM)
Reference	**57**	2.7	2.24
	58	3.2	0.25
1	**167**	3.6	4.80
2	**168**	4.1	2.15

4.5 Bicyclo[1.1.1]pentanes

Bicyclo[1.1.1]pentane (BCP) is a bridged bicyclic hydrocarbon compound that was first reported in 1964 by Wiberg and co-workers as part of a ring closure reaction of 3-bromocyclobutane-1-methyl bromide with sodium.[238,239] The reaction mixture was purified by gas chromatography and gave three main products: a mixture of hydrocarbons, a saturated hydrocarbon and 1,4-pentadiene. The saturated hydrocarbon was identified to be BCP by ^{1}H NMR spectroscopy and mass spectrometry. A review published in 2000 details the work carried out in this field since this time.[240]

Nowadays, BCP is commonly synthesised as a prefunctionalised derivative from 1,1-dibromo-2,2-bis(chloromethyl)cyclopropane *via* [1.1.1]propellane (Figure 4.18). Due to the volatile nature of the propellane intermediate, it is often prepared fresh and kept in solution. Common BCP derivatives from this route include *bis*-acids ($\mathsf{R} = \mathsf{R}' = CO_2H$),[241] *bis*-esters ($\mathsf{R} = \mathsf{R}' = CO_2Me$) and half-acids ($\mathsf{R} = CO_2H$, $\mathsf{R}' = CO_2Me$).

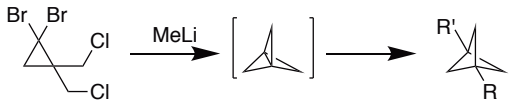

Figure 4.18: Common synthetic route to access functionalised bicyclo[1.1.1]pentanes. This proceeds *via* [1.1.1]propellane.

In a similar manner to cubane, the BCP motif has recently found use as a non-classical phenyl ring bioisostere.[242] While the size of the BCP motif is smaller than that of benzene and cubane (*vide supra*), its use as an effective phenyl bioisostere has been demonstrated in a number of cases. The phenyl ring in a γ-secretase inhibitor currently in development was replaced with the BCP motif resulting in a compound with not only equipotent enzyme inhibition, but also improved passive permeability, aqueous solubility and oral absorption characteristics (A, Figure 4.19).[243] In another case, a BCP replacement in a LpPLA2 inhibitor resulted in maintenance of potency while improving the compound's physicochemical properties (B).[244] BCP has also been used to synthesise an analogue of resveratrol that showed *in vivo* pharmacokinetic properties superior to the parent compound (C).[245] The improvements to the biological properties of the compounds in these examples suggested the use of the BCP motif may be advantageous for Series 4.

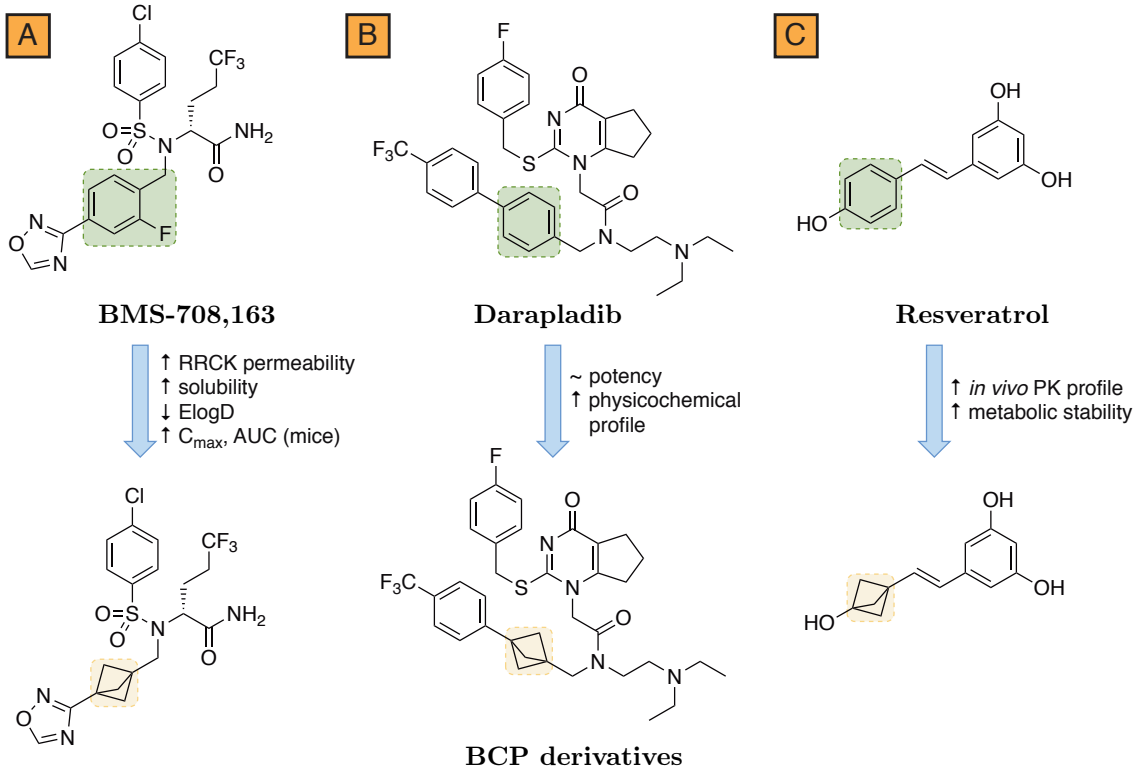

Figure 4.19: Examples of the use of BCP as a phenyl bioisostere. Replacements of phenyl rings with BCP have been shown to improve a range of biological properties while maintaining potency.

4.5.1 Synthesis of the Northwest BCP Series 4 Bioisosteres

Initial attempts at synthesising the Series 4 BCP bioisostere revolved around a report by Kokhan and co-workers that incorporated the BCP motif into a monofluorinated aliphatic label for ^{19}F NMR peptide studies (Figure 4.20).[246] A number of intermediates in this synthesis were attractive, the most notable being the *N*-Boc protected amino acid (orange box), which after reduction would yield the desired alcohol for coupling to the TP core. As it is not a necessity to have an enantiopure amine in the final building block, it could be envisioned that a Strecker reaction from the aldehyde intermediate would give the racemic amino acid in fewer steps.

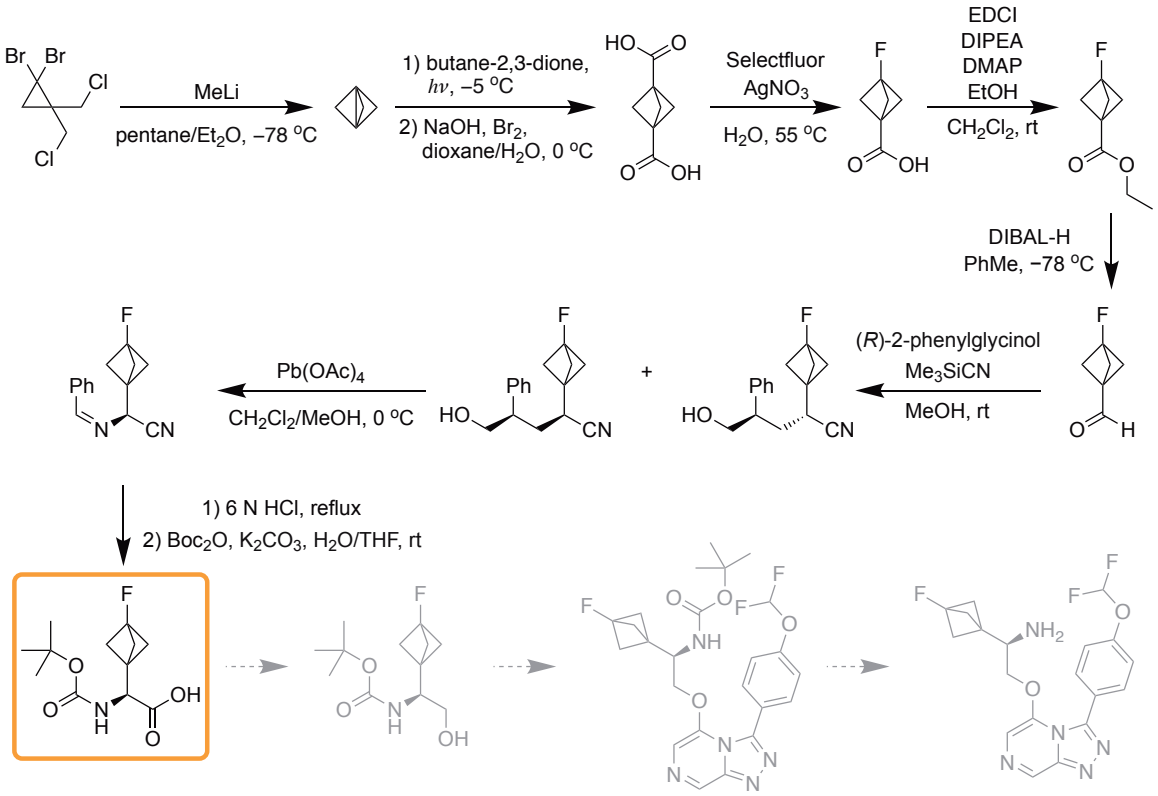

Figure 4.20: Reported route by Kokhan and co-workers for the synthesis of the BCP containing amino acid.

The first attempt to synthesise the [1.1.1]propellane intermediate followed a procedure outlined on *Organic Syntheses* in which MeLi was added dropwise to a solution of cyclopropane **169** in *n*-pentane at –78 °C (Figure 4.21). An ethereal solution of the propellane **170** was isolated by short-path vacuum distillation with the receiving flask cooled in liquid N_2.[247] Analysis of the ^{1}H NMR spectrum of the product showed only a trace amount of the desired propellane **170**. Slightly modified reaction conditions were tried, only using Et_2O and with higher reaction temperatures,[248] however no product could be identified by ^{1}H NMR spectroscopy. A final attempt followed procedures reported by Bunker and co-workers,[249] employing MeLi–LiBr as an alternative to MeLi. Encouragingly, this procedure resulted in isolation of the desired propellane

170 in 64% yield as judged by ^{1}H NMR spectroscopy. Apart from the residual Et_2O and pentane, the six equivalent protons from **170** exhibited a singlet at 2.04 ppm with the MeBr by-product appearing at 2.64 ppm. Rather than follow the same steps outlined above, it was found that the BCP aldehyde could be accessed in a more direct route *via* the BCP nitrile **171**.[250] This would again be a way of shortening the above synthesis to the desired alcohol nucleophile. The nitrile forming reaction was attempted on **170** but the ^{1}H NMR spectrum of the crude material was complicated by many signals and no desired product could be identified. While this reaction was unsuccessful, another opportunity emerged to access these BCP derivatives.

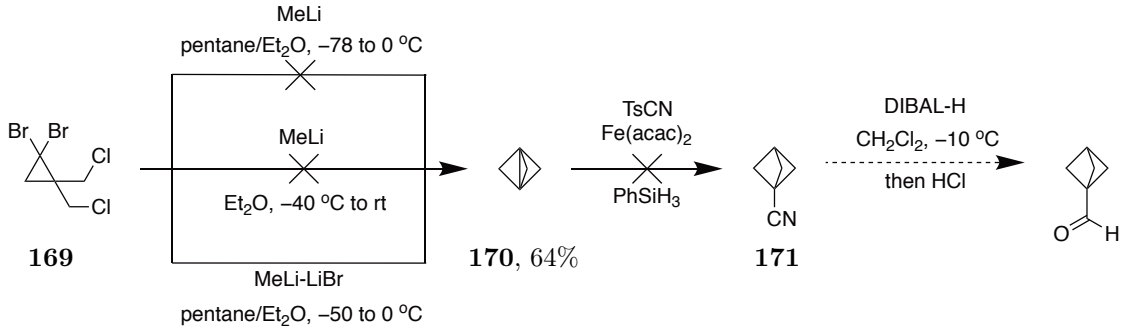

Figure 4.21: Attempted synthesis of the BCP aldehyde building block. The [1.1.1]propellane intermediate **170** was successfully synthesised but the following nitrile addition was unsuccessful.

Having seen the publication by Pfizer on γ-secretase inhibitors above, the corresponding author on the paper was contacted for information regarding BCP building blocks. Encouragingly, a number of BCP intermediates were suggested which could be obtained from Pfizer's Compound Transfer Program (CTP). This program allows researchers from around the world to request compounds from the Pfizer library for use in their own research free of charge. Ultimately, three of these were requested through the CTP for investigation within Series 4 and were kindly supplied (Figure 4.22).

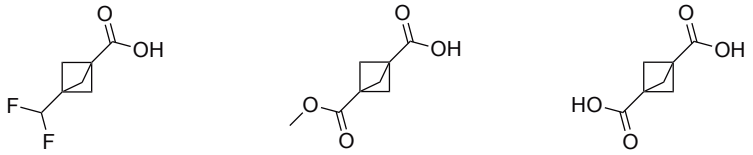

Figure 4.22: Three bicyclo[1.1.1]pentane building blocks obtained through Pfizer's Compound Transfer Program. 50 mg of the difluoromethyl-BCP and 1 g each of the half-acid and *bis*-acid were obtained through the CTP.

A number of transformations are known for the half-acid and *bis*-acid BCPs such as those shown in Figure 4.23. These include homologations, decarboxylations and reductions. From the perspective of desirable Series 4 derivatives, the most attractive of these building blocks would be the transformation of the half-acid **PF-06231780** to the mono-acid and the transformation of the

bis-acid **PF-06231780** to the fluoro-acid, since these would provide the most direct comparisons to existing Series 4 phenyl-containing analogues.

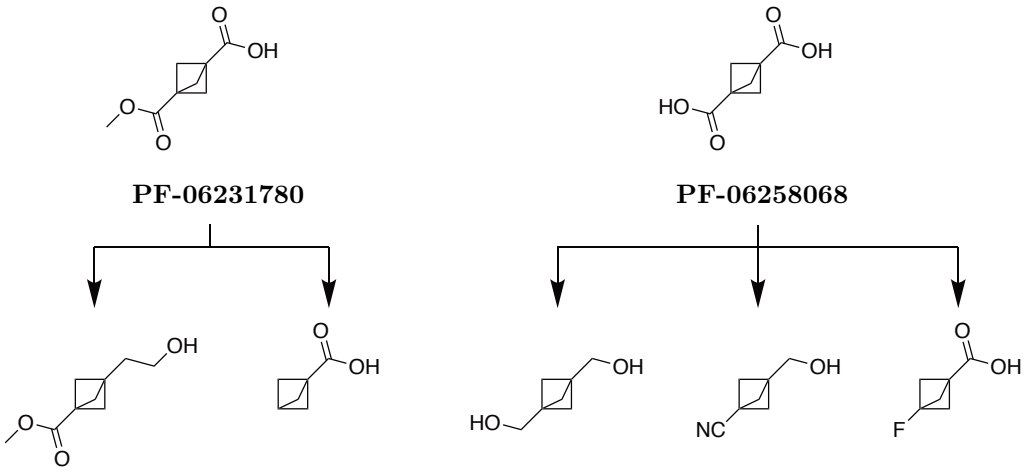

Figure 4.23: Some of the known transformations on half-acid and *bis*-acid BCPs. The acid containing products are the most useful for applications in Series 4.

Beginning with the half-acid **PF-06231780**, the carboxylic acid was converted to the acid chloride **172** in 94% yield using oxalyl chloride (Figure 4.24).[251] The original procedure reported by Dell and Tsanaktsidis for the Barton decarboxylation of **172** involved the use of benzene as a solvent.[252] As a safer alternative, toluene was used and the reaction successfully gave the mono-acid **173** in 27% yield. Unfortunately, due to time constraints and the small amount of material obtained from the reaction, no further transformations could be accomplished.

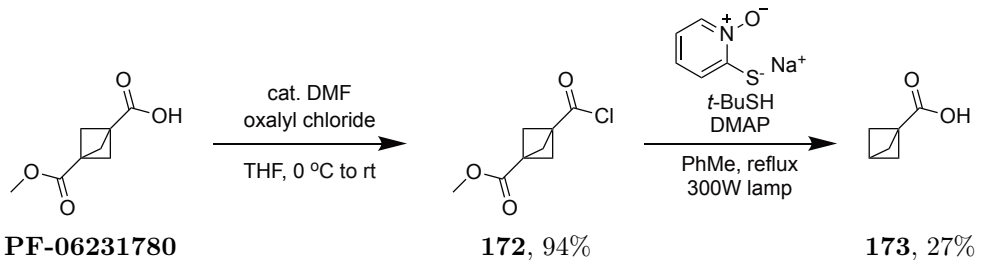

Figure 4.24: Conversion of the half-acid PF-06231780 to the mono-acid BCP. Synthesis of the acid chloride, followed by decarboxylation gave the desired mono-acid **173** in low yield. Not enough material was obtained for further transformations.

The following attempts to incorporate the BCP motif were made using the *bis*-acid **PF-06258068**. By following literature procedures for the silver-catalysed decarboxylative fluorination of the BCP *bis*-acid,[253] the fluoro-acid **174** was obtained in 41% yield (Figure 4.25). Homologation of the carboxylic acid was tried by following a patent procedure which utilised the Arndt-Eistert reaction.[254] The acid chloride was generated *in situ* from **174** using oxalyl chloride, then immediately reacted with TMS-diazomethane to form the diazoketone **175**. It was unclear by ^{1}H NMR spectroscopy whether the desired product had been successfully made, and due to the small scale of

these reactions, it was decided to carry this material through to the subsequent step. The following Wolff rearrangement was performed with catalytic silver benzoate to generate the ketene and in water to form the acid. It was, again, unclear whether or not the acid had been formed and ultimately, due to time constraints, these Series 4 BCP bioisostere compounds were no longer pursued.

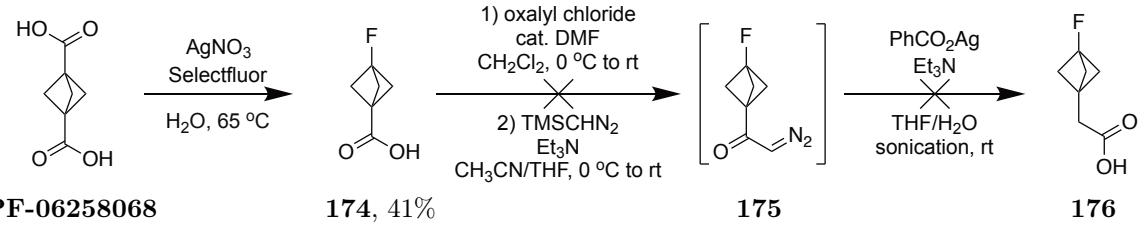

Figure 4.25: Conversion of the *bis*-acid PF-06258068 to the fluoro-acid BCP and attempted homologation. The fluoro-acid **174** was successfully made, however the homologation *via* an Arndt-Eistert reaction was ultimately unsuccessful.

Encouragingly, while there was only a small amount of the difluoromethyl-BCP (**PF-07040460**) that could be provided, the desired target compound was successfully synthesised from this material. The carboxylic acid was first reduced to the corresponding alcohol **177** in good yield (Figure 4.26). Nucleophilic displacement with this on the TP core **44** gave the desired final compound **178** in 27% yield. This BCP analogue would therefore act as a mimic for the corresponding northwest benzylic ether compound **57**.

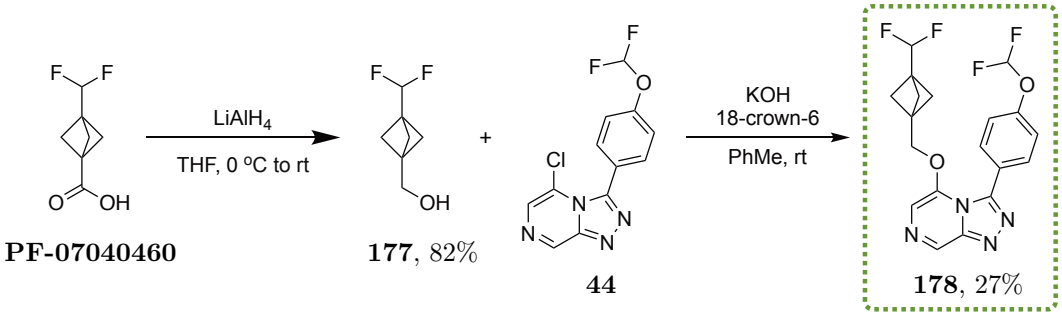

Figure 4.26: Synthesis of the difluoromethyl-BCP analogue. Reduction of the carboxylic acid, followed by nucleophilic displacement with TP core **44** gave the desired final compound.

Overall, the exploration of BCP as a phenyl bioisostere for Series 4 was met with a number of challenges. Many of the BCP building blocks did not contain UV active moieties or contained acidic groups. As a result, the monitoring and purification of these intermediates was less straightforward. Furthermore, a number of the reactions gave complex NMR spectra that provided limited information to determine the success of the reaction. Finally, the mass yields of these syntheses were relatively low. In some cases, rather that attempt to purify these complex mixtures, they were carried forward as crude materials. This ultimately led to even more complex mixtures than

desired.

4.5.2 Biological Evaluation

The successfully synthesised Series 4 BCP derivative **178** was evaluated for *in vitro* potency in comparison with the benzylic ether compound **57**. Both compounds exhibited similar potencies, however the BCP derivative was slightly less active (Entry 1) than the benzylic ether compound which had an IC_{50} of 2.24 μM (Table 4.5). It is notable that a majority of the cases which utilise the BCP motif as a phenyl bioisostere, such as the ones described in Figure 4.19, see improvements to the pharmacokinetic properties rather than to the *in vitro* activity (*vide infra*). Additionally, having demonstrated that compounds containing one methylene unit ether chains typically have lower potencies than those containing two methylene units, it could be envisioned that a BCP analogue with a two methylene unit ether chain would posses a more desirable potency. Unfortunately, due to time constraints and synthetic difficulties, such a compound was not obtained, yet it remains a clear target for further investigation.

Table 4.5: IC_{50} potency value of the northwest BCP analogue against *P. falciparum*. The potency observed was approximately equivalent to the phenyl-substituted comparator.

Entry	Compound	cLogP	IC_{50} (μM)
Reference	**57**	2.7	2.24
1	**178**	2.4	2.63

4.6 Other Hydrocarbon Cages

There are a large number of other hydrocarbon cages that are available for purchase or that can be accessed through synthesis. A selection of these were pursued in this study.

4.6.1 Synthesis of Northwest Miscellaneous Hydrocarbon Cage Series 4 Bioisosteres

A brief inspection of the Sigma-Aldrich catalogue for alcohol building blocks with hydrocarbon cages revealed three readily available compounds for potential nucleophilic displacement, namely: (1*R*)-(–)-nopol, (1*R*)-(–)-myrtenol and 5-norbornene-2-methanol (as a mixture of *endo* and *exo* isomers). Coupling of the nopol and norbornene alcohols with the TP core **44** proceeded smoothly to give the corresponding compounds **179** and **180** in good yields (Figure 4.27). In the case of the myrtenol alcohol, the desired product **181** was not obtained under either the standard or alternative reaction conditions, with the ^{1}H NMR spectrum of the reaction mixtures indicating only starting materials.

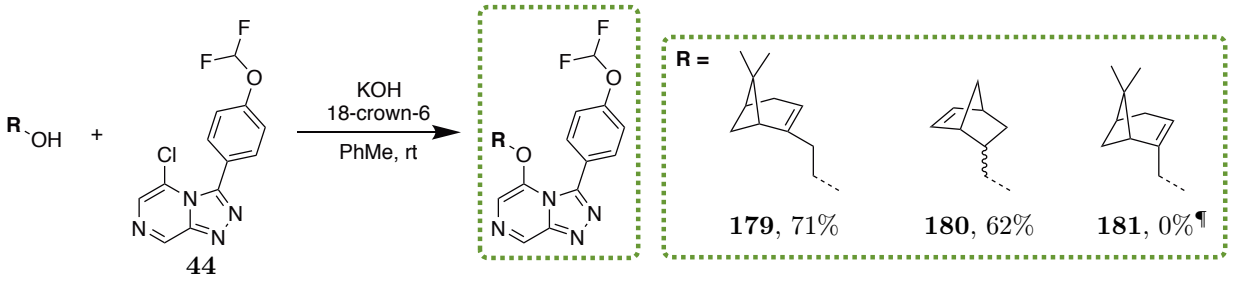

Figure 4.27: Incorporation of miscellaneous hydrocarbon cages. Nucleophilic displacement proceeded with all but the myrtenol alcohol. ¶Additional conditions: *t*-BuOK (1.2 equiv.), 1,4-dioxane, rt.

Coupling of the myrtenol alcohol to the hydrazine (**2**) and hydrazone (**55**) precursors of the TP core **44** was tried, however these were also unsuccessful (Figure 4.28). No further attempts were made to obtain the product due to the similarity of the cage to the nopol derivative **179** and the less desirable one methylene unit ether chain length.

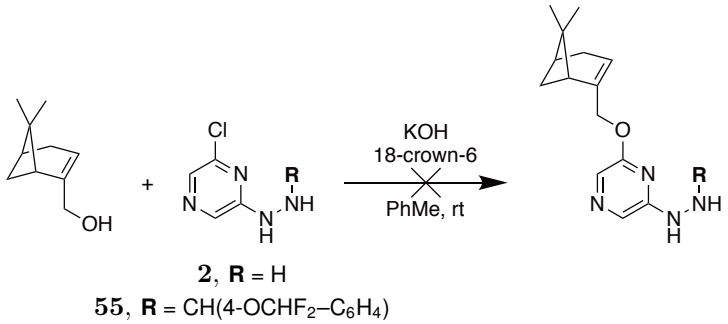

Figure 4.28: Attempted coupling of the myrtenol alcohol with the hydrazine and hydrazone precursors to the TP core 44. Both reactions were unsuccessful with only starting materials recovered.

4.6.2 Synthesis of Northwest Bird-Cage Series 4 Bioisostere

The final unique hydrocarbon cage for incorporation into Series 4 emerged after discussion with the Kassiou group at The University of Sydney. Pentacyclo[6.3.0.$0^{2,6}$.$0^{3,10}$.$0^{5,9}$]undecane (also know as D_3-trishomocubane) is one of a number of $C_{11}H_{14}$ trishomocubane isomers, closely related to adamanatane, that possess a relatively large cage size (5.5 Å H–H distance), high lipophilicity and conformational rigidity.[255] D_3-Trishomocubane was first synthesised in 1970 by Underwood and Ramamoorthy in a seven step process involving a Diels-Alder reaction with benzoquinone and cyclopentadiene, followed by cyclisation to the diketone upon irradiation with light, reduction to the diol, conversion to the dibromide, debromination to the diene, bromination and finally reduction to give D_3-trishomocubane (Figure 4.29).[256,257] Although less widely studied than adamantane, D_3-trishomocubane derivatives have been incorporated into biologically relevant compounds, including a treatment for Parkinson's disease and a compound with activity against dopamine receptors.[255,258]

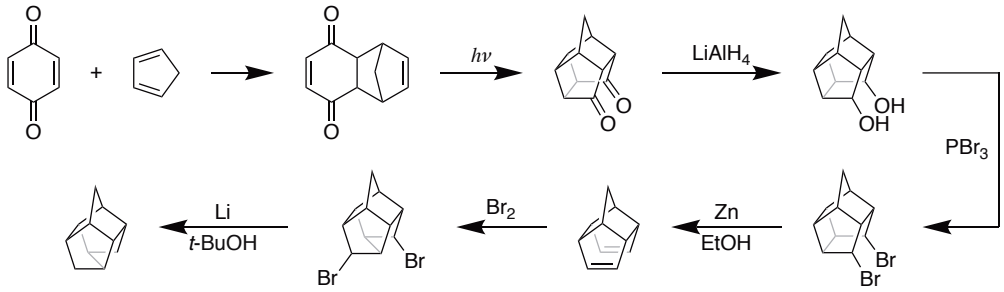

Figure 4.29: The Underwood and Ramamoorthy synthesis of D_3-trishomocubane. Initial formation of the Diels-Alder adduct, cyclisation by irradiation to the diketone, reduction and conversion to the dibromide, followed by HBr elimination using Zn, bromination and subsequent reduction gave a mix of the diene and the desired product, which could be separated on $AgNO_3$ doped silica.

Incorporation of the trishomocubane structure into a Series 4 compound revolved around the synthesis of the analogous pentacyclo[5.4.0.0^{2,6}.0^{3,10}.0^{5,9}]undecane derivative (also known as C_S-trishomocubane, referred throughout as the "bird-cage") shown in Figure 4.30. The monoketone **182** (provided by the Kassiou group and synthesised from Cookson's diketone) was condensed with Meldrum's acid following literature procedures to give compound **183**.[259] The alkene was reduced with $NaBH_4$ to give **184**, then converted to the carboxylic acid **185** and finally reduced to give the desired bird-cage alcohol intermediate **186** in 30% yield over the four steps. Final nucleophilic displacement on TP core **44** with **186** gave the final compound **187** in 31% yield.

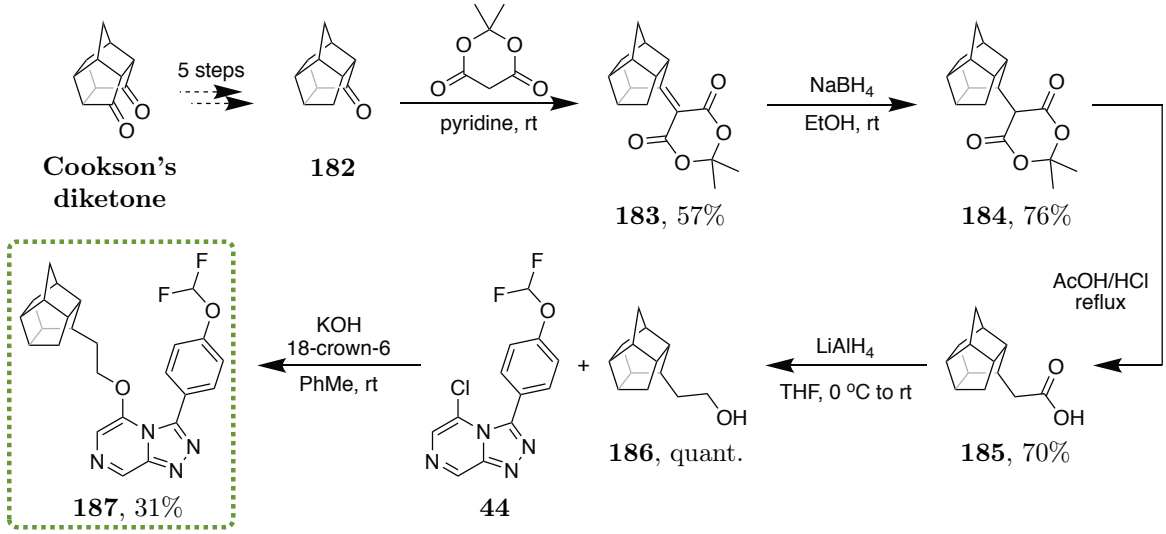

Figure 4.30: Synthesis of the northwest bird-cage derivative. Condensation of the monoketone with Meldrum's acid, reduction and decarboxylation gave the carboxylic acid **185**, which was further reduced and coupled with TP core **44** to give the final compound **187**.

4.6.3 Biological Evaluation

When evaluated for *in vitro* potency, these miscellaneous hydrocarbon cage isosteres were relatively well tolerated with higher activity seen with these analogues than the adamantane analogues but lower activity than the cubane analogues (Table 4.6). The norbornene-containing compound **180**

was the most potent of the set, which was interesting considering it possessed the less desirable one methylene unit ether chain (Entry 2). It is possible that this higher activity is influenced by the presence of both *endo* and *exo* isomers, which is unique to this compound.

Table 4.6: IC_{50} potency values of northwest miscellaneous hydrocarbon cage analogues against *P. falciparum*. All three hydrocarbon cage derivatives were relatively well tolerated.

Entry	Compound	cLogP	IC_{50} (μM)
Reference	**57**	2.7	2.24
	58	3.2	0.25
1	**179**	3.9	1.28
2	**180**	3.1	0.49
3	**187**	3.5	1.08

4.7 Carboranes

Carboranes are class of compounds consisting of a cluster of boron, carbon and hydrogen atoms arranged in a polyhedron. *Ortho*-carborane was first synthesised in 1963 by two groups independently in the United States[260,261] and is commonly prepared first by the reaction of decaborane ($B_{10}H_{14}$) and a weak Lewis acid (L = CH_3CN, RSR, R_3N) to generate *in situ* a Lewis acid decaborane ($B_{10}H_{12}L_2$), which is then reacted with acetylene to form *o*-carborane (Figure 4.31). Varying the acetylene allows for a wide range of substituted carboranyl derivatives to be synthesised. From *o*-carborane, the *meta*- and *para*-isomers can be generated by thermal isomerisation (*meta* at 420 °C; *para* at 600 °C). It is notable that while *o*- and *m*-carborane are available from chemical suppliers at a reasonable prices, the equipment required to obtain the *p*-isomer is far less common. As a result, obtaining this isomer can be quite expensive.

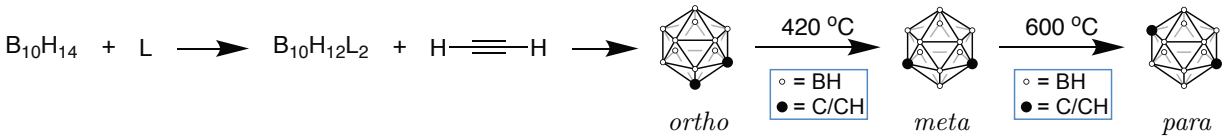

Figure 4.31: Route for the synthesis of *ortho*-carborane and its isomers. *In situ* generation of a Lewis acid decaborane, followed by reaction with acetylene gives *o*-carborane, the *m*- and *p*-isomers of which can be obtained by thermal isomerisation.

Due to the much larger size of carborane (*vide infra*) compared to a phenyl ring, it is perhaps less immediately obvious to medicinal chemists to use carborane as a phenyl bioisostere.[226,262,263] These carborane isomers are typically used in either the closed form, with all carbon and boron vertices (known as *closo*-carborane), or as the open form, with one boron vertex removed (known as *nido*-carborane). A prominent example of the application of a carborane bioisostere is that of the *closo*-carborane variant of tamoxifen (Figure 4.32).[264] The resulting carboranyl deriva-

tive showed high activity as an antiestrogen agent and was even found to be more stable than tamoxifen to decomposition. Another example is that of asborin, an *ortho*-carboranyl derivative of aspirin.[265] Interestingly in this case, the pharmacological profile of the resulting carboranyl derivative was changed drastically. Instead of acting as a selective cyclooxygenase (COX) enzyme inhibitor (like aspirin), asborin was instead found to be a potent inhibitor of the unrelated aldo/keto 1A1 reductase family.[266] In a similar manner to these closed forms, the open form has also shown potential as a phenyl replacement both in a carborane variant of tamoxifen[267] and trimethoprim.[268] In this latter case, the *nido* derivative was found to be less toxic than the *closo* derivative, however it also performed worse as a boron neutron capture therapy agent with poorer tumour retention and lower selectivity ratios for boron distribution in tumour versus normal tissues.

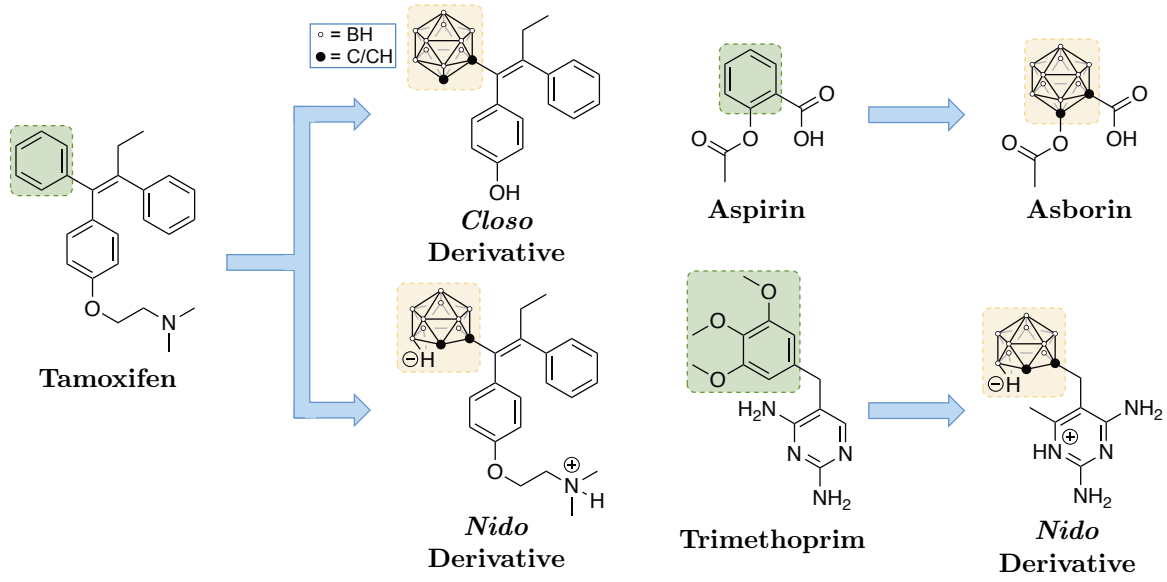

Figure 4.32: Examples of the use of carborane as a phenyl bioisostere. Replacement of a phenyl ring in known biologically relevant compounds with closed (*closo*) and open (*nido*) forms of carborane.

A key consideration for the use of carborane as a phenyl bioisostere is the choice of which isomer to use. The differences in the dipole moments of the carbon atoms in each isomer have an influence on the polarity and hydrophobicity of the compound (A, Figure 4.33).[269] In one case, a series of carborane-containing indomethacin derivatives was synthesised and evaluated for the ability to inhibit COX. It was found that the derivative containing the *o*-carborane was active against COX-2, while the other two carborane isomers were inactive when evaluated in a radioactivity assay (B).[270] Conversely, carborane isomers were incorporated into small molecule inhibitors of nicotinamide phosphoribosyltransferase (Nampt) with the results indicating similar potencies across multiple cancer cell lines (C).[271]

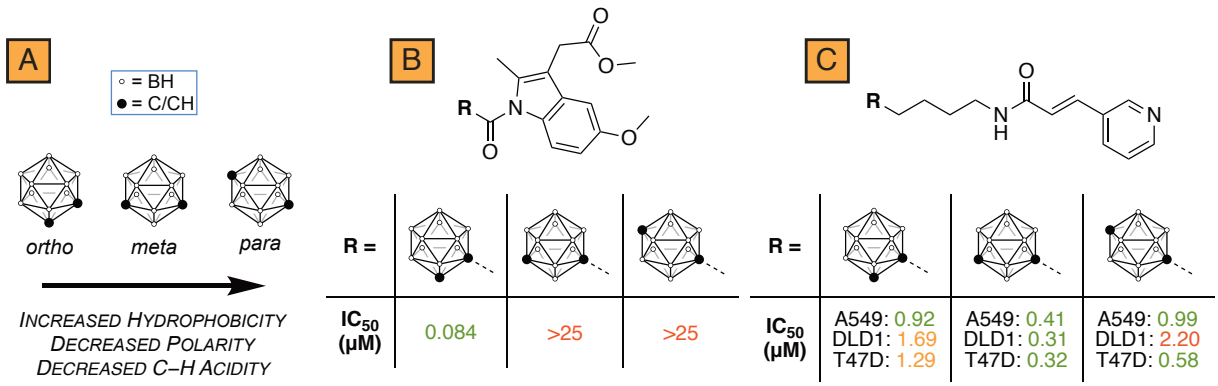

Figure 4.33: The effect of carborane isomerism on biological activity. (A) Each carborane isomer has unique hydrophobicity and polarity properties due to the difference in dipole moments of the carbon atoms. (B) Comparison of the carborane-containing indomethacin derivative showed only the *o*-carborane compound was active. (C) The carborane-containing Nampt inhibitors showed roughly similar potencies against three cancer cell lines (A549, DLD1 and T47D) across the three isomers.

4.7.1 Synthesis of the Series 4 Carborane Analogues

Following discussion with the Rendina group at The University of Sydney, samples of *o*-, *m*- and *p*-carborane were kindly provided for investigation as Series 4 phenyl bioisosteres. Following the procedure outlined by Li and co-workers,[272] *o*-carborane was lithiated using *n*-BuLi, with subsequent ring opening of oxetane by the organolithium intermediate, affording the *o*-carboranylethyl alcohol **188** in 66% yield (Figure 4.34). The *m*-carboranylethyl alcohol **189** was obtained in the same manner from *m*-carborane to give the corresponding alcohol in 23% yield. In the case of *p*-carborane, an alternative approach had to be taken, involving a benzyl protected alcohol, as there was a higher chance for the chain to be substituted at both carbons due to the more uniform distribution of electron density.[273] Following literature procedures,[274] *p*-carborane was lithiated and reacted with benzyl 2-bromoethyl ether to give the benzyl protected alcohol **190** in 47% yield. The subsequent literature benzyl deprotection method used hydrogen gas as a reagent but due to the inaccessibility of a hydrogen cylinder, an alternative procedure was used. One method reported by Mandal and McMurray used Et_3SiH and catalytic Pd–C to generate H_2 *in situ* to effect the hydrogenation.[275] This was applied to the deprotection of **190** which afforded the desired *p*-carboranylethyl alcohol **191** in 67% yield. With all three carborane alcohols in hand, each was coupled with TP core **44** to give the corresponding products **192**, **193** and **194** in low to moderate yields. Additionally, a small amount of the *o*-carborane product **192** was converted to its *nido*-form in a process reported by Yoo and co-workers,[276] by reaction with CsF in refluxing EtOH to give the caesium salt of the *nido*-carborane **195** in 65% yield.

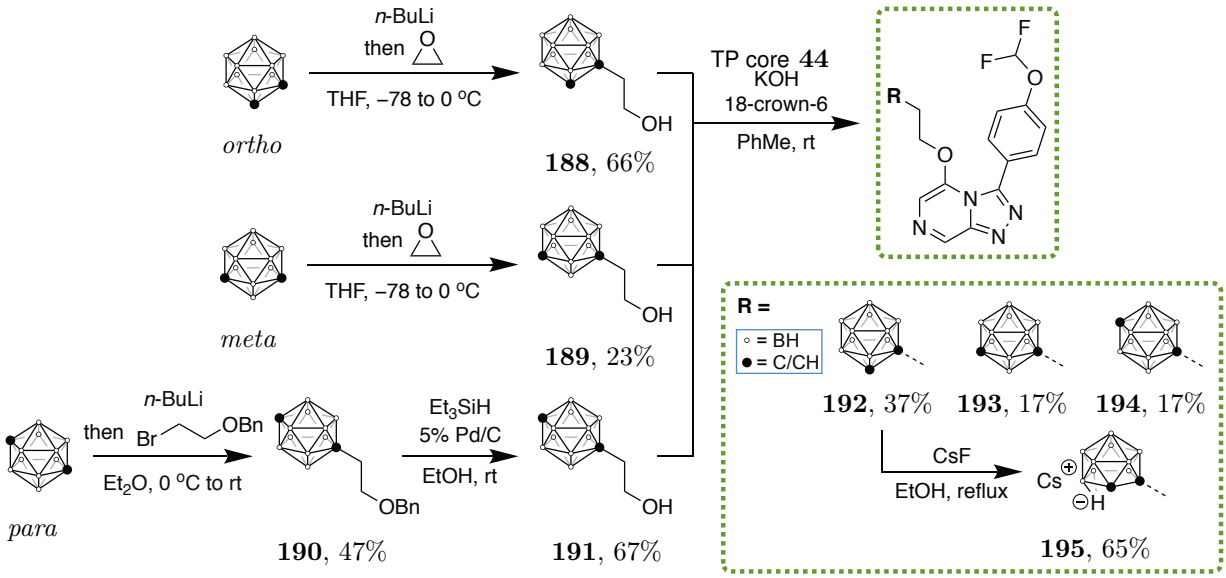

Figure 4.34: Synthesis of the northeast carborane compounds. The carborane alcohols, synthesised *via* the lithiated intermediates, were coupled with TP core **44** to give the final compounds. A small amount of compound **192** was converted to the *nido*-form as well.

4.7.2 Biological Evaluation

Striking results were seen when the carborane-containing analogues were evaluated for *in vitro* potency (Table 4.7). The *o*- and *m*-carborane (**192** and **193** respectively) showed potencies greater than not only all the previous phenyl bioisostere derivatives, but more importantly the parent phenyl compound **58** (Entries 1 and 2). A significant drop in potency was seen between the *m*- and *p*-carborane isomers (**193** and **194** respectively, Entries 2 and 3), however the general trend seen in potency was a decrease from *o*- to *m*- to *p*-carborane. It is thought that this trend is related to the difference in polarity and hydrophobicity of the three carborane isomers (*vide supra*). It appears that the more hydrophobic and less polar the carborane isomer is, the less potent the final compound. While it has been shown that the *nido*-form can act as a phenyl bioisostere, in our case, the *nido*-form **195** was shown to be less efficacious than the *closo*-form **192**, with the potency decreasing significantly (Entry 4). It is assumed that the removal of a carborane vertex, and thus breaking of the cage structure, results in a poorer phenyl ring mimic and reduced potency.

Table 4.7: IC_{50} potency values of northwest carborane analogues against *P. falciparum*. Unexpectedly, the *closo*-carborane analogues **192** and **193** were more potent than the parent phenyl compound, while the *p*-carborane isomer and the *nido*-carborane analogue were less potent. *cLogP values were calculated using ChemDraw Professional.

Entry	Compound	cLogP	IC_{50} (μM)
Reference	**58**	3.2	0.25
1	**192**	4.0*	0.05
2	**193**	-2.2*	0.12
3	**194**	-2.3*	2.00
4	**195**	-1.3*	2.29

The unexpectedly high potency seen with the carborane compounds prompted evaluation of cytotoxicity to ensure that the potency was not a result of generic toxicity. Such measurements showed that **192** and **195** were not cytotoxic at >10 μM in HepG2 cells.

4.8 Metabolic & Physicochemical Properties of Select Phenyl Bioisosteres

Having completed the set of Series 4 phenyl bioisostere analogues, select compounds (cubane **154**, BCP **178** and carborane **192**) were evaluated to determine the effect that phenyl replacement had on solubility and metabolic stability (Table 4.8). The reference compound used was **58**, which possessed a phenyl ring in the northwest position. The physicochemical properties that were measured were the kinetic solubilities at pH 6.5 and the distribution coefficient (LogD) at pH 7.4. The metabolic stability data included *in vitro* clearance and half-life measurements in both human and mouse liver microsomes (HLM and MLM respectively). In addition to this, the hepatic extraction ratio (E_H) was calculated for both humans and mice, which allowed for the clearance of each compound to be classified as either low (<0.3), intermediate (0.3–0.7) or high (0.7–0.95).

Table 4.8: Metabolic and physicochemical properties of select Series 4 phenyl bioisostere compounds. HLM: human liver microsomes. MLM: mouse liver microsomes. Sol.: aqueous solubility (μg/mL). CL_{int}: *in vitro* intrinsic clearance (mL/min/kg). $T_{1/2}$: half-life (min). E_H: hepatic extraction ratio. Data acquired by the Charman Laboratory at the Centre for Drug Candidate Optimisation, Monash University. *cLogP value was calculated using ChemDraw Professional.

Entry	Compound	cLogP	LogD (pH 7.4)	Sol. (pH 6.5)	HLM ($CL_{int}/T_{1/2}$)	MLM ($CL_{int}/T_{1/2}$)	E_H (H/M)
1	**58**	3.2	3.7	6.3 - 12.5	66/26	262/7	0.72/0.85
2	**154**	2.5	4.3	<1.6	197/9	573/3	0.89/0.92
3	**178**	2.4	3.6	6.3 - 12.5	9/190	26/66	0.27/0.36
4	**192**	4.0*	4.4	<1.6	249/7	>866/<2	0.91/>0.94

The effects on metabolic and physicochemical properties as a result of phenyl replacement by cubane have been mixed in the literature. While a number of cases have reported improvements

to solubility following cubane substitutions,[277] the case for metabolic stability is less consistent. There have been reports of increased[227] and decreased[278] metabolic stability as a result of phenyl replacement with cubane. In this case, when Series 4 cubane compound **154** was evaluated for its metabolic and physicochemical properties, it was seen to perform poorer than the parent phenyl compound **58**. The solubility at pH 6.5 was surprisingly low (<1.6 μg/mL) when compared to **58** (6.3 - 12.5 μg/mL), with an accompanying high clearance and short half-life in human liver microsomes (HLM) and mouse liver microsomes (MLM). When this compound was evaluated in rat cryopreserved hepatocytes (RCH), it showed an intermediate degradation rate, with low clearance and a short half-life. Similar results were seen with carborane compound **192**. It is possible the presence of the unsubstituted cubane is causing this reduction in pharmacokinetic properties when compared to the phenyl counterpart (in a similar manner to that shown above). While not done here, the synthesis of a substituted cubane analogue could lead to an improvement in these values. Encouragingly, the positive effect of the BCP bioisostere was demonstrated with the BCP analogue **178** which exhibited significant improvements to the pharmacokinetic properties. While the solubilities were seen to be within the same range for both compounds, the BCP analogue demonstrated a lower clearance and longer half-life in both HLM and MLM. Additionally, **178** was evaluated against RLM with similar improvements seen ($CL_{int}/T_{1/2}/E_H$ = 11/152/0.23).

It is highly suspected that clearance of the parent compound **58** occurs *via* benzylic oxidation, and that the removal of this phenyl ring was thought to slow this clearance (due to the absence of the benzylic position). With regards to the cubane analogue **154**, these results would suggest that the incorporation of cubane in place of phenyl has led to the shifting of the metabolic hotspot onto the cubane itself (*vide infra*), with the cubane now becoming the metabolic liability. This appears in contrast to the idea that cubane derivatives are more metabolically stable than phenyl rings due to the increased s-character caused by the strong (bond dissociation energy = 427 ± 17 kJ/mol)[279] and hindered tertiary C–H bonds making it less prone to metabolism by hydroxylation. It is clear in our case that such replacement did not lead to an improvement in metabolic stability.

4.9 Late-Stage Biofunctionalisation

An opportunity arose to have a number of Series 4 compounds evaluated in a late-stage biofunctionalisation experiment run at Pfizer by the laboratory of Scott Obach.[280] This process would allow for metabolites to be synthesised and isolated using liver microsomes as a way of probing sites of metabolic vulnerability.

The cubane and norbornene compounds (**154** and **180** respectively) were sent for evaluation in this assay. Liver microsomes were used to generate metabolites of each compound, the major product of which was isolated, characterised and sent for potency evaluation against the parasite 3D7 strain (Figure 4.35).[281]

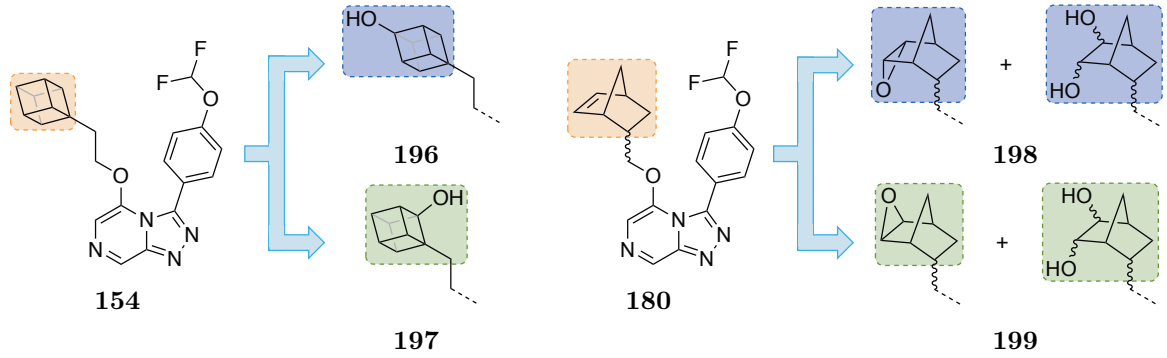

Figure 4.35: Late-stage biofunctionalisation performed on compounds 154 and 180. Hydroxylated metabolites **196** and **197** were obtained from **154** while epoxide metabolites **198** and **199** were obtained from **180**. Hydrolysis led to mixtures of the epoxides and the *cis*- and/or *trans*-diols.

In the case of cubane compound **154**, metabolism appeared to occur on the cubane cage itself (suggested by ^{1}H NMR spectroscopy and mass spectrometry; data were acquired by the Pfizer team and shared with the author immediately before submission. It may be seen in the NMR spectra that the methylene units of the linker chain are intact, strongly suggesting the oxidation has occurred on the cubane and not the linker.), with two hydroxylated derivatives **196** and **197** being identified. It is interesting to note that in an analogous case where metabolites were generated for a compound containing a phenyl ring,[280,281] hydroxylation did not occur on the phenyl ring but instead occurred at the benzylic position, as expected; i.e. the metabolites for the cubane derivatives are different to those for the analogous phenyl compounds. This is surprising, as cubane derivatives are thought to be quite metabolically stable, however in our system we are seeing the opposite of this, with preferential hydroxylation of the benzylic position in the phenyl case but apparently no benzylic hydroxylation in the case of cubane. In the case of the norbornene compound **180**, oxidation of the norbornene alkene resulted in two stereoisomeric epoxide derivatives, **198** and **199**, which were identified by NMR spectroscopy (1D and 2D) and HRMS. Interestingly, both epoxides were observed by NMR spectroscopy to slowly react with water resulting in hydrolysis to the corresponding *cis*- and/or *trans*-dihydrodiols, creating a mixture of epoxide and diol products. Attempts were made to push the conversion to the dihydrodiol products (using D_2O and DCO_2D) however no further conversion was seen. The potency of these compounds, as mixtures, was obtained before more efforts were made to separate the individual components.

All four biosynthesised products were evaluated for potency (**198** and **199** as mixtures of epoxide and diol in ratios that were not elucidated) and all were found to be inactive (Table 4.9).

Table 4.9: IC_{50} potency values of the late-stage biofunctionalisation products of 154 and 180 against *P. falciparum*. All metabolites were found to be inactive. Potencies in parentheses refer to the assay run at 10 fold dilution from the original compound concentration.

Entry	Compound	cLogP	IC_{50} (μM)
Reference	**154**	2.5	0.37
	180	3.1	0.49
1	**196**	1.7	>1
2	**197**	1.7	>3.3 (>1.1)
3	**198**	1.8	>9.8 (>0.98)
4	**199**	1.8	>11 (>1.1)

4.10 Size Comparison of Phenyl Biosisosteres

One aspect that is often discussed when using phenyl bioisosteres is how closely the structural dimensions of the replacing structure matches that of a phenyl ring. For instance, in a paper investigating the use of cubane as a phenyl bioisostere,[227] it is stated that the C–C distance across the diagonal of cubane (2.72 Å) is similar to the C–C distance across a benzene ring (2.79 Å). In another example on the use of BCP as a phenyl bioisostere,[243] a comparison is made of the same benzene C–C distance (2.8 Å) with the bridgehead C–C distance of a *para*-substituted BCP (1.7 Å). As a final case, in a review on carboranes as pharmacophores,[226] the van der Waals volumes of benzene (79 $Å^3$ stationary or 102 $Å^3$ rotating), adamantane (136 $Å^3$) and carborane isomers (141–148 $Å^3$) are compared.

It is clear that the information provided by these sources is fragmented and no one reference provides all the desired calculations. The best way to address this would be to gather deposited crystal structure files that contain the desired phenyl bioisosteres, and use a single program to analyse and calculate the structural dimensions. A more direct comparison could then be made between the different bioisosteres.

Many crystal structure viewing programs such as Mercury and PLATON allow for the calculation of bond lengths but few provide an intuitive way to calculate structural volumes. One such program which allows for the calculation of bond lengths, surface areas and volumes of structures all in one software package is UCSF Chimera. This, along with crystal structure files obtained from The Cambridge Crystallographic Data Centre (CCDC), were used to calculate the structural dimensions of the described phenyl bioisosteres (Figure 4.36). In cases where the crystal structure file contained multiple substructures, the desired structure could be isolated by deleting the

unwanted atoms prior to performing the area and volume calculations.

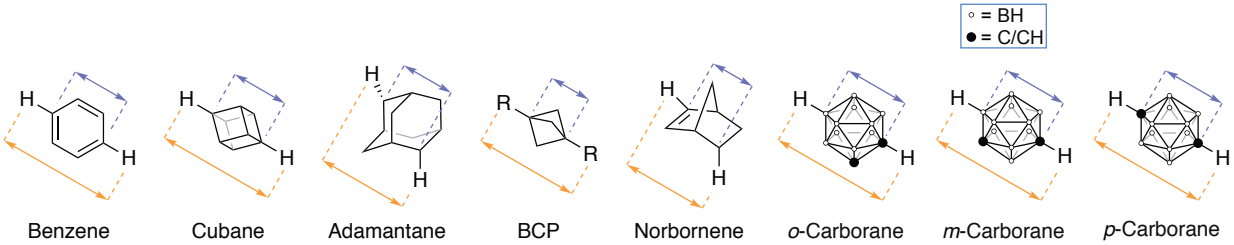

Structure (CCDC Identifier)	**C–C Distance (Å)**	**H–H Distance (Å)**	**Surface Area (Å^2)**	**Volume (Å^3)**
Benzene (ABELUO)	2.77 (2.70[282]; 2.79[227]; 2.82[277])	4.63 (5.90[234])	89.7	70.14 (79[226])
Cubane (CUBANE)	2.68 (2.70[282]; 2.72[227,277])	4.70	103	87.1
Adamantane (ADAMAN08)	3.53	4.92 (6.36[283]; 6.40[234])	126 (134[234])	119 (128[234]; 136[226])
BCP (HEHRUJ)	1.88 (1.70[243]; 1.85[277]; 1.90[282])	4.78†	80.2¶	61.4¶
Norbornene (HOBBOP)	2.89	4.64	101.3	84.76
***o*-Carborane** (TOKGIJ)	3.23*	5.26	135	127 (148[226])
***m*-Carborane** (TOKGOP)	3.20*	5.12	134	126 (143[226])
***p*-Carborane** (TOKGUV)	3.06	4.85 (5.35[284])	136	127 (141[226])

Figure 4.36: Structural information of select phenyl bioisosteres calculated using UCSF Chimera. C–C and H–H distances are indicated in purple and orange respectively. Where they exist, literature values are shown in parentheses. Surface areas and volumes were calculated using a model of the solvent-excluded molecular surface with hydrogen atoms included. R = terminal alkyne. †Alkyne C–C atom distance. ¶Surface area and volume calculated without alkyne substituents. *C–B distance.

It can be seen that among the literature reports, there is noticeable variation between the quoted values. For the most part, the atom distances are relatively consistent with those calculated using UCSF Chimera. When comparing the surface area and volume calculations, there is approximately a 10–15% increase with the literature values. More importantly, by using X-ray crystallography data in a single program to perform these calculations, more reliable comparisons can be made. It is noted that the BCP dimensions are an approximation and are expected to be smaller than stated. Nevertheless, it is surprising how well certain phenyl bioisosteres work when they are

incorporated into actual compounds given the sometimes significant differences in dimensions compared to a phenyl ring.

4.11 Concluding Remarks

A wide range of compounds was synthesised with the aim of probing the tolerability for bioisosteric replacement of the phenyl rings in the Series 4 compounds, with subsequent evaluation for biological activity (Figure 4.37).

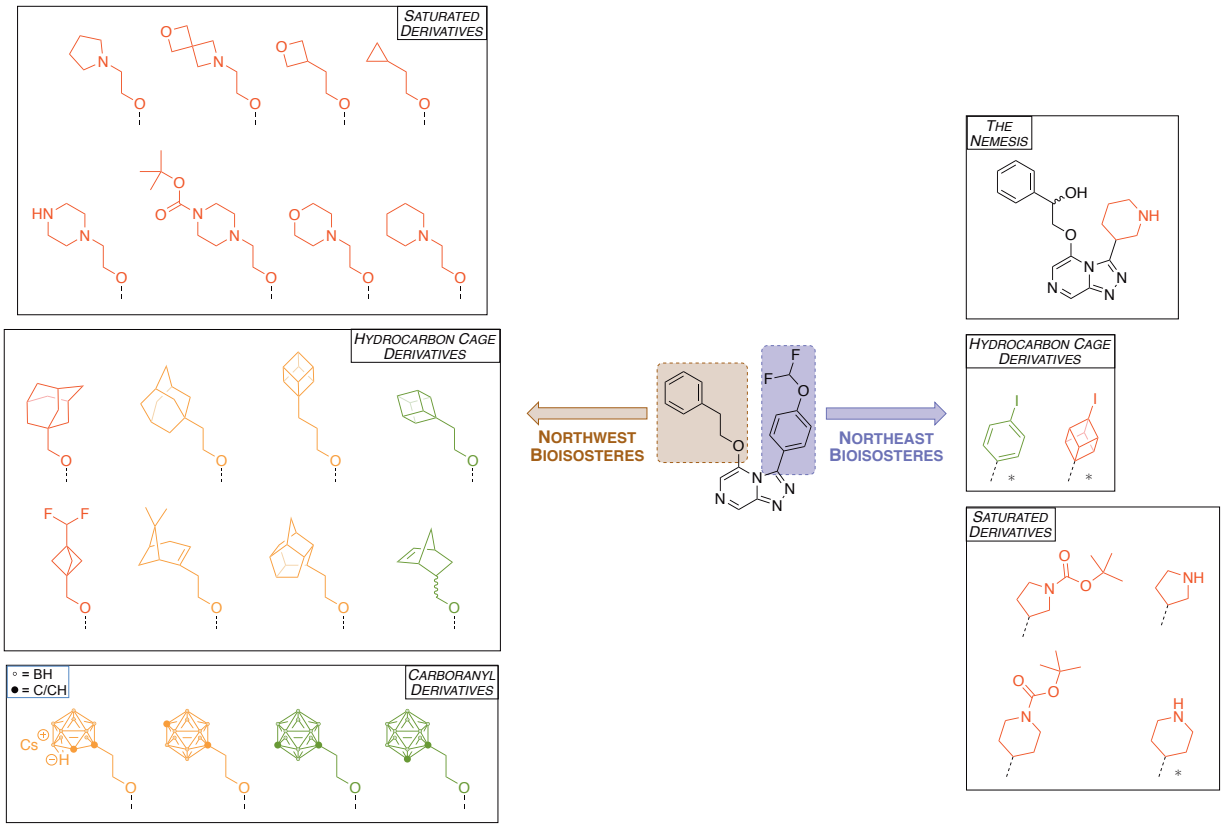

Figure 4.37: Summary of the SAR for compounds in this chapter. Colour coding: <1.0 μM = green, 1.0–2.5 μM = orange, >2.5 μM = red. *Compound has northwest 3,4-difluorophenyl ring instead.

A low tolerance was seen with all saturated heterocycle replacements in both the northwest and northeast positions, with all compounds being inactive. This was similarly the case with the northeast cubane replacements, suggesting a low tolerability for deplanarisation in the northeast position. Conversely, the northwest cubane replacements were well tolerated, with only a slight loss in potency when compared to the phenyl analogue. This would suggest that, while deplanarisation is tolerated in the northwest position, there must be a degree of rigidity within the structure to maintain potency. This was confirmed with replacements of the northwest phenyl ring with rigid hydrocarbon cages such as adamantane, BCP, nopol, norbornene and the bird-cage, all of which showed weak activity.

As a final point of investigation, carborane was evaluated for its ability to act as a phenyl bioisostere. Not only was the carborane replacement surprisingly well tolerated, it was the only case from the compounds described in this chapter in where the replacement resulted in an increase in potency when compared to the parent phenyl compound. This high potency was confirmed not to be a result of inherent cytotoxicity. As a general trend, the potency of the carborane isomers was a decrease from *o*- to *m*- to *p*-carborane. This appears to be in line with the increasing hydrophobicity and decreasing polarity across the isomers.

The cubane and carborane and BCP compounds (**154**, **178** and **192** respectively) were evaluated for their metabolic and physicochemical properties to determine whether these replacements led to an improvement in these properties when compared to the parent phenyl compound. Surprisingly, the analogues containing cubane and carborane replacements, designed to deplanarise the structure and remove benzylic metabolic hotspots, exhibited significant decreases in solubility and metabolic stability. Conversely, the BCP replacement led to a notable increase in these parameters when compared to the parent phenyl compound, with a much lower clearance and longer half-life in human, mouse and rat liver microsomes. The data acquired for the BCP compound **178** makes the analogous structure, containing a further methylene spacer in the linker, a high priority target for further investigation since it would be expected to have greater activity and improved solubility and clearance parameters.

The cubane and norbornene compounds (**154** and **180** respectively) were used to generate late-stage biofunctionalised metabolites using liver microsomes. Hydroxylation was seen to occur on the cubane cage itself which is in contrast to the corresponding phenyl compound, where oxidation occurs at the benzylic position. The norbornene compound produced two stereoisomeric epoxide compounds, both of which were seen to convert, to an extent, to the *cis*- and/or *trans*-dihydrodiols. All four metabolites were found to be inactive *in vitro*.

A more unified comparison of the structural dimensions of the phenyl bioisosteres discussed throughout this chapter was performed using UCSF Chimera. Using deposited crystal structure files from the CCDC, the calculated properties allowed for more direct comparisons between the different structures.

The following chapter will cover the evaluation of select compounds from Chapters 2, 3 and 4 to validate the mechanism of action for the Series 4 triazolopyrazines.

5. The Mechanism of Action of Series 4

This chapter covers the mechanism of action studies performed on the Series 4 triazolopyrazines. A brief survey of other novel mechanisms of action for antimalarials in development will be presented, followed by a discussion of the validation of the Series 4 mechanism of action, involving the protein target *Pf*ATP4.

5.1 Background

The mode/mechanism of action (MoA) may be defined as the interaction that a drug makes with its biological target in order to produce its pharmacological effect. Determination of the MoA of a potential drug candidate is a key step in any medicinal chemistry program as this may help guide optimisation of lead compounds or even influence the design of future target molecules. A number of methods exist for the determination of the MoA of new drugs.[285] Direct biochemical methods involve attaching chemical labels to drug molecules which allow them to be traced to their targets. Microscopy methods may be used to view the phenotypic changes that a drug creates when binding to a target.[286] Computational methods allow targets to be predicted based on pattern recognition with known reference compounds or genetic perturbations.[287] The use of omics-based methods has increased in recent years with the advent of CRISPR techniques and metabolomics approaches.[288,289] The recent development of *in vitro* evolution and whole genome analysis (IVIEWGA), which uses genome-based target discovery methods on compounds identified from the more conventional phenotypic screens, allows for even more drugs to be discovered.[290]

In the case of the malaria parasite, resistance to frontline antimalarial drugs is an ever present problem. As a result, the discovery and exploitation of novel MoAs has become a priority. Perhaps the most prominent example is that of artemisinin. First isolated in 1971 from the plant *Artemisia annua*,[22] artemisinin has been one of the most efficacious treatments for malaria for over 40 years. Resistance has been slow to develop, in part due to the use of artemisinin combination therapies (ACTs) where a fast-acting artemisinin derivative is combined with a complementary slow-acting drug from another class of compounds (examples include those described in Chapter 1). While the use of combination medicines helps, more reports of resistance to ACTs are emerging, highlighting the need to find new medicines.

The MoA of many of the most prominent antimalarials has been well studied.[291–293] For instance,

the structurally related quinoline drugs (such as quinine, mepacrine, chloroquine and mefloquine) have all been thought to act through the inhibition of haem detoxification.[17,44] More recently however, studies have shown that quinine and mefloquine bind to *P. falciparum* purine nucleoside phosphorylase (*Pf*PNP) in low nanomolar concentrations, suggesting this MoA plays a key role in their theraputic effect.[294] Still, there are certain antimalarial compounds that are used today for which the MoA is not precisely known. The MoA of artemisinin and its derivatives has been widely debated for many years with no clear conclusion.[295] The most generally accepted theory is that free radicals are generated through the activation of artemisinin by haem. These free radicals subsequently damage the proteins that are required for parasite survival.[296,297] Additional studies have emerged that identify other possible targets for artemisinins such as *P. falciparum* ATP6 (Ca^{2+} transporter) inhibition,[298] *P. falciparum* phosphatidylinositol-3-kinase (*Pf*PI3K) inhibition,[299] and the up-regulation of the unfolded protein response (UPR) pathways associated with parasite development.[300] Similarly, the MoA for piperaquine is not precisely known with research suggesting links to the generation of reactive oxygen species and the interference of electron transport within the parasite.[301,302]

5.2 Mechanisms of Action that Overcome Current Resistant Parasites

It is evident that developing new antimalarials based on the structures and MoAs of our existing treatments is not the most reliable strategy for combating the development of resistance. In order for future antimalarials to be most effective, they must not only show potent activity against the parasite, but also act through novel MoA pathways. By doing this, the chance of resistance emerging is minimised, thereby prolonging the use of the drug. Many of the compounds in Figure 1.5 have been identified as being highly efficacious against the malaria parasite with good safety profiles, physicochemical and pharmacokinetic properties. Most importantly, many of these compounds have been shown to act through novel MoAs, those of which are described in Table 5.1.[303]

Table 5.1: Novel MoAs of antimalarial drugs currently in development. A brief description of the MoA and an example compound for the target are given.

Target	Description of MoA	Example Compound
***Pf*eEF2**	The translational elongation factor 2 (eEF2) is one of the essential elongation factors responsible for the GTP-dependent translocation of the ribosome	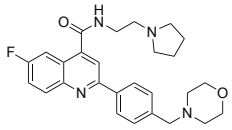 **M5717**[75]

	along mRNA. Also required for eukaryotic protein synthesis.	
***Pf*ATP4 (P-type Na^+–ATPase)**	The Na^+–ATPase transporter is responsible for the regulation of increasing Na^+ concentration within the parasite.	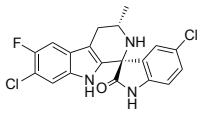 **KAE609**[121]
***Pf*ATP4 (V-type H^+–ATPase)**	The H^+–ATPase transporter is responsible for the regulation of decreasing H^+ concentration within the parasite.	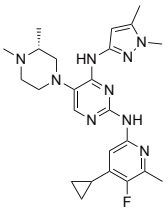 **MMV253**[78]
***Pf*PI(4)K**	Phosphatidylinositol 4-kinase (PI(4)K) is a eukaryotic enzyme responsible for the phosphorylation of lipids which allows the regulation of intracellular signalling and trafficking.	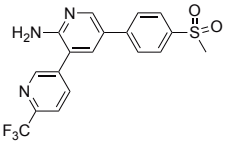 **MMV048**[84]
***Pf*DHODH**	Dihydroorotate dehydrogenase (DHODH) is an enzyme responsible for the biosynthetic oxidation of dihydroorotate (DHO) to ultimately generate pyrimidines, which are essential metabolites for parasitic replication in the human erythrocyte.	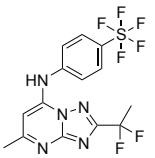 **DSM265**[124]
***Pf*DHFR**	Dihydrofolate reductase (DHFR) is an enzyme responsible for the catalytic recycling of folates, which is essential for a high parasitic replication rate.	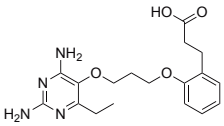 **P218**[95]
***Pf*cPheRS**	Cytosolic phenylalanyl-tRNA synthetase (cPheRS) is an enzyme involved in the synthesis of parasite proteins	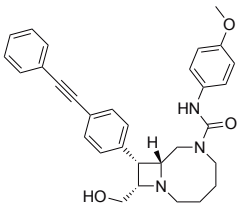 **BRD3444**[304]

***Pf*CPSF3**	The cleavage and polyadenylation specificity factor subunit 3 (CPSF3) is implicated in the cleavage of mRNA precursors prior to polyadenylation	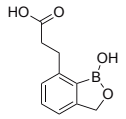 **AN3661**[88]
***Pf*CYTbc_1**	Cytochrome bc_1 (CYTbc_1) is an enzyme complex that transfers electrons from ubiquinol to cytochrome c and is a key component of the parasite respiratory chain	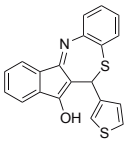 **BTZ**[305]

5.3 *P. falciparum* ATP4 Inhibiton

The most relevant of the above MoAs for the Series 4 triazolopyrazines is *Pf*ATP4 inhibition. An essential feature of the *P. falciparum* parasite is its ability to regulate its internal Na^+ and H^+ concentrations. An influx of Na^+ is regulated by using a P-type ATPase transporter (*Pf*ATP4) to shuttle Na^+ out of the cell,[306] while an analogous V-type ATPase transporter shuttles H^+ out of the cell to maintain an intracellular pH of ~7.3 (A, Figure 5.1).[307] Thus, disruption to these processes through the inhibition of the corresponding transporter will lead to the death of the parasite.

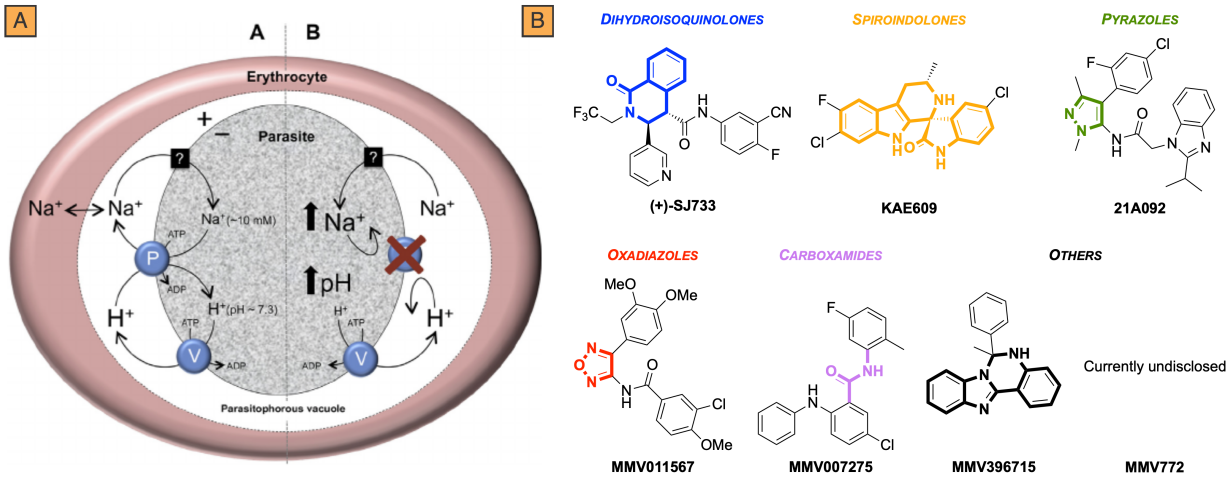

Figure 5.1: *P. falciparum* ATPase transporters (*Pf*ATP4) regulate Na^+ and H^+ through P- and V-type ATPases respectively. (A) Inhibition of *Pf*ATP4 leads to an increase in Na^+ concentration and a concomitant decrease in H^+ concentration. (Figure licence CC BY-NC-ND from N.J. Spillman & K. Kirk, 2015.[99]) (B) Representative compounds from a number of the structurally diverse chemotypes that have been shown to target *Pf*ATP4.

In 2014, the Kirk group at the Australian National University, utilised their assay for *Pf*ATP4 and screened the 400 compounds contained in the MMV Malaria Box, with a total of 28 compounds

being identified as inhibitors of *Pf*ATP4.[306] A striking observation from these results was the number of structurally diverse chemotypes that appeared to have the same molecular target (B, Figure 5.1). How such structural diversity of inhibitors against a single target can be possible is currently unclear as the structure of the *Pf*ATP4 protein has not yet been determined by X-ray crystallography, but a homology model has been developed using the closest mammalian homolog (sarco/endoplasmic reticulum Ca^{2+}-ATPase) to aid with this.[98] A standout from these chemotypes is the spiroindolone class of compounds, specifically KAE609, the discovery and hit to lead campaign of which is described in Chapter 1. This is perhaps the most promising of the *Pf*ATP4 inhibitors, having progressed into Phase IIb clinical trials. In order to determine the potential for KAE609 to cause drug resistance, resistant parasites were generated against a clone of the multidrug-resistant Dd2 strain.[121] Mutations were found in *pfatp4*, however the level of resistance was determined to be relatively low (about 4 times less potent) and it was confirmed that this resistance was specific to the spiroindolone class of compounds.

5.4 The Series 4 Triazolopyrazines Target *Pf*ATP4

When the series was first inherited in 2013, five of these inherited compounds were evaluated for their ability to act as inhibitors in the Kirk ion regulation assay as a means of identifying the MoA. The results revealed a good correlation between *in vitro* parasite-killing activity and disturbance of ion regulation (Figure 5.2). These results suggested that *Pf*ATP4 could be the molecular target for Series 4.

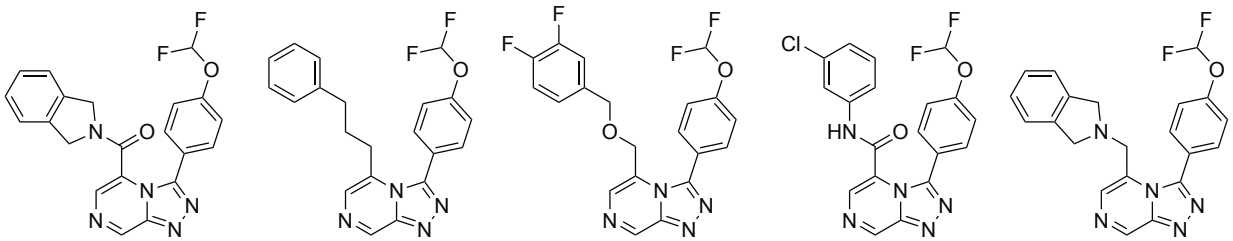

Figure 5.2: Set of five inherited compounds evaluated in the *Pf*ATP4 assay in 2013. Good correlation was seen between *in vitro* potency and ion regulation activity.

To probe this observation further, seven more inherited compounds were evaluated in 2014 (Figure 5.3). Encouragingly, excellent correlation was again seen between *in vitro* potency and ion regulation activity for this new set of compounds, supporting the previous results.

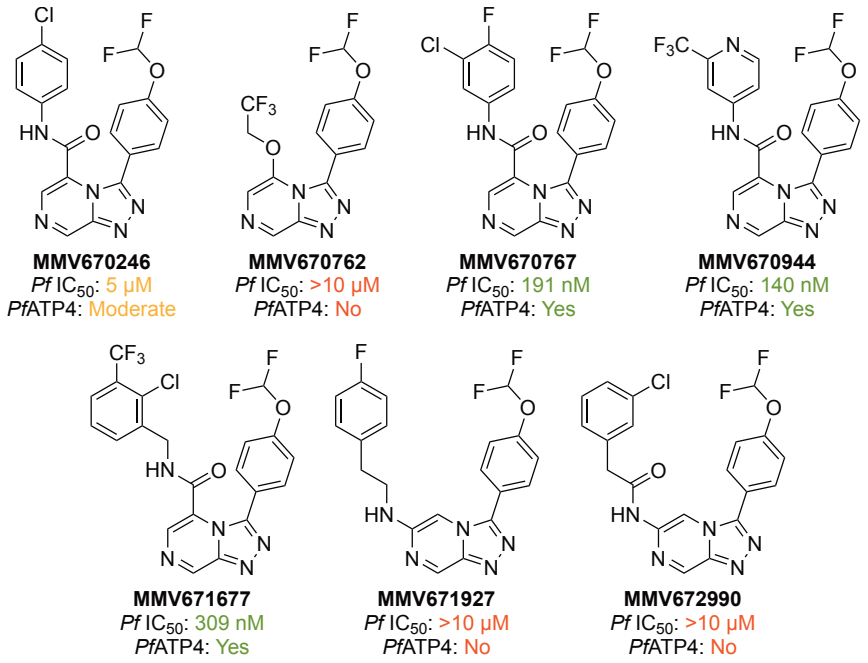

Figure 5.3: Set of seven inherited compounds evaluated in the *Pf*ATP4 assay. Again, good correlation was seen between *in vitro* potency and ion regulation activity.

Examination of the structural features among these two datasets showed that all twelve compounds possessed the same 4-$OCHF_2$ substituent on the northeast phenyl ring. Seven of the compounds contained an amide linker in the northwest position, with the remainder containing ethyl, amine or alkyl linkers. It is notable that none of these compounds possessed the two methylene unit chain ether linker, a key feature of many of the most potent Series 4 compounds.

5.5 Performing the *Pf*ATP4 Assay

A perfect opportunity to prove MoA further arose during the 2016 Frontrunners campaign (described in Chapter 2), which allowed these, and other newly synthesised compounds, to be evaluated for ion regulation ability. This time, following the synthesis of the compounds, rather than sending them for evaluation in the assay, they were taken by the author to the Kirk lab to perform the assay. All compounds were evaluated for both Na^+ and H^+ regulation.

5.5.1 Assay for Na^+ regulation

In order to evaluate the compounds for potential Na^+ ion regulation activity, 1 mM stock solutions in DMSO of each had to be made. The compounds were subsequently evaluated at concentrations of 1 μM and 5 μM. Positive (KAE609) and negative (DMSO) controls were used throughout the assay. To assay the intracellular Na^+ concentration ($[Na^+]_i$), trophozoite-stage *P. falciparum* parasites were loaded with Na^+-binding benzofuran isophthalate (SBFI) dye which enabled the change in sodium ion concentration within the parasite to be monitored by fluorescence spec-

troscopy. Two excitation wavelengths are used to measure the ($[Na^+]_i$). At 340 nm excitation, the dye is very sensitive to the ion concentration and at 380 nm the dye is near the isosbestic point (the wavelength at which the absorbance is at equilibrium and remains constant). The ratio of the fluorescence intensities from both wavelengths (340/380 nm) can therefore be used as an indicator of $[Na^+]_i$ over time (Figure 5.4).

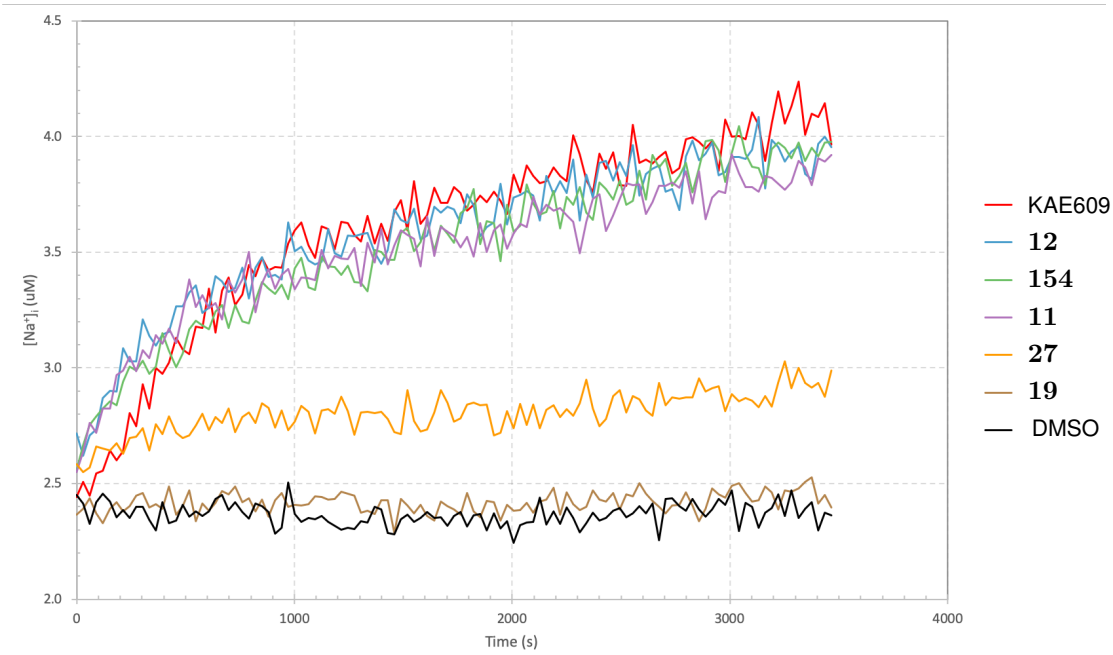

Figure 5.4: Representative graph of $[Na^+]_i$ over time for five test compounds compared with positive (KAE609) and negative (DMSO) controls. An increase in intracellular Na^+ concentration is consistent with inhibition of *Pf*ATP4.

For the positive control KAE609, the intracellular Na^+ concentration is seen to increase over time, consistent with inhibition of *Pf*ATP4. For the negative control DMSO, there is no change to the intracellular Na^+ concentration. Compounds **11**, **12** and **154** show an increase in $[Na^+]_i$ similar to the positive control, consistent with the high *in vitro* potencies of these compounds (0.14, 0.37 and 0.17 μM respectively). Compound **27** shows a moderate increase in $[Na^+]_i$ which is consistent with the lower activity (1.00 μM). Compound **19** shows no increase in $[Na^+]_i$ which is consistent with the compound being inactive (9.79 μM).

5.5.2 Assay for H^+ regulation

As the change in $[Na^+]_i$ is related to the change in intracellular H^+ concentration (i.e. pH_i) in the parasite, the above results were validated by performing the analogous H^+ ion regulation assay. Each compound was tested at a concentration of 1 μM, with the exception of select compounds which showed a notable difference in $[Na^+]_i$ when evaluated at 1 μM and 5 μM in the Na^+ ion regulation assay above. These were tested at a concentration of 5 μM instead. Positive (KAE609)

and negative (DMSO) controls were also used throughout the assay. This time, the parasites were loaded with 2',7'-bis(2-carboxyethyl)-5(6)-carboxyfluorescein (BCECF) dye which enabled the change in pH_i within the parasite to be monitored by fluorescence spectroscopy. Following the plateauing of the change in fluorescence caused by the test compound, an aliquot of concanamycin A was added and a rapid decrease in fluorescence was observed. In a similar manner to the Na^+ assay, two excitation wavelengths were used. At 490 nm, the measured fluorescence is pH sensitive whereas at 440 nm the fluorescence is pH insensitive. The ratio of the fluorescence intensities (490/440 nm) gives an indication of the pH_i over time (Figure 5.5).

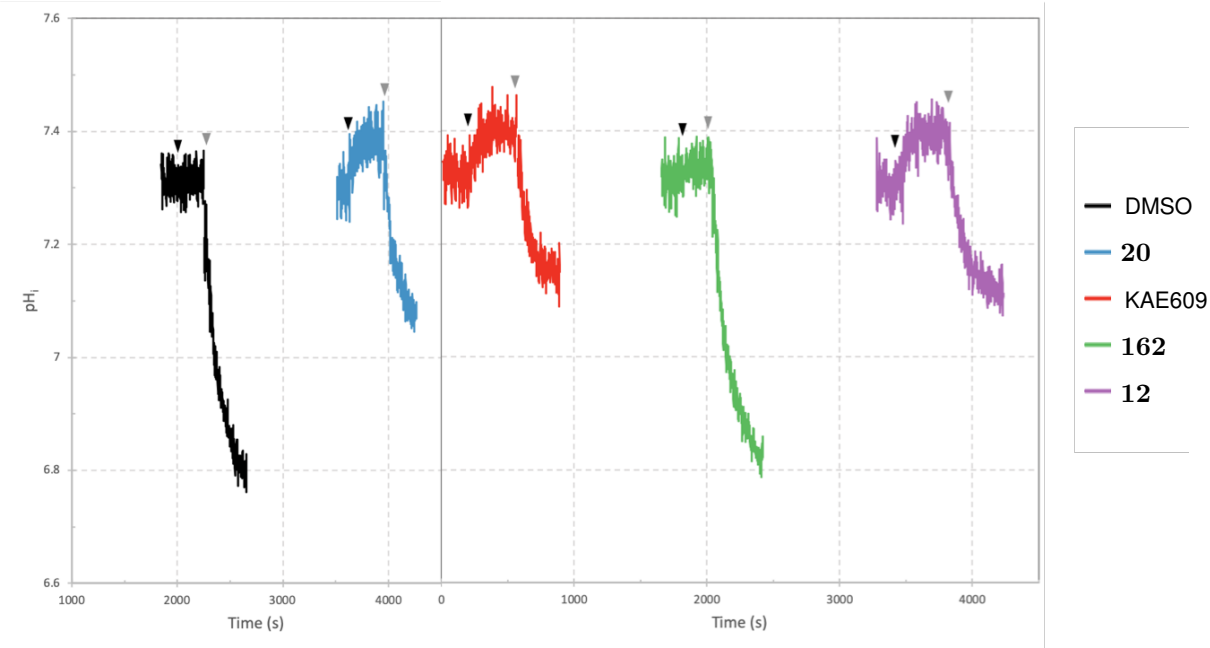

Figure 5.5: Representative graph of pH_i over time for three test compounds compared with positive (KAE609) and negative (DMSO) controls. A decrease in intracellular H^+ concentration is consistent with inhibition of *Pf*ATP4.

The black triangles (▼) indicate the time at which the compound of interest was added to the cuvette. An increase in pH_i following this time point (as for the KAE609 control and compounds **12** and **20**) indicates inhibition of the P-type transporter as the intracellular H^+ concentration decreases and the cell becomes more basic. This is consistent with the higher potencies for these two compounds (0.40 μM and 0.14 μM respectively). No increase in intracellular H^+ following this time point corresponds to no inhibition of *Pf*ATP4 (as for the DMSO control and compound **162**). This is consistent with the low potency of this compound (>10 μM). The grey triangles (▼) indicate the time at which concanamycin A was added to the cuvette. As concanamycin A is a known V-type H^+-ATPase inhibitor, following this time point, the pH_i should be seen to rapidly decrease as the intracellular environment becomes more acidic. This effect is more pronounced in cases where there is no inhibition of the Na^+-ATPase.

Since the information obtained from the Na^+ and H^+ regulation assays led to the same conclusion (i.e. inhibition of the P-type Na^+-ATPase can be identified by either an increase in $[Na^+]_i$ or an increase in pH), for simplicity the results discussed below refer to those obtained from the Na^+ regulation assay alone.

5.5.3 Further Validation of the MoA

All but one of the Frontrunner compounds showed the expected correlation between *in vitro* potency and ion regulation activity (Figure 5.6). The outlier compound **13** was shown to be quite potent *in vitro* (0.52 μM) but was found to be inactive in the ion regulation assay.

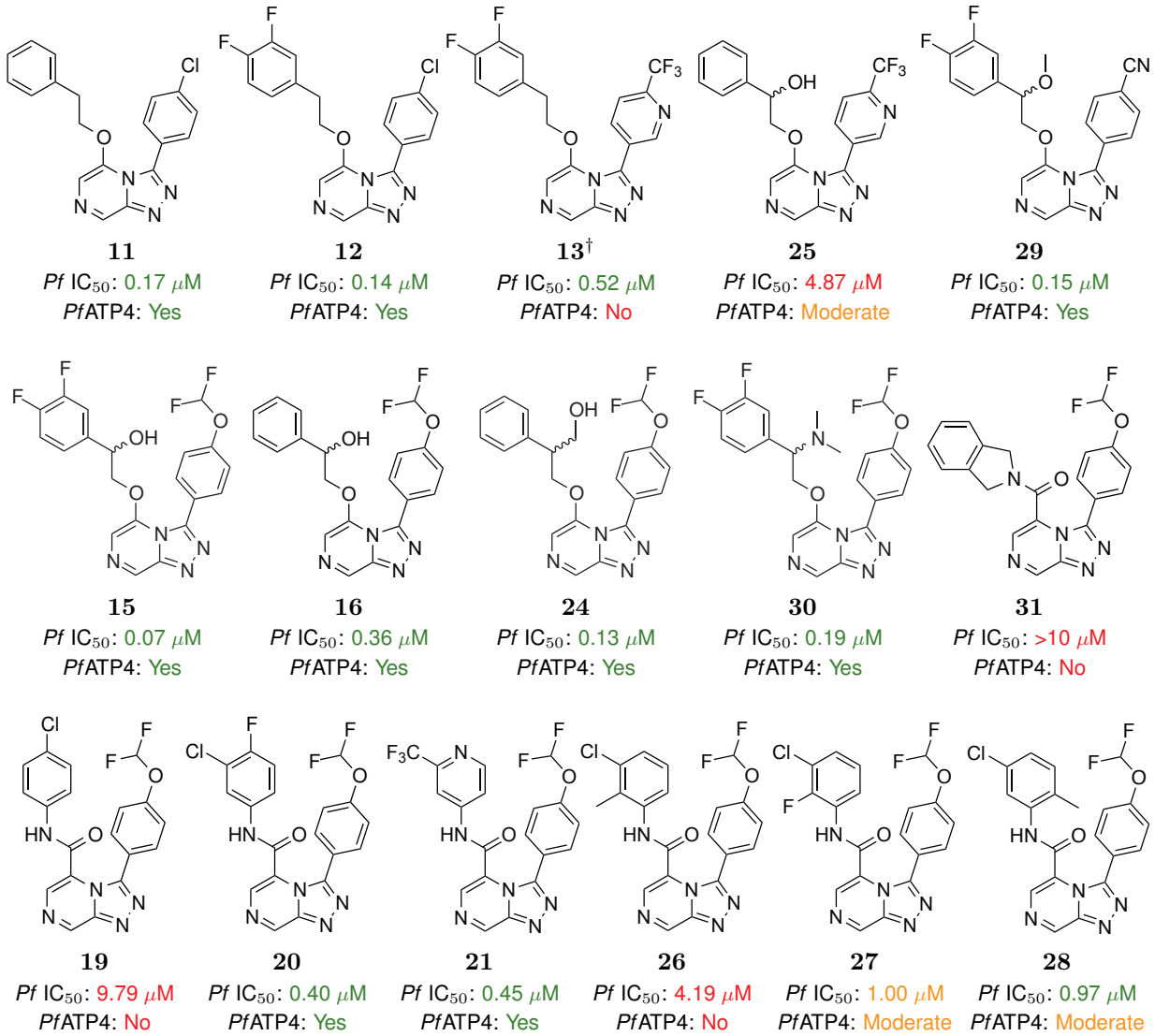

Figure 5.6: Evaluation of the Frontrunner compounds for *Pf*ATP4 activity. The majority of the results indicated good correlation between *in vitro* and ion regulation activity. †Outlier compound that did not show the expected correlation.

At the same time that the Frontrunners were being investigated, a set of compounds that were synthesised as part of Chapters 3 and 4 were evaluated for MoA as well (Figure 5.7). This more diverse range of compounds included a *tele*-substituted thioether **76**, oxidised thioethers **72** and **74**, ether-triazole-linked compounds **83**, **84** and **200** and northwest and northeast cubane bioisosteres **154**, **155**, **160** and **162**. Excellent correlation was seen among these compounds.

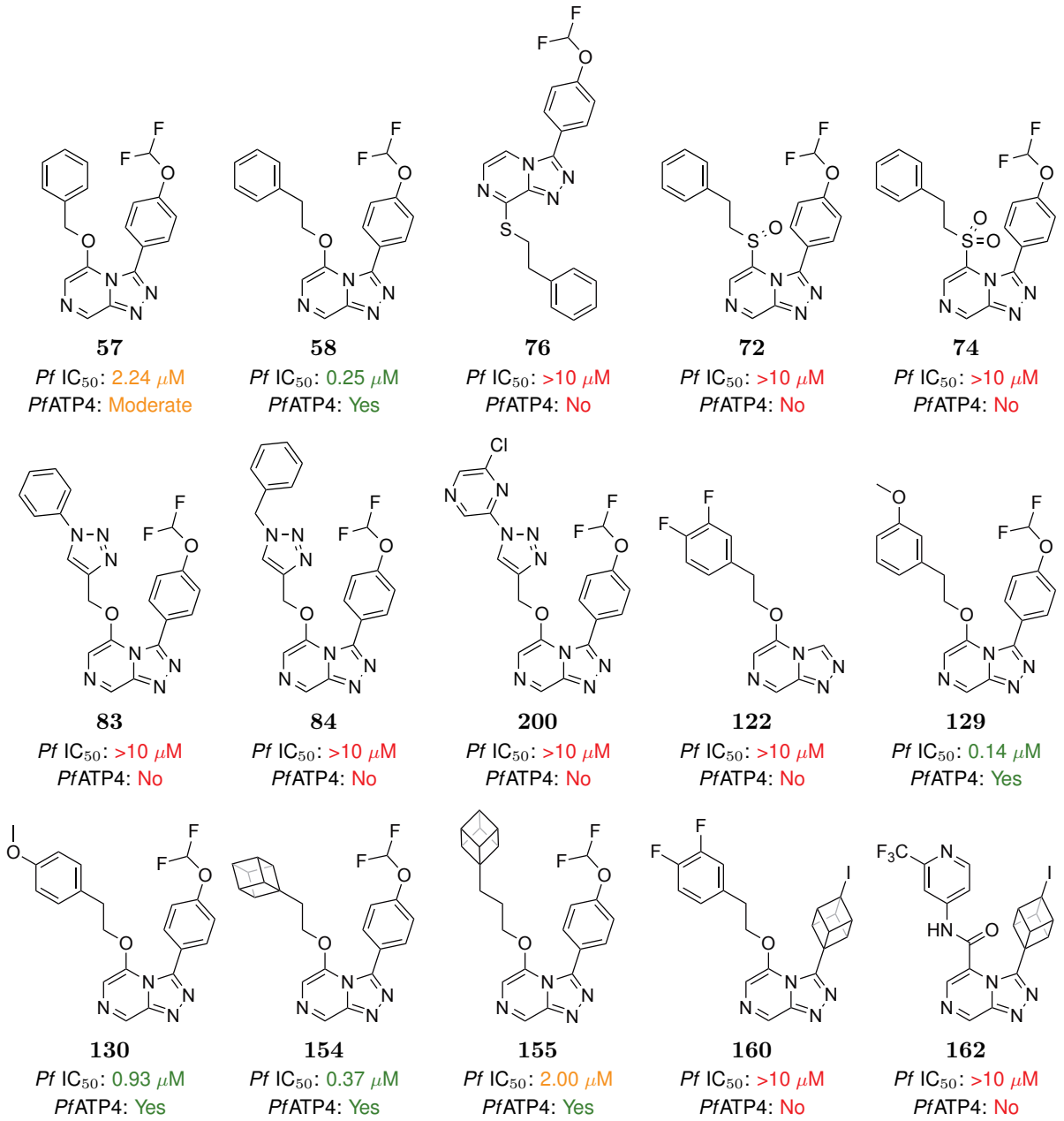

Figure 5.7: Evaluation of novel Series 4 compounds for *Pf*ATP4 activity. These results provide further evidence for *Pf*ATP4 as the Series 4 MoA.

Considering these combined results of compounds from 2013 to 2016, there is a high level of confidence that *Pf*ATP4 is the molecular target of the Series 4 triazolopyrazines, which adds to the already diverse range of chemotypes that have been found to target this protein. The potential of cross-resistance for Series 4 compounds was examined by the Kirk lab using three spiroindolone-

resistant parasites with known mutations in *pfatp4*.[308] It was found that the Series 4 compounds had reduced efficacy against all three resistant strains of *Pf*ATP4 compared to the parent Dd2 strain in a similar manner to KAE609, indicating cross-resistance with the spiroindolones. These results suggest the common mechanism of action, *Pf*ATP4, between these two structurally distinct classes of compounds. Even though some lead compounds from these chemotypes have progressed into clinical trials, this does not significantly impact the importance of Series 4 for this target. It remains the case that no molecule targeting *Pf*ATP4 has been approved for human use and, depending on the nature/extent of cross-resistance, should resistance develop for one of these lead compounds, it is possible that compounds from other classes will continue to be efficacious against *Pf*ATP4.

5.6 Establishing a Predictive Model for Series 4 *P. falciparum* Activity

Having gathered more data to support *Pf*ATP4 as the MoA for the Series 4 triazolopyrazines, it was thought appropriate to begin to develop a predictive model for *in vitro* activity to aid in the design of future Series 4 compounds, essentially to minimise the likelihood of spending resources on the synthesis of inactive Series 4 compounds. An initial attempt to develop a pharmacophore model was conducted by Dr. Murray Robertson in 2015 using known *Pf*ATP4 active and inactive compounds from the MMV Malaria Box.[309,310] Unfortunately, this model was unsuccessful, with the predictions correlating poorly with experimental potency results. It was suggested that this was due to overlapping binding sites and compound chirality not being taken into account.

In 2016, as a means to obtain a more predictive model for Series 4, a competition was established to better utilise the expertise of the OSM community.[311] This time, a more substantial list of active and inactive compounds was provided as a test set for the models (Test Set A: OSM Series 1 and 4 compounds, Test Set B: The Frontrunner compounds, Test Set C: Novel compounds synthesised in Chapters 3 and 4). There were ultimately six entrants and each created models based on different approaches (Table 5.2).

Table 5.2: Entrants and models created for the 2016 predictive modelling competition. Descriptions of the models were provided by each entrant.[312]

Entrant	Description of Model
Vito Spadavecchio	Created a library of common transformations as seen in the CHEMBL database of compounds (chembl_22_1), which amounted to ∼1.67 million compounds. After all of the SMIRKS/SMARTS patterns were extracted for all of the transformations, I was able to

	enumerate a new library of compounds based off of a lead Series 4 compound MMV669844. Next, this library was then applied to my MLP potency prediction algorithm; here, I used 'modelB.csv'; as my model, with the notable exception that all compounds in test set 'B' were labelled 'A', and thus included in on the training. The new compound potencies were then predicted; all compounds with submicromolar potency (e.g. $pIC_{50} < 0$) were then selected, and filtered for compounds with certain properties.
Ho Leung Ng	Tried to predict a binding site and the best fitting ligands: Used Cresset Forge to generate conformers and align with docking model of highly potent compounds, MMV670947, bound to homology model of *Pf*ATPase, pose #5, as described in my other notebook. That pose was used as the "Reference" for Forge. 3D alignments are generated with training set composed of Series 4 compounds, excluding those marked as Test Sets B and C, and those with log potency $\leq$5. The low potency compounds were excluded because assays did not provide precise values, only marking them "$<$ 5", for example. Test Set C was used as the "Prediction Set" by Forge.
Giovanni Cincilla	Developed several *Pf*ATP4 Ion Regulation Activity classification models using different strategies for modeling set sampling, different machine learning methods and different descriptors. Submitted the best performing one with which we achieved good general results: balanced accuracy (for actives) = 0.77, sensitivity (for actives) = 0.833, AUC (for actives) = 0.810.
James McCulloch	The final model is a meta classifier which uses the probability maps of upstream classifiers to produce an optimal composite classification. Each predictive model based on fingerprints or another SMILE based description vector such as DRAGON brings a certain amount of predictive power to the task of assessing likely molecular activity against *Pf*ATP4. The meta classifier combines the predictive power of each model in an optimal way to produce a more predictive composite model. It does this by taking as it's input the probability maps (the outputs) of other classifiers.

Davy Guan	A semi-supervised machine learning paradigm adapted from the machine learning algorithms implemented in the DeepChem project was used to construct QSAR models from both the labelled and unlabelled datasets. All molecules were featurised by either Graph convolutional techniques or with 1024 Bit ECFP4 descriptors. A 80/10/10 train, test, internal validation was used to split the Training dataset for model construction and internal validation before testing on the external validation dataset.
Jonathan Silva	Gradient boosting model (using xgboost) to predict actives and nonactives for the *Pf*ATP4 ion regulation assay. Data sampled to include only those in the vicinity of OSM S4 compounds.

Each model was evaluated for its ability to predict the activities of compounds against *Pf*ATP4 from a test set from the MMV Pathogen Box. These compounds had been evaluated by the Kirk lab, but the results were under embargo at the time.[313] The entrants were then provided with the molecular identifiers (e.g. SMILES strings) and asked to rank the compounds from most to least active. A panel of four judges (Prof. Matthew Todd, Dr. Alice Motion, Dr. Murray Robertson and Prof. Alexander Tropsha) then compared the top twenty predicted compounds from each model with the experimental results obtained from the Kirk lab to determine the winners of the competition. The end result was a tie for first place between the models developed by James McCulloch and Ho Leung Ng. Both were able to correctly predict two active compounds within their top twenty rankings and one active compound just outside the top twenty.[314]

Even though the resulting models from this initial round were not highly predictive, the success of the competition was demonstrated by eliciting six new solutions from the community, with each entrant using different approaches. Importantly, they all worked in an open manner and all data was shared.[312] Based on this, it was decided that a second round of the competition would be launched in 2019. With the publishing of the Kirk Pathogen Box results, this dataset could now be used for the improvement and development of new models, in addition to the existing OSM dataset. These new models could then be used to aid the synthetic design of Series 4 compounds, as well as screen libraries of commercially available compounds in order to identify new chemical scaffolds. This second round will be funded by a 2019 grant that will enable companies specialising in AI and machine learning methods to take part. These inputs were not available during the first round of the competition so the resulting models should provide new and interesting results when compared to those arising from the more traditional modelling methods from round one.

5.7 Concluding Remarks

The Frontrunner compounds were evaluated for ion regulation activity in order to validate the inherited results which suggested this to be the MoA for the Series 4 triazolopyrazines. Encouragingly, excellent correlation was seen between the *in vitro* potencies of the Frontrunner compounds and their ability to disrupt ion regulation. A more diverse set of compounds synthesised in Chapters 3 and 4 was also evaluated in this assay with the results also showing excellent correlation. Based on these combined data points, there is a high level of confidence that the MoA for Series 4 is through *Pf*ATP4 inhibition, adding to the already varied chemotypes that have been found against this target.

In order to design future Series 4 compounds more effectively, a competition was launched in 2016 with the goal of developing predictive models for *in vitro* activity. While the models from this first competition were found to perform better than the initial attempt made by Murray Robertson in 2015, they were still not highly predictive. A follow-up competition was planned to be launched in 2019, leveraging an expanded dataset of compounds which would be used to develop new models and improve the existing ones.

6. hERG Studies

This chapter covers the hERG studies performed on the Series 4 triazolopyrazines. The existing hERG dataset on Series 4 was examined with subsequent investigations made for how to reduce the hERG binding. With these ideas in mind, a series of compounds designed to minimise this binding were synthesised. The *in vitro* biological evaluation of these compounds is discussed, as well as the evaluation of hERG, metabolic and physicochemical properties.

6.1 hERG

The human ether-à-go-go related gene (hERG) codes for the $K_v11.1$ protein, which is a subunit of a potassium ion channel. There is often ambiguity with the nomenclature associated with these ion channels, but in most contexts the gene itself is commonly referred to as *hERG* (or *KCNH2* according to newer nomenclature), while the protein is referred to as hERG (or $K_v11.1$ according to newer nomenclature).[315] Nevertheless, this is one of the key ion channel proteins responsible for regulating the electrical activity of the heart through the efflux of K^+ ions from the heart muscle cells. This efflux of ions creates a change in voltage across the cell membrane (know as the cardiac action potential) which can be recorded and visualised as an electrocardiogram (ECG). The peaks and troughs, signified by letters P to T, represent the depolarisation and repolarisation of the cardiac action potential. The P wave represents the depolarisation of the atria, while the QRS complex and T wave respectively represent the depolarisation and repolarisation of the ventricles. The major risk associated with inhibition of this channel (either by mutation or by drug interaction) is the increased risk of irregular heartbeats, most commonly *torsades de pointes* (a specific form of polymorphic ventricular tachycardia), which can ultimately lead to cardiac arrest and sudden death. When viewed on an ECG, these irregular heartbeats are signified by the prolongation of the QT interval (Figure 6.1), which is a measure of the time taken for the depolarisation and repolarisation of the ventricles of the lower heart chambers, and is known as long QT syndrome (LQTS).[316] The increased time for repolarisation is mainly caused by inhibition of the rapid delayed rectified potassium current (I_K) which exports K^+ from the cells. A number of key reviews on this area have been published in recent years.[317–320]

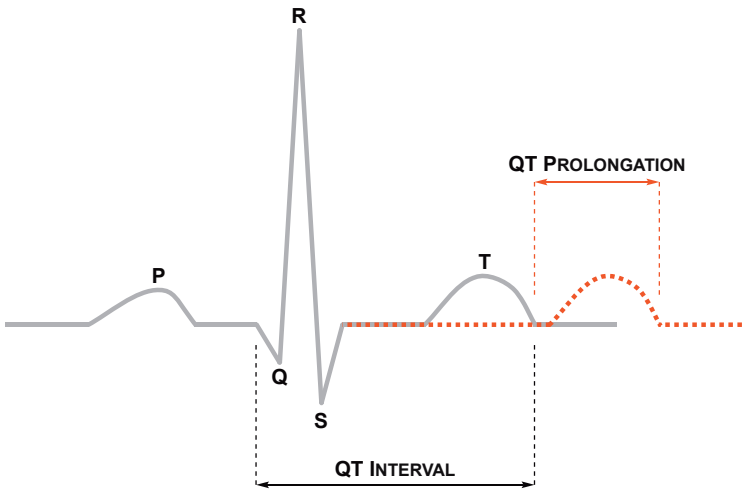

Figure 6.1: Electrocardiogram showing the prolongation of the QT interval as a result of hERG inhibition. This results in irregular heartbeats which can lead to cardiac arrest.

It is noteworthy that some drugs that were not designed for the treatment of arrhythmia have been found to block hERG, leading to QT prolongation. A prominent example is that of terfenadine. This antihistamine drug was first brought to market in 1982, but after cases of deaths as a result of taking terfenadine, it was found that it was blocking the hERG channel. As a result, it was subsequently withdrawn from commercial availability in 1997 (Figure 6.2).[321,322] Interestingly, the carboxylate derivative fexofenadine, which was first marketed in 1996, was found to not block hERG channels *in vitro*[323] but an isolated case was reported in 1999 where a patient taking the drug exhibited QT prolongation. A subsequent study indicated, however, that the QT prolongation was not due to interactions between fexofenadine and the hERG channels. Other examples of marketed dugs that saw withdrawals due to cases of hERG related cardiac issues include sertindole (antipsychotic)[324], cisapride (gastrointestinal prokinetic agent)[325] and astemizole (antihistaminic)[326], withdrawn in 1998, 2002 and 2003 respectively. Due to these concerns, and their associated expense, high-throughput screens have been developed to identify these potential problems at an earlier stage in the development process.[327]

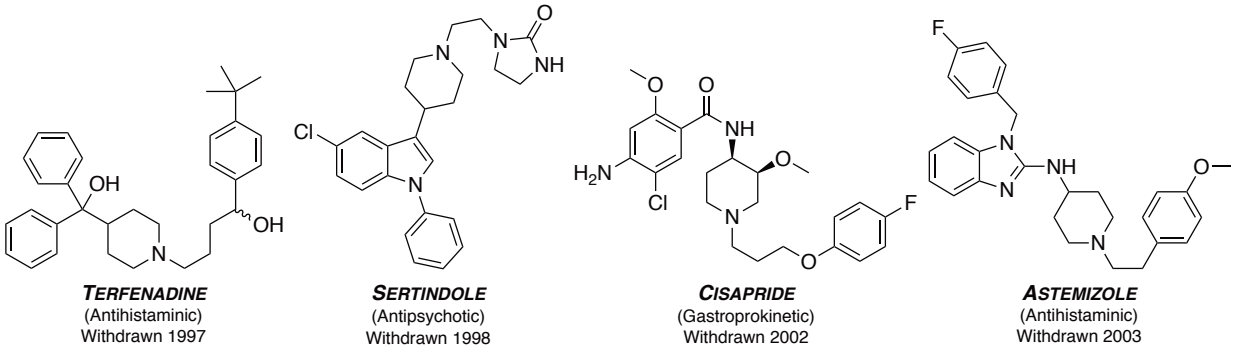

Figure 6.2: Drugs brought to market that were later found to inhibit the hERG ion channel. Due to these safety concerns the drugs were withdrawn from market.

For many years, the structure of the hERG channel remained unknown due to the difficulties associated with crystallising the complex structure. More recently however, Wang and MacKinnon were able to utilise cryo-electron microscopy to obtain a near-atomic resolution structure of the hERG channel (Figure 6.3).[328] The development of this technique was awarded the 2017 Nobel Prize in Chemistry.[329]

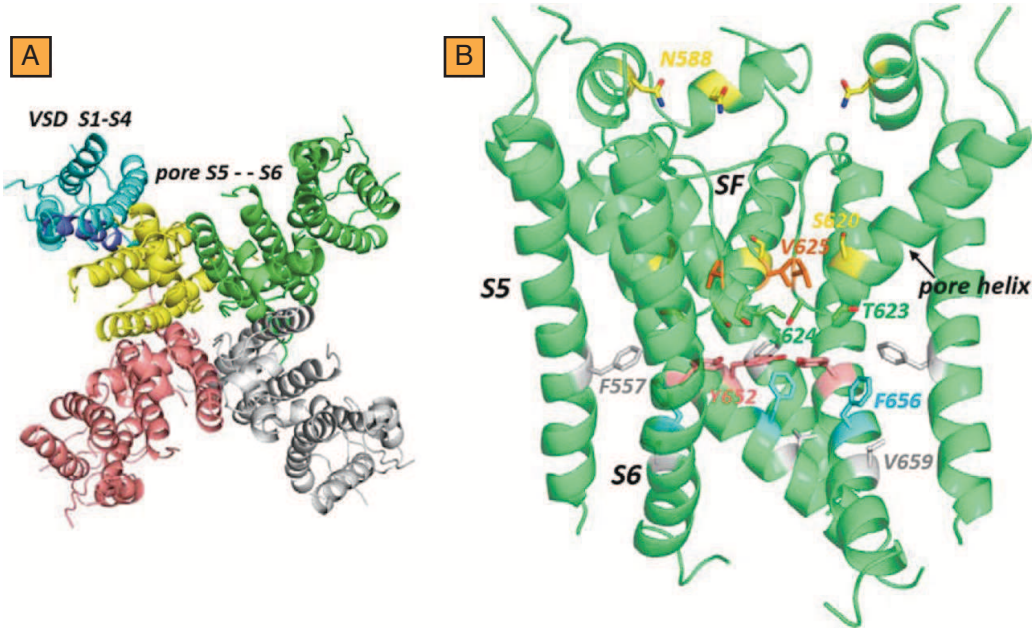

Figure 6.3: Open pore cryo-EM structure determined by Wang and MacKinnon[328] and reported by Helliwell and co-workers.[330] (A) Top-down view of the arrangement of subunits in the hERG tetramer. (B) Side-view of the pore domain. Figure license CC BY from Helliwell and co-workers, 2018.

6.2 Strategies to Reduce hERG Binding

With so many cases of hERG related withdrawals of already marketed drugs, the determination of potential hERG binding activity has become a crucial step in the preclinical stage of drug development. Studies have been conducted to better predict activity, with the following motifs identified to be common among hERG binders:[331]

- A positively ionisable, basic amine (pK_a >7.3)
- A hydrophobic or lipophilic structure (cLogP >3.7)
- The absence of negatively ionisable groups
- The absence of oxygen H-bond acceptors

Other chemical motifs, such as 1-(furan-2-carbonyl)piperazine, diarylthioether, arylchloride and sulfonamide have also been associated with hERG binding activity (Figure 6.4).[332,333]

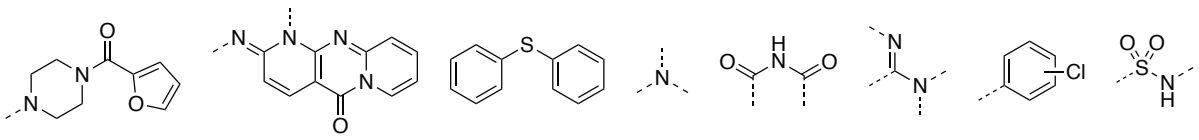

Figure 6.4: Additional substructures that have been suggested to cause hERG binding. These include common motifs such as tertiary amines, amidines, arylchlorides and sulfonamides.

With these features in mind, a number of general molecular features have been put forward that are said to decrease hERG binding activity (reducing the basicity of the amine, reducing the lipophilicity of the structure, introducing an acid moiety or introducing oxygen-centered H-bond acceptors).[334,335] The first three of these methods are described below. The hERG values are given as the negative log of the IC_{50} value in molar (pIC_{50}). It should be noted that hERG assays can provide different results based on the protocols used, and direct comparisons may not always be accurate. Methods are being developed to enable better comparisons between hERG assays.[336]

6.2.1 Reducing pK_a

Studies have suggested that hERG activity may be brought about by π–cation interactions between basic amines, common in many hERG blockers, and the aromatic residues within the hERG channel.[337,338] As these amines are typically protonated at physiological pH, reducing the pK_a of the amine would in turn lower the degree of π–cation interactions that can take place (Figure 6.5). While working on a series of 5-HT_{2A} antagonists, Fletcher and co-workers exploited pK_a to reduce hERG binding for their compounds.[339] While the introduction of a ketone at the β-position of the amine in **201a** led to a reduction of the pK_a and the hERG activity (**201b**), it was unfortunately found that this change led to degradation of the compound in polar solvents. In another example, where a series of potent indolylindazoylmaleimide-base protein kinase C-β (PKC-β) inhibitors was found to have hERG activity, it was identified that the basic tertiary alkylamine (in **202a**, essential for maintaining a high potency) was also responsible for the unwanted hERG affinity. Replacing this with a less basic morpholine moiety (**202b**) led to a compound with slightly less potent activity against the parent target, but a significantly reduced hERG affinity. In addition to these π–cation interactions, the related π–π and CH–π interactions have also been implicated in hERG binding.[340]

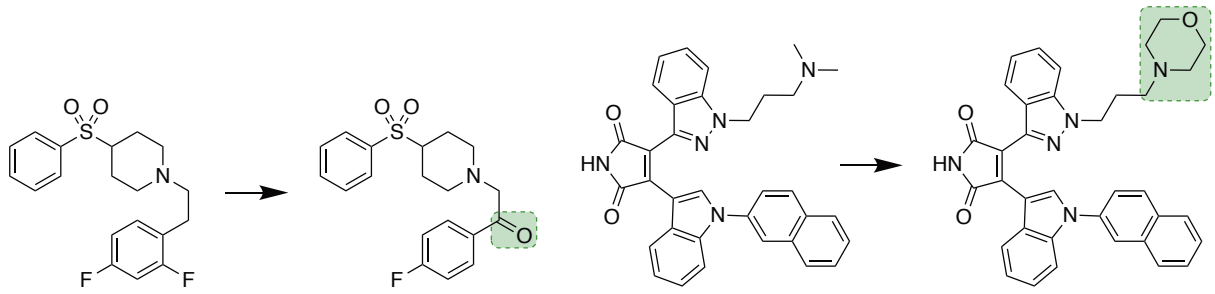

201a
hERG: 6.00
pK_a: 7.52

201b
hERG: 5.17
pK_a: 5.25

202a
hERG: 7.60
pK_a: 9.41

202b
hERG: 6.07
pK_a: 7.45

Figure 6.5: The strategy of reducing the pK_a of basic nitrogen atoms. Literature examples where modulating the pK_a led to decreased hERG affinity.

6.2.2 Reducing logP

Changing a compound's lipophilicity is a common method in medicinal chemistry for modulating key biological properties such as solubility and metabolic stability. It has been shown that this change can affect the hERG activity of the compound as well (Figure 6.6). When investigating a series of indolylquinolinone-based vascular endothelial growth factor receptor 2 (VEGFR-2) inhibitors, Fraley and co-workers encountered issues with hERG activity with their compounds.[341] Reducing lipophilicity by replacing the phenylether side-chain in **203a** (cLogP 3.47) with a piperazine amide group to give **203b** (cLogP 2.06) led to a reduction in hERG activity. In another example from Fletcher and co-workers, investigations into a series of 5-HT$_{2A}$ antagonists, the hERG activity was minimised by reducing the cLogP of their compounds.[339] In one case from this study, replacement of the chlorine atom in **204a** with a primary carboxamide (**204b**) reduced the lipophilicity and the hERG binding activity. The reduction in hERG activity from decreasing lipophilicity is said to be a result of the destabilisation of the interactions within a lipophilic ligand binding site in the hERG protein.[337,342] Modification of the logP may be considered as an extension to modification of the pK_a as reducing the basicity often alters the polarity of a compound too.

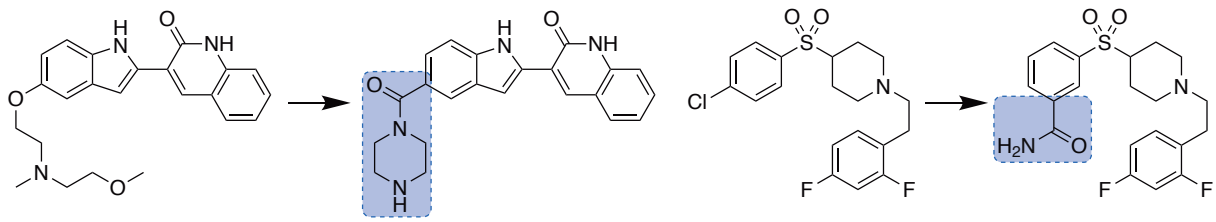

203a
hERG: 5.72
cLogP: 3.47

203b
hERG: <5.00
cLogP: 2.06

204a
hERG: 6.82
cLogP: 3.78

204b
hERG: 5.15
cLogP: 1.85

Figure 6.6: Reduction of compound lipophilicity (cLogP). Literature examples where modulating the cLogP led to decreased hERG affinity. This may be linked to changes to the pK_a as well.

6.2.3 Introducing Zwitterions/Acid Moieties

A compound's ability to create interactions within the hERG binding site can be prevented by inhibiting its ability to access this site in the first place, which can be achieved by limiting its membrane permeability through the introduction of zwitterionic moieties. As many drugs contain at least one nitrogen atom, a zwitterion can be formed by incorporating a carboxylic acid into the structure (Figure 6.7). As mentioned above, while terfenadine (**205a**) has been found to be a potent hERG blocker its carboxylate (and main metabolite), fexofenadine (**205b**), has been shown to have significantly reduced hERG affinity.[343] Introduction of a carboxylic acid to a human β-tryptase inhibitor (**206a**) led to a reduction of hERG activity (**206b**),[344] though with an accompanying large decrease in potency towards human β-tryptase. In another example, the dipeptidyl peptidase IV (DPPIV) inhibitor **207a** exhibited a 16-fold reduction in hERG activity when a carboxylic acid was introduced (**207b**), though this came at a cost to oral bioavailability (F).[345] Clearly then, while this strategy has been demonstrated to be effective in reducing hERG binding, the presence of an acid moiety may impact the overall potency of the compound or cause a reduction in oral bioavailability. A detailed investigation into the impact of introducing a carboxylic acid has been performed by Zhu and co-workers.[346] Additionally, a 2013 review analysed the ChEMBL database for hERG content and found that of the seven cases in which there was a transformation from H $\rightarrow$ CO_2H, all either reduced, or had no impact on, hERG binding. It was also noted that carboxylic acid-containing drugs were relatively uncommon.[347]

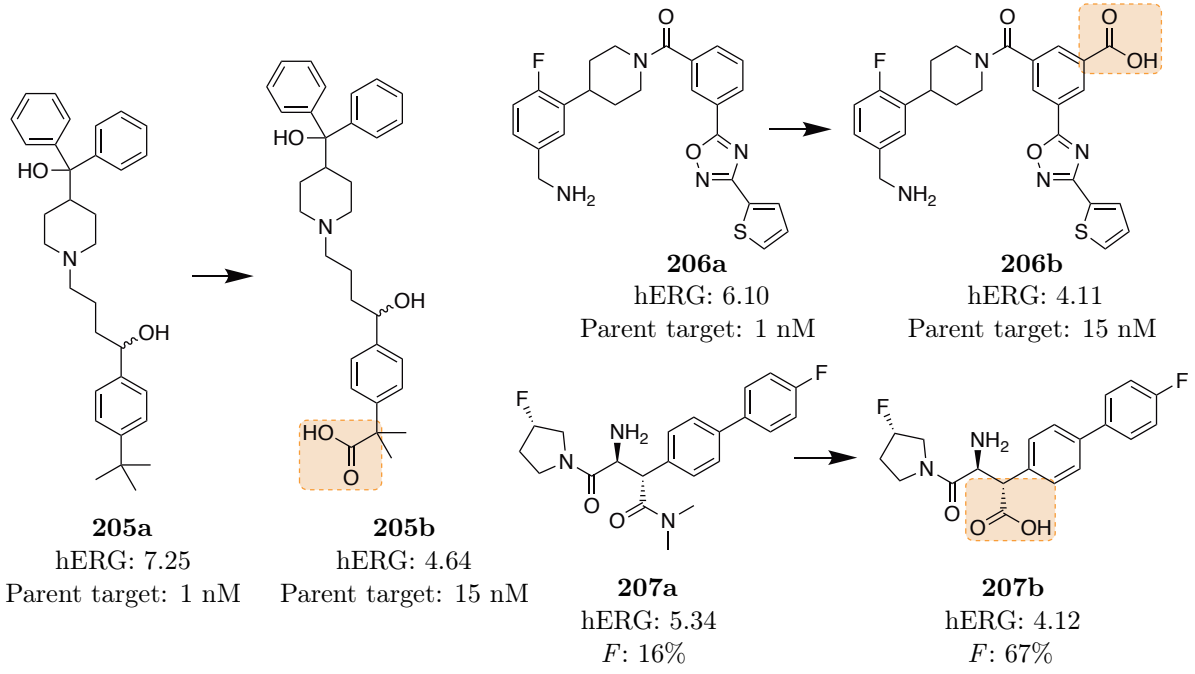

205a
hERG: 7.25
Parent target: 1 nM

205b
hERG: 4.64
Parent target: 15 nM

206a
hERG: 6.10
Parent target: 1 nM

206b
hERG: 4.11
Parent target: 15 nM

207a
hERG: 5.34
F: 16%

207b
hERG: 4.12
F: 67%

Figure 6.7: Incorporation of a carboxylic acid group. Literature examples of suppression of hERG binding affinity upon the inclusion of a carboxylic acid moiety.

6.3 Series 4 hERG Data

When the series was first inherited, two compounds (**MMV669844** and **MMV670944**) had been evaluated for hERG activity (Figure 6.8).[348] The hERG pIC_{50} values are classified as low (<5.00), moderate (5.00–5.20) or high (>5.20). While both compounds showed good potencies *in vitro*, they were found to have relatively high hERG affinity that prompted further investigation.

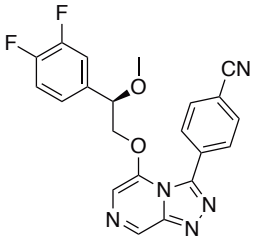

MMV669844
in vitro: 0.04 μM
hERG: 5.20

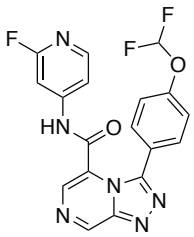

MMV670944
in vitro: 0.14 μM
hERG: 5.60

Figure 6.8: Two inherited compounds which had associated hERG data. Both were found to have undesirable hERG affinity.

A number of additional compounds were subsequently evaluated for hERG activity to determine whether this was an issue for the series as a whole (Figure 6.9).[349] Encouragingly, many of the compounds showed a much weaker hERG affinity.

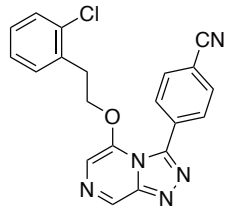

MMV639725
in vitro: 0.31 μM
hERG: <4.48

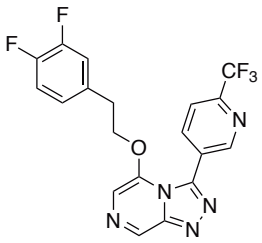

MMV670936
in vitro: 0.26 μM
hERG: <4.48

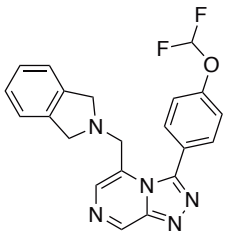

MMV669848
in vitro: 0.11 μM
hERG: <4.53

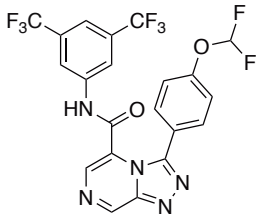

MMV675719
in vitro: 0.31 μM
hERG: 5.24

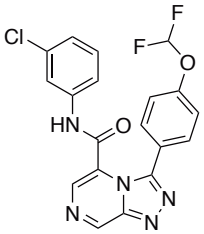

MMV669542
in vitro: 0.24 μM
hERG: 4.89

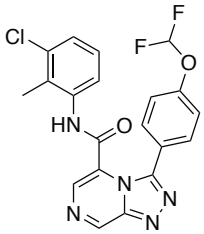

MMV675718
in vitro: >5 μM
hERG: 5.12

Figure 6.9: A further set of six compounds evaluated for hERG activity. These compounds were found to have weaker hERG affinity than the original two compounds.

Based on the differences among the ether-linked compounds above, it appears that the hERG activity seen with **MMV669844** could be attributed to the benzylic methoxy group. For the amide-linked compounds, it can be seen that changes to the pendant phenyl group have an influence on the hERG binding. It is likely that the presence of the pyridine nitrogen in **MMV670944** results in more π-cation interactions which translate to increased hERG binding. The strong hERG affinity seen with **MMV675719** could be explained by the increased lipophilicity from the two CF_3 groups. Similarly, for **MMV675718**, the additional methyl group (compared to **MMV669542**) increases the lipophilicity and hERG activity as well.

Three additional compounds that were synthesised in Chapter 3 (phenylalaninol compound **119**) and Chapter 4 (cubane and carborane compounds **154** and **192**) were evaluated for hERG activity in the hERG assay (Figure 6.10). All three compounds exhibited relatively strong hERG affinity.

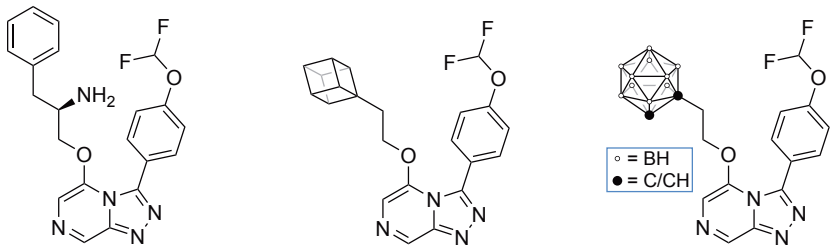

119
in vitro: 17 μM
hERG: 5.12

154
in vitro: 0.37 μM
hERG: 5.37

192
in vitro: 0.05 μM
hERG: 5.44

Figure 6.10: Three compounds synthesised throughout this thesis were evaluated. All were found to have relatively strong hERG affinity.

It is noted that while the hERG assays used to evaluate these different sets of Series 4 compounds did not use the exact same protocols, the values obtained give a rough indication of the activity which can be compared. Having seen such varied hERG data for Series 4, a targeted effort to minimise hERG binding was pursued with the strategies described above in mind.

6.4 The hERG Evador

In considering the three main methods to reduce hERG affinity, attempting to alter the pK_a of the nitrogens in the triazolopyrazine core was thought not to be a desirable strategy as it is known for the series as a whole that modifications to the triazolopyrazine core lead to a loss in *in vitro* potency. Similarly, the more general strategy of modifying the cLogP of the compound has been broadly explored as part of SAR studies and such changes (e.g. introducing OH or NH_2 groups) tend to impact dramatically the potency of the resulting compounds. Therefore, it was

decided to pursue the more focused strategy of introducing a zwitterionic species, specifically at the benzylic position of compound **58** to give compound **208** (Figure 6.11). In addition to the potential reduction in hERG activity, installing the carboxylic acid moiety at this position (rather than on the pendant phenyl ring) would have the additional benefit of blocking this metabolically labile site as well as increasing the overall solubility. This compound was named the "hERG Evador".[350,351] The synthesis of this compound would be based around the racemate, with the possibility of the two enantiomers being separated should the hERG Evador show potent *in vitro* activity.

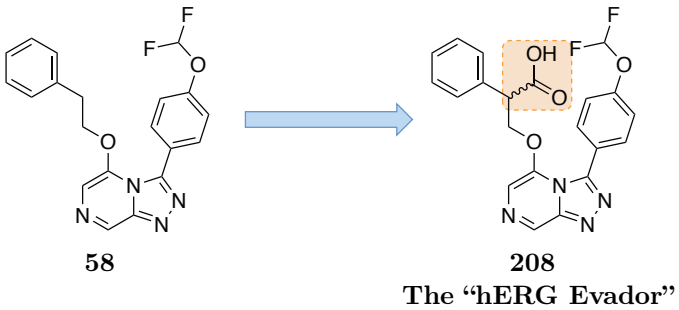

Figure 6.11: Introduction of a carboxylic acid into a Series 4 compound to minimise hERG binding. The ideal place of installation was thought to be at the benzylic position.

6.4.1 Synthesis of the "hERG Evador"

Initial studies towards the synthesis of the hERG Evador were conducted by students at Haverford College (Pennsylvania, USA) under the supervision of Robert Broadrup.[351,352] It was thought that the molecule could be readily synthesised by direct coupling of the commercially available tropic acid with TP core **44** (Figure 6.12). Interestingly, when this was performed, rather than isolating the desired compound **208**, a significant amount of an unknown by-product was isolated. This product, **209**, was later identified to be the result of displacement of the chlorine atom on the TP core with a hydroxy group (possibly due to intramolecular cyclisation of tropic acid).[353] Unfortunately, due to time constraints, the students were unable to pursue this further.

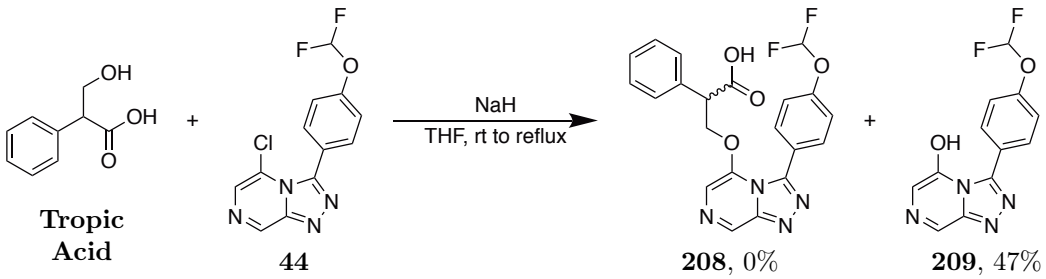

Figure 6.12: Direct nucleophilic displacement with tropic acid performed by students at Haverford College. While the desired product was not synthesised, a significant amount of the hydroxy displaced compound **209** was isolated.

It was thought that the issues with the coupling reaction could be avoided by protecting tropic acid's carboxylic acid as an ester, and converting it back to the acid after the coupling step. Accordingly, tropic acid was protected by esterification to give methyl ester **210** (Figure 6.13). Coupling was then attempted with TP core **44**, but no desired product was seen. The only isolated product (other than recovered starting materials) was identified to be the TP core in which the chlorine atom had been displaced by a methoxy group (**211**). This is likely to have resulted from hydrolysis of the ester under the basic reaction conditions and subsequent displacement of the chlorine atom by the methanol by-product.

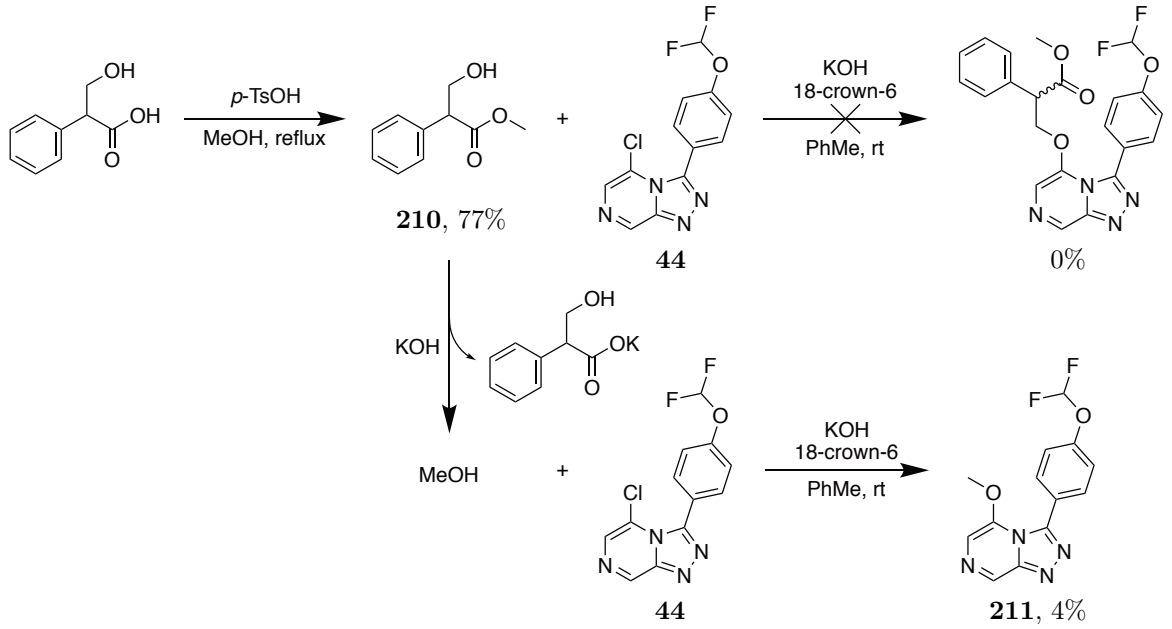

Figure 6.13: Attempted coupling of esterified tropic acid. The desired product was not seen, but a small amount of methoxy displacement product **211** was isolated.

With these results in mind, it was envisioned that the benzylic carboxylic acid could be accessed through a lengthier route *via* oxidation of a compound possessing a benzylic primary alcohol (in fact, Frontrunner compound **24**, Figure 6.14). The nucleophilic coupling partner for this compound could be accessed in a manner analogous to that used for the synthesis of the benzylic ketone compound **105** (described in Chapter 3, Figure 3.21), but with tropic acid as the starting material. To demonstrate this route, tropic acid was first esterified in EtOH to give the ethyl ester **212** in excellent yield (Figure 6.14). The primary alcohol was protected with a THP group (**213**) and the ester reduced with $LiAlH_4$ to give the desired alcohol nucleophile **214** in 22% yield. This was then coupled with TP core **44** to give the protected intermediate **215** in good yield. Finally, the THP group was removed with copper chloride to afford the benzylic primary alcohol compound **24** in good yield.

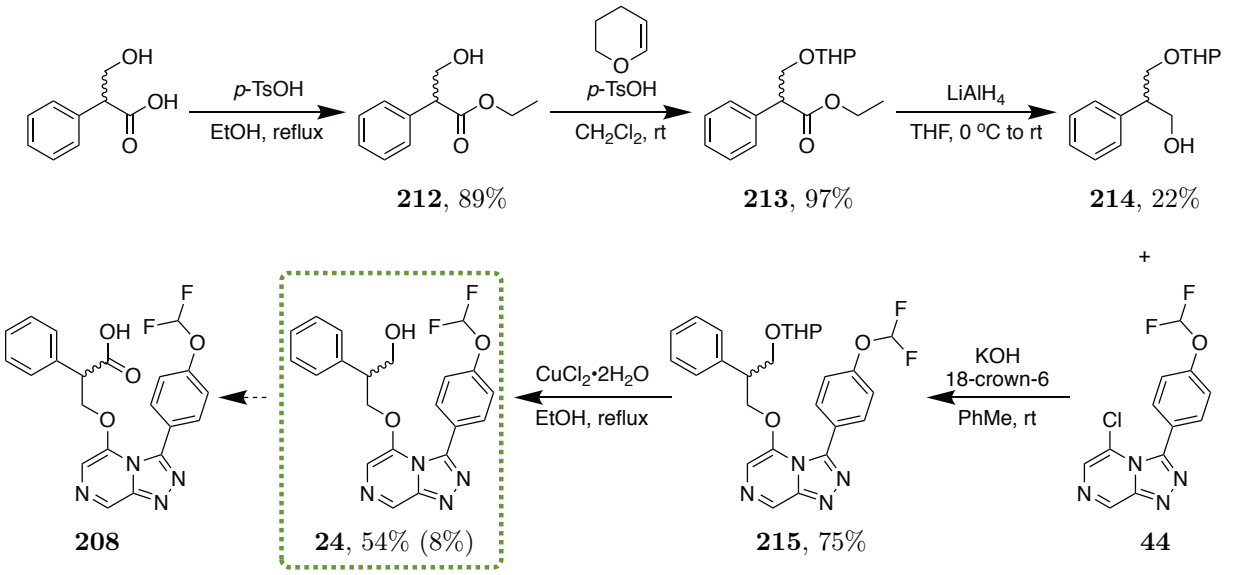

Figure 6.14: Synthesis of the benzylic primary alcohol compound 24 *en route* to the hERG Evador 208. The desired nucleophile was synthesised in three steps from tropic acid. Coupling with TP core **44** and THP deprotection gave the desired product. Final yield in brackets is the overall yield of the worst longest linear sequence starting from the nucleophile synthesis.

While this route provided the desired benzylic alcohol precursor compound **24** in 8% overall yield, it was thought that this compound could be obtained in a more step efficient manner, namely by direct coupling of the unprotected diol **216** with the TP core **44** (Figure 6.15). This would eliminate the steps required for protection and deprotection of the benzylic alcohol group. As such, reduction of the commercially available diethyl phenylmalonate with $LiAlH_4$ gave 2-phenylpropane-1,3-diol (**216**) in moderate yield. While coupling under KOH conditions proceeded to give the desired product, the yield was only 3% after two purifications of the final product by column chromatography. Approximately 46% of the crude material from this final reaction was identified to be a mixture of starting materials. It was later found that performing the same coupling reaction under *t*-BuOK conditions led to an improvement in overall yield (15%), however there was still a ∼40% mixture of starting materials remaining. It is evident from these reactions that, even though the direct coupling of the unprotected diol does give the desired product in a more step efficient manner, both reactions are still far from optimal.

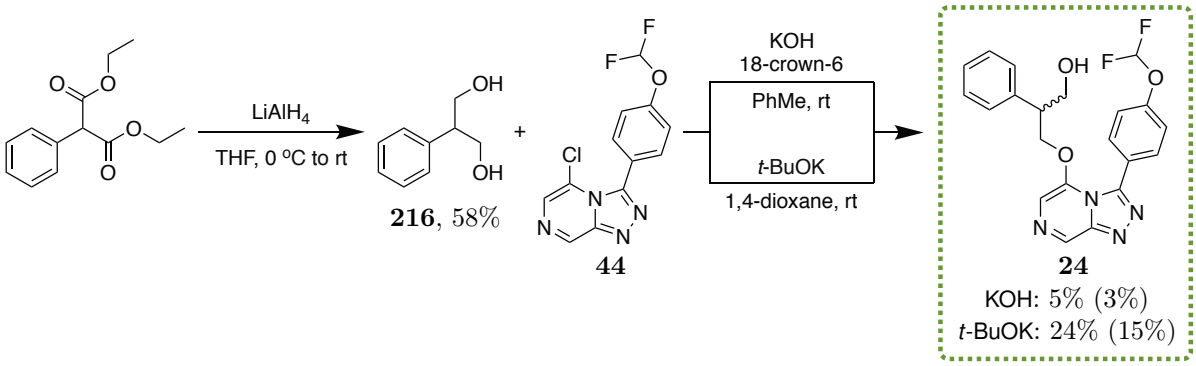

Figure 6.15: Alternative synthesis of the benzylic primary alcohol compound 24. Reduction of diethyl phenylmalonate, followed by direct coupling of the unprotected diol proceeded, albeit in lower yields. Final yield in brackets is the overall yield of the longest linear sequence starting from the core synthesis.

Nevertheless, with this alcohol intermediate in hand, attempts to oxidise the alcohol to the carboxylic acid were made. A survey of the literature for oxidations on analogous systems revealed a number of possible reaction conditions. A 1991 paper detailing the improved synthesis of 5-methylpyrazine-2-carboxylic acid described the transformation of 5-methylpyrazine-2-methanol to 5-methylpyrazine-2-carboxylic acid using potassium permanaganate (A, Figure 6.16).[354] Similarly, the transformation of 2-pyridine propanol to 3-(pyridin-2-yl)propanoic acid has been shown to proceed under similar conditions.[355] Other methods have utilised CrO_3 as a mixture with either H_5IO_6 (B)[356] or H_2SO_4 (C)[357,358].

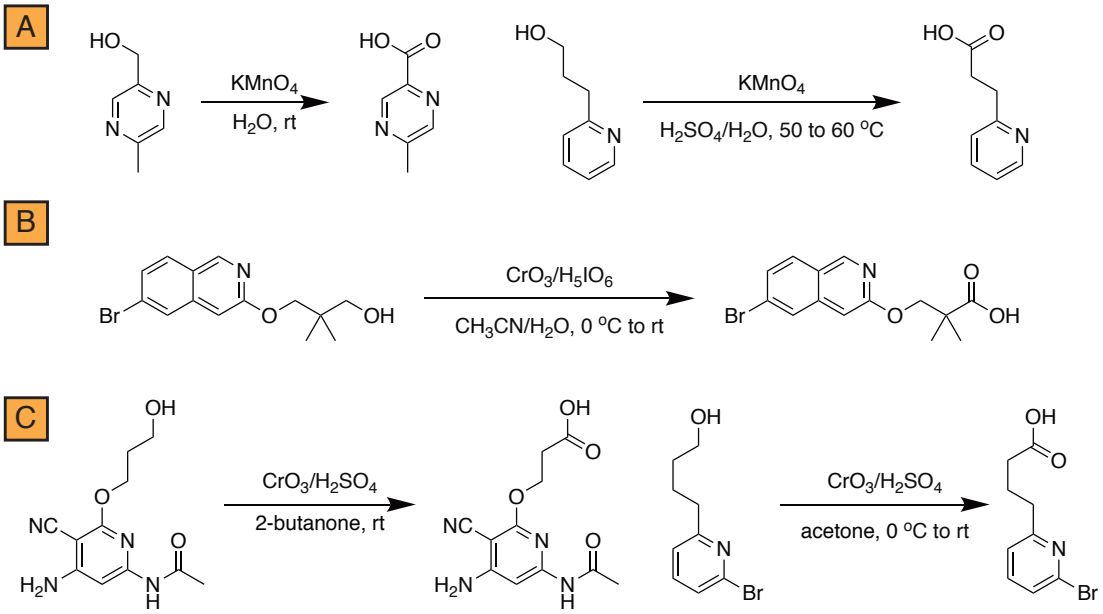

Figure 6.16: Literature examples for the oxidation of alcohols to carboxylic acids in systems containing a nitrogen heterocycle. Such oxidations can be performed with aqueous $KMnO_4$ solutions (A) or mixtures of CrO_3 with H_5IO_6 (B) or H_2SO_4 (C).

The oxidation of alcohol **24** to acid **208** was initially performed using the two $KMnO_4$ conditions shown above. Both procedures appeared to give the desired oxidised product as indicated by TLC, however isolation of the pure product was overall unsuccessful (Figure 6.17). As an alternative procedure, the oxidation was performed with a mixture of CrO_3 and H_2SO_4 (commonly known as the Jones oxidation). This time, the desired product was successfully isolated in 25% yield after two purifications by column chromatography.

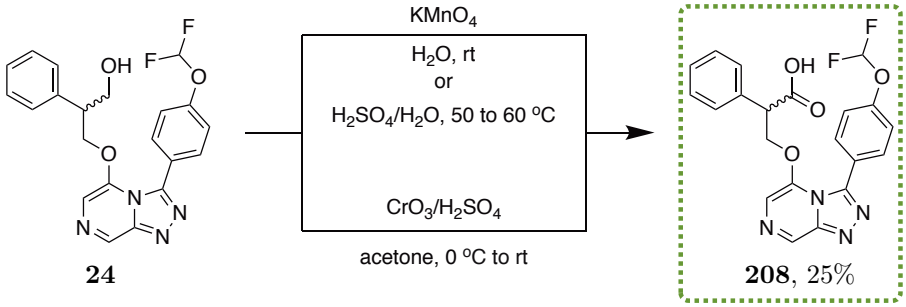

Figure 6.17: Synthesis of the hERG Evador. Oxidation of the benzylic primary alcohol with CrO_3/H_2SO_4 afforded the desired product in 25% yield.

6.5 Biological Evaluation: Part 1

With the hERG Evador **208** successfully synthesised, it and its two closely related analogues, **58** (without any benzylic substituent) and **24** (with a benzylic primary alcohol), were evaluated for *in vitro* potency, hERG binding activity and metabolic and physicochemical properties (Figure 6.18).

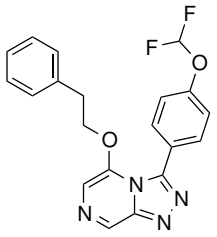

58
in vitro: 0.28 μM
hERG: 5.13

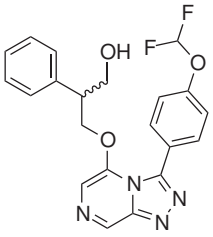

24
in vitro: 0.13 μM
hERG: 4.68

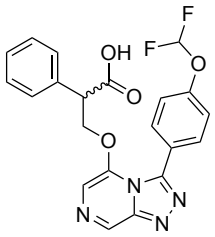

208
in vitro: 3.88 μM
hERG: <5.00

Compound	cLogP	LogD (pH 7.4)	Sol. (pH 6.5)	HLM ($CL_{int}/T_{1/2}$)	MLM ($CL_{int}/T_{1/2}$)	E_H (H/M)
58	3.2	3.7	6.3 - 12.5	66/26	262/7	0.72/0.85
24	2.7	2.8	12.5 - 25	49/35	36/5	0.66/0.89
208	2.3	1.3	25 - 50	<7/>255	<7/>255	<0.22/<0.13

Figure 6.18: *in vitro* IC_{50}, hERG pIC_{50} values and metabolic and physicochemical properties of the hERG Evador and related compounds. HLM: human liver microsomes. MLM: mouse liver microsomes. Sol.: aqueous solubility (μg/mL). CL_{int}: *in vitro* intrinsic clearance (mL/min/kg). $T_{1/2}$: half-life (min). E_H: hepatic extraction ratio

Encouragingly, when compared to **58** (pIC_{50} of 5.13), introduction of the carboxylic acid moiety (**208**) resulted in the desired reduction in hERG affinity (pIC_{50} of <5.00). This result appears to be consistent with the evidence that introduction of a carboxylic acid group helps to suppress hERG binding. In addition to this, the compound possessing a benzylic primary alcohol (**24**) also showed a significant reduction in hERG activity (pIC_{50} of 4.68) compared to **58**. Based on the rules described above, this decreased binding can be rationalised by the reduced lipophilicity/cLogP caused by the introduction of the alcohol moiety. Unfortunately, the hERG Evador was found to be significantly less potent *in vitro* (IC_{50} of 3.88 μM) than the comparison compounds **24** and **58**.

The carboxylic acid containing compound **208** showed excellent solubility at 25 - 50 μg/mL. It also possessed very low clearance and long half-life values equally across human and mouse liver microsomes. The benzylic primary alcohol compound **24** showed good solubility, however its clearance and long half-life was found to be comparably worse. In rat hepatocytes, the hERG Evador was also found to have low clearance (2 μL/min/10^6 cells) and a long half-life (224 min), compared to **24** which had a moderate clearance (13 μL/min/10^6 cells) and shorter half-life (29 min).

6.6 Synthesis of Substituted Phenyl Derivatives

Having demonstrated the significant improvement to hERG binding following the installation of a benzylic carboxylic acid group, and having discovered the excellent metabolic parameters for the hERG Evador, attempts were made to improve upon the *in vitro* potency. The obvious method to achieve this would be by making derivatives of the hERG Evador with substitutions on the northwest pendant phenyl ring. Even though the direct coupling of the diol to the TP core was shown to give the desired product in low yields, the phenyl substituted building blocks for this coupling could be accessed more readily and could be used in a slightly more step efficient synthesis (rather than synthesising the mono-protected diols for each analogue). For this reason, the synthesis involving coupling with the unprotected diol was used. While the unsubstituted 2-phenylpropane-1,3-diol is commercially available, derivatives with phenyl substitutions are less so. In order to investigate the phenyl substitution effect on potency, a robust route towards phenyl substituted 2-phenylpropane-1,3-diol derivatives had to be found. These diols could in theory be accessed *via* reduction of the corresponding diethyl phenylmalonate (*vide supra*), which could in turn be synthesised according to literature methods. Initial investigations were based around the 3,4-difluorophenyl derivative. One method for synthesising substituted diethyl phenylmalonate derivatives was described by Hennessy and Buchwald and involved a copper-catalysed arylation

of diethyl malonate and an aryl iodide.[359] Following this procedure, this reaction was performed with 1,2-difluoro-4-iodobenzene as the coupling partner (A, Figure 6.19).

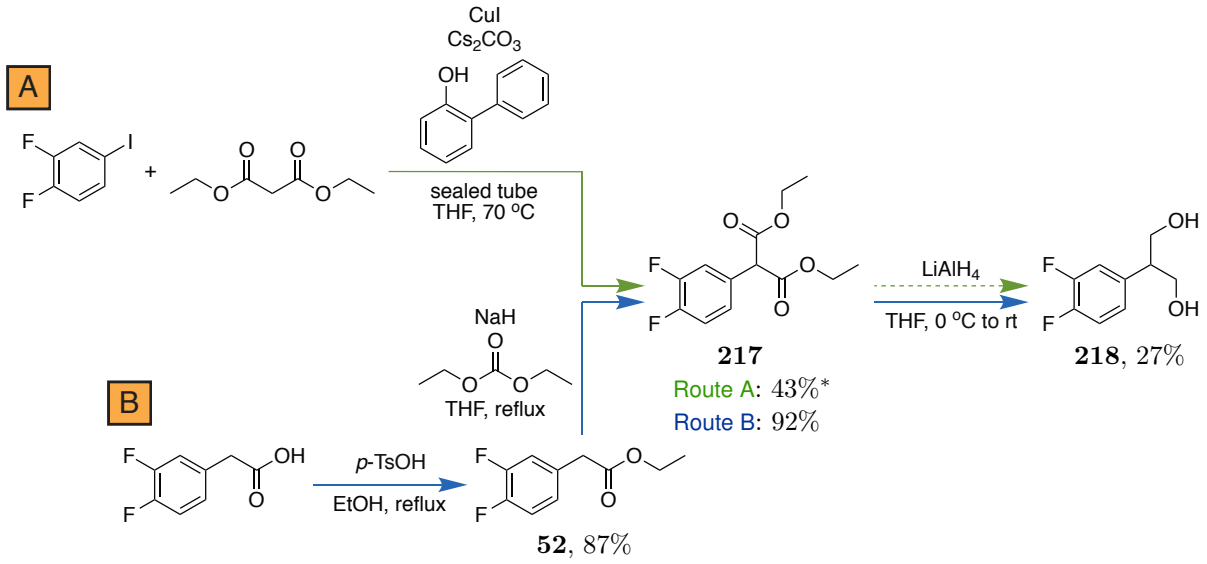

Figure 6.19: Synthesis of 2-(3,4-difluorophenyl)propane-1,3-diol *via* the diethyl malonate. (A) Initial attempt using copper-catalysed arylation of diethyl malonate and an aryl iodide to give the product **217**. *Product co-eluted with a significant amount of diethyl malonate. (B) Revised route gave greatly improved yields for the phenylmalonate ester in two simple steps.

While this reaction proceeded to give the desired coupling product **217** in 43% yield, the excess diethylmalonate starting material that was used was found to co-elute with the desired product during the purifications. Analysis of the ^{1}H NMR spectra of this mixture revealed that only 17% of the crude material was the desired product, with the remaining 83% being diethyl malonate. Even though it was possible to carry this mixture on to the following reduction step, this would have been relatively inefficient due to the larger amount of $LiAlH_4$ needed to reduce both **217** and the excess diethyl malonate. An alternative approach for the synthesis of diethyl phenylmalonate derivatives was found in a paper reporting the synthesis of 5,6,7,8-tetrahydro[1,2,4]triazolo[4,3-*a*]pyridine derivatives as γ-secretase modulators.[360] The step of interest involved the ethyl carboxylation of the α-position of ethyl 2-phenylacetate to give the diethyl phenylmalonate. These ethyl esters could be easily accessed *via* esterification of the corresponding 2-phenylacetic acid derivatives, many of which are commercially available. Beginning with 2-(3,4-difluorophenyl)acetic acid, esterification in EtOH gave the ethyl ester **52** in 87% yield (B, Figure 6.19). This was reacted with diethyl carbonate and NaH to form the diethyl phenylmalonate **217** in excellent yield. The two ester groups were reduced with $LiAlH_4$ to give the desired diol **218** in 27% yield.

Unfortunately, due to the small scale of these test reactions, not enough of the diol was available for coupling to the TP core, however, with this optimised route, a variety of other phenyl substituted diethyl phenylmalonate derivates were synthesised (Figure 6.20). Each 2-phenylacetic

acid derivative was esterified in EtOH to give the corresponding ethyl esters in *ca.* 93% yield. Subsequent ethyl carboxylation of the α-position afforded the diethyl phenylmalonate derivatives in *ca.* 76% yield.

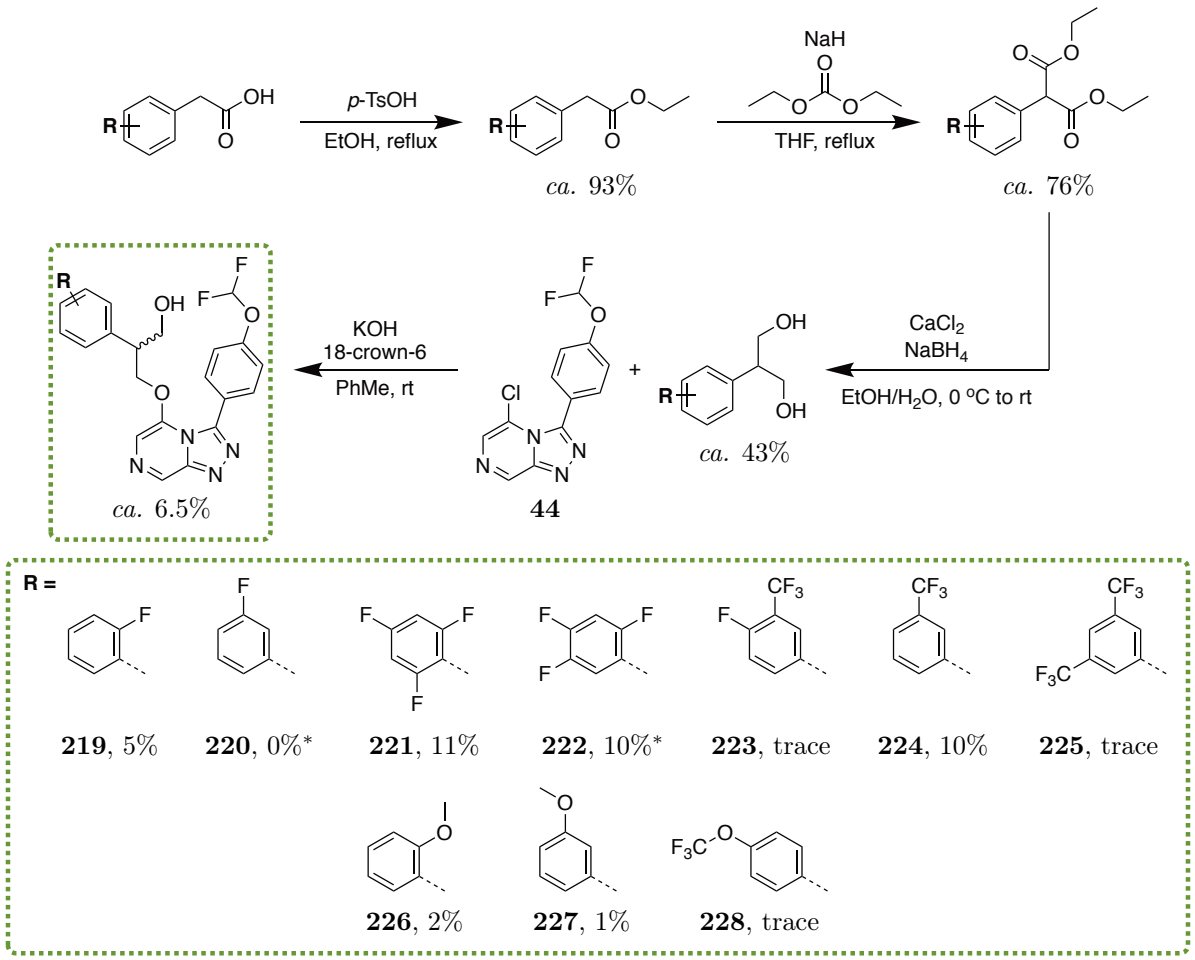

Figure 6.20: Synthesis of phenyl substituted derivatives of the hERG Evador. Good yields were seen with the improved route to the substituted diols, however very low yields were seen with the subsequent displacement step. *The *tele*-substitution product was also isolated (*vide infra*).

While the $LiAlH_4$ reduction step in Figure 6.19 provided the desired diol, it was thought the yield could be improved by using an alternative method. In a paper reporting the kilogram-scale synthesis of fingolimod, the authors performed an analogous reduction of a homologated diethyl phenylmalonate using $NaBH_4$ and $CaCl_2$ to give the corresponding diol in ~90% yield.[361] Encouragingly, applying these reduction conditions led to the desired diols in improved yields (*ca.* 43%). The final nucleophilic displacement step was performed using the KOH conditions (prior to the observation of improved yields when performed under *t*-BuOK conditions) to give the diol coupled products in low average yields of 6–7%.

Of the ten target compounds, six were isolated in high enough yields for biological evaluation. The remaining four were only isolated in trace amounts and were not evaluated for *in vitro*

potency. It was noted that in two cases, products of *tele*-substitution were identified and isolated (Figure 6.21).

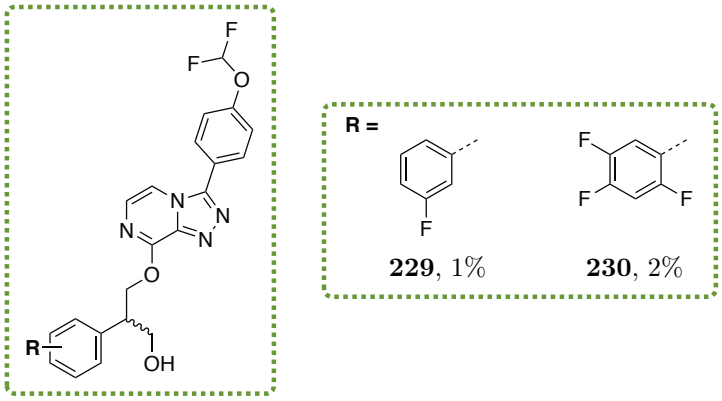

Figure 6.21: Two *tele*-substitution products identified from the diol coupling reactions above. Both were isolated in low yields.

Due to the low yields for these reactions, enough product was obtained from only one diol coupling (**221**) to carry out the subsequent oxidation step (Figure 6.22). Jones oxidation conditions provided the desired 2,4,6-trifluorophenyl derivative **231** of the hERG Evador in 25% yield.

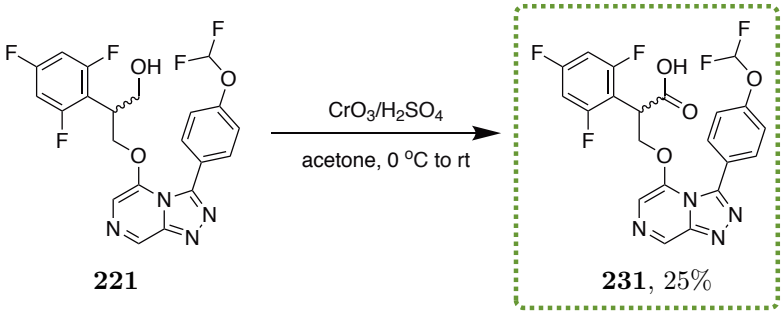

Figure 6.22: Oxidation of the 2,4,6-trifluorophenyl derivative of the hERG Evador. Jones oxidation gave the corresponding carboxylic acid product in 25% yield.

Having obtained a hERG Evador derivative possessing a phenyl ring with electron withdrawing groups, it was thought desirable to evaluate an analogue with electron donating substituents on the phenyl ring. Unfortunately, not enough of the methoxy substituted diol products above were obtained. Luckily, a 4-OMe substituted dimethyl phenylmalonate building block was found to be commercially available. This was reduced using $NaBH_4$ conditions to give the corresponding diol **232** in 54% yield (Figure 6.23). Coupling to the TP core **44** was performed using *t*-BuOK conditions to give the product **233** in 21% yield. This compound was then oxidised to give the 4-OMe analogue of the hERG Evador **234** in 23% yield.

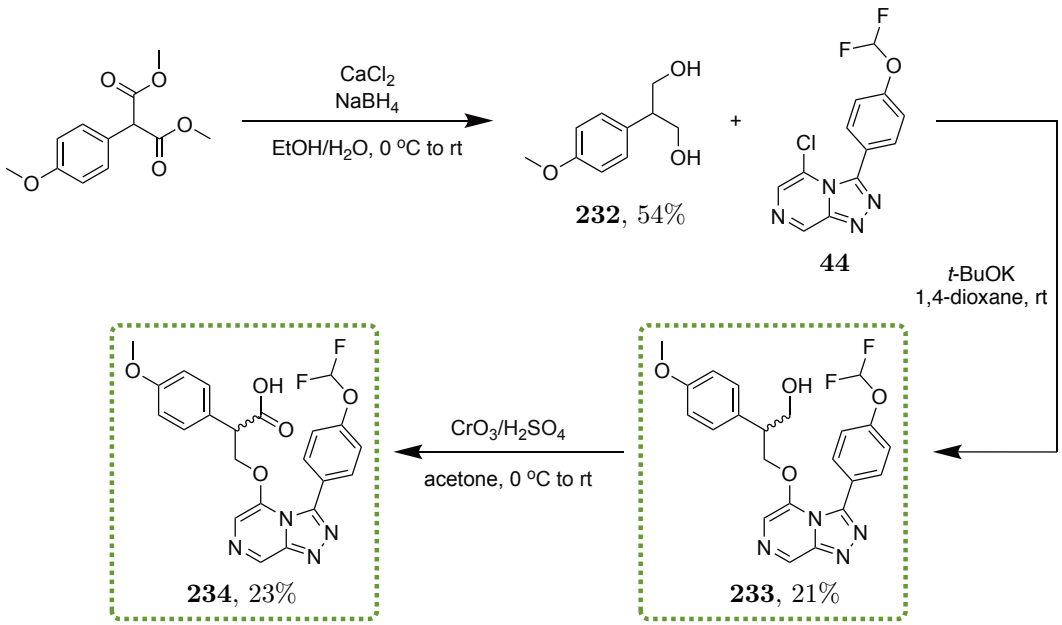

Figure 6.23: Synthesis of the hERG Evador derivative with an electron donating substituent on the pendant phenyl ring. Use of the *t*-BuOK conditions for the diol coupling step gave the product in improved yields.

Even though not all of the diol coupled derivatives in Figure 6.21 were synthesised in the desired amounts for biological evaluation, the ones that were made provided valuable SAR for this area. More importantly, two hERG Evador derivatives, with electron withdrawing and donating substituents on the pendant phenyl ring were made and were able to be tested for any improvements to *P. falciparum* activity.

6.7 Biological Evaluation: Part 2

Each of the benzylic primary alcohol and hERG Evador analogues were subsequently evaluated for *in vitro* activity (Table 6.1). In comparison with the parent benzylic primary alcohol compound **24**, the phenyl substituted analogues showed a range of activities, all of which were <1 μM. In these cases, both electron withdrawing groups (EWGs) and electron donating groups (EDGs) were well tolerated with the 3-CF_3 analogue (**224**) found to be the most potent of the set (Entry 6). Unsurprisingly, the *tele*-substitution product **230** was inactive (Entry 12). Unfortunately, not only were both hERG Evador analogues (**231** and **235**) inactive, but they were significantly less potent than the parent compound **208** (Entries 13 and 15). The addition of electron withdrawing or donating groups on the phenyl ring was seen to be detrimental to the activity, with EWGs more so. Nevertheless, it appears that phenyl substitution has a noticeable effect on the resulting potency of the hERG Evador analogue. It remains possible that the more potent derivatives found among the benzylic primary alcohol compounds (e.g. with 3-OMe and 3-CF_3 substituents) may provide better activity.

Table 6.1: IC_{50} potency values of the phenyl substituted benzylic primary alcohol analogues against *P. falciparum*. Potency was generally maintained among the benzylic primary alcohol derivatives. EWGs and EDGs were not well tolerated in the hERG Evador analogues with a significant loss in activity. N.D.: not determined.

Entry	Compound	cLogP	IC_{50} (μM)
Reference	**24**	2.7	0.13
	208	2.3	3.88
1	**219**	2.8	0.16
2	**220**	2.8	N.D.
3	**221**	3.0	0.89
4	**222**	3.0	0.19
5	**223**	3.6	N.D.
6	**224**	3.5	0.09
7	**225**	4.4	N.D.
8	**226**	2.6	0.30
9	**227**	2.6	0.12
10	**228**	3.8	N.D.
11	**229**	2.8	N.D.
12	**230**	3.0	9.69
13	**231**	2.6	>25
14	**233**	2.6	0.72
15	**234**	2.2	9.94

6.8 Concluding Remarks

The hERG binding affinity of a number of inherited Series 4 compounds has been found to be variable. In order to alleviate these concerns, a compound was designed based around examples in the literature which showed formation of a zwitterionic compound (i.e. incorporation of a carboxylic acid moiety) could lead to reduced hERG affinity. This Series 4 compound, named the "hERG Evador", possessing a benzylic carboxylic acid moiety, was synthesised *via* oxidation of the benzylic primary alcohol in Frontrunner compound **24**. Upon evaluation of its hERG affinity, a significant reduction was found when compared to the corresponding compound without benzylic substitution (**58**). While the hERG Evador also possessed excellent solubility, low clearance and a long half-life, this unfortunately came at the cost of a large loss in *in vitro* potency.

In an attempt to improve the potency, a number of phenyl substituted analogues of Frontrunner **24** were synthesised, with the aim of oxidising these to the corresponding carboxylic acids. Low yields were seen with the unoptimised diol coupling step, however a majority of the coupled products were isolated in sufficient yield to be evaluated for potency. The potency was generally maintained with the phenyl substituted benzylic alcohol analogues with the most potent compound having 3-CF_3 substitution (0.09 μM). Two hERG Evador derivatives were synthesised, one with electron withdrawing substituents (**231**) and one with an electron donating substituent (**234**) on the pendant phenyl ring. Unfortunately, both analogues led to a significant decrease in activity.

7. Open Source Malaria in the Undergraduate Laboratory

This chapter begins with an overview of the idea of crowdsourcing scientific research, and how openness can be utilised in synergy with this approach. The application of crowdsourced synthesis to the OSM project will be discussed with respect to its incorporation into a module for the first year Special Studies Program (SSP) in the School of Chemistry at The University of Sydney. For each year of the SSP course, the choice of target compounds, student syntheses and biological evaluation are discussed.

7.1 Crowdsourcing Chemical Synthesis

Crowdsourcing aims to involve the public in real research projects as a means of generating data and accelerating the research. Websites such as SciStarter,[362] citizenscience[363] and zooniverse[364] provide an easy way for the public to search for projects in which to participate.[132] While this idea has been applied to many areas of science including biology, physics and environmental science, its application to chemical synthesis has been less widespread. When considering the differences between openness and crowdsourcing, a key feature of an open source science project is the idea that anybody can contribute, no matter their scientific background. However, there is no guarantee that people will participate in the project.

The Distributed Drug Discovery (D3) program, created by Dr. William Scott at the Indiana University Purdue University Indianapolis in 2005 is one example of crowdsourced chemistry.[365–367] Scott's idea was to develop a low-cost strategy for the discovery of new drugs for neglected diseases by applying a distributed problem approach across the three key stages of drug discovery. For the first stage of identifying new candidates for further development, D3 have reached out to computational chemists around the world as a means to more effectively identify hit compounds to pursue. The second key stage involves the synthesis of the identified candidate compounds. For this step, D3 utilised undergraduate and graduate students in universities around the world to synthesise candidates.[368,369] The students involved in this process not only learn the techniques of synthetic chemistry, but also contribute to real research projects. The application of crowdsourcing to the final key stage (biological evaluation) is currently ongoing, but the goal is for biologists to develop simple and inexpensive assays that allow the students to become involved in the final stages of hit to lead drug discovery.

In 2008, while working on a way to convert sunlight into renewable hydrogen fuel *via* the pho-

toelectrolysis of water, Bruce Parkinson from the University of Wyoming applied crowdsourcing as a way to discover new semiconducting metal oxide catalysts for this process. He developed a simple combinatorial chemistry kit made with an inkjet printer, laser pointer and LEGO, naming it the Solar Hydrogen Activity Research Kit (SHArK). This kit allowed university and high school students to easily produce and test potential catalysts.[370] The first hit from the project emerged in 2014 when an undergraduate student from Gonzaga University discovered a promising p-type semiconductor which was further developed by the Parkinson group.[371]

In another example, the Drugs for Neglected Diseases *initiative* (DND*i*) launched the Open Synthesis Network (OSN) in 2015, a project aimed at involving masters and undergraduate students from universities around the world in drug research for neglected diseases.[372] There are currently 18 participating universities contributing to this project, from areas including India, the UK and the US, working to synthesise compounds that target visceral leishmaniasis and Chagas disease. Any compounds found to be efficacious against these diseases through this process will be developed further by DND*i* with the ultimate goal of producing new medicines. However, at this stage, the OSN is not a publicly open crowdsourcing project. While all members of the network are able to share and see all the data that has, and is currently being generated, members of the public cannot access this information.

It is notable that many examples of crowdsourced chemistry are not completely open: while anyone can participate in these projects, not everyone can see all that is happening within the project and as a consequence, there is a higher chance for unnecessary duplication. One solution to combining openness and crowdsourcing is to incorporate these approaches into an educational course such as a university lab class. Open source projects provide a perfect platform for this purpose, as everyone can see what else is happening within the project, and duplication is minimised. There are a number of benefits to crowdsourcing research projects like the ones described above. With more people working on synthesising molecules, more compounds can be identified and further developed, with the potential to greatly speed up this discovery and optimisation processes. These projects also benefit the universities involved, allowing students to take part in real research projects rather than resynthesising known targets that ultimately have no application beyond the learning gained in making them. However, for such a project to be incorporated into a university course, a number of considerations must be made, including how students would be assessed, and how to avoid plagiarism. Additionally, it is probable that the progress made by inexperienced undergraduate students will be lower than that of an individual postgrad, postdoc or CRO worker in the same period of time.

7.2 Open Source Malaria in an Undergraduate Laboratory

Dr. Alice Motion used these ideas to create a new crowdsourced undergraduate laboratory course at The University of Sydney in 2015, for students enrolled in the Special Studies Program (SSP).[373] The SSP is designed for high-achieving students in their first year of university, and this laboratory course enabled them to undertake more research-style experiments (in contrast to the standard experiments done in the regular first year course, in which the outcome is already known, or at least readily anticipated). The structure of this lab allows students to learn new experimental techniques at a much earlier stage in their degree and get more hands on experience with the uncertainties of scientific research.

Having worked in the OSM project for a number of years, Alice saw this as an opportunity to apply crowdsourcing to the project by tasking the students with the synthesis of novel antimalarial compounds for Series 4. The simplicity and robustness of the synthetic route to the TP core make it suitable for undergraduates to perform, and allows them to learn important techniques such as TLC analysis of reaction mixtures and NMR spectroscopy. The target compounds chosen for the SSP class focussed on simple Series 4 analogues that explored missing SAR using commercially available reagents; these were feasible because the essential features of the synthesis had been worked out for previous analogues (Figure 7.1). Each year, the class of 50–60 students was divided into four groups and under the guidance of a postgraduate demonstrator, each group was tasked with synthesising an assigned compound over four lab sessions of three hours each. As a demonstrator to this course between 2016 and 2018, I collaborated with Dr. Motion on the selection of suitable target compounds, design of synthetic routes, and purification of student products, and was lead demonstrator for this component of the class.

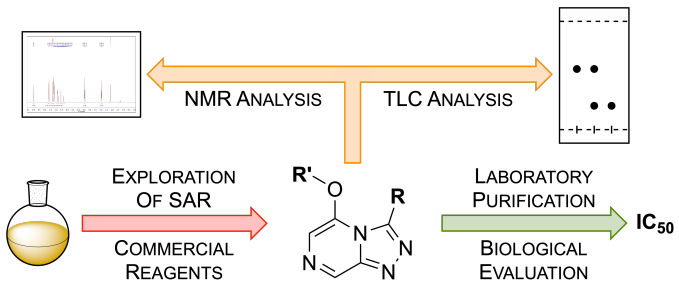

Figure 7.1: Overall aim of the SSP student OSM projects. Beginning from commercial reagents, students would synthesise Series 4 analogues with variation in the northeast (**R**) and northwest (**OR′**) positions to explore SAR (⇨). Under the guidance of a demonstrator, TLC and NMR would be conducted throughout (⇨), with the final compounds purified in the research lab and sent for biological evaluation (⇨).

Compounds were designed to explore the northeast and northwest moieties (Figure 7.2). Each week, the SSP students carried out one step of the synthesis, beginning from the hydrazine **2** which was provided from the research lab (due to the lengthy reaction conditions and hazardous reagents required for its synthesis). The students would then set up the subsequent reaction and monitor its progress by TLC throughout the session. When the reaction was determined to be complete, a work-up was performed and the crude product isolated for the following week. Although learning the techniques of column chromatography is key for any drug discovery project, the time frame of the course did not allow for the students to purify their own final compounds. Rather, the students would learn about the theory of column chromatography, while the crude final products made by the undergraduate students were purified in the research lab at the end of the route, and sent for biological evaluation. Once bioassay results were obtained, students would be notified of the *in vitro* potencies of their compounds and discuss these with their demonstrators. Throughout this process, the students would use the hydrazone intermediate to learn about recrystallisation and NMR techniques. In addition, the structure of this course allows the students to interact with demonstrators and academics directly to discuss aspects of the research being conducted, such as reaction mechanisms and the impact of open source research, and for their work to be openly available to comment from the wider community. At the conclusion of the OSM module, the undergraduate students summarised and presented their findings in a video or poster presentation.

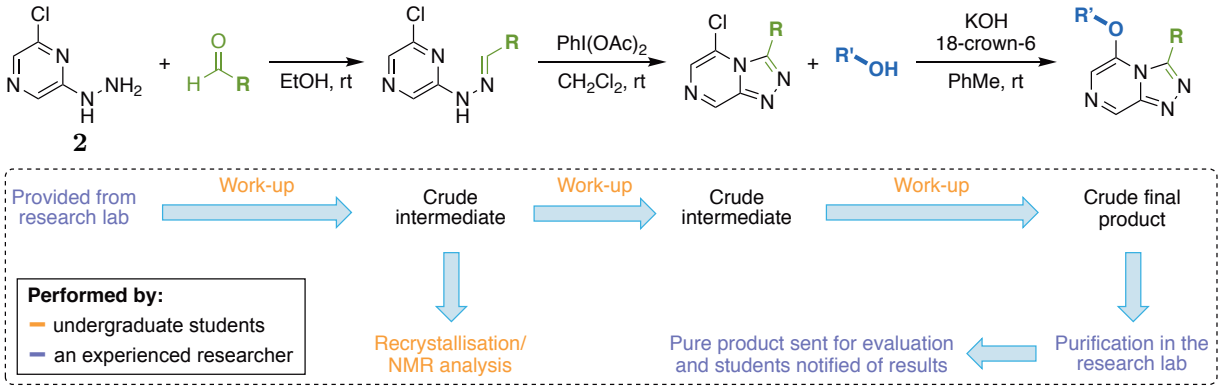

Figure 7.2: Outline of the synthetic route used by the students to synthesise new Series 4 compounds. The initial starting material was provided, with the aldehyde (**RCHO**) or alcohol (**R′OH**) varied based on the need to explore a particular area of SAR.

7.3 Class of 2015

The first class of students to undertake this course explored an aspect that was, surprisingly, missing from the inherited data: the effect that the position of substitution on the northeast phenyl ring has on potency against *P. falciparum* (Figure 7.3).[373]

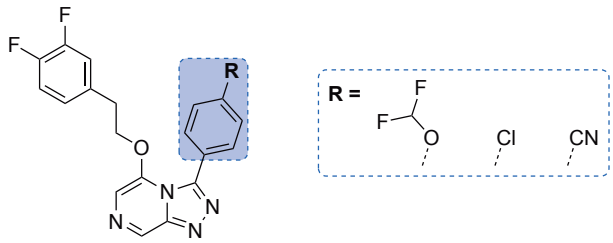

Figure 7.3: The majority of the inherited compounds incorporated a 4-$OCHF_2$ group on the northeast phenyl ring. A small number had either 4-Cl or 4-CN groups. The reason for these substitution patterns was not clear.

All of the inherited compounds with phenyl rings in the northeast position were either unsubstituted, or substituted only at the 4-position with $OCFH_2$, Cl or CN groups. No 2- or 3-substituted compounds were present in the dataset. To investigate this further, students were tasked with synthesising derivatives with varying chloro-substitution, due to the relative affordability and availability of the required chlorobenzaldehyde isomers. Accordingly, students carried out the condensation step using either benzaldehyde or one of its 2-, 3- and 4-chloro derivatives to give the corresponding hydrazone intermediates. Cyclisation of these crude products led to the corresponding TP cores. Finally, nucleophilic displacement of chloride from the respective TP cores using 2-phenylethanol gave the final compounds **236**–**239** (Figure 7.4). The final crude mixtures were purified in the research lab and sent for bioactivity evaluation.

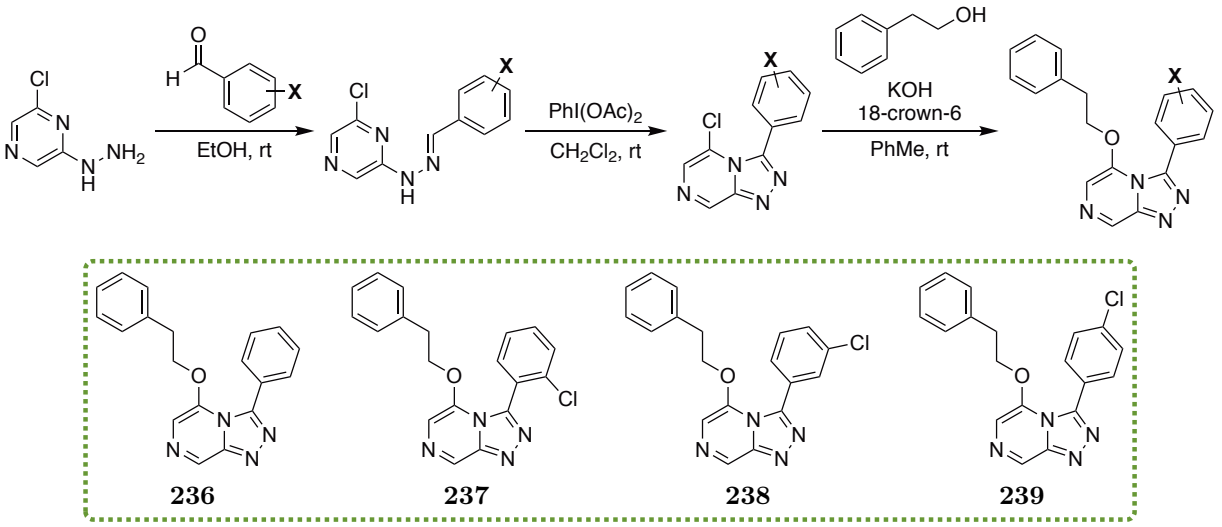

Figure 7.4: Series 4 compounds synthesised with the SSP class of 2015. Compounds with monochlorinated northeast phenyl rings were successfully synthesised by the students, with a bare phenyl ring compound prepared as a control.

It was found that the substitution position of the halide on the northeast phenyl ring was very important to activity (Table 7.1). When compared to the control compound with a bare phenyl ring **236**, substitution at the 2- and 3-positions (**237** and **238** respectively) led to a decrease in potency (Entries 1–3). However, when the chlorine atom was attached at the 4-position (**239**),

significantly higher potency was seen than for the phenyl control **236** (Entry 4).

Table 7.1: IC_{50} potency values of northeast chlorophenyl isomers against *P. falciparum*. The chlorine substitution position greatly influences the potency, with 4-substitution ideal.

Entry	Compound	cLogP	IC_{50} (μM)
1	**236**	3.0	1.60
2	**237**	3.6	>5
3	**238**	3.6	>2.5
4	**239**	3.6	0.057

As these compounds were the first examples of analogues with alternative substitution pattens on the northeast phenyl ring, they provided the OSM project with valuable SAR data, which not only validated the use of 4-substitution in the inherited compounds, but also provided a rationale for further investigations into substitution patterns on this ring.

7.4 Class of 2016

The following year, with the 2016 class of students we sought to build upon the previous year's results by investigating further halide substitution effects on the northeast phenyl ring.[374] Having created a highly potent compound in **239**, which possessed a 4-substituted phenyl ring, we wondered whether it was the *presence* of substituents at the 2- and 3-positions or the *absence* of a 4-chloro substituent that was the cause of the inactivity. Two aspects were explored: firstly, replacement of the chlorine with fluorine, and secondly, how additional substitution (as well as a 4-chloro group) would impact the potency. A set of four new aldehydes was chosen, each with either a fluorine or chlorine at the 4-position, and three of which possessing an additional fluorine or chlorine at the 2- or 3-position. By following the synthetic route carried out in the previous year, condensation of **2** with the relevant disubstituted chlorobenzaldehydes (2,4- or 3,4-dichloro) or fluorinated benzaldehydes (4-fluoro or 3,4-difluoro) gave the corresponding hydrazones, which were cyclised to give the respective TP cores. Following nucleophilic displacement with 2-phenylethanol, the desired crude final products **240**–**243** were obtained (Figure 7.5), purified and sent for potency evaluation.

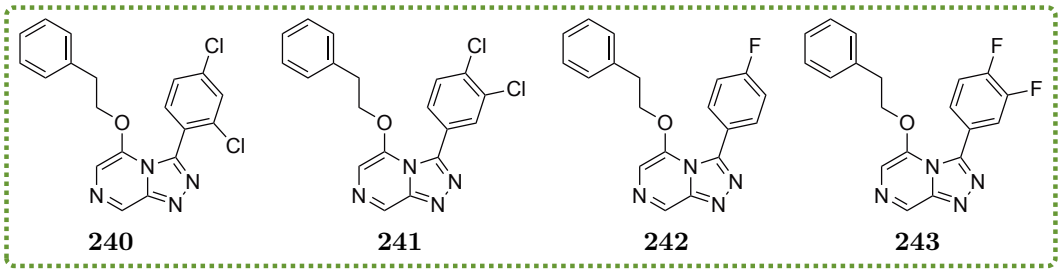

Figure 7.5: Series 4 compounds synthesised with the SSP class of 2016. Building on the 2015 results, compounds with chlorinated and fluorinated northeast phenyl rings were successfully synthesised by the students.

While all four compounds showed similar submicromolar activity, none were found to improve upon the lead 4-chloro compound from the 2015 set (Table 7.2). However, compared with the inactive 2- and 3-substituted compounds (**237** and **238**), addition of a halide at the 4-position led to a recovery of activity (Entries 6, 7 and 9). Activity was maintained when replacing the chlorine at the 4-position with a fluorine (Entry 3).

Table 7.2: IC_{50} potency values of northeast chlorophenyl and fluorophenyl isomers against *P. falciparum*. These results confirmed the importance of substitution in the 4-position for maintaining activity, but showed that additional halogen substitution elsewhere on the ring was tolerated as well.

Entry	Compound	cLogP	IC_{50} (μM)
1	**240**	4.2	0.26
2	**241**	4.2	0.71
3	**242**	3.1	0.37
4	**243**	3.2	0.58

The combined results from the 2015 and 2016 crowdsourcing experiments confirmed the importance of substitution at the 4-position, and validated the continued use of northeast phenyl rings with substituents at this position.

7.5 Class of 2017

Following the success of the previous two years' investigations of the importance of substitution on the northeast phenyl ring, we shifted the focus for the class of 2017, choosing target compounds to extend the work being carried out on phenyl bioisosteres described in Chapter 4.[375] This year, the students would aim to make, not four, but eight compounds. Two TP cores would be made based on the most potent compounds from the previous years (4-chloro compound **239** and 2,4-dichloro compound **241**), with the northwest phenyl ring to be varied using one of four hydrocarbon cages (adamantane, nopol, norbornene and myrtenol). Each demonstrator group began by synthesising the two TP cores, first by condensation of 4-chloro and 2,4-dichloro substituted benzaldehyde with **2**, followed by cyclisation to form the respective triazolopyrazines. Groups were then assigned a

hydrocarbon cage to perform the final nucleophilic displacement with each of their two cores, leading to compounds **244**–**251** (Figure 7.6).

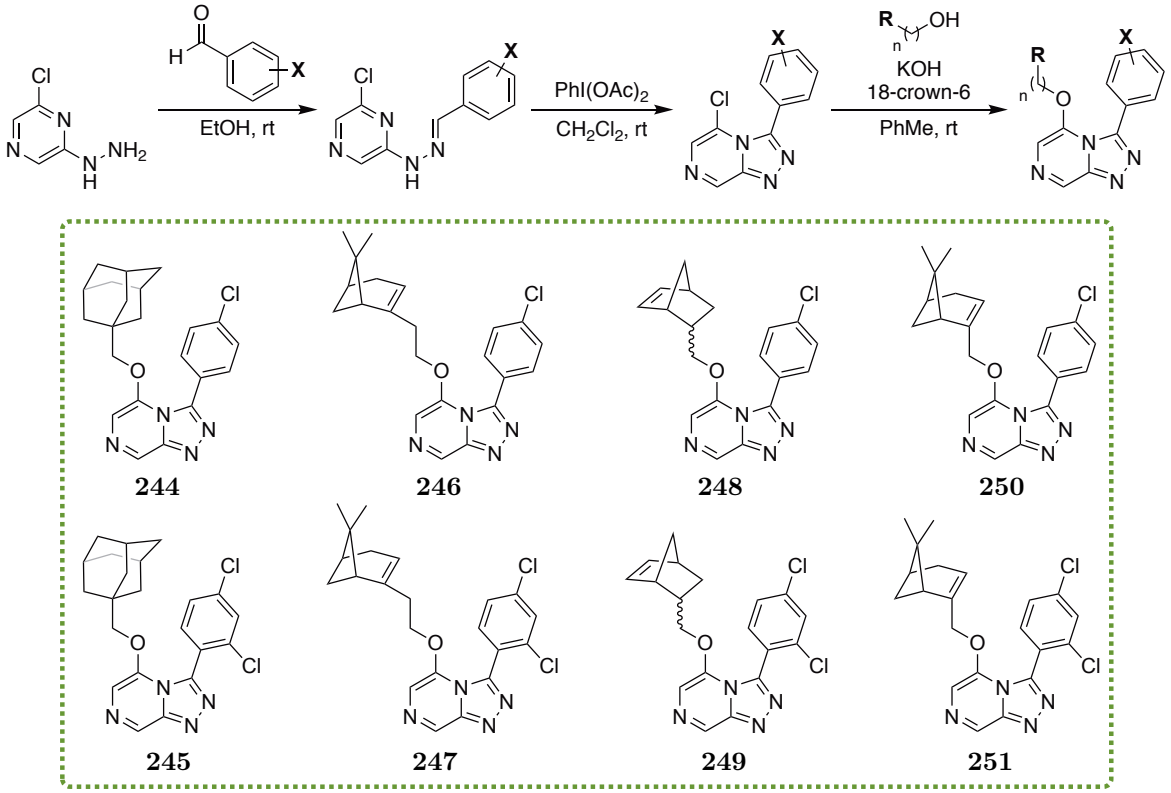

Figure 7.6: Series 4 compounds synthesised with the SSP class of 2017. The scope was expanded in 2017, with eight target compounds based upon replacement of the northwest phenyl ring with hydrocarbon cages.

While compounds **244**–**249** were made successfully, unexpectedly for the students and their demonstrators, displacement reactions performed using the myrtenol nucleophile (to give compounds **250** and **251**) were unsuccessful, with no reaction seen by TLC, using either TP core. The ^{1}H NMR spectra of the crude material from these reactions indicated only starting materials present. Additional investigations were performed in the research lab (see Chapter 4) but were ultimately inconclusive. As a result, these two compounds were not pursued any further.

Upon evaluation of the 2017 compounds for potency, it was found that a majority were inactive (Table 7.3). As a general trend, compounds with 2,4-dichloro substitution on the northeast phenyl ring (Entries 2, 4 and 6) were less potent than those with the simpler 4-chloro substitution (Entries 1, 3 and 5). The nopol derivative **246** was moderately active but still less so than the corresponding northwest phenyl analogue **239**. Norbornene compound **248**, which was obtained as a mixture of *endo* and *exo* isomers, was the most potent of this set (Entry 5).

Table 7.3: IC_{50} potency values of northwest hydrocarbon cage compounds against *P. falciparum*. These hydrocarbon replacements led to a decrease in activity, similar to that seen with the examples discussed in Chapter 4.

Entry	Compound	cLogP	IC_{50} (μM)
1	**244**	4.0	2.53
2	**245**	4.7	8.00
3	**246**	4.3	1.05
4	**247**	5.0	8.24
5	**248**	3.1	0.62
6	**249**	3.7	9.55
7	**250**	3.9	Not isolated
8	**251**	4.5	Not isolated

Overall, all SSP phenyl bioisostere analogues from the class of 2017 were found to be less potent than those possessing a 4-$OCHF_2$-substituted phenyl ring (see Chapter 4).

7.6 Class of 2018

For the class of 2018, we maintained our focus on replacements of the phenyl rings, but this time used saturated heterocycles in place of hydrocarbon cages. Investigation returned to the northeast position, and the number of target compounds reduced to a more manageable four (one per group).[376] It was noted that in the original dataset, two inherited compounds incorporated saturated heterocycles in the northeast position, one bearing an *N*-acyl piperidine moiety **MMV668961** and the other bearing a tetrahydropyran moiety **MMV668959** (the heteroatoms at the 4-position of the heterocycle in both cases). Both of these analogues were shown to be inactive (Figure 7.7). It was thought important to validate these results given that 4-substituted phenyl rings in the northeast position (which these heterocycles mimic) have be shown to be beneficial for potency, and deplanarisation should aid in compound solubility (see Chapter 4).

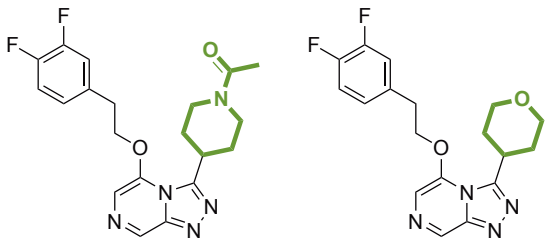

MMV668961 >10 μM **MMV668959** >10 μM

Figure 7.7: Inherited compounds possessing northeast saturated heterocycles. Both northeast *N*-acetylpiperidine and tetrahydropyran analogues are inactive.

Four analogues were proposed to investigate these data. The compounds contain 5- and 6-membered nitrogen (*N*-Boc protected) and oxygen heterocycles in the northeast position. For

simplicity, the 3,4-difluorophenyl moiety present in the northwest position of the inherited compounds was replaced with an unsubstituted phenyl ring, as for previous SSP campaigns. To ensure all the students could be assessed on performing the same reactions, the deprotection of the compounds possessing *N*-Boc groups would not be conducted by the students, but competed subsequently in the research lab instead. The respective aldehydes were condensed with **2**, cyclised, and reacted with 2-phenylethanol to give the four target compounds **148**–**151** (Figure 7.8).

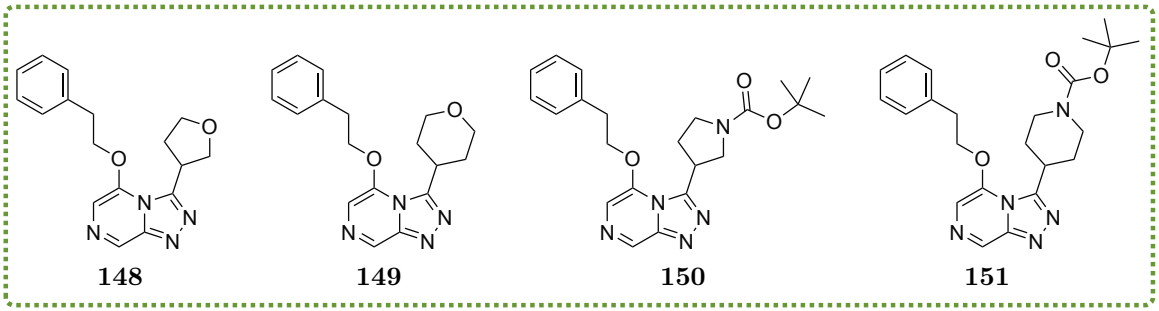

Figure 7.8: Series 4 compounds synthesised with the SSP class of 2018. The 2018 target compounds were based upon replacement of the northeast phenyl ring with saturated heterocycles. The *N*-Boc protected compounds would be deprotected in the research lab prior to biological evaluation.

Once the undergraduate students had completed the synthesis of their crude final compounds, purification was attempted in the research lab as per previous years. Surprisingly, even after three columns (one regular-phase and two reversed-phase) on each of the compounds, none were pure enough for biological evaluation. It was decided that each of the four compounds would need to be resynthesised with purification of every intermediate to ensure the compounds were made. The reactions were repeated by the author, with intermediates and final products successfully purified and characterised by NMR spectrometry and mass spectrometry (see Chapter 4). Ultimately, when these resynthesised compounds were evaluated for *in vitro* potency, all were found to be non-potent (all >10 μM), confirming the inactivity of inherited compounds **MMV668961** and **MMV668959**.

During the purification and characterisation of these compounds, a number of discrepancies were found between the spectra obtained for the products synthesised by the students and those made in the research lab. Firstly, when comparing the hydrazone intermediates for each compound, one key signal was observed at a significantly different chemical shift. In a representative example, the signal around ~8.5–8.0 ppm (indicated by a black box) shifted from 7.99 ppm in the student synthesised sample to 8.15 ppm in the research lab sample (Figure 7.9).

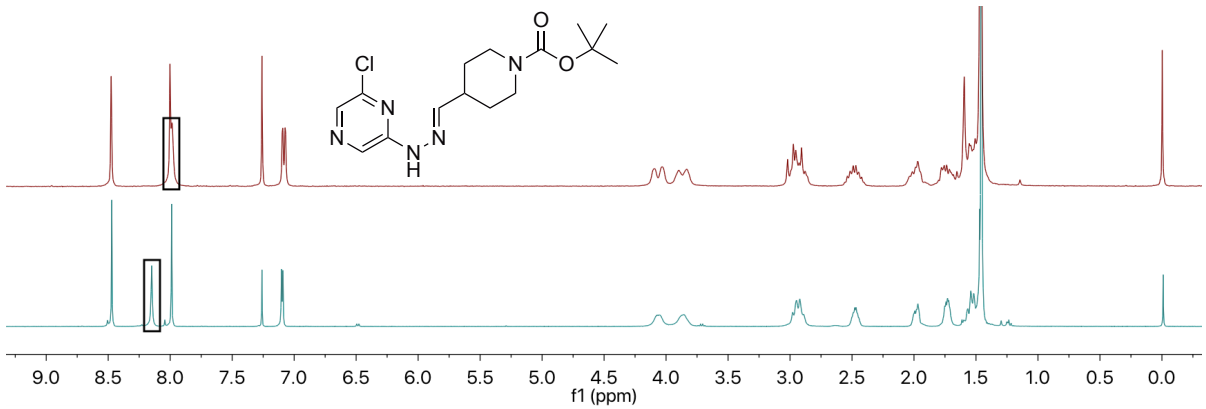

Figure 7.9: Representative comparison between a student synthesised hydrazone and a research lab resynthesised hydrazone. The signal in the black box was seen to shift between the two samples. This was confirmed to be a result of compound concentration in the analysed sample.

This signal was identified to arise from the hydrazone NH proton, and throughout all student samples was seen shifted upfield by ~0.5 ppm relative to the peak in the spectra from the equivalent samples arising from the research lab. The discrepancy was initially attributed to the presence of the two isomeric products of the C=N double bond, and potentially a different distribution of the isomers arising from the two preparations. However, the *E*-isomer is the thermodynamic product, and the reaction conditions used for the student and research syntheses were essentially the same, so it is highly unlikely that the less stable *Z*-isomer formed in one case and not the other. When the ^{1}H NMR spectrum of a sample containing a mixture of both products was obtained, only one signal at 7.97 ppm was seen. This outcome confirmed that the observed difference was not due to the presence of isomers but in fact due to a difference in concentrations between the two samples used for NMR spectroscopy (an explanation first suggested by A/Prof. Chase Smith).[376] It was rationalised that the student samples were run at a lower concentration than the research samples. The chemical shifts of OH and NH protons are known to be dependent on a number of factors, one of which is sample concentration. At higher concentrations, there is increased intermolecular hydrogen bonding which translates to more deshielding and a downfield shift.[377]

A second discrepancy was seen when comparing samples of the final products made in the student lab versus the research lab. The ^{1}H NMR spectra arising from the SSP products (spectra in red) and the resynthesised products (spectra in blue) revealed a number of key differences (Figure 7.10), suggesting the compounds made by the students were in fact different products. The spectra obtained from the research samples appear to be typical to those of other Series 4 compounds, while the spectra from the student samples showed consistent differences not previously seen with compounds from this series.

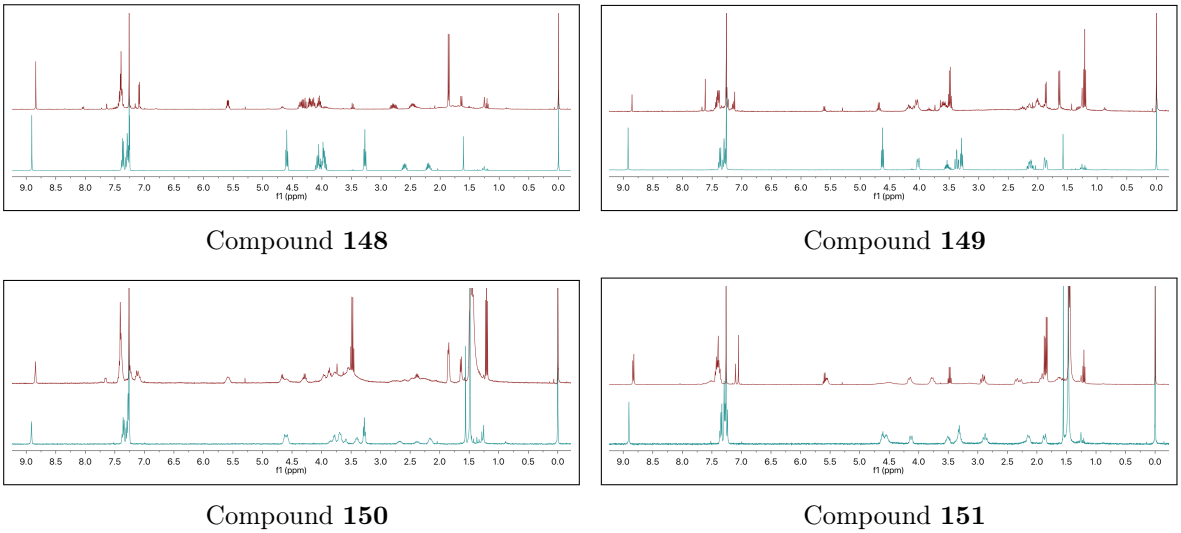

Compound **148** Compound **149**

Compound **150** Compound **151**

Figure 7.10: NMR spectroscopic comparison of student compounds (after purification) and resynthesised compounds. Key differences include: change in position of signals at ∼9.0 ppm, shift between aromatic signals at ∼7.3 ppm, multiple differences between aliphatic signals at ∼6.0–1.0 ppm.

The most notable differences are as follows: there are slight differences in shifts for the pyrazine signal at ∼9.0 ppm, there are slight differences in shifts for the phenyl signals at ∼7.3 ppm, additional signals are present in the student compounds at ∼7.0 ppm, there are differences in shifts for all aliphatic signals between ∼6.0–1.0 ppm, and there is an absence of the triplets corresponding to the northwest methylene chain in the student compounds.

To confirm that this was not a concentration effect (as seen above), a mixture of the student product and the resynthesised product was analysed by ^{1}H NMR spectroscopy. Signals from both compounds were present in the mixed sample, ruling out a concentration effect as a cause for these changes. With so many differences between the NMR spectra, it was anticipated that the low-resolution mass spectra for the student compounds would be different to the expected mass. However this was not the case as each compound showed the expected mass for the desired products. Investigations to determine the identity of the student-synthesised products are ongoing. with attempts at recrystallisation to solve their X-ray structures.[376]

7.7 Concluding Remarks

The use of crowdsourced chemical synthesis was demonstrated by incorporating OSM into a module for the SSP laboratory class at the University of Sydney. Every year since 2015, groups of students synthesised novel Series 4 compounds for biological evaluation which allowed for important new SAR data to be obtained.

A number of challenges were overcome throughout these classes. One set of compounds in 2017 could not be synthesised, and as a result, a subgroup of students were not able to be assessed

on final yields of their compounds. While this might result in deduction of marks in a regular laboratory class, by taking into considering the novel nature of the reactions being performed within this class, student performance could be assessed not solely on the basis of synthetic yields, but instead by the proficiency with which they were able to perform the reactions and communicate results. These are arguably more important skills for students to learn, as high yields are not the only important aspect of chemical research. In a similar manner, even though the target compounds were not synthesised by the class of 2018, students could be assessed on their ability to perform reactions and report the results.

Another notable aspect of conducting open research in an undergraduate laboratory class is the potential for plagiarism, not only from fellow students, but also from the work of past students on the course, or researchers elsewhere in the world working in the open towards similar targets. This unique context offers an excellent opportunity to teach the students about the importance of proper citation of others' results, and appropriate referencing to previous work even if unpublished. As a result, the assessment of students throughout this course is weighted towards their ongoing performance during the lab sessions and the quality of the written records of their experiments.

When running an undergraduate lab course in such a way, it is important to obtain feedback from the students to refine and develop the course further. Anonymous student feedback from Unit of Study Surveys (USS) for the OSM module between 2015 and 2018 particularly highlight the lab classes, with students describing the course as being "challenging but enjoyable", "like playing with lego and solving riddles, and pretty intellectually rewarding", and "different and very stimulating". Many students enjoyed the research aspects of the course and the real world applications of their work. As a more personal reflection on time spent as a demonstrator for this course, I found it an extremely enjoyable and rewarding experience. This course has allowed me to develop as a researcher by providing the opportunity to mentor students and convey my own research in an effective manner.

The OSM module in the SSP course will continue to develop in the coming years, with new compounds synthesised based on areas of missing SAR. When work on Series 4 concludes, the course is readily adapted to other open source projects, building on the approaches developed and lessons learned with the OSM module.

8. Conclusions and Future Work

8.1 Conclusions

Throughout this work, a large range of novel Series 4 compounds was synthesised. This began with the resynthesis of a number of high value targets, named the Frontrunners, in order to obtain a more complete set of biological data including *in vitro* potency, solubility, metabolic stability and mechanism of action measurements. The evaluation of the resynthesised compounds began with *in vitro* potency, the results of which were consistent with the inherited and previously obtained data. Having acquired a more complete set of metabolic and physicochemical properties for these compounds, a number of key observations were made. Compounds possessing a northwest pendant 3,4-difluorophenyl ring were found to be generally more potent than those with an unsubstituted pendant phenyl ring. Similarly, compounds with a 4-Cl or 4-$OCHF_2$ substituted phenyl ring in the northeast triazole position were beneficial for potency. Benzylic substitution of the ether-linked compounds was favoured with improvements to both solubility and metabolic stability. The amide-linked compounds were no longer pursued due to the lower potency, solubility and higher metabolic clearance relative to the ether-linked compounds. This campaign also highlighted the impact that open science can have on conducting scientific research. The process undertaken to obtain the dimethylamine Frontrunner compound **30** was an excellent example of the benefits of community-accelerated synthesis and an advantage of working in an open manner. It could be imagined that without such inputs from the community, the amount of time and resources spent to get to the same point would be increased.

While investigating thioether-linked compounds, discrepancies were found in the ^{1}H NMR spectra of an existing compound. This originally isolated inactive compound was confirmed to be an alternative product, where the thioether was substituted at the 8-position of the pyrazine ring (Figure 8.1). The desired 5-substituted product was isolated and found to have moderate potency. The *tele*-substitution phenomenon has since been observed among amine-linked Series 4 compounds as well.

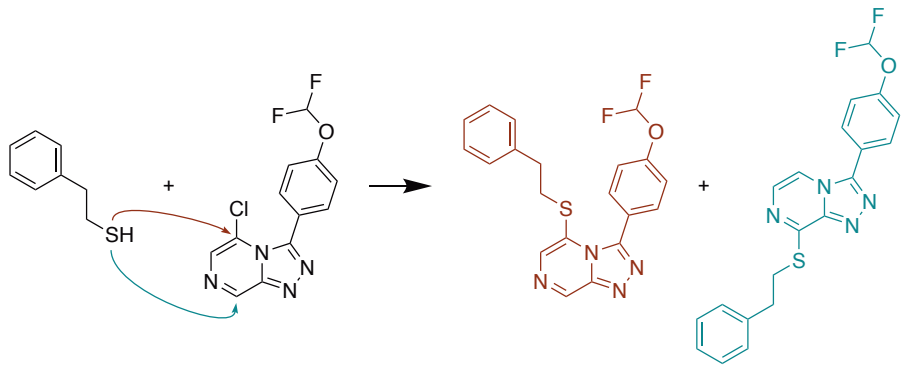

Figure 8.1: The unexpected identification of *tele*-substitution products during the synthesis of thioether-linked compounds. This observation led to the correction of a number of existing Series 4 compounds which had originally been misassigned.

Exploration of different linkers between the pyrazine ring and the northwest pendant phenyl group confirmed that an ether linker of two methylene units was key to maintaining activity. The use of other carbon chain lengths, triazoles, sulfoxides and sulfones as linkers were found to be poorly tolerated. Substitution at the benzylic position with amines and alcohols was generally beneficial for activity with the additional benefit of blocking this metabolically labile position and aiding compound solubility. Finally, the investigations into northeast substitutions validated the continued use of the 4-$OCHF_2$ group on the northeast phenyl ring (Figure 8.2).

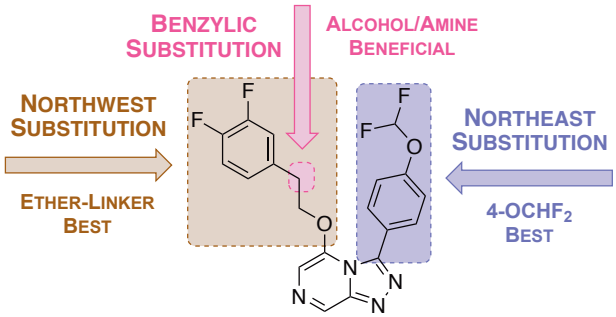

Figure 8.2: Key results from the exploration of Series 4 SAR. A number of key validations were made including the use of an ether-linker in the northwest position and the use of a 4-$OCHF_2$ substituted phenyl ring in the northeast position. Additionally, benzylic substitution was generally found to be beneficial.

In an attempt to improve the physicochemical properties of the Series 4 compounds, exploration into the reduction of aromaticity and deplanarisation through the use of phenyl bioisosteres was conducted (Figure 8.3). It was found that simple saturated ring systems were poorly tolerated in both the northwest and northeast positions. Interestingly, when replacing the phenyl rings with cubane, the potency was maintained when substituted at the northwest position but not at the northeast position. These results suggest a relatively low tolerability for deplanarisation in the northeast position and prompted further investigation into the former position. When using rigid hydrocarbon cages such as adamantane and norbornene, only a slight reduction in potency was

seen confirming the higher tolerability for deplanarisation in this position. A surprising result was seen upon the incorporation of carborane isomers in the northwest position, with the resulting compounds showing improved potency when compared with the parent phenyl compound. Unfortunately, when examining the cubane (**154**) and carborane (**192**) compounds for solubility and metabolic stability, they were both found to be detrimental to both these areas. Conversely, the BCP compound **178** was found to possess significantly improved physicochemical and metabolic properties.

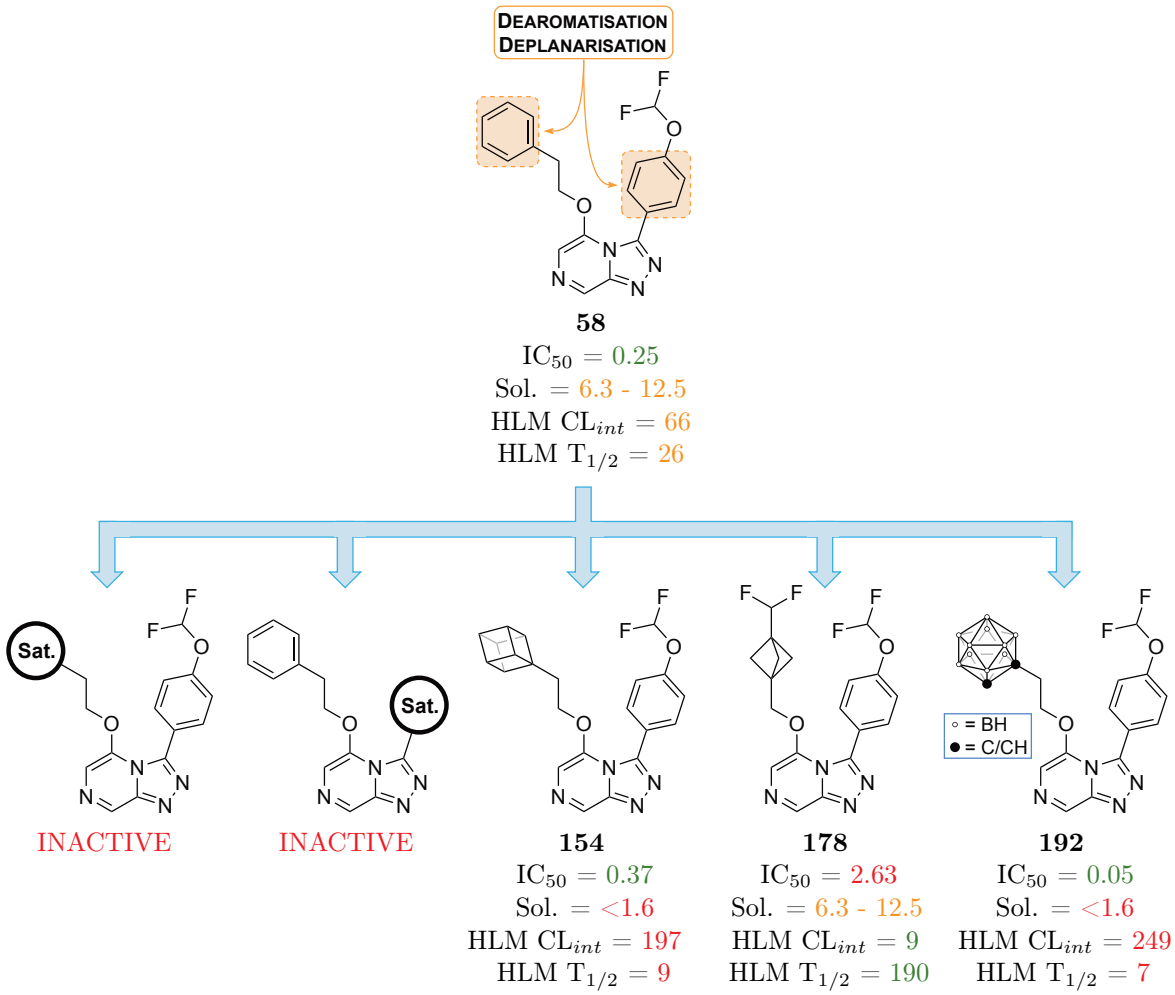

Figure 8.3: Key results from the exploration of phenyl bioisosteres. Saturated ring systems were poorly tolerated in both northwest and northeast positions, whereas the more rigid caged systems were better tolerated. The BCP derivative was found to have improved the solubility and metabolic stability when compared to the phenyl, cubane and carborane derivatives. Units: IC_{50} (μM); Sol. (μg/mL); CL_{int} (mL/min/kg); $T_{1/2}$ (min).

Validation of the suspected Series 4 mechanism of action was performed using compounds synthesised throughout this thesis. Excellent correlation was seen between *in vitro* potency and ion regulation activity in *Pf*ATP4. An initial crowdsourcing competition to predict active compounds was successfully ran, which paved the way for the launch of a second round involving the

application of machine learning approaches.

Having seen variable results for Series 4 hERG activity, a directed effort was made to alleviate these concerns. These investigations revolved around reports where incorporation of a carboxylic acid led to a reduction in hERG binding. It was found that, following installation of a carboxylic acid at the benzylic position (**208**) of a standard ether-linked Series 4 compound (**58**), a significant reduction in hERG activity was seen, along with a concomitant increase in solubility and metabolic stability Unfortunately, this came at a cost to *in vitro* potency. In an attempt to improve upon this aspect, a range of phenyl substituted analogues was synthesised. Unfortunately, while the benzylic alcohol intermediates performed well with IC_{50} values <1 μM, the two hERG Evador analogues were found to be significantly less potent.

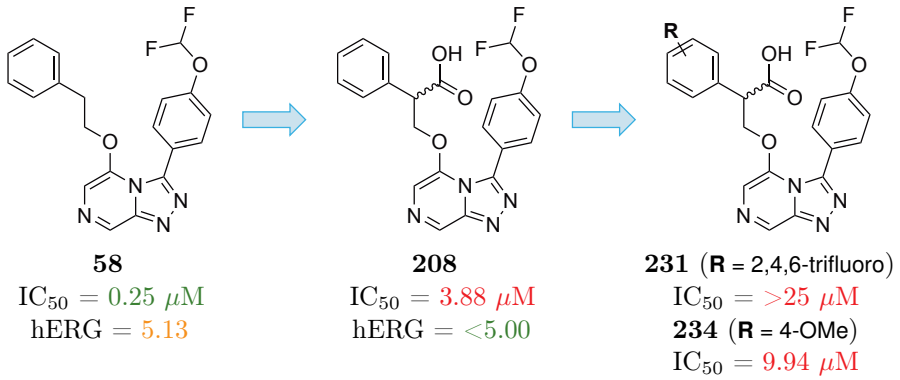

Figure 8.4: Key results from the exploration of Series 4 hERG activity. Installation of a carboxylic acid into a Series 4 compound was found to alleviate the concerns related to hERG binding, but this came with an accompanied decrease in *in vitro* potency.

The application of crowdsourced chemical synthesis to the OSM project was made possible *via* several initiatives including The University of Sydney's Special Studies Program. Over the span of five years, students have synthesised around twenty novel Series 4 compounds. These compounds have contributed to the greater dataset of Series 4 and have provided valuable information about SAR that were previously unexplored. The challenges associated with teaching and assessing work done in such an open manner was addressed with a larger focus put on the abilities of the students to perform in the lab and convey their experimental results.

8.2 Future Work

Following the observation that *tele*-substitution products may arise from the reaction of nucleophiles with the TP core, investigations have begun which aim to better explain this phenomenon.[378] Evaluation of the potential for these *tele*-substitution products to act against indications other than malaria have begun which might indicate a broader usefulness for the divergent

synthetic routes available from nucleophilic displacement on an aza-aromatic core.[379]

After screening a wide range of phenyl bioisosteres, the BCP analogue was identified as possessing significantly improved physicochemical and metabolic properties. The less desirable potency is attributed to the one methylene unit ether chain. Future efforts will be made to synthesise the corresponding two methylene unit ether chain analogue to provide a compound with better all-round biological properties (Figure 8.5).

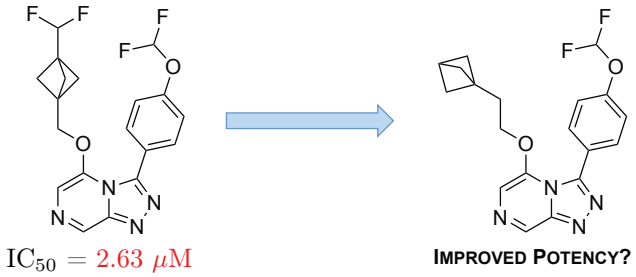

Figure 8.5: The two methylene unit BCP derivative proposed to possess better activity. This proposed compound would posses the improved physicochemical properties of the one methylene unit chain BCP derivative and a potency closer to the corresponding two methylene unit chain phenyl compound.

While preliminary studies conducted on Series 4 have revealed cross-resistance with KAE609,[161] further studies revolving around omics-based approaches (such as genomics, proteomics and epigenomics)[380] may be considered to identify potential off-target interactions. For example, proteomics approaches have recently been applied on the indoloquinoline antimalarial ICL-M to reveal important information about its MoA.[381] It is notable however that such studies are typically expensive to conduct. The entries resulting from the second round of the modelling competition must be evaluated to determine the accuracy of prediction for each model. Should these models be successful, they will become a valuable tool not only for the design of Series 4 compounds, but also for the identification of novel scaffolds which have the potential to target *Pf*ATP4.

The ultimate goal of the OSM project remains to be progression of the first open source discovered compound into clinical trials. Progress has been made in this regard, with a lead compound having been identified.[382] The remaining physicochemical and safety data must be obtained and optimisation of the synthetic route towards this compound may be conducted. Should a late lead be progressed into the clinical phase, subsequent strategies may be developed, using Series 4 as a real example, of how the later stages of open source drug discovery may be operated and funded.

9. Experimental Details

9.1 General Experimental Details

Room temperature (rt) typically varies between 15–25 °C. Reagents were purchased from either Sigma–Aldrich, Alfa Aesar, Acros, Merck, Fischer Scientific, Matrix Scientific, Ajax or Fluorochem. Unless otherwise specified, the reagents were used without further purification. Anhydrous conditions: glassware was dried at >130 °C for >12 h, assembled hot and allowed to cool under a high vacuum where appropriate or purged with inert gas. Anhydrous solvents were obtained from the PureSolv system or by drying over activated 3 Å molecular sieves. Nitrogen gas was dried over silica and calcium chloride. Argon gas was used as acquired. The phrase *in vacuo* corresponds to ∼1 mbar on a Schlenk line. Reduced pressure means under rotary evaporation at 40 °C from 900–50 mbar. Flash chromatography was performed on Davisil Grace Davison 40–63 μm (230–400 mesh) silica gel or on a Biotage Isolera One. Analytical thin layer chromatography was performed on Merck Silica Gel 60 F_{254} precoated aluminium plates (0.2 mm) and visualised with UV irradiation (254 nm) and potassium permanganate, anisaldehyde or ninhydrin staining. High temperature reactions were carried out in silicone oil baths, controlled by temperature probe in the oil bath.

9.2 General Analytical and Preparative Instrumentation and Notation

Melting points (m.p.) were recorded on a Stanford Research Systems OptiMelt at 1 °C min^{-1} (capillaries ø = 1.5–1.6 mm, 90 mm) or a Stuart SMP10 at 2 °C min^{-1} (capillaries ø = 1.8–1.9 mm, 100 mm). Infrared spectroscopy was carried out on a Bruker Alpha-E (attenuated total reflectance) without atmospheric compensation and processed using OPUS 7.0 software. Samples were analysed neat. Nuclear magnetic resonance spectroscopy was carried out at 300 K on Bruker spectrometers: either AVANCE 200 (^{1}H at 200 MHz), AVANCE 300 (^{1}H at 300 MHz, ^{13}C at 75 MHz), AVANCE III 400 (^{1}H at 400 MHz, ^{13}C at 101 MHz) or AVANCE III 500 (^{1}H at 500 MHz, ^{13}C at 126 MHz). Spectra were processed using Bruker Topspin or Mestrelab Research Mnova. Deuterated solvents ($CDCl_3$, DMSO-d_6, CD_3OD, acetone-d_6) obtained from the Cambridge Isotope Laboratories. ^{1}H and ^{13}C chemical shifts are reported in parts per million (ppm) with respect to TMS at 0.00 ppm. The chemical shifts of the spectra were calibrated to residual solvent peaks (^{1}H: $CHCl_3$ 7.26 ppm, DMSO 2.50 ppm, MeOH 3.31 ppm, $(CH_3)_2CO$ 2.05 ppm, TMS 0.00 ppm; ^{13}C: $CHCl_3$ 77.16 ppm, DMSO 39.52 ppm, MeOH 49.00 ppm, $(CH_3)_2CO$ 39.52 ppm, TMS 0.00 ppm). ^{1}H signal multiplicity is reported as: singlet (s), doublet (d),

triplet (t), quartet (q), pentet (p) and combinations thereof, or multiplet (m). Broad signals are designated broad (br). Coupling constants (J) are reported in Hertz (Hz). Integrals are relative. $_{app}$ = apparent when the multiplicity was unexpected, e.g. coincidental or unresolved. Low resolution mass spectrometry (m/z) was carried out on a Finnigan quadrupole ion trap mass spectrometer using electrospray ionisation (ESI) or atmospheric-pressure chemical ionisation (APCI). High resolution mass spectrometry (HRMS) was performed on a Bruker 7T FT-ICR using ESI or APCI. Positive and negative detection is indicated by the charge of the ion, e.g. $[M+H]^+$ indicates positive ion detection. Analytical liquid chromatography-mass spectrometry (LCMS) was performed on an Agilent Infinity 1290 II system consisting of a quaternary pump (G7111A) and a diode array detector WR (G7115A) coupled to a InfinityLab LC/MSD (G6125B) using ESI. An Agilent ZORBAX Eclipse XDB-C18 column (5 μm, 4.6 × 150 mm) was eluted at a flow rate of 1 mL/min with a mobile phase of 0.1% formic acid in H_2O and 0.1% formic acid in MeCN. Preparative LCMS was performed on a combined Agilent Infinity 1260 II and Infinity 1290 II system consisting of a preparative binary pump (G7161A) and a multiple wavelength detector (G7165A) coupled to a InfinityLab LC/MSD (G6125B) using ESI and a preparative open-bed fraction collector (G7159B). An Agilent PrepHT XDB-C18 column (7 μm, 21.2 × 250 mm) was eluted at a flow rate of 15 or 25 mL/min with a mobile phase of 0.1% formic acid in H_2O and 0.1% formic acid in MeCN.

9.3 General Synthetic Procedures

General Procedure 1: Displacement of chloride with hydrazine

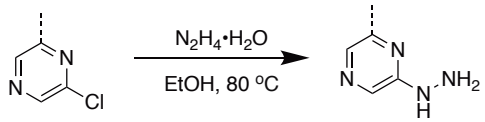

Chloropyrazine (1 equiv.) was stirred in EtOH (345 mM). Hydrazine monohydrate (2 equiv.) was added and the reaction stirred at 80 °C until completion as indicated by TLC. The solvent was removed under reduced pressure, then the residue diluted with H_2O and EtOAc. The organic layer was separated and the aqueous layer extracted with EtOAc (3 ×). The combined organic layers were washed with brine, dried (Na_2SO_4), filtered and concentrated under reduced pressure to give the corresponding displacement product which was carried forward without further purification unless otherwise stated.

General Procedure 2: Condensation of hydrazine with an aldehyde

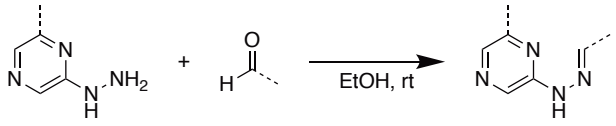

The product from General Procedure 1 (1 equiv.) was stirred into EtOH (112 mM). Aldehyde (1 equiv.) was added and the reaction stirred at rt until completion as indicated by TLC. The solvent was removed under reduced pressure to give the corresponding condensation product which was carried forward without further purification unless otherwise stated.

General Procedure 3: Oxidative cyclisation of a hydrazone

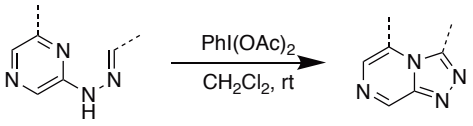

The product from General Procedure 2 (1 equiv.) was stirred into CH_2Cl_2 (112 mM). $PhI(OAc)_2$ (1 equiv.) was added and the reaction stirred at rt until completion as indication by TLC. The reaction was quenched with sat. aq. $NaHCO_3$, diluted with CH_2Cl_2 and the organic layer separated. The aqueous layer was extracted with CH_2Cl_2 (3 $\times$) and the combined organic layers were washed with brine, dried ($MgSO_4$), filtered and concentrated under reduced pressure to give the corresponding crude material which was purified by flash chromatography on silica to give the corresponding cyclisation product.

General Procedure 4: Nucleophilic displacement of Cl from the TP core

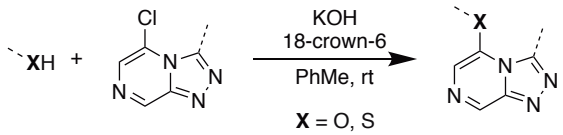

Nucleophile (1.0 equiv.) was dissolved in PhMe (168 mM) along with the product from General Procedure 3 (1.0 equiv.), KOH (3.0 equiv.) and 18-crown-6 (0.1 equiv.). The reaction mixture was allowed to stir at rt until completion as indicated by TLC. The reaction was diluted with H_2O, then extracted with EtOAc. The organic layers were washed with H_2O until the aqueous layer became neutral, followed by brine, dried ($MgSO_4$), filtered and concentrated under reduced pressure to give the crude material, which was purified by flash chromatography on silica to give the corresponding displacement product.

General Procedure 5: CuAAC reaction

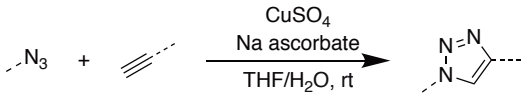

Azide (1 equiv.) and alkyne alcohol (1 equiv.) were added to a 1:1 THF/H_2O mixture. The reaction was backfilled with N_2 (5 ×). Copper sulfate pentahydrate (10 mol%) and sodium ascorbate (25 mol%) were added and the reaction backfilled with N_2 (3 ×). The reaction mixture was allowed to stir at rt until completion as indicated by TLC. The reaction mixture was extracted with EtOAc and the combined organic layers were washed with H_2O, dried (Na_2SO_4), filtered and concentrated under reduced pressure to give the corresponding addition product that was used without further purification unless otherwise stated.

General Procedure 6: Ester to alcohol reduction with $LiAlH_4$

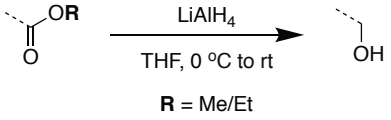

Ester (1 equiv.) was dissolved in anhydrous THF (566 mM) and cooled to 0 °C. $LiAlH_4$ (1 M in THF, 0.64 equiv.) was added dropwise and the reaction mixture stirred for 10 min at 0 °C, then at rt overnight. The reaction was cooled in an ice bath. Excess LAH was quenched with EtOAc dropwise, then sat. aq. Rochelle's salt was added. The mixture was stirred at 0 °C, then at rt until two distinct layers were seen. The organic layer was separated and the aqueous layer extracted with EtOAc (3 ×). The combined organic layers were dried ($MgSO_4$), filtered and concentrated under reduced pressure to give the corresponding reduction product that was used without further purification unless otherwise stated.

General Procedure 7: Esterification of a carboxylic acid

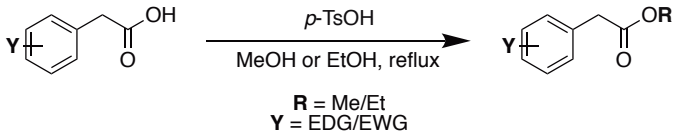

Carboxylic acid (1.00 equiv.) and *p*-TsOH (0.02 equiv.) were dissolved in MeOH or EtOH (1.45 M) and the reaction heated to reflux overnight. The reaction was cooled to rt and the solvent removed. EtOAc was added to the residue and the organic layer washed with H_2O, sat. aq. $NaHCO_3$, brine, dried ($MgSO_4$), filtered and concentrated under reduced pressure to give the corresponding ester product that was used without further purification unless otherwise stated.

General Procedure 8: Ethyl carboxylation of an ethyl ester

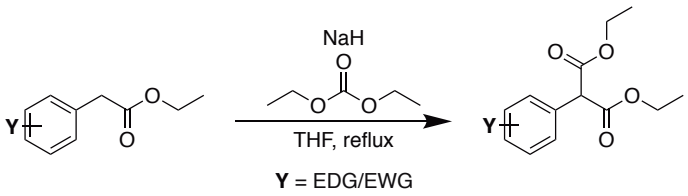

The product from General Procedure 7 (1.00 equiv.) was dissolved in THF (0.36 M). NaH (60% dispersion in mineral oil, 2.05 equiv.) and diethyl carbonate (5.10 equiv.) were added and the reaction heated to reflux for 1 h. The reaction was cooled to rt, quenched with sat. aq. NH_4Cl and extracted with EtOAc. The combined organic layers were washed with brine, dried (Na_2SO_4), filtered through a pad of silica and concentrated under reduced pressure to give the crude material, which was purified by flash chromatography on silica to give the corresponding carboxylated product.

General Procedure 9: Bis-ester to diol reduction with $NaBH_4$

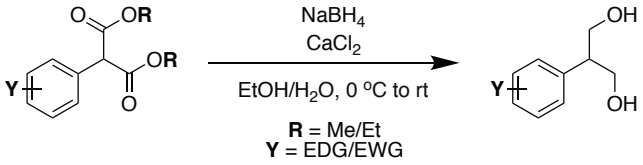

Ester (1.00 equiv.) was dissolved in EtOH (1.28 M) and a solution of $CaCl_2$ (2.93 equiv.) in H_2O (0.53 M) was added. The suspension was cooled to 0 °C and $NaBH_4$ (5.90 equiv.) was added portionwise keeping the temperature at 0–5 °C. The reaction mixture was allowed to stir for 2 h at 0 °C then stirred at rt overnight. The pH was adjusted to 5–6 with 1 M HCl and the EtOH removed under reduced pressure. The aqueous solution was extracted with EtOAc (3 ×) and the combined organic layers were dried (Na_2SO_4), filtered and concentrated under reduced pressure to give the crude material, which was purified by flash chromatography on silica to give the corresponding reduction product.

9.4 Synthesis and Characterisation of Compounds from Chapter 2

5-Chloro-3-(4-chlorophenyl)-[1,2,4]triazolo[4,3-*a*]pyrazine 252

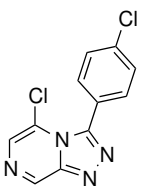

Prepared according to General Procedure 3 from: (*E*)-2-chloro-6-(2-(4-chlorobenzylidene)hydrazinyl)pyrazine (synthesised by Dr. Alice Motion, 750 mg, 2.81 mmol) to give the crude title compound as a red powder (1.23 g); purified by automated flash chromatography on silica (Biotage Isolera, 12–100% EtOAc in hexanes) to give *the title compound* as a pale orange powder (659 mg, 89%); $\mathbf{R_f}$ 0.19 (50% EtOAc

in hexanes); **m.p.** 180–183 °C; **^{1}H NMR** (300 MHz, $CDCl_3$) δ: 9.29 (s, 1H), 7.86 (s, 1H), 7.55 (d, *J* 8.6, 2H), 7.48 (d, *J* 8.5, 2H); **^{13}C NMR** (75 MHz, $CDCl_3$) δ: 147.2, 143.0, 137.2, 132.6, 129.8, 128.3, 125.1, 121.8; ***m/z*** (ESI+) 287 ($[M+Na]^+$, 100%); **HRMS** (ESI+) found 286.98617 $[M+Na]^+$, $C_{11}H_6Cl_2N_4Na^+$ requires 286.98617.

3-(4-Chlorophenyl)-5-phenethoxy-[1,2,4]triazolo[4,3-*a*]pyrazine 11

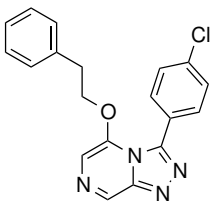

Prepared according to General Procedure 4 from: 2-phenylethanol (136 mL, 1.13 mmol) and **252** (300 mg, 1.13 mmol) to give the crude title compound as a brown solid (386 mg); purified by automated flash chromatography on silica (Biotage Isolera, 12–100% EtOAc in hexanes) to give *the title compound* as a yellow powder (279 mg, 70%); $\mathbf{R_f}$ 0.06 (50% EtOAc in hexanes); **m.p.** 128–130 °C; **^{1}H NMR** (300 MHz, $CDCl_3$) δ: 8.97 (s, 1H), 7.55 (d, *J* 8.5, 2H), 7.38 (d, *J* 8.5, 2H), 7.30 (s, 1H), 7.25–7.16 (m, 3H), 7.01–6.75 (m, 2H), 4.44 (t, *J* 6.5, 2H), 2.95 (t, *J* 6.5, 2H); **^{13}C NMR** (75 MHz, DMSO-d_6) δ: 147.4, 145.3, 143.8, 137.2, 135.0, 134.7, 132.4, 128.6, 128.2, 127.6, 126.7, 126.4, 108.9, 71.2, 33.8; ***m/z*** (ESI+) 373 ($[M+Na]^+$, 100%), 723 ($[2M+Na]^+$, 89%); **HRMS** (ESI+) found 373.08253 $[M+Na]^+$, $C_{19}H_{15}ClN_4ONa^+$ requires 373.08262.

6-Chloro-*N*-(4-chlorophenyl)pyrazine-2-carboxamide 253

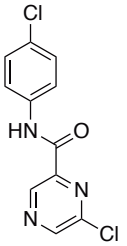

6-Chloropyrazine-2-carboxylic acid (1.00 g, 6.31 mmol, 1.0 equiv.), 4-chloroaniline (805 mg, 6.31 mmol, 1.0 equiv.) and DIPEA (2.20 mL, 12.6 mmol, 2.0 equiv.) were dissolved in DMF (10 mL) and cooled to 0 °C. T3P (50% in EtOAc, 5.60 mL, 1.5 equiv.) was added dropwise with stirring, and the reaction mixture was kept at 0 °C for 15 min, then stirred at rt for 22 h. The reaction mixture was diluted with EtOAc (20 mL) and washed with sat. aq. $NaHCO_3$ (3 × 20 mL). The combined aqueous layers were extracted with EtOAc (2 × 20 mL) and the combined organic layers washed with H_2O (10 mL), brine (10 mL), and concentrated under reduced pressure to give the crude title compound as a pale brown solid (1.21 g); purified by automated flash chromatography on silica (Biotage Isolera, 12–100% EtOAc in hexanes) to give *the title compound* as pale brown crystals (853 mg, 40%); $\mathbf{R_f}$ 0.63 (50% EtOAc in hexanes); **m.p.** 148–151 °C (lit.[383] 145–146 °C); **^{1}H NMR** (300 MHz, $CDCl_3$) δ: 9.38 (br s, 2H), 8.82 (s, 1H), 7.71 (d, *J* 8.8, 2H), 7.36 (d, *J* 8.8, 2H); ***m/z*** (ESI+) 290 ($[M+Na]^+$, 67%), 555 ($[2M+Na]^+$, 100%); **HRMS** (ESI+) found 289.98591 $[M+Na]^+$, $C_{11}H_7Cl_2N_3ONa^+$ requires 289.98582. Spectroscopic data matched those in the literature.[383]

N-(4-Chlorophenyl)-6-hydrazinylpyrazine-2-carboxamide 254

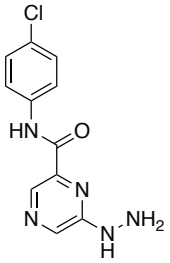

Prepared according to General Procedure 1 from: **253** (4.00 g, 14.9 mmol) to give the crude title compound as a yellow solid (3.45 g); this intermediate, though novel, was carried forward without purification or complete characterisation; $\mathbf{R_f}$ 0.15 (50% EtOAc in hexanes); **^{1}H NMR** (400 MHz, DMSO-d$_6$) δ: 10.46 (s, 1H), 8.50 (s, 1H), 8.31 (s, 1H), 8.19 (s, 1H), 7.87 (d, *J* 8.9, 2H), 7.45 (d, *J* 8.9, 2H), 4.63 (br s, 2H); **^{13}C NMR** (101 MHz, DMSO-d$_6$) δ: 162.5, 155.0, 141.0, 137.1, 135.6, 129.8, 128.7, 127.8, 121.9.

(*E*)-*N*-(4-Chlorophenyl)-6-(2-(4-(difluoromethoxy)benzylidene)hydrazinyl)pyrazine-2-carboxamide 255

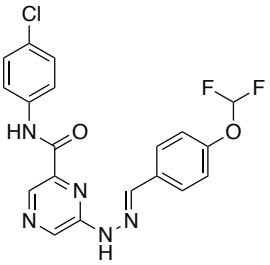

Prepared according to General Procedure 2 from: **254** (150 mg, 0.57 mmol) and 4-(difluoromethoxy)benzaldehyde (75.2 μL, 0.57 mmol) to give the crude title compound as a yellow powder (253 mg); this intermediate, though novel, was carried forward without purification or complete characterisation; $\mathbf{R_f}$ 0.49 (5% MeOH in CH_2Cl_2); **^{1}H NMR** (400 MHz, DMSO-d$_6$) δ: 11.41 (s, 1H), 10.46 (s, 1H), 8.83 (s, 1H), 8.59 (s, 1H), 8.13 (s, 1H), 7.82 (dd, *J* 8.9 & 2.9, 4H), 7.44 (d, *J* 8.9, 2H), 7.26 (t, *J* 73.8, 1H), 7.23 (d, *J* 8.6, 2H); **^{13}C NMR** (101 MHz, DMSO-d$_6$) δ: 162.5, 151.8, 151.2, 142.3, 141.6, 137.2, 134.3, 133.6, 131.7, 129.0, 128.5, 128.2, 122.0, 119.1, 116.4 (t, *J* 258.0).

N-(4-Chlorophenyl)-3-(4-(difluoromethoxy)phenyl)-[1,2,4]triazolo[4,3-*a*]pyrazine-5-carboxamide 19

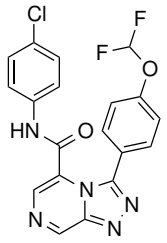

Prepared according to General Procedure 3 from: **255** (111 mg, 0.27 mmol) to give the crude title compound as an orange solid (1.16 g); purified by trituration with MeOH to give *the title compound* as a white powder (398 mg, 49%); $\mathbf{R_f}$ 0.25 (5% MeOH in CH_2Cl_2); **m.p.** >300 °C; **^{1}H NMR** (300 MHz, DMSO-d$_6$) δ: 10.85 (s, 1H), 9.65 (s, 1H), 8.30 (s, 1H), 7.63 (d, *J* 7.9, 2H), 7.54–6.69 (m, 7H); **^{13}C NMR** (75 MHz, DMSO-d$_6$) δ: 157.2, 152.0, 146.8, 146.0, 145.7, 136.3, 130.3, 130.2, 128.4, 128.2, 124.5, 124.0, 121.1, 118.3, 115.9 (t, *J* 258.3); ***m/z*** (ESI+) 438 ($[M+Na]^+$, 100%); **HRMS** (ESI+) found 438.05398 $[M+Na]^+$, $C_{19}H_{12}ClF_2N_5O_2Na^+$ requires 438.05402.

6-Chloro-*N*-(3-chloro-4-fluorophenyl)pyrazine-2-carboxamide 256

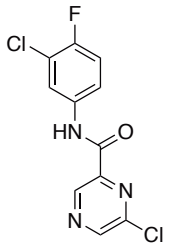

6-Chloropyrazine-2-carboxylic acid (500 mg, 3.15 mmol, 1.0 equiv.), 3-chloro-4-fluoroaniline (459 mg, 3.15 mmol, 1.0 equiv.) and DIPEA (1.10 mL, 6.31 mmol, 2.0 equiv.) were dissolved in DMF (5 mL) and cooled to 0 °C. T3P (50% in EtOAc, 2.82 mL, 1.5 equiv.) was added dropwise with stirring, and the reaction mixture was kept at 0 °C for 15 min, then stirred at rt for 1 h. The reaction mixture was diluted with EtOAc (20 mL) and washed with sat. aq. $NaHCO_3$ (3 × 20 mL). The combined aqueous layers were extracted with EtOAc (2 × 20 mL) and the combined organic layers washed with H_2O (10 mL), brine (10 mL), and concentrated under reduced pressure to give the crude title compound as a light brown solid (1.04 g); this intermediate, though novel, was carried forward without purification or complete characterisation; $\mathbf{R_f}$ 0.91 (100% EtOAc); **^{1}H NMR** (200 MHz, DMSO-d$_6$) δ: 10.86 (s, 1H), 9.23 (s, 1H), 9.07 (s, 1H), 8.15 (dd, *J* 6.8 & 2.4, 1H), 7.94–7.77 (m, 1H), 7.44 (t, *J* 9.1, 1H).

***N*-(3-Chloro-4-fluorophenyl)-6-hydrazinylpyrazine-2-carboxamide 257**

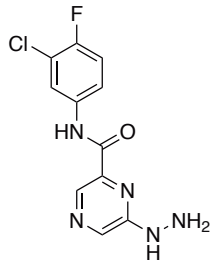

Prepared according to General Procedure 1 from: **256** (976 mg, 3.41 mmol) to give the crude title compound as a yellow solid (644 mg); this intermediate, though novel, was carried forward without purification or characterisation; $\mathbf{R_f}$ 0.31 (100% EtOAc).

(*E*)-*N*-(3-Chloro-4-fluorophenyl)-6-(2-(4-(difluoromethoxy)benzylidene)hydrazinyl) pyrazine-2-carboxamide 258

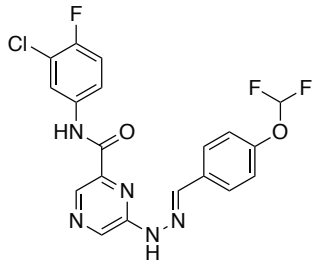

Prepared according to General Procedure 2 from: **257** (325 mg, 1.15 mmol) and 4-(difluoromethoxy)benzaldehyde (0.15 mL, 1.15 mmol) to give the crude title compound as a bright yellow solid (567 mg); this intermediate, though novel, was carried forward without purification or characterisation; $\mathbf{R_f}$ 0.49 (50% EtOAc in hexanes).

_N_-(3-Chloro-4-fluorophenyl)-3-(4-(difluoromethoxy)phenyl)-[1,2,4]triazolo[4,3-_a_] pyrazine-5-carboxamide 20

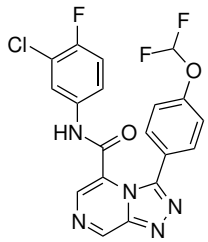

Prepared according to General Procedure 3 from: **258** (500 mg, 1.15 mmol) to give the crude title compound as an orange solid (663 mg); purified by automated flash chromatography on silica (Biotage Isolera, 25–100% EtOAc in hexanes) to give *the title compound* as an off-white powder (191 mg, 38%); $\mathbf{R_f}$ 0.30 (100% EtOAc); **m.p.** 266–269 °C; **^{1}H NMR** (300 MHz, DMSO-d$_6$) δ: 10.93 (s, 1H), 9.66 (s, 1H), 8.30 (s, 1H), 7.63 (d, *J* 8.4, 2H), 7.51 (d, *J* 6.5, 1H), 7.31 (t, *J* 9.0, 1H), 7.43–6.82 (m, 4H); **^{13}C NMR** (75 MHz, DMSO-d$_6$) δ: 157.3, 155.5, 152.1, 146.8, 146.2, 145.7, 134.4, 130.4, 130.3, 124.3, 124.0, 121.1, 120.0 (d, *J* 6.9), 119.1 (d, *J* 18.4), 118.2, 116.8 (d, *J* 22.0), 115.8; ***m/z*** (ESI+) 434 ([M+H]$^+$, 27%), 466 ([M+CH$_3$OH+H]$^+$, 100%); **HRMS** (ESI+) found 434.06305 [M+H]$^+$, $C_{19}H_{11}ClF_3N_5O_2H^+$ requires 434.06261.

5-(2-Phenyl-2-((tetrahydro-2_H_-pyran-2-yl)oxy)ethoxy)-3-(6-(trifluoromethyl) pyridin-3-yl)-[1,2,4]triazolo[4,3-_a_]pyrazine 107

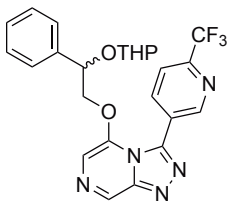

Prepared according to General Procedure 4 from: **103** (300 mg, 1.35 mmol) and 5-chloro-3-(6-(trifluoromethyl)pyridin-3-yl)-[1,2,4]triazolo[4,3-*a*]pyrazine (synthesised by Dr. Alice Motion, 404 mg, 1.35 mmol) to give the crude title compound as a dark olive green sludge (706 mg); purified by automated flash chromatography on silica (Biotage Isolera, 25–100% EtOAc in hexanes) to give *the title compound* as a dark olive green powder (363 mg, 55%); this intermediate, though novel, was carried forward without characterisation; $\mathbf{R_f}$ 0.53 (100% EtOAc).

1-Phenyl-2-((3-(6-(trifluoromethyl)pyridin-3-yl)-[1,2,4]triazolo[4,3-_a_]pyrazin-5-yl) oxy)ethan-1-ol 25

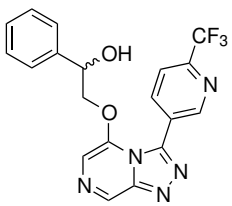

Compound **107** (200 mg, 0.41 mmol, 1 equiv.) was dissolved in EtOH (5 mL). $CuCl_2{\cdot}2H_2O$ (3.51 mg, 0.02 mmol, 5 mol%) was added and the mixture heated at reflux for 2 h. The solvent was removed and the residue directly purified by automated flash chromatography on silica (Biotage Isolera, 25–100% EtOAc in hexanes) to give *the title compound* as an olive green powder (145 mg, 88%); $\mathbf{R_f}$ 0.28 (100% EtOAc); **m.p.** 145–148 °C; **^{1}H NMR** (300 MHz, $CDCl_3$) δ: 9.13 (s, 1H), 8.98 (br s, 1H), 8.30 (d, *J* 8.0, 1H), 7.77 (d, *J* 8.0, 1H), 7.37 (s, 1H), 7.31 (br s, 5H), 4.92 (br s, 1H), 4.44–4.21 (m, 2H), 3.59 (s, 1H); **^{13}C NMR** (75 MHz, $CDCl_3$) δ: 151.3, 148.9, 148.5, 143.8, 143.5, 139.8, 139.0, 136.5, 129.0, 127.0, 126.1, 123.3, 119.8, 119.6, 109.3, 75.4, 71.6; ***m/z*** (ESI+) 402 ([M+H]$^+$, 100%); **HRMS** (ESI+) found 402.11810 [M+H]$^+$, $C_{19}H_{14}F_3N_5O_2H^+$ requires 402.11724.

(6-Chloropyrazin-2-yl)(isoindolin-2-yl)methanone 37

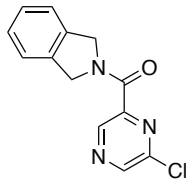

6-Chloropyrazine-2-carboxylic acid (1.00 g, 6.31 mmol, 1.0 equiv.), isoindoline (0.72 mL, 6.31 mmol, 1.0 equiv.) and DIPEA (2.20 mL, 12.6 mmol, 2.0 equiv.) were dissolved in DMF (10 mL) and cooled to 0 °C. T3P (50% in EtOAc, 5.60 mL, 1.5 equiv.) was added dropwise with stirring, and the reaction mixture was kept at 0 °C for 15 min, then stirred at rt for 19 h. The reaction mixture was diluted with EtOAc (20 mL) and washed with sat. aq. $NaHCO_3$ (3 × 20 mL). The combined aqueous layers were extracted with EtOAc (2 × 20 mL) and the combined organic layers washed with H_2O (10 mL), brine (10 mL), and concentrated under reduced pressure to give the crude title compound as a brown solid (1.67 g); this intermediate, though novel, was carried forward without purification or complete characterisation; $\mathbf{R_f}$ 0.88 (100% EtOAc); **^{1}H NMR** (300 MHz, $CDCl_3$) δ: 9.18 (s, 1H), 8.71 (s, 1H), 7.47–6.94 (m, 4H), 5.26 (s, 2H), 5.05 (s, 2H); **^{13}C NMR** (75 MHz, $CDCl_3$) δ: 162.5, 147.6, 147.1, 145.9, 143.9, 136.9, 135.0, 127.9, 127.8, 122.8, 122.7, 54.9, 54.0 (mixture of amide rotamers).

(6-Hydrazinylpyrazin-2-yl)(isoindolin-2-yl)methanone 259

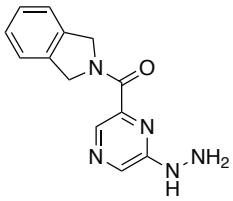

Prepared according to General Procedure 1 from: **37** (1.50 g, 5.78 mmol) to give the crude title compound as an orange solid (1.30 g); this intermediate, though novel, was carried forward without purification or characterisation; $\mathbf{R_f}$ 0.30 (100% EtOAc).

(*E*)-(6-(2-(4-(Difluoromethoxy)benzylidene)hydrazinyl)pyrazin-2-yl)(isoindolin-2-yl) methanone 260

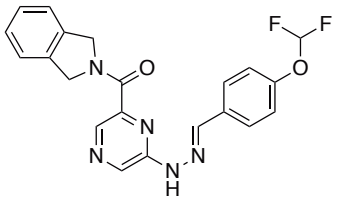

Prepared according to General Procedure 2 from: **259** (1.00 g, 3.92 mmol) and 4-(difluoromethoxy)benzaldehyde (0.52 mL, 3.92 mmol) to give the crude title compound as a yellow solid (1.62 g) that was carried forward without further purification or complete characterisation; a small amount of crude material was purified by trituration with CH_2Cl_2 to give *the title compound* as a yellow powder (30.2 mg); $\mathbf{R_f}$ 0.30 (50% EtOAc in hexanes); **m.p.** 218–220 °C; **^{1}H NMR** (400 MzHz, DMSO-d_6) δ: 11.36 (s, 1H), 8.72 (s, 1H), 8.36 (s, 1H), 8.10 (s, 1H), 7.81 (d, *J* 8.8, 2H), 7.43–7.40 (m, 1H), 7.34–7.29 (m, 3H), 7.26 (t, *J* 73.9, 1H), 7.23 (d, *J* 8.7, 2H), 5.11 (s, 2H), 4.89 (s, 2H); **^{13}C NMR** (101 MHz, DMSO-d_6) δ: 164.5, 151.6 (t, *J* 3.1), 151.0, 145.7, 140.9, 137.3, 135.4, 134.3, 131.94, 131.91, 128.3, 127.7, 127.6, 123.1, 122.8, 119.1, 116.3 (t, *J* 257.9), 54.2, 52.9 (mixture of amide rotamers).

(3-(4-(Difluoromethoxy)phenyl)-[1,2,4]triazolo[4,3-*a*]pyrazin-5-yl)(isoindolin-2-yl) methanone 31

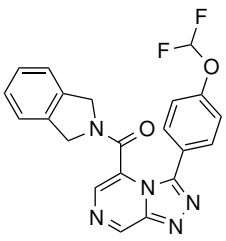

Prepared according to General Procedure 3 from: **260** (1.40 g, 3.42 mmol) to give the crude title compound as a viscous dark orange liquid (1.86 g); purified by automated flash chromatography on silica (Biotage Isolera, 12–100% EtOAc in hexanes) to give *the title compound* as a yellow powder (671 mg, 48%); $\mathbf{R_f}$ 0.35 (100% EtOAc); **m.p.** 158–161 °C; **^{1}H NMR** (300 MHz, $CDCl_3$) δ: 9.43 (s, 1H), 8.01 (s, 1H), 7.45 (d, *J* 8.7, 2H), 7.35–7.17 (m, 4H), 6.99 (d, *J* 8.6, 2H), 6.46 (t, *J* 73.0, 1H), 4.51 (s, 2H), 4.37 (br s, 2H); **^{13}C NMR** (75 MHz, $CDCl_3$) δ: 158.7, 152.7, 146.9, 145.9, 135.0, 134.1, 130.8, 129.4, 128.5, 128.2, 124.0, 122.9, 122.9, 122.6, 119.4, 115.3 (t, *J* 262.2), 53.3, 52.1 (mixture of amide rotamers); ***m/z*** (ESI+) 430 ($[M+Na]^+$, 100%); **HRMS** (ESI+) found 430.10851 $[M+Na]^+$, $C_{21}H_{15}F_2N_5O_2Na^+$ requires 430.10862.

Methyl 6-chloropyrazine-2-carboxylate 34

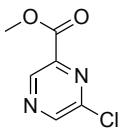

To a solution of 6-chloropyrazine-2-carboxylic acid (2.00 g, 12.6 mmol) in MeOH (32 mL) was added conc. HCl (0.25 mL). The mixture was heated at 80 °C. The reaction was cooled to rt and the solvent removed. The residue was diluted with EtOAc and washed with a sat. aq. $NaHCO_3$, dried (Na_2SO_4), filtered and concentrated under reduced pressure to give the crude title compound as a dark brown liquid (1.94 g); carried forward without further purification or characterisation; $\mathbf{R_f}$ 0.76 (100% EtOAc).

(6-Chloropyrazin-2-yl)methanol 33

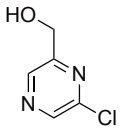

To a solution of **34** (353 mg, 2.05 mmol, 1 equiv.) in H_2O (5 mL) was added $NaBH_4$ (387 mg, 10.2 mmol, 5 equiv.) portionwise at 0 °C. The reaction was warmed to rt and stirred for 30 min, followed by addition of sat. aq. K_2CO_3 (10 mL) and EtOH (5 mL). The resulting mixture was stirred for 1 h then extracted with EtOAc (2 ×). The combined organic layers were dried (Na_2SO_4), filtered and concentrated under reduced pressure to give the crude title compound as an orange solid (275 mg); purified by automated flash chromatography on silica (Biotage Isolera, 25–100% EtOAc in hexanes) to give *the title compound* as a white solid (102 mg, 35%); carried forward without complete characterisation; $\mathbf{R_f}$ 0.12 (50% EtOAc in hexanes); **m.p.** 62–69 °C; **^{1}H NMR** (300 MHz, $CDCl_3$) δ: 8.58 (s, 1H), 8.52 (s, 1H), 4.83 (d, *J* 5.4, 2H), 3.12–2.75 (m, 1H); **^{13}C NMR** (75 MHz, $CDCl_3$) δ: 155.4, 148.8, 143.4, 140.4, 62.8. Compound reported in the literature but no NMR characterisation data were provided.[384]

2-((6-Chloropyrazin-2-yl)methyl)isoindoline 36

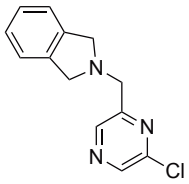

To a stirred solution of **33** (250 mg, 1.73 mmol, 1.0 equiv.) and MsCl (160 μL, 208 mmol, 1.2 equiv.) in CH_2Cl_2 (10 mL) at 0 °C, was added Et_3N (1.21 mL, 8.65 mmol, 5.0 equiv.) dropwise. After 1 h the reaction was diluted with H_2O (12 mL) and extracted with CH_2Cl_2 (3 ×). The combined organic layers were washed with H_2O (2 ×), brine (2 ×), dried (Na_2SO_4), filtered and concentrated under reduced pressure to give the crude mesylate **35** as a red liquid (154 mg); $\mathbf{R_f}$ 0.89 (50% EtOAc in hexanes); compound **35** (70.0 mg, 0.31 mmol) was dissolved in DMF (3 mL). Isoindoline (53.5 μL, 0.47 mmol) and Et_3N (65.7 μL, 0.47 mmol) were added and the reaction stirred at rt overnight. The reaction mixture was diluted with H_2O and EtOAc. The aqueous layer was extracted with EtOAc (4 ×) and the combined organic layers were washed with H_2O (2 ×), brine (2 ×) and concentrated under reduced pressure to give the crude title compound as a dark brown liquid (104 mg); this intermediate, though novel, was carried forward without purification or complete characterisation; $\mathbf{R_f}$ 0.85 (100% EtOAc); **^{1}H NMR** (200 MHz, $CDCl_3$) δ: 8.68 (s, 1H), 8.50 (s, 1H), 7.20 (br s, 4H), 4.10 (s, 2H), 4.05 (s, 4H).

2-(3,4-Difluorophenyl)-2-(dimethylamino)acetonitrile 48

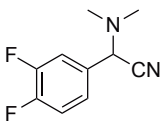

To a solution of 3,4-difluorobenzaldehyde (2.00 mL, 18.1 mmol, 1.0 equiv.) in MeOH (50 mL) was added dimethylamine (6.52 mL, 36.3 mmol, 2.0 equiv.) and stirred at rt. The reaction was cooled to 0 °C and TMSCN (2.95 mL, 23.6 mmol, 1.3 equiv.) was added slowly and stirred. After completion, as indicated by TLC (10% EtOAc in hexanes), the solvent was removed and the residue directly purified by automated flash chromatography on silica (Biotage Isolera, 2–20% EtOAc in hexanes) to give *the title compound* as a yellow liquid (3.40 g, 96%); this intermediate, though novel, was carried forward without complete characterisation; $\mathbf{R_f}$ 0.46 (10% EtOAc in hexanes); **^{1}H NMR** (300 MHz, $CDCl_3$) δ: 7.39 (ddd, *J* 10.2, 7.3 & 2.0, 1H), 7.34–7.27 (m, 1H), 7.20 (dt, *J* 9.7 & 8.1, 1H), 4.81 (s, 1H), 2.32 (s, 6H); **^{13}C NMR** (75 MHz, $CDCl_3$) δ: 150.62 (dd, *J* 249.4 & 11.5), 150.55 (dd, *J* 246.0 & 11.3), 130.9 (dd, *J* 5.5 & 3.7), 123.8 (dd, *J* 6.6 & 3.7), 117.6 (dd, *J* 17.6 & 0.9), 117.1 (dd, *J* 18.9 & 0.9), 114.5, 62.2 (d, *J* 1.8), 41.7.

2-(3,4-Difluorophenyl)-2-(dimethylamino)acetic acid 49

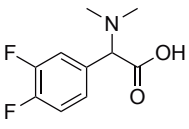

A mixture of **48** (1.00 g, 5.10 mmol) and HCl (6 M, 32 mL) was stirred at 90 °C for 4 h. The mixture was cooled to rt and the solvent was removed to give the crude title compound as a pale yellow solid; trituration with CH_2Cl_2 gave *the title compound* as an off-white powder (738 mg, 67%); this intermediate, though novel, was

carried forward without purification or characterisation; $\mathbf{R_f}$ 0.70 (25% EtOAc in hexanes).

Ethyl 2-(3,4-difluorophenyl)acetate 52

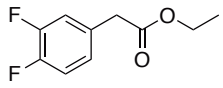

Prepared according to General Procedure 7 from: 3,4-difluorophenylacetic acid (5.00 g, 29.1 mmol 1 equiv.) to give the crude title compound as a clear pale yellow oil (5.95 g); carried forward without further purification; $\mathbf{R_f}$ 0.85 (50% EtOAc in hexanes); **^{1}H NMR** (200 MHz, $CDCl_3$) δ: 7.20–6.87 (m, 3H), 4.16 (q, J 7.1, 2H), 3.56 (s, 2H), 1.25 (t, J 7.1, 3H); **^{13}C NMR** (75 MHz, $CDCl_3$) δ: 171.0, 150.2 (dd, J 248.0 & 12.7), 149.7 (dd, J 247.3 & 12.6), 133.1–128.9 (m), 125.4 (dd, J 5.9 & 3.7 Hz), 118.3 (d, J 17.6), 117.2 (d, J 17.3), 61.2, 40.4, 14.1. Spectroscopic data matched those in the literature.[385]

Ethyl 2-bromo-2-(3,4-difluorophenyl)acetate 53

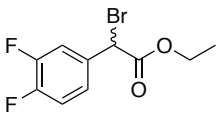

Compound **52** (2.00 g, 10.0 mmol, 1.00 equiv.) was dissolved in α,α,α-trifluorotoluene (10 mL). NBS (1.83 g, 10.3 mmol, 1.03 equiv.) and HBr (48% aq., 4 drops) were added and the reaction heated to 80 °C for 19 h. The reaction was cooled to rt, filtered and concentrated under reduced pressure to give the crude title compound as a yellow liquid (2.13 g); carried forward without further purification; $\mathbf{R_f}$ 0.65 (10% EtOAc in hexanes); **^{1}H NMR** (200 MHz, $CDCl_3$) δ: 7.55–7.36 (m, 1H), 7.34–7.03 (m, 2H), 5.27 (s, 1H), 4.26 (qd, J 7.1 & 2.0, 2H), 1.30 (t, J 7.1, 3H). Spectroscopic data matched those in the literature.[385]

Ethyl 2-(3,4-difluorophenyl)-2-(dimethylamino)acetate 54

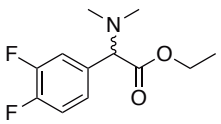

Compound **53** (500 mg, 1.79 mmol, 1 equiv.) was dissolved in DMF (5 mL). Dimethylamine solution (33% in alcohol, 0.32 mL, 1.79 mmol, 1 equiv.) and K_2CO_3 (743 mg, 5.37 mmol, 3 equiv.) were added and the reaction stirred at rt for 2 h. The mixture was filtered and the solvent removed. The residue was partitioned between EtOAc and H_2O. The aqueous layer was extracted with EtOAc and the combined organic layers were washed with brine, dried (Na_2SO_4), filtered and concentrated under reduced pressure to give the crude title compound as a yellow oil (410 mg); this intermediate, though novel, was carried forward without purification or complete characterisation; $\mathbf{R_f}$ 0.22 (10% EtOAc in hexanes); **^{1}H NMR** (200 MHz, $CDCl_3$) δ: 7.41–7.15 (m, 1H), 7.15–6.90 (m, 2H), 4.29–3.99 (m, 2H), 3.74 (s, 1H), 2.17 (s, 6H), 1.16 (t, J 7.1, 3H).

2-(3,4-Difluorophenyl)-2-(dimethylamino)ethan-1-ol 47

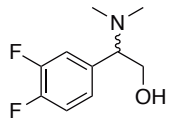

Prepared according to General Procedure 6 from: **54** (450 mg, 1.85 mmol, 1 equiv.) to give the crude title compound as a yellow oil (245 mg); this intermediate, though novel, was carried forward without purification or complete characterisation; $\mathbf{R_f}$ 0.06 (50% EtOAc in hexanes); **^{1}H NMR** (200 MHz, $CDCl_3$) δ: 7.23–6.79 (m, 3H), 3.91–3.76 (m, 1H), 3.67 (dd, *J* 10.8 & 5.1, 1H), 3.48 (dd, *J* 8.2 & 5.2, 1H), 2.47 (s, 1H), 2.20 (s, 6H).

2-((3-(4-(Difluoromethoxy)phenyl)-[1,2,4]triazolo[4,3-*a*]pyrazin-5-yl)oxy)-1-(3,4-difluorophenyl)-*N*,*N*-dimethylethan-1-amine 30

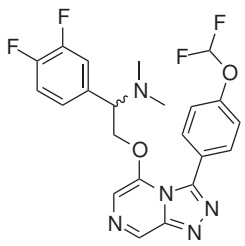

Prepared according to General Procedure 4 from: **47** (200 mg, 0.99 mmol) and **44** (295 mg, 0.99 mmol) to give the crude title compound as dark brown solid (372 mg); purified by automated flash chromatography on silica (Biotage Isolera, 25–100% EtOAc in hexanes) to give *the title compound* as a brown powder (169 mg, 37%); $\mathbf{R_f}$ 0.25 (100% EtOAc); **m.p.** 132–135 °C; **^{1}H NMR** (400 MHz, DMSO-d_6) δ: 9.04 (s, 1H), 7.72 (d, *J* 8.7, 2H), 7.65 (s, 1H), 7.37 (t, *J* 73.7, 1H), 7.27 (d, *J* 8.7, 2H), 7.31–7.20 (m, 1H), 7.03 (ddd, *J* 11.7, 8.0 & 1.8, 1H), 6.91–6.79 (m, 1H), 4.95–4.46 (m, 2H), 3.55 (t, *J* 5.9, 1H), 2.00 (s, 6H); **^{13}C NMR** (101 MHz, DMSO-d_6) δ: 151.8 (t, *J* 3.3), 147.4, 147.3, 145.5, 143.7, 134.9 (dt, *J* 39.2 & 4.5), 132.4, 125.0 (dd, *J* 6.1 & 3.3), 124.5, 117.6, 117.0 (d, *J* 17.0), 116.6 (d, *J* 17.0), 116.1 (t, *J* 258.4), 109.0, 70.6, 65.7, 41.8 (two phenyl C–F signals expected between 155 and 148 ppm; observed for compound **97**; too weak to be seen); ***m/z*** (ESI+) 462 ($[M+H]^+$, 100%); **HRMS** (ESI+) found 462.15604 $[M+H]^+$, $C_{22}H_{19}F_4N_5O_2H^+$ requires 462.15476.

9.5 Synthesis and Characterisation of Compounds from Chapter 3

2-Chloro-6-hydrazinylpyrazine 2

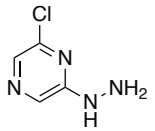

Prepared according to General Procedure 1 from: 2,6-dichloropyrazine (22.3 g, 150 mmol) to give the crude title compound as fine yellow needles (19.7 g); carried forward without further purification; $\mathbf{R_f}$ 0.12 (30% EtOAc in hexanes); **m.p.** 133–135 °C (lit.[183] 136–139 °C); **^{1}H NMR** (300 MHz; $CDCl_3$) δ: 8.13 (s, 1H), 7.89 (s, 1H), 6.38 (s, 1H), 3.86 (s, 2H); **^{13}C NMR** (75 MHz; $CDCl_3$) δ: 156.4, 146.7, 132.4, 129.0. Spectroscopic data matched those in the literature.[183]

(*E*)-2-Chloro-6-(2-(4-(difluoromethoxy)benzylidene)hydrazinyl)pyrazine 55

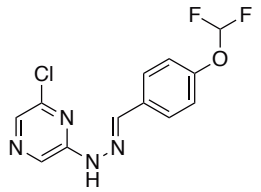

Prepared according to General Procedure 2 from: **2** (2.10 g, 14.5 mmol) and 4-(difluoromethoxy)benzaldehyde (1.92 mL, 14.5 mmol) to give the crude title compound as a pale yellow powder (4.40 g); purified by recrystallisation from EtOAc to give *the title compound* as light brown crystals (3.29 g, 76%); $\mathbf{R_f}$ 0.63 (25% EtOAc in hexanes); this intermediate, though novel, was carried forward without complete characterisation; **m.p.** 197–200 °C; **^{1}H NMR** (300 MHz, DMSO-d$_6$) 11.55 (s, 1H), 8.56 (s, 1H), 8.05 (d, *J* 5.2, 2H), 7.79 (d, *J* 8.5, 2H), 7.29 (t, *J* 73.9, 1H), 7.22 (d, *J* 8.4, 2H); **^{13}C NMR** (75 MHz, DMSO-d$_6$) δ: 152.3, 151.7, 145.6, 141.6, 132.4, 131.5, 128.8, 128.3, 118.8, 116.2 (t, *J* 257.9).

5-Chloro-3-(4-(difluoromethoxy)phenyl)-[1,2,4]triazolo[4,3-*a*]pyrazine 44

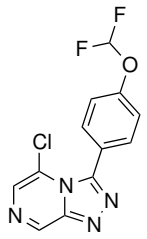

Prepared according to General Procedure 3 from: **55** (6.70 g, 22.4 mmol) to give the crude title compound as a reddish-brown solid (10.3 g); purified by automated flash chromatography on silica (Biotage Isolera, 12–100% EtOAc in hexanes) to give *the title compound* as a reddish-brown solid (4.91 g, 73%); this intermediate, though novel, was carried forward without complete characterisation; $\mathbf{R_f}$ 0.42 (50% EtOAc in hexanes); **m.p.** 130–133 °C; **^{1}H NMR** (300 MHz, $CDCl_3$) δ: 9.34 (s, 1H), 7.88 (s, 1H), 7.65 (d, *J* 7.6, 2H), 7.27 (d, *J* 7.7, 2H), 6.64 (t, *J* 73.1, 1H); **^{13}C NMR** (75 MHz, $CDCl_3$) δ: 153.2, 147.4, 147.3, 143.2, 133.2, 130.0, 123.8, 122.0, 118.8, 115.6 (t, *J* 261.4).

3-(4-(Difluoromethoxy)phenyl)-5-phenoxy-[1,2,4]triazolo[4,3-*a*]pyrazine 56

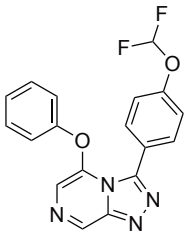

Prepared according to General Procedure 4 from: phenol (31.7 mg, 0.34 mmol) and **44** (100 mg, 0.34 mmol); the solvent was removed and the residue directly purified by automated flash chromatography on silica (Biotage Isolera, 25–100% EtOAc in hexanes) to give *the title compound* as an off-white powder (44.9 mg, 38%); $\mathbf{R_f}$ 0.41 (100% EtOAc); **m.p.** 113–117 °C; **^{1}H NMR** (400 MHz, $CDCl_3$) δ: 9.12 (s, 1H), 7.72 (d, *J* 8.7, 2H), 7.36 (t, *J* 7.9, 2H), 7.25–7.19 (m, 2H), 7.15 (d, *J* 8.6, 2H), 6.93 (d, *J* 8.0, 2H), 6.54 (t, *J* 73.3, 1H); **^{13}C NMR** (101 MHz, $CDCl_3$) δ: 153.1, 152.6 (t_{app}, *J* 2.8), 148.2, 146.5, 142.7, 138.4, 132.3, 130.6, 126.5, 124.4, 118.8, 115.7 (t, *J* 261.0), 114.2 (1 obscured signal); **^{19}F NMR** (376 MHz, $CDCl_3$) δ: -81.36; ***m/z*** (ESI+) 377 ($[M+Na]^+$, 100%); **HRMS** (ESI+) found 355.09979 $[M+H]^+$, $C_{18}H_{12}F_2N_4O_2H^+$ requires 355.10011.

5-(Benzyloxy)-3-(4-(difluoromethoxy)phenyl)-[1,2,4]triazolo[4,3-*a*]pyrazine 57

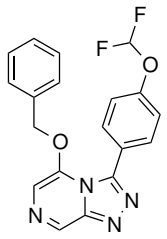

Prepared according to General Procedure 4 from: benzyl alcohol (70.0 μL, 0.67 mmol) and **44** (200 mg, 0.67 mmol) to give the crude title compound as a brown solid (205 mg); purified by automated flash chromatography on silica (Biotage Isolera, 25–100% EtOAc in hexanes) to give *the title compound* as a pale yellow powder (135 mg, 54%); $\mathbf{R_f}$ 0.08 (50% EtOAc in hexanes); **m.p.** 152–156 °C; **^{1}H NMR** (300 MHz, $CDCl_3$) δ: 9.02 (s, 1H), 7.58 (d, *J* 8.5, 2H), 7.42 (s, 1H), 7.38–7.22 (m, 3H), 7.07 (d, *J* 7.3, 2H), 6.95 (d, *J* 8.4, 2H), 6.46 (t, *J* 73.4, 1H), 5.19 (s, 2H); **^{13}C NMR** (75 MHz, $CDCl_3$) δ: 152.4, 147.9, 146.5, 143.9, 136.7, 132.9, 132.5, 129.3, 128.8, 128.2, 124.5, 118.3, 115.7 (t, *J* 260.4), 108.9, 72.9; ***m/z*** (ESI+) 391 ($[M+Na]^+$, 100%), 759 ($[2M+Na]^+$, 77%); **HRMS** (ESI+) 391.09746 $[M+Na]^+$, $C_{19}H_{14}F_2N_4O_2Na^+$ requires 391.09772.

3-(4-(Difluoromethoxy)phenyl)-5-phenethoxy-[1,2,4]triazolo[4,3-*a*]pyrazine 58

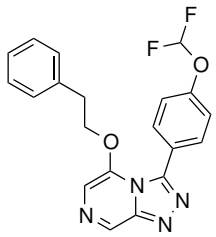

Prepared according to General Procedure 4 from: 2-phenylethanol (80.8 μL, 0.67 mmol) and **44** (200 mg, 0.67 mmol) to give the crude title compound as a brown solid (264 mg); purified by automated flash chromatography on silica (Biotage Isolera, 25–100% EtOAc in hexanes) to give *the title compound* as a pale yellow powder (189 mg, 73%); $\mathbf{R_f}$ 0.10 (50% EtOAc in hexanes); **m.p.** 115–117 °C; **^{1}H NMR** (300 MHz, $CDCl_3$) δ: 8.99 (s, 1H), 7.63 (d, *J* 8.7, 2H), 7.30 (s, 1H), 7.25–7.08 (m, 5H), 6.95–6.80 (m, 2H), 6.56 (t, *J* 73.3, 1H), 4.44 (t, *J* 6.5, 2H), 2.94 (t, *J* 6.5, 2H); **^{13}C NMR** (75 MHz, $CDCl_3$) δ: 152.4, 147.8, 146.2, 143.9, 136.4, 136.2, 132.4, 128.7, 128.4, 127.0, 124.8, 118.6, 115.5 (t, *J* 261.3), 108.3, 71.2, 34.4; ***m/z*** (ESI+) 405 ($[M+Na]^+$, 100%), 787 ($[2M+Na]^+$, 71%); **HRMS** (ESI+) 405.11312 $[M+Na]^+$, $C_{20}H_{16}F_2N_4O_2Na^+$ requires 405.11332.

3-(4-(Difluoromethoxy)phenyl)-5-(3-phenylpropoxy)-[1,2,4]triazolo[4,3-*a*]pyrazine 59

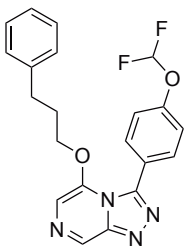

Prepared according to General Procedure 4 from: 3-phenylpropanol (45.9 μL, 0.34 mmol) and **44** (100 mg, 0.34 mmol); the solvent was removed and the residue directly purified by automated flash chromatography on silica (Biotage Isolera, 25–100% EtOAc in hexanes) to give *the title compound* as a dark yellow crystalline powder (111 mg, 83%); $\mathbf{R_f}$ 0.42 (100% EtOAc); **m.p.** 153–157 °C; **^{1}H NMR** (400 MHz, $CDCl_3$) δ: 9.03 (s, 1H), 7.75 (d, *J* 8.8, 2H), 7.32–7.16 (m, 6H), 6.96 (d, *J* 7.0, 2H), 6.47 (t, *J* 73.3, 1H), 4.19 (t, *J* 5.9, 2H), 2.35 (t, *J* 7.6, 2H), 1.96 (dt, *J* 8.4 & 6.4, 2H); **^{13}C NMR** (101 MHz, $CDCl_3$) δ: 152.7, 147.9, 146.3, 144.2, 140.0, 136.5, 132.6, 128.8, 128.3, 126.6, 125.2, 118.6, 115.7 (t, *J* 261.0), 108.4, 70.1, 31.6, 29.9; **^{19}F NMR** (376 MHz,

$CDCl_3$) δ: -81.33; ***m/z*** (ESI+) 419 ($[M+Na]^+$, 100%); **HRMS** (ESI+) found 397.14685 $[M+H]^+$, $C_{21}H_{18}F_2N_4O_2H^+$ requires 397.14706.

3-(4-(Difluoromethoxy)phenyl)-5-(2-phenoxyethoxy)-[1,2,4]triazolo[4,3-*a*]pyrazine 60

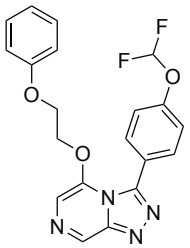

Prepared according to General Procedure 4 from: 2-phenoxyethanol (42.1 μL, 0.34 mmol) and **44** (100 mg, 0.34 mmol); the solvent was removed and the residue directly purified by automated flash chromatography on silica (Biotage Isolera, 25–100% EtOAc in hexanes) to give *the title compound* as a light brown powder (63.6 mg, 47%); $\mathbf{R_f}$ 0.26 (100% EtOAc); **m.p.** 190–194 °C; **^{1}H NMR** (400 MHz, $CDCl_3$) δ: 9.05 (s, 1H), 7.72 (d, *J* 8.7, 2H), 7.44–7.29 (m, 3H), 7.06 (t, *J* 7.4, 1H), 6.83 (dd, *J* 15.5 & 8.3, 4H), 6.02 (t, *J* 73.5, 1H), 5.07–4.29 (m, 2H), 4.24–3.83 (m, 2H); **^{13}C NMR** (101 MHz, $CDCl_3$) δ: 157.9, 152.6, 147.9, 146.7, 144.0, 137.0, 132.7, 130.0, 124.5, 121.9, 117.9, 115.6 (t, *J* 259.8), 114.1, 108.4, 69.4, 64.9; **^{19}F NMR** (376 MHz, $CDCl_3$) δ: -81.42; ***m/z*** (ESI+) 421 ($[M+Na]^+$, 100%); **HRMS** (ESI+) found 399.12600 $[M+H]^+$, $C_{20}H_{16}F_2N_4O_3H^+$ requires 399.12632.

5-(Benzylthio)-3-(4-(difluoromethoxy)phenyl)-[1,2,4]triazolo[4,3-*a*]pyrazine 63

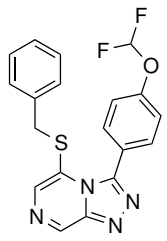

Prepared according to General Procedure 4 from: benzyl mecaptan (39.6 μL, 337 μmol) and **44** (100 mg, 337 μmol) to give the crude title compound as a orange solid; purified by automated flash chromatography on silica (Biotage Isolera, 12–100% EtOAc in hexanes) to give **63** as a light brown powder (18.1 mg, 14%); **m.p.** 231–233 °C; **^{1}H NMR** (300 MHz, $CDCl_3$) δ: 9.27 (s, 1H), 7.83–7.58 (m, 3H), 7.34–7.09 (m, 5H), 7.10–6.81 (m, 2H), 6.52 (t, *J* 73.1, 1H), 3.73 (s, 2H); **^{13}C NMR** (75 MHz, $CDCl_3$) δ: 153.2, 147.8, 146.6, 143.5, 134.4, 134.2, 133.5, 129.0, 128.7, 128.3, 127.0, 124.1, 118.5, 115.6 (t, *J* 261.6), 40.2; ***m/z*** (ESI+) 385 ($[M+H]^+$, 66%), 407 ($[M+Na]^+$, 100%), 791 ($[2M+Na]^+$, 51%); **HRMS** (ESI+) found 385.09255 $[M+H]^+$, $C_{19}H_{14}F_2N_4OSH^+$ requires 385.09291.

3-(4-(Difluoromethoxy)phenyl)-5-(phenethylthio)-[1,2,4]triazolo[4,3-*a*]pyrazine 64

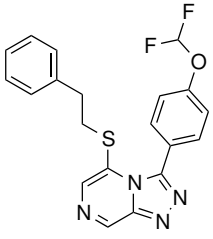

Prepared according to General Procedure 4 from: 2-phenylethanethiol (45.1 μL, 337 μmol) and **44** (100 mg, 337 μmol) to give the crude title compound as a orange solid; purified by automated flash chromatography on silica (Biotage Isolera, 12–100% EtOAc in hexanes) to give **64** as a light yellow powder (49.8 mg, 37%); **m.p.** 78–83 °C; **^{1}H NMR** (400 MHz, $CDCl_3$) δ: 9.21 (s, 1H), 7.76 (s, 1H), 7.64 (d, *J* 8.7, 2H), 7.25–7.18 (m, 5H), 7.00–6.95 (m, 2H), 6.64 (t, *J* 73.1, 1H), 2.92 (t, *J*

7.4, 2H), 2.76 (t, *J* 7.3, 2H); **^{13}C NMR** (101 MHz, $CDCl_3$) δ: 153.1, 147.6, 146.4, 142.3, 138.3, 133.5, 131.3, 128.7, 128.6, 128.4, 127.1, 124.1, 118.3, 115.6 (t, *J* 261.4), 35.8, 34.6; ***m/z*** (ESI+) 421 ($[M+Na]^+$, 100%); **HRMS** (ESI+) found 399.10816 $[M+H]^+$, $C_{20}H_{16}F_2N_4OSH^+$ requires 399.10856.

2-(Benzylsulfinyl)-6-chloropyrazine 67

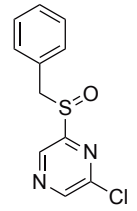

NaH (60% dispersion in mineral oil, 1.60 g, 67.1 mmol) was added to benzyl mercaptan (8.00 mL, 67.1 mmol) in PhMe (64 mL). The mixture was heated to reflux for 1 h, then cooled to rt and a solution of 2,6-dichloropyrazine (10.0 g, 67.1 mmol) in PhMe (64 mL) was added. The mixture was heated to reflux for 24 h, cooled to rt, then washed with H_2O (80 mL). The organic layer was separated, dried (Na_2SO_4), filtered and concentrated under reduced pressure to give the crude sulfide as a yellow liquid (16.9 g). H_2O_2 (30% in H_2O, 1.04 mL, 33.8 mmol, 4 equiv.) was slowly added to the crude sulfide (2.00 g, 8.45 mmol, 1 equiv.) in glacial AcOH (10 mL). The reaction mixture was stirred at rt until completion as indicated by TLC (25% EtOAc in hexanes). The solution was neutralised with NaOH (4 M) and extracted with CH_2Cl_2. The organic layer was dried (Na_2SO_4), filtered and concentrated under reduced pressure to give a cloudy orange liquid (2.00 g); purified by automated flash chromatography on silica (Biotage Isolera, 12–100% EtOAc in hexanes) to give *the title compound* as a large yellow crystals (628 mg, 29%); this intermediate, though novel, was carried forward without complete characterisation; $\mathbf{R_f}$ 0.65 (25% EtOAc in hexanes); **m.p.** 92–99 °C; **^{1}H NMR** (500 MHz, $CDCl_3$) δ: 8.63 (s, 1H), 8.62 (s, 1H), 7.46–7.15 (m, 3H), 7.07–7.02 (m, 2H), 4.42 (d, *J* 13.3, 1H), 4.14 (d, *J* 13.3, 1H); **^{13}C NMR** (75 MHz, $CDCl_3$) δ: 159.3, 148.5, 145.7, 140.5, 130.4, 128.9, 128.7, 128.4, 60.0; ***m/z*** (ESI+) 253 ($[M+H]^+$, 100%).

2-Chloro-6-(phenethylsulfinyl)pyrazine 68

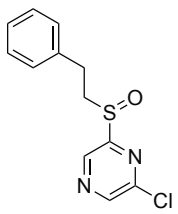

NaH (60% dispersion in mineral oil, 403 mg, 16.8 mmol) was added to phenylethyl mercaptan (2.25 mL, 16.8 mmol) in PhMe (16 mL). The mixture was heated to reflux for 1 h, then cooled to rt and a solution of 2,6-dichloropyrazine (2.50 g, 16.8 mmol) in PhMe (16 mL) was added. The mixture was heated to reflux for 24 h, cooled to rt, then washed with H_2O (30 mL). The organic layer was separated, dried (Na_2SO_4), filtered and concentrated under reduced pressure to give the crude sulfide as a yellow liquid (3.56 g). H_2O_2 (30% in H_2O, 2.18 mL, 71.0 mmol, 5 equiv.) was slowly added to the crude sulfide (3.56 g, 14.2 mmol, 1 equiv.) in glacial AcOH (15 mL). The reaction mixture was stirred at rt until completion as indicated by TLC (25% EtOAc in hexanes). The solution was neutralised with NaOH (4 M) and extracted with CH_2Cl_2. The organic layer was dried

(Na_2SO_4), filtered and concentrated under reduced pressure to give a cloudy yellow liquid (3.50 g); purified by automated flash chromatography on silica (Biotage Isolera, 6–50% EtOAc in hexanes) to give *the title compound* as a viscous orange liquid (888 mg, 23%); this intermediate, though novel, was carried forward without complete characterisation; $\mathbf{R_f}$ 0.20 (25% EtOAc in hexanes); **^{1}H NMR** (300 MHz, $CDCl_3$) δ: 9.12 (s, 1H), 8.70 (s, 1H), 8.09–6.45 (m, 5H), 3.73–2.94 (m, 4H); ***m/z*** (ESI+) 289 ($[2M+Na]^+$, 97%), 555 ($[2M+Na]^+$, 100%).

2-(Benzylsulfonyl)-6-chloropyrazine 69

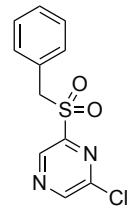

NaH (60% dispersion in mineral oil, 1.60 g, 67.1 mmol) was added to benzyl mercaptan (8.00 mL, 67.1 mmol) in PhMe (64 mL). The mixture was heated to reflux for 1 h, then cooled to rt and a solution of 2,6-dichloropyrazine (10.0 g, 67.1 mmol) in PhMe (64 mL) was added. The mixture was heated to reflux for 24 h, cooled to rt, then washed with H_2O (80 mL). The organic layer was separated, dried (Na_2SO_4), filtered and concentrated under reduced pressure to give the crude sulfide as a yellow liquid (16.9 g). The crude sulfide (4.91 g, 20.7 mmol) in glacial AcOH (50 mL) was added to a solution of $KMnO_4$ (3.50 g) in H_2O (28 mL) and the mixture was stirred at rt for 1 h. The mixture was adjusted to pH 7 with sat. aq. NH_4OH solution (40 mL) then filtered, extracted with $CHCl_3$ (3 × 100 mL), dried (Na_2SO_4), filtered and concentrated under reduced pressure to give a cloudy yellow liquid (3.14 g); purified by automated flash chromatography on silica (Biotage Isolera, 6–75% EtOAc in hexanes) to give *the title compound* as large white crystals (1.31 g, 24%); $\mathbf{R_f}$ 0.30 (25% EtOAc in hexanes); **m.p.** 84–92 °C (lit.[181] 86–87 °C); **IR** ν_{max} (film) /cm^{-1} 1334, 1119; **^{1}H NMR** (300 MHz, $CDCl_3$) δ: 8.85 (s, 1H), 8.79 (s, 1H), 7.71–6.67 (m, 5H), 4.65 (s, 2H); **^{13}C NMR** (75 MHz, $CDCl_3$) δ: 151.2, 149.3, 148.7, 141.4, 131.2, 129.4, 129.1, 126.4, 59.0; ***m/z*** (ESI+) 291 ($[M+Na]^+$, 100%), 559 ($[2M+Na]^+$, 74%); **HRMS** (ESI+) found 290.99692 $[M+Na]^+$, $C_{11}H_9ClN_2O_2SNa^+$ requires 290.99652. Compound reported in the literature but no NMR or mass spectrometry characterisation data were provided.[181]

2-Chloro-6-(phenethylsulfonyl)pyrazine 70

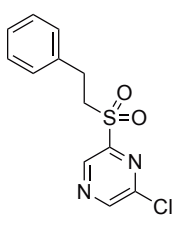

NaH (60% dispersion in mineral oil, 403 mg, 16.8 mmol) was added to phenylethyl mercaptan (2.25 mL, 16.8 mmol) in PhMe (16 mL). The mixture was heated to reflux for 1 h, then cooled to rt and a solution of 2,6-dichloropyrazine (2.50 g, 16.8 mmol) in PhMe (16 mL) was added. The mixture was heated to reflux for 24 h, cooled to rt, then washed with H_2O (30 mL). The organic layer was separated, dried (Na_2SO_4), filtered and concentrated under reduced pressure to give the crude sulfide as a yellow liquid (3.92 g). The crude sulfide (3.92 g, 15.6 mmol) in glacial AcOH (40 mL)

was added to a solution of $KMnO_4$ (2.5 g) in H_2O (20 mL) and the mixture was stirred at rt for 1 h. The mixture was adjusted to pH 7 with sat. NH_4OH solution (40 mL) then filtered, extracted with $CHCl_3$ (3 × 100 mL), dried (Na_2SO_4), filtered and concentrated under reduced pressure to give an orange semi-solid (1.23 g); purified by automated flash chromatography on silica (Biotage Isolera, 6–50% EtOAc in hexanes) to give *the title compound* as a large white crystals (547 mg, 12%); this intermediate, though novel, was carried forward without complete characterisation; $\mathbf{R_f}$ 0.52 (25% EtOAc in hexanes); **m.p.** 92–100 °C; **^{1}H NMR** (200 MHz, $CDCl_3$) δ: 9.04 (s, 1H), 8.72 (s, 1H), 7.98–6.81 (m, 5H), 3.90–3.59 (m, 2H), 3.28–3.04 (m, 2H).

2-(Benzylsulfinyl)-6-hydrazinylpyrazine 261

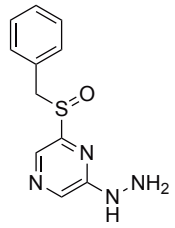

Prepared according to General Procedure 1 from: **67** (500 mg, 1.98 mmol) to give the crude title compound as a yellow powder (538 mg); this intermediate, though novel, was carried forward without purification or characterisation; $\mathbf{R_f}$ 0.00 (25% EtOAc in hexanes).

2-Hydrazinyl-6-(phenethylsulfinyl)pyrazine 262

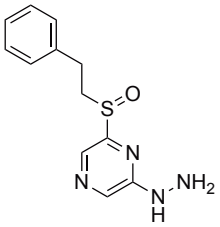

Prepared according to General Procedure 1 from: **68** (467 mg, 1.75 mmol) to give the crude title compound as a viscous yellow liquid (488 mg); this intermediate, though novel, was carried forward without purification or characterisation; $\mathbf{R_f}$ 0.03 (50% EtOAc in hexanes).

2-(Benzylsulfonyl)-6-hydrazinylpyrazine 263

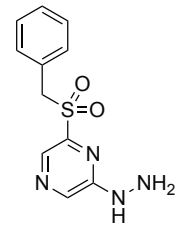

Prepared according to General Procedure 1 from: **69** (503 mg, 1.86 mmol) to give the crude title compound as a yellow powder (483 mg); this intermediate, though novel, was carried forward without purification or complete characterisation; $\mathbf{R_f}$ 0.06 (50% EtOAc in hexanes); **^{1}H NMR** (400 MHz, DMSO-d$_6$) δ: 8.86 (s, 1H), 8.31 (s, 1H), 7.92 (s, 1H), 7.41–7.10 (m, 3H), 7.26–7.19 (m, 2H), 4.74 (s, 2H), 4.55 (s, 2H); **^{13}C NMR** (101 MHz, DMSO-d$_6$) δ: 156.1, 148.4, 131.1, 128.4, 128.26, 128.34, 128.0, 57.1 (1 obscured signal).

2-Hydrazinyl-6-(phenethylsulfonyl)pyrazine 264

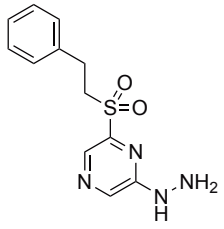

Prepared according to General Procedure 1 from: **70** (444 mg, 1.57 mmol) to give the crude title compound as a yellow powder (400 mg); this intermediate, though novel, was carried forward without purification or characterisation; $\mathbf{R_f}$ 0.08 (50% EtOAc in hexanes).

(*E*)-2-(Benzylsulfinyl)-6-(2-(4-(difluoromethoxy)benzylidene)hydrazinyl) pyrazine 265

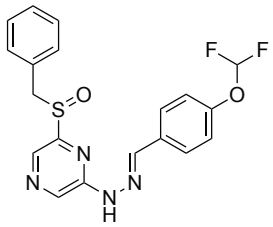

Prepared according to General Procedure 2 from: **261** (200 mg, 0.81 mmol) and 4-(difluoromethoxy)benzaldehyde (107 μL, 0.81 mmol) to give the crude title compound as a pale yellow powder (348 mg); carried forward without further purification; $\mathbf{R_f}$ 0.83 (50% EtOAc in hexanes); **^{1}H NMR** (500 MHz, DMSO-d$_6$) δ: 11.71 (br s, 1H), 8.73 (s, 1H), 8.12 (s, 1H), 7.95 (s, 1H), 7.83 (d, *J* 8.7, 2H), 7.30–7.28 (m, 3H), 7.24 (d, *J* 8.6, 2H), 7.23 (t, *J* 73.9, 1H), 7.10–7.04 (m 2H), 4.46 (d, *J* 13.1, 1H), 4.16 (d, *J* 13.1, 1H); **^{13}C NMR** (126 MHz, DMSO-d$_6$) δ: 155.6, 151.7, 151.7, 141.6, 132.7, 131.5, 130.9, 130.4, 129.7, 128.4, 128.3, 128.1, 118.9, 116.2 (t, *J* 257.8), 58.6; ***m/z*** (ESI+) 425 ([M+Na]$^+$, 100%); **HRMS** (ESI+) found 425.08579 [M+Na]$^+$, $C_{19}H_{16}F_2N_4O_2SNa^+$ requires 425.08542.

(*E*)-2-(2-(4-(Difluoromethoxy)benzylidene)hydrazinyl)-6-(phenethylsulfinyl) pyrazine 266

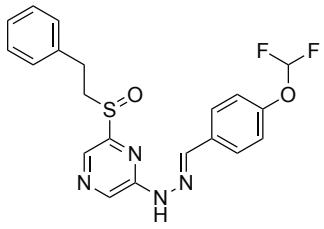

Prepared according to General Procedure 2 from: **262** (480 mg, 1.83 mmol) and 4-(difluoromethoxy)benzaldehyde (242 μL, 1.83 mmol) to give the crude title compound as a yellow powder (752 mg); purified by automated flash chromatography on silica (Biotage Isolera, 12–100% EtOAc in hexanes) to give *the title compound* as a yellow powder (327 mg, 43%); this intermediate, though novel, was carried forward without complete characterisation; $\mathbf{R_f}$ 0.55 (50% EtOAc in hexanes); **m.p.** 165–173 °C; **^{1}H NMR** (200 MHz, $CDCl_3$) δ: 8.90 (s, 1H), 8.66 (s, 1H), 8.60 (s, 1H), 7.88 (s, 1H), 7.77 (d, *J* 8.6, 2H), 7.43–7.15 (m, 7H), 6.62 (t, *J* 73.4, 1H), 3.54–3.11 (m, 3H), 3.00 (dq, *J* 14.3, 6.7 & 6.3, 1H).

(*E*)-2-(Benzylsulfonyl)-6-(2-(4-(difluoromethoxy)benzylidene)hydrazinyl) pyrazine 267

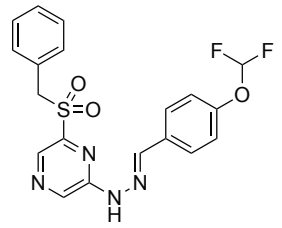

Prepared according to General Procedure 2 from: **263** (100 mg, 0.38 mmol) and 4-(difluoromethoxy)benzaldehyde (50.0 μL, 0.38 mmol) to give the crude title compound as a pale yellow powder (157 mg); purified by trituration with CH_2Cl_2 to give *the title compound* as a light brown powder (140 mg, 88%); $\mathbf{R_f}$ 0.81 (75% EtOAc in hexanes); **m.p.** 238–242 °C; **^{1}H NMR** (500 MHz, DMSO-d$_6$) δ: 11.99 (br s, 1H), 8.93 (s, 1H), 8.24 (s, 1H), 8.14 (s, 1H), 7.85 (d, *J* 8.7, 2H), 7.37–7.32 (m, 3H), 7.31 (t, *J* 73.9, 1H), 7.27–7.21 (m, 4H), 4.74 (s, 2H); **^{13}C NMR** (126 MHz, DMSO-d$_6$) δ: 152.0, 151.8, 148.5, 142.3, 135.7, 131.9, 131.4, 131.2, 128.6, 128.5, 127.6, 118.9, 118.3, 116.2, 58.0; ***m/z*** (ESI+) 441 ([M+Na]$^+$, 100%); **HRMS** (ESI+) found 441.08074 [M+Na]$^+$, $C_{19}H_{16}F_2N_4O_3SNa^+$ requires 441.08034.

(*E*)-2-(2-(4-(Difluoromethoxy)benzylidene)hydrazinyl)-6-(phenethylsulfonyl) pyrazine 268

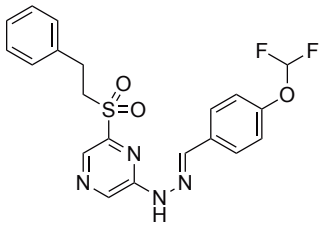

Prepared according to General Procedure 2 from: **264** (400 mg, 1.44 mmol) and 4-(difluoromethoxy)benzaldehyde (190 μL, 1.44 mmol) to give the crude title compound as a pale yellow powder (348 mg); purified by automated flash chromatography on silica (Biotage Isolera, 12–100% EtOAc in hexanes) to give *the title compound* as a yellow powder (275 mg, 44%); this intermediate, though novel, was carried forward without complete characterisation; $\mathbf{R_f}$ 0.74 (50% EtOAc in hexanes); **^{1}H NMR** (300 MHz; $CDCl_3$) δ: 8.97 (s, 1H), 8.67 (s, 1H), 8.42 (s, 1H), 7.80 (s, 1H), 7.72 (d, *J* 8.7, 2H), 7.42–7.05 (m, 7H), 6.57 (t, *J* 73.4, 1H), 3.40–3.69 (m, 2H), 3.33–3.01 (m, 2H).

5-(Benzylsulfinyl)-3-(4-(difluoromethoxy)phenyl)-[1,2,4]triazolo[4,3-*a*]pyrazine 71

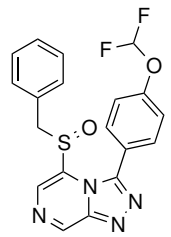

Prepared according to General Procedure from: **265** (150 mg, 0.37 mmol) to give the crude title compound as an orange solid (172 mg); purified by automated flash chromatography on silica (Biotage Isolera, 12–100% EtOAc in hexanes) to give *the title compound* as a pale yellow powder (30.0 mg, 20%); $\mathbf{R_f}$ 0.13 (50% EtOAc in hexanes); **m.p.** 227–228 °C; **^{1}H NMR** (300 MHz, $CDCl_3$) δ: 9.46 (s, 1H), 8.19 (s, 1H), 7.78 (d, *J* 8.4, 2H), 7.41 (d, *J* 8.0, 2H), 7.17 (t, *J* 7.5, 3H), 6.70 (t, *J* 72.4, 1H), 6.53 (d, *J* 7.7, 2H), 3.64 (dd, *J* 106.7 & 13.3, 2H); **^{13}C NMR** (500 MHz, DMSO-d$_6$) δ: 153.5, 146.4, 145.9, 145.8, 134.9, 133.8, 130.2, 129.0, 128.6, 128.4, 128.3, 122.8, 118.2, 116.1 (t, *J* 257.9), 59.8; **^{19}F NMR** (471 MHz, DMSO-d$_6$) δ: -83.25; ***m/z*** (ESI+) 401 ([M+H]$^+$, 41%), 423 ([M+Na]$^+$, 100%);

HRMS (ESI+) found 423.07010 $[M+Na]^+$, $C_{19}H_{14}F_2N_4O_2SNa^+$ requires 423.06982.

5-(Phenethylsulfinyl)-3-(4-(difluoromethoxy)phenyl)-[1,2,4]triazolo[4,3-*a*]pyrazine 72

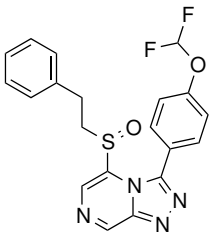

Prepared according to General Procedure 3 from: **266** (300 mg, 0.72 mmol) to give the crude title compound as a pale orange solid (292 mg); purified by automated flash chromatography on silica (Biotage Isolera, 18–100% EtOAc in hexanes) to give *the title compound* as an off-white powder (262 mg, 88%); $\mathbf{R_f}$ 0.40 (75% EtOAc in hexanes); **m.p.** 151–154 °C; **^{1}H NMR** (300 MHz, $CDCl_3$) δ: 9.43 (s, 1H), 8.52 (s, 1H), 7.67 (d, *J* 8.8, 2H), 7.32 (d, *J* 8.7, 2H), 7.17 (m, 4H), 6.82 (m, 1H), 6.65 (t, *J* 72.5, 1H), 2.99–2.54 (m, 4H); **^{13}C NMR** (75 MHz, $CDCl_3$) δ: 153.7, 146.5, 146.4, 146.0, 137.0, 133.9, 132.7, 130.0, 128.8, 128.2, 127.1, 122.3, 119.6, 115.3 (t, *J* 262.9), 55.2, 27.6; ***m/z*** (ESI+) 437 ($[M+Na]^+$, 100%); **HRMS** (ESI+) found 437.08558 $[M+Na]^+$, $C_{20}H_{16}F_2N_4O_2SNa^+$ requires 437.08542.

5-(Benzylsulfonyl)-3-(4-(difluoromethoxy)phenyl)-[1,2,4]triazolo[4,3-*a*]pyrazine 73

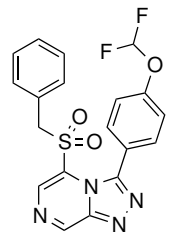

Prepared according to General Procedure 3 from: **267** (100 mg, 0.24 mmol) to give the crude title compound as an orange solid (69.6 mg); purified by automated flash chromatography on silica (Biotage Isolera, 12–100% EtOAc in hexanes) to give *the title compound* as a pale yellow powder (24.9 mg, 25%); insufficient material remaining for complete characterisation; $\mathbf{R_f}$ 0.24 (50% EtOAc in hexanes); **m.p.** 222–224 °C; **^{1}H NMR** (300 MHz, $CDCl_3$) δ: 9.56 (s, 1H), 8.41 (s, 1H), 7.76 (d, *J* 8.6, 2H), 7.38 (d, *J* 8.4, 2H), 7.44–7.18 (m, 3H), 6.88 (d, *J* 7.4, 2H), 6.69 (t, *J* 72.7, 1H), 4.02 (s, 2H); ***m/z*** (ESI–) 415 ($[M-H]^-$, 100%); **HRMS** (ESI+) found 417.08306 $[M+H]^+$, $C_{19}H_{14}F_2N_4O_3SH^+$ requires 417.08278.

5-(Phenethylsulfonyl)-3-(4-(difluoromethoxy)phenyl)-[1,2,4]triazolo[4,3-*a*]pyrazine 74

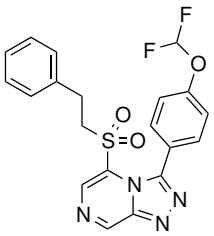

Prepared according to General Procedure 3 from: **268** (275 mg, 0.64 mmol) to give the crude title compound as a pale yellow solid (332 mg); purified by automated flash chromatography on silica (Biotage Isolera, 12–100% EtOAc in hexanes) to give *the title compound* as a white powder (179 mg, 65%); $\mathbf{R_f}$ 0.43 (50% EtOAc in hexanes); **m.p.** 142–143 °C; **^{1}H NMR** (300 MHz, $CDCl_3$) δ: 9.50 (s, 1H), 8.62 (s, 1H), 7.65 (d, *J* 8.7, 2H), 7.39–7.11 (m, 6H), 6.89 (m, 1H), 6.61 (t, *J* 72.8, 1H), 3.03 (ddd, *J* 8.4, 6.1 & 1.8, 2H), 2.88 (ddd, *J* 8.3, 6.1 & 1.8, 2H); **^{13}C NMR** (75 MHz, $CDCl_3$) δ: 153.4, 150.4, 147.3, 144.4, 141.5, 136.5, 130.2, 129.3, 128.8, 128.3, 126.8, 120.8, 118.9, 115.5 (t, *J* 262.6), 54.6, 28.9; ***m/z*** (ESI+) 453 ($[M+Na]^+$, 100%); **HRMS** (ESI+) found

431.09863 $[M+H]^+$, $C_{20}H_{16}F_2N_4O_3SH^+$ requires 431.09838.

8-(Benzylthio)-3-(4-(difluoromethoxy)phenyl)-[1,2,4]triazolo[4,3-*a*]pyrazine 75

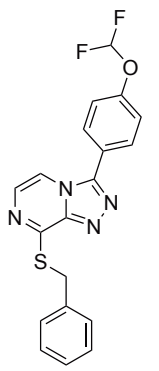

Isolated from the same reaction as for **63** to give *the title compound* as a light brown powder (102 mg, 78%); **m.p.** 176–180 °C; **^{1}H NMR** (400 MHz, $CDCl_3$) δ: 7.89–7.81 (m, 3H), 7.73 (d, *J* 4.8, 1H), 7.47 (d, *J* 7.1, 2H), 7.40–7.20 (m, 5H), 6.62 (t, *J* 73.0, 1H), 4.61 (s, 2H); **^{13}C NMR** (101 MHz, $CDCl_3$) δ: 155.5, 152.9, 147.2, 144.4, 136.7, 130.1, 130.07, 129.4, 128.7, 127.6, 123.1, 120.5, 115.6 (t, *J* 262.0), 111.4, 33.4; ***m/z*** (ESI+) 385 ($[M+H]^+$, 66%), 407 ($[M+Na]^+$, 100%), 791 ($[2M+Na]^+$, 33%); **HRMS** (ESI+) found 385.09261 $[M+H]^+$, $C_{19}H_{14}F_2N_4OSH^+$ requires 385.09291.

3-(4-(Difluoromethoxy)phenyl)-8-(phenethylthio)-[1,2,4]triazolo[4,3-*a*]pyrazine 76

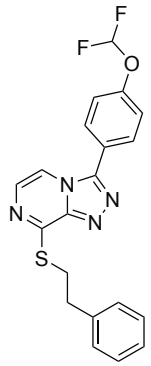

Isolated from the same reaction as for **64** to give *the title compound* as a light yellow powder (75.4 mg, 56%); **m.p.** 154–155 °C; **^{1}H NMR** (300 MHz, $CDCl_3$) δ: 7.89–7.73 (m, 3H), 7.68 (d, *J* 4.8, 1H), 7.36–7.11 (m, 7H), 6.57 (t, *J* 73.0, 1H), 3.55 (dd, *J* 8.7 & 6.8, 2H), 3.06 (dd, *J* 8.7 & 6.8, 2H); **^{13}C NMR** (75 MHz, $CDCl_3$) δ: 155.6, 152.8, 147.2, 144.5, 140.0, 130.13, 130.06, 128.74, 128.66, 126.7, 123.0, 120.4, 115.5 (t, *J* 261.9), 111.2, 35.4, 30.5; ***m/z*** (ESI+) 421 ($[M+Na]^+$, 100%); **HRMS** (ESI+) found 399.10815 $[M+H]^+$, $C_{20}H_{16}F_2N_4OSH^+$ requires 399.10856.

5-Azido-3-(4-(difluoromethoxy)phenyl)-[1,2,4]triazolo[4,3-*a*]pyrazine 77

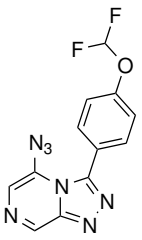

Compound **44** (2.00 g, 6.47 mmol, 1 equiv.) and NaN_3 (1.75 g, 27.0 mmol, 4 equiv.) were stirred in anhydrous DMF (40 mL) at rt for 3 h. The reaction was diluted with EtOAc (50 mL) and washed H_2O (5 × 50 mL), brine (2 × 50 mL), dried ($MgSO_4$), filtered and concentrated under reduced pressure to give the crude title compound as a viscous black liquid (1.61 g); purified by automated flash chromatography on silica (Biotage Isolera, 12–100% EtOAc in hexanes) to give *the title compound* as a black powder (1.40 g, 69%); this intermediate, though novel, was carried forward without complete characterisation; $\mathbf{R_f}$ 0.31 (50% EtOAc in hexanes); **^{1}H NMR** (200 MHz, $CDCl_3$) δ: 9.17 (s, 1H), 7.75 (s, 1H), 7.70 (d, *J* 8.8, 2H), 7.28 (d, obscured by solvent peak, 2H), 6.64 (t, *J* 73.2, 1H).

5-(4-Phenyl-1*H*-1,2,3-triazol-1-yl)-3-(4-(difluoromethoxy)phenyl)-[1,2,4]triazolo[4,3-*a*]pyrazine 78

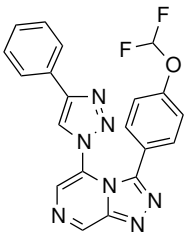

Compound **77** (54.6 mg, 0.18 mmol, 1.0 equiv.) and phenyl acetylene (20.0 μL, 0.18 mmol, 1.0 equiv.) were dissolved in H_2O (1 mL) and THF (1 mL). $CuSO_4{\cdot}5H_2O$ (63.0 mg, 0.25 mmol, 1.4 equiv.) and Na ascorbate (100 mg, 0.50 mmol, 2.8 equiv.) were added and the reaction stirred at rt. The reaction was diluted with CH_2Cl_2, washed with H_2O (2 ×), brine, dried ($MgSO_4$), filtered and concentrated under reduced pressure to give the crude title compound as a brown liquid (31.6 mg); purified by automated flash chromatography on silica (Biotage Isolera, 18–100% EtOAc in hexanes) to give *the title compound* as a dark orange solid (6.90 mg, 9%); insufficient material remaining for complete characterisation; **^{1}H NMR** (500 MHz, CD_3OD) δ: 9.62 (s, 1H), 8.32 (s, 1H), 8.31 (s, 1H), 7.67–7.61 (m, 2H), 7.49–7.36 (m, 3H), 7.31 (d, *J* 8.7, 2H), 6.94 (d, *J* 8.6, 2H), 6.23 (t, *J* 73.5, 1H); ***m/z*** (ESI+) 378 ($[M\text{-}N_2+H]^+$, 100%), 406 ($[M+H]^+$, 25%); **HRMS** (ESI+) found 428.10422 $[M+Na]^+$, $C_{20}H_{13}F_2N_7ONa^+$ requires 428.10422.

Azidobenzene 79

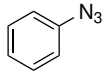

To a solution of aniline (0.30 mL, 3.29 mmol, 1.0 equiv.) in 50% AcOH (15 mL) was slowly added $NaNO_2$ (341 mg, 4.94 mmol, 1.5 equiv.) below 0 °C within 15 min. The reaction was vigorously stirred at 0 °C for 1 h. NaN_3 (321 mg, 4.94 mmol, 1.5 equiv.) was added at 0 °C in portions. The resulting solution was stirred at 0 °C for a further 1 h, followed by dilution with ice cold H_2O (40 mL) and extraction with EtOAc (3 × 25 mL). The combined organic layers were washed with sat. aq. $NaHCO_3$ (3 × 15 mL), brine (2 × 15 mL), dried (Na_2SO_4), filtered and concentrated under reduced pressure to give the crude title compound as a dark brown liquid (57.9 mg); carried forward without further purification or characterisation; $\mathbf{R_f}$ 0.87 (50% EtOAc in hexanes).

(Azidomethyl)benzene 80

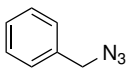

Benzyl chloride (1.00 mL, 8.69 mmol, 1.0 equiv.) and NaN_3 (678 mg, 10.4 mmol, 1.2 equiv.) were stirred in anhydrous DMF (20 mL) at rt for 6 h. The reaction was diluted with EtOAc (50 mL) and washed with sat. aq. $NaHCO_3$ (50 mL). The aqueous layer was extracted with EtOAc (50 mL) and the combined organic layers were washed with H_2O (50 mL), brine (50 mL), dried (Na_2SO_4), filtered and concentrated under reduced pressure to give the crude title compound as a clear liquid (1.30 g); carried forward without further purification; **IR** ν_{max} (film) /cm^{-1} 2089; **^{1}H NMR** (300 MHz, $CDCl_3$) δ: 6.95–7.62 (m, 5H), 4.24 (s, 2H); **^{13}C NMR** (75 MHz, $CDCl_3$) δ: 135.4, 128.8, 128.3, 128.2, 54.8. Spectroscopic data matched those in

the literature.[386]

(1-Phenyl-1*H*-1,2,3-triazol-4-yl)methanol 81

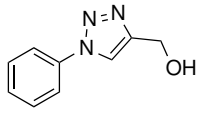

Prepared according to General Procedure 5 from: **79** (57.9 mg, 0.49 mmol) and propargyl alcohol (28.0 μL, 0.49 mmol) to give the crude title compound as orange crystals (68.3 mg); carried forward without further purification; $\mathbf{R_f}$ 0.09 (50% EtOAc in hexanes); **^{1}H NMR** (300 MHz, $CDCl_3$) δ: 8.00 (s, 1H), 7.70 (d, *J* 7.8, 2H), 7.57–7.37 (m, 3H), 4.88 (s, 2H), 3.46 (s, 1H); **^{13}C NMR** (75 MHz, $CDCl_3$) δ: 148.6, 137.1, 129.9, 129.0, 120.7, 120.3, 56.5; ***m/z*** (ESI+) 198 ($[M+Na]^+$, 100%), 373 ($[2M+Na]^+$, 45%); **HRMS** (ESI+) found 198.06382 $[M+Na]^+$, $C_9H_9N_3ONa^+$ requires 198.06382. Spectroscopic data matched those in the literature.[387]

(1-Benzyl-1*H*-1,2,3-triazol-4-yl)methanol 82

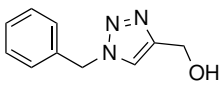

Prepared according to General Procedure 5 from: **80** (580 mg, 4.33 mmol) and propargyl alcohol (250 μL, 4.33 mmol) to give the crude title compound as a yellow oil (68.3 mg); purified by automated flash chromatography on silica (Biotage Isolera, 18–100% EtOAc in hexanes) to give *the title compound* as a white powder (538 mg, 66%); $\mathbf{R_f}$ 0.20 (75% EtOAc in hexanes); **^{1}H NMR** (300 MHz, $CDCl_3$) δ: 7.46 (s, 1H), 7.38–7.16 (m, 5H), 5.48 (s, 2H), 4.73 (s, 2H) (alcohol OH signal not seen); **^{13}C NMR** (75 MHz, $CDCl_3$) δ: 148.2, 134.5, 129.1, 128.7, 128.1, 121.9, 56.1, 54.2; ***m/z*** (ESI+) 212 ($[M+Na]^+$, 70%), 401 ($[2M+Na]^+$, 100%); **HRMS** (ESI+) found 212.07945 $[M+Na]^+$, $C_{10}H_{11}N_3ONa^+$ requires 212.07942. Spectroscopic data matched those in the literature.[388]

3-(4-(Difluoromethoxy)phenyl)-5-((1-phenyl-1*H*-1,2,3-triazol-4-yl)methoxy)-[1,2,4]triazolo[4,3-*a*]pyrazine 83

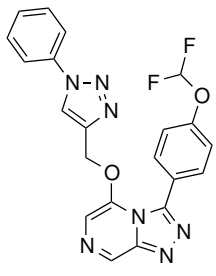

Prepared according to General Procedure 4 from: **81** (50.0 mg, 0.29 mmol) and **44** (85.0 mg, 0.29 mmol) to give the crude title compound as a pale yellow solid (109 mg); purified by automated flash chromatography on silica (Biotage Isolera, 0–10% MeOH in CH_2Cl_2) to give *the title compound* as an orange powder (86 mg, 70%); $\mathbf{R_f}$ 0.21 (100% EtOAc); **m.p.** 172–175 °C; **^{1}H NMR** (300 MHz, $CDCl_3$) δ: 9.08 (s, 1H), 7.75–7.61 (m, 5H), 7.61–7.45 (m, 4H), 7.07 (d, *J* 8.3, 2H), 6.43 (t, *J* 73.3, 1H), 5.46 (s, 2H); **^{13}C NMR** (75 MHz, DMSO-d_6) δ: 151.8, 147.5, 145.6, 143.5, 141.3, 136.3, 135.6, 132.6, 129.9, 128.9, 124.4, 123.5, 120.2, 117.1, 116.0 (t, *J* 258.3), 109.5, 63.7; ***m/z*** (ESI+) 458 ($[M+Na]^+$, 100%); **HRMS** (ESI+) found 458.11441 $[M+Na]^+$, $C_{21}H_{15}F_2N_7O_2Na^+$ requires 458.11475.

5-((1-Benzyl-1*H*-1,2,3-triazol-4-yl)methoxy)-3-(4-(difluoromethoxy)phenyl)-[1,2,4] triazolo[4,3-*a*]pyrazine 84

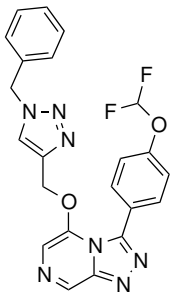

Prepared according to General Procedure 4 from: **82** (159 mg, 0.84 mmol) and **44** (250 mg, 0.84 mmol) to give the crude title compound as a pale brown solid (346 mg); purified by automated flash chromatography on silica (Biotage Isolera, 0–10% MeOH in CH_2Cl_2) to give *the title compound* as a pale yellow powder (331 mg, 87%); $\mathbf{R_f}$ 0.03 (50% EtOAc in hexanes); **m.p.** 109–111 °C; **^{1}H NMR** (300 MHz, $CDCl_3$) δ: 8.98 (s, 1H), 7.56 (d, *J* 8.7, 2H), 7.42 (s, 1H), 7.39–7.26 (m, 3H), 7.23–7.15 (m, 2H), 7.11 (s, 1H), 6.97 (d, *J* 8.4, 2H), 6.53 (t, *J* 73.4, 1H), 5.43 (s, 2H), 5.26 (s, 2H); **^{13}C NMR** (75 MHz, $CDCl_3$) δ: 152.3, 147.9, 146.4, 143.5, 140.7, 137.1, 134.1, 132.7, 129.4, 129.2, 128.3, 124.7, 123.4, 118.3, 115.8 (t, *J* 260.8), 109.1, 64.1, 54.5; ***m/z*** (ESI+) 472 ($[M+H]^+$, 100%); **HRMS** (ESI+) found 472.12966 $[M+Na]^+$, $C_{22}H_{17}F_2N_7O_2Na^+$ requires 472.13042.

1-(3,4-Difluorophenyl)ethan-1-one 94

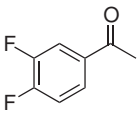

1-(3,4-Difluorophenyl)ethan-1-ol (1.50 g, 9.48 mmol, 1.0 equiv.) was dissolved in CH_2Cl_2 (15 mL). HIO_3 (1.84 g, 10.4 mmol, 1.1 equiv.) and TEMPO (74.1 mg, 0.47 mmol, 5 mol%) were added and the reaction stirred under Ar at rt for 19 h. The reaction was poured into an aqueous solution of $Na_2S_2O_3$ (50 mL) and extracted with a 1:1 mixture of Et_2O:hexane (3 × 50 mL). The combined organic layers were washed with brine, dried (Na_2SO_4), filtered and concentrated under reduced pressure to give the crude title compound as an orange liquid (1.39 g); purified by automated flash chromatography on silica (Biotage Isolera, 6–50% EtOAc in hexanes) to give *the title compound* as a clear red liquid (1.04 g, 70%); $\mathbf{R_f}$ 0.69 (25% EtOAc in hexanes); **^{1}H NMR** (200 MHz, $CDCl_3$) δ: 7.98–7.61 (m, 2H), 7.28 (q, *J* 9.4 & 9.0, 1H), 2.62 (s, 3H). Spectroscopic data matched those in the literature.[389]

2-(3,4-Difluorophenyl)-2,2-dimethoxyethan-1-ol 95

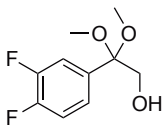

To a solution of KOH (2.70 g, 48.0 mmol, 10 equiv.) in MeOH (30 mL) was added **94** (750 mg, 4.80 mmol, 1.0 equiv.) dropwise over 15 min at 0 °C. $PhI(OAc)_2$ (3.09 g, 9.61 mmol, 2.0 equiv.) was added in small portions over 20 min and the resulting solution stirred at rt for 23 h. The solvent was removed and the residue dissolved and H_2O and extracted with EtOAc (3 ×). The combined organic layers were washed with brine, dried (Na_2SO_4), filtered and concentrated under reduced pressure to give the crude title compound as a brown liquid (1.41 g); carried forward without further purification or complete characterisation; $\mathbf{R_f}$ 0.11 (10% EtOAc in hexanes); **^{1}H NMR** (200 MHz, $CDCl_3$) δ: 7.53–6.85 (m, 3H), 3.78 (s, 2H), 3.25 (s, 6H) (alcohol OH signal not seen). Compound reported in the literature but no

characterisation data were provided.[195]

1-(3,4-Difluorophenyl)-2-hydroxyethan-1-one 96

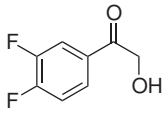

Compound **95** (1.00 g, 4.58 mmol, 1 equiv.) was dissolved in 3:1 THF:H_2O (10 mL) and *p*-TsOH (1.58 g, 9.17 mmol, 2 equiv.) was added. The mixture was stirred at reflux for 2 h. The reaction was quenched with H_2O and extracted with EtOAc (3 ×). The combined organic layers were washed with brine, dried (Na_2SO_4), filtered and concentrated under reduced pressure to give the crude title compound as a yellow solid (803 mg); purified by dissolving in EtOAc and filtering insoluble impurities to give *the title compound* as a light brown powder (516 mg, 65%); carried forward without complete characterisation; $\mathbf{R_f}$ 0.48 (50% EtOAc in hexanes); **^{1}H NMR** (200 MHz, $CDCl_3$) δ: 7.90–7.57 (m, 2H), 7.44–7.19 (m, 1H), 4.84 (s, 2H) (alcohol OH signal not seen). Compound reported in the literature but no characterisation data were provided.[390]

2-((3-(4-(Difluoromethoxy)phenyl)-[1,2,4]triazolo[4,3-*a*]pyrazin-5-yl)oxy)-1-(3,4-difluorophenyl)ethan-1-one 97

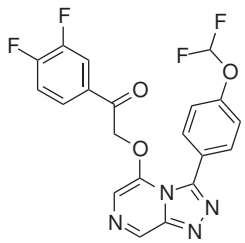

Compound **98** (100 mg, 0.21 mmol, 1 equiv.) was dissolved in 3:1 THF:H_2O (10 mL) and *p*-TsOH (72.0 mg, 0.42 mmol, 2 equiv.) was added. The mixture was stirred at reflux. The condenser was removed and the THF allowed to boil off to give a mixture of black sludge and H_2O. The reaction was quenched with H_2O and extracted with EtOAc (3 ×). The combined organic layers were washed with brine, dried (Na_2SO_4), filtered and concentrated under reduced pressure to give the crude title compound as a brown solid (94.1 mg); purified by automated flash chromatography on silica (Biotage Isolera, 25–100% EtOAc in hexanes) to give a light brown powder (50.4 mg, 56%); repurified by preparative TLC (5% MeOH in CH_2Cl_2) to give *the title compound* as an off-white powder (24.0 mg, 27%); $\mathbf{R_f}$ 0.49 (5% MeOH in CH_2Cl_2); **m.p.** 192–200 °C; **^{1}H NMR** (500 MHz, DMSO-d$_6$) δ: 9.11 (s, 1H), 8.06–7.98 (m, 1H), 7.90–7.78 (m, 1H), 7.83 (d, *J* 8.8, 2H), 7.71 (s, 1H), 7.63 (dt, *J* 10.1 & 8.4, 1H), 7.34 (t, *J* 73.7, 1H), 7.23 (d, *J* 8.7, 2H), 5.85 (s, 2H); **^{13}C NMR** (126 MHz, DMSO-d$_6$) δ: 190.2, 153.1 (dd, *J* 254.9 & 12.8), 152.0 (t, *J* 2.9), 149.4 (dd, *J* 247.9 & 13.0), 147.5, 145.8, 143.5, 135.7, 132.5, 131.3–130.5 (m), 126.2 (dd, *J* 7.9 & 3.2), 124.4, 118.2 (d, *J* 17.9), 117.7 (d, *J* 18.1), 117.4, 115.1 (d, *J* 257.8), 109.9, 72.3; ***m/z*** (ESI+) 455 ($[M+Na]^+$, 100%); **HRMS** (ESI+) found 455.07297 $[M+Na]^+$, $C_{20}H_{12}F_4N_4O_3Na^+$ requires 455.07377.

3-(4-(Difluoromethoxy)phenyl)-5-(2-(3,4-difluorophenyl)-2,2-dimethoxyethoxy)-[1,2,4]triazolo[4,3-*a*]pyrazine 98

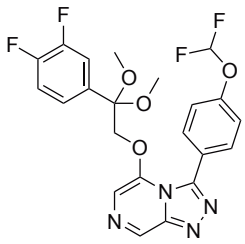

Prepared according to General Procedure 4 from: **95** (167 mg, 0.77 mmol) and **44** (227 mg, 0.77 mmol) to give the crude title compound as a brown solid (321 mg); purified by automated flash chromatography on silica (Biotage Isolera, 25–100% EtOAc in hexanes) to give *the title compound* as a light brown powder (221 mg, 60%); $\mathbf{R_f}$ 0.58 (100% EtOAc); **m.p.** 148–153 °C; **^{1}H NMR** (300 MHz, $CDCl_3$) δ: 8.97 (s, 1H), 7.65 (d, *J* 8.6, 2H), 7.33 (d, *J* 8.5, 2H), 7.25 (br s, 1H), 7.03–6.82 (m, 1H), 6.69 (t, *J* 73.3, 1H), 6.75–6.58 (m, 2H), 4.32 (s, 2H), 3.18 (s, 6H); **^{13}C NMR** (75 MHz, $CDCl_3$) δ: 152.5, 147.8, 146.2, 143.6, 137.1, 134.7, 132.3, 124.8, 122.9 (dd, *J* 6.2 & 3.5), 119.2, 117.1 (d, *J* 17.5), 116.6 (d, *J* 18.9), 115.7 (t, *J* 261.7), 108.6, 99.5, 71.2, 49.1 (two phenyl C–F signals expected between 155 and 148 ppm; observed for compound **97**; too weak to be seen); ***m/z*** (ESI+) 501 ($[M+Na]^+$, 100%); **HRMS** (ESI+) found 501.11602 $[M+Na]^+$, $C_{22}H_{18}F_4N_4O_4Na^+$ requires 501.11562.

(2-(3,4-Difluorophenyl)-1,3-dioxolan-2-yl)methanol 99

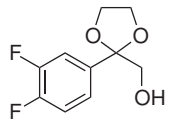

Compound **96** (100 mg, 0.58 mmol, 1.0 equiv.) was dissolved in PhMe (5 mL). *p*-TsOH (40.0 mg, 0.23 mmol, 0.4 equiv.) and ethylene glycol (162 μL, 2.90 mmol, 5.0 equiv.) were added and the reaction heated to reflux. The reaction was cooled to rt and the solvent removed. The residue was partitioned between H_2O and CH_2Cl_2 and the organic layer separated, dried ($MgSO_4$), filtered and concentrated under reduced pressure to give the crude title compound as a yellow oil (119 mg); this intermediate, though novel, was carried forward without purification or characterisation; $\mathbf{R_f}$ 0.04 (50% EtOAc in hexanes, $KMnO_4$ stain).

3-(4-(Difluoromethoxy)phenyl)-5-((2-(3,4-difluorophenyl)-1,3-dioxolan-2-yl) methoxy)-[1,2,4]triazolo[4,3-*a*]pyrazine 100

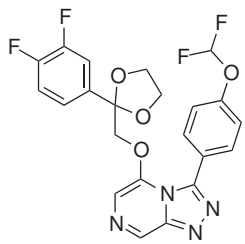

Prepared according to General Procedure 4 from: **99** (50.0 mg, 0.23 mmol) and **44** (68.6 mg, 0.23 mmol) to give the crude title compound as a green solid (95.0 mg); purified by automated flash chromatography on silica (Biotage Isolera, 25–100% EtOAc in hexanes) to give *the title compound* as a an off-white powder (8.10 mg, 7%); $\mathbf{R_f}$ 0.25 (100% EtOAc); **m.p.** 150–155 °C; **^{1}H NMR** (400 MHz, $CDCl_3$) δ: 9.04 (s, 1H), 7.73 (d, *J* 8.9, 2H), 7.37 (s, 1H), 7.28 (d, *J* 8.9, 2H), 7.12–6.87 (m, 3H), 6.64 (t, *J* 73.2, 1H), 4.30 (s, 2H), 3.83–3.79 (m, 2H), 3.79–3.76 (m, 2H); **^{13}C NMR** (101 MHz, $CDCl_3$) δ: 152.3, 152.5–149.3 (4 peaks), 151.8–148.4 (4 peaks), 148.0, 146.4,

144.0, 137.1, 135.9–135.2 (m), 132.5, 124.9, 122.4 (dd, *J* 6.6 & 3.8), 119.2, 117.5 (d, *J* 17.3), 115.7 (d, *J* 19.0), 115.6 (t, *J* 261.8), 109.1, 106.3, 73.2, 65.4; ***m/z*** (ESI+) 499 ($[M+Na]^+$, 100%); **HRMS** (ESI+) found 499.10048 $[M+Na]^+$, $C_{22}H_{16}F_4N_4O_4Na^+$ requires 499.09999.

Ethyl 2-hydroxy-2-phenylacetate 101

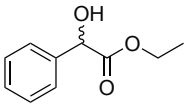

Prepared according to General Procedure 7 from: DL-Mandelic acid (10.0 g, 65.7 mmol, 1 equiv.) to give the crude title compound as a clear yellow oil (12.3 g); carried forward without further purification; $\mathbf{R_f}$ 0.55 (25% EtOAc in hexanes); **IR** ν_{max} (film) /cm^{-1} 3453, 1728; **^{1}H NMR** (400 MHz, $CDCl_3$) δ: 7.46–7.40 (m, 2H), 7.40–7.29 (m, 3H), 5.16 (s, 1H), 4.34–4.09 (m, 2H), 3.64 (br s, 1H), 1.22 (t, *J* 7.1, 3H); **^{13}C NMR** (101 MHz, $CDCl_3$) δ: 173.7, 138.6, 128.6, 128.4, 126.6, 73.0, 62.2, 14.1. Spectroscopic data matched those in the literature.[391]

Ethyl 2-phenyl-3-((tetrahydro-2*H*-pyran-2-yl)oxy)propanoate 102

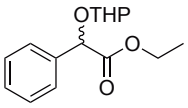

Compound **101** (10.0 g, 5.55 mmol, 1.0 equiv.) was dissolved in CH_2Cl_2 (200 mL). *p*-TsOH (1.91 g, 1.11 mmol, 0.2 equiv.) and 3,4-dihydro-2*H*-pyran (5.57 mL, 61.0 mmol, 1.1 equiv.) were added and the reaction stirred at rt. The reaction was quenched with ice cold H_2O (80 mL) and the organic layer separated. The aqueous layer was extracted with CH_2Cl_2 (3 × 50 mL) and the combined organic layers washed with H_2O (50 mL), brine (40 mL), dried ($MgSO_4$), filtered and concentrated under reduced pressure to give the crude title compound as a black oil (14.1 g); carried forward without further purification or complete characterisation; $\mathbf{R_f}$ 0.76 (25% EtOAc in hexanes); **^{1}H NMR** (400 MHz, $CDCl_3$) δ: 7.53–7.42 (m, 2H), 7.41–7.27 (m, 3H), 5.26 (d, *J* 41.6, 1H), 4.74 (dt, *J* 120.7 & 3.3, 1H), 4.16 (ddtd, *J* 18.0, 14.5, 7.6 & 3.7, 2H), 3.71 (ddd, *J* 11.2, 9.9 & 3.2, 1H), 3.60–3.42 (m, 1H), 2.01–1.38 (m, 6H), 1.20 (t, *J* 7.1, 3H). Compound reported in the literature but no characterisation data were provided.[392]

2-Phenyl-2-((tetrahydro-2*H*-pyran-2-yl)oxy)ethan-1-ol 103

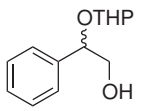

Prepared according to General Procedure 6 from: **102** (12.0 g, 45.4 mmol, 1 equiv.) to give the crude title compound as a dark red oil (11.3 g); purified by automated flash chromatography on silica (Biotage Isolera, 25–100% EtOAc in hexanes) to give *the title compound* as a dark red oil (3.24 g, 32%); **^{1}H NMR** (400 MHz, $CDCl_3$, present as a mixture of diastereomers) δ: 7.47–7.06 (m, 10H), 4.91 (t, *J* 3.6, 1H), 4.82 (dd, *J* 8.3 & 3.7, 1H), 4.73 (dd, *J* 6.9 & 4.9, 1H), 4.52 (dd, *J* 5.7 & 2.8, 1H), 4.22–3.20 (m, 8H), 3.04 (d_{app}, *J* 10.8, 1H), 2.25 (br s, 1H), 2.13–1.32 (m, 12H); **^{13}C NMR** (101 MHz, $CDCl_3$, present

as a mixture of diastereomers) δ: 140.0, 138.9, 128.6, 128.4, 128.1, 127.7, 126.9, 126.8, 99.2, 98.0, 80.8, 79.9, 67.7, 66.8, 63.8, 62.7, 31.1, 30.7, 25.4, 25.36, 20.4, 19.5. Spectroscopic data matched those in the literature.[393,394]

3-(4-(Difluoromethoxy)phenyl)-5-(2-phenyl-2-((tetrahydro-2*H*-pyran-2-yl)oxy) ethoxy)-[1,2,4]triazolo[4,3-*a*]pyrazine 104

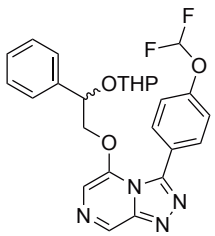

Prepared according to General Procedure 4 from: **103** (206 mg, 0.93 mmol) and **44** (275 mg, 0.93 mmol) to give the crude title compound as a black sludge (477 mg); purified by automated flash chromatography on silica (Biotage Isolera, 25–100% EtOAc in hexanes) to give *the title compound* as a brown powder (201 mg, 45%); this intermediate, though novel, was carried forward without characterisation; $\mathbf{R_f}$ 0.42 (100% EtOAc).

2-((3-(4-(Difluoromethoxy)phenyl)-[1,2,4]triazolo[4,3-*a*]pyrazin-5-yl)oxy)-1-phenylethan-1-ol 16

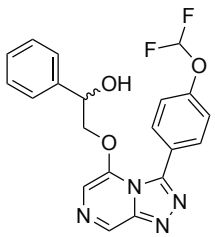

Compound **104** (100 mg, 0.21 mmol, 1 equiv.) was dissolved in EtOH (2 mL). $CuCl_2{\cdot}2H_2O$ (1.77 mg, 0.01 mmol, 5 mol%) was added and the mixture heated at reflux for 3 h. The solvent was removed and the residue dissolved in EtOAc, washed with H_2O, brine, dried ($MgSO_4$), filtered and concentrated under reduced pressure to give the crude title compound as a dark brown liquid (90.0 mg); purified by automated flash chromatography on silica (Biotage Isolera, 25–100% EtOAc in hexanes) to give *the title compound* as a brown powder (65.2 mg, 79%); $\mathbf{R_f}$ 0.27 (100% EtOAc); **m.p.** 85–90 °C; **^{1}H NMR** (300 MHz, $CDCl_3$) δ: 8.92 (br s, 1H), 7.75 (d, J 8.0, 2H), 7.27 (d_{app}, J 28.7, 8H), 6.62 (t, J 73.3, 1H), 4.91 (br s, 1H), 4.31 (d, J 5.0, 2H), 3.26 (br s, 1H); **^{13}C NMR** (75 MHz, $CDCl_3$) δ: 152.5, 147.7, 146.4, 144.0, 139.0, 136.5, 132.6, 128.9, 128.7, 126.2, 124.8, 118.8, 115.7 (t, J 261.4), 108.8, 75.2, 71.5; ***m/z*** (ESI+) 399 ($[M+H]^+$, 100%); **HRMS** (ESI+) 399.12603 $[M+H]^+$, $C_{20}H_{16}F_2N_4O_3H^+$ requires 399.12628.

2-((3-(4-(Difluoromethoxy)phenyl)-[1,2,4]triazolo[4,3-*a*]pyrazin-5-yl)oxy)-1-phenylethan-1-one 105

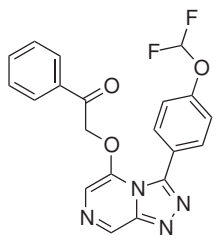

Compound **16** (2.00 g, 5.02 mmol, 1.0 equiv.) was dissolved in anhydrous CH_2Cl_2 (30 mL) and MnO_2 (21.8 g, 251 mmol, 50 equiv.) was added and the reaction stirred at reflux. The mixture was filtered through celite and the celite washed with EtOAc. The filtrate was concentrated under reduced pressure to give the crude title compound as a brown solid (1.65 g); purified by automated flash chromatograph on silica (Biotage Isolera, 25–100% EtOAc in hexanes) to give *the title compound* as a brown powder (741 mg, 37%); **m.p.** 120–128 °C; **^{1}H NMR** (400 MHz, $CDCl_3$) δ: 8.99 (s, 1H), 7.84 (dd_{app}, *J* 8.3 & 1.1, 2H), 7.78 (d, *J* 8.8, 2H), 7.65 (t, *J* 7.5, 1H), 7.49 (t, *J* 7.8, 2H), 7.22 (s, 1H), 7.14 (d, *J* 8.7, 2H), 6.57 (t, *J* 73.4, 1H), 5.49 (s, 2H); **^{13}C NMR** (101 MHz, $CDCl_3$) δ: 190.4, 152.5, 147.9, 146.6, 143.5, 137.1, 134.9, 133.4, 132.5, 129.3, 128.0, 124.7, 118.5, 115.7 (t, *J* 260.6), 109.2, 71.3; ***m/z*** (ESI+) 419 ($[M+Na]^+$, 100%), 815 ($[2M+Na]^+$, 13%); **HRMS** (ESI+) found 419.09273 $[M+Na]^+$, $C_{20}H_{14}F_2N_4O_3Na^+$ requires 419.09262.

2-Morpholino-2-phenylethan-1-ol 269

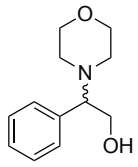

To a mixture of styrene oxide (571 μL, 4.99 mmol, 1.00 equiv.) and morpholine (459 μL, 5.24 mmol, 1.05 equiv.) was added $Mg(ClO_4)_2$ (22.3 mg, 99.9 μmol, 2 mol%). The reaction mixture was allowed to stir at rt for 3 h, following which EtOAc was added and the organic layer washed with H_2O, dried (Na_2SO_4), filtered and concentrated under reduced pressure to give the crude title compound as a clear colourless oil (914 mg); carried forward without further purification or characterisation; $\mathbf{R_f}$ 0.33 (100% EtOAc).

4-(2-((3-(4-(Difluoromethoxy)phenyl)-[1,2,4]triazolo[4,3-*a*]pyrazin-5-yl)oxy)-1-phenylethyl)morpholine 108

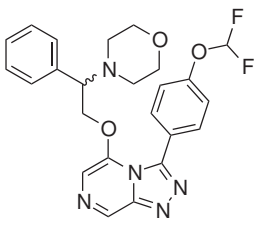

Prepared according to General Procedure 4 from: **269** (100 mg, 0.48 mmol) and **44** (143 mg, 0.48 mmol) to give the crude title compound as a brown solid (215 mg); purified by automated flash chromatography on silica twice (Biotage Isolera, 0–10% MeOH in CH_2Cl_2, then 0–5% MeOH in CH_2Cl_2) to give a pale yellow powder; repurified by preparative TLC (4% MeOH in CH_2Cl_2) to give *the title compound* as a pale yellow powder (58.6 mg, 26%); $\mathbf{R_f}$ 0.03 (100% EtOAc); **m.p.** 150–158 °C; **^{1}H NMR** (400 MHz, $CDCl_3$) δ: 9.01 (s, 1H), 7.60 (d, *J* 8.7, 2H), 7.31 (s, 1H), 7.30–7.27 (m, 3H), 7.20 (d, *J* 8.6, 2H), 7.09–6.95 (m, 2H), 6.63 (t, *J* 73.1, 1H), 4.50 (ddd, *J* 36.1, 10.2 & 5.7, 2H), 3.56 (t, *J* 4.6, 4H), 3.49 (t, *J* 5.6, 1H), 2.22 (tq, *J* 11.4, 5.7 & 4.6, 4H);

^{13}C NMR (101 MHz, $CDCl_3$) δ: 152.4, 147.9, 146.3, 143.9, 136.8, 132.5, 128.9, 128.5, 128.2, 125.0, 119.1, 115.7 (t, *J* 261.7), 108.7, 71.9, 68.1, 67.0, 51.3 (1 obscured signal); ***m/z*** (ESI+) 490 ($[M+Na]^+$, 100%); **HRMS** (ESI+) found 490.16655 $[M+Na]^+$, $C_{24}H_{23}F_2N_5O_3Na^+$ requires 490.16612.

Ethyl 2-(3,4-difluorophenyl)-2-(ethyl(methyl)amino)acetate 109

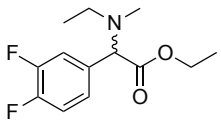

Compound **53** (600 mg, 2.15 mmol, 1 equiv.) was dissolved in DMF (6 mL). *N*-Ethylmethylamine (0.18 mL, 2.15 mmol, 1 equiv.) and K_2CO_3 (891 mg, 6.45 mmol, 3 equiv.) were added and the reaction stirred at rt. The reaction was filtered and the solvent removed. The residue was partitioned between EtOAc and H_2O. The aqueous layer was extracted with EtOAc and the combined organic layers were washed with brine, dried (Na_2SO_4), filtered and concentrated under reduced pressure to give the crude title compound as a dark yellow oil (474 mg); this intermediate, though novel, was carried forward without purification or complete characterisation; $\mathbf{R_f}$ 0.45 (10% EtOAc in hexanes; **^{1}H NMR** (200 MHz, $CDCl_3$) δ: 7.44–7.24 (m, 1H), 7.21–6.99 (m, 2H), 4.31–4.04 (m, 3H), 2.68–2.31 (m, 2H), 2.23 (s, 3H), 1.23 (t, *J* 7.1, 3H), 1.05 (t, *J* 7.1, 3H).

Ethyl 2-(diethylamino)-2-(3,4-difluorophenyl)acetate 110

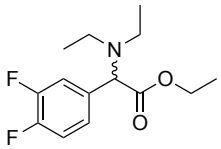

Compound **53** (600 mg, 2.15 mmol, 1 equiv.) was dissolved in DMF (6 mL). Diethylamine (0.22 mL, 2.15 mmol, 1 equiv.) and K_2CO_3 (891 mg, 6.45 mmol, 3 equiv.) were added and the reaction stirred at rt. The reaction was filtered and the solvent removed. The residue was partitioned between EtOAc and H_2O. The aqueous layer was extracted with EtOAc and the combined organic layers were washed with brine, dried (Na_2SO_4), filtered and concentrated under reduced pressure to give the crude title compound as a dark yellow oil (481 mg); this intermediate, though novel, was carried forward without purification or complete characterisation; $\mathbf{R_f}$ 0.61 (10% EtOAc in hexanes; **^{1}H NMR** (200 MHz, $CDCl_3$) δ: 7.41–7.23 (m, 1H), 7.22–7.04 (m, 2H), 4.40 (s, 1H), 4.18 (dtt, *J* 10.8, 7.2 & 3.7, 2H), 2.59 (q, *J* 7.1, 4H), 1.24 (t, *J* 7.1, 3H), 0.99 (t, *J* 7.1, 6H).

2-(3,4-Difluorophenyl)-2-(ethyl(methyl)amino)ethan-1-ol 270

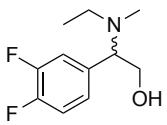

Prepared according to General Procedure 6 from: **109** (350 mg, 1.36 mmol) to give the crude title compound as an orange oil (300 mg); purified by automated flash chromatography on silica (Biotage Isolera, 12–100% EtOAc in hexanes) to give *the title compound* as a clear yellow oil (32.9 mg, 11%); this intermediate, though novel, was carried forward without complete characterisation; $\mathbf{R_f}$ 0.09 (50% EtOAc in hexanes; **^{1}H NMR**

(400 MHz, $CDCl_3$) δ: 7.12 (dt, J 10.2 & 8.3, 1H), 7.03 (ddd, J 11.3, 7.7 & 2.1, 1H), 6.92 (ddt, J 8.0, 3.8 & 1.8, 1H), 3.85 (dd, J 10.3 & 8.8, 1H), 3.77–3.56 (m, 2H), 2.85 (br s, 1H), 2.42 (ddq, J 74.1, 12.4 & 7.1, 2H), 2.16 (s, 3H), 1.08 (t, J 7.1, 3H); **^{13}C NMR** (101 MHz, $CDCl_3$) δ: 150.2 (dd, J 248.5 & 12.5), 150.0 (dd, J 248.5 & 12.6), 133.5 (t, J 4.4), 125.0 (dd, J 6.1 & 3.6), 117.7 (d, J 17.0), 117.1 (d, J 17.0), 67.7, 60.9, 48.0, 36.6, 13.0.

2-(Diethylamino)-2-(3,4-difluorophenyl)ethan-1-ol 112

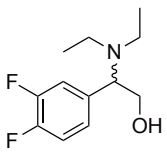

Prepared according to General Procedure 6 from: **110** (350 mg, 1.29 mmol) to give the crude title compound as an orange oil (291 mg); this intermediate, though novel, was carried forward without purification or complete characterisation; $\mathbf{R_f}$ 0.24 (50% EtOAc in hexanes; **^{1}H NMR** (200 MHz, $CDCl_3$) δ: 7.25–6.82 (m, 3H), 4.02–3.51 (m, 3H), 2.98–2.10 (m, 4H), 1.08 (t, J 7.1, 6H) (alcohol OH signal not seen).

2-((3-(4-(Difluoromethoxy)phenyl)-[1,2,4]triazolo[4,3-*a*]pyrazin-5-yl)oxy)-1-(3,4-difluorophenyl)-*N*-ethyl-*N*-methylethan-1-amine 113

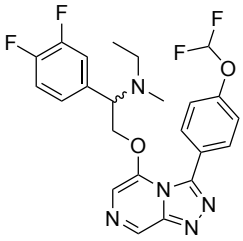

Prepared according to General Procedure 4 from: **111** (20.0 mg, 92.9 μmol) and **44** (27.6 mg, 92.9 μmol) to give the crude title compound as a brown solid; purified by automated flash chromatography on silica (Biotage Isolera, 1–10% MeOH in CH_2Cl_2) to give *the title compound* as a dark orange powder (13.3 mg, 30%); insufficient material remaining for complete characterisation; $\mathbf{R_f}$ 0.12 (100% EtOAc); **^{1}H NMR** (200 MHz, $CDCl_3$) δ: 9.03 (s, 1H), 7.61 (d, J 8.7, 2H), 7.32 (s, 1H), 7.19 (d, J 8.6, 2H), 7.10–6.92 (m, 1H), 6.80–6.64 (m, 2H), 6.62 (t, J 73.2, 1H), 4.45 (dq, J 7.5, 4.0 & 3.4, 2H), 3.63 (t, J 5.7, 1H), 2.39–2.20 (m, 2H), 2.10 (s, 3H), 0.97 (t, J 7.1, 3H); ***m/z*** (ESI+) 476 ($[M+H]^+$, 100%); **HRMS** (ESI+) found 476.17066 $[M+H]^+$, $C_{23}H_{21}F_4N_5O_2H^+$ requires 476.17041.

2-((3-(4-(Difluoromethoxy)phenyl)-[1,2,4]triazolo[4,3-*a*]pyrazin-5-yl)oxy)-1-(3,4-difluorophenyl)-*N*,*N*-diethylethan-1-amine 114

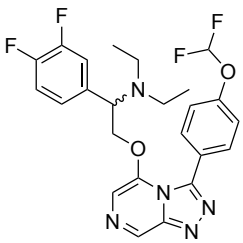

Prepared according to General Procedure 4 from: **112** (30.0 mg, 131 μmol) and **44** (38.8 mg, 131 μmol) to give the crude title compound as a brown solid; purified by automated flash chromatography on silica (Biotage Isolera, 25–100% EtOAc in hexanes) to give *the title compound* as a yellow powder (40.1 mg, 63%); insufficient material remaining for complete characterisation; $\mathbf{R_f}$ 0.33 (100% EtOAc); **^{1}H NMR** (200 MHz, $CDCl_3$) δ: 9.04 (s, 1H), 7.57 (d, J 8.6, 2H), 7.34 (s, 1H), 7.13 (d, J 8.5, 2H), 7.08–6.88 (m, 1H), 6.83–6.62 (m, 2H), 6.41 (t, J 73.1,

1H), 4.64–4.25 (m, 2H), 3.85 (t, *J* 5.7, 1H), 2.68–2.19 (m, 4H), 0.95 (t, *J* 7.1, 6H); ***m/z*** (ESI+) 512 ([M+Na]$^+$, 100%); **HRMS** (ESI+) found 512.16767 [M+Na]$^+$, $C_{24}H_{23}F_4N_5O_2Na^+$ requires 512.16801.

tert-Butyl (*R*)-(1-hydroxy-3-phenylpropan-2-yl)carbamate 115

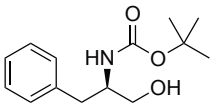

To a solution of (*R*)-2-amino-3-phenylpropan-1-ol (200 mg, 1.32 mmol, 1.0 equiv.) in CH_2Cl_2 (3.5 mL) was added Boc_2O (0.33 mL, 1.45 mmol, 1.1 equiv.) at 0 °C. The reaction was warmed to rt and stirred overnight. Sat. aq. NH_4Cl (6 mL) was added and the organic layer separated. The aqueous layer was extracted with CH_2Cl_2 (2 × 8 mL) and the combined organic layers were dried (Na_2SO_4), filtered and concentrated under reduced pressure to give the crude title compound as a yellow solid (594 mg); purified automated flash chromatograph on silica (Biotage Isolera, 12–50% EtOAc in hexanes) to give *the title compound* as a white powder (250 mg, 75%); $\mathbf{R_f}$ 0.63 (100% EtOAc, $KMnO_4$ stain); **m.p.** 100–105 °C; **^{1}H NMR** (400 MHz, $CDCl_3$) δ: 7.34–7.27 (m, 2H), 7.25–7.18 (m, 3H), 4.76 (d, *J* 8.1, 1H), 3.87 (br s, 1H), 3.60 (ddt, *J* 46.1, 10.5 & 4.6, 2H), 2.84 (d, *J* 7.2, 2H), 2.44 (br s, 1H), 1.41 (s, 9H); **^{13}C NMR** (101 MHz, $CDCl_3$) δ: 156.3, 138.0, 129.4, 128.7, 126.7, 79.9, 64.5, 53.9, 37.6, 28.5. Spectroscopic data matched those in the literature.[395]

tert-Butyl (*S*)-(1-hydroxy-3-phenylpropan-2-yl)carbamate 116

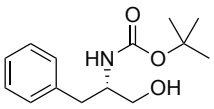

To a solution of (*S*)-2-amino-3-phenylpropan-1-ol (200 mg, 1.32 mmol, 1.0 equiv.) in CH_2Cl_2 (3.5 mL) was added Boc_2O (0.33 mL, 1.45 mmol, 1.1 equiv.) at 0 °C. The reaction was warmed to rt and stirred overnight. Sat. aq. NH_4Cl (6 mL) was added and the organic layer separated. The aqueous layer was extracted with CH_2Cl_2 (2 × 8 mL) and the combined organic layers were dried (Na_2SO_4), filtered and concentrated under reduced pressure to give the crude title compound as a yellow solid (413 mg); purified automated flash chromatograph on silica (Biotage Isolera, 12–50% EtOAc in hexanes) to give *the title compound* as a white powder (301 mg, 91%); $\mathbf{R_f}$ 0.68 (100% EtOAc, $KMnO_4$ stain); **m.p.** 105–110 °C; **^{1}H NMR** (400 MHz, $CDCl_3$) δ: 7.33–7.27 (m, 2H), 7.25–7.19 (m, 3H), 4.77 (d, *J* 8.0, 1H), 3.87 (br s, 1H), 3.60 (ddt, *J* 45.1, 10.5 & 4.6, 2H), 2.84 (d, *J* 7.1, 2H), 2.46 (br s, 1H), 1.41 (s, 9H); **^{13}C NMR** (101 MHz, $CDCl_3$) δ: 156.3, 138.0, 129.4, 128.7, 126.7, 79.9, 64.5, 53.9, 37.7, 28.5. Spectroscopic data matched those in the literature.[395]

tert-Butyl (_R_)-(1-((3-(4-(difluoromethoxy)phenyl)-[1,2,4]triazolo[4,3-_a_]pyrazin-5-yl) oxy)-3-phenylpropan-2-yl)carbamate 117

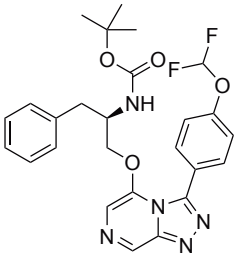

Prepared according to General Procedure 4 from: **115** (200 mg, 0.80 mmol) and **44** (236 mg, 0.80 mmol) to give the crude title compound as a black sludge (408 mg); purified by automated flash chromatography on silica (Biotage Isolera, 25–100% EtOAc in hexanes) to give *the title compound* as a dark brown powder (135 mg, 33%); $\mathbf{R_f}$ 0.59 (100% EtOAc); **m.p.** 78–82 °C; **^{1}H NMR** (400 MHz, $CDCl_3$) δ: 9.06 (s, 1H), 7.78 (d, *J* 8.6, 2H), 7.36 (d, *J* 8.5, 2H), 7.26–7.18 (m, 3H), 7.23 (s, 1H), 6.92 (d, *J* 6.3, 2H), 6.57 (t, *J* 72.8, 1H), 4.33–3.91 (m, 4H), 2.35 (ddd, *J* 71.6, 13.7 & 7.5, 2H), 1.42 (s, 9H); **^{13}C NMR** (101 MHz, $CDCl_3$) δ: 154.9, 152.7, 147.8, 145.8, 143.9, 136.9, 136.4, 132.5, 128.98, 128.95, 127.2, 125.5, 119.2, 115.6 (t, *J* 262.5), 108.6, 80.4, 71.0, 50.3, 37.2, 28.4; **^{19}F NMR** (376 MHz, $CDCl_3$) δ: -81.34; ***m/z*** (ESI+) 534 ($[M+Na]^+$, 100%); **HRMS** (ESI+) found 512.20948 $[M+H]^+$, $C_{26}H_{27}F_2N_5O_4H^+$ requires 512.21039.

tert-Butyl (_S_)-(1-((3-(4-(difluoromethoxy)phenyl)-[1,2,4]triazolo[4,3-_a_]pyrazin-5-yl) oxy)-3-phenylpropan-2-yl)carbamate 118

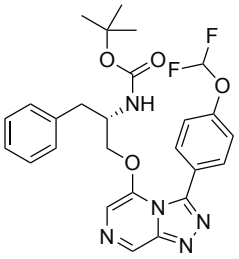

Prepared according to General Procedure 4 from: **116** (200 mg, 0.80 mmol) and **44** (236 mg, 0.80 mmol) to give the crude title compound as a black sludge; purified by automated flash chromatography on silica (Biotage Isolera, 25–100% EtOAc in hexanes) to give *the title compound* as a dark brown powder (169 mg, 42%); $\mathbf{R_f}$ 0.57 (100% EtOAc); **m.p.** 78–82 °C; **^{1}H NMR** (500 MHz, $CDCl_3$) δ: 9.05 (s, 1H), 7.77 (d, *J* 8.6, 2H), 7.35 (d, *J* 8.4, 2H), 7.29–7.15 (m, 3H), 6.92 (d, *J* 6.7, 2H), 6.56 (t, *J* 72.9, 1H), 4.29–3.93 (m, 4H), 2.35 (ddd, *J* 88.6, 13.7 & 7.5, 2H), 1.42 (s, 9H) (amine NH signal not seen); **^{13}C NMR** (126 MHz, $CDCl_3$) δ: 154.9, 152.7, 147.8, 145.8, 143.9, 136.9, 136.4, 132.5, 128.99, 128.95, 127.2, 125.6, 119.2, 115.6 (t, *J* 262.0), 108.6, 80.4, 71.0, 50.3, 37.2, 28.4; **^{19}F NMR** (471 MHz, $CDCl_3$) δ: -81.34; ***m/z*** (ESI+) 534 ($[M+Na]^+$, 100%); **HRMS** (ESI+) found 534.19172 $[M+Na]^+$, $C_{26}H_{27}F_2N_5O_4Na^+$ requires 534.19233.

(*R*)-1-((3-(4-(Difluoromethoxy)phenyl)-[1,2,4]triazolo[4,3-*a*]pyrazin-5-yl)oxy)-3-phenylpropan-2-amine 119

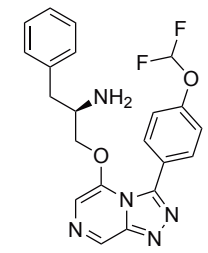

Compound **117** (85.0 mg, 0.17 mmol, 1.00 equiv.) was dissolved in CH_2Cl_2 (0.48 mL). TFA (0.14 mL, 1.86 mmol, 11.2 equiv.) was added and the reaction stirred at rt overnight. The solvent was removed and the residue directly purified by automated flash chromatography on silica twice (Biotage Isolera, 25–100% EtOAc in hexanes, then 0–10% MeOH in CH_2Cl_2) to give a brown semi-solid (53.1 mg, 78%); repurified by automated reversed-phase flash chromatography on silica (Biotage Isolera, 5–100% MeOH in H_2O) to give *the title compound* as a light yellow powder (20.1 mg, 29%); **m.p.** 142–148 °C; **^{1}H NMR** (500 MHz, CD_3OD) δ: 8.98 (s, 1H), 7.83 (d, *J* 8.7, 2H), 7.46 (s, 1H), 7.36 (d, *J* 8.6, 2H), 7.27 (t, *J* 7.4, 2H), 7.20 (t, *J* 7.4, 1H), 7.07 (d, *J* 7.1, 2H), 6.94 (t, *J* 73.5, 1H), 4.14 (ddd, *J* 40.9, 9.2 & 5.0, 2H), 3.16 (br s, 1H), 2.60–2.31 (m, 2H) (amine NH_2 signal not seen); **^{13}C NMR** (126 MHz, CD_3OD) δ: 154.5, 148.9, 147.5, 146.1, 138.8, 136.4, 133.8, 130.2, 129.7, 127.7, 126.1, 119.4, 117.4 (t, *J* 259.1), 110.0, 75.6, 52.4, 40.3; **^{19}F NMR** (471 MHz, CD_3OD) δ: -84.15; ***m/z*** (ESI+) 412 ($[M+H]^+$, 16%), 434 ($[M+Na]^+$, 100%), 845 ($[2M+Na]^+$, 9%); **HRMS** (ESI+) found 412.15765 $[M+H]^+$, $C_{21}H_{19}F_2N_5O_2H^+$ requires 412.15796.

(*S*)-1-((3-(4-(Difluoromethoxy)phenyl)-[1,2,4]triazolo[4,3-*a*]pyrazin-5-yl)oxy)-3-phenylpropan-2-amine 120

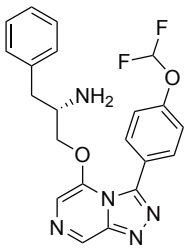

Compound **118** (85.0 mg, 0.17 mmol, 1.00 equiv.) was dissolved in CH_2Cl_2 (0.48 mL). TFA (0.14 mL, 1.86 mmol, 11.2 equiv.) was added and the reaction stirred at rt overnight. The solvent was removed and the residue directly purified by automated flash chromatography on silica (Biotage Isolera, 0–10% MeOH in CH_2Cl_2) to give a pale yellow powder (131 mg, >100%); repurified by automated reversed-phase flash chromatography on silica (Biotage Isolera, 5–100% MeOH in H_2O) to give *the title compound* as an off-white powder (18.2 mg, 27%); **m.p.** 142–148 °C; **^{1}H NMR** (500 MHz, CD_3OD) δ: 8.98 (s, 1H), 7.83 (d, *J* 8.7, 2H), 7.46 (s, 1H), 7.36 (d, *J* 8.6, 2H), 7.27 (t, *J* 7.4, 2H), 7.20 (t, *J* 7.4, 1H), 7.07 (d, *J* 7.1, 2H), 6.94 (t, *J* 73.5, 1H), 4.14 (ddd, *J* 41.1, 9.2 & 5.1, 2H), 3.16 (p, *J* 6.1, 1H), 2.64–2.34 (m, 2H) (amine NH_2 signal not seen); **^{13}C NMR** (126 MHz, CD_3OD) δ: 154.5, 148.9, 147.5, 146.1, 138.9, 136.4, 133.8, 130.2, 129.7, 127.7, 126.1, 119.4, 117.4 (t, *J* 259.0), 110.0, 75.6, 52.4, 40.3; **^{19}F NMR** (471 MHz, CD_3OD) δ: -84.15; ***m/z*** (ESI+) 412 ($[M+H]^+$, 34%), 434 ($[M+Na]^+$, 100%), 845 ($[2M+Na]^+$, 12%); **HRMS** (ESI+) found 412.15730 $[M+H]^+$, $C_{21}H_{19}F_2N_5O_2H^+$ requires 412.15796.

5-Chloro-[1,2,4]triazolo[4,3-*a*]pyrazine 121

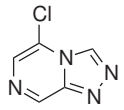

Compound **2** (7.00 g, 48.4 mmol, 1.0 equiv.) was suspended in PhMe (140 mL). Triethyl orthoformate (16.1 mL, 96.8 mmol, 2.0 equiv.) and *p*-TsOH (1.67 g, 9.68 mmol, 0.2 equiv.) were added and the reaction heated at reflux for 3 h. The solvent was removed under reduced pressure and the residue directly purified by automated flash chromatography on silica (Biotage Isolera, 25–100% EtOAc in hexanes) to give *the title compound* as a light brown powder (3.30 g, 44%); $\mathbf{R_f}$ 0.12 (50% EtOAc in hexanes); **m.p.** 168–172 °C; **^{1}H NMR** (400 MHz, DMSO-d$_6$) δ: 9.69 (s, 1H), 9.44 (s, 1H), 8.16 (s, 1H); **^{13}C NMR** (101 MHz, DMSO-d$_6$) δ: 145.6, 141.7, 136.0, 127.7, 121.2. Spectroscopic data matched those in the literature.[183]

5-(3,4-Difluorophenethoxy)-[1,2,4]triazolo[4,3-*a*]pyrazine 122

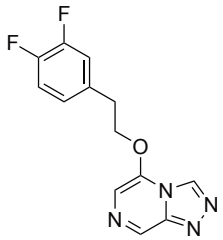

Prepared according to General Procedure 4 from: 2-(3,4-difluorophenyl)ethan-1-ol (174 mg, 1.10 mmol) and **121** (170 mg, 1.10 mmol) to give the crude title compound as a yellow solid (174 mg); purified by automated flash chromatography on silica (Biotage Isolera, 25–100% EtOAc in hexanes) to give *the title compound* as a greenish-yellow powder (118 mg, 39%); $\mathbf{R_f}$ 0.18 (100% EtOAc); **m.p.** 206–211 °C; **^{1}H NMR** (500 MHz, DMSO-d$_6$) δ: 9.43 (s, 1H), 9.04 (s, 1H), 7.64 (s, 1H), 7.54 (ddd, *J* 11.9, 7.9 & 2.1, 1H), 7.37 (dt, *J* 10.9 & 8.5, 1H), 7.31–7.22 (m, 1H), 4.64 (t, *J* 6.5, 2H), 3.19 (t, *J* 6.5, 2H); **^{13}C NMR** (126 MHz, DMSO-d$_6$) δ: 149.2 (dd, *J* 244.9 & 12.6), 148.3 (dd, *J* 244.0 & 12.5), 145.8, 142.3, 135.3 (dd, *J* 6.1 & 3.8), 134.5, 133.1, 126.1, 118.2 (d, *J* 16.9), 117.2 (d, *J* 16.8), 108.3, 70.8, 33.4; ***m/z*** (ESI+) 299 ([M+Na]$^+$, 100%); **HRMS** (ESI+) found 299.07126 [M+Na]$^+$, $C_{13}H_{10}F_2N_4ONa^+$ requires 299.07152.

(*E*)-2-(2-Benzylidenehydrazinyl)-6-chloropyrazine 123

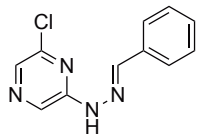

Prepared according to General Procedure 2 from: benzaldehyde (0.18 mL, 1.73 mmol) and **2** (250 mg, 1.73 mmol); filtered and triturated with Et_2O to give *the title compound* as a yellow powder (253 mg, 63%); carried forward without purification or complete characterisation; $\mathbf{R_f}$ 0.77 (25% EtOAc in hexanes); **m.p.** 210–217 °C; **^{1}H NMR** (400 MHz, DMSO-d$_6$) δ: 11.58 (s, 1H), 8.57 (s, 1H), 8.08 (s, 1H), 8.05 (s, 1H), 7.73 (d, *J* 6.9, 2H), 7.49–7.33 (m, 3H); **^{13}C NMR** (101 MHz, DMSO-d$_6$) δ: 152.3, 145.5, 142.7, 134.4, 132.3, 129.4, 128.8, 126.6 (1 obscured signal). Compound reported in the literature but no NMR characterisation data were provided.[183]

5-Chloro-3-phenyl-[1,2,4]triazolo[4,3-*a*]pyrazine 124

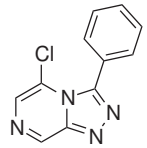

Prepared according to General Procedure 3 from: **123** (220 mg, 0.95 mmol) to give the crude title compound as an orange powder; trituration with Et_2O gave *the title compound* as an orange powder (189 mg, 87%); carried forward without purification or characterisation; $\mathbf{R_f}$ 0.16 (50% EtOAc in hexanes).

5-(3,4-Difluorophenethoxy)-3-phenyl-[1,2,4]triazolo[4,3-*a*]pyrazine 125

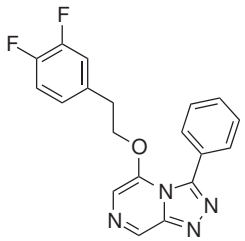

Prepared according to General Procedure 4 from: 2-(3,4-difluorophenyl)ethan-1-ol (103 mg, 0.65 mmol) and **124** (150 mg, 0.65 mmol) to give the crude title compound as an orange solid (90.0 mg); purified by automated flash chromatography on silica (Biotage Isolera, 25–100% EtOAc in hexanes) to give *the title compound* as a yellow powder (16.4 mg, 7%); $\mathbf{R_f}$ 0.20 (100% EtOAc); **m.p.** 100–110 °C; **^{1}H NMR** (500 MHz, $CDCl_3$) δ: 9.03 (s, 1H), 7.70 (ddd, *J* 7.5, 4.2 & 1.6, 2H), 7.66–7.38 (m, 3H), 7.27 (s, 1H), 7.06–6.82 (m, 1H), 6.41 (ddd, *J* 13.3, 6.8 & 4.6, 2H), 4.37 (t, *J* 6.0, 2H), 2.86 (t, *J* 6.0, 2H); **^{13}C NMR** (126 MHz, $CDCl_3$) δ: 150.2 (dd, *J* 248.7 & 12.7), 149.5 (dd, *J* 247.9 & 12.5), 147.8, 147.2, 144.0, 136.8, 133.6 (dd, *J* 5.4 & 4.1), 131.0, 130.9, 130.3, 128.0, 124.6 (dd, *J* 5.9 & 3.6), 117.8 (d, *J* 17.2), 117.4 (d, *J* 17.1), 108.2, 71.1, 34.0; ***m/z*** (ESI+) 375 ($[M+Na]^+$, 100%); **HRMS** (ESI+) found 375.10307 $[M+Na]^+$, $C_{19}H_{14}F_2N_4ONa^+$ requires 375.10279.

(*E*)-2-Chloro-6-(2-(4-(pentafluoro-λ^6-sulfanyl)benzylidene)hydrazinyl)pyrazine 126

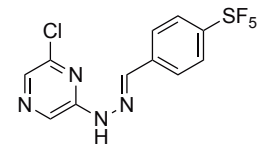

Prepared according to General Procedure 2 from: 4-(pentafluorosulfanyl) benzaldehyde (1.50 g, 6.46 mmol) and **2** (934 mg, 6.46 mmol) to give the crude title compound as a yellow powder (2.59 g); purified by recrystallisation from EtOH to give *the title compound* as light brown crystals (1.76 g, 76%); this intermediate, though novel, was carried forward without complete characterisation; $\mathbf{R_f}$ 0.68 (25% EtOAc in hexanes); **m.p.** 237–243 °C; **^{1}H NMR** (400 MHz, $CDCl_3$) δ: 8.67 (s, 1H), 8.41 (br s, 1H), 8.11 (s, 1H), 7.94–7.67 (m, 5H).

5-Chloro-3-(4-(pentafluoro-λ^6-sulfanyl)phenyl)-[1,2,4]triazolo[4,3-*a*]pyrazine 127

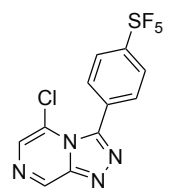

Prepared according to General Procedure 3 from: **126** (1.50 g, 4.18 mmol) to give the crude title compound as a light orange solid (2.17 g); purified by recrystallisation from EtOH to give *the title compound* as orange plates (881 mg, 59%); this intermediate, though novel, was carried forward without complete characterisation; **m.p.** 178–182 °C; **^{1}H NMR** (400 MHz, $CDCl_3$) δ: 9.38 (s, 1H), 7.94 (s, 1H), 7.94 (d, *J*

8.8, 2H), 7.78 (d, *J* 8.6, 2H); **^{13}C NMR** (101 MHz, $CDCl_3$) δ: 155.5, 147.4, 146.4, 143.1, 131.9, 130.3, 130.2, 125.8, 121.8.

3-(4-(Pentafluoro-λ^6-sulfanyl)phenyl)-5-phenethoxy-[1,2,4]triazolo[4,3-*a*]pyrazine 128

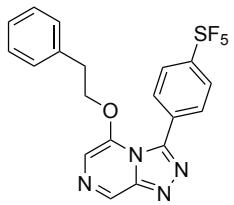

Prepared according to General Procedure 4 from: 2-phenylethanol (33.6 μL, 0.28 mmol) and **127** (100 mg, 0.28 mmol) to give the crude title compound as a dark brown solid (129 mg); purified by automated flash chromatography on silica (Biotage Isolera, 25–100% EtOAc in hexanes) to give *the title compound* as a brown powder (103 mg, 83%); $\mathbf{R_f}$ 0.37 (100% EtOAc); **m.p.** 136–141 °C; **^{1}H NMR** (400 MHz, $CDCl_3$) δ: 9.03 (s, 1H), 7.79 (d, *J* 8.9, 2H), 7.72 (d, *J* 8.7, 2H), 7.38 (s, 1H), 7.23–7.16 (m, 3H), 6.95–6.82 (m, 2H), 4.51 (t, *J* 6.3, 2H), 2.97 (t, *J* 6.3, 2H). **^{13}C NMR** (101 MHz, $CDCl_3$) δ: 154.8, 154.6, 148.0, 145.4, 143.8, 136.5, 136.1, 131.1, 128.9, 128.4, 127.2, 125.5 (p, *J* 4.5), 108.8, 71.4, 34.4; ***m/z*** (ESI+) 465 ($[M+Na]^+$, 100%); **HRMS** (ESI+) found 465.07835 $[M+Na]^+$, $C_{19}H_{15}F_5N_4OSNa^+$ requires 465.07789.

3-(4-(Difluoromethoxy)phenyl)-5-(3-methoxyphenethoxy)-[1,2,4]triazolo[4,3-*a*] pyrazine 129

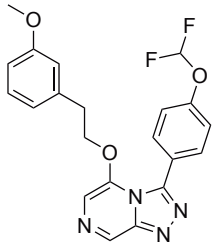

Prepared according to General Procedure 4 from: 3-methoxyphenethyl alcohol (0.12 mL, 0.84 mmol) and **44** (250 mg, 0.84 mmol); the solvent was removed and the residue directly purified by automated flash chromatography on silica (Biotage Isolera, 25–100% EtOAc in hexanes) to give *the title compound* as an orange powder (130 mg, 37%); $\mathbf{R_f}$ 0.31 (100% EtOAc); **m.p.** 107–112 °C; **^{1}H NMR** (300 MHz, $CDCl_3$) δ: 9.00 (s, 1H), 7.63 (d, *J* 8.8, 2H), 7.31 (s, 1H), 7.15 (d_{app}, *J* 8.5, 3H), 6.79–6.70 (m, 1H), 6.58 (t, *J* 73.4, 1H), 6.51–6.45 (m, 2H), 4.44 (t, *J* 6.5, 2H), 3.75 (s, 3H), 2.92 (t, *J* 6.5, 2H); **^{13}C NMR** (75 MHz, $CDCl_3$) δ: 160.0, 152.6, 147.9, 146.4, 144.0, 137.8, 136.5, 132.5, 129.8, 124.9, 120.8, 118.6, 115.8 (t, *J* 260.8 Hz), 114.9, 111.9, 108.5, 71.1, 55.3, 34.5; ***m/z*** (ESI+) 435 ($[M+Na]^+$, 100%); **HRMS** (ESI+) found 435.12413 $[M+Na]^+$, $C_{21}H_{18}F_2N_4O_3Na^+$ requires 435.12392.

3-(4-(Difluoromethoxy)phenyl)-5-(4-methoxyphenethoxy)-[1,2,4]triazolo[4,3-*a*] pyrazine 130

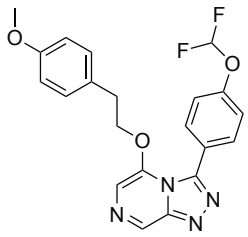

Prepared according to General Procedure 4 from: 4-methoxyphenethyl alcohol (128 mg, 0.84 mmol) and **44** (250 mg, 0.84 mmol); the solvent was removed and the residue directly purified by automated flash chromatography on silica (Biotage Isolera, 25–100% EtOAc in hexanes) to give *the title compound* as an orange powder (138 mg, 40%); $\mathbf{R_f}$ 0.32 (100% EtOAc); **m.p.** 134–138 °C; **^{1}H NMR** (300 MHz, $CDCl_3$) δ: 9.00 (s, 1H), 7.66 (d, *J* 8.7, 2H), 7.30 (s, 1H), 7.20 (d, *J* 8.6, 2H), 6.81–6.69 (m, 4H), 6.58 (t, *J* 73.3, 1H), 4.39 (t, *J* 6.5, 2H), 3.76 (s, 3H), 2.88 (t, *J* 6.5, 2H); **^{13}C NMR** (75 MHz, $CDCl_3$) δ: 158.8, 152.5, 147.9, 146.4, 144.0, 136.5, 132.6, 129.6, 128.2, 125.0, 118.7, 115.7 (t, *J* 261.1), 114.2, 108.4, 71.6, 55.4, 33.8; ***m/z*** (ESI+) 435 ($[M+Na]^+$, 100%); **HRMS** (ESI+) found 435.12414 $[M+Na]^+$, $C_{21}H_{18}F_2N_4O_3Na^+$ requires 435.12392.

1,4-Phenylenedimethanol 131

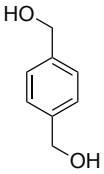

Terephthalaldehyde (1.00 g, 7.46 mmol, 1.0 equiv.) was dissolved in EtOH (20 mL) and $NaBH_4$ (423 mg, 11.2 mmol, 1.5 equiv.) was added portionwise. The reaction was stirred at rt for 1 h. The solvent was removed and the residue taken up in H_2O, extracted with Et_2O, dried (Na_2SO_4), filtered and concentrated under reduced pressure to give the crude title compound as a white solid (456 mg); purified by recrystallisation from Et_2O to give *the title compound* as white needles (340 mg, 33%); $\mathbf{R_f}$ 0.24 (50% EtOAc in hexanes); **m.p.** 122–126 °C (lit.[204] 117–118 °C); **^{1}H NMR** (400 MHz, DMSO-d_6) δ: 7.25 (s, 4H), 5.12 (t, *J* 5.7, 2H), 4.47 (d, *J* 5.6, 4H); **^{13}C NMR** (101 MHz, DMSO-d_6) δ: 140.9, 126.2, 62.8. Spectroscopic data matched those in the literature.[204]

(4-(((3-(4-(Difluoromethoxy)phenyl)-[1,2,4]triazolo[4,3-*a*]pyrazin-5-yl)oxy)methyl) phenyl)methanol 132

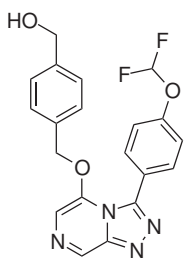

t-BuOK (22.7 mg, 0.20 mmol, 1.2 equiv.) was added portionwise to a stirred solution of **131** (46.6 mg, 0.34 mmol, 1.0 equiv.) in 1,4-dioxane (3 mL) at 0 °C. **44** (50.0 mg, 0.17 mmol, 0.5 equiv.) was added and the reaction allowed to warm to rt and stirred for 4 h. CH_2Cl_2 and K_2CO_3 were added and the mixture was filtered and concentrated under reduced pressure to give the crude title compound as a yellow solid (71.1 mg); purified by automated flash chromatography on silica (Biotage Isolera, 25–100% EtOAc in hexanes) to give a white powder (15.2 mg, 23%); repurified by preparative TLC (5% MeOH in CH_2Cl_2) to give *the title compound* as a white powder (10.0

mg, 15%); $\mathbf{R_f}$ 0.13 (100% EtOAc); **m.p.** 167–169 °C; **^{1}H NMR** (400 MHz, $CDCl_3$) δ: 9.03 (s, 1H), 7.58 (d, *J* 8.6, 2H), 7.42 (s, 1H), 7.32 (d, *J* 7.8, 2H), 7.07 (d, *J* 7.9, 2H), 6.95 (d, *J* 8.5, 2H), 6.50 (t, *J* 73.4, 1H), 5.18 (s, 2H), 4.73 (s, 2H), 2.00 (br s, 1H); **^{13}C NMR** (101 MHz, $CDCl_3$) δ: 152.4, 147.9, 146.5, 143.9, 142.5, 136.8, 132.5, 132.1, 128.6, 127.3, 124.6, 118.3, 115.8 (t, *J* 260.5), 108.9, 72.8, 64.8; ***m/z*** (ESI+) 421 ($[M+Na]^+$, 100%); **HRMS** (ESI+) found 421.10875 $[M+Na]^+$, $C_{20}H_{16}F_2N_4O_3Na^+$ requires 421.10827.

9.6 Synthesis and Characterisation of Compounds from Chapter 4

5-(2-cyclopropylethoxy)-3-(4-(difluoromethoxy)phenyl)-[1,2,4]triazolo[4,3-*a*] pyrazine 133

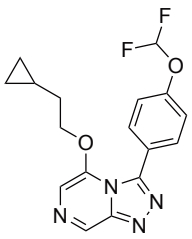

Prepared according to General Procedure 4 from: 2-cyclopropylethanol (50.0 mg, 0.58 mmol) and **44** (172 mg, 0.58 mmol) to give the crude title compound as a black solid (230 mg); purified by automated flash chromatography on silica (Biotage Isolera, 25–100% EtOAc in hexanes) to give an orange solid; repurifed by preparative TLC (75% EtOAc in hexanes) to give *the title compound* as a yellow powder (42.3 mg, 21%); $\mathbf{R_f}$ 0.58 (100% EtOAc); **m.p.** 120–124 °C; **^{1}H NMR** (400 MHz, $CDCl_3$) δ: 9.03 (s, 1H), 7.71 (d, *J* 8.8, 2H), 7.32 (s, 1H), 7.23 (d, *J* 8.7, 2H), 6.60 (t, *J* 73.2, 1H), 4.25 (t, *J* 6.3, 2H), 1.51 (q, *J* 6.4, 2H), 0.54–0.19 (m, 3H), -0.01–-0.10 (m, 2H); **^{13}C NMR** (101 MHz, $CDCl_3$) δ: 152.5, 148.0, 146.4, 144.4, 136.2, 132.6, 125.1, 118.8, 115.7 (t, *J* 261.4), 108.3, 71.3, 33.5, 7.4, 4.3; **^{19}F NMR** (376 MHz, $CDCl_3$) δ: -81.43; ***m/z*** (ESI+) 369 ($[M+Na]^+$, 100%), 715 ($[2M+Na]^+$, 35%); **HRMS** (ESI+) found 347.13130 $[M+H]^+$, $C_{17}H_{16}F_2N_4O_2H^+$ requires 347.13141.

2-(Oxetan-3-yl)ethan-1-ol 272

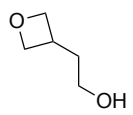

Lithium 2-(oxetan-3-yl)acetate (150 mg) was converted to the free acid by addition of conc. HCl and extraction with EtOAc to give a colourless oil (125 mg). Prepared according to General Procedure 6 from: free acid (100 mg, 0.86 mmol) to give the crude title compound as a yellow oil (41.4 mg); carried forward without purification or characterisation.

3-(4-(Difluoromethoxy)phenyl)-5-(2-(oxetan-3-yl)ethoxy)-[1,2,4]triazolo[4,3-*a*] pyrazine 134

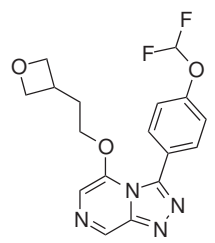

Prepared according to General Procedure 4 from: **272** (35.0 mg, 0.34 mmol) and **44** (102 mg, 0.34 mmol) to give the crude title compound as a brown solid (108 mg); purified by automated flash chromatography on silica (Biotage Isolera, 1–10% MeOH in CH_2Cl_2) to give *the title compound* as an orange powder (21.6 mg, 17%); $\mathbf{R_f}$ 0.06 (100% EtOAc); **m.p.** 110–114 °C; **^{1}H NMR** (400 MHz, $CDCl_3$) δ: 9.04 (s, 1H), 7.68 (d, *J* 8.7, 2H), 7.30 (s, 1H), 7.25 (d, *J* 7.5, 2H), 6.62 (t, *J* 73.1, 1H), 4.21–3.96 (m, 2H), 3.91–3.71 (m, 1H), 3.65 (q_{app}, *J* 7.7, 1H), 3.48 (dd_{app}, *J* 9.0 & 7.0, 1H), 3.34 (dd, *J* 9.1 & 4.7, 1H), 2.47 (hept, *J* 7.1, 1H), 1.86 (dtd, *J* 12.9, 8.1 & 5.2, 1H), 1.42 (td, *J* 13.0 & 7.6, 1H); **^{13}C NMR** (101 MHz, $CDCl_3$) δ: 152.4, 147.8, 146.2, 144.0, 136.8, 132.4, 125.2, 119.0, 115.6 (t, *J* 262.0), 108.4, 72.3, 69.8, 67.5, 38.3, 28.4; ***m/z*** (ESI+) 385 ($[M+Na]^+$, 100%), 747 ($[2M+Na]^+$, 47%); **HRMS** (ESI+) found 385.10867 $[M+Na]^+$, $C_{17}H_{16}F_2N_4O_3Na^+$ requires 385.10827.

6-(2-((3-(4-(Difluoromethoxy)phenyl)-[1,2,4]triazolo[4,3-*a*]pyrazin-5-yl)oxy)ethyl)-2 -oxa-6-azaspiro[3.3]heptane 135

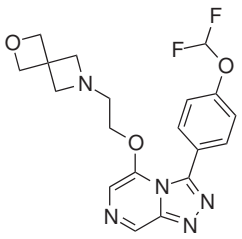

Prepared according to General Procedure 4 from: 2-[2-oxa-6-azaspiro[3.3]heptan-6-yl]ethan-1-ol (100 mg, 0.70 mmol) and **44** (207 mg, 0.70 mmol) to give the crude title compound as a brown solid (234 mg); purified by automated flash chromatography on silica (Biotage Isolera, 1–10% MeOH in CH_2Cl_2) to give *the title compound* as a light brown powder (145 mg, 52%); $\mathbf{R_f}$ 0.07 (5% MeOH in CH_2Cl_2); **m.p.** 136–141 °C; **^{1}H NMR** (400 MHz, $CDCl_3$) δ: 9.03 (s, 1H), 7.75 (d, *J* 8.8, 2H), 7.28 (s, 1H), 7.26 (d, *J* 8.8, 2H), 6.64 (t, *J* 73.0, 1H), 4.62 (s, 4H), 4.16 (t, *J* 5.2, 2H), 3.09 (s, 4H), 2.58 (t, *J* 5.2, 2H); **^{13}C NMR** (101 MHz, $CDCl_3$) δ: 152.2, 147.9, 146.3, 144.0, 136.7, 132.7, 125.1, 119.0, 115.5 (t, *J* 262.4), 108.6, 81.0, 70.0, 64.2, 56.4, 39.5; ***m/z*** (ESI+) 426 ($[M+Na]^+$, 100%); **HRMS** (ESI+) found 426.13533 $[M+Na]^+$, $C_{19}H_{19}F_2N_5O_3Na^+$ requires 426.13482.

3-(4-(Difluoromethoxy)phenyl)-5-(2-(pyrrolidin-1-yl)ethoxy)-[1,2,4]triazolo[4,3-*a*] pyrazine 136

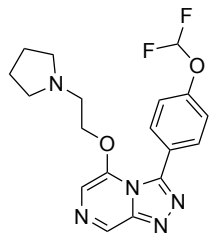

Prepared according to General Procedure 4 from: 1-(2-hydroxyethyl) pyrrolidine (59.1 μL, 0.51 mmol) and **44** (150 mg, 0.51 mmol); the solvent was removed and the residue directly purified by automated flash chromatography on silica (Biotage Isolera, 1–10% MeOH in CH_2Cl_2) to give *the title compound* as a brown powder (70.2 mg, 37%); $\mathbf{R_f}$ 0.12 (5% MeOH in CH_2Cl_2); **m.p.** 96–102 °C; **^{1}H NMR** (400 MHz, CD_3OD) δ: 8.98 (s, 1H), 7.80 (d, *J* 8.8, 2H), 7.54 (s, 1H), 7.33 (d, *J* 8.8, 2H), 7.00 (t, *J* 73.5, 1H), 4.43 (t, *J* 5.2, 2H), 2.77 (t, *J* 5.2, 2H), 2.32 (t, *J* 6.5, 4H), 1.87–1.59 (m, 4H); **^{13}C NMR** (101 MHz, CD_3OD) δ: 151.9, 149.5, 149.1, 146.0, 136.3, 134.0, 125.9, 119.5, 117.4 (t, *J* 259.5), 110.1, 71.3, 55.1, 54.6, 24.2; ***m/z*** (ESI+) 398 ($[M+Na]^+$, 100%); **HRMS** (ESI+) found 376.15819 $[M+H]^+$, $C_{18}H_{19}F_2N_5O_2H^+$ requires 376.15796.

3-(4-(Difluoromethoxy)phenyl)-5-(2-(piperidin-1-yl)ethoxy)-[1,2,4]triazolo[4,3-*a*] pyrazine 137

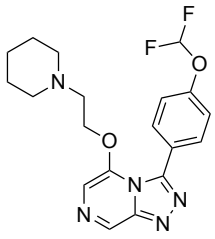

Prepared according to General Procedure 4 from: 1-(2-hydroxyethyl) piperidine (67.1 μL, 0.51 mmol) and **44** (150 mg, 0.51 mmol); the solvent was removed and the residue directly purified by automated flash chromatography on silica (Biotage Isolera, 1–10% MeOH in CH_2Cl_2) to give *the title compound* as a brown powder (70.2 mg, 36%); $\mathbf{R_f}$ 0.21 (5% MeOH in CH_2Cl_2); **m.p.** 123–129 °C; **^{1}H NMR** (400 MHz, CD_3OD) δ: 8.97 (s, 1H), 7.79 (d, *J* 8.7, 2H), 7.53 (s, 1H), 7.33 (d, *J* 8.7, 2H), 7.01 (t, *J* 73.5, 1H), 4.43 (t, *J* 5.1, 2H), 2.63 (t, *J* 5.1, 2H), 2.21 (br s_{app}, 4H), 1.73–1.35 (m, 4H), 1.41–1.33 (m, 2H); **^{13}C NMR** (101 MHz, CD_3OD) δ: 154.3, 149.0, 147.8, 146.0, 136.2, 133.9, 125.9, 119.4, 117.4 (t, *J* 259.4), 110.1, 70.3, 57.7, 55.4, 26.5, 24.7; ***m/z*** (ESI+) 412 ($[M+Na]^+$, 100%); **HRMS** (ESI+) found 390.17370 $[M+H]^+$, $C_{19}H_{21}F_2N_5O_2H^+$ requires 390.17361.

4-(2-((3-(4-(Difluoromethoxy)phenyl)-[1,2,4]triazolo[4,3-*a*]pyrazin-5-yl)oxy)ethyl) morpholine 138

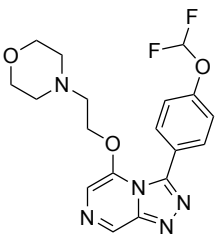

Prepared according to General Procedure 4 from: 4-(2-hydroxyethyl) morpholine (61.2 μL, 0.51 mmol) and **44** (150 mg, 0.51 mmol); the solvent was removed and the residue directly purified by automated flash chromatography on silica (Biotage Isolera, 1–10% MeOH in CH_2Cl_2) to give *the title compound* as a light brown powder (141 mg, 71%); $\mathbf{R_f}$ 0.26 (5% MeOH in CH_2Cl_2); **m.p.** 160–164 °C; **^{1}H NMR** (400 MHz, CD_3OD) δ: 8.97 (s, 1H), 7.80 (d, *J* 8.8, 2H),

7.53 (s, 1H), 7.33 (d, *J* 8.7, 2H), 7.00 (t, *J* 73.5, 1H), 4.42 (t, *J* 5.1, 2H), 3.62–3.42 (m, 4H), 2.61 (t, *J* 5.0, 2H), 2.37–2.04 (m, 4H); **^{13}C NMR** (101 MHz, CD_3OD) δ: 154.3, 150.1, 149.0, 146.1, 136.2, 134.0, 125.9, 119.4, 117.5 (t, *J* 259.3), 110.1, 70.2, 67.7, 57.5, 54.5; ***m/z*** (ESI+) 414 ($[M+Na]^+$, 100%); **HRMS** (ESI+) found 392.15301 $[M+H]^+$, $C_{18}H_{19}F_2N_5O_3H^+$ requires 392.15287.

tert-Butyl 4-(2-hydroxyethyl)piperazine-1-carboxylate 139

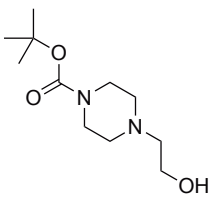

A solution of Boc_2O (2.18 mL, 9.45 mmol, 1.23 equiv.) in CH_2Cl_2 (7 mL) was added dropwise to a solution of 1-(2-hydroxyethyl)piperazine (1.00 g, 7.68 mmol, 1.00 equiv.) in CH_2Cl_2 (10 mL) at 0 °C. The reaction was warmed to rt and stirred for 2 h. Sat. aq. NH_4Cl (6 mL) was added and the organic layer separated. The aqueous layer was extracted with CH_2Cl_2 (2 × 8 mL) and the combined ojrganic layers were dried (Na_2SO_4), filtered and concentrated under reduced pressure to give the crude title compound as a cloudy yellow residue; purified by DCVC (25–100% EtOAc in hexanes) to give *the title compound* as a clear oil that crystallised on standing (674 mg, 38%); $\mathbf{R_f}$ 0.05 (100% EtOAc, $KMnO_4$ stain); **m.p.** 45–52 °C; **IR** ν_{max} (film) /cm^{-1} 3426, 2974, 2933, 2868, 2812, 1695; **^{1}H NMR** (300 MHz, $CDCl_3$) δ: 3.61 (t, *J* 5.4, 2H), 3.42 (t, *J* 5.1, 4H), 2.54 (t, *J* 5.4, 2H), 2.44 (t, *J* 5.1, 4H), 1.45 (s, 9H) (alcohol OH signal not seen); **^{13}C NMR** (75 MHz, $CDCl_3$) δ: 154.8, 79.8, 59.5, 57.9, 52.9, 28.6 (1 obscured signal). Spectroscopic data matched those in the literature.[396]

tert-Butyl 4-(2-((3-(4-(difluoromethoxy)phenyl)-[1,2,4]triazolo[4,3-*a*]pyrazin-5-yl) oxy)ethyl)piperazine-1-carboxylate 140

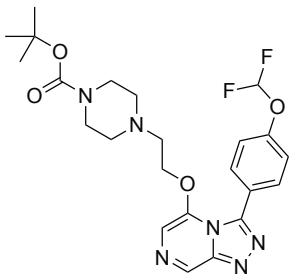

Prepared according to General Procedure 4 from: **139** (200 mg, 0.87 mmol) and **44** (258 mg, 0.87 mmol) to give the crude title compound as a brown semi-solid (422 mg); purified by automated flash chromatography on silica (Biotage Isolera, 2–20% MeOH in CH_2Cl_2) to give *the title compound* as a yellow powder with trace amounts of inseparable **139** (205 mg, 48%); $\mathbf{R_f}$ 0.01 (100% EtOAc); **m.p.** 134–139 °C; **^{1}H NMR** (400 MHz, $CDCl_3$) δ: 9.04 (s, 1H), 7.74 (d, *J* 8.8, 2H), 7.32 (s, 1H), 7.24 (d, *J* 8.8, 2H), 6.62 (t, *J* 73.1, 1H), 4.30 (t, *J* 5.2, 2H), 3.33–3.18 (m, 4H), 2.59 (t, *J* 5.2, 2H), 2.25–2.05 (m, 4H), 1.45 (s, 9H); **^{13}C NMR** (101 MHz, $CDCl_3$) δ: 154.7, 152.4, 147.9, 146.4, 144.0, 136.7, 132.6, 125.1, 118.9, 115.6 (t, *J* 262.0), 108.6, 80.0, 69.0, 56.1, 53.1, 28.5 (1 obscured signal); **^{19}F NMR** (376 MHz, $CDCl_3$) δ: -81.50; ***m/z*** (ESI+) 513 ($[M+Na]^+$, 100%); **HRMS** (ESI+) found 491.22134 $[M+H]^+$, $C_{23}H_{28}F_2N_6O_4H^+$ requires 491.22129.

3-(4-(Difluoromethoxy)phenyl)-5-(2-(piperazin-1-yl)ethoxy)-[1,2,4]triazolo[4,3-*a*] pyrazine 141

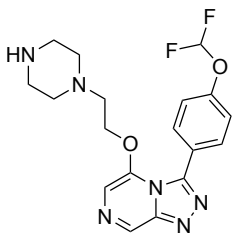

Compound **140** (150 mg, 0.31 mmol, 1.00 equiv.) was dissolved in CH_2Cl_2 (0.88 mL). TFA (0.26 mL, 3.42 mmol, 11.2 equiv.) was added and the reaction stirred at rt overnight. The solvent was removed and the residue directly purified by automated flash chromatography on silica (Biotage Isolera, 2–15% MeOH in CH_2Cl_2) to give *the title compound* as a light yellow powder (106 mg, 89%); **m.p.** 140–148 °C; **^{1}H NMR** (400 MHz, CD_3OD) δ: 8.99 (s, 1H), 7.81 (d, *J* 8.8, 2H), 7.53 (s, 1H), 7.35 (d, *J* 8.7, 2H), 7.03 (t, *J* 73.5, 1H), 4.42 (t, *J* 5.0, 2H), 3.16–2.94 (m, 4H), 2.70 (t, *J* 5.0, 2H), 2.58–2.35 (m, 4H) (amine NH signal not seen); **^{13}C NMR** (101 MHz, CD_3OD) δ: 154.2, 149.0, 147.8, 146.0, 136.3, 134.0, 126.0, 119.4, 117.4 (t, *J* 259.5), 110.1, 70.1, 56.6, 50.6, 44.8; ***m/z*** (ESI+) 413 ([M+Na]$^+$, 100%); **HRMS** (ESI+) found 319.16873 [M+H]$^+$, $C_{18}H_{20}F_2N_6O_2H^+$ requires 391.16886.

***tert*-Butyl (*E*)-3-((2-(6-chloropyrazin-2-yl)hydrazinylidene)methyl)piperidine-1 -carboxylate 142**

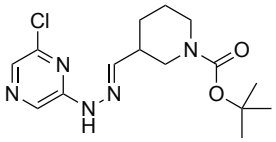

Prepared according to General Procedure 2 from: 1-boc-3-piperidinecarboxaldehyde (1.00 g, 4.69 mmol) and **2** (678 mg, 4.69 mmol); filtered and washed with EtOH to give *the title compound* as an off-white powder (900 mg, 57%); this intermediate, though novel, was carried forward without purification or complete characterisation; **R_f** 0.54 (25% EtOAc in hexanes); **m.p.** 182–184 °C; **^{1}H NMR** (400 MHz, $CDCl_3$) δ: 8.47 (s, 1H), 8.24 (s, 1H), 7.98 (s, 1H), 7.10 (d, *J* 4.2, 1H), 4.06 (br s, 1H), 3.87 (br s, 1H), 2.93 (q, *J* 12.6, 2H), 2.47 (dq, *J* 9.4 & 4.9, 1H), 1.98 (dd, *J* 9.6 & 4.2, 1H), 1.73 (dt, *J* 8.1 & 4.2, 1H), 1.60–1.45 (m, 2H), 1.45 (s, 9H); ***m/z*** (ESI+) 362 ([M+Na]$^+$, 100%); **HRMS** (ESI+) found 362.13483 [M+Na]$^+$, $C_{15}H_{22}ClN_5O_2Na^+$ requires 362.13542.

***tert*-Butyl 3-(5-chloro-[1,2,4]triazolo[4,3-*a*]pyrazin-3-yl)piperidine-1-carboxylate 143**

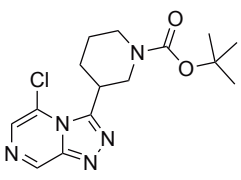

Prepared according to General Procedure 3 from: **142** (800 mg, 2.35 mmol) to give the crude title compound as a dark red oil (1.27 g); purified by automated flash chromatography on silica (Biotage Isolera, 12–100% EtOAc in hexanes) to give *the title compound* as an orange powder (513 mg, 65%); this intermediate, though novel, was carried forward without complete characterisation; **R_f** 0.18 (50% EtOAc in hexanes); **m.p.** 128–132 °C; **^{1}H NMR** (300 MHz, $CDCl_3$) δ: 9.22 (s, 1H), 7.83 (s, 1H), 4.51 (d, *J* 13.5, 1H), 4.16 (s, 1H), 3.82 (t, *J* 10.8, 1H), 3.42–3.21 (m, 1H), 2.89 (s, 1H), 2.32 (d, *J* 13.2, 1H), 2.27–2.02 (m, 1H), 1.93 (dq, *J* 13.4 & 3.2, 1H), 1.77–1.57 (m, 1H), 1.45 (s, 9H); ***m/z***

(ESI+) 360 ([M+Na]$^+$, 100%); **HRMS** (ESI+) found 360.11951 [M+Na]$^+$, $C_{15}H_{20}ClN_5O_2Na^+$ requires 360.11977.

tert-Butyl 3-(5-(2-phenyl-2-((tetrahydro-2*H*-pyran-2-yl)oxy)ethoxy)-[1,2,4]triazolo [4,3-*a*]pyrazin-3-yl)piperidine-1-carboxylate 144

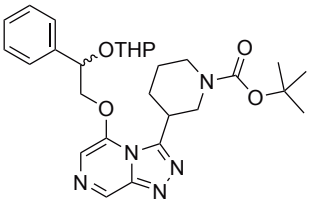

Prepared according to General Procedure 4 from: **103** (98.7 mg, 0.44 mmol) and **143** (150 mg, 0.44 mmol) to give the crude title compound as black liquid (240 mg); purified by automated flash chromatography on silica (Biotage Isolera, 25–100% EtOAc in hexanes) to give *the title compound* as a light brown powder (84.9 mg, 36%); this intermediate, though novel, was carried forward without complete characterisation; $\mathbf{R_f}$ 0.43 (100% EtOAc); **m.p.** 82–87 °C; ***m/z*** (ESI+) 546 ([M+Na]$^+$, 100%); **HRMS** (ESI+) found 524.28645 [M+H]$^+$, $C_{28}H_{37}N_5O_5H^+$ requires 524.28675.

1-Phenyl-2-((3-(piperidin-3-yl)-[1,2,4]triazolo[4,3-*a*]pyrazin-5-yl)oxy)ethan-1-ol 145

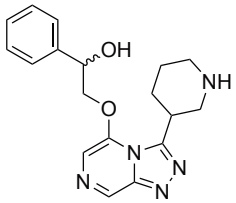

Compound **144** (55.0 mg, 105 μmol, 1.00 equiv.) was dissolved in CH_2Cl_2 (0.31 mL). TFA (90.6 μL, 1.18 mmol, 11.2 equiv.) was added and the reaction stirred at rt overnight. The reaction mixture was directly purified by automated flash chromatography on silica (Biotage Isolera, 0–10% MeOH in CH_2Cl_2) to give a sticky white solid (41.4 mg, >100%); repurified by automated reversed-phase flash chromatography on silica (Biotage Isolera, 5–100% MeOH in H_2O) to give *the title compound* as a hygroscopic yellow solid (23.4 mg, 66%); **^{1}H NMR** (500 MHz, CD_3OD) δ: 8.89 (s, 1H), 7.60–7.49 (m, 3H), 7.43 (t, *J* 7.6, 2H), 7.35 (t, *J* 7.4, 1H), 5.25 (dd, *J* 8.1 & 3.2, 1H), 4.68–4.44 (m, 2H), 4.19 (tt, *J* 8.2 & 4.1, 1H), 3.78–3.56 (m, 3H), 3.41–3.32 (m, 1H), 3.24 (ddt, *J* 17.5, 9.7 & 4.2, 1H), 2.29 (dq, *J* 9.3, 5.2 & 4.0, 1H), 2.05 (dtd, *J* 13.2, 8.8 & 3.9, 1H), 1.91 (dqt, *J* 23.6, 9.4 & 4.1, 3H); **^{13}C NMR** (126 MHz, CD_3OD, present as a mixture of diastereomers, ∼1:0.75 *maj*/*min*) δ: 149.1$^{(min)}$, 149.0$^{(maj)}$, 148.8$^{(maj)}$, 148.7$^{(min)}$, 146.03$^{(maj)}$, 146.00$^{(min)}$, 141.6$^{(min)}$, 141.4$^{(maj)}$, 136.28$^{(maj)}$, 136.26$^{(min)}$, 129.8, 129.40$^{(maj)}$, 129.36$^{(min)}$, 127.53$^{(maj)}$, 127.49$^{(min)}$, 110.1$^{(maj)}$, 110.0$^{(min)}$, 76.6$^{(maj)}$, 76.4$^{(min)}$, 72.7$^{(maj)}$, 72.4$^{(min)}$, 47.9$^{(maj)}$, 47.6$^{(min)}$, 45.35$^{(maj)}$, 45.31$^{(min)}$, 33.3$^{(min)}$, 33.2$^{(maj)}$, 29.3$^{(min)}$, 28.9$^{(maj)}$, 21.9$^{(min)}$, 21.7$^{(maj)}$; ***m/z*** (ESI+) 340 ([M+H]$^+$, 100%); **HRMS** (ESI+) found 340.17539 [M+H]$^+$, $C_{18}H_{21}N_5O_2H^+$ requires 340.17680.

tert-Butyl 3-(5-(3,4-difluorophenethoxy)-[1,2,4]triazolo[4,3-_a_]pyrazin-3-yl)piperidine-1-carboxylate 146

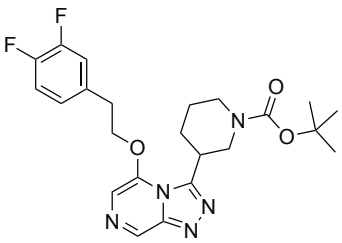

Prepared according to General Procedure 4 from: 2-(3,4-difluorophenyl)ethan-1-ol (46.8 mg, 0.30 mmol) and **143** (100 mg, 0.30 mmol) to give the crude title compound as a dark red oil (136 mg); purified by automated flash chromatography on silica (Biotage Isolera, 25–100% EtOAc in hexanes) to give *the title compound* as a yellow powder (77.8 mg, 57%); this intermediate, though novel, was carried forward without complete characterisation; $\mathbf{R_f}$ 0.24 (100% EtOAc); **m.p.** 149–153 °C; ***m/z*** (ESI+) 482 ($[M+Na]^+$, 100%); **HRMS** (ESI+) found 460.21549 $[M+H]^+$, $C_{23}H_{27}F_2N_5O_3H^+$ requires 460.21547.

5-(3,4-Difluorophenethoxy)-3-(piperidin-3-yl)-[1,2,4]triazolo[4,3-_a_]pyrazine 147

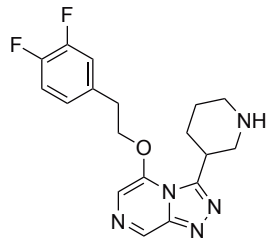

Compound **146** (42.0 mg, 91.4 μmol, 1.00 equiv.) was dissolved in CH_2Cl_2 (0.24 mL). TFA (78.9 μL, 1.02 mmol, 11.2 equiv.) was added and the reaction stirred at rt overnight. The solvent was removed and the residue directly purified by automated flash chromatography on silica (Biotage Isolera, 0–10% MeOH in CH_2Cl_2) to give a sticky yellow solid (43.1 mg, >100%); repurified by automated reversed-phase flash chromatography on silica (Biotage Isolera, 5–100% MeOH in H_2O) to give *the title compound* as a hygroscopic white powder (32.9 mg, 100%); **m.p.** 152–158 °C; **^{1}H NMR** (500 MHz, CD_3OD) δ: 8.88 (s, 1H), 7.54 (s, 1H), 7.34 (ddd, *J* 11.2, 7.7 & 1.8, 1H), 7.29–7.21 (m, 1H), 7.20–7.14 (m, 1H), 4.71 (ddt, *J* 34.7, 9.7 & 6.8, 2H), 4.08 (tt, *J* 7.9 & 4.1, 1H), 3.78–3.57 (m, 2H), 3.40–3.26 (m, 4H), 3.23 (ddd, *J* 12.4, 8.8 & 3.6, 1H), 2.12 (ddd, *J* 13.1, 7.0 & 3.6, 1H), 1.85 (dtd, *J* 20.1, 10.2, 9.7 & 3.5, 2H), 1.75 (ddq, *J* 14.5, 9.1, 5.0 & 4.5, 1H); **^{13}C NMR** (126 MHz, CD_3OD) δ: 151.6 (dd, *J* 246.8 & 12.7), 150.6 (dd, *J* 245.8 & 12.6), 149.0, 148.7, 145.8, 136.3, 135.8 (dd, *J* 5.8 & 4.0), 126.4 (dd, *J* 6.2 & 3.5), 118.7 (d, *J* 17.4), 118.5 (d, *J* 17.3), 110.0, 72.3, 47.5, 45.2, 34.7, 33.0, 29.3, 21.5; **^{19}F NMR** (471 MHz, CD_3OD) δ: -140.23, -143.27; ***m/z*** (ESI+) 360 ($[M+H]^+$, 100%); **HRMS** (ESI+) found 360.16159 $[M+H]^+$, $C_{18}H_{19}F_2N_5OH^+$ requires 360.16304.

(_E_)-2-Chloro-6-(2-((tetrahydrofuran-3-yl)methylene)hydrazinyl)pyrazine 273

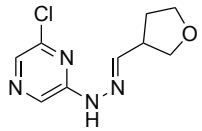

Prepared according to General Procedure 2 from: tetrahydrofuran-3-carbaldehyde (50% in H_2O, 800 mg, 1.88 mmol) and **2** (578 mg, 1.88 mmol); purified by automated flash chromatography on silica (Biotage Isolera, 6–50% EtOAc in hexanes) to give *the title compound* as an off-white powder (662 mg, 73%); $\mathbf{R_f}$ 0.28 (25% EtOAc in hexanes); **m.p.** 135–138 °C; **^{1}H NMR** (400 MHz, $CDCl_3$) δ: 8.46 (s, 1H), 8.40

(s, 1H), 7.98 (s, 1H), 7.14 (d, *J* 5.9, 1H), 3.95 (ddd, *J* 13.8, 8.4 & 6.6, 2H), 3.89–3.71 (m, 2H), 3.17 (dq, *J* 13.8 & 6.3, 1H), 2.20 (dtd, *J* 12.8, 7.8 & 5.4, 1H), 2.10–1.95 (m, 1H); **^{13}C NMR** (101 MHz, $CDCl_3$) δ: 152.0, 146.2, 146.0, 134.0, 129.1, 70.9, 68.2, 42.0, 30.6; ***m/z*** (ESI+) 249 ($[M+Na]^+$, 100%); **HRMS** (ESI+) found 227.06911 $[M+H]^+$, $C_9H_{11}ClN_4OH^+$ requires 227.06942.

(*E*)-2-Chloro-6-(2-((tetrahydro-2*H*-pyran-4-yl)methylene)hydrazinyl)pyrazine 274

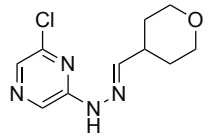

Prepared according to General Procedure 2 from: 4-formyltetrahydropyran (200 mg, 1.75 mmol) and **2** (253 mg, 1.75 mmol); filtered and washed with EtOH to give *the title compound* as a brown powder (284 mg, 67%); $\mathbf{R_f}$ 0.33 (25% EtOAc in hexanes); **m.p.** 160–168 °C; **^{1}H NMR** (400 MHz, $CDCl_3$) δ: 8.47 (s, 1H), 8.40 (s, 1H), 7.98 (s, 1H), 7.09 (d, *J* 4.7, 1H), 4.01 (dt, *J* 11.1 & 3.5, 2H), 3.47 (td, *J* 11.5 & 2.2, 2H), 2.72–2.40 (m, 1H), 1.85–1.73 (m, 2H), 1.73–1.57 (m, 2H); **^{13}C NMR** (101 MHz, $CDCl_3$) δ: 152.2, 148.3, 146.1, 133.8, 129.2, 67.3, 37.9, 30.1; ***m/z*** (ESI+) 263 ($[M+Na]^+$, 100%); **HRMS** (ESI+) found 241.08477 $[M+H]^+$, $C_{10}H_{13}ClN_4OH^+$ requires 241.08507.

tert-Butyl (*E*)-3-((2-(6-chloropyrazin-2-yl)hydrazinylidene)methyl)pyrrolidine-1-carboxylate 275

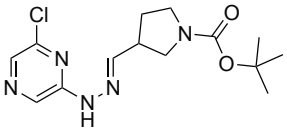

Prepared according to General Procedure 2 from: 1-boc-3-pyrrolidinecarbaldehyde (200 mg, 1.00 mmol) and **2** (145 mg, 1.00 mmol); purified by automated flash chromatography on silica (Biotage Isolera, 6–50% EtOAc in hexanes) to give *the title compound* as an off-white powder (215 mg, 66%); $\mathbf{R_f}$ 0.27 (25% EtOAc in hexanes); **m.p.** 124–128 °C; **^{1}H NMR** (400 MHz, $CDCl_3$) δ: 8.47 (s, 1H), 8.45 (s, 1H), 7.98 (s, 1H), 7.16 (d, *J* 4.3, 1H), 3.61 (dt, *J* 20.6 & 9.8, 1H), 3.54–3.44 (m, 1H), 3.44–3.32 (m, 2H), 3.09 (s, 1H), 2.18–2.06 (m, 1H), 2.06–1.90 (m, 1H), 1.46 (s, 9H); **^{13}C NMR** (101 MHz, $CDCl_3$) δ: 154.6, 152.0, 146.2, 144.9, 134.0, 129.1, 79.6, 48.9, 45.2, 41.4, 40.5, 28.6; ***m/z*** (ESI+) 348 ($[M+Na]^+$, 100%); **HRMS** (ESI+) found 348.11936 $[M+Na]^+$, $C_{14}H_{20}ClN_5O_2Na^+$ requires 348.11977.

tert-Butyl (*E*)-4-((2-(6-chloropyrazin-2-yl)hydrazinylidene)methyl)piperidine-1-carboxylate 276

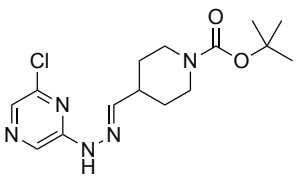

Prepared according to General Procedure 2 from: 1-boc-4-piperidinecarboxaldehyde (400 mg, 1.88 mmol) and **2** (271 mg, 1.88 mmol); filtered and washed with EtOH to give *the title compound* as a light brown powder (352 mg, 55%); $\mathbf{R_f}$ 0.52 (25% EtOAc in hexanes); **m.p.** 179–183 °C; **^{1}H NMR** (400 MHz, $CDCl_3$) δ: 8.47 (s, 1H), 8.15 (s, 1H), 7.99 (s, 1H), 7.09 (s, 1H), 4.06

(br s, 1H), 3.85 (br s, 1H), 2.93 (q, *J* 12.2, 2H), 2.47 (dq, *J* 9.3 & 4.5, 1H), 1.99 (dd, *J* 9.2 & 3.8, 1H), 1.74 (dd, *J* 8.6 & 3.9, 1H), 1.66–1.44 (m, 2H), 1.46 (s, 9H); **^{13}C NMR** (101 MHz, $CDCl_3$) δ: 154.9, 152.1, 146.2, 145.1, 134.0, 129.2, 79.9, 38.7, 28.6, 28.5, 24.4; ***m/z*** (ESI+) 362 ($[M+Na]^+$, 100%); **HRMS** (ESI+) found 362.13500 $[M+Na]^+$, $C_{15}H_{22}ClN_5O_2Na^+$ requires 362.13542.

5-Chloro-3-(tetrahydrofuran-3-yl)-[1,2,4]triazolo[4,3-*a*]pyrazine 277

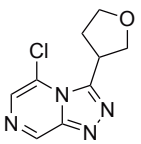

Prepared according to General Procedure 3 from: **273** (600 mg, 2.65 mmol) to give the crude title compound as a brownish-red solid (816 mg); purified by automated flash chromatography on silica (Biotage Isolera, 12–100% EtOAc in hexanes) to give *the title compound* as a pale yellow powder (457 mg, 77%); $\mathbf{R_f}$ 0.06 (50% EtOAc in hexanes); **m.p.** 99–102 °C; **^{1}H NMR** (400 MHz, $CDCl_3$) δ: 9.22 (s, 1H), 7.83 (s, 1H), 4.42 (dq, *J* 8.7 & 6.3, 1H), 4.30 (dd, *J* 8.5 & 7.3, 1H), 4.24–4.17 (m, 1H), 4.17–4.11 (m, 1H), 4.05 (td, *J* 8.1 & 5.9, 1H), 2.77 (ddt, *J* 12.2, 7.9 & 6.0, 1H), 2.48 (dddd, *J* 12.5, 8.7, 7.8 & 6.5, 1H); **^{13}C NMR** (101 MHz, $CDCl_3$) δ: 149.8, 147.8, 143.4, 129.4, 121.3, 72.9, 68.6, 37.7, 32.4; ***m/z*** (ESI+) 247 ($[M+Na]^+$, 100%); **HRMS** (ESI+) found 225.05378 $[M+H]^+$, $C_9H_9ClN_4OH^+$ requires 225.05377.

5-Chloro-3-(tetrahydro-2*H*-pyran-4-yl)-[1,2,4]triazolo[4,3-*a*]pyrazine 278

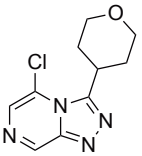

Prepared according to General Procedure 3 from: **274** (230 mg, 0.96 mmol) to give the crude title compound as a dark orange solid (293 mg); purified by automated flash chromatography on silica (Biotage Isolera, 12–100% EtOAc in hexanes) to give *the title compound* as pale yellow crystalline powder (145 mg, 63%); $\mathbf{R_f}$ 0.06 (50% EtOAc in hexanes); **m.p.** 185–193 °C; **^{1}H NMR** (400 MHz, $CDCl_3$) δ: 9.23 (s, 1H), 7.82 (s, 1H), 4.27–4.09 (m, 2H), 3.95 (tt, *J* 11.3 & 3.7, 1H), 3.61 (td, *J* 11.7 & 2.1, 2H), 2.45–2.21 (m, 2H), 2.17–2.03 (m, 2H); **^{13}C NMR** (101 MHz, $CDCl_3$) δ: 151.9, 147.4, 143.4, 129.5, 121.4, 67.5, 34.3, 32.4; ***m/z*** (ESI+) 261 ($[M+Na]^+$, 100%); **HRMS** (ESI+) found 239.06928 $[M+H]^+$, $C_{10}H_{11}ClN_4OH^+$ requires 239.06942.

***tert*-Butyl 3-(5-chloro-[1,2,4]triazolo[4,3-*a*]pyrazin-3-yl)pyrrolidine-1-carboxylate 279**

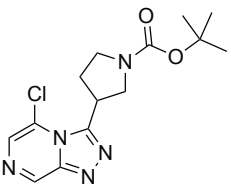

Prepared according to General Procedure 3 from: **275** (160 mg, 0.49 mmol) to give the crude title compound as an orange solid (157 mg); purified by automated flash chromatography on silica (Biotage Isolera, 12–100% EtOAc in hexanes) to give *the title compound* as a pale yellow powder (101 mg, 63%); $\mathbf{R_f}$ 0.07 (50% EtOAc in hexanes); **m.p.** 157–160 °C; **^{1}H NMR** (400 MHz, $CDCl_3$) δ: 9.23 (s, 1H), 7.84 (s, 1H), 4.45–4.32 (m, 1H), 4.00–3.70 (m, 3H), 3.55 (dt, *J* 10.7 & 7.3, 1H), 2.90–2.50 (m, 1H), 2.54–2.35 (m, 1H), 1.46 (s, 9H); **^{13}C NMR** (101 MHz, $CDCl_3$) δ: 154.4, 149.3, 147.7, 143.3,

129.5, 121.3, 79.8, 51.4 (d, *J* 57.4), 45.6, 36.7 (d, *J* 85.9), 31.2 (d, *J* 63.2), 28.6; ***m/z*** (ESI+) 346 ([M+Na]$^+$, 100%); **HRMS** (ESI+) found 346.10403 [M+Na]$^+$, $C_{14}H_{18}ClN_5O_2Na^+$ requires 346.10412.

tert-Butyl 4-(5-chloro-[1,2,4]triazolo[4,3-*a*]pyrazin-3-yl)piperidine-1-carboxylate 280

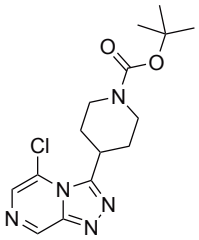

Prepared according to General Procedure 3 from: **276** (300 mg, 0.88 mmol) to give the crude title compound as a black solid (347 mg); purified by automated flash chromatography on silica (Biotage Isolera, 12–100% EtOAc in hexanes) to give *the title compound* as a pale yellow powder (245 mg, 82%); $\mathbf{R_f}$ 0.14 (50% EtOAc in hexanes); **m.p.** 112–116 °C; **^{1}H NMR** (400 MHz, $CDCl_3$) δ: 9.21 (s, 1H), 7.82 (s, 1H), 4.50 (d, *J* 12.5, 1H), 4.16 (s, 1H), 3.81 (t, *J* 10.8, 1H), 3.28 (t, *J* 11.8, 1H), 2.88 (s, 1H), 2.31 (d, *J* 13.2, 1H), 2.12 (qd, *J* 12.8 & 3.6, 1H), 1.91 (dq, *J* 9.7 & 3.0, 1H), 1.64 (q, *J* 11.6 & 10.8, 1H), 1.44 (s, 9H); **^{13}C NMR** (101 MHz, $CDCl_3$) δ: 154.5, 150.2, 147.3, 143.3, 129.4, 121.6, 80.1, 35.6, 31.0, 28.6, 25.0; ***m/z*** (ESI+) 360 ([M+Na]$^+$, 100%); **HRMS** (ESI+) found 360.11974 [M+Na]$^+$, $C_{15}H_{20}ClN_5O_2Na^+$ requires 360.11977.

5-Phenethoxy-3-(tetrahydrofuran-3-yl)-[1,2,4]triazolo[4,3-*a*]pyrazine 148

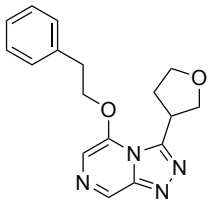

Prepared according to General Procedure 4 from: 2-phenylethanol (107 μL, 0.89 mmol) and **277** (200 mg, 0.89 mmol); the solvent was removed and the residue directly purified by automated flash chromatography on silica (Biotage Isolera, 25–100% EtOAc in hexanes) to give *the title compound* as a yellow powder (205 mg, 74%); $\mathbf{R_f}$ 0.11 (100% EtOAc); **m.p.** 127–133 °C; **^{1}H NMR** (400 MHz, $CDCl_3$) δ: 8.91 (s, 1H), 7.41–7.33 (m, 2H), 7.30 (td, *J* 8.3, 7.8 & 4.0, 3H), 7.25 (s, 1H), 4.89–4.48 (m, 2H), 4.37–3.73 (m, 5H), 3.27 (t, *J* 6.6, 2H), 2.86–2.47 (m, 1H), 2.31–2.10 (m, 1H); **^{13}C NMR** (101 MHz, $CDCl_3$) δ: 148.5, 147.9, 144.1, 136.8, 136.2, 129.2, 128.7, 127.6, 107.8, 72.7, 71.1, 68.5, 37.6, 35.1, 31.8; ***m/z*** (ESI+) 333 ([M+Na]$^+$, 100%); **HRMS** (ESI+) found 311.14994 [M+H]$^+$, $C_{17}H_{18}N_4O_2H^+$ requires 311.15025.

5-Phenethoxy-3-(tetrahydro-2*H*-pyran-4-yl)-[1,2,4]triazolo[4,3-*a*]pyrazine 149

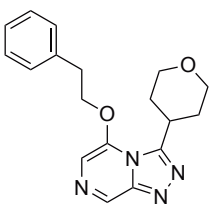

Prepared according to General Procedure 4 from: 2-phenylethanol (50.2 μL, 0.42 mmol) and **278** (100 mg, 0.42 mmol); the solvent was removed and the residue directly purified by automated flash chromatography on silica (Biotage Isolera, 25–100% EtOAc in hexanes) to give *the title compound* as a pale yellow powder (95.2 mg, 70%); $\mathbf{R_f}$ 0.10 (100% EtOAc); **m.p.** 146–149 °C; **^{1}H NMR** (400 MHz, $CDCl_3$)

δ: 8.92 (s, 1H), 7.42–7.35 (m, 2H), 7.33–7.26 (m, 4H), 4.62 (t, J 6.7, 2H), 4.37–3.87 (m, 2H), 3.53 (tt, J 11.4 & 3.8, 1H), 3.37 (td, J 11.7 & 2.1, 2H), 3.29 (t, J 6.6, 2H), 2.24–2.06 (m, 2H), 1.95–1.78 (m, 2H); **^{13}C NMR** (101 MHz, $CDCl_3$) δ: 150.9, 147.6, 144.2, 136.9, 136.0, 129.2, 128.6, 127.6, 107.8, 70.6, 67.5, 34.8, 34.2, 32.0; ***m/z*** (ESI+) 347 ($[M+Na]^+$, 100%); **HRMS** (ESI+) found 325.16558 $[M+H]^+$, $C_{18}H_{20}N_4O_2H^+$ requires 325.16590.

tert-Butyl 3-(5-phenethoxy-[1,2,4]triazolo[4,3-*a*]pyrazin-3-yl)pyrrolidine-1-carboxylate 150

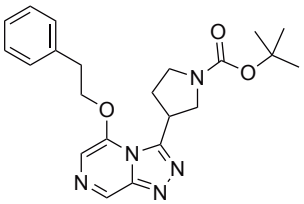

Prepared according to General Procedure 4 from: 2-phenylethanol (25.9 μL, 0.22 mmol) and **279** (70.0 mg, 0.22 mmol); the solvent was removed and the residue directly purified by automated flash chromatography on silica (Biotage Isolera, 25–100% EtOAc in hexanes) to give *the title compound* as a pale yellow powder (38.7 mg, 44%); **R_f** 0.14 (100% EtOAc); **m.p.** 123–126 °C; **^{1}H NMR** (400 MHz, $CDCl_3$) δ: 8.91 (s, 1H), 7.47–7.04 (m, 6H), 4.60 (d_{app}, J 17.1, 2H), 3.79 (d_{app}, J 7.0, 1H), 3.69 (s, 2H), 3.40 (br s, 1H), 3.27 (t, J 7.0, 2H), 2.67 (br s, 1H), 2.38 (br s, 1H), 2.16 (br s, 1H), 1.49 (s, 9H); **^{13}C NMR** (126 MHz, $CDCl_3$) δ: 154.6, 154.4, 148.1, 147.9, 147.8, 144.1, 136.8, 136.7, 136.2, 136.1, 129.2, 129.1, 128.6, 128.5, 127.6, 127.5, 108.0, 107.9, 79.7, 71.0, 51.5, 50.9, 45.7, 45.4, 37.0, 36.2, 35.12, 35.07, 30.9, 30.3, 28.7 (mixture of amide rotamers); ***m/z*** (ESI+) 432 ($[M+Na]^+$, 100%); **HRMS** (ESI+) found 432.20002 $[M+Na]^+$, $C_{22}H_{27}N_5O_3Na^+$ requires 432.20061.

tert-Butyl 4-(5-phenethoxy-[1,2,4]triazolo[4,3-*a*]pyrazin-3-yl)piperidine-1-carboxylate 151

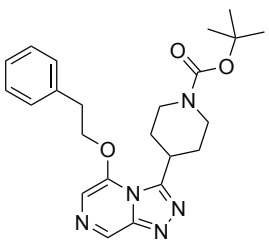

Prepared according to General Procedure 4 from: 2-phenylethanol (70.9 μL, 0.59 mmol) and **280** (200 mg, 0.59 mmol); the solvent was removed and the residue directly purified by automated flash chromatography on silica (Biotage Isolera, 25–100% EtOAc in hexanes) to give *the title compound* as a pale yellow powder (174 mg, 69%); **R_f** 0.26 (100% EtOAc); **m.p.** 145–149 °C; **^{1}H NMR** (400 MHz, $CDCl_3$) δ: 8.89 (s, 1H), 7.56–7.10 (m, 6H), 4.80–4.41 (m, 2H), 4.26–4.04 (m, 1H), 3.56–3.40 (m, 1H), 3.37–3.15 (m, 2H), 2.87 (t, J 12.2, 2H), 2.13 (d_{app}, J 10.7, 2H), 1.86 (dq, J 9.3 & 2.8, 1H), 1.59–1.39 (m, 2H), 1.46 (s, 9H); **^{13}C NMR** (101 MHz, $CDCl_3$) δ: 154.7, 149.0, 147.5, 144.3, 136.5, 129.0, 128.9, 127.3, 107.8, 79.9, 71.4, 48.7, 44.7, 35.5, 34.7, 28.6, 25.2; ***m/z*** (ESI+) 446 ($[M+Na]^+$, 100%); **HRMS** (ESI+) found 424.23386 $[M+H]^+$, $C_{23}H_{29}N_5O_3H^+$ requires 424.23432.

5-Phenethoxy-3-(pyrrolidin-3-yl)-[1,2,4]triazolo[4,3-*a*]pyrazine 152

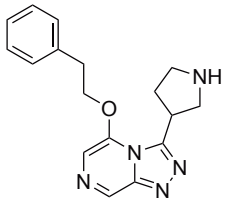

Compound **150** (20.0 mg, 48.8 μmol, 1.00 equiv.) was dissolved in CH_2Cl_2 (0.13 mL). TFA (42.1 μL, 0.55 mmol, 11.2 equiv.) was added and the reaction stirred at rt overnight. The solvent was removed and the residue directly purified by automated flash chromatography on silica (Biotage Isolera, 2–10% MeOH in CH_2Cl_2) to give a clear oil (21.2 mg, >100%); repurified by automated reversed-phase flash chromatography on silica (Biotage Isolera, 5–100% MeOH in H_2O) to give *the title compound* as a white powder (9.1 mg, 60%); **m.p.** 78–85 °C; **^{1}H NMR** (400 MHz, $CDCl_3$) δ: 8.88 (s, 1H), 7.40–7.33 (m, 2H), 7.33–7.26 (m, 3H), 7.23 (s, 1H), 4.59 (t, *J* 6.6, 2H), 3.86 (ddt, *J* 8.7, 7.5 & 3.6, 1H), 3.27 (t, *J* 6.6, 2H), 3.30–3.17 (m, 2H), 3.00 (dq, *J* 41.7 & 7.5, 2H), 2.45 (br s, 1H), 2.34–2.18 (m, 1H), 2.16–1.94 (m, 1H); **^{13}C NMR** (101 MHz, $CDCl_3$) δ: 150.7, 147.8, 144.3, 136.7, 136.3, 129.1, 128.7, 127.5, 107.7, 70.9, 53.6, 47.4, 37.9, 35.1, 32.6; ***m/z*** (ESI+) 310 ($[M+H]^+$, 100%); **HRMS** (ESI+) found 310.16593 $[M+H]^+$, $C_{17}H_{19}N_5OH^+$ requires 310.16624.

5-Phenethoxy-3-(piperidin-4-yl)-[1,2,4]triazolo[4,3-*a*]pyrazine 153

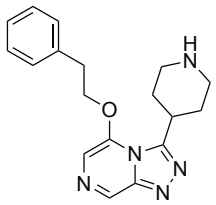

Compound **151** (100 mg, 0.24 mmol, 1.00 equiv.) was dissolved in CH_2Cl_2 (0.62 mL). TFA (0.2 mL, 2.64 mmol, 11.2 equiv.) was added and the reaction stirred at rt overnight. The solvent was removed and the residue directly purified by automated flash chromatography on silica (Biotage Isolera, 2–10% MeOH in CH_2Cl_2) to give a white solid (107 mg, >100%); repurified by automated reversed-phase flash chromatography on silica (Biotage Isolera, 5–100% MeOH in H_2O) to give *the title compound* as a white powder (61.7 mg, 81%); **m.p.** 175–180 °C; **^{1}H NMR** (400 MHz, $CDCl_3$) δ: 8.90 (s, 1H), 7.48–6.67 (m, 6H), 4.77–4.40 (m, 2H), 4.04 (dt, *J* 8.1 & 4.4, 1H), 3.68–3.51 (m, 2H), 3.39–3.23 (m, 3H), 3.09 (ddd, *J* 12.5, 9.0 & 4.1, 1H), 2.33–1.90 (m, 1H), 1.90–1.64 (m, 3H) (amine NH signal not seen); **^{13}C NMR** (101 MHz, $CDCl_3$) δ: 147.5, 147.4, 143.9, 136.4, 136.0, 129.1, 128.7, 127.4, 108.5, 71.2, 46.9, 44.1, 34.5, 32.0, 29.2, 21.1; ***m/z*** (ESI+) 324 ($[M+H]^+$, 100%); **HRMS** (ESI+) found 324.18134 $[M+H]^+$, $C_{18}H_{21}N_5OH^+$ requires 324.18189.

5-(2-(Cuban-1-yl)ethoxy)-3-(4-(difluoromethoxy)phenyl)-[1,2,4]triazolo[4,3-*a*] pyrazine 154

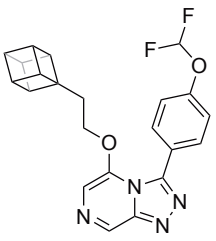

Prepared according to General Procedure 4 from: 2-cubylethanol (19.0 mg, 0.12 mmol) and **44** (37.0 mg, 0.12 mmol) to give the crude title compound as a brown solid (40.0 mg); purified by automated flash chromatography on silica (Biotage Isolera, 18–100% EtOAc in hexanes) to give *the title compound* as a pale yellow powder (28.0 mg, 55%); $\mathbf{R_f}$ 0.35 (75% EtOAc in hexanes); **m.p.** 146–149 °C; **^{1}H NMR** (300 MHz, $CDCl_3$) δ: 9.05 (s, 1H), 7.73 (d, *J* 8.7, 2H), 7.33 (s, 1H), 7.24 (d, *J* 8.6, 2H), 6.61 (t, *J* 73.2, 1H), 4.26 (t, *J* 6.5, 2H), 3.98 (ddq, *J* 7.2, 4.6 & 2.2, 1H), 3.78 (q, *J* 5.0, 3H), 3.54 (ddd, *J* 5.7, 4.4 & 2.3, 3H), 1.95 (t, *J* 6.5, 2H); **^{13}C NMR** (75 MHz, $CDCl_3$) δ: 152.5, 147.9, 146.4, 144.2, 136.3, 132.7, 124.9, 119.1, 118.6, 115.7, 112.2, 108.4, 68.2, 55.7, 48.6, 48.3, 44.3, 31.8; ***m/z*** (ESI+) 431 ($[M+Na]^+$, 100%), 839 ($[2M+Na]^+$, 23%); **HRMS** (ESI) found 431.12913 $[M+Na]^+$, $C_{22}H_{18}F_2N_4O_2Na^+$ requires 431.12902.

5-(3-(Cuban-1-yl)propoxy)-3-(4-(difluoromethoxy)phenyl)-[1,2,4]triazolo[4,3-*a*] pyrazine 155

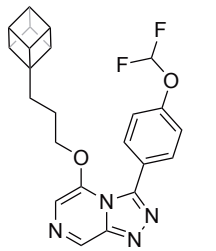

Prepared according to General Procedure 4 from: 3-cubylpropanol (20.0 mg, 0.12 mmol) and **44** (37.0 mg, 0.12 mmol) to give the crude title compound as a brown solid (45.0 mg); purified by automated flash chromatography on silica (Biotage Isolera, 18–100% EtOAc in hexanes) to give *the title compound* as a light brown powder (24.0 mg, 47%); $\mathbf{R_f}$ 0.33 (75% EtOAc in hexanes); **m.p.** 128–132 °C; **^{1}H NMR** (300 MHz, $CDCl_3$) δ: 9.06 (s, 1H), 7.72 (d, *J* 8.7, 2H), 7.32 (s, 1H), 7.23 (d, *J* 8.5, 2H), 6.59 (t, *J* 73.2, 1H), 4.22 (t, *J* 6.2, 2H), 4.04 (qt, *J* 4.5 & 2.2, 1H), 3.86 (q, *J* 5.1, 3H), 3.63 (dt, *J* 5.4 & 2.3, 3H), 1.75 (s, 4H); **^{13}C NMR** (75 MHz, $CDCl_3$) δ: 152.6, 147.9, 146.3, 144.3, 136.3, 132.5, 125.1, 119.2, 118.6, 115.7, 112.2, 108.4, 71.4, 58.2, 48.7, 48.2, 44.1, 29.1, 23.6; ***m/z*** (ESI+) 445 ($[M+Na]^+$, 100%), 867 ($[2M+Na]^+$, 13%); **HRMS** (ESI+) found 445.14481 $[M+Na]^+$, $C_{23}H_{20}F_2N_4O_2Na^+$ requires 445.14462.

1-Iodo-4-(hydroxymethyl)cubane 156

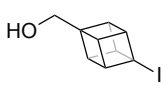

4-Iodocubanecarboxylic acid (200 mg, 0.73 mmol) was dissolved in anhydrous THF (7 mL) under Ar and cooled to 0 °C. Borane dimethyl sulfide complex (0.23 mL, 1.16 mmol) was added and the reaction stirred at 0 °C for 20 min, then at rt for 4 h. The solution was quenched with H_2O and stirred overnight. After adding EtOAc, the solution was washed with H_2O, brine, dried ($MgSO_4$), filtered and concentrated under reduced pressure to give the crude title compound as a white solid (162 mg); carried forward without further purification;

$\mathbf{R_f}$ 0.80 (100% EtOAc); **^{1}H NMR** (300 MHz, $CDCl_3$) δ: 4.21 (dd, J 5.8 & 4.4, 3H), 4.04 (dd, J 5.8 & 4.2, 3H), 3.77 (s, 2H) (alcohol OH signal not seen); **^{13}C NMR** (75 MHz, $CDCl_3$) δ: 63.2, 59.1, 54.8, 48.0, 39.0. Spectroscopic data matched those in the literature.[229]

1-Iodocubane-4-carboxaldehyde 157

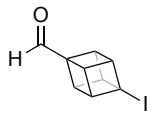

A stirring solution of oxalyl chloride (63.8 μL, 0.75 mmol) in anhydrous CH_2Cl_2 (1 mL) was prepared under Ar at –78 °C. Anhydrous DMSO (0.11 mL, 1.54 mmol) in anhydrous CH_2Cl_2 (1 mL) was added dropwise. After 20 min at –78 °C, a solution of **156** (162 mg, 0.62 mmol) in anhydrous CH_2Cl_2 (4.25 mL) was added dropwise under Ar. The mixture was maintained at –78 °C for 1.5 h, then anhydrous Et_3N (0.39 mL, 2.80 mmol) was added. The mixture was warmed to rt and quenched with H_2O (4 mL). The aqueous layer was extracted with CH_2Cl_2 (2 × 4 mL) and the combined organic layers washed with H_2O (4 mL), brine (4 mL), dried ($MgSO_4$), filtered and concentrated under reduced pressure to give the crude title compound as an off-white solid (161 mg); purified by automated flash chromatography on silica (Biotage Isolera, 12–100% EtOAc in hexanes) to give *the title compound* as a white solid (130 mg, 81%); $\mathbf{R_f}$ 0.84 (50% EtOAc in hexanes); **m.p.** 124–130 °C (lit.[229] 106–109 °C); **^{1}H NMR** (300 MHz, $CDCl_3$) δ: 9.74 (s, 1H), 4.56–4.47 (m, 3H), 4.33–4.25 (m, 3H); **^{13}C NMR** (75 MHz, $CDCl_3$) δ: 197.1, 62.8, 54.8, 49.0, 35.6. Spectroscopic data matched those in the literature.[229]

2-Chloro-6-(2-((*E*)-((2*r*,3*R*,4*r*,5*S*)-4-iodocuban-1-yl)methylene)hydrazinyl) pyrazine 158

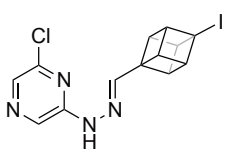

Prepared according to General Procedure 2 from: **2** (33.6 mg, 0.23 mmol) and **157** (60.0 mg, 0.23 mmol) to give the crude title compound as an off-white powder (90.1 mg); this intermediate, though novel, was carried forward without purification or characterisation; $\mathbf{R_f}$ 0.73 (2% MeOH in CH_2Cl_2).

5-Chloro-3-(4-iodocuban-1-yl)-[1,2,4]triazolo[4,3-*a*]pyrazine 159

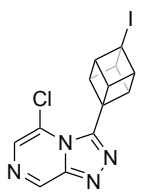

Prepared according to General Procedure 3 from: **158** (80.0 mg, 0.21 mmol) to give the crude title compound as a dark orange solid (110 mg); purified by automated flash chromatography on silica (Biotage Isolera, 0–10% MeOH in CH_2Cl_2) to give *the title compound* as a brown powder (62.0 mg, 78%); $\mathbf{R_f}$ 0.37 (2% MeOH in CH_2Cl_2); **m.p.** decomposed >150 °C; **^{1}H NMR** (300 MHz, $CDCl_3$) δ: 9.20 (s, 1H), 7.87 (s, 1H), 4.95–4.56 (m, 3H), 4.54–4.12 (m, 3H); **^{13}C NMR** (75 MHz, $CDCl_3$) δ: 147.7, 142.8, 129.1, 120.9, 54.7, 53.0, 51.7, 50.4, 34.5; ***m/z*** (ESI+) 405 ($[M+Na]^+$, 100%); **HRMS** (ESI+) found 404.93752

$[M+Na]^+$, $C_{13}H_8ClIN_4Na^+$ requires 404.93744.

5-(3,4-Difluorophenethoxy)-3-(4-iodocuban-1-yl)-[1,2,4]triazolo[4,3-*a*]pyrazine 160

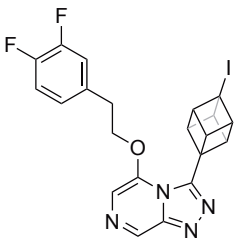

Prepared according to General Procedure 4 from: 2-(3,4-difluorophenyl) ethanol (20.7 mg, 0.13 mmol) and **159** (50.0 mg, 0.13 mmol) to give the crude title compound as an orange solid (81.4 mg); purified by automated flash chromatography on silica (Biotage Isolera, 25–100% EtOAc in hexanes) to give *the title compound* as a brown powder (19.9 mg, 30%); $\mathbf{R_f}$ 0.23 (100% EtOAc); **m.p.** 147–153 °C; **^{1}H NMR** (300 MHz, $CDCl_3$) δ: 8.86 (s, 1H), 7.47–6.73 (m, 4H), 4.64–4.35 (m, 5H), 4.26 (br s, 3H), 3.16 (t, *J* 7.5, 2H); **^{13}C NMR** (75 MHz, $CDCl_3$) δ: 156.4, 152.2, 151.7, 148.3, 146.3, 143.3, 136.7, 132.2, 124.9, 118.0, 108.1, 71.4, 54.9, 52.4, 52.2, 35.4, 34.2; ***m/z*** (ESI+) 527 ($[M+Na]^+$, 100%); **HRMS** (ESI+) found 527.01503 $[M+Na]^+$, $C_{21}H_{15}F_2IN_4ONa^+$ requires 527.01512.

6-(2-((*E*)-((2*r*,3*R*,4*r*,5*S*)-4-Iodocuban-1-yl)methylene)hydrazinyl)-*N*-(2-(trifluoromethyl)pyridin-4-yl)pyrazine-2-carboxamide 161

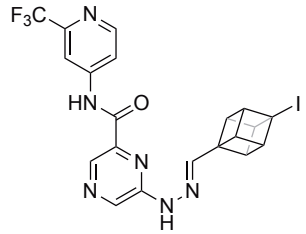

Prepared according to General Procedure 2 from: 6-hydrazinyl-*N*-(2-(trifluoromethyl)pyridin-4-yl)pyrazine-2-carboxamide (synthesised by Dr. Alice Motion, 57.8 mg, 0.19 mmol) and **157** (50.0 mg, 0.19 mmol) to give the crude title compound as a brown powder (109 mg); this intermediate, though novel, was carried forward without purification or characterisation; $\mathbf{R_f}$ 0.24 (50% EtOAc in hexanes).

3-(4-Iodocuban-1-yl)-*N*-(2-(trifluoromethyl)pyridin-4-yl)-[1,2,4]triazolo[4,3-*a*] pyrazine-5-carboxamide 162

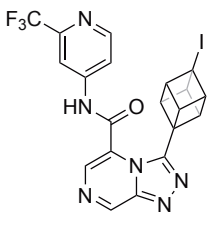

Prepared according to General Procedure 3 from: **161** (90.0 mg, 0.17 mmol) to give the crude title compound as a brown solid (171 mg); purified by automated flash chromatography on silica (Biotage Isolera, 25–100% EtOAc in hexanes, 0–20% MeOH in CH_2Cl_2) to give *the title compound* as a brown powder (34.0 mg, 38%); $\mathbf{R_f}$ 0.15 (100% EtOAc); **m.p.** decomposed >150 °C; **^{1}H NMR** (500 MHz, $CDCl_3$) δ: 11.88 (s, 1H), 9.59 (s, 1H), 8.79 (d, *J* 5.5, 1H), 8.43 (s, 1H), 8.24 (d, *J* 1.9, 1H), 8.07 (dd, *J* 5.5 & 1.8, 1H), 4.65–4.54 (m, 3H), 4.37–4.13 (m, 3H); **^{13}C NMR** (126 MHz, $CDCl_3$) δ: 160.4, 151.8, 147.6, 147.4, 146.7, 146.3, 137.1, 131.0, 130.7, 123.2, 116.5, 110.7, 54.6, 52.4, 51.7, 35.6; ***m/z*** (APCI+) 537 ($[M+H]^+$, 100%); **HRMS** (APCI+) found 537.01345 $[M+H]^+$, $C_{20}H_{12}F_3IN_6OH^+$ requires 537.01418.

4-Iodobenzaldehyde 163

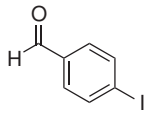

1,3-Dimethyl-2-imidazolidinone (15 mL) was added to 4-bromobenzaldehyde (1.00 g, 5.40 mmol, 1.0 equiv.), KI (8.07 g, 48.6 mmol 9.0 equiv.) and CuI (3.19 g, 17.8 mmol, 3.1 equiv.). The mixture was purged with N_2 and heated with vigorous stirring at 200 °C for 23 h. After cooling to rt, brine and ice were added and the reaction was placed in an ice bath for 3 h. The precipitated inorganic salts were removed by filtration and the filtrate extracted with Et_2O. The combined organic layers were washed with brine, dried (Na_2SO_4), filtered and concentrated under reduced pressure to give the crude title compound as a dark orange liquid (1.32 g); purified by automated flash chromatography on silica (Biotage Isolera, 12–75% EtOAc in hexanes) to give *the title compound* as a yellow powder (263 mg, 21%); $\mathbf{R_f}$ 0.87 (50% EtOAc in hexanes); **m.p.** 72–79 °C (lit.[397] 77–78 °C); **^{1}H NMR** (400 MHz, $CDCl_3$) δ: 9.96 (s, 1H), 7.91 (d, *J* 8.2, 2H), 7.59 (d, *J* 8.5, 2H); **^{13}C NMR** (101 MHz, $CDCl_3$) δ: 191.5, 138.6, 135.7, 130.9, 103.0. Spectroscopic data matched those in the literature.[230]

(*E*)-2-Chloro-6-(2-(4-iodobenzylidene)hydrazinyl)pyrazine 166

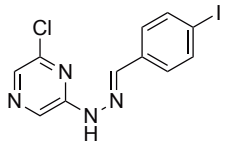

Prepared according to General Procedure 2 from: **163** (175 mg, 0.75 mmol) and **2** (109 mg, 0.75 mmol) to give the crude title compound as a light yellow powder (200 mg); this intermediate, though novel, was carried forward without purification or characterisation; $\mathbf{R_f}$ 0.26 (10% EtOAc in hexanes).

5-Chloro-3-(4-iodophenyl)-[1,2,4]triazolo[4,3-*a*]pyrazine 164

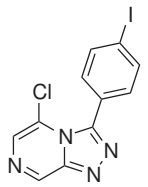

Prepared according to General Procedure 3 from: **166** (200 mg, 0.56 mmol) to give the crude title compound as a brown powder (270 mg); purified by automated flash chromatography on silica (Biotage Isolera, 12–100% EtOAc in hexanes) to give *the title compound* as a light brown powder (157 mg, 79%); this intermediate, though novel, was carried forward without complete characterisation; $\mathbf{R_f}$ 0.42 (50% EtOAc in hexanes); **m.p.** decomposed >200 °C; **^{1}H NMR** (300 MHz, $CDCl_3$) δ: 9.34 (s, 1H), 7.88 (d_{app}, *J* 5.8, 3H), 7.37 (d, *J* 7.9, 2H).

5-(3,4-Difluorophenethoxy)-3-(4-iodophenyl)-[1,2,4]triazolo[4,3-*a*]pyrazine 165

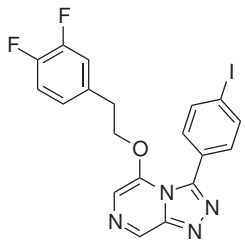

Prepared according to General Procedure 4 from: 2-(3,4-difluorophenyl)ethan-1-ol (44.4 mg, 0.28 mmol) and **164** (100 mg, 0.28 mmol) to give the crude title compound as a brown solid (125 mg); purified by automated flash chromatography on silica (Biotage Isolera, 25–100% EtOAc in hexanes) to give *the title compound* as a pale yellow powder (81.1 mg, 61%); $\mathbf{R_f}$ 0.50 (100% EtOAc); **m.p.** 155–157 °C; **^{1}H NMR** (300 MHz, $CDCl_3$) δ: 9.02 (s, 1H), 7.83 (d, *J* 7.7, 2H), 7.40 (d, *J* 7.6, 2H), 7.31 (s, 1H), 7.00 (q, *J* 8.7, 1H), 6.54 (t, *J* 9.2, 2H), 4.42 (t, *J* 5.9, 3H), 2.92 (t, *J* 5.8, 3H); **^{13}C NMR** (101 MHz, $CDCl_3$) δ: 150.3 (dd, *J* 249.0 & 12.7), 149.5 (dd, *J* 248.0 & 12.5), 147.9, 146.3, 143.8, 137.1, 136.8, 133.3 (dd, *J* 5.6 & 4.0), 132.3, 127.4, 124.5 (dd, *J* 6.1 & 3.6), 117.5 (d, *J* 17.4), 117.4 (d, *J* 17.3), 108.5, 96.7, 70.9, 33.9; ***m/z*** (ESI+) 501 ($[M+Na]^+$, 100%); **HRMS** (ESI+) found 500.99862 $[M+Na]^+$, $C_{19}H_{13}F_2IN_4ONa^+$ requires 500.99942.

5-(((3*r*,5*r*,7*r*)-Adamantan-1-yl)methoxy)-3-(4-(difluoromethoxy)phenyl)-[1,2,4]triazolo[4,3-*a*]pyrazine 167

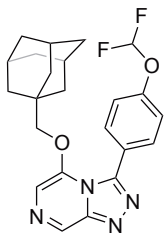

Prepared according to General Procedure 4 from: 1-adamantanemethanol (100 mg, 0.60 mmol) and **44** (178 mg, 0.60 mmol) to give the crude title compound as a brown solid (215 mg); purified by automated flash chromatography on silica (Biotage Isolera, 25–100% EtOAc in hexanes) to give *the title compound* as a yellow powder (140 mg, 55%); $\mathbf{R_f}$ 0.53 (100% EtOAc); **m.p.** 210–219 °C; **^{1}H NMR** (400 MHz, $CDCl_3$) δ: 9.01 (s, 1H), 7.67 (d, *J* 8.7, 2H), 7.29 (s, 1H), 7.26 (d, *J* 8.7, 2H), 6.59 (t, *J* 73.2, 1H), 3.71 (s, 2H), 1.88 (br s, 3H), 1.67 (d, *J* 12.3, 3H), 1.48 (d, *J* 11.6, 3H), 1.26 (d_{app}, *J* 2.5, 6H); **^{13}C NMR** (101 MHz, $CDCl_3$) δ: 152.6, 147.9, 146.0, 144.9, 136.2, 132.4, 125.5, 118.9, 115.7 (t, *J* 261.2), 108.7, 81.6, 38.8, 36.6, 33.6, 27.8; ***m/z*** (ESI+) 449 ($[M+Na]^+$, 100%), 875 ($[2M+Na]^+$, 44%); **HRMS** (ESI+) found 449.17606 $[M+Na]^+$, $C_{23}H_{24}F_2N_4O_2Na^+$ requires 449.17595.

5-(2-((1*s*,3*s*)-Adamantan-1-yl)ethoxy)-3-(4-(difluoromethoxy)phenyl)-[1,2,4]triazolo[4,3-*a*]pyrazine 168

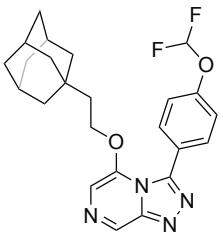

Prepared according to General Procedure 4 from: 1-adamantaneethanol (250 mg, 1.39 mmol) and **44** (411 mg, 1.39 mmol) to give the crude title compound as a dark brown solid (680 mg); purified by automated flash chromatography on silica (Biotage Isolera, 25–100% EtOAc in hexanes) to give *the title compound* as a light brown powder (363 mg, 59%); $\mathbf{R_f}$ 0.63 (100% EtOAc); **m.p.** 182–185 °C; **^{1}H NMR** (400 MHz, $CDCl_3$) δ: 9.00 (s, 1H), 7.73–7.64 (m, 2H), 7.29 (s, 1H),

7.25–7.20 (m, 2H), 6.61 (t, *J* 73.2, 1H), 4.24 (t, *J* 6.7, 2H), 1.87 (s, 3H), 1.66 (d, *J* 12.3, 3H), 1.52 (d, *J* 11.4, 3H), 1.39 (t, *J* 6.7, 2H), 1.29 (d, *J* 2.4, 6H); **^{13}C NMR** (101 MHz, $CDCl_3$) δ: 152.5, 147.9, 146.4, 144.2, 136.2, 132.7, 125.1, 118.7, 115.6 (t, *J* 261.6), 108.3, 67.5, 42.3, 41.9, 36.8, 31.7, 28.5; ***m/z*** (ESI+) 463 ($[M+Na]^+$, 100%); **HRMS** (ESI+) found 463.19161 $[M+Na]^+$, $C_{24}H_{26}F_2N_4O_2Na^+$ requires 463.19160.

[1.1.1]Propellane 170

Pentane (1.68 mL) and Et_2O (0.25 mL) were added 1,1-dibromo-2,2-bis(chloromethyl) cyclopropane (95% purity, 2.00 g, 6.40 mmol, 1.0 equiv.) and the mixture cooled to –50 °C (isopropanol/dry ice bath). MeLi·LiBr solution (1.5 M in Et_2O, 10.2 mL, 15.4 mmol, 2.4 equiv.) was added dropwise keeping the temperature around –50 °C (no higher than –40 °C). After the addition, the bath was replaced with an ice bath and the mixture allowed to warm to 0 °C. After 2 h, the volatile material was transferred under short-path vacuum distillation (distillation flask kept at 0 °C in an ice bath) to a receiving flask cooled to –78 °C (dry ice/acetone) to give an Et_2O solution of *the title compound* as a clear colourless liquid (0.685 M, 272 mg, 64%); yield by ^{1}H NMR calculated according to literature procedures;[249] carried forward without further purification; **^{1}H NMR** (300 MHz, $CDCl_3$) δ: 2.04 (s, 6H). Spectroscopic data matched those in the literature.[249]

Methyl 3-(chlorocarbonyl)bicyclo[1.1.1]pentane-1-carboxylate 172

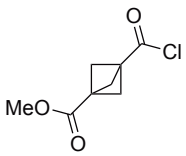

3-(Methoxycarbonyl)bicyclo[1.1.1]pentane-1-carboxylic acid (250 mg, 1.47 mmol, 1.0 equiv.) was dissolved in THF (17.3 mL, 85 mM) and cooled to 0 °C. Oxalyl chloride (149 μL, 1.76 mmol, 1.2 equiv.) was added, followed by DMF (3 drops). The reaction was allowed to stir at 0 °C for several minutes, then stirred at rt for 6 h. The solvent was removed and the crude product azeotroped several times with heptane to give *the title compound* as an off-white solid (261 mg, 94%); carried forward without further purification; **^{1}H NMR** (400 MHz, $CDCl_3$) δ: 3.69 (s, 3H), 2.35 (s, 6H); **^{13}C NMR** (101 MHz, $CDCl_3$) δ: 174.8, 169.7, 53.0, 52.0, 37.7, 37.6. Spectroscopic data matched those in the literature.[398]

Bicyclo[1.1.1]pentane-1-carboxylic acid 173

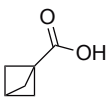

To a stirred suspension of 2-mercaptopyridine *N*-oxide sodium salt (94.9 mg, 0.64 mmol, 1.2 equiv.) in anhydrous PhMe (1.5 mL) was added *t*-BuSH (0.15 mL, 1.33 mmol, 2.5 equiv.) and DMAP (several mg). The mixture was deoxygenated then heated to reflux under an inert atmosphere. A solution of **172** (100 mg, 0.53 mmol, 1.0 equiv.) in

anhydrous PhMe (1.5 mL) was added dropwise while the reaction was irradiated with a 300 W lamp. After 3 h at reflux, the reaction was cooled to rt and treated with excess sat. aq. $Ca(ClO_2)$ and stirred for 2 h. The solution was washed with H_2O (3 ×) and the combined aqueous layers extracted with CH_2Cl_2. The combined organic layers were washed with brine, dried ($MgSO_4$), filtered and concentrated under reduced pressure to give a black liquid. The residue treated with a solution of excess KOH in 50% aq. MeOH at rt for 2-3 days. The solution was concentrated, diluted with H_2O and extracted with CH_2Cl_2 to give the disulfide by-product. The aqueous layer was acidified and extracted with CH_2Cl_2 to give *the title compound* as dark brown sludge (15.8 mg, 27%); carried forward without further purification; **^{1}H NMR** (400 MHz, $CDCl_3$) δ: 2.43 (s, 1H), 2.11 (s, 6H) (acid OH signal not seen); **^{13}C NMR** (101 MHz, $CDCl_3$) δ: 174.9, 51.6, 42.6, 27.9. Spectroscopic data matched those in the literature.[399]

3-Fluorobicyclo[1.1.1]pentane-1-carboxylic acid 174

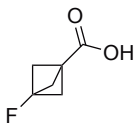

A flask was charged with bicyclo[1.1.1]pentane-1,3-dicarboxylic acid (500 mg, 3.20 mmol, 1.0 equiv.), $AgNO_3$ (40.8 mg, 0.24 mmol, 7.5 mol%) and Selectfluor (2.84 g, 8.01 mmol, 2.5 equiv.) and flushed with Ar under a condenser. Deoxygenated H_2O (16 mL, 0.2 M) was added and the reaction stirred at 65 °C for 19 h. The reaction was cooled to rt and extracted with Et_2O (3 ×). The organic layer was dried (Na_2SO_4), filtered and concentrated under reduced pressure to give a brown solid. The residue was dissolved in pentane, filtered slowly and the filtrate concentrated under reduced pressure to give *the title compound* as white plates (171 mg, 41%); **m.p.** 126–129 °C; **^{1}H NMR** (400 MHz, $CDCl_3$) δ: 2.40 (d, *J* 2.4, 6H) (acid OH signal not seen); **^{13}C NMR** (101 MHz, $CDCl_3$) δ: 175.6 (d, *J* 36.8), 74.8 (d, *J* 328.9), 55.7 (d, *J* 22.1), 28.2 (d, *J* 48.0); **^{19}F NMR** (376 MHz, $CDCl_3$) δ: -149.85. Spectroscopic data matched those in the literature.[253]

(3-(Difluoromethyl)bicyclo[1.1.1]pentan-1-yl)methanol 177

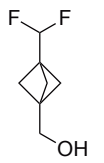

3-(Difluoromethyl)bicyclo[1.1.1]pentane-1-carboxylic acid (25.8 mg, 159 μmol, 1.0 equiv.) was dissolved in THF (72.3 μL, 2.2 M) and cooled to 0 °C. $LiAlH_4$ (1 M in THF, 239 μL, 239 μmol, 1.5 equiv.) was added and the reaction allowed to warm to rt and stirred for 3 h. The reaction was quenched with H_2O (18 μL) and anhydrous Na_2SO_4 (103 mg) and stirred for 20 min. The mixture was filtered, washed with THF and the filtrate concentrated under reduced pressure to give the crude title compound as a pale yellow oil (19.6 mg); this intermediate, though novel, was carried forward without purification or complete characterisation; $\mathbf{R_f}$ 0.34 (25% EtOAc in hexanes, $KMnO_4$ stain); **^{1}H NMR** (200 MHz, $CDCl_3$) δ: 5.70 (t, *J* 56.5, 1H), 3.66 (s, 2H), 1.81 (s, 6H) (alcohol OH signal not seen).

3-(4-(Difluoromethoxy)phenyl)-5-((3-(difluoromethyl)bicyclo[1.1.1]pentan-1-yl) methoxy)-[1,2,4]triazolo[4,3-*a*]pyrazine 178

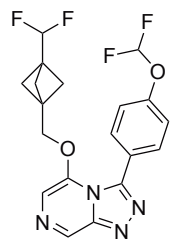

Prepared according to General Procedure 4 from: **177** (15.0 mg, 101 μmol) and **44** (30.0 mg, 101 μmol); the solvent was removed and the residue directly purified by automated flash chromatography on silica (Biotage Isolera, 25–100% EtOAc in hexanes) to give *the title compound* as a yellow powder (11.1 mg, 27%); $\mathbf{R_f}$ 0.40 (100% EtOAc); **m.p.** 129–134 °C; **^{1}H NMR** (500 MHz, $CDCl_3$) δ: 9.05 (s, 1H), 7.69 (d, *J* 8.8, 2H), 7.29 (d, *J* 8.7, 2H), 7.28 (s, 1H), 6.61 (t, *J* 73.0, 1H), 5.62 (t, *J* 56.3, 1H), 4.20 (s, 2H), 1.63 (s, 6H); **^{13}C NMR** (126 MHz, $CDCl_3$) δ: 152.2, 147.8, 146.1, 144.2, 136.8, 132.4, 125.5, 119.5, 115.6, 112.6, 108.5, 70.4, 47.6 (t, *J* 3.9), 39.0, 37.2; ***m/z*** (ESI+) 431 ($[M+Na]^+$, 100%); **HRMS** (ESI+) found 409.12812 $[M+H]^+$, $C_{19}H_{16}F_4N_4O_2H^+$ requires 409.12822.

3-(4-(Difluoromethoxy)phenyl)-5-(2-((1*R*,5*S*)-6,6-dimethylbicyclo[3.1.1]hept-2-en-2-yl)ethoxy)-[1,2,4]triazolo[4,3-*a*]pyrazine 179

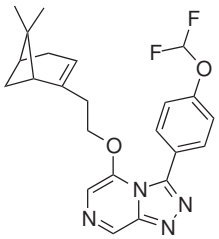

Prepared according to General Procedure 4 from: (1*R*)-(–)-nopol (57.6 μL, 0.34 mmol) and **44** (100 mg, 0.34 mmol); the solvent was removed and the residue directly purified by automated flash chromatography on silica (Biotage Isolera, 25–100% EtOAc in hexanes) to give *the title compound* as a light red powder (103 mg, 71%); $\mathbf{R_f}$ 0.49 (100% EtOAc); **m.p.** 134–137 °C; **^{1}H NMR** (400 MHz, $CDCl_3$) δ: 9.01 (s, 1H), 7.71 (d, *J* 8.8, 2H), 7.29 (s, 1H), 7.24 (d, *J* 8.8, 2H), 6.61 (t, *J* 73.3, 1H), 4.97 (dt, *J* 2.9 & 1.3, 1H), 4.29–4.11 (m, 2H), 2.39–2.22 (m, 3H), 2.13 (br s, 1H), 2.07 (br s, 1H), 2.05–1.98 (m, 1H), 1.83 (td, *J* 5.7 & 1.5, 1H), 1.20 (s, 3H), 0.98 (d_{app}, *J* 8.6, 1H), 0.63 (s, 3H); **^{13}C NMR** (101 MHz, $CDCl_3$) δ: 152.5, 148.0, 146.4, 144.1, 142.4, 136.4, 132.6, 125.1, 120.0, 118.7, 115.7 (t, *J* 261.3), 108.4, 69.3, 45.5, 40.7, 38.1, 35.5, 31.7, 31.4, 26.3, 21.1; ***m/z*** (ESI+) 449 ($[M+Na]^+$, 100%), 875 ($[2M+Na]^+$, 33%); **HRMS** (ESI+) found 449.17597 $[M+Na]^+$, $C_{23}H_{24}F_2N_4O_2Na^+$ requires 449.17595.

5-(((1*S*,2*S*,4*S*)-Bicyclo[2.2.1]hept-5-en-2-yl)methoxy)-3-(4-(difluoromethoxy)phenyl)-[1,2,4]triazolo[4,3-*a*]pyrazine 180

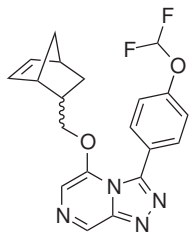

Prepared according to General Procedure 4 from: 5-norbornene-2-methanol (40.8 μL, 0.34 mmol) and **44** (100 mg, 0.34 mmol); the solvent was removed and the residue directly purified by automated flash chromatography on silica (Biotage Isolera, 25–100% EtOAc in hexanes) to give *the title compound* (present as a mixture of *endo* and *exo* isomers) as a yellow powder (80.0 mg, 62%); $\mathbf{R_f}$ 0.63 (100% EtOAc); **m.p.** 122–128 °C; **^{1}H NMR** (400 MHz, $CDCl_3$, present as a mixture of *endo* and *exo* isomers, ∼1:0.78 *maj/min*) δ: 9.01 (s, 1H$^{(min)}$), 9.00 (s, 1H$^{(maj)}$), 7.72 (d, *J* 8.7, 4H$^{(comb)}$), 7.37–7.14 (m, 6H$^{(comb)}$), 6.61 (t, *J* 73.2, 1H$^{(min)}$), 6.59 (t, *J* 73.2, 1H$^{(maj)}$), 6.15 (dd, *J* 5.7 & 3.0, 1H$^{(maj)}$), 6.06 (dd, *J* 5.7 & 3.0, 1H$^{(min)}$), 5.90 (dd, *J* 5.8 & 3.2, 1H$^{(min)}$), 5.74 (dd, *J* 5.7 & 2.8, 1H$^{(maj)}$), 4.09 (ddd, *J* 140.2, 8.8 & 6.2, 2H$^{(min)}$), 3.88 (dt, *J* 90.9 & 9.1, 2H$^{(maj)}$), 2.89–2.65 (m, 2H$^{(comb)}$), 2.43–2.20 (m, 3H$^{(comb)}$), 1.71 (ddd, *J* 12.4, 9.1 & 3.7, 1H$^{(maj)}$), 1.64 (dq, *J* 9.5 & 4.8, 1H$^{(min)}$), 1.47–1.35 (m, 1H$^{(comb)}$), 1.34–1.23 (m, 1H$^{(comb)}$), 1.21–1.12 (m, 3H$^{(comb)}$), 1.10–0.99 (m, 1H$^{(min)}$), 0.47 (ddd, *J* 11.7, 4.1 & 2.6, 1H$^{(maj)}$); **^{13}C NMR** (101 MHz, $CDCl_3$, present as a mixture of *endo* and *exo* isomers) δ: 152.4, 152.3, 147.9, 146.3, 146.3, 144.24, 144.22, 138.6, 137.3, 136.3, 136.1, 135.7, 132.6, 132.5, 131.5, 129.1, 128.7, 125.3, 125.1, 119.1, 118.7, 115.7 (t, *J* 261.6), 115.6 (t, *J* 261.9), 108.2, 75.0, 74.4, 49.4, 44.8, 43.7, 43.4, 42.3, 41.6, 38.1, 37.9, 29.4, 28.9; ***m/z*** (ESI+) 407 ([M+Na]$^+$, 100%); **HRMS** (ESI+) found 407.12942 [M+Na]$^+$, $C_{20}H_{18}F_2N_4O_2Na^+$ requires 407.12900.

2,2-Dimethyl-5-(octahydro-1*H*-2,4,1-(epiethane[1,1,2]triyl)cyclobuta[*cd*]pentalen-7-ylidene)-1,3-dioxane-4,6-dione 183

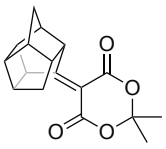

Octahydro-1*H*-2,4,1-(epiethane[1,1,2]triyl)cyclobuta[*cd*]pentalen-7-one (150 mg, 0.94 mmol, 1.0 equiv.) was dissolved in pyridine (1 mL) and isopropylidene malonate (162 mg, 1.12 mmol, 1.2 equiv.) was added. The mixture was agitated several times within the first hour to dissolve the acid, then left to stand for 5 days. The reaction mixture was poured over H_2O (20 mL) and the precipitate filtered to give the crude title compound as a white powder (153 mg); carried forward without further purification; a small amount of crude material was purified by recrystallisation from 50% aq. acetone to give *the title compound* as white plates; **m.p.** 160–164 °C (lit.[259] 157–158 °C); **IR** ν_{max} (film) /cm^{-1} 1726, 1606; **^{1}H NMR** (400 MHz, $CDCl_3$) δ: 4.24 (ddd, *J* 8.4, 5.9 & 2.4, 1H), 4.16–3.98 (m, 1H), 3.18 (td, *J* 8.6 & 3.5, 1H), 2.94 (d, *J* 10.1, 1H), 2.79 (q, *J* 6.4 & 6.0, 1H), 2.66 (q, *J* 7.0 & 6.4, 1H), 2.58–2.45 (m, 2H), 1.92 (d, *J* 10.9, 1H), 1.71 (d, *J* 5.3, 6H), 1.52 (d, *J* 10.9, 1H), 1.40–1.15 (m, 2H); **^{13}C NMR** (101 MHz, $CDCl_3$) δ: 194.6, 161.2, 161.0, 111.5, 103.9, 50.8, 50.6, 47.8, 47.5, 44.2, 43.0, 42.8, 39.8,

36.9, 30.9, 27.7, 27.1. Spectroscopic data matched those in the literature.[259]

2,2-Dimethyl-5-(octahydro-1*H*-2,4,1-(epiethane[1,1,2]triyl)cyclobuta[*cd*]pentalen-7-yl)-1,3-dioxane-4,6-dione 184

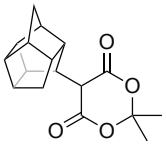

Compound **183** (120 mg, 0.42 mmol, 1.0 equiv.) was suspended in EtOH (8 mL) and $NaBH_4$ (17.4 mg, 0.42 mmol, 1.1 equiv.) was added portionwise keeping the temperature below 30 °C. The reaction mixture was allowed to stir for 1 h then filtered. The filtrate was reduced to half the volume and poured onto a H_2O (8 mL) and AcOH (0.13 mL) mixture and left to stand for 2 h. The solid was filtered, washed with H_2O and dried *in vacuo* to give the crude title compound as white crystals (91.8 mg); carried forward without further purification; a small amount of crude material was purified by recrystallisation from 50% aq. acetone to give *the title compound* as white plates; **m.p.** 138–143 °C (lit.[259] 136–137 °C); **IR** ν_{max} (film) /cm^{-1} 1742; **^{1}H NMR** (400 MHz, $CDCl_3$) δ: 3.91 (d, *J* 9.9, 1H), 3.05–2.73 (m, 2H), 2.59 (qd, *J* 12.2, 10.8 & 4.8, 3H), 2.47 (d, *J* 8.8, 1H), 2.24 (br d, *J* 17.9, 2H), 1.92 (dt, *J* 9.9 & 3.1, 1H), 1.81 (d, *J* 13.2, 1H), 1.73 (d, *J* 8.1, 6H), 1.70 (s_{app}, 1H), 1.30–1.08 (m, 2H); **^{13}C NMR** (101 MHz, $CDCl_3$) δ: 166.0, 165.8, 105.4, 47.4, 46.4, 46.3, 44.3, 42.5, 42.1, 41.7, 41.5, 38.4, 36.4, 34.1, 29.2, 28.8, 28.3. Spectroscopic data matched those in the literature.[259]

2-(Octahydro-1*H*-2,4,1-(epiethane[1,1,2]triyl)cyclobuta[*cd*]pentalen-7-yl)acetic acid 185

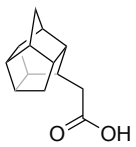

Compound **184** (65.0 mg, 0.23 mmol) was dissolved in a mixture of AcOH (0.5 mL) and conc. HCl (0.1 mL) and heated at reflux for 2.5 h. The reaction was cooled to rt and poured onto H_2O (3.75 mL), cooled in ice, filtered and washed with H_2O to give the crude title compound as an off-white powder (32.5 mg); carried forward without further purification; a small amount of crude material was purified by recrystallisation from hexane to give *the title compound* as white crystals; **^{1}H NMR** (300 MHz, $CDCl_3$) δ: 2.82–2.49 (m, 6H), 2.30 (br s, 1H), 2.27–2.14 (m, 4H), 1.93 (tt, *J* 6.8 & 2.8, 1H), 1.69 (s, 1H), 1.68–1.59 (m, 1H), 1.17 (d, *J* 10.7, 1H), 1.03 (dt, *J* 12.7 & 3.5, 1H). Spectroscopic data matched those in the literature.[259]

2-(Octahydro-1*H*-2,4,1-(epiethane[1,1,2]triyl)cyclobuta[*cd*]pentalen-7-yl)ethan-1-ol 186

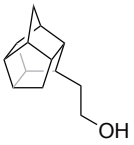

Prepared according to General Procedure **6** from: **185** (25.0 mg, 0.12 mmol) to give the crude title compound as a clear oil (25.6 mg); this intermediate, though novel, was carried forward without purification or characterisation.

3-(4-(Difluoromethoxy)phenyl)-5-(2-(octahydro-1*H*-2,4,1-(epiethane[1,1,2]triyl) cyclobuta[*cd*]pentalen-7-yl)ethoxy)-[1,2,4]triazolo[4,3-*a*]pyrazine 187

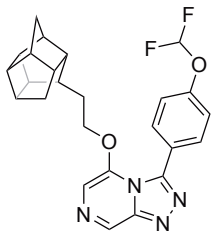

Prepared according to General Procedure 4 from: **186** (20.0 mg, 0.11 mmol) and **44** (31.2 mg, 0.11 mmol); the solvent was removed and the residue directly purified by automated flash chromatography on silica (Biotage Isolera, 25–100% EtOAc in hexanes) to give *the title compound* as a light brown powder (14.5 mg, 31%); $\mathbf{R_f}$ 0.35 (100% EtOAc); **m.p.** 136–142 °C; **^{1}H NMR** (400 MHz, $CDCl_3$) δ: 9.02 (s, 1H), 7.70 (d, *J* 8.8, 2H), 7.29 (s, 1H), 7.23 (d, *J* 8.7, 2H), 6.61 (t, *J* 73.2, 1H), 4.18 (tq, *J* 5.8 & 2.5, 2H), 2.60 (q, *J* 6.5, 1H), 2.48 (dq, *J* 27.4 & 6.8, 2H), 2.30 (dt, *J* 7.8 & 4.0, 1H), 2.25–2.19 (m, 1H), 2.19–2.13 (m, 1H), 2.01–1.97 (m, 1H), 1.91 (q, *J* 6.5, 2H), 1.68–1.49 (m, 4H), 1.18–1.05 (m, 2H); **^{13}C NMR** (101 MHz, $CDCl_3$) δ: 148.0, 146.4, 145.8, 144.3, 136.3, 132.5, 125.1, 118.6, 115.7, 108.4, 71.2, 47.4, 47.0, 44.5, 42.3, 41.8, 41.5, 38.8, 38.4, 36.3, 34.2, 28.7, 28.6; ***m/z*** (ESI+) 473 ($[M+Na]^+$, 100%); **HRMS** (ESI+) found 451.19408 $[M+H]^+$, $C_{25}H_{24}F_2N_4O_2H^+$ requires 451.19401.

***o*-Carboranylethyl alcohol 188**

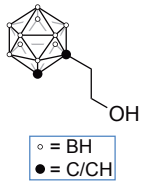

To a solution of *o*-carborane (100 mg, 0.69 mmol, 1 equiv.) in anhydrous THF (2.25 mL) was added *n*-BuLi (1.6 M in hexanes, 0.43 mL, 0.69 mmol, 1 equiv.) at –78 °C under N_2. Stirring was continued for 30 min, then ethylene oxide (2.5 M in THF, 0.42 mL, 1.04 mmol, 1.5 equiv.) was added dropwise. Stirring was continued for 1 h at 0 °C, then the reaction was quenched with sat. aq. NH_4Cl (1 mL). The aqueous phase was extracted with EtOAc (3 × 1.5 mL) and the combined organic layers dried (Na_2SO_4), filtered and concentrated under reduced pressure to give the crude title compound as a cloudy white liquid (156 mg); purified by automated flash chromatography on silica (Biotage Isolera, 5–40% EtOAc in hexanes) to give *the title compound* as a white solid (110 mg, 66%); **^{1}H NMR** (400 MHz, $CDCl_3$) δ: 3.98 (br s, 1H), 3.79 (t, *J* 5.9, 2H), 2.49 (t, *J* 5.9, 2H), 2.80–1.42 (m, 11H); **^{13}C NMR** (101 MHz, $CDCl_3$) δ: 73.2, 60.8, 60.7, 39.9; ***m/z*** (ESI–) 189 ($[M-H]^-$, 100%); **HRMS** (ESI–) found 189.20580 $[M-H]^-$, $C_4H_{15}B_{10}O^-$ requires 189.20589. Spectroscopic data matched those in the literature.[400]

m-Carboranylethyl alcohol 189

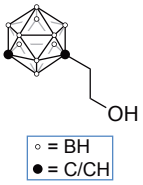

To a solution of *m*-carborane (100 mg, 0.69 mmol, 1 equiv.) in anhydrous THF (2.25 mL) was added *n*-BuLi (1.6 M in hexanes, 0.43 mL, 0.69 mmol, 1 equiv.) at –78 °C under N_2. Stirring was continued for 30 min, then ethylene oxide (2.5 M in THF, 0.42 mL, 1.04 mmol, 1.5 equiv.) was added dropwise. Stirring was continued for 1 h at 0 °C, then the reaction was quenched with sat. aq. NH_4Cl (1 mL). The aqueous phase was extracted with EtOAc (3 × 1.5 mL) and the combined organic layers dried (Na_2SO_4), filtered and concentrated under reduced pressure to give the crude title compound as a white solid (160 mg); purified by automated flash chromatography on silica (Biotage Isolera, 6–50% EtOAc in hexanes) to give *the title compound* as a white solid (30.7 mg, 23%); $\mathbf{R_f}$ 0.47 (25% EtOAc in hexanes, $KMnO_4$ stain); ^{1}**H NMR** (200 MHz, $CDCl_3$) δ: 3.88–3.32 (m, 2H), 2.94 (s, 1H), 2.51–2.00 (m, 2H), 3.29–0.71 (m, 11H); ***m/z*** (APCI+) 191 ($[M+H]^+$, 100%); **HRMS** (ESI–) found 189.20582 $[M-H]^-$, $C_4H_{15}B_{10}O^-$ requires 189.20589. Spectroscopic data matched those in the literature.[401]

1-(2-Benzyloxyethyl)-1,12-dicarba-closo-dodecaborane 190

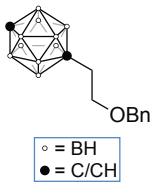

To a solution of *p*-carborane (120 mg, 0.83 mmol, 1.0 equiv.) in anhydrous Et_2O (2.88 mL) was added *n*-BuLi (1.6 M in hexanes, 572 μL, 0.92 mmol, 1.1 equiv.) at 0 °C under Ar. The reaction mixture was allowed to stir at rt for 1 h, then benzyl 2-bromoethyl ether (163 μL, 1.00 mmol, 1.2 equiv.) was added and the reaction stirred for 16 h. The reaction was cooled to 0 °C, quenched with H_2O and diluted with EtOAc. The organic layer was washed with H_2O, brine, dried (Na_2SO_4), filtered and concentrated under reduced pressure to give the crude title compound as a yellow oil (325 mg); purified by automated flash chromatography on silica (Biotage Isolera, 6–50% EtOAc in hexanes) to give *the title compound* as a clear colourless oil (108 mg, 47%); $\mathbf{R_f}$ 0.83 (10% EtOAc in hexanes, $KMnO_4$ stain); ^{1}**H NMR** (200 MHz, $CDCl_3$) δ: 7.63–6.97 (m, 5H), 4.40 (s, 2H), 3.26 (t, *J* 7.2, 2H), 2.64 (br s, 1H), 1.95 (t, *J* 7.1, 2H), 3.72–0.63 (m, 10H). Spectroscopic data matched those in the literature.[274]

p-Carboranylethyl alcohol 191

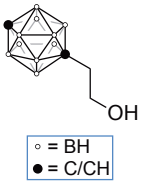

Compound **190** (90 mg, 0.32 mmol, 1.00 equiv.) and 5% Pd/C (34.4 mg, 0.02 mmol, 0.05 equiv.) were suspended in EtOH (2 mL). The reaction purged with Ar and Et_3SiH (0.52 mL, 3.23 mmol, 10.0 equiv.) was added dropwise and the reaction stirred at rt for 19 h. The mixture was filtered through a pad of celite and concentrated under reduced pressure to give the crude title compound as a pale yellow solid

(40.7 mg); carried forward without further purification; $\mathbf{R_f}$ 0.26 (10% EtOAc in hexanes, $KMnO_4$ stain); **^{1}H NMR** (400 MHz, $CDCl_3$) δ: 3.45 (t, J 7.0, 2H), 2.66 (br s, 1H), 2.91–1.26 (m, 11H), 1.90 (t, J 7.0, 2H). Spectroscopic data matched those in the literature.[400]

5-((1,2-Dicarba-closo-decaborane-1-yl)ethoxy)-3-(4-(difluoromethoxy)phenyl)-[1,2,4]triazolo[4,3-*a*]pyrazine 192

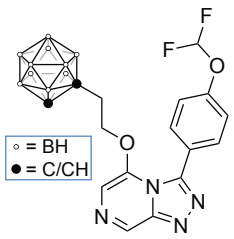

Prepared according to General Procedure 4 from: **188** (50.0 mg, 0.27 mmol) and **44** (78.8 mg, 0.27 mmol) to give the crude title compound as a brown liquid (117 mg); purified by automated flash chromatography on silica (Biotage Isolera, 25–100% EtOAc in hexanes) to give *the title compound* as a light brown powder (43.6 mg, 37%); $\mathbf{R_f}$ 0.17 (100% EtOAc); **m.p.** 179–184 °C; **^{1}H NMR** (400 MHz, $CDCl_3$) δ: 9.10 (s, 1H), 7.69 (d, J 8.8, 2H), 7.33 (s, 1H), 7.29 (d, J 8.7, 2H), 6.66 (t, J 72.7, 1H), 4.32 (t, J 5.6, 2H), 2.55 (t, J 5.6, 2H), 3.11–1.14 (m, 11H); **^{13}C NMR** (101 MHz, $CDCl_3$) δ: 152.6, 147.9, 145.8, 142.9, 137.8, 132.5, 124.8, 119.3, 115.4 (t, J 263.3), 108.7, 71.0, 68.5, 60.1, 36.4; ***m/z*** (ESI+) 449 ($[M+H]^+$, 20%), 471 ($[M+Na]^+$, 100%); **HRMS** (ESI+) found 471.26102 $[M+Na]^+$, $C_{16}H_{22}B_{10}F_2N_4O_2Na^+$ requires 471.26142.

5-((1,7-Dicarba-closo-decaborane-1-yl)ethoxy)-3-(4-(difluoromethoxy)phenyl)-[1,2,4]triazolo[4,3-*a*]pyrazine 193

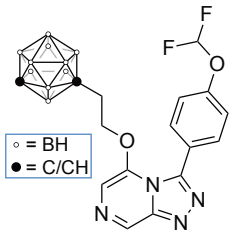

Prepared according to General Procedure 4 from: **189** (20.0 mg, 106 μmol) and **44** (31.5 mg, 106 μmol); the solvent was removed and the residue directly purified by automated flash chromatography on silica (Biotage Isolera, 25–100% EtOAc in hexanes) to give a yellow powder (11.1 mg, 23%); repurified by automated reversed-phase flash chromatography on silica (Biotage Isolera, 5–100% MeOH in H_2O) to give *the title compound* as a light yellow powder (8.3 mg, 17%); $\mathbf{R_f}$ 0.36 (100% EtOAc); **m.p.** 158–162 °C; **^{1}H NMR** (400 MHz, $CDCl_3$) δ: 9.07 (s, 1H), 7.69 (d, J 8.7, 2H), 7.31–7.24 (m, 3H), 6.63 (t, J 73.1, 1H), 4.16 (t, J 6.5, 2H), 2.25 (t, J 6.5, 2H), 3.28–0.98 (m, 11H); **^{13}C NMR** (101 MHz, $CDCl_3$) δ: 152.6, 147.9, 146.3, 143.3, 137.4, 132.5, 125.0, 119.2, 115.6 (t, J 262.0), 108.7, 71.2, 68.9, 55.5, 34.8; **^{19}F NMR** (376 MHz, $CDCl_3$) δ: -81.47; ***m/z*** (ESI+) 471 ($[M+Na]^+$, 100%); **HRMS** (ESI+) found 449.27839 $[M+H]^+$, $C_{16}H_{22}B_{10}F_2N_4O_2H^+$ requires 449.27948.

5-((1,12-Dicarba-closo-decaborane-1-yl)ethoxy)-3-(4-(difluoromethoxy)phenyl)-[1,2,4]triazolo[4,3-*a*]pyrazine 194

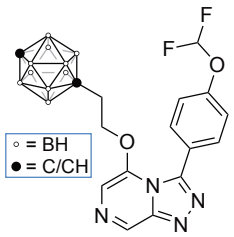

Prepared according to General Procedure 4 from: **191** (20.0 mg, 106 μmol) and **44** (31.5 mg, 106 μmol); the solvent was removed and the residue directly purified by automated flash chromatography on silica (Biotage Isolera, 25–100% EtOAc in hexanes) to give *the title compound* light brown powder (16.2 mg, 34%); $\mathbf{R_f}$ 0.43 (100% EtOAc); **m.p.** 137–143 °C; **^{1}H NMR** (500 MHz, $CDCl_3$) δ: 9.05 (s, 1H), 7.65 (d, J 8.7, 2H), 7.25 (d, J 8.8, 1H), 7.23 (s, 1H), 6.63 (t, J 73.1, 1H), 3.98 (t, J 6.6, 2H), 1.91 (t, J 6.6, 2H), 2.86–1.05 (m, 11H); **^{13}C NMR** (126 MHz, $CDCl_3$) δ: 152.6, 147.9, 146.4, 143.3, 137.2, 132.5, 124.9, 119.0, 115.7 (t, J 261.7), 108.6, 70.8, 68.6, 59.2, 36.4; ***m/z*** (ESI+) 449 ($[M+H]^+$, 100%); **HRMS** (ESI+) found 449.28061 $[M+H]^+$, $C_{16}H_{22}B_{10}F_2N_4O_2H^+$ requires 449.27948.

5-((7,8-Dicarba-nido-undecaborane-7-yl)ethoxy)-3-(4-(difluoromethoxy)phenyl)-[1,2,4]triazolo[4,3-*a*]pyrazine 195

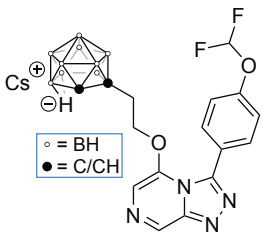

Compound **192** (20.0 mg, 44.6 μmol, 1 equiv.) and CsF (20.3 mg, 134 μmol, 3 equiv.) were dissolved in EtOH (1 mL) and heated to reflux for 25 h. The solvent was removed. Acetone (2 mL) was added, the solution filtered through a fritted glass funnel, washed several times with acetone and the solvent removed to give the crude product as an off-white solid (27.4 mg); purified by automated flash chromatography on silica (Biotage Isolera, 2–10% MeOH in CH_2Cl_2) to give *the title compound* as a yellow powder (16.4 mg, 65%); $\mathbf{R_f}$ 0.13 (10% MeOH in CH_2Cl_2); **m.p.** 181–190 °C; **^{1}H NMR** (500 MHz, CD_3OD) δ: 8.94 (s, 1H), 7.76 (d, J 8.9, 2H), 7.50 (s, 1H), 7.28 (d, J 8.9, 2H), 6.91 (t, J 73.8, 1H), 4.56 (s, 2H), 4.46–4.29 (m, 2H), 1.94–1.65 (m, 2H) (carborane BH signals not seen); **^{13}C NMR** (126 MHz, CD_3OD) δ: 154.6, 149.0, 148.0, 146.3, 135.6, 133.9, 125.6, 119.2, 117.7 (t, J 257.9), 109.9, 74.2, 38.8 (carborane C signals not seen); ***m/z*** (ESI+) 484 ($[M+2Na]^+$, 100%); **HRMS** (ESI+) found 484.23813 $[M+2Na]^+$, $C_{16}H_{22}B_9CsF_2N_4O_2Na_2^+$ requires 484.23746.

9.7 Synthesis and Characterisation of Compounds from Chapter 6

Methyl 3-hydroxy-2-phenylpropanoate 210

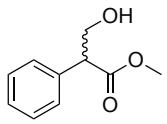

Prepared according to General Procedure 7 from: tropic acid (1.00 g, 6.02 mmol, 1 equiv.) to give *the title compound* as a clear colourless oil (831 mg, 77%); carried forward without further purification; **^{1}H NMR** (400 MHz, $CDCl_3$) δ: 7.94–7.10 (m, 5H), 4.13 (dd, *J* 10.4 & 8.3, 1H), 3.93–3.78 (m, 2H), 3.71 (s, 3H) (alcohol OH signal not seen); **^{13}C NMR** (101 MHz, $CDCl_3$) δ: 173.7, 135.7, 129.0, 128.3, 127.9, 64.7, 54.1, 52.3. Spectroscopic data matched those in the literature.[402]

3-(4-(Difluoromethoxy)phenyl)-5-methoxy-[1,2,4]triazolo[4,3-*a*]pyrazine 211

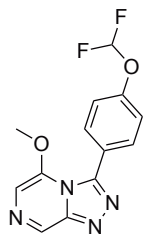

By-product from the reaction of **210** (182 mg, 1.01 mmol, 1 equiv.) with **44** (300 mg, 1.01 mmol, 1 equiv.) according to General Procedure 4; purified by automated flash chromatography on silica (Biotage Isolera, 25–100% EtOAc in hexanes) to give *the title compound* as a yellow powder (16.0 mg, 4%); **m.p.** 91–95 °C; **^{1}H NMR** (400 MHz, $CDCl_3$) δ: 9.04 (s, 1H), 7.72 (d, *J* 8.7, 2H), 7.33 (s, 1H), 7.24 (d, *J* 8.6, 2H), 6.62 (t, *J* 73.3, 1H), 4.01 (s, 3H); **^{13}C NMR** (101 MHz, $CDCl_3$) δ: 152.6, 147.9, 146.5, 144.9, 136.8, 132.4, 124.9, 118.7, 115.7 (t, *J* 260.9), 108.0, 57.3; ***m/z*** (ESI+) 293 ($[M+H]^+$, 100%); **HRMS** (ESI+) found 293.08405 $[M+H]^+$, $C_{13}H_{10}F_2N_4O_2H^+$ requires 293.08446.

Ethyl 3-hydroxy-2-phenylpropanoate 212

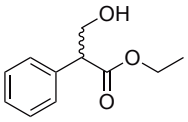

Prepared according to General Procedure 7 from: tropic acid (500 mg, 3.01 mmol, 1 equiv.) to give *the title compound* as a clear oil (604 mg, >100%); carried forward without further purification; $\mathbf{R_f}$ 0.66 (50% EtOAc in hexanes); **^{1}H NMR** (200 MHz, $CDCl_3$) δ: 7.58–7.08 (m, 5H), 4.37–3.98 (m, 3H), 3.91–3.71 (m, 2H), 1.22 (t, *J* 7.1, 3H) (alcohol OH signal not seen). Spectroscopic data matched those in the literature.[403]

Ethyl 2-phenyl-3-((tetrahydro-2*H*-pyran-2-yl)oxy)propanoate 213

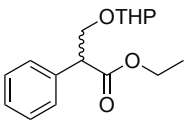

Compound **212** (4.78 g, 24.6 mmol, 1.0 equiv.) was dissolved in CH_2Cl_2 (123 mL). *p*-TsOH (848 mg, 4.92 mmol, 0.2 equiv.) and 3,4-dihydro-2*H*-pyran (2.47 mL, 27.1 mmol, 1.1 equiv.) were added and the reaction stirred at rt overnight. The reaction was quenched with ice cold H_2O (80 mL) and the organic layer separated. The aqueous layer was extracted with CH_2Cl_2 (3 × 50 mL) and the combined organic layers washed with

H_2O (50 mL), brine (40 mL), dried ($MgSO_4$), filtered and concentrated under reduced pressure to give the crude title compound as a brown oil (14.1 g); this intermediate, though novel, was carried forward without purification or characterisation; $\mathbf{R_f}$ 0.84 (50% EtOAc in hexanes).

2-Phenyl-3-((tetrahydro-2*H*-pyran-2-yl)oxy)propan-1-ol 214

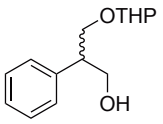

Prepared according to General Procedure 6 from: **213** (6.00 g, 21.6 mmol, 1 equiv.) to give the crude title compound as a orange oil (4.98 g); purified by automated flash chromatography on silica (Biotage Isolera, 25–100% EtOAc in hexanes) to give *the title compound* as a clear pale yellow oil (1.11 g, 22%); $\mathbf{R_f}$ 0.29 (25% EtOAc in hexanes); **^{1}H NMR** (200 MHz, $CDCl_3$) δ: 7.75–6.58 (m, 5H), 4.61 (br s, 1H), 4.35–3.62 (m, 6H), 3.63–3.42 (m, 1H), 3.37–3.04 (m, 1H), 2.75–2.49 (m, 1H), 1.87–1.54 (m, 4H) (alcohol OH signal not seen). Spectroscopic data matched those in the literature.[404]

3-(4-(Difluoromethoxy)phenyl)-5-(2-phenyl-3-((tetrahydro-2*H*-pyran-2-yl)oxy) propoxy)-[1,2,4]triazolo[4,3-*a*]pyrazine 215

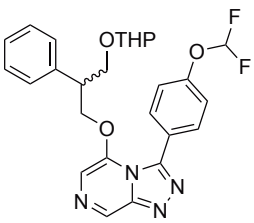

Prepared according to General Procedure 4 from: **214** (983 mg, 4.16 mmol) and **44** (1.23 g, 4.16 mmol) to give the crude title compound as a black sludge (2.13 mg); purified by automated flash chromatography on silica (Biotage Isolera, 25–100% EtOAc in hexanes) to give *the title compound* as a sticky brown solid (1.56 mg, 75%); this intermediate, though novel, was carried forward without characterisation; $\mathbf{R_f}$ 0.41 (100% EtOAc).

3-((3-(4-(Difluoromethoxy)phenyl)-[1,2,4]triazolo[4,3-*a*]pyrazin-5-yl)oxy)-2-phenyl propan-1-ol 24

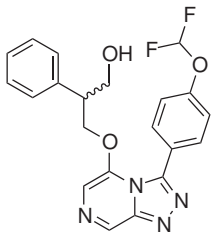

Compound **215** (1.50 g, 2.82 mmol, 1 equiv.) was dissolved in EtOH (30 mL). $CuCl_2{\cdot}2H_2O$ (24.0 mg, 0.14 mmol, 5 mol%) was added and the mixture heated to reflux for 1 h. The solvent was removed and CH_2Cl_2 was added to the residue. The solid was filtered, washed with CH_2Cl_2 and dried *in vacuo* to give *the title compound* as a light brown powder (683 mg, 54%); $\mathbf{R_f}$ 0.18 (100% EtOAc); **m.p.** 154–160 °C; **^{1}H NMR** (400 MHz, DMSO-d$_6$) δ: 9.05 (br s, 1H), 7.66 (d, *J* 8.8, 2H), 7.63 (br s, 1H), 7.35 (t, *J* 73.7, 1H), 7.26–7.12 (m, 5H), 6.98 (dd, *J* 7.4 & 2.0, 2H), 4.80 (t, *J* 5.3, 1H), 4.68–4.38 (m, 2H), 3.39 (t, *J* 5.8, 2H), 2.99 (p, *J* 6.3, 1H); **^{13}C NMR** (101 MHz, DMSO-d$_6$) δ: 151.9, 146.2, 145.2, 139.6, 135.0, 132.4, 128.1, 127.9, 126.6, 124.8, 117.7, 116.2 (t, *J* 258.1), 108.8, 71.7, 61.8, 46.6; ***m/z*** (ESI+) 435 ([M+Na]$^+$, 100%); **HRMS** (ESI+) found 435.12445 [M+Na]$^+$, $C_{21}H_{18}F_2N_4O_3Na^+$ requires 435.12392.

2-Phenylpropane-1,3-diol 216

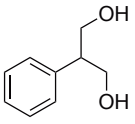

Prepared according to General Procedure 6 from: diethyl phenylmalonate (8.00 g, 33.9 mmol, 1.00 equiv.) with $LiAlH_4$ (1 M in THF, 77.2 mL, 77.2 mmol, 2.28 equiv.) to give the crude title compound as a clear yellow oil; purified by automated flash chromatography on silica (Biotage Isolera, 0–10% MeOH in CH_2Cl_2) to give *the title compound* as a clear colourless oil (2.98 g, 58%); **^{1}H NMR** (200 MHz, $CDCl_3$) δ: 7.43–7.16 (m, 5H), 4.11–3.82 (m, 4H), 3.24–3.00 (m, 1H), 2.09 (br s, 2H). Spectroscopic data matched those in the literature.[405]

3-((3-(4-(Difluoromethoxy)phenyl)-[1,2,4]triazolo[4,3-*a*]pyrazin-5-yl)oxy)-2-phenyl propanoic acid 208

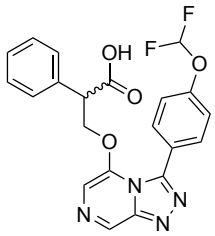

Compound **24** (100 mg, 0.24 mmol, 1 equiv.) was dissolved in acetone (4.33 mL) and cooled to 0 °C. Jones reagent (2.5 M, 194 μL, 0.48 mmol, 2 equiv.) was added in 3 portions (64.7 μL each) with 20 min intervals between additions. After stirring for 20 min, the reaction was quenched with excess isopropanol and stirred for a further 10 min. The mixture was diluted with H_2O and the organic solvents removed. The aqueous phase was diluted with H_2O and extracted with EtOAc (4 ×), washed with brine, dried (Na_2SO_4), filtered and concentrated under reduced pressure to give the crude title compound as a brownish-yellow solid (97.7 mg); purified by manual column chromatograph on silica (75–100% EtOAc in hexanes) to give *the title compound* as an off-white powder (25.7 mg, 25%); **m.p.** 115–120 °C; **IR** ν_{max} (film) /cm^{-1} 1716; **^{1}H NMR** (400 MHz, DMSO-d$_6$) δ: 9.06 (s, 1H), 7.72 (d, *J* 8.8, 2H), 7.69 (s, 1H), 7.33 (t, *J* 73.6, 1H), 7.31–7.26 (m, 5H), 7.14–7.10 (m, 2H), 4.79 (t, *J* 9.0, 1H), 4.64–4.36 (m, 1H), 3.80 (dd, *J* 8.4, 5.6, 1H), 3.38 (dd$_{app}$, *J* 14.1 & 7.1, 1H); **^{13}C NMR** (101 MHz, DMSO-d$_6$) δ: 171.9, 152.0, 147.4, 145.5, 143.6, 135.4, 135.1, 132.3, 128.6, 128.0, 127.7, 124.5, 117.7, 116.3, 109.0, 71.1, 49.6; ***m/z*** (ESI+) 449 ([M+Na]$^+$, 41%), 471 ([M-H+2Na]$^+$, 100%); **HRMS** (ESI+) found 427.12162 [M+H]$^+$, $C_{21}H_{16}F_2N_4O_4H^+$ requires 427.12124.

Diethyl 2-(3,4-difluorophenyl)malonate 217

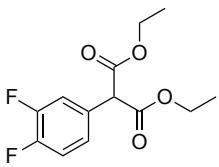

Prepared according to General Procedure 8 from: **52** (1.00 g, 5.00 mmol, 1.00 equiv.) to give the crude title compound as a brown liquid (2.68 g); purified by automated flash chromatography on silica (Biotage Isolera, 0–10% EtOAc in hexanes) to give *the title compound* as a clear yellow oil (1.25 g, 92%); **^{1}H NMR** (200 MHz, $CDCl_3$) δ: 7.46–6.98 (m, 3H), 4.55 (s, 1H), 4.19 (q, *J* 7.1, 4H), 1.28 (q, *J* 7.3, 6H). Spectroscopic data matched those in the literature.[360]

2-(3,4-Difluorophenyl)propane-1,3-diol 218

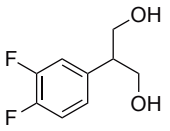

Prepared according to General Procedure 6 from: **217** (1.00 g, 3.67 mmol, 1 equiv.) with $LiAlH_4$ (1 M in THF, 11.0 mL, 11.0 mmol, 3 equiv.) to give the crude title compound as a clear colourless oil (666 mg); purified by automated flash chromatography on silica (Biotage Isolera, 25–100% EtOAc in hexanes) to give *the title compound* as a clear colourless oil (189 mg, 27%); this intermediate, though novel, was carried forward without complete characterisation; $\mathbf{R_f}$ 0.12 (50% EtOAc in hexanes); **^{1}H NMR** (200 MHz, $CDCl_3$) δ: 7.23–6.80 (m, 3H), 4.07–3.83 (m, 4H), 3.05 (p, *J* 6.4, 1H), 2.15–1.92 (m, 2H).

Ethyl 2-(2-fluorophenyl)acetate 281

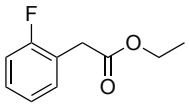

Prepared according to General Procedure 7 from: 2-(2-fluorophenyl)acetic acid (2.00 g, 13.0 mmol) to give *the title compound* as a clear colourless oil (2.25 g, 95%); carried forward without further purification; $\mathbf{R_f}$ 0.81 (25% EtOAc in hexanes); **^{1}H NMR** (200 MHz, $CDCl_3$) δ: 7.42–7.15 (m, 2H), 7.16–6.93 (m, 2H), 4.16 (q, *J* 7.1, 2H), 3.65 (s, 2H), 1.24 (t, *J* 7.1, 3H). Spectroscopic data matched those in the literature.[406]

Ethyl 2-(3-fluorophenyl)acetate 282

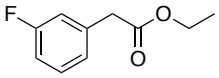

Prepared according to General Procedure 7 from: 2-(3-fluorophenyl)acetic acid (2.00 g, 13.0 mmol) to give *the title compound* as a clear colourless oil (2.11 g, 89%); carried forward without further purification or characterisation; $\mathbf{R_f}$ 0.89 (25% EtOAc in hexanes).

Ethyl 2-(2,4,6-trifluorophenyl)acetate 283

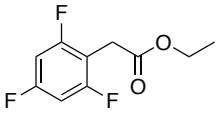

Prepared according to General Procedure 7 from: 2-(2,4,6-trifluorophenyl) acetic acid (600 mg, 3.16 mmol) to give *the title compound* as a clear colourless oil (630 mg, 91%); carried forward without further purification or characterisation; $\mathbf{R_f}$ 0.85 (25% EtOAc in hexanes).

Ethyl 2-(2,4,5-trifluorophenyl)acetate 284

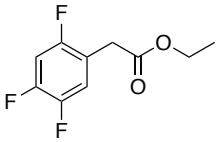

Prepared according to General Procedure 7 from: 2-(2,4,5-trifluorophenyl) acetic acid (1.00 g, 5.26 mmol) to give *the title compound* as a clear colourless oil (1.08 g, 94%); carried forward without further purification or characterisation; $\mathbf{R_f}$ 0.95 (25% EtOAc in hexanes).

Ethyl 2-(4-fluoro-3-(trifluoromethyl)phenyl)acetate 285

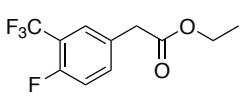

Prepared according to General Procedure 7 from: 2-(4-fluoro-3-(trifluoromethyl)phenyl)acetic acid (1.00 g, 4.50 mmol) to give *the title compound* as a clear colourless oil (1.03 g, 91%); this intermediate, though novel, was carried forward without purification or characterisation; $\mathbf{R_f}$ 0.82 (25% EtOAc in hexanes).

Ethyl 2-(3-(trifluoromethyl)phenyl)acetate 286

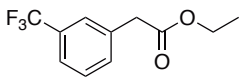

Prepared according to General Procedure 7 from: 2-(3-(trifluoromethyl) phenyl)acetic acid (1.00 g, 4.90 mmol) to give *the title compound* as a clear colourless oil (1.05 g, 92%); carried forward without further purification or characterisation; $\mathbf{R_f}$ 0.81 (25% EtOAc in hexanes).

Ethyl 2-(3,5-bis(trifluoromethyl)phenyl)acetate 287

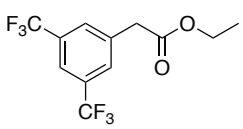

Prepared according to General Procedure 7 from: 2-(3,5-bis(trifluoromethyl) phenyl)acetic acid (1.00 g, 3.67 mmol) to give *the title compound* as a clear colourless oil (1.03 g, 94%); carried forward without further purification or characterisation; $\mathbf{R_f}$ 0.85 (25% EtOAc in hexanes).

Ethyl 2-(2-methoxyphenyl)acetate 288

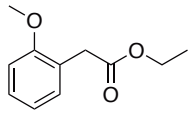

Prepared according to General Procedure 7 from: 2-(2-methoxyphenyl)acetic acid (1.00 g, 6.02 mmol) to give *the title compound* as a clear colourless oil (1.10 g, 94%); carried forward without further purification or characterisation; $\mathbf{R_f}$ 0.89 (25% EtOAc in hexanes).

Ethyl 2-(3-methoxyphenyl)acetate 289

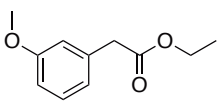

Prepared according to General Procedure 7 from: 2-(3-methoxyphenyl)acetic acid (1.00 g, 6.02 mmol) to give *the title compound* as a clear colourless oil (1.11 g, 95%); carried forward without further purification or characterisation; $\mathbf{R_f}$ 0.86 (25% EtOAc in hexanes).

Ethyl 2-(4-(trifluoromethoxy)phenyl)acetate 290

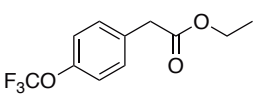

Prepared according to General Procedure 7 from: 2-(4-(trifluoromethoxy) phenyl)acetic acid (600 mg, 2.73 mmol) to give *the title compound* as a clear pale yellow oil (615 g, 91%); carried forward without further purification or characterisation; $\mathbf{R_f}$ 0.70 (25% EtOAc in hexanes).

Diethyl 2-(2-fluorophenyl)malonate 291

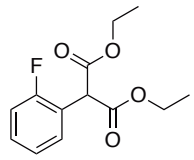

Prepared according to General Procedure 8 from: **281** (2.00 g, 11.0 mmol) to give the crude title compound as an opaque white liquid (6.41 g); purified by automated flash chromatography on silica (Biotage Isolera, 0–15% EtOAc in hexanes) to give *the title compound* as a clear colourless oil (2.56 g, 92%); $\mathbf{R_f}$ 0.51 (10% EtOAc in hexanes); **^{1}H NMR** (200 MHz, $CDCl_3$) δ: 7.47 (td, J 7.5 & 1.6, 1H), 7.39–7.26 (m, 1H), 7.22–6.98 (m, 2H), 4.97 (s, 1H), 4.59–3.94 (m, 4H), 1.27 (t, J 7.1, 6H). Spectroscopic data matched those in the literature.[407]

Diethyl 2-(3-fluorophenyl)malonate 292

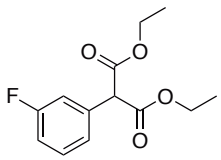

Prepared according to General Procedure 8 from: **282** (2.00 g, 11.0 mmol) to give the crude title compound as an orange liquid (6.22 g); purified by automated flash chromatography on silica (Biotage Isolera, 0–15% EtOAc in hexanes) to give *the title compound* as a clear pale yellow oil (2.03 g, 73%); carried forward without characterisation; $\mathbf{R_f}$ 0.42 (10% EtOAc in hexanes).

Diethyl 2-(2,4,6-trifluorophenyl)malonate 293

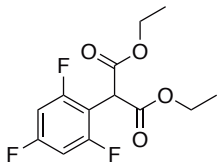

Prepared according to General Procedure 8 from: **283** (550 mg, 2.52 mmol) to give the crude title compound as a yellow oil (1.59 g); purified by automated flash chromatography on silica (Biotage Isolera, 0–15% EtOAc in hexanes) to give *the title compound* as a clear pale yellow oil (515 mg, 70%); carried forward without characterisation; $\mathbf{R_f}$ 0.44 (10% EtOAc in hexanes).

Diethyl 2-(2,4,5-trifluorophenyl)malonate 294

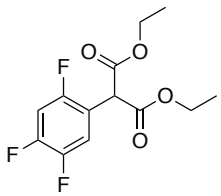

Prepared according to General Procedure 8 from: **284** (800 mg, 3.67 mmol) to give the crude title compound as a clear yellow oil (1.75 g); purified by automated flash chromatography on silica (Biotage Isolera, 0–15% EtOAc in hexanes) to give *the title compound* as a clear pale yellow oil (946 mg, 89%); carried forward without characterisation; $\mathbf{R_f}$ 0.52 (10% EtOAc in hexanes).

Diethyl 2-(4-fluoro-3-(trifluoromethyl)phenyl)malonate 295

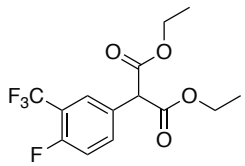

Prepared according to General Procedure 8 from: **285** (800 mg, 3.20 mmol) to give the crude title compound as a clear orange oil (1.66 g); purified by automated flash chromatography on silica (Biotage Isolera, 0–15% EtOAc in hexanes) to give *the title compound* as a clear yellow oil (512 mg, 50%); this

intermediate, though novel, was carried forward without characterisation; $\mathbf{R_f}$ 0.34 (10% EtOAc in hexanes).

Diethyl 2-(3-(trifluoromethyl)phenyl)malonate 296

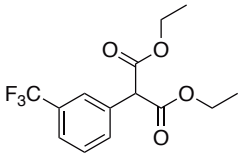

Prepared according to General Procedure 8 from: **286** (800 mg, 3.54 mmol) to give the crude title compound as a clear orange oil (1.65 g); purified by automated flash chromatography on silica (Biotage Isolera, 0–15% EtOAc in hexanes) to give *the title compound* as a clear colourless oil (756 mg, 72%); carried forward without characterisation; $\mathbf{R_f}$ 0.42 (10% EtOAc in hexanes).

Diethyl 2-(3,5-bis(trifluoromethyl)phenyl)malonate 297

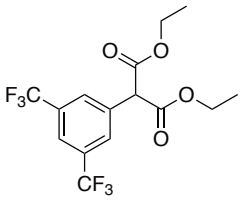

Prepared according to General Procedure 8 from: **287** (800 mg, 2.66 mmol) to give the crude title compound as a clear orange oil (1.50 g); purified by automated flash chromatography on silica (Biotage Isolera, 0–15% EtOAc in hexanes) to give *the title compound* as a clear yellow oil (775 mg, 78%); carried forward without characterisation; $\mathbf{R_f}$ 0.50 (10% EtOAc in hexanes).

Diethyl 2-(2-methoxyphenyl)malonate 298

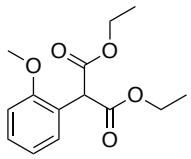

Prepared according to General Procedure 8 from: **288** (800 mg, 4.12 mmol) to give the crude title compound as a clear pale yellow oil (2.09 g); purified by automated flash chromatography on silica (Biotage Isolera, 0–15% EtOAc in hexanes) to give *the title compound* as a clear colourless oil (846 mg, 77%); carried forward without characterisation; $\mathbf{R_f}$ 0.27 (10% EtOAc in hexanes).

Diethyl 2-(3-methoxyphenyl)malonate 299

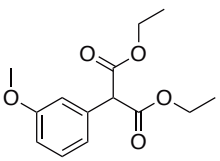

Prepared according to General Procedure 8 from: **289** (800 mg, 4.12 mmol) to give the crude title compound as a clear pale yellow oil (2.11 g); purified by automated flash chromatography on silica (Biotage Isolera, 0–15% EtOAc in hexanes) to give *the title compound* as a clear pale yellow oil (918 mg, 83%); carried forward without characterisation; $\mathbf{R_f}$ 0.31 (10% EtOAc in hexanes).

Diethyl 2-(4-(trifluoromethoxy)phenyl)malonate 300

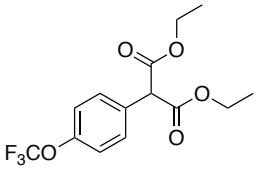

Prepared according to General Procedure 8 from: **290** (550 mg, 2.22 mmol) to give the crude title compound as a clear yellow oil (1.23 g); purified by automated flash chromatography on silica (Biotage Isolera, 0–15% EtOAc in hexanes) to give *the title compound* as a clear pale yellow oil (542 mg, 76%); carried forward without characterisation; $\mathbf{R_f}$ 0.47 (10% EtOAc in hexanes).

2-(2-Fluorophenyl)propane-1,3-diol 301

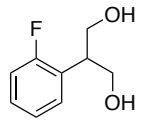

Prepared according to General Procedure 9 from: **291** (1.00 g, 3.93 mmol) to give the crude title compound as a viscous clear colourless oil (640 mg); purified by automated flash chromatography on silica (Biotage Isolera, 25–100% EtOAc in hexanes) to give *the title compound* as a viscous clear colourless oil (295 mg, 44%); this intermediate, though novel, was carried forward without complete characterisation; $\mathbf{R_f}$ 0.09 (25% EtOAc in hexanes); **^{1}H NMR** (400 MHz, $CDCl_3$) δ: 7.36–7.16 (m, 2H), 7.15–6.99 (m, 2H), 4.12 (dt, *J* 14.3 & 5.3, 2H), 3.98 (ddd, *J* 29.1, 10.7 & 6.5, 2H), 3.50–3.37 (m, 1H), 2.61 (br s, 2H); **^{19}F NMR** (376 MHz, $CDCl_3$) δ: -117.58.

2-(3-Fluorophenyl)propane-1,3-diol 302

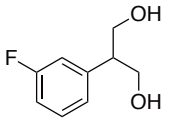

Prepared according to General Procedure 9 from: **292** (1.00 g, 3.93 mmol) to give the crude title compound as a viscous clear colourless oil (586 mg); purified by automated flash chromatography on silica (Biotage Isolera, 25–100% EtOAc in hexanes) to give *the title compound* as a viscous clear colourless oil (229 mg, 34%); this intermediate, though novel, was carried forward without complete characterisation; $\mathbf{R_f}$ 0.08 (25% EtOAc in hexanes); **^{1}H NMR** (400 MHz, $CDCl_3$) δ: 7.33–7.24 (m, 1H), 7.05–6.89 (m, 3H), 4.16–3.86 (m, 4H), 3.07 (p, *J* 7.1 & 6.4, 1H), 2.51 (br s, 2H); **^{19}F NMR** (376 MHz, $CDCl_3$) δ: -112.68.

2-(2,4,6-Trifluorophenyl)propane-1,3-diol 303

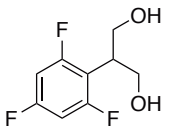

Prepared according to General Procedure 9 from: **293** (300 mg, 1.03 mmol) to give the crude title compound as a clear colourless oil (250 mg); purified by automated flash chromatography on silica (Biotage Isolera, 25–100% EtOAc in hexanes) to give *the title compound* as a white powder (79.0 mg, 37%); this intermediate, though novel, was carried forward without characterisation; $\mathbf{R_f}$ 0.09 (25% EtOAc in hexanes).

2-(2,4,5-Trifluorophenyl)propane-1,3-diol 304

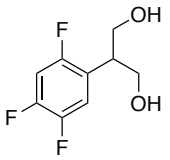

Prepared according to General Procedure 9 from: **294** (900 mg, 3.10 mmol) to give the crude title compound as a clear pale yellow oil (394 mg); purified by automated flash chromatography on silica (Biotage Isolera, 25–100% EtOAc in hexanes) to give *the title compound* as a viscous clear colourless oil (181 mg, 28%); this intermediate, though novel, was carried forward without complete characterisation; $\mathbf{R_f}$ 0.11 (25% EtOAc in hexanes); **^{1}H NMR** (400 MHz, $CDCl_3$) δ: 7.29–7.13 (m, 1H), 6.92 (td, *J* 9.8 & 6.7, 1H), 3.98 (d, *J* 5.9, 4H), 3.35 (p, *J* 6.1, 1H), 2.05 (br s, 2H).

2-(4-Fluoro-3-(trifluoromethyl)phenyl)propane-1,3-diol 305

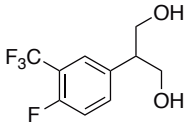

Prepared according to General Procedure 9 from: **295** (450 mg, 1.40 mmol) to give the crude title compound as a viscous clear colourless oil (358 mg); purified by automated flash chromatography on silica (Biotage Isolera, 25–100% EtOAc in hexanes) to give *the title compound* as a viscous pale yellow oil (217 mg, 65%); this intermediate, though novel, was carried forward without complete characterisation; $\mathbf{R_f}$ 0.03 (25% EtOAc in hexanes); **^{1}H NMR** (400 MHz, $CDCl_3$) δ: 7.55–7.37 (m, 2H), 7.17 (t, *J* 9.4, 1H), 4.34–3.81 (m, 4H), 3.19–3.06 (m, 1H), 1.94 (br s, 2H).

2-(3-(Trifluoromethyl)phenyl)propane-1,3-diol 306

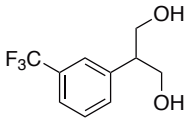

Prepared according to General Procedure 9 from: **296** (700 mg, 2.30 mmol) to give the crude title compound as a viscous clear colourless oil (293 mg); purified by automated flash chromatography on silica (Biotage Isolera, 25–100% EtOAc in hexanes) to give *the title compound* as a viscous clear colourless oil (108 mg, 21%); this intermediate, though novel, was carried forward without complete characterisation; $\mathbf{R_f}$ 0.08 (25% EtOAc in hexanes); **^{1}H NMR** (400 MHz, $CDCl_3$) δ: 7.56–7.50 (m, 2H), 7.46 (d, *J* 4.7, 2H), 4.02 (dtt, *J* 16.3, 11.1 & 5.4, 4H), 3.16 (p, *J* 6.4, 1H), 1.99 (t, *J* 5.2, 2H).

2-(3,5-Bis(trifluoromethyl)phenyl)propane-1,3-diol 307

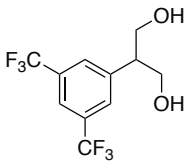

Prepared according to General Procedure 9 from: **297** (700 mg, 1.88 mmol) to give the crude title compound as a viscous clear colourless oil (489 mg); purified by automated flash chromatography on silica (Biotage Isolera, 25–100% EtOAc in hexanes) to give *the title compound* as a viscous clear colourless oil (54.9 mg, 10%); $\mathbf{R_f}$ 0.06 (25% EtOAc in hexanes); **^{1}H NMR** (400 MHz, $CDCl_3$) δ: 7.79 (s, 1H), 7.76 (s, 2H), 4.04 (d_{app}, *J* 5.6, 4H), 3.20 (p, *J* 6.5, 1H), 1.99 (br s, 2H). Spectroscopic data matched those in the literature.[405]

2-(2-Methoxyphenyl)propane-1,3-diol 308

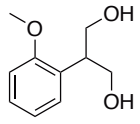

Prepared according to General Procedure 9 from: **298** (800 mg, 3.00 mmol) to give the crude title compound as a viscous clear colourless oil (554 mg); purified by automated flash chromatography on silica (Biotage Isolera, 25–100% EtOAc in hexanes) to give *the title compound* as a viscous clear colourless oil (306 mg, 56%); $\mathbf{R_f}$ 0.05 (25% EtOAc in hexanes); **^{1}H NMR** (400 MHz, $CDCl_3$) δ: 7.20 (ddd, J 22.4, 7.6 & 1.5, 2H), 6.99–6.81 (m, 2H), 4.09–3.89 (m, 4H), 3.83 (s, 3H), 3.55 (ddd, J 12.7, 7.4 & 5.3, 1H) (diol OH signals not seen). Spectroscopic data matched those in the literature.[408]

2-(3-Methoxyphenyl)propane-1,3-diol 309

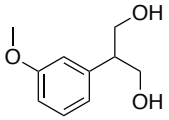

Prepared according to General Procedure 9 from: **299** (850 mg, 3.19 mmol) to give the crude title compound as a viscous clear colourless oil (573 mg); purified by automated flash chromatography on silica (Biotage Isolera, 25–100% EtOAc in hexanes) to give *the title compound* as a viscous clear colourless oil (300 mg, 52%); carried forward without characterisation; $\mathbf{R_f}$ 0.06 (25% EtOAc in hexanes).

2-(4-(Trifluoromethoxy)phenyl)propane-1,3-diol 310

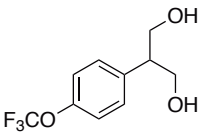

Prepared according to General Procedure 9 from: **300** (400 mg, 1.25 mmol) to give the crude title compound as an opaque white liquid (326 mg); purified by automated flash chromatography on silica (Biotage Isolera, 25–100% EtOAc in hexanes) to give *the title compound* as a white solid (240 mg, 81%); this intermediate, though novel, was carried forward without characterisation; $\mathbf{R_f}$ 0.09 (25% EtOAc in hexanes).

3-((3-(4-(Difluoromethoxy)phenyl)-[1,2,4]triazolo[4,3-*a*]pyrazin-5-yl)oxy)-2-(2-fluorophenyl)propan-1-ol 219

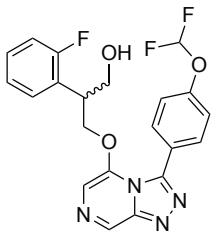

Prepared according to General Procedure 4 from: **301** (57.4 mg, 0.34 mmol) and **44** (100 mg, 0.34 mmol) to give the crude title compound as a dark brown solid (84.1 mg); purified by preparative reversed-phase LCMS (5–100% MeCN in H_2O) to give *the title compound* as a light brown powder (6.60 mg, 5%); insufficient material remaining for complete characterisation; **^{1}H NMR** (400 MHz, $CDCl_3$) δ: 9.02 (s, 1H), 7.55 (d, J 8.6, 2H), 7.40 (s, 1H), 7.34–7.20 (m, 1H), 7.12 (d, J 8.5, 2H), 7.08–6.99 (m, 2H), 6.94 (t, J 7.6, 1H), 6.61 (t, J 73.3, 1H), 4.59 (p, J 9.4, 2H), 3.64 (ddd, J 32.9, 10.9 & 6.0, 2H), 3.43 (p, J 6.3, 1H) (alcohol OH signal not seen); ***m/z*** (ESI+) 431 ($[M+H]^+$, 100%); **HRMS** (ESI+) found 431.13196 $[M+H]^+$, $C_{21}H_{17}F_3N_4O_3H^+$ requires 431.13255.

3-((3-(4-(Difluoromethoxy)phenyl)-[1,2,4]triazolo[4,3-*a*]pyrazin-5-yl)oxy)-2-(2,4,6-trifluorophenzyl)propan-1-ol 221

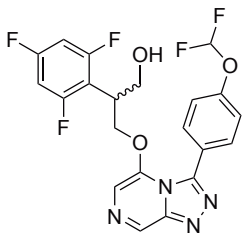

Prepared according to General Procedure 4 from: **303** (68.0 mg, 0.33 mmol) and **44** (97.9 mg, 0.33 mmol) to give the crude title compound as a dark brown solid (107 mg); purified by automated flash chromatography on silica (Biotage Isolera, 25–100% EtOAc in hexanes) to give *the title compound* as a yellow powder (17.3 mg, 11%); insufficient material remaining for complete characterisation; **m.p.** 140–146 °C; **^{1}H NMR** (500 MHz, $CDCl_3$) δ: 9.05 (s, 1H), 7.58 (d, *J* 8.7, 2H), 7.39 (s, 1H), 7.16 (d, *J* 8.6, 2H), 6.64 (t, *J* 73.3, 1H), 6.61 (t, *J* 8.5, 2H), 4.85–4.49 (m, 2H), 3.73–3.59 (m, 2H), 3.54 (p, *J* 7.0, 1H) (alcohol OH signal not seen); ***m/z*** (ESI+) 467 ($[M+H]^+$, 100%); **HRMS** (ESI+) found 467.11377 $[M+H]^+$, $C_{21}H_{15}F_5N_4O_3H^+$ requires 467.11371.

3-((3-(4-(difluoromethoxy)phenyl)-[1,2,4]triazolo[4,3-a]pyrazin-5-yl)oxy)-2-(2,4,5-trifluorophenyl)propan-1-ol 222

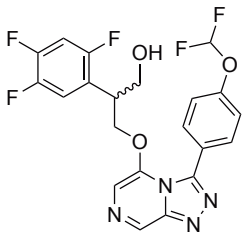

Prepared according to General Procedure 4 from: **304** (85.0 mg, 0.41 mmol) and **44** (122 mg, 0.41 mmol) to give the crude title compound as a dark brown solid (178 mg); purified by preparative reversed-phase LCMS (5–95% MeCN in H_2O) to give an orange solid (46.2 mg, 24%); repurified by automated reversed-phase flash chromatography on silica (Biotage Isolera, 5–75% MeCN in H_2O) to give *the title compound* as a white powder (18.6 mg, 10%); insufficient material remaining for complete characterisation; **^{1}H NMR** (400 MHz, $CDCl_3$) δ: 9.03 (s, 1H), 7.61 (d, *J* 8.7, 2H), 7.38 (s, 1H), 7.20 (d, *J* 8.6, 2H), 6.90 (td, *J* 9.8 & 6.6, 1H), 6.73 (ddd, *J* 10.5, 8.5 & 6.8, 1H), 6.62 (t, *J* 73.1, 1H), 4.62–4.37 (m, 2H), 3.68–3.54 (m, 2H), 3.37 (p, *J* 6.2, 1H) (alcohol OH signal not seen); ***m/z*** (ESI+) 467 ($[M+H]^+$, 100%); **HRMS** (ESI+) found 467.11453 $[M+H]^+$, $C_{21}H_{15}F_5N_4O_3H^+$ requires 467.11371.

3-((3-(4-(Difluoromethoxy)phenyl)-[1,2,4]triazolo[4,3-*a*]pyrazin-5-yl)oxy)-2-(4-fluoro-3-(trifluoromethyl)phenyl)propan-1-ol 223

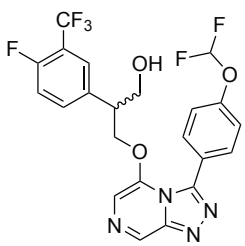

Prepared according to General Procedure 4 from: **305** (65.3 mg, 0.27 mmol) and **44** (81.3 mg, 0.27 mmol) to give the crude title compound as a dark brown solid (133 mg); purified by preparative reversed-phase LCMS (5–95% MeCN in H_2O) to give a pale yellow solid (5.00 mg, 4%); repurified by automated reversed-phase flash chromatography on silica (Biotage Isolera, 5–75% MeCN in H_2O) to give *the title compound* as a light brown powder (trace amounts); the data obtained suggested the desired product was formed, however there was insufficient material

remaining for complete characterisation; ***m/z*** (ESI+) 499 ($[M+H]^+$, 100%).

3-((3-(4-(Difluoromethoxy)phenyl)-[1,2,4]triazolo[4,3-*a*]pyrazin-5-yl)oxy)-2-(3-(trifluoromethyl)phenyl)propan-1-ol 224

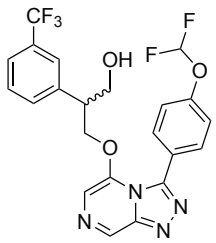

Prepared according to General Procedure 4 from: **306** (28.4 mg, 0.13 mmol) and **44** (38.3 mg, 0.13 mmol) to give the crude title compound as a dark brown solid (58.6 mg); purified by preparative reversed-phase LCMS (5–100% MeCN in H_2O) to give *the title compound* as a light brown powder (6.70 mg, 10%); insufficient material remaining for complete characterisation; **^{1}H NMR** (500 MHz, $CDCl_3$) δ: 9.05 (s, 1H), 7.61 (d, *J* 8.7, 2H), 7.54 (d, *J* 7.8, 1H), 7.41 (d, *J* 7.9, 1H), 7.39 (s, 1H), 7.32 (br s, 1H), 7.18 (d, *J* 8.6, 2H), 7.15 (d, *J* 7.9, 1H), 6.62 (t, *J* 73.1, 1H), 4.56 (ddd, *J* 54.3, 9.3 & 6.7, 2H), 3.61 (ddt, *J* 42.2, 11.1 & 5.6, 2H), 3.15 (p, *J* 6.2, 1H) (alcohol OH signal not seen); ***m/z*** (ESI+) 481 ($[M+H]^+$, 100%); **HRMS** (ESI+) found 481.13071 $[M+H]^+$, $C_{22}H_{17}F_5N_4O_3H^+$ requires 481.12936.

2-(3,5-Bis(trifluoromethyl)phenyl)-3-((3-(4-(difluoromethoxy)phenyl)-[1,2,4]triazolo[4,3-a]pyrazin-5-yl)oxy)propan-1-ol 225

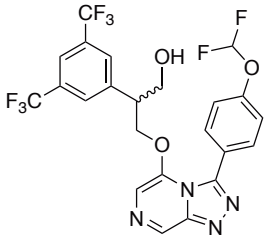

Prepared according to General Procedure 4 from: **307** (29.3 mg, 0.10 mmol) and **44** (30.2 mg, 0.10 mmol) to give the crude title compound as a dark brown solid (46.5 mg); purified by preparative reversed-phase LCMS (5–95% MeCN in H_2O) to give *the title compound* as a light brown powder (trace amounts); the data obtained suggested the desired product was formed, however there was insufficient material remaining for complete characterisation; ***m/z*** (ESI+) 549 ($[M+H]^+$, 100%).

3-((3-(4-(Difluoromethoxy)phenyl)-[1,2,4]triazolo[4,3-*a*]pyrazin-5-yl)oxy)-2-(2-methoxyphenyl)propan-1-ol 226

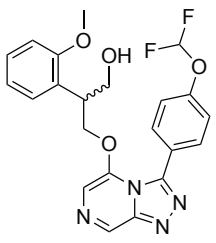

Prepared according to General Procedure 4 from: **308** (88.7 mg, 0.49 mmol) and **44** (144 mg, 0.49 mmol) to give the crude title compound as a dark brown solid (177 mg); purified by preparative reversed-phase LCMS (5–100% MeCN in H_2O) to give *the title compound* as an off-white powder (4.1 mg, 2%); insufficient material remaining for complete characterisation; **^{1}H NMR** (400 MHz, $CDCl_3$) δ: 9.02 (s, 1H), 7.59 (d, *J* 8.7, 2H), 7.39 (s, 1H), 7.29–7.22 (m, 1H), 7.12 (d, *J* 8.6, 2H), 6.88 (t, *J* 7.8, 3H), 6.60 (t, *J* 73.4, 1H), 4.56 (d, *J* 6.5, 2H), 3.82 (s, 3H), 3.71–3.46 (m, 3H) (alcohol OH signal not seen); ***m/z*** (ESI+) 443 ($[M+H]^+$, 100%); **HRMS** (ESI+) found

433.15332 $[M+H]^+$, $C_{22}H_{20}F_2N_4O_4H^+$ requires 443.15254.

3-((3-(4-(Difluoromethoxy)phenyl)-[1,2,4]triazolo[4,3-*a*]pyrazin-5-yl)oxy)-2-(3-methoxyphenyl)propan-1-ol 227

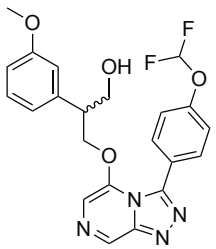

Prepared according to General Procedure 4 from: **309** (104 mg, 0.57 mmol) and **44** (170 mg, 0.57 mmol) to give the crude title compound as a dark brown solid (211 mg); purified by preparative reversed-phase LCMS (5–100% MeCN in H_2O) to give *the title compound* as a light brown powder (3.1 mg, 1%); insufficient material remaining for complete characterisation; **^{1}H NMR** (400 MHz, $CDCl_3$) δ: 9.03 (s, 1H), 7.57 (d, *J* 8.6, 2H), 7.38 (s, 1H), 7.22 (t, *J* 8.2, 1H), 7.14 (d, *J* 8.5, 2H), 6.87–6.77 (m, 2H), 6.61–6.57 (m, 1H), 6.53 (t, *J* 73.4, 1H), 4.52 (ddd, *J* 30.4, 9.3 & 7.1, 2H), 3.79 (s, 3H), 3.57 (ddd, *J* 44.7, 10.8 & 5.8, 2H), 3.12–3.01 (m, 1H) (alcohol OH signal not seen); ***m/z*** (ESI+) 443 ($[M+H]^+$, 100%); **HRMS** (ESI+) found 443.15274 $[M+H]^+$, $C_{22}H_{20}F_2N_4O_4H^+$ requires 443.15254.

3-((3-(4-(difluoromethoxy)phenyl)-[1,2,4]triazolo[4,3-a]pyrazin-5-yl)oxy)-2-(4-(trifluoromethoxy)phenyl)propan-1-ol 228

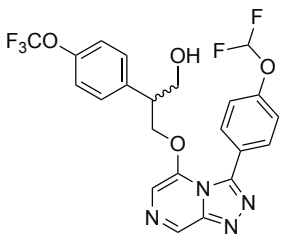

Prepared according to General Procedure 4 from: **310** (100 mg, 0.42 mmol) and **44** (126 mg, 0.42 mmol) to give the crude title compound as a dark brown solid (176 mg); purified by preparative reversed-phase LCMS (5–100% MeCN in H_2O) to give a light brown powder (2.1 mg, 1%); repurified by automated reversed-phase flash chromatography on silica (Biotage Isolera, 5–75% MeCN in H_2O) to give *the title compound* as a pale yellow solid (trace amounts); the data obtained suggested the desired product was formed, however there was insufficient material remaining for complete characterisation; ***m/z*** (ESI+) 497 ($[M+H]^+$, 100%).

3-((3-(4-(Difluoromethoxy)phenyl)-[1,2,4]triazolo[4,3-*a*]pyrazin-8-yl)oxy)-2-(3-fluorophenyl)propan-1-ol 229

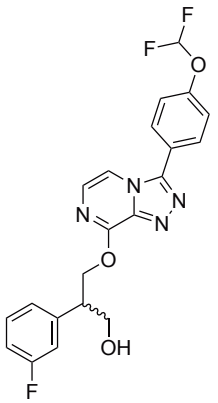

Isolated from the reaction of **302** (80.0 mg, 0.47 mmol, 1 equiv.) with **44** (139 mg, 0.47 mmol, 1 equiv.) according to General Procedure 4; purified by preparative reversed-phase LCMS (5–100% MeCN in H_2O) to give a light brown powder (2.3 mg, 1%); repurified by automated reversed-phase flash chromatography on silica (Biotage Isolera, 5–75% MeCN in H_2O) to give *the title compound* as a light brown powder (1.8 mg, 1%); insufficient material remaining for complete characterisation; **^{1}H NMR** (400 MHz, $CDCl_3$) δ: 7.86 (d, *J* 8.7, 2H), 7.80 (d, *J* 4.9, 1H), 7.41 (d, *J* 4.9, 1H), 7.37 (d, *J* 8.6, 2H), 7.37–7.29 (m, 1H), 7.20 (d_{app}, *J* 7.6, 1H), 7.14 (dt, *J* 10.3 & 2.2, 1H), 7.04–6.91 (m, 1H), 6.63 (t, *J* 72.9, 1H), 5.15–4.84 (m, 2H), 4.04 (br s, 2H), 3.66–3.40 (m, 1H) (alcohol OH signal not seen); ***m/z*** (ESI+) 431 ($[M+H]^+$, 100%); **HRMS** (ESI+) found 431.13367 $[M+H]^+$, $C_{21}H_{17}F_3N_4O_3H^+$ requires 431.13255.

3-((3-(4-(Difluoromethoxy)phenyl)-[1,2,4]triazolo[4,3-*a*]pyrazin-8-yl)oxy)-2-(2,4,5-trifluorophenyl)propan-1-ol 230

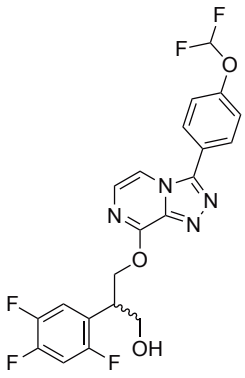

Isolated from the same reaction as for **311** to give *the title compound* as a white powder (4.5 mg, 2%); insufficient material remaining for complete characterisation; **^{1}H NMR** (400 MHz, $CDCl_3$) δ: 7.86 (d, *J* 8.7, 2H), 7.82 (d, *J* 4.9, 1H), 7.47–7.38 (m, 1H), 7.42 (d, *J* 4.9, 1H), 7.37 (d, *J* 8.6, 2H), 6.95 (td, *J* 9.8 & 6.6, 1H), 6.63 (t, *J* 72.9, 1H), 5.06–4.78 (m, 2H), 4.03 (br s, 2H), 3.78 (dq, *J* 10.7 & 5.1, 1H), 2.65 (br s, 1H); ***m/z*** (ESI+) 467 ($[M+H]^+$, 100%); **HRMS** (ESI+) found 467.11353 $[M+H]^+$, $C_{21}H_{15}F_5N_4O_3H^+$ requires 467.11371.

3-((3-(4-(difluoromethoxy)phenyl)-[1,2,4]triazolo[4,3-*a*]pyrazin-5-yl)oxy)-2-(2,4,6-trifluorophenyl)propanoic acid 231

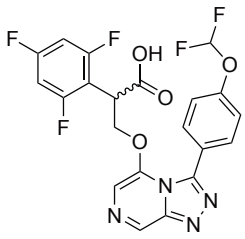

Compound **221** (10.0 mg, 21.4 μmol, 1 equiv.) was dissolved in acetone (0.38 mL) and cooled to 0 °C. Jones reagent (2.5 M, 17.2 μL, 42.9 μmol, 2 equiv.) was added in 3 portions (5.72 μL each) with 20 min intervals between additions. After stirring for 20 min, the reaction was quenched with excess isopropanol and stirred for a further 10 min. The mixture was diluted with H_2O and the organic solvents removed. The aqueous phase was diluted with H_2O

and extracted with EtOAc (4 ×), washed with brine, dried (Na_2SO_4), filtered and concentrated under reduced pressure to give the crude title compound as a yellow powder (10.6 mg); purified by preparative reversed-phase LCMS (5–95% MeCN in H_2O) to give *the title compound* as a light brown powder (2.6 mg, 25%); insufficient material remaining for complete characterisation; **^{1}H NMR** (500 MHz, acetone-d_6) δ: 8.95 (s, 1H), 7.74 (d, *J* 8.7, 2H), 7.66 (s, 1H), 7.26 (d, *J* 8.2, 2H), 7.04–6.86 (m, 2H), 6.69 (t, *J* 73.3, 1H), 5.19–4.97 (m, 1H), 4.69–4.52 (m, 1H), 4.31 (br s, 1H) (acid OH signal not seen); ***m/z*** (ESI+) 481 ($[M+H]^+$, 100%); **HRMS** (ESI+) found 481.09320 $[M+H]^+$, $C_{21}H_{13}F_5N_4O_4H^+$ requires 481.09297.

2-(4-Methoxyphenyl)propane-1,3-diol 232

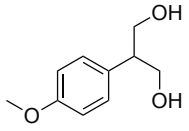

Prepared according to General Procedure 9 from: 1,3-dimethyl 2-(4-methoxyphenyl)propanedioate (500 mg, 2.10 mmol) to give the crude title compound as a viscous clear colourless oil (474 mg); purified by automated flash chromatography on silica (Biotage Isolera, 25–100% EtOAc in hexanes) to give *the title compound* as a white powder (206 mg, 54%); $\mathbf{R_f}$ 0.05 (25% EtOAc in hexanes); **^{1}H NMR** (500 MHz, $CDCl_3$) δ: 7.16 (d, J 8.7, 2H), 6.88 (d, *J* 8.7, 2H), 4.11–3.85 (m, 4H), 3.79 (s, 3H), 3.07 (ddd, *J* 13.2, 7.5 & 5.7, 1H), 2.01 (br s, 2H); **^{13}C NMR** (126 MHz, $CDCl_3$) δ: 158.9, 131.2, 129.2, 114.4, 66.4, 55.4, 49.1. Spectroscopic data matched those in the literature.[405]

3-((3-(4-(Difluoromethoxy)phenyl)-[1,2,4]triazolo[4,3-*a*]pyrazin-5-yl)oxy)-2-(4-methoxyphenyl)propan-1-ol 233

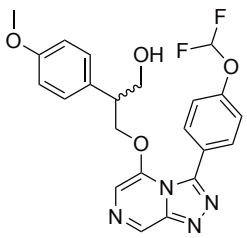

t-BuOK (185 mg, 1.65 mmol, 2.0 equiv.) was added portionwise to a stirred solution of **232** (150 mg, 0.82 mmol, 1.0 equiv.) in 1,4-dioxane (15 mL, 55 mM) at rt. **44** (195 mg, 0.66 mmol, 0.8 equiv.) was added and the reaction allowed to warm to rt and stirred for 1 h. CH_2Cl_2 and K_2CO_3 were added and the mixture was filtered and concentrated under reduced pressure to give the crude title compound as a dark brown sludge (400 mg); purified by automated flash chromatography on silica (Biotage Isolera, 25–100% EtOAc in hexanes) to give *the title compound* as yellow powder (75.1 mg, 21%); **m.p.** 75–80 °C; **^{1}H NMR** (400 MHz, $CDCl_3$) δ: 9.02 (s, 1H), 7.59 (d, *J* 8.6, 2H), 7.36 (s, 1H), 7.17 (d, *J* 8.6, 2H), 6.92 (d, *J* 8.7, 2H), 6.82 (d, *J* 8.6, 2H), 6.62 (t, *J* 73.3, 1H), 4.49 (ddd, *J* 33.4, 9.3 & 6.9, 2H), 3.79 (s, 3H), 3.55 (ddd, *J* 41.0, 10.9 & 6.2, 2H), 3.06 (p, *J* 6.5, 1H); **^{13}C NMR** (101 MHz, $CDCl_3$) δ: 159.3, 147.9, 146.2, 144.7, 144.1, 136.6, 132.4, 129.4, 128.9, 125.1, 119.0, 114.5, 108.6, 71.5, 63.6, 55.4, 46.2 (1 obscured signal); ***m/z*** (ESI+) 443 ($[M+H]^+$, 100%); **HRMS** (ESI+) found 443.15399 $[M+H]^+$, $C_{22}H_{20}F_2N_4O_4H^+$ requires 443.15254.

3-((3-(4-(Difluoromethoxy)phenyl)-[1,2,4]triazolo[4,3-*a*]pyrazin-5-yl)oxy)-2-(4-methoxyphenyl)propanoic acid 234

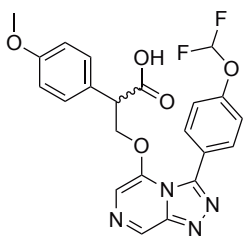

Compound **233** (40.0 mg, 90.4 μmol, 1 equiv.) was dissolved in acetone (1.61 mL) and cooled to 0 °C. Jones reagent (2.5 M, 72.3 μL, 181 μmol, 2 equiv.) was added in 3 portions (24.1 μL each) with 20 min intervals between additions. After stirring for 20 min, the reaction was quenched with excess isopropanol and stirred for a further 10 min. The mixture was diluted with H_2O and the organic solvents removed. The aqueous phase was diluted with H_2O and extracted with EtOAc (4 ×), washed with brine, dried (Na_2SO_4), filtered and concentrated under reduced pressure to give the crude title compound as a yellow powder (37.0 mg); purified by automated reversed-phase flash chromatography on silica (5–75% MeCN in H_2O) to give *the title compound* as an off-white powder (9.50 mg, 23%); insufficient material remaining for complete characterisation; $\mathbf{R_f}$ 0.18 (10% MeOH in CH_2Cl_2); **^{1}H NMR** (400 MHz, CD_3OD) δ: 8.93 (s, 1H), 7.68 (d, *J* 8.7, 2H), 7.55 (s, 1H), 7.25 (d, *J* 8.7, 2H), 7.06 (t, *J* 73.7, 1H), 7.05 (d, *J* 8.6, 2H), 6.76 (d, *J* 8.7, 2H), 4.60 (br s, 1H), 4.44 (t, *J* 8.3, 1H), 3.74 (s, 3H), 3.65 (t, *J* 7.2, 1H) (acid OH signal not seen); ***m/z*** (ESI+) 457 ($[M+H]^+$, 100%); **HRMS** (ESI+) found 457.13211 $[M+H]^+$, $C_{22}H_{18}F_2N_4O_5H^+$ requires 457.13180.

10. References

[1] World Health Organization. Malaria Fact Sheet. http://www.who.int/mediacentre/factsheets/fs094/en/, Accessed 19 Apr 2016.

[2] World Health Organization. World Malaria Report 2018. https://www.who.int/malaria/publications/world-malaria-report-2018/en/, Accessed 27 Nov 2018.

[3] S. I. Hay, A. A. Abajobir, K. H. Abate, *et al.* Global, Regional, and National Disability-Adjusted Life-Years (DALYs) for 333 Diseases and Injuries and Healthy Life Expectancy (HALE) for 195 Countries and Territories, 1990–2016: A Systematic Analysis for the Global Burden of Disease Study 2016. *Lancet* **2017**, *390*, 1260–1344. DOI: 10.1016/S0140-6736(17)32130-X.

[4] C. Cheney. Fight against malaria stalling and could reverse, warns 2017 World Malaria Report. https://www.devex.com/news/fight-against-malaria-stalling-and-could-reverse-warns-2017-world-malaria-report-91636, Accessed 24 Mar 2018.

[5] T. Mwangi. Global malaria report reveals Africa's hits and missed: here's what to do. http://theconversation.com/global-malaria-report-reveals-africas-hits-and-misses-heres-what-to-do-88577, Accessed 24 Mar 2018.

[6] Medicines for Malaria Venture. Definitions and symptoms. https://www.mmv.org/malaria-medicines/definitions-and-symptoms, Accessed 20 Jun 2019.

[7] W. Chin, P. G. Contacos, G. R. Coatney, *et al.* A Naturally Acquired Quotidian-Type Malaria in Man Transferable to Monkeys. *Science* **1965**, *149*, 865–865. DOI: 10.1126/science.149.3686.865.

[8] Centers for Disease Control and Prevention. Lifecycle. https://www.cdc.gov/malaria/about/biology/index.html, Accessed 29 Apr 2019.

[9] J. Achan, A. O. Talisuna, A. Erhart, *et al.* Quinine, an Old Anti-Malarial Drug in a Modern World: Role in the Treatment of Malaria. *Malar. J.* **2011**, *10*, 144. DOI: 10.1186/1475-2875-10-144.

[10] D. Bunnag, J. Karbwang, K. Na-Bangchang, *et al.* Quinine-Tetracycline for Multidrug Resistant Falciparum Malaria. *Southeast Asian J. Trop. Med. Public Health* **1996**, *27*, 15–18.

[11] R. Green. A Report on Fifty Cases of Malaria Treated with Atebrin. A New Synthetic Drug.

Lancet **1932**, *219*, 826–829. DOI: 10.1016/s0140-6736(00)56672-0.

[12] P. J. Weina. From Atabrine in World War II to Mefloquine in Somalia: The Role of Education in Preventive Medicine. *Mil. Med.* **1998**, *163*, 635–639.

[13] F. Loeb, W. Clark, G. Coatney, *et al.* Activity of a New Antimalarial Agent, Chloroquine (SN 7618). *JAMA* **1946**, *130*, 1069. DOI: 10.1001/jama.1946.02870160015006.

[14] M. Mushtaque and Shahjahan. Reemergence of Chloroquine (CQ) Analogs as Multi-Targeting Antimalarial Agents: A Review. *Eur. J. Med. Chem.* **2015**, *90*, 280–295. DOI: 10.1016/j.ejmech.2014.11.022.

[15] C. Trenholme, R. Williams, R. Desjardins, *et al.* Mefloquine (WR 142,490) in the Treatment of Human Malaria. *Science* **1975**, *190*, 792–794. DOI: 10.1126/science.1105787.

[16] P. Brasseur, M. Danis, S. R. Moyou, *et al.* High Level of Sensitivity to Chloroquine of 72 *Plasmodium Falciparum* Isolates from Southern Cameroon in January 1985. *Am. J. Trop. Med. Hyg.* **1986**, *35*, 711–716. DOI: 10.4269/ajtmh.1986.35.711.

[17] M. Foley and L. Tilley. Quinoline Antimalarials: Mechanisms of Action and Resistance. *Int. J. Parasitol.* **1997**, *27*, 231–240. DOI: 10.1016/s0020-7519(96)00152-x.

[18] R. L. Nevin and A. M. Croft. Psychiatric Effects of Malaria and Anti-Malarial Drugs: Historical and Modern Perspectives. *Malaria Journal* **2016**, *15*. DOI: 10.1186/s12936-016-1391-6.

[19] T. M. Cosgriff, R. E. Desjardins, C. L. Pamplin, *et al.* Evaluation of the Antimalarial Activity of the Phenanthrenemethanol Halofantrine (WR 171,669)*. *Am. J. Trop. Med. Hyg.* **1982**, *31*, 1075–1079. DOI: 10.4269/ajtmh.1982.31.1075.

[20] A. M. Croft. A Lesson Learnt: The Rise and Fall of Lariam and Halfan. *J. R. Soc. Med.* **2007**, *100*, 170–174. DOI: 10.1258/jrsm.100.4.170.

[21] World Health Organization. Model List of Essential Medicines. `http://www.who.int/medicines/publications/essentialmedicines/en/`, Accessed 13 Dec 2018.

[22] Qinghaosu Antimalaria Coordinating Research Group. Antimalarial Studies on Qinghaosu. *Chin. Med. J. (Engl.)* **1979**, *92*, 811–816.

[23] Nobelprize.org. The Nobel Prize in Physiology or Medicine 2015. `https://www.nobelprize.org/prizes/medicine/2015/summary/`, Accessed 24 Mar 2018.

[24] R. T. Eastman and D. A. Fidock. Artemisinin-Based Combination Therapies: A Vital Tool in Efforts to Eliminate Malaria. *Nat. Rev. Microbiol.* **2009**, *7*, 864–874. DOI: 10.1038/nrmicro2239.

[25] H. Noedl, Y. Se, K. Schaecher, *et al.* Evidence of Artemisinin-Resistant Malaria in Western Cambodia. *N. Engl. J. Med.* **2008**, *359*, 2619–2620. DOI: 10.1056/nejmc0805011.

[26] R. Amato, R. D. Pearson, J. Almagro-Garcia, *et al.* Origins of the Current Outbreak of Multidrug-Resistant Malaria in Southeast Asia: A Retrospective Genetic Study. *Lancet Infect. Dis.* **2018**, *18*, 337–345. DOI: 10.1016/s1473-3099(18)30068-9.

[27] F. H. S. Curd, D. G. Davey and F. L. Rose. Studies on Synthetic Antimalarial Drugs. *Ann. Trop. Med. Parasitol.* **1945**, *39*, 208–216. DOI: 10.1080/00034983.1945.11685237.

[28] A. T. Hudson and A. W. Randall. Naphthoquinone Derivatives, **1991**. US5053432A.

[29] M. Fry and M. Pudney. Site of Action of the Antimalarial Hydroxynaphthoquinone, 2-[trans-4-(4'-chlorophenyl)cyclohexyl]-3-hydroxy-1,4-naphthoquinone (566C80). *Biochem. Pharmacol.* **1992**, *43*, 1545–1553. DOI: 10.1016/0006-2952(92)90213-3.

[30] I. K. Srivastava and A. B. Vaidya. A Mechanism for the Synergistic Antimalarial Action of Atovaquone and Proguanil. *Antimicrob. Agents Chemother.* **1999**, *43*, 1334–1339.

[31] Medicines for Malaria Venture. US FDA approves *Krintafel* (tafenoquine) for the radical cure of *P. vivax* malaria. `https://www.mmv.org/newsroom/press-releases/us-fda-approves-krintafel-tafenoquine-radical-cure-p-vivax-malaria`, **2018**, Accessed 25 Sept 2018.

[32] Y. A. Ebstie, S. M. Abay, W. T. Tadesse, *et al.* Tafenoquine and its Potential in the Treatment and Relapse Prevention of *Plasmodium vivax* Malaria: The Evidence to Date. *Drug Des. Dev. Ther.* **2016**, *10*, 2387–2399. DOI: 10.2147/dddt.s61443.

[33] L. Chen, F. Y. Qu and Y. C. Zhou. Field Observations on the Antimalarial Piperaquine. *Chin. Med. J. (Engl.)* **1982**, *95*, 281–286.

[34] J. L. Vennerstrom, W. Y. Ellis, A. L. Ager, *et al.* Bisquinolines. 1. N,N-Bis(7-chloroquinolin-4-yl)alkanediamines with Potential Against Chloroquine-Resistant Malaria. *J. Med. Chem.* **1992**, *35*, 2129–2134. DOI: 10.1021/jm00089a025.

[35] P. B. Russell and G. H. Hitchings. 2,4-Diaminopyrimidines as Antimalarials. III. 5-Aryl Derivatives. *J. Am. Chem. Soc.* **1951**, *73*, 3763–3770. DOI: 10.1021/ja01152a060.

[36] Nobelprize.org. The Nobel Prize in Physiology or Medicine 1988. `https://www.nobelprize.org/prizes/medicine/1988/summary/`, Accessed 19 June 2018.

[37] A. Laing. Treatment of Acute Falciparum Malaria with Sulphorthodimethoxine (Fansil). *Br. Med. J.* **1965**, *1*, 905–907.

[38] V. Lumb, M. K. Das, N. Singh, *et al.* Multiple Origins of *Plasmodium falciparum* Dihydropteroate Synthetase Mutant Alleles Associated with Sulfadoxine Resistance in India. *Antimicrob. Agents Chemother.* **2011**, *55*, 2813–2817. DOI: 10.1128/aac.01151-10.

[39] X. Y. Zheng, Y. Xia, F. H. Gao, *et al.* Synthesis of 7351, a New Antimalarial Drug. *Acta Pharmacol. Sin.* **1979**, *14*, 736–737.

[40] C. Chang, T. Lin-Hua and C. Jantanavivat. Studies on a New Antimalarial Compound: Pyronaridine. *Trans. R. Soc. Trop. Med. Hyg.* **1992**, *86*, 7–10. DOI: 10.1016/0035-9203(92)90414-8.

[41] S. L. Croft, S. Duparc, S. J. Arbe-Barnes, *et al.* Review of Pyronaridine Anti-Malarial Properties and Product Characteristics. *Malar. J.* **2012**, *11*, 270. DOI: 10.1186/1475-2875-11-270.

[42] R. W. Berliner, D. P. Earle, J. V. Taggart, *et al.* Studies on the Chemotheraphy of the Human Malarias. VI. The Physiological Disposition, Antimalarial Activity, and Toxicity of Several Derivatives of 4-Aminoquinoline. *J. Clin. Invest.* **1948**, *27*, 98–107. DOI: 10.1172/jci101980.

[43] F. Bompart, J.-R. Kiechel, R. Sebbag, *et al.* Innovative Public-Private Partnerships to Maximize the Delivery of Anti-Malarial Medicines: Lessons Learned from the ASAQ Winthrop Experience. *Malar. J.* **2011**, *10*, 143. DOI: 10.1186/1475-2875-10-143.

[44] J. M. Combrinck, T. E. Mabotha, K. K. Ncokazi, *et al.* Insights into the Role of Heme in the Mechanism of Action of Antimalarials. *ACS Chem. Biol.* **2012**, *8*, 133–137. DOI: 10.1021/cb300454t.

[45] L. Cui and X.-Z. Su. Discovery, Mechanisms of Action and Combination Therapy of Artemisinin. *Expert Rev. Anti Infect. Ther.* **2009**, *7*, 999–1013. DOI: 10.1586/eri.09.68.

[46] Medicines for Malaria Venture. MMV-supported projects. `https://www.mmv.org/research-development/mmv-supported-projects`, Accessed 27 Feb 2019.

[47] T. Wells and W. Gutteridge. *Negleted Diseases and Drug Discovery.* RSC, **2012**.

[48] J. N. Burrows, S. Duparc, W. E. Gutteridge, *et al.* New Developments in Anti-Malarial Target Candidate and Product Profiles. *Malar. J.* **2017**, *16*, 1–29. DOI: 10.1186/s12936-016-1675-x.

[49] G. D. Shanks, M. D. Edstein and D. Jacobus. Evolution from Double to Triple-Antimalarial Drug Combinations. *Trans. R. Soc. Trop. Med. Hyg.* **2014**, *109*, 182–188. DOI: 10.1093/trstmh/tru199.

[50] M. Mishra, V. K. Mishra, V. Kashaw, *et al.* Comprehensive Review on Various Strategies for Antimalarial Drug Discovery. *Eur. J. Med. Chem.* **2017**, *125*, 1300–1320. DOI: 10.1016/j.ejmech.2016.11.025.

[51] M. A. Phillips, J. N. Burrows, C. Manyando, *et al.* Malaria. *Nat. Rev. Dis. Primers* **2017**, *3*, 17050. DOI: 10.1038/nrdp.2017.50.

[52] J. Okombo and K. Chibale. Recent Updates in the Discovery and Development of Novel Antimalarial Drug Candidates. *MedChemComm* **2018**, *9*, 437–453. DOI: 10.1039/c7md00637c.

[53] E. A. Ashley and A. P. Phyo. Drugs in Development for Malaria. *Drugs* **2018**, *78*, 861–879. DOI: 10.1007/s40265-018-0911-9.

[54] P. M. O'Neill, A. E. Shone, D. Stanford, *et al.* Synthesis, Antimalarial Activity, and Preclinical Pharmacology of a Novel Series of 4'-Fluoro and 4'-Chloro Analogues of Amodiaquine. Identification of a Suitable "Back-Up" Compound for *N-tert*-Butyl Isoquine. *J. Med. Chem.* **2009**, *52*, 1828–1844. DOI: 10.1021/jm8012757.

[55] S. Bora, D. Chetia and A. Prakash. Synthesis and Antimalarial Activity Evaluation of Some Isoquine Analogues. *Med. Chem. Res.* **2010**, *20*, 1632–1637. DOI: 10.1007/s00044-010-9460-9.

[56] P. M. O'Neill, B. K. Park, A. E. Shone, *et al.* Candidate Selection and Preclinical Evaluation of *N-tert*-Butyl Isoquine (GSK369796), An Affordable and Effective 4-Aminoquinoline Antimalarial for the 21st Century. *J. Med. Chem.* **2009**, *52*, 1408–1415. DOI: 10.1021/jm8012618.

[57] M. A. Powles, J. Allocco, L. Yeung, *et al.* MK-4815, A Potential New Oral Agent for Treatment of Malaria. *Antimicrob. Agents Chemother.* **2012**, *56*, 2414–2419. DOI: 10.1128/aac.05326-11.

[58] C. Singh and S. K. Puri. Substituted 1,2,4-Trioxanes as Antimalarial Agents and a Process of Producing the Substituted 1,2,4-Trioxanes, **2001**. US6316493B1.

[59] N. Shafiq, S. Rajagopalan, H. N. Kushwaha, *et al.* Single Ascending Dose Safety and Pharmacokinetics of CDRI-97/78: First-in-Human Study of a Novel Antimalarial Drug. *Malar. Res. Treat.* **2014**, *2014*, 1–10. DOI: 10.1155/2014/372521.

[60] J. D. McChesney, D. N. Nanayakkara, M. Bartlett, *et al.* Preparation of 8-(Aminoalkylamino)quinolines as Parasiticides, **1997**. WO1997036590A1.

[61] B. L. Tekwani and L. A. Walker. 8-Aminoquinolines: Future Role as Antiprotozoal Drugs. *Curr. Opin. Infect. Dis.* **2006**, *19*, 623–631. DOI: 10.1097/qco.0b013e328010b848.

[62] N. P. D. Nanayakkara, A. L. Ager, M. S. Bartlett, *et al.* Antiparasitic Activities and Toxicities of Individual Enantiomers of the 8-Aminoquinoline 8-[(4-Amino-1-Methylbutyl)Amino]-6-Methoxy-4-Methyl-5-[3,4-Dichlorophenoxy]Quinoline Succinate. *Antimicrob. Agents Chemother.* **2008**, *52*, 2130–2137. DOI: 10.1128/aac.00645-07.

[63] S. R. Marcsisin, J. C. Sousa, G. A. Reichard, *et al.* Tafenoquine and NPC-1161B Require CYP 2D Metabolism for Anti-Malarial Activity: Implications for the 8-Aminoquinoline Class of Anti-Malarial Compounds. *Malar. J.* **2014**, *13*, 1–9. DOI: 10.1186/1475-2875-13-2.

[64] R. K. Haynes, B. Fugmann, J. Stetter, *et al.* Artemisone–A Highly Active Antimalarial Drug of the Artemisinin Class. *Angew. Chem. Int. Ed.* **2006**, *45*, 2082–2088. DOI: 10.1002/anie.200503071.

[65] L. Vivas, L. Rattray, L. B. Stewart, *et al.* Antimalarial Efficacy and Drug Interactions of the Novel Semi-Synthetic Endoperoxide Artemisone *in vitro* and *in vivo*. *J. Antimicrob. Chemother.* **2007**, *59*, 658–665. DOI: :10.1093/jac/dkl563.

[66] J. Nagelschmitz, B. Voith, G. Wensing, *et al.* First Assessment in Humans of the Safety, Tolerability, Pharmacokinetics, and Ex Vivo Pharmacodynamic Antimalarial Activity of the New Artemisinin Derivative Artemisone. *Antimicrob. Agents Chemother.* **2008**, *52*, 3085–3091. DOI: 10.1128/AAC.01585-07.

[67] W. C. Chan, D. H. W. Chan, K. W. Lee, *et al.* Evaluation and Optimization of Synthetic Routes from Dihydroartemisinin to the Alkylamino-Artemisinins Artemiside and Artemisone: A Test of *N*-Glycosylation Methodologies on a Lipophilic Peroxide. *Tetrahedron* **2018**, *74*, 5156–5171. DOI: 10.1016/j.tet.2018.04.027.

[68] D. Coertzen, J. Reader, M. van der Watt, *et al.* Artemisone and Artemiside Are Potent Panreactive Antimalarial Agents That Also Synergize Redox Imbalance in *Plasmodium falciparum* Transmissible Gametocyte Stages. *Antimicrob. Agents Chemother.* **2018**, *62*. DOI: 10.1128/AAC.02214-17.

[69] O. Nicolas, D. Margout, N. Taudon, *et al.* Pharmacological Properties of a New Antimalarial Bisthiazolium Salt, T3, and a Corresponding Prodrug, TE3. *Antimicrob. Agents Chemother.* **2005**, *49*, 3631–3639. DOI: 10.1128/aac.49.9.3631-3639.2005.

[70] N. L. Drake, H. J. Creech, J. A. Garman, *et al.* Synthetic Antimalarials. The Preparation of Certain 4-Aminoquinolines. *J. Am. Chem. Soc.* **1946**, *68*, 1208–1213. DOI: 10.1021/ja01211a021.

[71] S. Ramanathan-Girish, P. Catz, M. R. Creek, *et al.* Pharmacokinetics of the Antimalarial

Drug, AQ-13, in Rats and Cynomolgus Macaques. *Int. J. Toxicol.* **2004**, *23*, 179–189. DOI: 10.1080/10915810490471352.

[72] F. E. Sáenz, T. Mutka, K. Udenze, *et al.* Novel 4-Aminoquinoline Analogs Highly Active against the Blood and Sexual Stages of *Plasmodium In Vivo* and *In Vitro*. *Antimicrob. Agents Chemother.* **2012**, *56*, 4685–4692. DOI: 10.1128/aac.01061-12.

[73] F. Mzayek, H. Deng, F. J. Mather, *et al.* Randomized Dose-Ranging Controlled Trial of AQ-13, a Candidate Antimalarial, and Chloroquine in Healthy Volunteers. *PLoS Clin. Trials* **2007**, *2*, e6. DOI: 10.1371/journal.pctr.0020006.

[74] O. A. Koita, L. Sangaré, H. D. Miller, *et al.* AQ-13, An Investigational Antimalarial, versus Artemether plus Lumefantrine for the Treatment of Uncomplicated *Plasmodium falciparum* Malaria: A Randomised, Phase 2, Non-Inferiority Clinical Trial. *Lancet Infect. Dis.* **2017**, *17*, 1266–1275. DOI: 10.1016/s1473-3099(17)30365-1.

[75] B. Baragaña, I. Hallyburton, M. C. S. Lee, *et al.* A Novel Multiple-Stage Antimalarial Agent that Inhibits Protein Synthesis. *Nature* **2015**, *522*, 315–320. DOI: 10.1038/nature14451.

[76] B. Baragaña, N. R. Norcross, C. Wilson, *et al.* Discovery of a Quinoline-4-carboxamide Derivative with a Novel Mechanism of Action, Multistage Antimalarial Activity, and Potent in Vivo Efficacy. *J. Med. Chem.* **2016**, *59*, 9672–9685. DOI: 10.1021/acs.jmedchem.6b00723.

[77] J. N. Burrows, R. H. van Huijsduijnen, J. J. Möhrle, *et al.* Designing the Next Generation of Medicines for Malaria Control and Eradication. *Malar. J.* **2013**, *12*, 1–20. DOI: 10.1186/1475-2875-12-187.

[78] S. Hameed, S. Solapure, V. Patil, *et al.* Triaminopyrimidine is a Fast-Killing and Long-Acting Antimalarial Clinical Candidate. *Nat. Commun.* **2015**, *6*, 1–11. DOI: 10.1038/ncomms7715.

[79] Medicines for Malaria Venture. MMV and Zydus join forces to develop new antimalarial. `https://www.mmv.org/newsroom/press-releases/mmv-and-zydus-join-forces-develop-new-antimalarial`, **2017**, accessed 17 June 2018.

[80] C. L. Manach, A. T. Nchinda, T. Paquet, *et al.* Identification of a Potential Antimalarial Drug Candidate from a Series of 2-Aminopyrazines by Optimization of Aqueous Solubility and Potency across the Parasite Life Cycle. *J. Med. Chem.* **2016**, *59*, 9890–9905. DOI: 10.1021/acs.jmedchem.6b01265.

[81] Y. Younis, F. Douelle, T.-S. Feng, *et al.* 3,5-Diaryl-2-aminopyridines as a Novel Class of Orally Active Antimalarials Demonstrating Single Dose Cure in Mice and Clinical Candidate Potential. *J. Med. Chem.* **2012**, *55*, 3479–3487. DOI: 10.1021/jm3001373.

[82] D. G. Cabrera, F. Douelle, Y. Younis, *et al.* Structure–Activity Relationship Studies of Orally Active Antimalarial 3,5-Substituted 2-Aminopyridines. *J. Med. Chem.* **2012**, *55*, 11022–11030. DOI: 10.1021/jm301476b.

[83] Y. Younis, F. Douelle, D. G. Cabrera, *et al.* Structure–Activity-Relationship Studies around the 2-Amino Group and Pyridine Core of Antimalarial 3,5-Diarylaminopyridines Lead to a Novel Series of Pyrazine Analogues with Oral in Vivo Activity. *J. Med. Chem.* **2013**, *56*, 8860–8871. DOI: 10.1021/jm401278d.

[84] C. W. McNamara, M. C. S. Lee, C. S. Lim, *et al.* Targeting *Plasmodium* PI(4)K to Eliminate Malaria. *Nature* **2013**, *504*, 248–253. DOI: 10.1038/nature12782.

[85] Y.-K. Zhang, J. J. Plattner, Y. R. Freund, *et al.* Synthesis and Structure–Activity Relationships of Novel Benzoxaboroles as a New Class of Antimalarial Agents. *Bioorg. Med. Chem. Lett.* **2011**, *21*, 644–651. DOI: 10.1016/j.bmcl.2010.12.034.

[86] Y.-K. Zhang, J. J. Plattner, E. E. Easom, *et al.* Benzoxaborole Antimalarial Agents. Part 5. Lead Optimization of Novel Amide Pyrazinyloxy Benzoxaboroles and Identification of a Preclinical Candidate. *J. Med. Chem.* **2017**, *60*, 5889–5908. DOI: 10.1021/acs.jmedchem.7b00621.

[87] Y.-K. Zhang, J. J. Plattner, E. E. Easom, *et al.* Benzoxaborole Antimalarial Agents. Part 4. Discovery of Potent 6-(2-(Alkoxycarbonyl)pyrazinyl-5-oxy)-1,3-dihydro-1-hydroxy-2,1-benzoxaboroles. *J. Med. Chem.* **2015**, *58*, 5344–5354. DOI: 10.1021/acs.jmedchem.5b00678.

[88] E. Sonoiki, C. L. Ng, M. C. S. Lee, *et al.* A Potent Antimalarial Benzoxaborole Targets a *Plasmodium falciparum* Cleavage and Polyadenylation Specificity Factor Homologue. *Nat. Commun.* **2017**, *8*, 14574. DOI: 10.1038/ncomms14574.

[89] S. Pegoraro, M. Duffey, T. D. Otto, *et al.* SC83288 is a Clinical Development Candidate for the Treatment of Severe Malaria. *Nat. Commun.* **2017**, *8*, 1–15. DOI: 10.1038/ncomms14193.

[90] J. Leban, S. Pegoraro, M. Dormeyer, *et al.* Sulfonyl-Phenyl-Ureido Benzamidines: A Novel Structural Class of Potent Antimalarial Agents. *Bioorg. Med. Chem. Lett.* **2004**, *14*, 1979–1982. DOI: 10.1016/j.bmcl.2004.01.083.

[91] M. Duffey, C. P. Sanchez and M. Lanzer. Profiling of the Anti-Malarial Drug Candidate SC83288 Against Artemisinins in *Plasmodium falciparum*. *Malar. J.* **2018**, *17*, 1–10. DOI: 10.1186/s12936-018-2279-4.

[92] S. J. Burgess, J. X. Kelly, S. Shomloo, *et al.* Synthesis, Structure-Activity Relationship, and Mode-of-Action Studies of Antimalarial Reversed Chloroquine Compounds. *J. Med. Chem.*

2010, *53*, 6477–6489. DOI: 10.1021/jm1006484.

[93] S. J. Burgess, A. Selzer, J. X. Kelly, *et al.* A Chloroquine-like Molecule Designed to Reverse Resistance in *Plasmodium falciparum*. *J. Med. Chem.* **2006**, *49*, 5623–5625. DOI: 10.1021/jm060399n.

[94] G. Wirjanata, B. F. Sebayang, F. Chalfein, *et al.* Contrasting *Ex Vivo* Efficacies of "Reversed Chloroquine" Compounds in Chloroquine-Resistant *Plasmodium falciparum* and *P. vivax* Isolates. *Antimicrob. Agents Chemother.* **2015**, *59*, 5721–5726. DOI: 10.1128/aac.01048-15.

[95] Y. Yuthavong, B. Tarnchompoo, T. Vilaivan, *et al.* Malarial Dihydrofolate Reductase as a Paradigm for Drug Development Against a Resistance-Compromised Target. *Proc. Natl. Acad. Sci. U.S.A.* **2012**, *109*, 16823–16828. DOI: 10.1073/pnas.1204556109.

[96] W. A. Guiguemde, A. A. Shelat, D. Bouck, *et al.* Chemical Genetics of *Plasmodium falciparum*. *Nature* **2010**, *465*, 311–315. DOI: 10.1038/nature09099.

[97] D. M. Floyd, P. Stein, Z. Wang, *et al.* Hit-to-Lead Studies for the Antimalarial Tetrahydroisoquinolone Carboxanilides. *J. Med. Chem.* **2016**, *59*, 7950–7962. DOI: 10.1021/acs.jmedchem.6b00752.

[98] M. B. Jiménez-Díaz, D. Ebert, Y. Salinas, *et al.* (+)-SJ733, A Clinical Candidate for Malaria that Acts Through ATP4 to Induce Rapid Host-Mediated Clearance of *Plasmodium*. *Proc. Natl. Acad. Sci. U.S.A.* **2014**, *111*, E5455–E5462. DOI: 10.1073/pnas.1414221111.

[99] N. J. Spillman and K. Kirk. The Malaria Parasite Cation ATPase *Pf*ATP4 and its Role in the Mechanism of Action of a New Arsenal of Antimalarial Drugs. *Int. J. Parasitol. Drugs Drug Resist.* **2015**, *5*, 149–162. DOI: 10.1016/j.ijpddr.2015.07.001.

[100] C. Boss, H. Aissaoui, N. Amaral, *et al.* Discovery and Characterization of ACT-451840: An Antimalarial Drug with a Novel Mechanism of Action. *ChemMedChem* **2016**, *11*, 1995–2014. DOI: 10.1002/cmdc.201600298.

[101] A. L. Bihan, R. de Kanter, I. Angulo-Barturen, *et al.* Characterization of Novel Antimalarial Compound ACT-451840: Preclinical Assessment of Activity and Dose–Efficacy Modeling. *PLoS Med.* **2016**, *13*, 1–24. DOI: 10.1371/journal.pmed.1002138.

[102] A. Krause, J. Dingemanse, A. Mathis, *et al.* Pharmacokinetic/Pharmacodynamic Modelling of the Antimalarial Effect of Actelion-451840 in an Induced Blood Stage Malaria Study in Healthy Subjects. *Br. J. Clin. Pharmacol.* **2016**, *82*, 412–421. DOI: 10.1111/bcp.12962.

[103] S. A. Charman, S. Arbe-Barnes, I. C. Bathurst, *et al.* Synthetic Ozonide Drug Candidate

OZ439 Offers New Hope for a Single-Dose Cure of Uncomplicated Malaria. *Proc. Natl. Acad. Sci. U.S.A.* **2011**, *108*, 4400–4405. DOI: 10.1073/pnas.1015762108.

[104] J. L. Vennerstrom, S. Arbe-Barnes, R. Brun, *et al.* Identification of an Antimalarial Synthetic Trioxolane Drug Development Candidate. *Nature* **2004**, *430*, 900–904. DOI: 10.1038/nature02779.

[105] Y. Dong, S. Wittlin, K. Sriraghavan, *et al.* The Structure-Activity Relationship of the Antimalarial Ozonide Arterolane (OZ277). *J. Med. Chem.* **2010**, *53*, 481–491. DOI: 10.1021/jm901473s.

[106] Y. Dong, J. Chollet, H. Matile, *et al.* Spiro and Dispiro-1,2,4-trioxolanes as Antimalarial Peroxides: Charting a Workable Structure-Activity Relationship Using Simple Prototypes. *J. Med. Chem.* **2005**, *48*, 4953–4961. DOI: 10.1021/jm049040u.

[107] Y. Dong, Y. Tang, J. Chollet, *et al.* Effect of Functional Group Polarity on the Antimalarial Activity of Spiro and Dispiro-1,2,4-trioxolanes. *Bioorg. Med. Chem.* **2006**, *14*, 6368–6382. DOI: 10.1016/j.bmc.2006.05.041.

[108] M. Kaiser, S. Wittlin, A. Nehrbass-Stuedli, *et al.* Peroxide Bond-Dependent Antiplasmodial Specificity of Artemisinin and OZ277 (RBx11160). *Antimicrob. Agents Chemother.* **2007**, *51*, 2991–2993. DOI: 10.1128/aac.00225-07.

[109] Y. Dong, X. Wang, S. Kamaraj, *et al.* Structure–Activity Relationship of the Antimalarial Ozonide Artefenomel (OZ439). *J. Med. Chem.* **2017**, *60*, 2654–2668. DOI: 10.1021/acs.jmedchem.6b01586.

[110] A. P. Phyo, P. Jittamala, F. H. Nosten, *et al.* Antimalarial Activity of Artefenomel (OZ439), a Novel Synthetic Antimalarial Endoperoxide, in Patients with *Plasmodium falciparum* and *Plasmodium vivax* Malaria: An Open-Label Phase 2 Trial. *Lancet Infect. Dis.* **2016**, *16*, 61–69. DOI: 10.1016/s1473-3099(15)00320-5.

[111] A. Gautam, T. Ahmed, P. Sharma, *et al.* Pharmacokinetics and Pharmacodynamics of Arterolane Maleate Following Multiple Oral Doses in Adult Patients with *P. falciparum* Malaria. *J. Clin. Pharmacol.* **2011**, *51*, 1519–1528. DOI: 10.1177/0091270010385578.

[112] N. Valecha, S. Krudsood, N. Tangpukdee, *et al.* Arterolane Maleate Plus Piperaquine Phosphate for Treatment of Uncomplicated *Plasmodium falciparum* Malaria: A Comparative, Multicenter, Randomized Clinical Trial. *Clin. Infect. Dis.* **2012**, *55*, 663–671. DOI: 10.1093/cid/cis475.

[113] J. Jourdan, H. Matile, E. Reift, *et al.* Monoclonal Antibodies that Recognize the Alkylation

Signature of Antimalarial Ozonides OZ277 (Arterolane) and OZ439 (Artefenomel). *ACS Infect. Dis.* **2015**, *2*, 54–61. DOI: 10.1021/acsinfecdis.5b00090.

[114] E. L. Allman, H. J. Painter, J. Samra, *et al.* Metabolomic Profiling of the Malaria Box Reveals Antimalarial Target Pathways. *Antimicrob. Agents Chemother.* **2016**, *60*, 6635–6649. DOI: 10.1128/aac.01224-16.

[115] J. J. Moehrle, S. Duparc, C. Siethoff, *et al.* First-in-Man Safety and Pharmacokinetics of Synthetic Ozonide OZ439 Demonstrates an Improved Exposure Profile Relative to Other Peroxide Antimalarials. *Br. J. Clin. Pharmacol.* **2013**, *75*, 535–548. DOI: 10.1111/j.1365-2125.2012.04368.x.

[116] J. S. McCarthy, M. Baker, P. O'Rourke, *et al.* Efficacy of OZ439 (Artefenomel) Against Early *Plasmodium falciparum* Blood-Stage Malaria Infection in Healthy Volunteers. *J. Antimicrob. Chemother.* **2016**, *71*, 2620–2627. DOI: 10.1093/jac/dkw174.

[117] D. Plouffe, A. Brinker, C. McNamara, *et al. In silico* Activity Profiling Reveals the Mechanism of Action of Antimalarials Discovered in a High-Throughput Screen. *Proc. Natl. Acad. Sci. U.S.A.* **2008**, *105*, 9059–9064. DOI: 10.1073/pnas.0802982105.

[118] A. Nagle, T. Wu, K. Kuhen, *et al.* Imidazolopiperazines: Lead Optimization of the Second-Generation Antimalarial Agents. *J. Med. Chem.* **2012**, *55*, 4244–4273. DOI: 10.1021/jm300041e.

[119] T. Wu, A. Nagle, K. Kuhen, *et al.* Imidazolopiperazines: Hit to Lead Optimization of New Antimalarial Agents. *J. Med. Chem.* **2011**, *54*, 5116–5130. DOI: 10.1021/jm2003359.

[120] K. L. Kuhen, A. K. Chatterjee, M. Rottmann, *et al.* KAF156 is an Antimalarial Clinical Candidate with Potential for Use in Prophylaxis, Treatment, and Prevention of Disease Transmission. *Antimicrob. Agents Chemother.* **2014**, *58*, 5060–5067. DOI: 10.1128/aac.02727-13.

[121] M. Rottmann, C. McNamara, B. K. S. Yeung, *et al.* Spiroindolones, a Potent Compound Class for the Treatment of Malaria. *Science* **2010**, *329*, 1175–1180. DOI: 10.1126/science.1193225.

[122] B. K. S. Yeung, B. Zou, M. Rottmann, *et al.* Spirotetrahydro β-Carbolines (Spiroindolones): A New Class of Potent and Orally Efficacious Compounds for the Treatment of Malaria. *J. Med. Chem.* **2010**, *53*, 5155–5164. DOI: 10.1021/jm100410f.

[123] N. J. White, S. Pukrittayakamee, A. P. Phyo, *et al.* Spiroindolone KAE609 for Falciparum and Vivax Malaria. *N. Engl. J. Med.* **2014**, *371*, 403–410. DOI: 10.1056/nejmoa1315860.

[124] J. M. Coteron, M. Marco, J. Esquivias, *et al.* Structure-Guided Lead Optimization of Triazolopyrimidine-Ring Substituents Identifies Potent *Plasmodium falciparum* Dihydroorotate Dehydrogenase Inhibitors with Clinical Candidate Potential. *J. Med. Chem.* **2011**, *54*, 5540–5561. DOI: 10.1021/jm200592f.

[125] J. S. McCarthy, J. Lotharius, T. RÃijckle, *et al.* Safety, Tolerability, Pharmacokinetics, and Activity of the Novel Long-Acting Antimalarial DSM265: A Two-Part First-in-Human Phase 1a/1b Randomised Study. *Lancet Infect. Dis.* **2017**, *17*, 626–635. DOI: 10.1016/s1473-3099(17)30171-8.

[126] P. Kraker, D. Leony, W. Reinhardt, *et al.* The Case for an Open science in Technology Enhanced Learning. *Int. J. Technology Enhanced Learning* **2011**, *3*, 643. DOI: 10.1504/IJTEL.2011.045454.

[127] OpenScience ASAP. What is Open Science? `http://opensciencеasap.org/open-science/`, Accessed 26 Mar 2018.

[128] C. Franzoni and H. Sauermann. Crowd Science: The Organization of Scientific Research in Open Collaborative Projects. *Research Policy* **2014**, *43*, 1–20. DOI: 10.1016/j.respol.2013.07.005.

[129] S. Cooper, F. Khatib, A. Treuille, *et al.* Predicting Protein Structures with a Multiplayer Online Game. *Nature* **2010**, *466*, 756–760. DOI: 10.1038/nature09304.

[130] F. Khatib, F. DiMaio, S. Cooper, *et al.* Crystal Structure of a Monomeric Retroviral Protease Solved by Protein Folding Game Players. *Nat. Struct. Mol. Biol.* **2011**, *18*, 1175–1177. DOI: 10.1038/nsmb.2119.

[131] C. B. Eiben, J. B. Siegel, J. B. Bale, *et al.* Increased Diels-Alderase Activity Through Backbone Remodeling Guided by Foldit Players. *Nat. Biotechnol.* **2012**, *30*, 190–192. DOI: 10.1038/nbt.2109.

[132] M. Nielsen. *Reinventing Discovery: The New Era of Networked Science*. Princeton University Press, **2012**.

[133] A. M. Edwards, C. Bountra, D. J. Kerr, *et al.* Open Access chemical and Clinical Probes to Support Drug Discovery. *Nat. Chem. Biol.* **2009**, *5*, 436–440. DOI: 10.1038/nchembio0709-436.

[134] S. Müller, S. Ackloo, C. H. Arrowsmith, *et al.* Donated Chemical Probes for Open Science. *eLife* **2018**, *7*. DOI: 10.7554/eLife.34311.

[135] The Structural Genomics Consortium. Chemical Probes. `https://www.thesgc.org/chemical-probes`, Accessed 7 May 2019.

[136] The Structural Genomics Consortium. Donated chemical probes. `https://www.thesgc.org/node/565599`, Accessed 7 May 2019.

[137] J. G. Moffat, F. Vincent, J. A. Lee, *et al.* Opportunities and Challenges in Phenotypic Drug Discovery: An Industry Perspective. *Nat. Rev. Drug Discov.* **2017**, *16*, 531–543. DOI: 10.1038/nrd.2017.111.

[138] G. E. Croston. The Utility of Target-Based Discovery. *Expert Opin. Drug Discov.* **2017**, *12*, 427–429. DOI: 10.1080/17460441.2017.1308351.

[139] F.-J. Gamo, L. M. Sanz, J. Vidal, *et al.* Thousands of Chemical Starting Points for Antimalarial Lead Identification. *Nature* **2010**, *465*, 305–310. DOI: 10.1038/nature09107.

[140] ChEMBL-NTD. Deposited Set 2: Novartis GNF Whole Cell Dataset (20th May 2010). `https://chembl.gitbook.io/chembl-ntd/downloads/deposited-set-2-novartis-gnf-whole-cell-dataset-20th-may-2010`, Accessed 19 Feb 2019.

[141] Medicines for Malaria Venture. The Malaria Box. `https://www.mmv.org/mmv-open/malaria-box`, Accessed 19 Feb 2019.

[142] T. Spangenberg, J. N. Burrows, P. Kowalczyk, *et al.* The Open Access Malaria Box: A Drug Discovery Catalyst for Neglected Diseases. *PLoS One* **2013**, *8*, 1–8. DOI: 10.1371/journal.pone.0062906.

[143] W. C. V. Voorhis, J. H. Adams, R. Adelfio, *et al.* Open Source Drug Discovery with the Malaria Box Compound Collection for Neglected Diseases and Beyond. *PLoS Pathog.* **2016**, *12*, 1–23. DOI: 10.1371/journal.ppat.1005763.

[144] Medicines for Malaria Venture. The Pathogen Box. `https://www.mmv.org/mmv-open/pathogen-box`, Accessed 19 Feb 2019.

[145] S. Duffy, M. L. Sykes, A. J. Jones, *et al.* Screening the Medicines for Malaria Venture Pathogen Box across Multiple Pathogens Reclassifies Starting Points for Open-Source Drug Discovery. *Antimicrob. Agents Chemother.* **2017**, *61*, 1–22. DOI: 10.1128/AAC.00379-17.

[146] J. Spalenka, S. Escotte-Binet, A. Bakiri, *et al.* Discovery of New Inhibitors of *Toxoplasma gondii* via the Pathogen Box. *Antimicrob. Agents Chemother.* **2017**, *62*, 1–10. DOI: 10.1128/AAC.01640-17.

[147] Medicines for Malaria Venture. The Pandemic Response Box. `https://www.mmv.org/mmv-`

open/pandemic-response-box, Accessed 19 Feb 2019.

[148] Y. Antonova-Koch, S. Meister, M. Abraham, *et al.* Open-Source Discovery of Chemical Leads for Next-Generation Chemoprotective Antimalarials. *Science* **2018**, *362*, 1–8. DOI: 10.1126/science.aat9446.

[149] The Synaptic Leap. Open Source Drug Discovery for Malaria. http://www.thesynapticleap.org/node/343, Accessed 27 Mar 2018.

[150] Open Source Malaria. Open Source Malaria. http://opensourcemalaria.org/, Accessed 27 Mar 2018.

[151] Open Source Malaria GitHub. Open Source Malaria Series 4 GitHub. https://github.com/OpenSourceMalaria/Series4, Accessed 15 Aug 2019.

[152] Twitter. Open Source Malaria Twitter. https://twitter.com/o_s_m?lang=en, Accessed 15 Aug 2019.

[153] Open Source Malaria GitHub. Lab Notebooks. https://github.com/OpenSourceMalaria/Series4/wiki/Sources-of-Data#lab-notebooks, Accessed 15 Aug 2019.

[154] A. E. Williamson, P. M. Ylioja, M. N. Robertson, *et al.* Open Source Drug Discovery: Highly Potent Antimalarial Compounds Derived from the Tres Cantos Arylpyrroles. *ACS Cent. Sci.* **2016**, *2*, 687–701. DOI: 10.1021/acscentsci.6b00086.

[155] M. McConville, J. Fernández, Í. Angulo-Barturen, *et al.* Carbamoyl Triazoles, Known Serine Protease Inhibitors, Are a Potent New Class of Antimalarials. *J. Med. Chem.* **2015**, *58*, 6448–6455. DOI: 10.1021/acs.jmedchem.5b00434.

[156] Medicines for Malaria Venture. Potential new class of antimalarials now open source. http://www.mmv.org/newsroom/news/potential-new-class-antimalarials-now-open-source, **2018**, Accessed 19 Apr 2016.

[157] PubChem. Primary QHTS for Delayed Death Inhibitors of the Malarial Parasite Plastid, 48 Hour Incubation. https://pubchem.ncbi.nlm.nih.gov/bioassay/504832#section=Top, Accessed 26 Feb 2019.

[158] J.-X. Ren, N.-N. Gao, X.-S. Cao, *et al.* Homology Modeling and Virtual Screening for Inhibitors of Lipid Kinase PI(4)K from *Plasmodium*. *Biomed. Pharmacother.* **2016**, *83*, 798–808. DOI: 10.1016/j.biopha.2016.07.048.

[159] A.-M. Zeeman, S. M. van Amsterdam, C. W. McNamara, *et al.* KAI407, A Potent Non-8-Aminoquinoline Compound that Kills *Plasmodium cynomolgi* Early Dormant Liver

Stage Parasites *In Vitro*. *Antimicrob. Agents Chemother.* **2013**, *58*, 1586–1595. DOI: 10.1128/AAC.01927-13.

[160] L. Dembele, X. Ang, M. Chavchich, *et al.* The *Plasmodium* PI(4)K Inhibitor KDU691 Selectively Inhibits Dihydroartemisinin-Pretreated *Plasmodium falciparum* Ring-Stage Parasites. *Sci. Rep.* **2017**, *7*, 1–9. DOI: 10.1038/s41598-017-02440-6.

[161] Open Source Malaria GitHub. Similarity of Series 4 Compounds to KAI407. `https://github.com/OpenSourceMalaria/OSM_To_Do_List/issues/147`, Accessed 7 May 2019.

[162] Open Source Malaria GitHub. Sources of Data. `https://github.com/OpenSourceMalaria/Series4/wiki/Sources-of-Data`, Accessed 29 Apr 2019.

[163] K. Kirk. Ion Regulation in the Malaria Parasite. *Annu. Rev. Microbiol.* **2015**, *69*, 341–359. DOI: 10.1146/annurev-micro-091014-104506.

[164] Open Source Malaria GitHub. Synthesis of the Ether-Linked Series. `https://github.com/OpenSourceMalaria/Series4/wiki/Synthesis-of-the-Ether-Linked-Series`, Accessed 15 Aug 2019.

[165] J. M. Ubels. Synthesis of Novel Triazolopyrazines as Candidate Antimalarials. Honours thesis, The University of Sydney, (Sydney, Australia), **2014**, `https://github.com/OpenSourceMalaria/Series4/blob/master/Student%20Reports/2014%20Honours%20Thesis%20Ubels.pdf`.

[166] T. MacDonald. Development of Routes to Access and Functionalise [1,2,4]Triazolo[4,3-*a*]pyrazine Amides as New Antimalarial Compounds. Honours thesis, The University of Sydney, (Sydney, Australia), **2014**, `https://github.com/OpenSourceMalaria/Series4/blob/master/Student%20Reports/2014%20Honours%20Thesis%20MacDonald.pdf`.

[167] openmolecules.org. DataWarrior. `http://www.openmolecules.org/datawarrior/`, Accessed 26 Aug 2019.

[168] Medicines for Malaria Venture. Information for scientists - Frontrunner template: late leads. `https://www.mmv.org/research-development/information-scientists`, Accessed 2 Feb 2020.

[169] Open Source Malaria GitHub. The Frontrunners. `https://github.com/OpenSourceMalaria/OSM_To_Do_List/issues/400`, Accessed 23 Jan 2019.

[170] The OSM Blog. Appeal for assistance on methods for difluoromethylation of AEW 103. `http://malaria.ourexperiment.org/the_osm_blog/8470/post.html`, Accessed 2

Feb 2019.

[171] P.-Q. Huang, S.-H. Xiang, J. Xu, *et al.* Amide Activation by Tf_2O: Reduction of Amides to Amines by $NaBH_4$ under Mild Conditions. *Synlett* **2010**, *2010*, 1829–1832. DOI: 10.1055/s-0030-1258111.

[172] Y. Mizutani, H. Tanimoto, T. Morimoto, *et al.* Double Nucleophilic N-Alkylation of α-Oxime-Esters with Grignard Reagents. *Tetrahedron Lett.* **2012**, *53*, 5903–5906. DOI: 10.1016/j.tetlet.2012.08.091.

[173] Open Source Malaria GitHub. Troubles with the synthesis of MMV670437 (dimethylamine) for the Frontrunners. `https://github.com/OpenSourceMalaria/OSM_To_Do_List/issues/435`, Accessed 23 Jan 2019.

[174] A. W. Stamford, E. J. Gilbert and J. N. Cumming. Pyrrolidine-Fused Thiadiazine Dioxide Compounds as BACE Inhibitors, Compositions, and their Use, **2012**. WO2012138590A1.

[175] C. Chen, B. Eastman, A. Gosberg, *et al.* Fused Ring Heterocycle Kinase Modulators, **2008**. WO2008124848A1.

[176] R. W. Evans, J. R. Zbieg, S. Zhu, *et al.* Simple Catalytic Mechanism for the Direct Coupling of α-Carbonyls with Functionalized Amines: A One-Step Synthesis of Plavix. *J. Am. Chem. Soc.* **2013**, *135*, 16074–16077. DOI: 10.1021/ja4096472.

[177] R. Laufer, G. Ng, Y. Liu, *et al.* Discovery of Inhibitors of the Mitotic Kinase TTK based on *N*-(3-(3-Sulfamoylphenyl)-1*H*-indazol-5-yl)-acetamides and carboxamides. *Bioorg. Med. Chem.* **2014**, *22*, 4968–4997. DOI: 10.1016/j.bmc.2014.06.027.

[178] M. J. Delves, U. Straschil, A. Ruecker, *et al.* Routine *in vitro* Culture of *P. falciparum* Gametocytes to Evaluate Novel Transmission-Blocking Interventions. *Nat. Protoc.* **2016**, *11*, 1668–1680. DOI: 10.1038/nprot.2016.096.

[179] Y. Li, Q. Meng, M. Yang, *et al.* Current Trends in Drug Metabolism and Pharmacokinetics. *Acta Pharm. Sin. B* **2019**, *9*, 1113–1144. DOI: 10.1016/j.apsb.2019.10.001.

[180] K.-M. Roy. *Sulfones and Sulfoxides.* In Ullmann's Encyclopedia of Industrial Chemistry, **2000**.

[181] C. Cheeseman and R. Godwin. Pyrazines. Part III. Some Nucleophilic Substitution Reactions of Chloropyrazines. *J. Chem. Soc. C* **1971**, 2973–2976. DOI: 10.1039/J39710002973.

[182] H. Golchoubian and F. Hosseinpoor. Effective Oxidation of Sulfides to Sulfoxides with Hydrogen Peroxide under Transition-Metal-Free Conditions. *Molecules* **2007**, *12*, 304–311.

DOI: 10.3390/12030304.

[183] J. Bradac, Z. Furek, D. Janezic, *et al.* Heterocycles. 167. Telesubstitution and Other Transformations of Imidazo[1,2-a]- and s-Triazolo[4,3-a]pyrazines. *J. Org. Chem.* **1977**, *42*, 4197–4201. DOI: 10.1021/jo00862a005.

[184] J. Suwiński and K. Świerczek. *cine*- and *tele*-Substitution Reactions. *Tetrahedron* **2001**, *57*, 1639–1662. DOI: 10.1016/s0040-4020(00)01067-x.

[185] M. Tišler. *tele*-Substitutions in Heterocyclic Chemistry. *Acta Chim. Slov.* **2011**, *58*, 9–13.

[186] J. W. Suwiński. *cine*- and *tele*-Substitution Reactions: Review of Work from 2002-2016. *Arkivoc* **2017**, *2017*, 402–435. DOI: 10.24820/ark.5550190.p010.215.

[187] B. Verček, B. Stanovnik and M. Tišler. Products of Abnormal Substitution of s-Triazolo(1,5-*a*)pyrazines. *Tetrahedron Lett.* **1974**, *15*, 4539–4542. DOI: 10.1016/s0040-4039(01)92213-0.

[188] Open Source Malaria GitHub. OSM Series 4 - Next Round of Synthesis. `https://github.com/OpenSourceMalaria/OSM_To_Do_List/issues/358`, Accessed 6 Mar 2019.

[189] C.-H. Zhou and Y. Wang. Recent Researches in Triazole Compounds as Medicinal Drugs. *Curr. Med. Chem.* **2012**, *19*, 239–280. DOI: 10.2174/092986712803414213.

[190] R. D. Taylor, M. MacCoss and A. D. G. Lawson. Rings in Drugs. *J. Med. Chem.* **2014**, *57*, 5845–5859. DOI: 10.1021/jm4017625.

[191] H.-Z. Zhang, G. Damu, G.-X. Cai, *et al.* Current Developments in the Syntheses of 1,2,4-Triazole Compounds. *Curr. Org. Chem.* **2014**, *18*, 359–406. DOI: 10.2174/13852728113179990025.

[192] M. S. Singh, S. Chowdhury and S. Koley. Advances of Azide-Alkyne Cycloaddition-Click Chemistry Over the Recent Decade. *Tetrahedron* **2016**, *72*, 5257–5283. DOI: 10.1016/j.tet.2016.07.044.

[193] N. Schultheiss, C. Barnes and E. Bosch. From Molecular Design to Supramolecular Design: Synthesis and Size-Selective Coordination Chemistry of 1,2-Bis(2'-pyrazineethynyl) Benzene. *Cryst. Growth Des.* **2003**, *3*, 573–580. DOI: 10.1021/cg034036p.

[194] D. A. Smith, C. Allerton, A. S. Kalgutkar, *et al. Parmacokinetics And Metabolism In Drug Design.* John Wiley & Sons, Ltd, **2012**.

[195] B. Lagu, T. M. Dhar, D. Nagarathnam, *et al.* Oxazolidinones as α1A Receptor Antagonists, **1997**. US6159990A.

[196] S. Imai and H. Togo. Synthetic Utility of Iodic Acid in the Oxidation of Benzylic Alcohols to Aromatic Aldehydes and Ketones. *Tetrahedron* **2016**, *72*, 6948–6954. DOI: 10.1016/j.tet.2016.09.019.

[197] J. Wang, C. Zhang, Z. Qu, *et al.* Copper(II) Chloride Dihydrate: A Catalytic Agent for the Deprotection of Tetrahydropyranyl Ethers (THP Ethers) and 1-Ethoxyethyl Ethers (EE Ethers). *J. Chem. Res. (S)* **1999**, 294–295. DOI: 10.1039/A900262F.

[198] A. A. Jafari and Moradgholi. $Mg(ClO_4)_2$, an Efficient Catalyst for Synthesis of β-Amino Alcohols by Ring Opening of Epoxides with Amines under Solvent-Free Conditions. *Synth. Commun.* **2011**, *41*, 594–602. DOI: 10.1080/00397911003629473.

[199] Triazolopyrazine Series. Synthesis of (R)-1-((3-(4-chlorophenyl)-[1,2,4]triazolo[4,3-a]pyrazin-5-yl)oxy)-3-phenylpropan-2-amine. `http://malaria.ourexperiment.org/triazolopyrazine_se/10883/`, Accessed 30 Jan 2019.

[200] Open Source Malaria GitHub. Griffith Uni 2017 Trimester 2 Undergrad Projects. `https://github.com/OpenSourceMalaria/OSM_To_Do_List/issues/508`, Accessed 4 Feb 2019.

[201] Open Source Malaria GitHub. GU Project 6: Synthesis of phenylalaninol ether side-chain. `https://github.com/OpenSourceMalaria/OSM_To_Do_List/issues/523`, Accessed 30 Jan 2019.

[202] G. C. Moraski, R. Bristol, N. Seeger, *et al.* Preparation and Evaluation of Potent Pentafluorosulfanyl Substituted Anti-Tuberculosis Compounds. *ChemMedChem* **2017**, *12*, 1108–1115. DOI: 10.1002/cmdc.201700170.

[203] B. El-Haj, S. Ahmed, M. Garawi, *et al.* Linking Aromatic Hydroxy Metabolic Functionalization of Drug Molecules to Structure and Pharmacologic Activity. *Molecules* **2018**, *23*, 2119. DOI: 10.3390/molecules23092119.

[204] A. Modak, T. Naveen and D. Maiti. An Efficient Dehydroxymethylation Reaction by a Palladium Catalyst. *Chem. Commun.* **2013**, *49*, 252–254. DOI: 10.1039/c2cc36951f.

[205] M. Ishikawa and Y. Hashimoto. Improvement in Aqueous Solubility in Small Molecule Drug Discovery Programs by Disruption of Molecular Planarity and Symmetry. *J. Med. Chem.* **2011**, *54*, 1539–1554. DOI: 10.1021/jm101356p.

[206] M. A. Walker. Novel Tactics for Designing Water-Soluble Molecules in Drug Discovery. *Expert Opin. Drug Discovery* **2014**, *9*, 1421–1433. DOI: 10.1517/17460441.2014.960839.

[207] T. J. Ritchie and S. J. Macdonald. Heterocyclic Replacements for Benzene: Maximising

ADME Benefits by Considering Individual Ring Isomers. *Eur. J. Med. Chem.* **2016**, *124*, 1057–1068. DOI: 10.1016/j.ejmech.2016.10.029.

[208] I. Langmuir. Isomorphism, Isosterism and Covalence. *J. Am. Chem. Soc.* **1919**, *41*, 1543–1559. DOI: 10.1021/ja02231a009.

[209] H. Friedman. Influence of Isosteric Replacements Upon Biological Activity. NAS-NRS. **1951**, *206*, 295–358.

[210] N. A. Meanwell. Synopsis of Some Recent Tactical Application of Bioisosteres in Drug Design. *J. Med. Chem.* **2011**, *54*, 2529–2591. DOI: 10.1021/jm1013693.

[211] M. F. Sowaileh, R. A. Hazlitt and D. A. Colby. Application of the Pentafluorosulfanyl Group as a Bioisosteric Replacement. *ChemMedChem* **2017**, *12*, 1481–1490. DOI: 10.1002/cmdc.201700356.

[212] E. Bonandi, M. S. Christodoulou, G. Fumagalli, *et al.* The 1,2,3-Triazole Ring as a Bioisostere in Medicinal Chemistry. *Drug Discov. Today* **2017**, *22*, 1572–1581. DOI: 10.1016/j.drudis.2017.05.014.

[213] N. A. Meanwell. Fluorine and Fluorinated Motifs in the Design and Application of Bioisosteres for Drug Design. *J. Med. Chem.* **2018**, *61*, 5822–5880. DOI: 10.1021/acs.jmedchem.7b01788.

[214] P. K. Mykhailiuk. Saturated Bioisosteres of Benzene: Where to go Next? *Org. Biomol. Chem.* **2019**, *17*, 2839–2849. DOI: 10.1039/C8OB02812E.

[215] G. S. Prakash and F. Wang. Fluorine: The New Kingpin of Drug Discovery. *Chim. Oggi* **2012**, *30*, 30–36.

[216] E. Vitaku, D. T. Smith and J. T. Njardarson. Analysis of the Structural Diversity, Substitution Patterns, and Frequency of Nitrogen Heterocycles among U.S. FDA Approved Pharmaceuticals. *J. Med. Chem.* **2014**, *57*, 10257–10274. DOI: 10.1021/jm501100b.

[217] M. D. Delost, D. T. Smith, B. J. Anderson, *et al.* From Oxiranes to Oligomers: Architectures of U.S. FDA Approved Pharmaceuticals Containing Oxygen Heterocycles. *J. Med. Chem.* **2018**, *61*, 10996–11020. DOI: 10.1021/acs.jmedchem.8b00876.

[218] Open Source Malaria GitHub. The Nemesis – proposed synthesis Haverford College. `https://github.com/OpenSourceMalaria/OSM_To_Do_List/issues/409`, Accessed 9 Apr 2019.

[219] Open Source Malaria GitHub. Starting Synthesis of "The Nemesis". `https://github.com/OpenSourceMalaria/OSM_To_Do_List/issues/430`, Accessed 21 Apr 2019.

[220] Open Source Malaria GitHub. Finishing up "The Nemesis". `https://github.com/OpenSourceMalaria/OSM_To_Do_List/issues/466`, Accessed 21 Apr 2019.

[221] P. E. Eaton and T. W. Cole. Cubane. *J. Am. Chem. Soc.* **1964**, *86*, 3157–3158. DOI: 10.1021/ja01069a041.

[222] N. B. Chapman, J. M. Key and K. J. Toyne. The Preparation and Properties of Cage Polycyclic Systems. I. Pentacyclo[5.3.0.$0^{2,5}$.$0^{3,9}$.$0^{4,8}$]decane and Pentacyclo[4.3.0.$0^{2,5}$.$0^{3,8}$.$0^{4,7}$]nonane Derivatives. *J. Org. Chem.* **1970**, *35*, 3860–3867. DOI: 10.1021/jo00836a062.

[223] M. J. Falkiner, S. W. Littler, K. J. McRae, *et al.* Pilot-Scale Production of Dimethyl 1,4-Cubanedicarboxylate. *Org. Process Res. Dev.* **2013**, *17*, 1503–1509. DOI: 10.1021/op400181g.

[224] K. F. Biegasiewicz, J. R. Griffiths, G. P. Savage, *et al.* Cubane: 50 Years Later. *Chemical Reviews* **2015**, *115*, 6719–6745. DOI: 10.1021/cr500523x.

[225] T. A. Reekie, C. M. Williams, L. M. Rendina, *et al.* Cubanes in Medicinal Chemistry. *J. Med. Chem.* **2018**, *62*, 1078–1095. DOI: 10.1021/acs.jmedchem.8b00888.

[226] M. Scholz and E. Hey-Hawkins. Carbaboranes as Pharmacophores: Properties, Synthesis, and Application Strategies. *Chem. Rev.* **2011**, *111*, 7035–7062. DOI: 10.1021/cr200038x.

[227] B. Chalmers, H. Xing, S. Houston, *et al.* Validating Eaton's Hypothesis: Cubane as a Benzene Bioisostere. *Angew. Chem. Int. Ed.* **2016**, *55*, 3580–3585. DOI: 10.1002/ange.201510675.

[228] Open Source Malaria GitHub. Cubane? `https://github.com/OpenSourceMalaria/OSM_To_Do_List/issues/379`, Accessed 10 July 2018.

[229] J. Griffiths, J. Tsanaktsidis, G. Savage, *et al.* Thermochemical Properties of Iodinated Cubane Derivatives. *Thermochim. Acta* **2010**, *499*, 15–20. DOI: 10.1016/j.tca.2009.10.015.

[230] K.-I. Yamashita, M. Tsuboi, M. S. Asano, *et al.* Facile Aromatic Finkelstein Iodination (AFI) Reaction in 1,3-Dimethyl-2-imidazolidinone (DMI). *Synth. Commun.* **2011**, *42*, 170–175. DOI: 10.1080/00397911.2010.523152.

[231] V. Prelog and R. Seiwerth. Über die Synthese des Adamantans. *Eur. J. Inorg. Chem.* **1941**, *74*, 1644–1648. DOI: 10.1002/cber.19410741004.

[232] P. von R. Schleyer. A Simple Preparation of Adamantane. *J. Am. Chem. Soc.* **1957**, *79*, 3292–3292. DOI: 10.1021/ja01569a086.

[233] G. A. Olah and O. Farooq. Superacid-Catalyzed Isomerization of *endo*- to *exo*-Trimethylenenorbornane (Tetrahydrodicyclopentadiene) and to Adamantane. *J. Org. Chem.* **1986**, *51*, 5410–5413. DOI: 10.1021/jo00376a067.

[234] G. Lamoureux and G. Artavia. Use of the Adamantane Structure in Medicinal Chemistry. *Curr. Med. Chem.* **2010**, *17*, 2967–2978. DOI: 10.2174/092986710792065027.

[235] A. D. Brown, M. E. Bunnage, P. A. Glossop, *et al.* The Discovery of Long Acting β_2-Adrenoreceptor Agonists. *Bioorg. Med. Chem. Lett.* **2007**, *17*, 4012–4015. DOI: 10.1016/j.bmcl.2007.04.081.

[236] A. D. Brown, M. E. Bunnage, P. A. Glossop, *et al.* The Discovery of Adamantyl-derived, Inhaled, Long Acting β_2-Adrenoreceptor Agonists. *Bioorg. Med. Chem. Lett.* **2008**, *18*, 1280–1283. DOI: 10.1016/j.bmcl.2008.01.034.

[237] X. Bao, Y. Sun, C. Bao, *et al.* Design, Synthesis and Evaluation of *N*-Hydroxypropenamides Based on Adamantane to Overcome Resistance in NSCLC. *Bioorg. Chem.* **2019**, *86*, 696–704. DOI: 10.1016/j.bioorg.2019.02.047.

[238] K. B. Wiberg, D. S. Connor and G. M. Lampman. The Reaction of 3-Bromocyclobutane-1-methyl Bromide with Sodium: Bicyclo[1. 1. 1]pentane. *Tetrahedron Lett.* **1964**, *5*, 531–534. DOI: 10.1016/S0040-4039(00)73269-2.

[239] K. B. Wiberg and D. S. Connor. Bicyclo[1.1.1]pentane. *J. Am. Chem. Soc.* **1966**, *88*, 4437–4441. DOI: 10.1021/ja00971a025.

[240] M. D. Levin, P. Kaszynski and J. Michl. Bicyclo[1.1.1]pentanes, [*n*]Staffanes, [1.1.1]Propellanes, and Tricyclo[2.1.0.0^{2,5}]pentanes. *Chem. Rev.* **2000**, *100*, 169–234. DOI: 10.1021/cr990094z.

[241] P. Kaszynski and J. Michl. A Practical Photochemical Synthesis of Bicyclo[1.1.1]pentane-1,3-dicarboxylic acid. *J. Org. Chem.* **1988**, *53*, 4593–4594. DOI: 10.1021/jo00254a038.

[242] J. Kanazawa and M. Uchiyama. Recent Advances in the Synthetic Chemistry of Bicyclo[1.1.1]pentane. *Synlett* **2018**, *30*, 1–11. DOI: 10.1055/s-0037-1610314.

[243] A. F. Stepan, C. Subramanyam, I. V. Efremov, *et al.* Application of the Bicyclo[1.1.1]pentane Motif as a Nonclassical Phenyl Ring Bioisostere in the Design of a Potent and Orally Active γ-Secretase Inhibitor. *J. Med. Chem.* **2012**, *55*, 3414–3424. DOI: 10.1021/jm300094u.

[244] N. D. Measom, K. D. Down, D. J. Hirst, *et al.* Investigation of a Bicyclo[1.1.1]pentane as a Phenyl Replacement within an LpPLA2 Inhibitor. *ACS Med. Chem. Lett.* **2016**, *8*, 43–48.

DOI: 10.1021/acsmedchemlett.6b00281.

[245] Y. L. Goh, Y. T. Cui, V. Pendharkar, *et al.* Toward Resolving the Resveratrol Conundrum: Synthesis and *in Vivo* Pharmacokinetic Evaluation of BCP–Resveratrol. *ACS Med. Chem. Lett.* **2017**, *8*, 516–520. DOI: 10.1021/acsmedchemlett.7b00018.

[246] S. O. Kokhan, A. V. Tymtsunik, S. L. Grage, *et al.* Design, Synthesis, and Application of an Optimized Monofluorinated Aliphatic Label for Peptide Studies by Solid-State ^{19}F NMR Spectroscopy. *Angew. Chem. Int. Ed.* **2016**, *55*, 14788–14792. DOI: 10.1002/anie.201608116.

[247] [1.1.1]Propellane. *Org. Synth.* **1998**, *75*, 98. DOI: 10.15227/orgsyn.075.0098.

[248] J. Belzner, U. Bunz, K. Semmler, *et al.* Concerning the Synthesis of [1.1.1]Propellane. *Chem. Ber.* **1989**, *122*, 397–398. DOI: 10.1002/cber.19891220233.

[249] K. D. Bunker, N. W. Sach, Q. Huang, *et al.* Scalable Synthesis of 1-Bicyclo[1.1.1]pentylamine via a Hydrohydrazination Reaction. *Org. Lett.* **2011**, *13*, 4746–4748. DOI: 10.1021/ol201883z.

[250] K. D. Bunker. Propellane Derivatives and Synthesis, **2015**. WO2015134710A1.

[251] A. Maderna, C. Subramanyam, L. N. Tumey, *et al.* Bifunctional Cytotoxic Agents Containing the CTI Pharmacophore, **2016**. US20160271270A1.

[252] E. Della and J. Tsanaktsidis. Decarboxylation of Bridgehead Carboxylic Acids by the Barton Procedure. *Aust. J. Chem.* **1986**, *39*, 2061. DOI: 10.1071/CH9862061.

[253] Y. L. Goh and V. A. Adsool. Radical Fluorination Powered Expedient Synthesis of 3-Fluorobicyclo[1.1.1]pentan-1-amine. *Org. Biomol. Chem.* **2015**, *13*, 11597–11601. DOI: 10.1039/C5OB02066B.

[254] K. D. Bunker, C. Guo, M. C. Grier, *et al.* Bicyclic compounds, **2015**. US20160075654A1.

[255] I. A. Levandovsky, D. I. Sharapa, O. A. Cherenkova, *et al.* The Chemistry of D_3-Trishomocubane. *Russ. Chem. Rev.* **2010**, *79*, 1005–1026. DOI: 10.1070/rc2010v079n11abeh004119.

[256] G. R. Underwood and B. Ramamoorthy. Chemical Studies of Caged Compounds. The Synthesis of Hexacyclo[5,4,0,$0^{2,6}$,$0^{3,10}$,$0^{5,9}$,$0^{8,11}$]undecane, "Homopentaprismane". *J. Chem. Soc. D* **1970**, *0*, 12b–13. DOI: 10.1039/c2970000012b.

[257] G. R. Underwood and B. Ramamoorthy. Chemical Studies of Caged Compounds. II The Synthesis of Pentacyclo[6,3,0,$0^{2,6}$,$0^{3,10}$,$0^{5,9}$]undecane: Trishomocubane. *Tetrahedron Lett.* **1970**, *11*, 4125–4127. DOI: 10.1016/s0040-4039(01)98683-6.

[258] S. D. Banister, I. A. Moussa, C. Beinat, *et al.* Trishomocubane as a Scaffold for the Development of Selective Dopamine Transporter (DAT) Ligands. *Bioorg. Med. Chem. Lett.* **2011**, *21*, 38–41. DOI: 10.1016/j.bmcl.2010.11.075.

[259] A. M. Aleksandrov, T. J. Pehk, A. E. Petrenko, *et al.* Accessible Route to 4-Substituted "Bird-Cage" Hydrocarbon Derivatives. *J. Org. Chem.* **1994**, *59*, 3709–3711. DOI: 10.1021/jo00092a038.

[260] T. L. Heying, J. W. Ager, S. L. Clark, *et al.* A New Series of Organoboranes. I. Carboranes from the Reaction of Decaborane with Acetylenic Compounds. *Inorg. Chem.* **1963**, *2*, 1089–1092. DOI: 10.1021/ic50010a002.

[261] M. M. Fein, J. Bobinski, N. Mayes, *et al.* Carboranes. I. The Preparation and Chemistry of 1-Isopropenylcarborane and its Derivatives (a New Family of Stable Clovoboranes). *Inorg. Chem.* **1963**, *2*, 1111–1115. DOI: 10.1021/ic50010a007.

[262] J. F. Valliant, K. J. Guenther, A. S. King, *et al.* The Medicinal Chemistry of Carboranes. *Coord. Chem. Rev.* **2002**, *232*, 173–230. DOI: 10.1016/s0010-8545(02)00087-5.

[263] F. Issa, M. Kassiou and L. M. Rendina. Boron in Drug Discovery: Carboranes as Unique Pharmacophores in Biologically Active Compounds. *Chem. Rev.* **2011**, *111*, 5701–5722. DOI: 10.1021/cr2000866.

[264] M. L. Beer, J. Lemon and J. F. Valliant. Preparation and Evaluation of Carborane Analogues of Tamoxifen. *J. Med. Chem.* **2010**, *53*, 8012–8020. DOI: 10.1021/jm100758j.

[265] M. Scholz, K. Bensdorf, R. Gust, *et al.* Asborin: The Carbaborane Analogue of Aspirin. *ChemMedChem* **2009**, *4*, 746–748. DOI: 10.1002/cmdc.200900072.

[266] M. Scholz, M. Steinhagen, J. T. Heiker, *et al.* Asborin Inhibits Aldo/Keto Reductase 1A1. *ChemMedChem* **2010**, *6*, 89–93. DOI: 10.1002/cmdc.201000368.

[267] J. F. Valliant, P. Schaffer, K. A. Stephenson, *et al.* Synthesis of Boroxifen, A *Nido*-Carborane Analogue of Tamoxifen. *J. Org. Chem.* **2002**, *67*, 383–387. DOI: 10.1021/jo0158229.

[268] R. C. Reynolds, S. R. Campbell, R. G. Fairchild, *et al.* Novel Boron-Containing, Nonclassical Antifolates: Synthesis and Preliminary Biological and Structural Evaluation. *J. Med. Chem.* **2007**, *50*, 3283–3289. DOI: 10.1021/jm0701977.

[269] Z. J. Lesnikowski. Boron Units as Pharmacophores - New Applications and Opportunities of Boron Cluster Chemistry. *Collect. Czech. Chem. Commun.* **2007**, *72*, 1646–1658. DOI: 10.1135/cccc20071646.

[270] M. Scholz, A. L. Blobaum, L. J. Marnett, *et al.* *ortho*-Carbaborane Derivatives of Indomethacin as Cyclooxygenase (COX)-2 Selective Inhibitors. *Bioorg. Med. Chem.* **2012**, *20*, 4830–4837. DOI: 10.1016/j.bmc.2012.05.063.

[271] M. W. Lee, Y. V. Sevryugina, A. Khan, *et al.* Carboranes Increase the Potency of Small Molecule Inhibitors of Nicotinamide Phosphoribosyltranferase. *J. Med. Chem.* **2012**, *55*, 7290–7294. DOI: 10.1021/jm300740t.

[272] K. Li, Y. Wang, G. Yang, *et al.* Oxa, Thia, Heterocycle, and Carborane Analogues of SQ109: Bacterial and Protozoal Cell Growth Inhibitors. *ACS Infect. Dis.* **2015**, *1*, 215–221. DOI: 10.1021/acsinfecdis.5b00026.

[273] L. I. Zakharkin, V. N. Kalinin and L. S. Podvisotskaya. The Comparative Reactivity of ortho-, meta-, and para-Carboranes. *Russ. Chem. Bull.* **1970**, *19*, 1227–1231. DOI: 10.1007/BF00852664.

[274] S. Fujii, A. Kano, C. Songkram, *et al.* Synthesis and Structure–Activity Relationship of *p*-Carborane-Based Non-Secosteroidal Vitamin D Analogs. *Bioorg. Med. Chem.* **2014**, *22*, 1227–1235. DOI: 10.1016/j.bmc.2014.01.015.

[275] P. K. Mandal and J. S. McMurray. Pd–C-Induced Catalytic Transfer Hydrogenation with Triethylsilane. *J. Org. Chem.* **2007**, *72*, 6599–6601. DOI: 10.1021/jo0706123.

[276] J. Yoo, J.-W. Hwang and Y. Do. Facile and Mild Deboronation *o*-Carboranes Using Cesium Fluoride. *Inorg. Chem.* **2001**, *40*, 568–570. DOI: 10.1021/ic000768k.

[277] Y. P. Auberson, C. Brocklehurst, M. Furegati, *et al.* Improving Nonspecific Binding and Solubility: Bicycloalkyl Groups and Cubanes as *para*-Phenyl Bioisosteres. *ChemMedChem* **2017**, *12*, 590–598. DOI: 10.1002/cmdc.201700082.

[278] K. C. Nicolaou, D. Vourloumis, S. Totokotsopoulos, *et al.* Synthesis and Biopharmaceutical Evaluation of Imatinib Analogues Featuring Unusual Structural Motifs. *ChemMedChem* **2015**, *11*, 31–37. DOI: 10.1002/cmdc.201500510.

[279] Y. Feng, L. Liu, J.-T. Wang, *et al.* Homolytic C–H and N–H Bond Dissociation Energies of Strained Organic Compounds. *J. Org. Chem.* **2004**, *69*, 3129–3138. DOI: 10.1021/jo035306d.

[280] Open Source Malaria GitHub. Late Stage Functionalisation of Series 4 Compounds Through Biosynthesis. `https://github.com/OpenSourceMalaria/OSM_To_Do_List/issues/513`, Accessed 21 Apr 2019.

[281] Open Source Malaria GitHub. Update on Scott Obach's Biofunctionalisation Experiments.

https://github.com/OpenSourceMalaria/Series4/issues/13, Accessed 21 Apr 2019.

[282] D. Bandak, O. Babii, R. Vasiuta, *et al.* Design and Synthesis of Novel ^{19}F-Amino Acid: A Promising ^{19}F NMR Label for Peptide Studies. *Org. Lett.* **2015**, *17*, 226–229. DOI: 10.1021/ol503300m.

[283] N. Morel-Desrosiers and J.-P. Morel. Standard Molar Enthalpies, Volumes, and Heat Capacities of Adamantane in Cyclohexane, n-Hexane, and Carbon Tetrachloride. Interpretation using the Scaled-Particle Theory. *J. Solution Chem.* **1979**, *8*, 579–592. DOI: 10.1007/BF00715998.

[284] R. K. Bohn and M. D. Bohn. Molecular Structures of 1,2-, 1,7-, and 1,12-Dicarba-closo-dodecaborane(12), $B_{10}C_2H_{12}$. *Inorg. Chem.* **1971**, *10*, 350–355. DOI: 10.1021/ic50096a026.

[285] M. Schenone, V. Dančík, B. K. Wagner, *et al.* Target Identification and Mechanism of Action in Chemical Biology and Drug Discovery. *Nat. Chem. Biol.* **2013**, *9*, 232–240. DOI: 10.1038/nchembio.1199.

[286] V. Fetz, H. Prochnow, M. Brönstrup, *et al.* Target identification by Image Analysis. *Nat. Prod. Rep.* **2016**, *33*, 655–667. DOI: 10.1039/C5NP00113G.

[287] Y.-F. Dai and X.-M. Zhao. A Survey on the Computational Approaches to Identify Drug Targets in the Postgenomic Era. *Biomed Res. Int.* **2015**, *2015*, 1–9. DOI: 10.1155/2015/239654.

[288] J. H. Woo, Y. Shimoni, W. S. Yang, *et al.* Elucidating Compound Mechanism of Action by Network Perturbation Analysis. *Cell* **2015**, *162*, 441–451. DOI: 10.1016/j.cell.2015.05.056.

[289] M. Kampmann. Elucidating Drug Targets and Mechanisms of Action by Genetic Screens in Mammalian Cells. *Chem. Commun.* **2017**, *53*, 7162–7167. DOI: 10.1039/C7CC02349A.

[290] M. R. Luth, P. Gupta, S. Ottilie, *et al.* Using *in Vitro* Evolution and Whole Genome Analysis To Discover Next Generation Targets for Antimalarial Drug Discovery. *ACS Infect. Dis.* **2018**, *4*, 301–314. DOI: 10.1021/acsinfecdis.7b00276.

[291] P. H. Schlesinger, D. J. Krogstad and B. L. Herwaldt. Antimalarial Agents: Mechanisms of Action. *Antimicrob. Agents Chemother.* **1988**, *32*, 793–798.

[292] A. Saifi. Antimalarial Drugs: Mode of Action and Status of Resistance. *Afr. J. Pharm. Pharmacol.* **2013**, *7*, 148–156. DOI: 10.5897/AJPPX12.015.

[293] S. Parija and H. Antony. Antimalarial Drug Resistance: An Overview. *Trop. Parasitol.* **2016**, *6*, 30. DOI: 10.4103/2229-5070.175081.

[294] J. M. Dziekan, H. Yu, D. Chen, *et al.* Identifying Purine Nucleoside Phosphorylase as the

Target of Auinine using Cellular Thermal Shift Assay. *Sci. Transl. Med.* **2019**, *11*, eaau3174. DOI: 10.1126/scitranslmed.aau3174.

[295] P. M. O'Neill, V. E. Barton and S. A. Ward. The Molecular Mechanism of Action of Artemisinin - The Debate Continues. *Molecules* **2010**, *15*, 1705–1721. DOI: 10.3390/molecules15031705.

[296] J. Wang, C.-J. Zhang, W. N. Chia, *et al.* Haem-Activated Promiscuous Targeting of Artemisinin in *Plasmodium falciparum*. *Nat. Commun.* **2015**, *6*. DOI: 10.1038/ncomms10111.

[297] L. Tilley, J. Straimer, N. F. Gnädig, *et al.* Artemisinin Action and Resistance in *Plasmodium falciparum*. *Trends Parasitol.* **2016**, *32*, 682–696. DOI: 10.1016/j.pt.2016.05.010.

[298] A. Shandilya, S. Chacko, B. Jayaram, *et al.* A Plausible Mechanism for the Antimalarial Activity of Artemisinin: A Computational Approach. *Sci. Rep.* **2013**, *3*. DOI: 10.1038/srep02513.

[299] A. Mbengue, S. Bhattacharjee, T. Pandharkar, *et al.* A Molecular Mechanism of Artemisinin Resistance in *Plasmodium falciparum* Malaria. *Nature* **2015**, *520*, 683–687. DOI: 10.1038/nature14412.

[300] S. Mok, E. A. Ashley, P. E. Ferreira, *et al.* Population Transcriptomics of Human Malaria Parasites Reveals the Mechanism of Artemisinin Resistance. *Science* **2014**, *347*, 431–435. DOI: 10.1126/science.1260403.

[301] D. R. Hill, J. K. Baird, M. E. Parise, *et al.* Primaquine: Report from CDC Expert Meeting on Malaria Chemoprophylaxis I. *Am. J. Trop. Med. Hyg.* **2006**, *75*, 402–415. DOI: 10.4269/ajtmh.2006.75.402.

[302] D. Fernando, C. Rodrigo and S. Rajapakse. Primaquine in Vivax Malaria: An Update and Review on Management Issues. *Malar. J.* **2011**, *10*, 351. DOI: 10.1186/1475-2875-10-351.

[303] A. R. Gomes, M. Ravenhall, E. D. Benavente, *et al.* Genetic Diversity of Next Generation Antimalarial Targets: A Baseline for Drug Resistance Surveillance Programmes. *Int. J. Parasitol. Drugs Drug Resist.* **2017**, *7*, 174–180. DOI: 10.1016/j.ijpddr.2017.03.001.

[304] N. Kato, E. Comer, T. Sakata-Kato, *et al.* Diversity-Oriented Synthesis Yields Novel Multistage Antimalarial Inhibitors. *Nature* **2016**, *538*, 344–349. DOI: 10.1038/nature19804.

[305] C. K. Dong, S. Urgaonkar, J. F. Cortese, *et al.* Identification and Validation of Tetracyclic Benzothiazepines as *Plasmodium falciparum* Cytochrome bc_1 Inhibitors. *Chem. Biol.* **2011**,

18, 1602–1610. DOI: 10.1016/j.chembiol.2011.09.016.

[306] A. M. Lehane, M. C. Ridgway, E. Baker, *et al.* Diverse Chemotypes Disrupt Ion Homeostasis in the Malaria Parasite. *Mol. Microbiol.* **2014**, *94*, 327–339. DOI: 10.1111/mmi.12765.

[307] K. J. Saliba and K. Kirk. pH Regulation in the Intracellular Malaria Parasite, *Plasmodium falciparum*. *J. Biol. Chem.* **1999**, *274*, 33213–33219. DOI: 10.1074/jbc.274.47.33213.

[308] Biological Evaluation of Compounds. Evaluation of Series 4 Compounds vs ATP-Resistant Mutants. `http://malaria.ourexperiment.org/biological_data/11448/post.html`, Accessed 30 Jun 2019.

[309] Pharmacophore Modelling of OSM Compounds. Pharmacophore Modelling of the Malaria Box PfATP4 Active Compounds. `http://malaria.ourexperiment.org/pharmacophore_modelling_/7971/post.html`, Accessed 28 May 2019.

[310] Pharmacophore Modelling of OSM Compounds. Using the Pharmacophore Model to search Commercial Compounds for new leads. `http://malaria.ourexperiment.org/pharmacophore_modelling_/12498/post.html`, Accessed 28 May 2019.

[311] Open Source Malaria GitHub. COMPETITION: A Predictive Model For Series Four. `https://github.com/OpenSourceMalaria/OSM_To_Do_List/issues/421`, Accessed 28 May 2019.

[312] Google Sheets. Summary of Competition Entries. `https://docs.google.com/spreadsheets/d/1pY6sYXIw66jnzUO3CoP8HceYdDjLRvwg5_pLkBY1Wek/edit?usp=sharing`, Accessed 12 Jun 2019.

[313] A. S. M. Dennis, J. E. O. Rosling, A. M. Lehane, *et al.* Diverse Antimalarials from Whole-Cell Phenotypic Screens Disrupt Malaria Parasite Ion and Volume Homeostasis. *Sci. Rep.* **2018**, *8*. DOI: 10.1038/s41598-018-26819-1.

[314] Open Source Malaria GitHub. Competition Results! `https://github.com/OpenSourceMalaria/OSM_To_Do_List/issues/538`, Accessed 12 Jun 2019.

[315] G. A. Gutman. International Union of Pharmacology. LIII. Nomenclature and Molecular Relationships of Voltage-Gated Potassium Channels. *Pharmacol. Rev.* **2005**, *57*, 473–508. DOI: 10.1124/pr.57.4.10.

[316] M. Recanatini, E. Poluzzi, M. Masetti, *et al.* QT Prolongation Through hERG K^+ Channel Blockade: Current Knowledge and Strategies for the Early Prediction During Drug Development. *Med. Res. Rev.* **2004**, *25*, 133–166. DOI: 10.1002/med.20019.

[317] M. Perry, M. Sanguinetti and J. Mitcheson. Revealing the Structural Basis of Action of

hERG Potassium Channel Activators and Blockers. *J. Physiol. (Lond.)* **2010**, *588*, 3157–3167. DOI: 10.1113/jphysiol.2010.194670.

[318] J. I. Vandenberg, M. D. Perry, M. J. Perrin, *et al.* hERG K^+ Channels: Structure, Function, and Clinical Significance. *Physiol. Rev.* **2012**, *92*, 1393–1478. DOI: 10.1152/physrev.00036.2011.

[319] J. M. Kratz, U. Grienke, O. Scheel, *et al.* Natural Products Modulating the hERG Channel: Heartaches and Hope. *Nat. Prod. Rep.* **2017**, *34*, 957–980. DOI: 10.1039/c7np00014f.

[320] J. I. Vandenberg, E. Perozo and T. W. Allen. Towards a Structural View of Drug Binding to hERG K^+ Channels. *Trends Pharmacol. Sci.* **2017**, *38*, 899–907. DOI: 10.1016/j.tips.2017.06.004.

[321] M.-L. Roy, R. Dumaine and A. M. Brown. HERG, a Primary Human Ventricular Target of the Nonsedating Antihistamine Terfenadine. *Circulation* **1996**, *94*, 817–823. DOI: 10.1161/01.CIR.94.4.817.

[322] H. Suessbrich, S. Waldegger, F. Lang, *et al.* Blockade of HERG Channels Expressed in *Xenopus* Oocytes by the Histamine Receptor Antagonists Terfenadine and Astemizole. *FEBS Lett.* **1996**, *385*, 77–80. DOI: 10.1016/0014-5793(96)00355-9.

[323] C. Scherer, C. Lerche, N. Decher, *et al.* The Antihistamine Fexofenadine does not Affect I_{Kr} Currents in a Case Report of Drug-Induced Cardiac Arrythmia. *Br. J. Pharmacol.* **2002**, *137*, 892–900. DOI: 10.1038/sj.bjp.0704873.

[324] D. Rampe, M. K. Murawsky, J. Grau, *et al.* The Antipsychotic Agent Sertindole is a High Affinity Antagonist of the Human Cardiac Potassium Channel HERG. *J. Pharmacol. Exp. Ther.* **1998**, *286*, 788–793.

[325] D. Rampe, M.-L. Roy, A. Dennis, *et al.* A Mechanism for the Proarrhythmic Effects of Cisapride (Propulsid): High Affinity Blockade of the Human Cardiac Potassium Channel HERG. *FEBS Lett.* **1997**, *417*, 28–32. DOI: 10.1016/S0014-5793(97)01249-0.

[326] Z. Zhou, V. R. Vorperian, Q. Gong, *et al.* Block of HERG Potassium Channels by the Antihistamine Astemizole and its Metabolites Desmethylastemizole and Norastemizole. *J. Cardiovasc. Electrophysiol.* **1999**, *10*, 836–843. DOI: 10.1111/j.1540-8167.1999.tb00264.x.

[327] B. Wible, P. Hawryluk, E. Ficker, *et al.* HERG-Lite: A Novel Comprehensive High-Throughput Screen for Drug-Induced hERG Risk. *J. Pharmacol. Toxicol. Meth.* **2005**, *52*, 136–145. DOI: 10.1016/j.vascn.2005.03.008.

[328] W. Wang and R. MacKinnon. Cryo-EM Structure of the Open Human *Ether-à-go-go*-Related K^+ Channel hERG. *Cell* **2017**, *169*, 422–430.e10. DOI: 10.1016/j.cell.2017.03.048.

[329] Nobelprize.org. The Nobel Prize in Chemistry 2017. `https://www.nobelprize.org/prizes/chemistry/2017/summary/`, Accessed 5 Apr 2018.

[330] M. V. Helliwell, Y. Zhang, A. E. Harchi, *et al.* Structural Implications of hERG K^+ Channel Block by a High-Affinity Minimally Structured Blocker. *J. Biol. Chem.* **2018**, *293*, 7040–7057. DOI: 10.1074/jbc.ra117.000363.

[331] T. Sato, H. Yuki, K. Ogura, *et al.* Construction of an Integrated Database for hERG Blocking Small Molecules. *PLoS One* **2018**, *13*, e0199348. DOI: 10.1371/journal.pone.0199348.

[332] F. Du, J. J. Babcock, H. Yu, *et al.* Global Analysis Reveals Families of Chemical Motifs Enriched for hERG Inhibitors. *PLoS One* **2015**, *10*, e0118324. DOI: 10.1371/journal.pone.0118324.

[333] C. Zhang, Y. Zhou, S. Gu, *et al. In silico* Prediction of hERG Potassium Channel Blockage by Chemical Category Approaches. *Toxicol. Res.* **2016**, *5*, 570–582. DOI: 10.1039/C5TX00294J.

[334] C. Jamieson, E. M. Moir, Z. Rankovic, *et al.* Medicinal Chemistry of hERG Optimizations: Highlights and Hang-Ups. *J. Med. Chem.* **2006**, *49*, 5029–5046. DOI: 10.1021/jm060379l.

[335] L. Di and E. Kerns. *Drug-like Properties: Concepts, Structure Design and Methods: From ADME to Toxicity Optimization.* Elsevier Science, **2008**.

[336] W. Lee, M. J. Windley, M. D. Perry, *et al.* Protocol-Dependent Differences in IC_{50} Values Measured in Human Ether-Á-Go-Go–Related Gene Assays Occur in a Predictable Way and Can Be Used to Quantify State Preference of Drug Binding. *Mol. Pharmacol.* **2019**, *95*, 537–550. DOI: 10.1124/mol.118.115220.

[337] J. S. Mitcheson, J. Chen, M. Lin, *et al.* A Structural Basis for Drug-Induced Long QT Syndrome. *Proc. Natl. Acad. Sci. U.S.A.* **2000**, *97*, 12329–12333. DOI: 10.1073/pnas.210244497.

[338] R. A. Pearlstein, R. J. Vaz, J. Kang, *et al.* Characterization of HERG Potassium Channel Inhibition using CoMSiA 3D QSAR and Homology Modeling Approaches. *Bioorg. Med. Chem. Lett.* **2003**, *13*, 1829–1835. DOI: 10.1016/S0960-894X(03)00196-3.

[339] S. R. Fletcher, F. Burkamp, P. Blurton, *et al.* 4-(Phenylsulfonyl)piperidines: Novel, Selective, and Bioavailable 5-HT_{2A} Receptor Antagonists. *J. Med. Chem.* **2002**, *45*, 492–503. DOI: 10.1021/jm011030v.

[340] Y. N. Imai, S. Ryu and S. Oiki. Docking Model of Drug Binding to the Human Ether-à-go-

go Potassium Channel Guided by Tandem Dimer Mutant Patch-Clamp Data: A Synergic Approach. *J. Med. Chem.* **2009**, *52*, 1630–1638. DOI: 10.1021/jm801236n.

[341] M. E. Fraley, K. L. Arrington, C. A. Buser, *et al.* Optimization of the Indolyl Quinolinone Class of KDR (VEGFR-2) Kinase Inhibitors. *Bioorg. Med. Chem. Lett.* **2004**, *14*, 351–355. DOI: 10.1016/j.bmcl.2003.11.007.

[342] D. Fernandez, A. Ghanta, G. W. Kauffman, *et al.* Physicochemical Features of the hERG Channel Drug Binding Site. *J. Biol. Chem.* **2003**, *279*, 10120–10127. DOI: 10.1074/jbc.M310683200.

[343] D. Rampe, B. Wible, A. M. Brown, *et al.* Effects of Terfenadine and its Metabolites on a Delayed Rectifier K^+ Channel Cloned from Human Heart. *Mol. Pharmacol.* **1993**, *44*, 1240–1245.

[344] R. J. Vaz, Z. Gao, J. Pribish, *et al.* Design of Bivalent Ligands Using Hydrogen Bond Linkers: Synthesis and Evaluation of Inhibitors for Human β-Tryptase. *Bioorg. Med. Chem. Lett.* **2004**, *14*, 6053–6056. DOI: 10.1016/j.bmcl.2004.09.065.

[345] S. D. Edmondson, A. Mastracchio, M. Beconi, *et al.* Potent and Selective Proline Derived Dipeptidyl Peptidase IV Inhibitors. *Bioorg. Med. Chem. Lett.* **2004**, *14*, 5151–5155. DOI: 10.1016/j.bmcl.2004.07.056.

[346] B.-Y. Zhu, Z. J. Jia, P. Zhang, *et al.* Inhibitory Effect of Carboxylic Acid Group on hERG Binding. *Bioorg. Med. Chem. Lett.* **2006**, *16*, 5507–5512. DOI: 10.1016/j.bmcl.2006.08.039.

[347] P. Czodrowski. hERG Me Out. *J. Chem. Inf. Model.* **2013**, *53*, 2240–2251. DOI: 10.1021/ci400308z.

[348] Biological Evaluation of Compounds. hERG Data for MMV669844 and MMV670944. `http://malaria.ourexperiment.org/biological_data/9562`, Accessed 14 May 2019.

[349] Biological Evaluation of Compounds. Compounds sent for evaluation against the hERG ion channel at AstraZeneca. `http://malaria.ourexperiment.org/biological_data/11081`, Accessed 14 May 2019.

[350] Open Source Malaria GitHub. Meeting Discussion Point 3: Potency. `https://github.com/OpenSourceMalaria/OSM_To_Do_List/issues/390`, Accessed 1 Jul 2019.

[351] Open Source Malaria GitHub. The hERG Evador – proposed synthesis Haverford College. `https://github.com/OpenSourceMalaria/OSM_To_Do_List/issues/405`, Accessed 13 May 2019.

[352] Open Source Malaria GitHub. Start Synthesis of "the hERG Evador". https://github.com/OpenSourceMalaria/OSM_To_Do_List/issues/427, Accessed 13 May 2019.

[353] Open Source Malaria GitHub. Really confusing NMR for hERG evador: carboxylic acid proton coupled to a triplet??? https://github.com/OpenSourceMalaria/OSM_To_Do_List/issues/451, Accessed 10 July 2018.

[354] I. Iovel, Y. Goldberg and M. Shymanska. An Improved Synthesis of 5-Methylpyrazine-2-carboxylic acid. *Org. Prep. Proced. Int.* **1991**, *23*, 188–190. DOI: 10.1080/00304949109458308.

[355] Y. Yuan, S. A. Zaidi, O. Elbegdorj, *et al.* Design, Synthesis, and Biological Evaluation of 14-Heteroaromatic-Substituted Naltrexone Derivatives: Pharmacological Profile Switch from Mu Opioid Receptor Selectivity to Mu/Kappa Opioid Receptor Dual Selectivity. *J. Med. Chem.* **2013**, *56*, 9156–9169. DOI: 10.1021/jm4012214.

[356] C. Aciro, V. A. Steadman, S. N. Pettit, *et al.* Macrocyclic Inhibitors of Flaviviridae Viruses, **2013**. WO2013185090A1.

[357] B. G. Szczepankiewicz, C. Kosogof, L. T. J. Nelson, *et al.* Aminopyridine-Based c-Jun N-Terminal Kinase Inhibitors with Cellular Activity and Minimal Cross-Kinase Activity. *J. Med. Chem.* **2006**, *49*, 3563–3580. DOI: 10.1021/jm060199b.

[358] W. E. Bondinell, J. F. Callahan, W. F. Huffman, *et al.* Platelet Aggregation Inhibiting Compounds, **1998**. US6028087A.

[359] E. J. Hennessy and S. L. Buchwald. A General and Mild Copper-Catalyzed Arylation of Diethyl Malonate. *Org. Lett.* **2002**, *4*, 269–272. DOI: 10.1021/ol017038g.

[360] T. Takai, T. Koike, M. Nakamura, *et al.* Discovery of Novel 5,6,7,8-Tetrahydro[1,2,4]triazolo[4,3-*a*]pyridine Derivatives as γ-Secretase Modulators (Part 2). *Bioorg. Med. Chem.* **2016**, *24*, 3192–3206. DOI: 10.1016/j.bmc.2016.05.040.

[361] A. N. Balaev, A. A. Busel and V. E. Fedorov. Kilogram-Scale Pilot Synthesis of Fingolimod. *Pharm. Chem. J.* **2017**, *51*, 476–479. DOI: 10.1007/s11094-017-1636-x.

[362] SciStarter. SciStarter. https://scistarter.org, Accessed 26 Aug 2019.

[363] Citizen Science Association. Citizen Science Association. https://www.citizenscience.org, Accessed 26 Aug 2019.

[364] Zooniverse. Zooniverse. https://www.zooniverse.org, Accessed 26 Aug 2019.

[365] W. L. Scott and M. J. O'Donnell. Distributed Drug Discovery, Part 1: Linking Academia

and Combinatorial Chemistry to Find Drug Leads for Developing World Diseases. *J. Comb. Chem.* **2009**, *11*, 3–13. DOI: 10.1021/cc800183m.

[366] W. L. Scott, J. Alsina, C. O. Audu, *et al.* Distributed Drug Discovery, Part 2: Global Rehearsal of Alkylating Agents for the Synthesis of Resin-Bound Unnatural Amino Acids and Virtual D^3 Catalog Construction. *J. Comb. Chem.* **2009**, *11*, 14–33. DOI: 10.1021/cc800184v.

[367] W. L. Scott, C. O. Audu, J. L. Dage, *et al.* Distributed Drug Discovery, Part 3: Using D^3 Methodology to Synthesize Analogs of an Anti-Melanoma Compound. *J. Comb. Chem.* **2009**, *11*, 34–43. DOI: 10.1021/cc800185z.

[368] P. Zajdel, J. Król, K. Grychowska, *et al.* Solid-Phase Synthesis of Arylpiperazine Derivatives and Implementation of the Distributed Drug Discovery (D3) Project in the Search for CNS Agents. *Molecules* **2011**, *16*, 4104–4121. DOI: 10.3390/molecules16054104.

[369] W. L. Scott, R. E. Denton, K. A. Marrs, *et al.* Distributed Drug Discovery: Advancing Chemical Education through Contextualized Combinatorial Solid-Phase Organic Laboratories. *J. Chem. Educ.* **2015**, *92*, 819–826. DOI: 10.1021/ed500135n.

[370] Parkinson Research Group. The SHArK Project. `http://www.uwyo.edu/parkinson/shark_project.html`, Accessed 7 May 2019.

[371] J. G. Rowley, T. D. Do, D. A. Cleary, *et al.* Combinatorial Discovery Through a Distributed Outreach Program: Investigation of the Photoelectrolysis Activity of p-Type Fe, Cr, Al Oxides. *ACS Appl. Mater. Interfaces* **2014**, *6*, 9046–9052. DOI: 10.1021/am406045j.

[372] Drugs for Neglected Diseases *initiative*. Open Synthesis Network. `https://www.dndi.org/diseases-projects/open-innovation/open-synthesis-network/`, Accessed 7 May 2019.

[373] The OSM Blog. Alice Williamson's Open Source Undergrad Lab Course. `http://malaria.ourexperiment.org/the_osm_blog/11566/Alice_Williamsons_Open_Source_Undergrad_Lab_Course.html`, Accessed 12 July 2018.

[374] The OSM Blog. Special Studies Program Results: First Year Drug Design and Synthesis at The University of Sydney. `http://malaria.ourexperiment.org/the_osm_blog/14151/Special_Studies_Program_Results_First_Year_Drug_Design_and_Synthesis_at_The_University_of_Sydney.html`, Accessed 12 July 2018.

[375] Open Source Malaria GitHub. Special Studies Program (SSP) 2017. `https://github.com/OpenSourceMalaria/OSM_To_Do_List/issues/514`, Accessed 12 July 2018.

[376] Open Source Malaria GitHub. 2018 SSP Compounds. `https://github.com/OpenSourceMalaria/Series4/issues/53`, Accessed 6 May 2019.

[377] E. Breitmaier. *Structure Elucidation by NMR in Organic Chemistry*. John Wiley & Sons, Ltd, **2002**.

[378] Open Source Malaria GitHub. The Aussies - unexpected products from substitution down under. `https://github.com/OpenSourceMalaria/Series4/issues/46`, Accessed 12 Jul 2019.

[379] Open Source Malaria GitHub. KinomeScan of Series 4 and telesubstitution compounds. `https://github.com/OpenSourceMalaria/Series4/issues/69`, Accessed 12 Jul 2019.

[380] A. N. Cowell and E. A. Winzeler. Advances in Omics-Based Methods to Identify Novel Targets for Malaria and other Parasitic Protozoan Infections. *Genome Med.* **2019**, *11*. DOI: 10.1186/s13073-019-0673-3.

[381] K. Rujimongkon, M. Mungthin, J. Tummatorn, *et al.* Proteomic Analysis of *Plasmodium falciparum* Response to Isocryptolepine Derivative. *PLoS One* **2019**, *14*, e0220871. DOI: 10.1371/journal.pone.0220871.

[382] Open Source Malaria GitHub. Remaining Data Needed for OHOH Compound(s). `https://github.com/OpenSourceMalaria/Series4/issues/67`, Accessed 12 Jul 2019.

[383] M. Dolezal, R. Vicik, M. Miletin, *et al.* Synthesis and Antimycobacterial, Antifungal, and Photosynthesis-Inhibiting Evaluation of some Anilides of Substituted Pyrazine-2-carboxylic acids. *Chem. Pap. - Chem. Zvesti* **2000**, *54*, 245–248.

[384] Z. D. Konteatis, J. Popovici-Muller, J. M. Travins, *et al.* Therapeutically active compounds and their methods of use, **2015**. WO2015003640A1.

[385] L. Mattiello, C. D. Luca and L. Rampazzo. Electrochemistry of some Ethyl α-bromo(dihalophenyl)acetates and Electrochemical Synthesis of Diastereoisomeric Diethyl 2,3-bis(dihalogenophenyl)succinates. *J. Chem. Soc., Perkin Trans. 2* **1990**, 1041–1044. DOI: 10.1039/p29900001041.

[386] J. Pietruszka and G. Solduga. Enantiomerically Pure Cyclopropylamines from Cyclopropylboronic Esters. *Eur. J. Org. Chem.* **2009**, *2009*, 5998–6008. DOI: 10.1002/ejoc.200900882.

[387] N. Boechat, V. F. Ferreira, S. B. Ferreira, *et al.* Novel 1,2,3-Triazole Derivatives for Use Against *Mycobacterium tuberculosis* H37Rv (ATCC 27294) Strain. *J. Med. Chem.* **2011**, *54*, 5988–5999. DOI: 10.1021/jm2003624.

[388] H. Sharghi, R. Khalifeh and M. M. Doroodmand. Copper Nanoparticles on Charcoal for Multicomponent Catalytic Synthesis of 1,2,3-Triazole Derivatives from Benzyl Halides or Alkyl Halides, Terminal Alkynes and Sodium Azide in Water as a "Green" Solvent. *Adv. Synth. Catal.* **2009**, *351*, 207–218. DOI: 10.1002/adsc.200800612.

[389] S. Xu, Z. Yun, Y. Feng, *et al.* Zeolite Y Nanoparticle Assemblies with High Activity in the Direct Hydration of Terminal Alkynes. *RSC Adv.* **2016**, *6*, 69822–69827. DOI: 10.1039/c6ra11489j.

[390] M. Ellermann, S. N. Gradl, C. C. Kopitz, *et al.* Dihydrooxadiazinones, **2019**. WO2019025562A1.

[391] A. R. Katritzky, S. K. Singh, C. Cai, *et al.* Direct Synthesis of Esters and Amides from Unprotected Hydroxyaromatic and -aliphatic Carboxylic Acids. *J. Org. Chem.* **2006**, *71*, 3364–3374. DOI: 10.1021/jo052293q.

[392] W. J. Brouillette, E. E. Smissman and G. L. Grunewald. *N*-Acylcarbamates as Intermediates in Synthetic Approaches to a Bicyclic Trimethylene-Bridged 2,4-Oxazolidinedione and Hydantoin. *J. Org. Chem.* **1979**, *44*, 839–843. DOI: 10.1021/jo01319a039.

[393] S. A. Nieuwenhuis, L. B. Vertegaal, M. C. de Zoete, *et al.* Acid-catalyzed solvolysis of Polyenol Ethers. III. Effect of the Alkoxy Moiety. *Tetrahedron* **1994**, *50*, 13207–13230. DOI: 10.1016/S0040-4020(01)89330-3.

[394] J.-D. Hamel and J.-F. Paquin. Au-Catalyzed Intramolecular Hydroalkoxylation of *gem*-Difluorinated Alkynols. *J. Fluorine Chem.* **2018**, *216*, 11–23. DOI: 10.1016/j.jfluchem.2018.09.009.

[395] H. Ji, H. Li, P. Martásek, *et al.* Discovery of Highly Potent and Selective Inhibitors of Neuronal Nitric Oxide Synthase by Fragment Hopping. *J. Med. Chem.* **2009**, *52*, 779–797. DOI: 10.1021/jm801220a.

[396] A. del Prado, R. Navarro, P. Levkin, *et al.* Dual Stimuli-Responsive Polyamines Derived from *N*-Vinylpyrrolidones Through CuAAC Click Chemistry. *J. Polym. Sci., Part A: Polym. Chem.* **2015**, *54*, 1098–1108. DOI: 10.1002/pola.27949.

[397] H. Yang, Y. Li, M. Jiang, *et al.* General Copper-Catalyzed Transformations of Functional Groups from Arylboronic Acids in Water. *Chem. Eur. J.* **2011**, *17*, 5652–5660. DOI: 10.1002/chem.201003711.

[398] E. W. Della and D. K. Taylor. Synthesis of Some Bridgehead-Bridgehead-Disubstituted Bicyclo[1.1.1]pentanes. *J. Org. Chem.* **1994**, *59*, 2986–2996. DOI: 10.1021/jo00090a015.

[399] M. T. Hossain and J. W. Timberlake. Synthesis of Bisbicyclo[1.1.1]pentyldiazene. The Smallest Bridgehead Diazene. *J. Org. Chem.* **2001**, *66*, 6282–6285.

[400] J. Nekvinda, B. Grüner, D. Gabel, *et al.* Host-Guest Chemistry of Carboranes: Synthesis of Carboxylate Derivatives and Their Binding to Cyclodextrins. *Chem. Eur. J.* **2018**, *24*, 12970–12975. DOI: 10.1002/chem.201802134.

[401] H. K. Agarwal, B. Buszek, K. G. Ricks, *et al.* Synthesis of *closo*-1,7-Carboranyl Alkyl Amines. *Tetrahedron Lett.* **2011**, *52*, 5664–5667. DOI: 10.1016/j.tetlet.2011.08.101.

[402] G. Deguest, L. Bischoff, C. Fruit, *et al.* Anionic, in Situ Generation of Formaldehyde: A Very Useful and Versatile Tool in Synthesis. *Org. Lett.* **2007**, *9*, 1165–1167. DOI: 10.1021/ol070145b.

[403] R. Soengas and A. Estévez. Convenient Procedure for the Indium-Mediated Hydroxymethylation of Active Bromo Compounds: Transformation of Ketones into α-Hydroxymethyl Nitroalkanes. *Synlett* **2010**, *2010*, 2625–2627. DOI: 10.1055/s-0030-1258581.

[404] K. Masutani, T. Minowa, Y. Hagiwara, *et al.* Cyanation of Alcohols with Diethyl Cyanophosphonate and 2,6-Dimethyl-1,4-benzoquinone by a New Type of Oxidation–Reduction Condensation. *Bull. Chem. Soc. Jpn.* **2006**, *79*, 1106–1117. DOI: 10.1246/bcsj.79.1106.

[405] W. F. Bailey, K. M. Lambert, Z. D. Stempel, *et al.* Controlling the Conformational Energy of a Phenyl Group by Tuning the Strength of a Nonclassical CH···O Hydrogen Bond: The Case of 5-Phenyl-1,3-dioxane. *J. Org. Chem.* **2016**, *81*, 12116–12127. DOI: 10.1021/acs.joc.6b02428.

[406] A. J. Boddy, D. P. Affron, C. J. Cordier, *et al.* Rapid Assembly of Saturated Nitrogen Heterocycles in One-Pot: Diazo-Heterocycle "Stitching" by N-H Insertion and Cyclization. *Angew. Chem. Int. Ed.* **2018**, *58*, 1458–1462. DOI: 10.1002/anie.201812925.

[407] X. Xie, G. Cai and D. Ma. CuI/l-Proline-Catalyzed Coupling Reactions of Aryl Halides with Activated Methylene Compounds. *Org. Lett.* **2005**, *7*, 4693–4695. DOI: 10.1021/ol0518838.

[408] N. Ríos-Lombardía, E. Busto, E. García-Urdiales, *et al.* Enzymatic Desymmetrization of Prochiral 2-Substituted-1,3-Diamines: Preparation of Valuable Nitrogenated Compounds. *J. Org. Chem.* **2009**, *74*, 2571–2574. DOI: 10.1021/jo8025912.

[409] V. Mersch-Sundermann, S. Knasmüller, X.-J. Wu, *et al.* Use of a Human-Derived Liver Cell Line for the Detection of Cytoprotective, Antigenotoxic and Cogenotoxic Agents. *Toxicology* **2004**, *198*, 329–340. DOI 10.1016/j.tox.2004.02.009.

[410] C. D. Bevan and R. S. Lloyd. A High-Throughput Screening Method for the Determination of Aqueous Drug Solubility Using Laser Nephelometry in Microtiter Plates. *Anal. Chem.* **2000**, *72*, 1781–1787. DOI: 10.1021/ac9912247.

[411] F. Lombardo, M. Y. Shalaeva, K. A. Tupper, *et al.* ElogDoct: A Tool for Lipophilicity Determination in Drug Discovery. 2. Basic and Neutral Compounds. *J. Med. Chem.* **2001**, *44*, 2490–2497. DOI: 10.1021/jm0100990.

[412] B. J. Ring, J. Y. Chien, K. K. Adkison, *et al.* PhRMA CPCDC Initiative on Predictive Models of Human Pharmacokinetics, Part 3: Comparative Assessement of Prediction Methods of Human Clearance. *J. Pharm. Sci.* **2011**, *100*, 4090–4110. DOI: 10.1002/jps.22552.

[413] R. S. Obach. Prediction of Human Clearance of Twenty-Nine Drugs from Hepatic Microsomal Intrinsic Clearance Data: An Examination of In Vitro Half-Life Approach and Nonspecific Binding to Microsomes. *Drug Metab. Dispos.* **1999**, *27*, 1350–1359.

A. Supporting NMR Data for Novel Final Compounds

Images of the ^{1}H NMR and ^{13}C NMR spectra for the final compounds synthesised in this thesis. Residual solvent peaks are indicated by red peak labels unless obscured by compound peaks. The complete set of raw data files (NMR and mass spectra) for intermediates and final compounds synthesised in this thesis are available to download at DOI: 10.25910/5d7af492b2c63. A complete PDF copy of the ELN entries for all experiments carried out in this thesis is also available to download at this link.

A.1 3-(4-Chlorophenyl)-5-phenethoxy-[1,2,4]triazolo[4,3-*a*]pyrazine 11

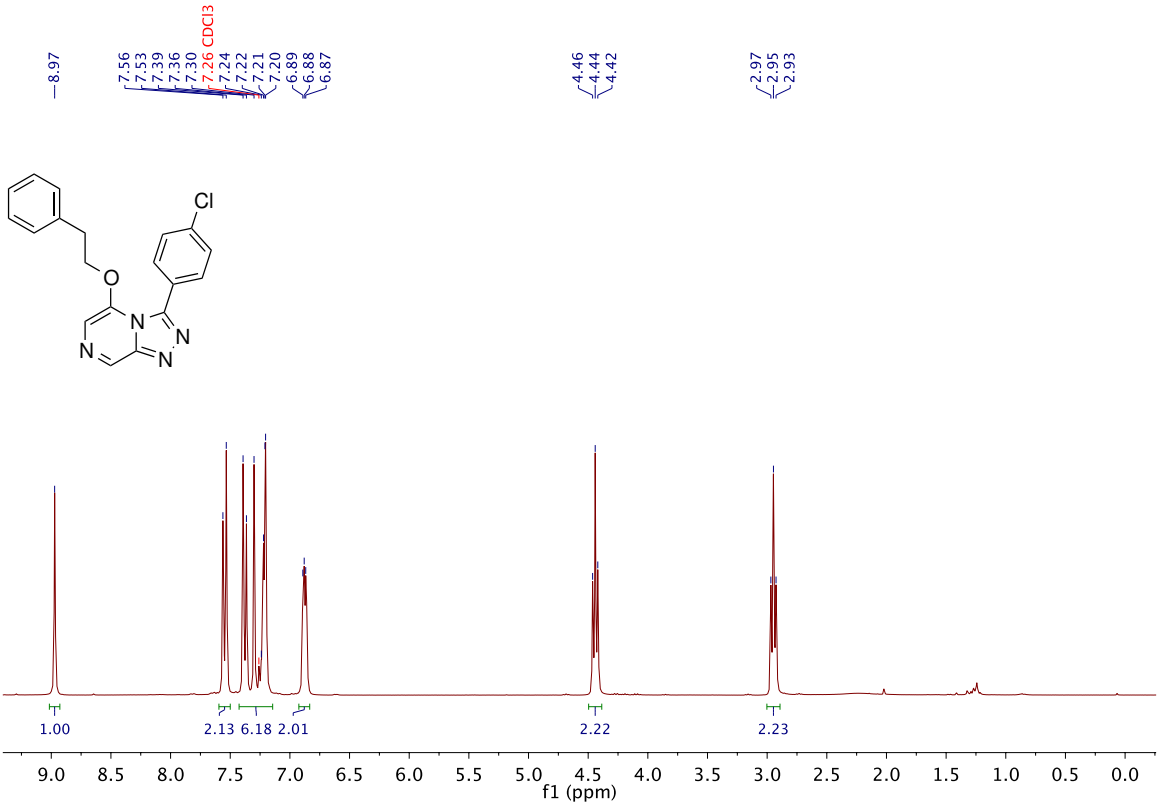

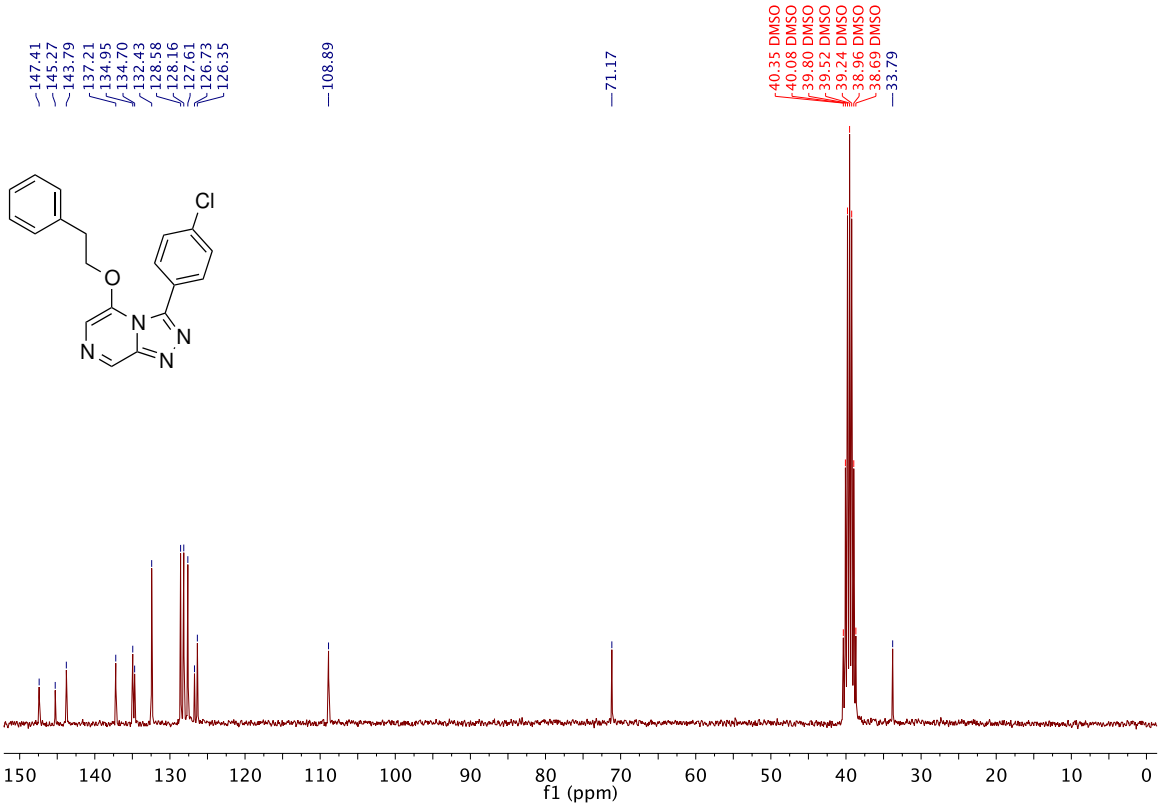

A.2 *N*-(4-Chlorophenyl)-3-(4-(difluoromethoxy)phenyl)-[1,2,4]triazolo[4,3-*a*] pyrazine-5-carboxamide 19

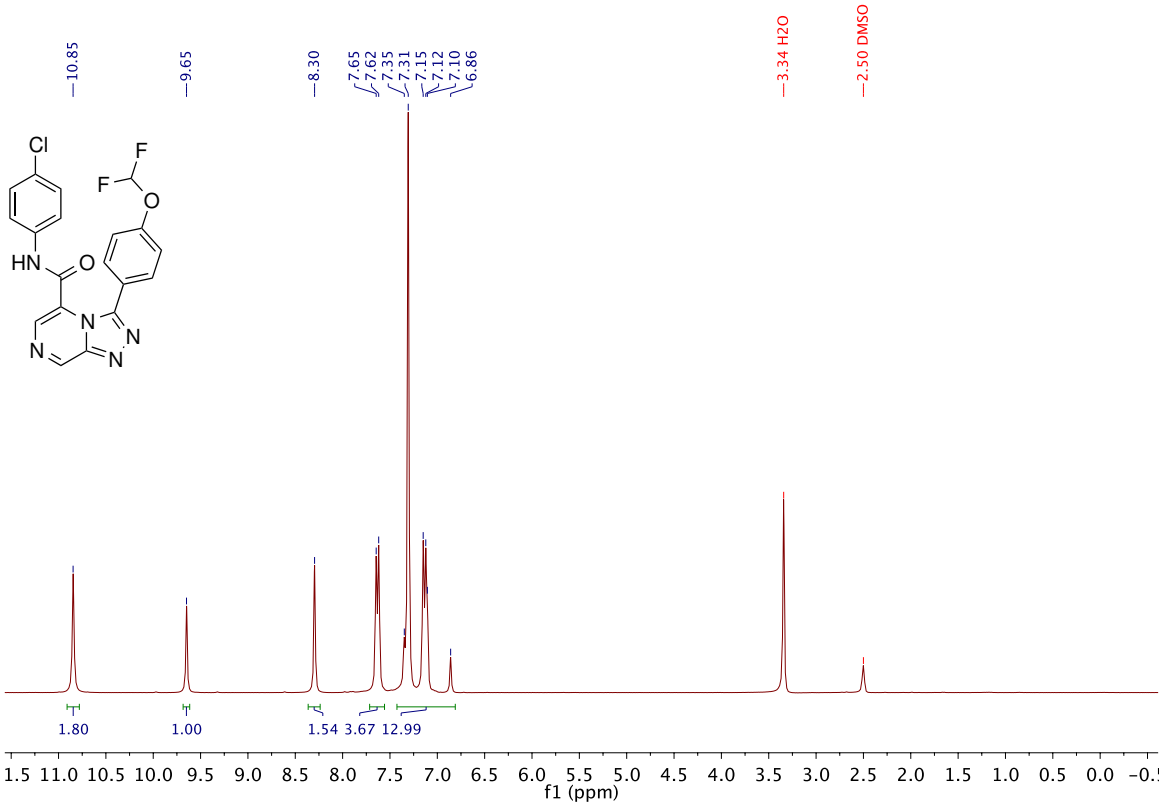

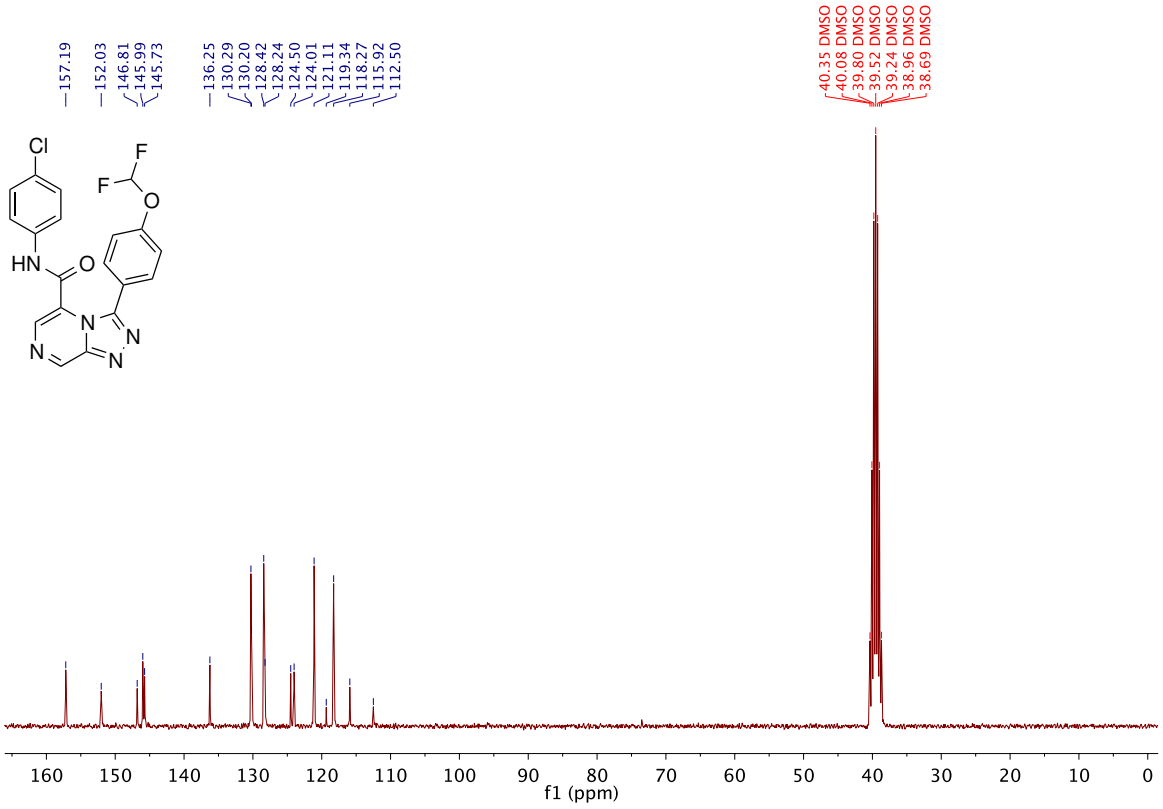

A.3 *N*-(3-Chloro-4-fluorophenyl)-3-(4-(difluoromethoxy)phenyl)-[1,2,4]triazolo[4,3-*a*]pyrazine-5-carboxamide 20

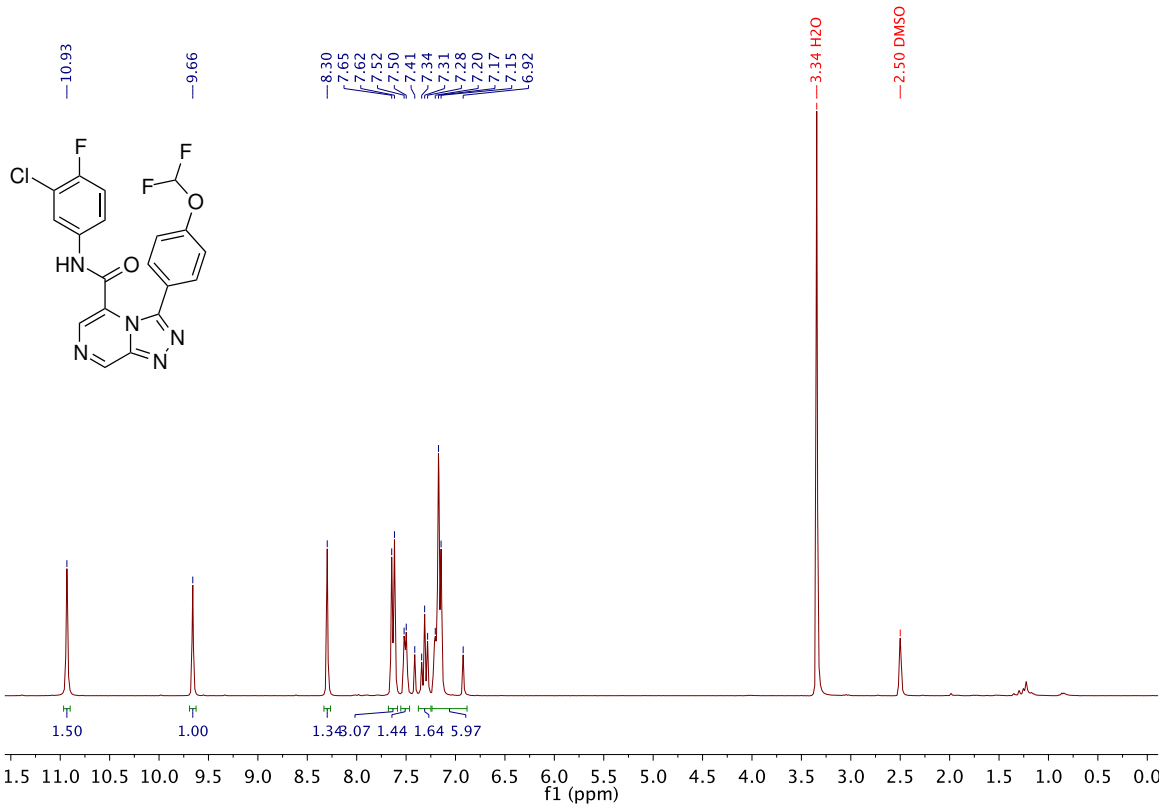

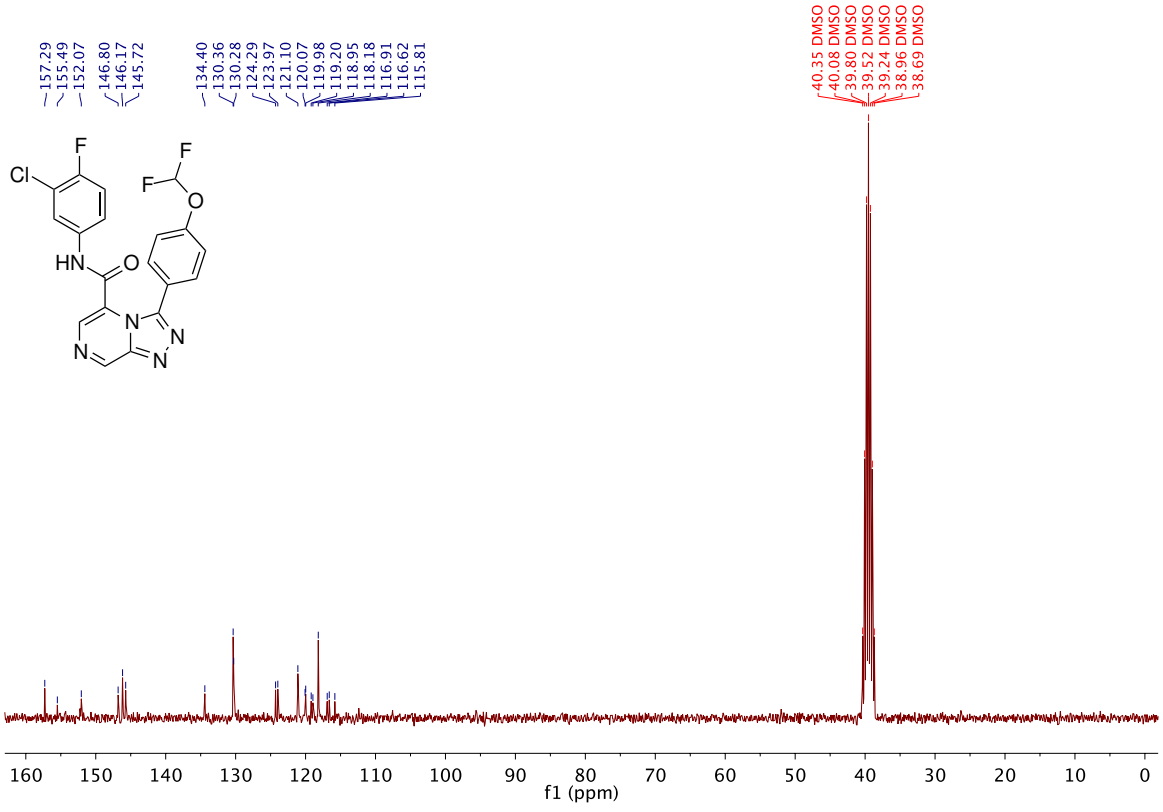

A.4 (3-(4-(Difluoromethoxy)phenyl)-[1,2,4]triazolo[4,3-*a*]pyrazin-5-yl) (isoindolin-2-yl)methanone 31

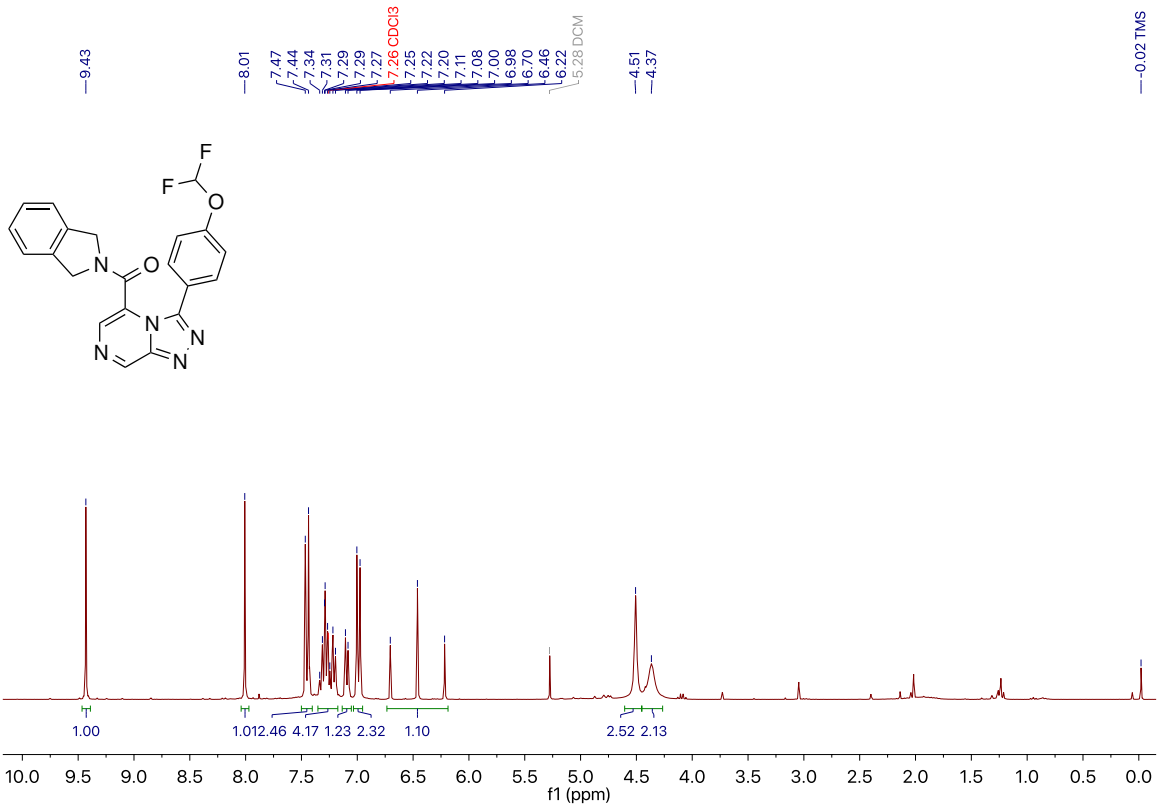

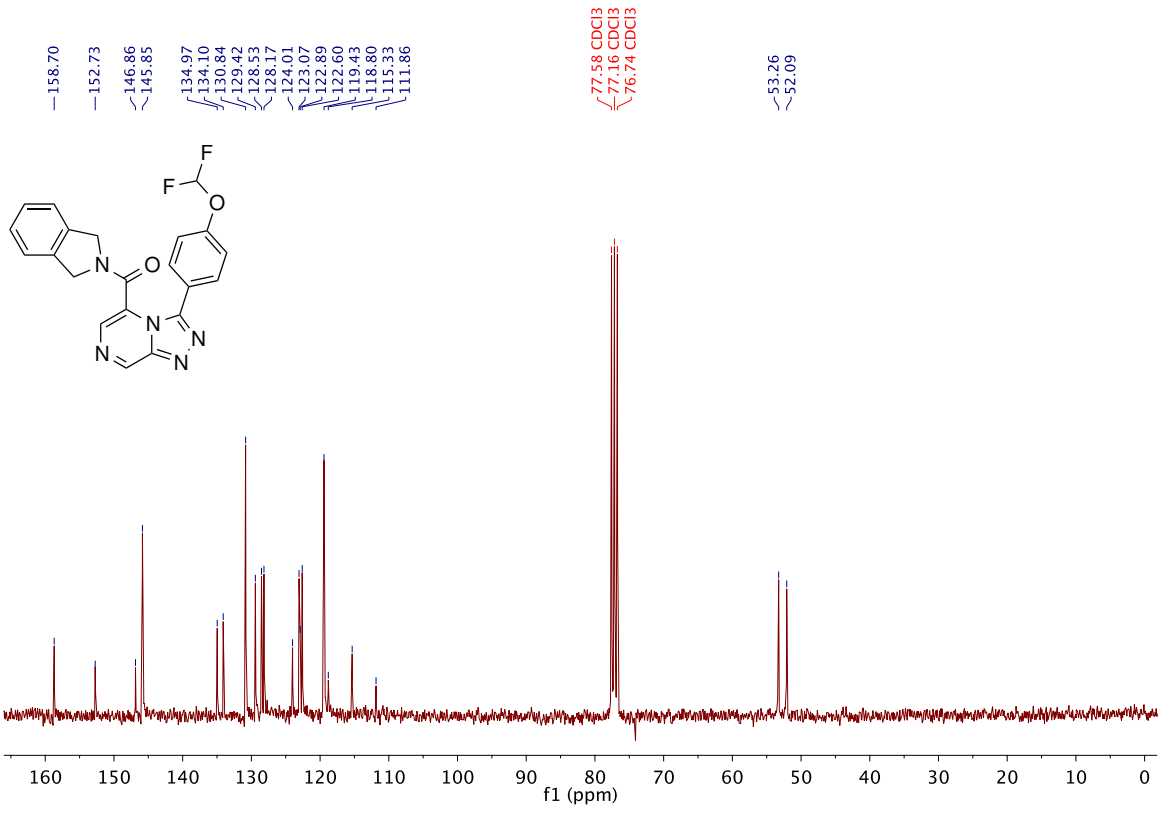

A.5 2-((3-(4-(Difluoromethoxy)phenyl)-[1,2,4]triazolo[4,3-*a*]pyrazin-5-yl) oxy)-1-(3,4-difluorophenyl)-*N*,*N*-dimethylethan-1-amine 30

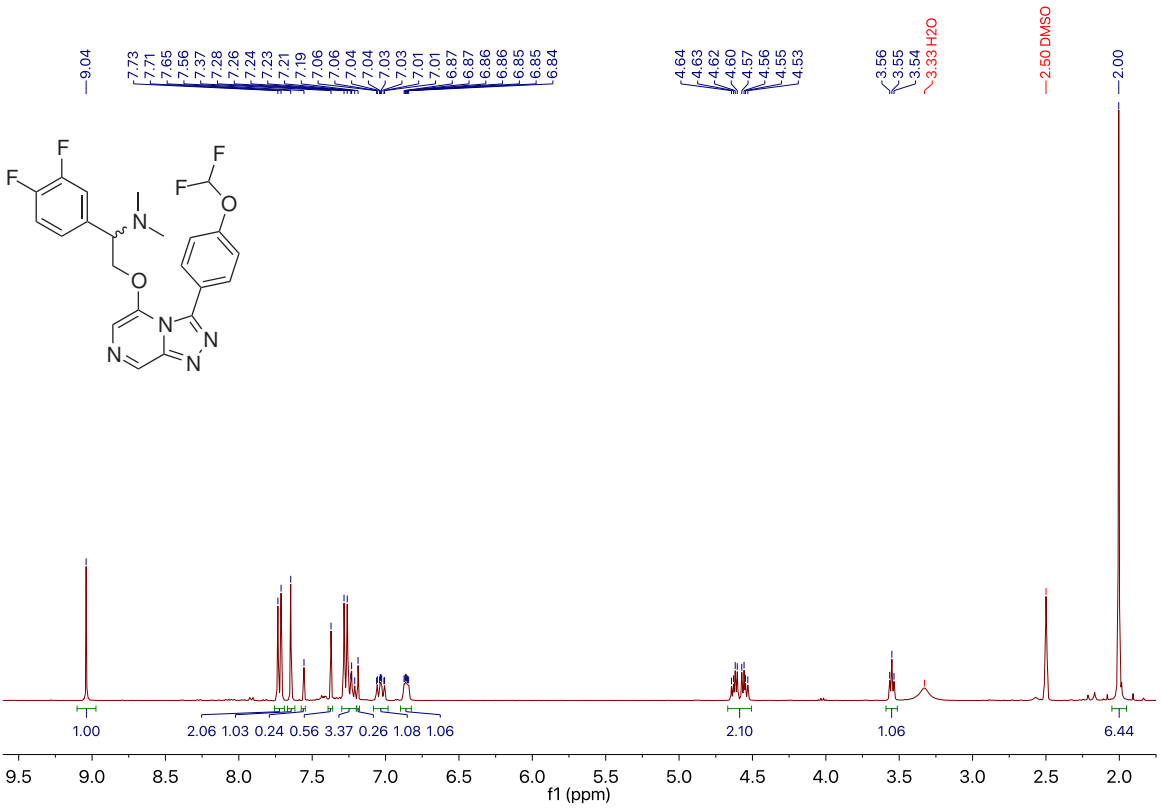

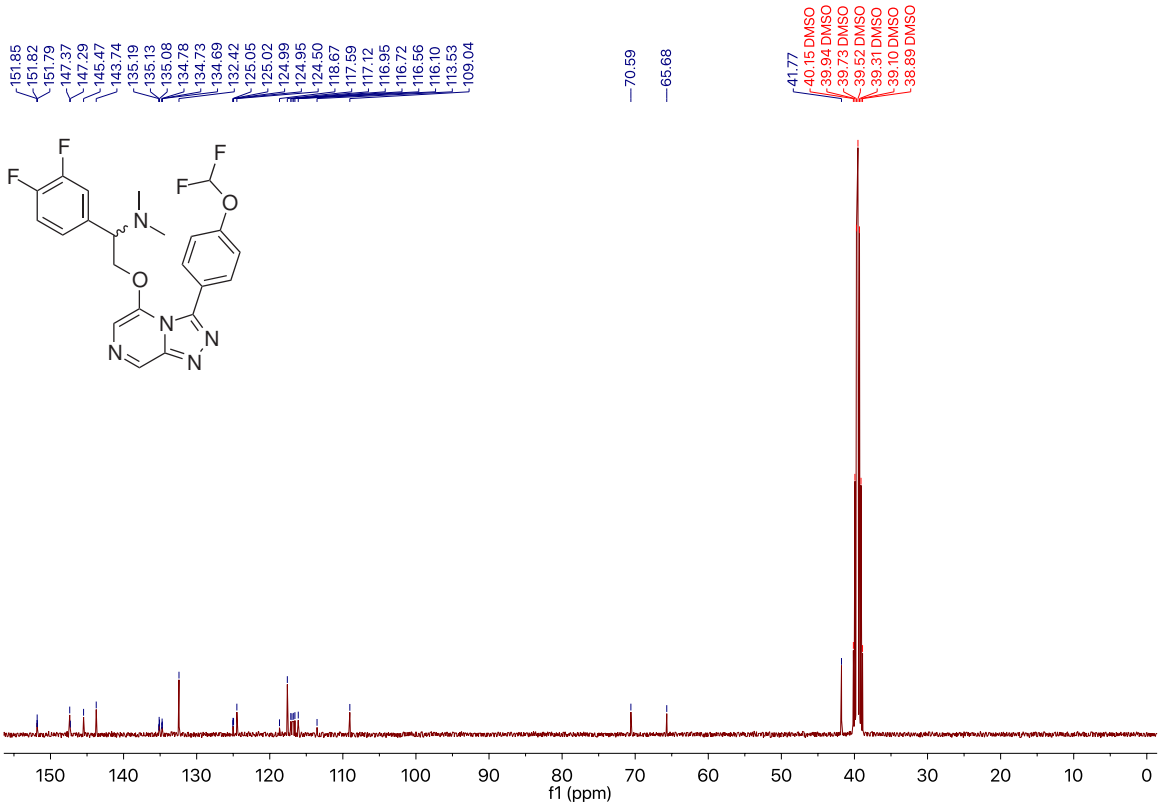

A.6 3-(4-(Difluoromethoxy)phenyl)-5-phenoxy-[1,2,4]triazolo[4,3-*a*] pyrazine 56

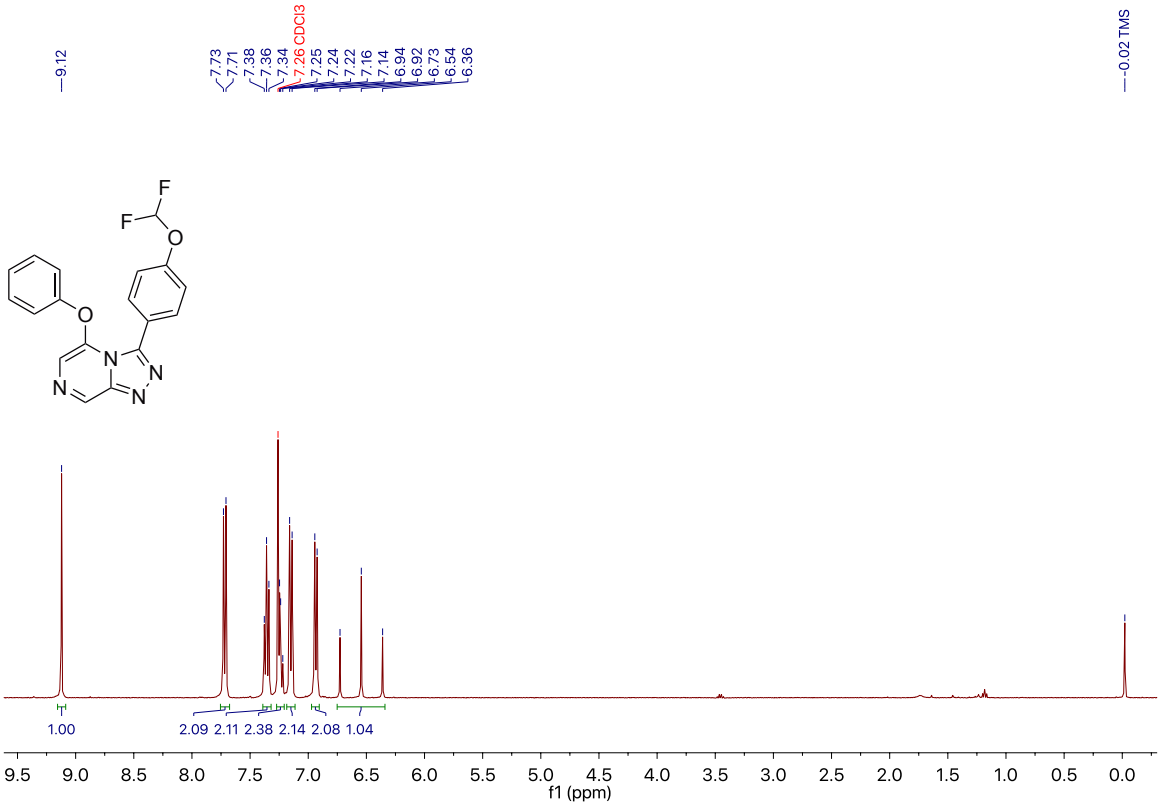

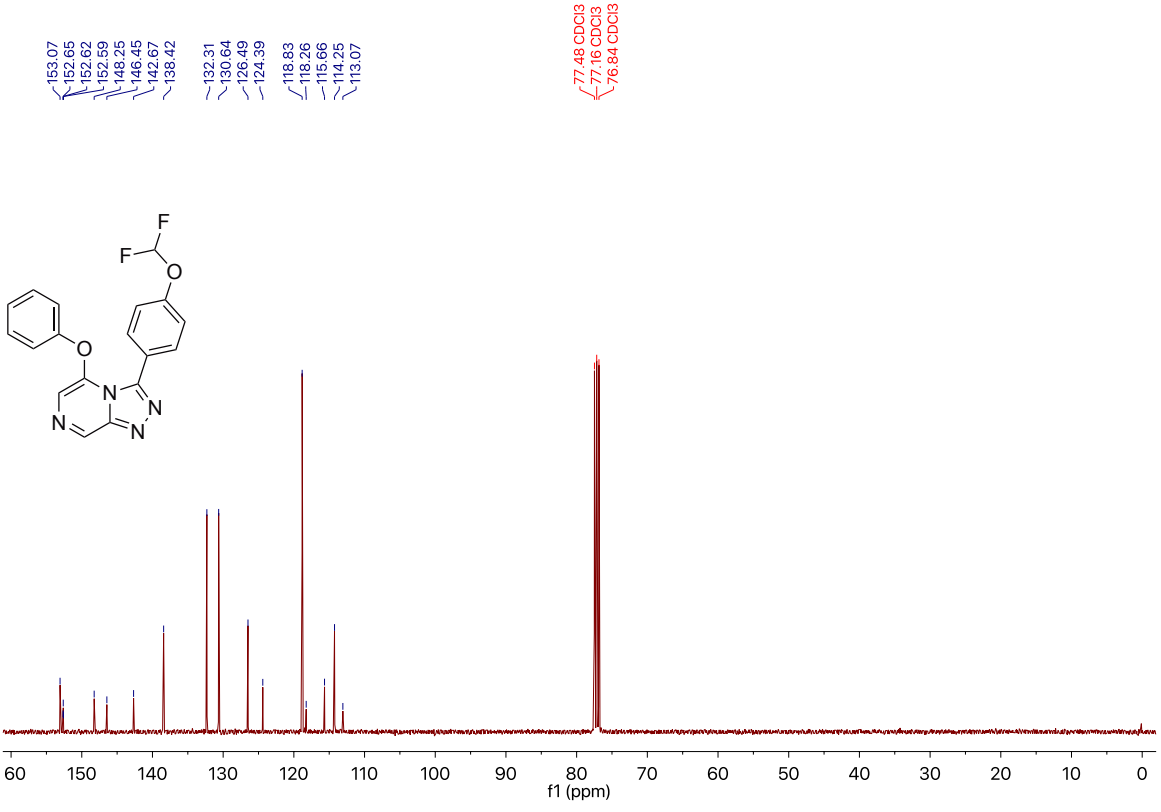

A.7 5-(Benzyloxy)-3-(4-(difluoromethoxy)phenyl)-[1,2,4]triazolo[4,3-*a*] pyrazine 57

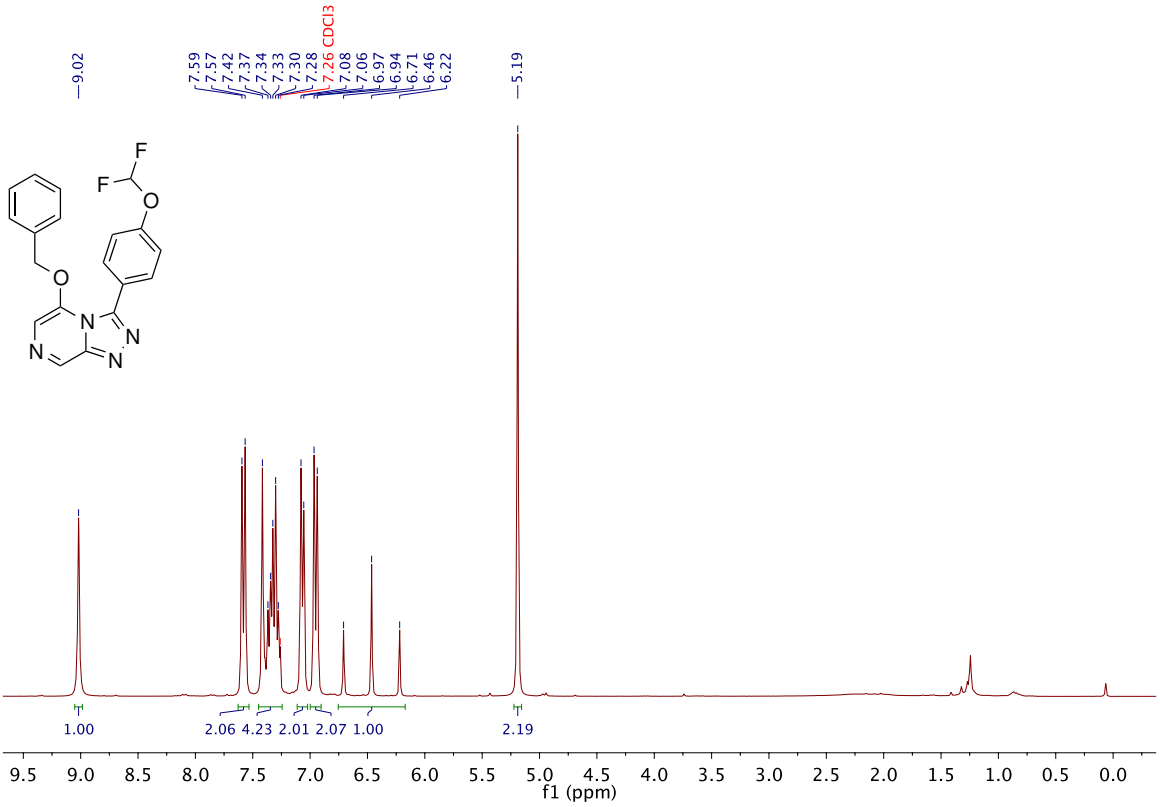

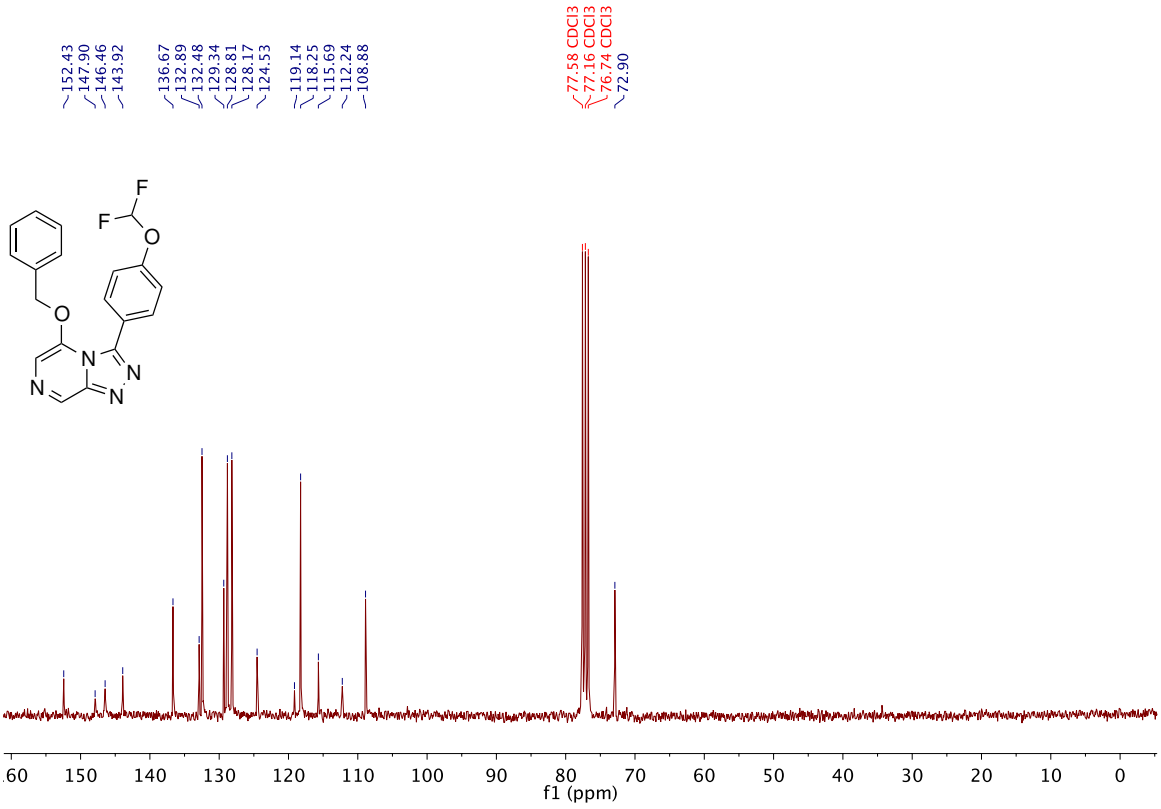

A.8 3-(4-(Difluoromethoxy)phenyl)-5-phenethoxy-[1,2,4]triazolo[4,3-*a*] pyrazine 58

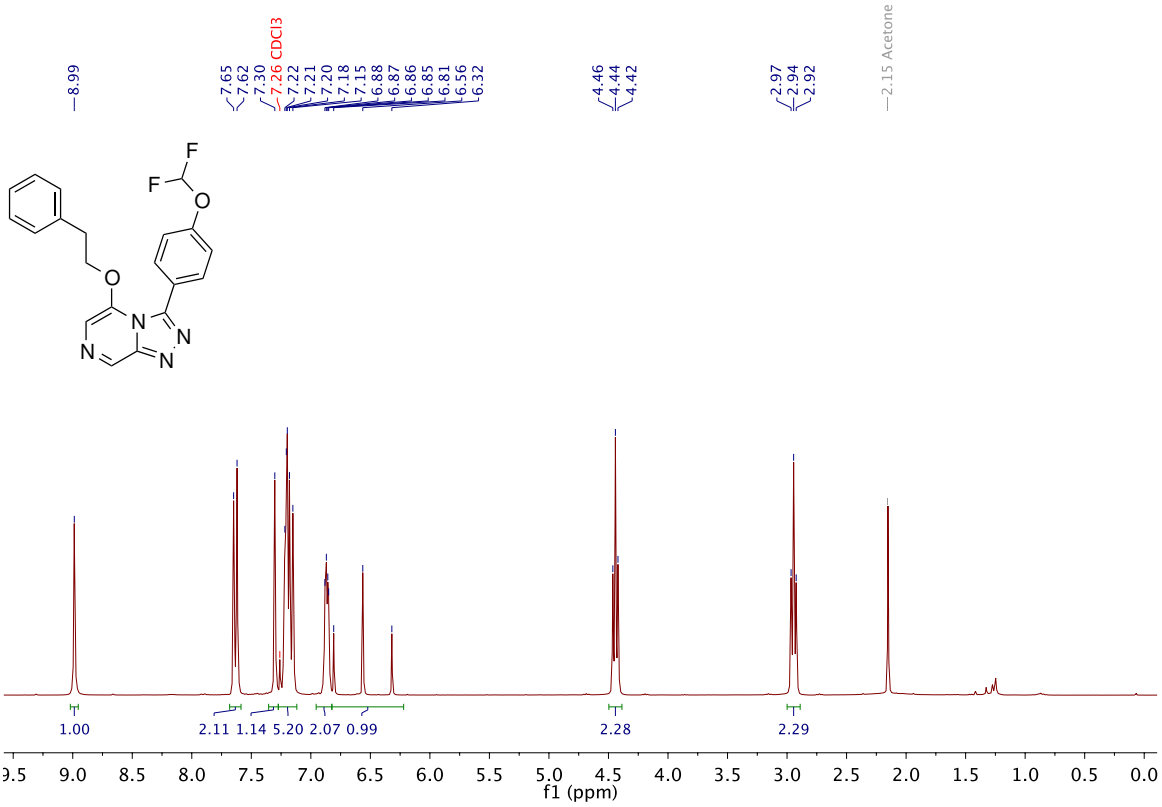

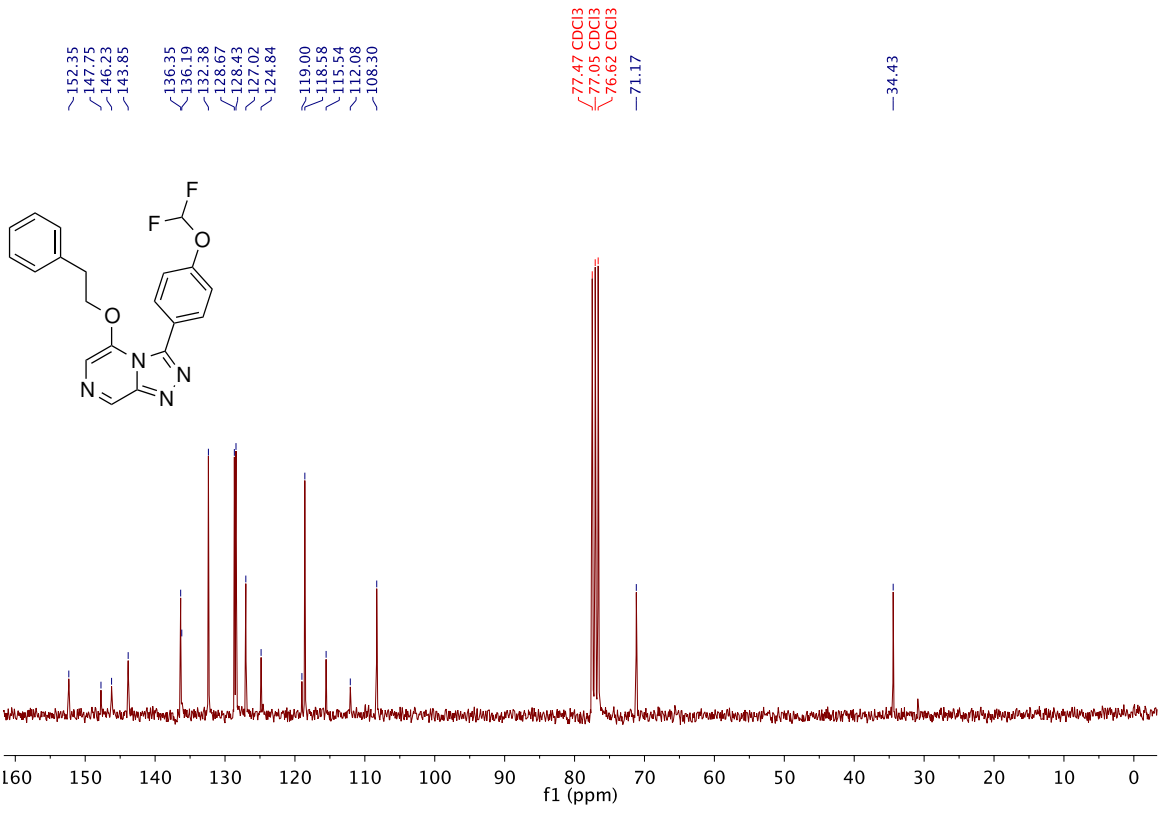

A.9 3-(4-(Difluoromethoxy)phenyl)-5-(3-phenylpropoxy)-[1,2,4]triazolo [4,3-*a*]pyrazine 59

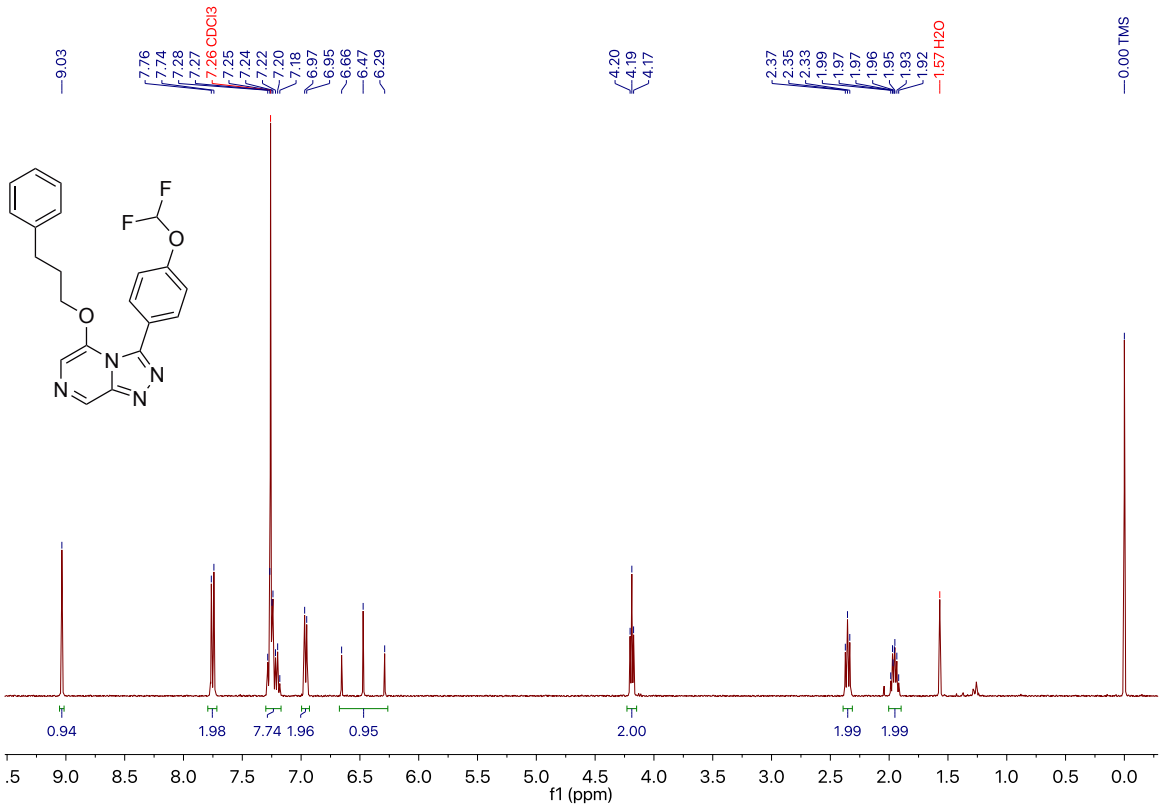

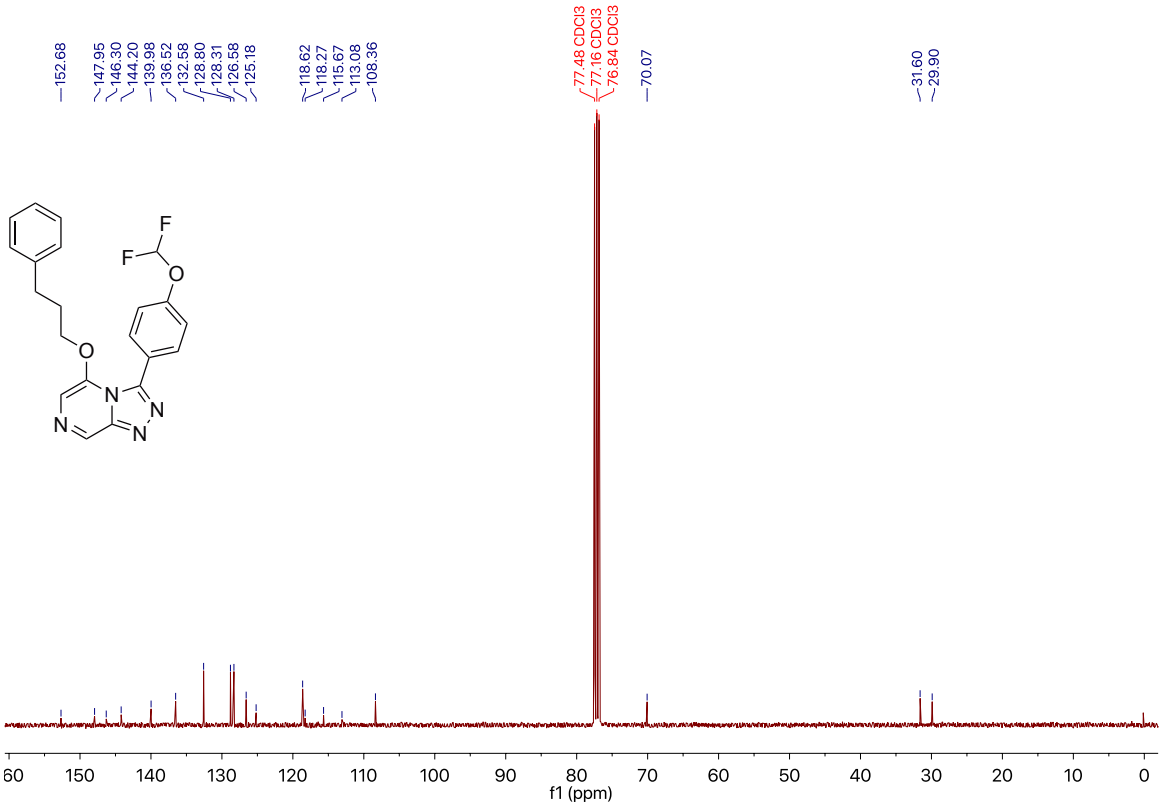

A.10 3-(4-(Difluoromethoxy)phenyl)-5-(2-phenoxyethoxy)-[1,2,4]triazolo [4,3-*a*]pyrazine 60

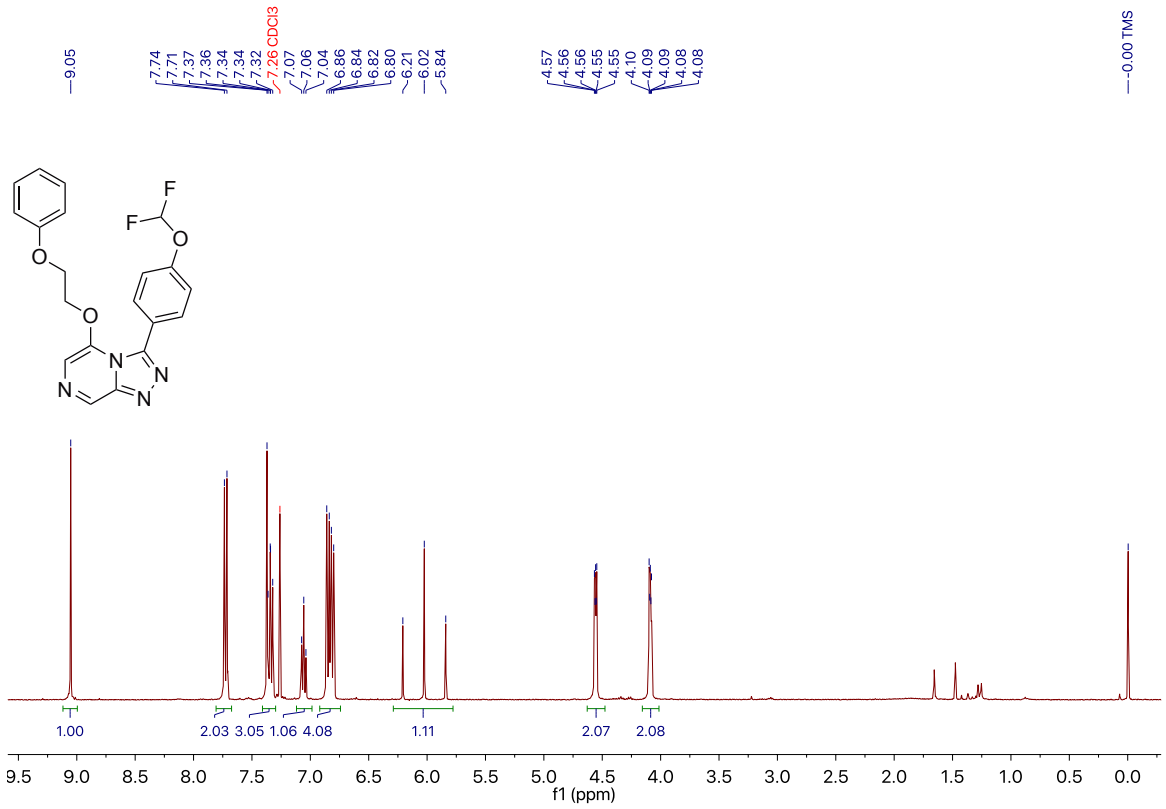

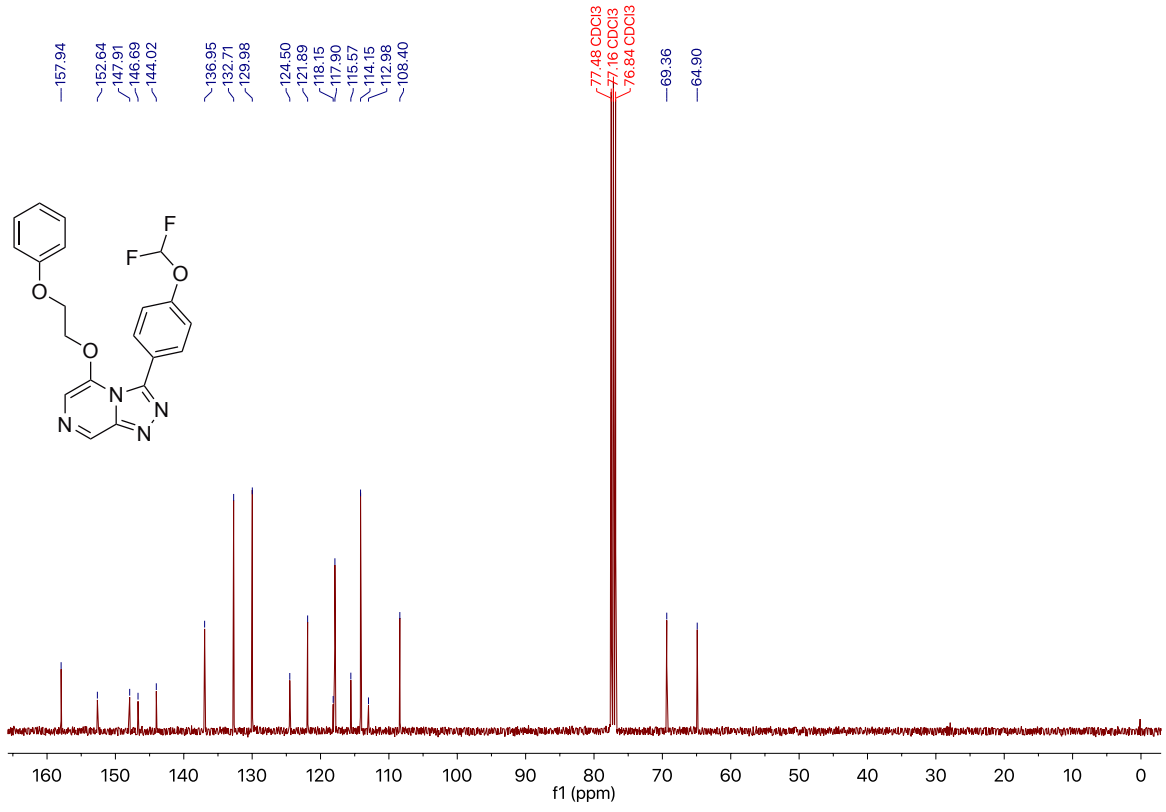

A.11 5-(Benzylthio)-3-(4-(difluoromethoxy)phenyl)-[1,2,4]triazolo[4,3-*a*] pyrazine 63

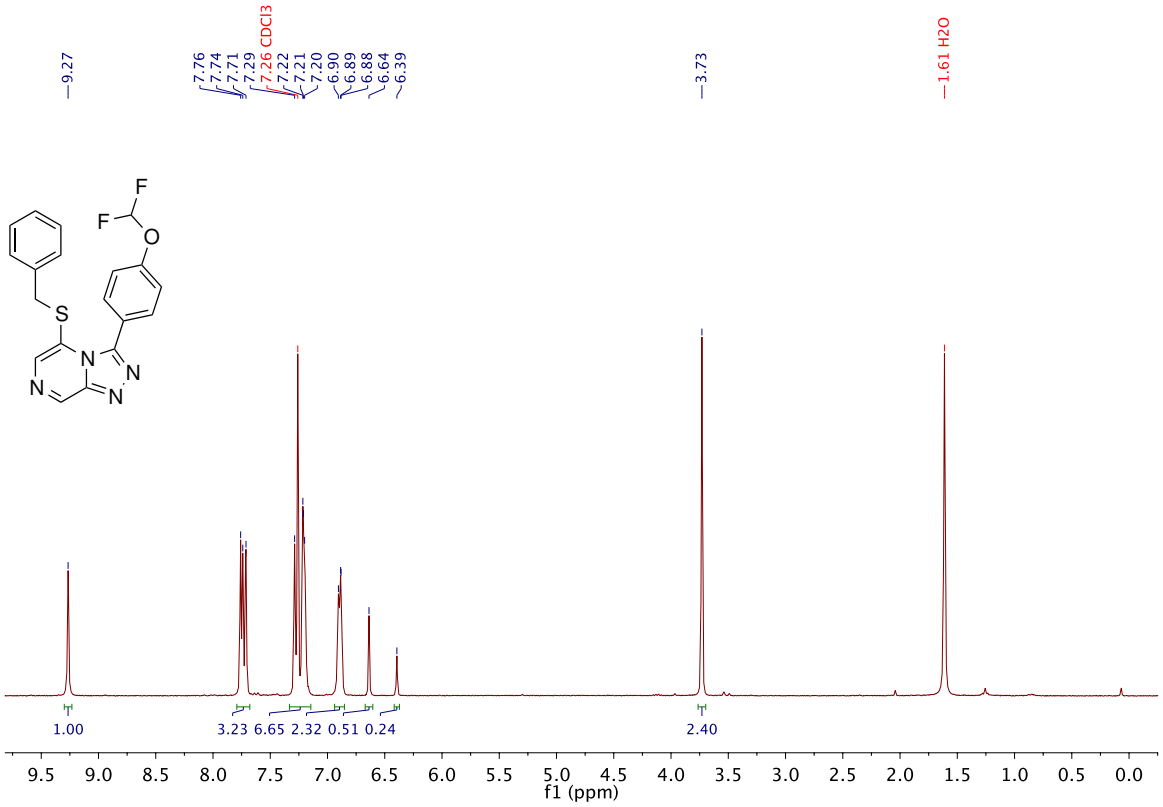

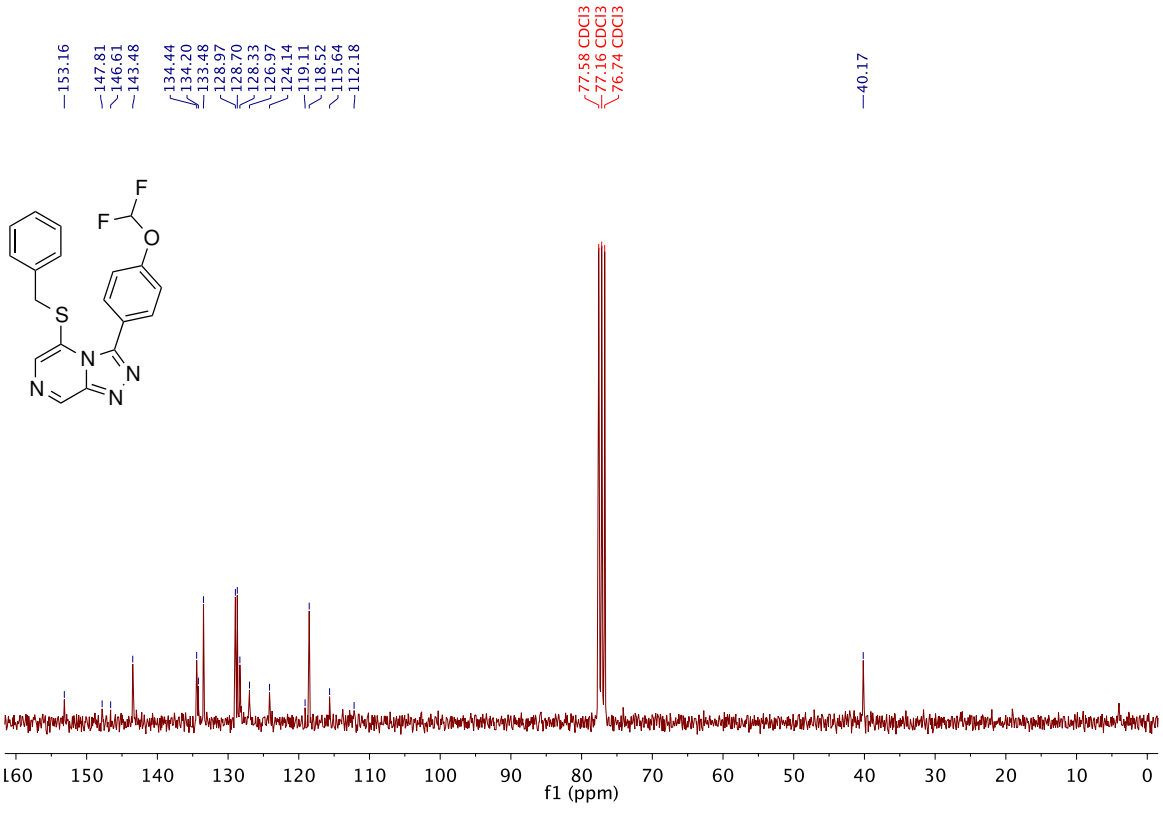

A.12 3-(4-(Difluoromethoxy)phenyl)-5-(phenethylthio)-[1,2,4]triazolo[4,3-*a*] pyrazine 64

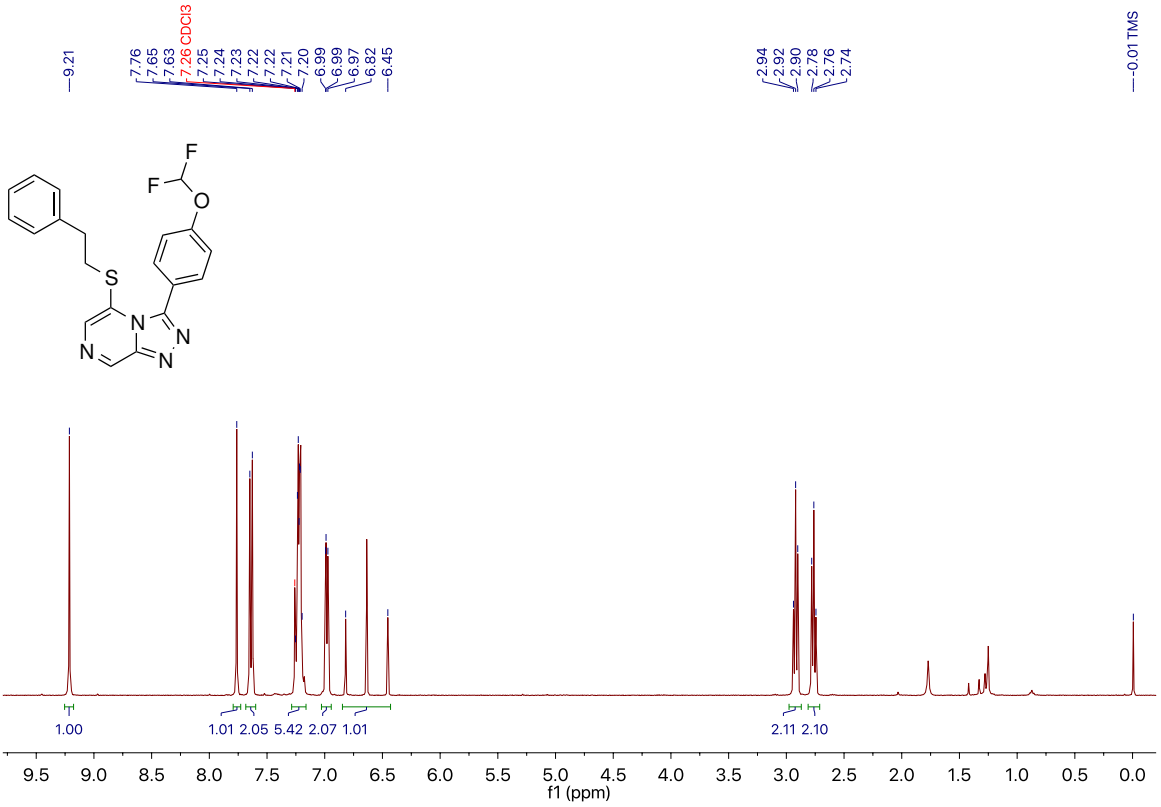

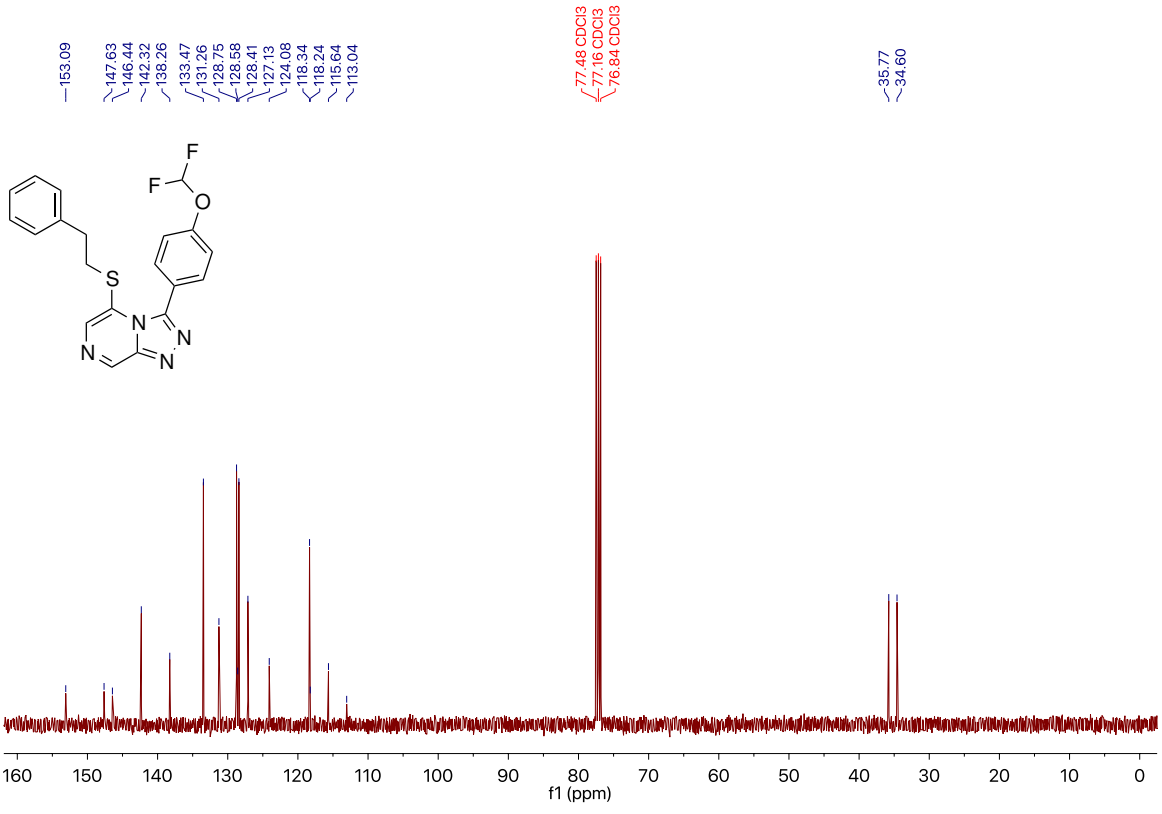

A.13 5-Benzylsulfinyl-3-(4-(difluoromethoxy)phenyl)-[1,2,4]triazolo[4,3-*a*] pyrazine 71

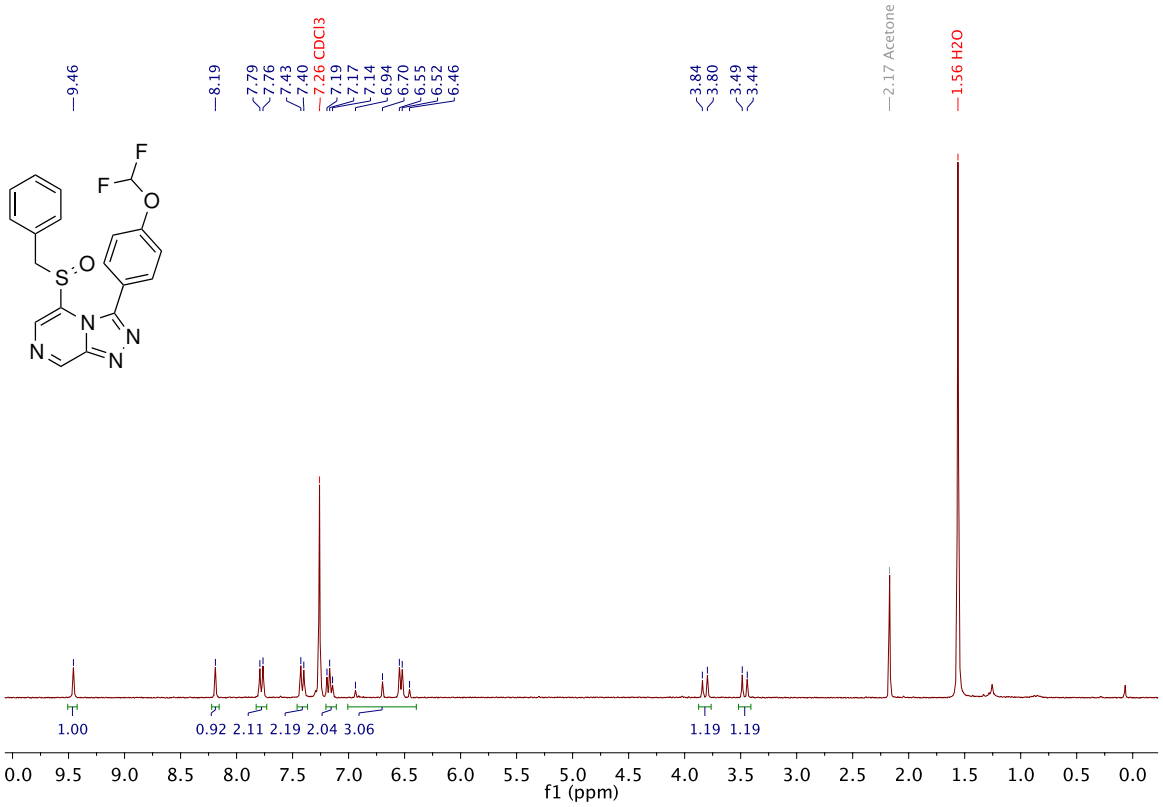

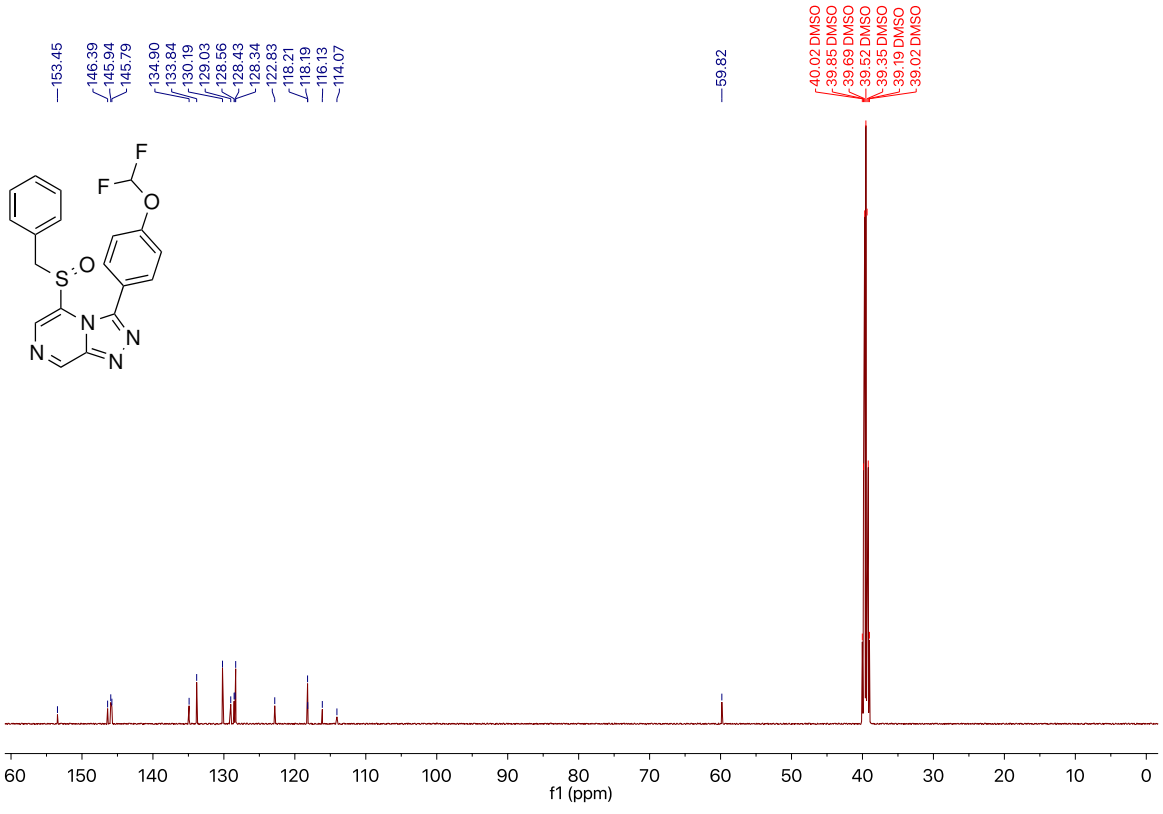

A.14 5-(Phenethylsulfinyl)-3-(4-(difluoromethoxy)phenyl)-[1,2,4]triazolo [4,3-*a*]pyrazine 72

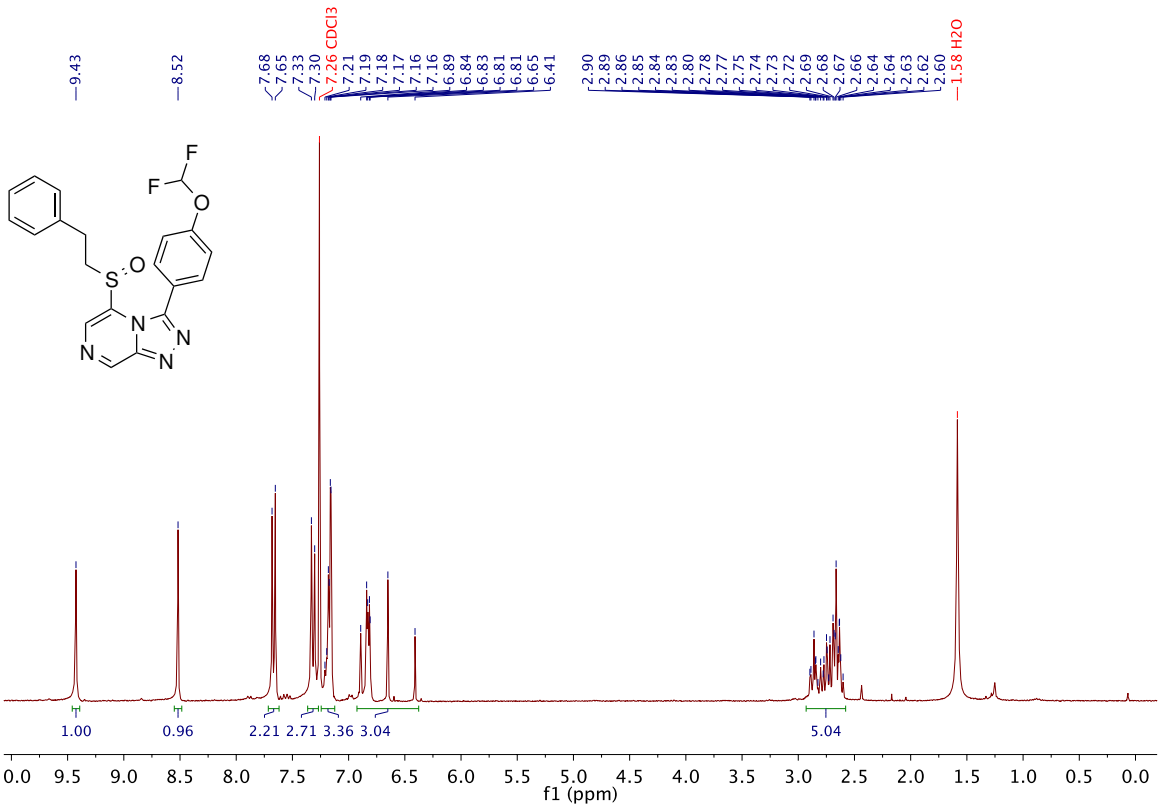

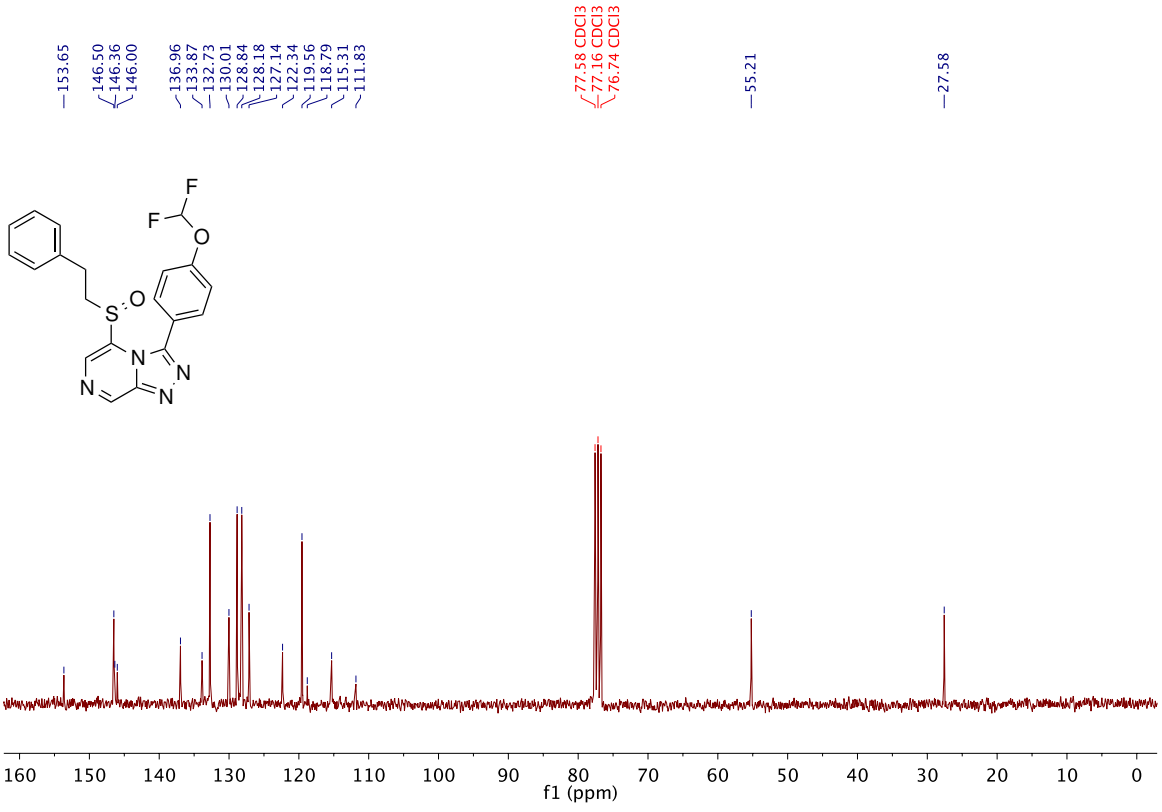

A.15 5-(Phenethylsulfonyl)-3-(4-(difluoromethoxy)phenyl)-[1,2,4]triazolo [4,3-*a*]pyrazine 74

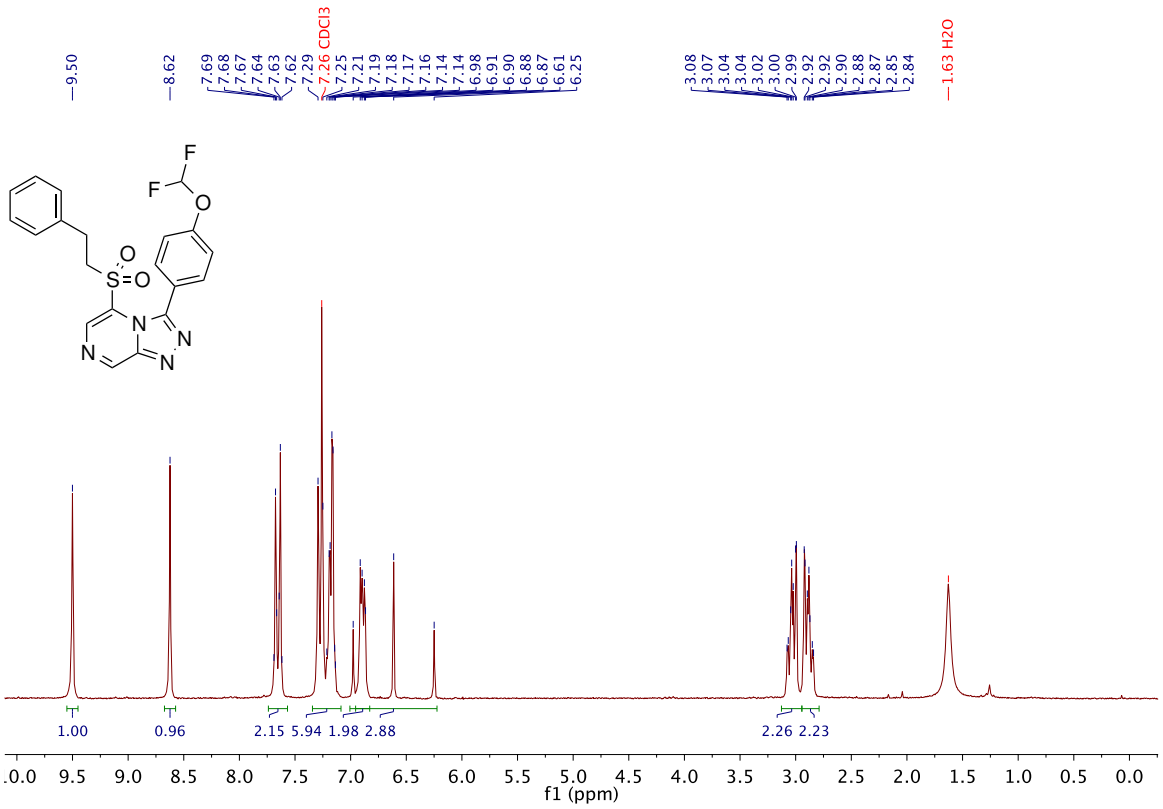

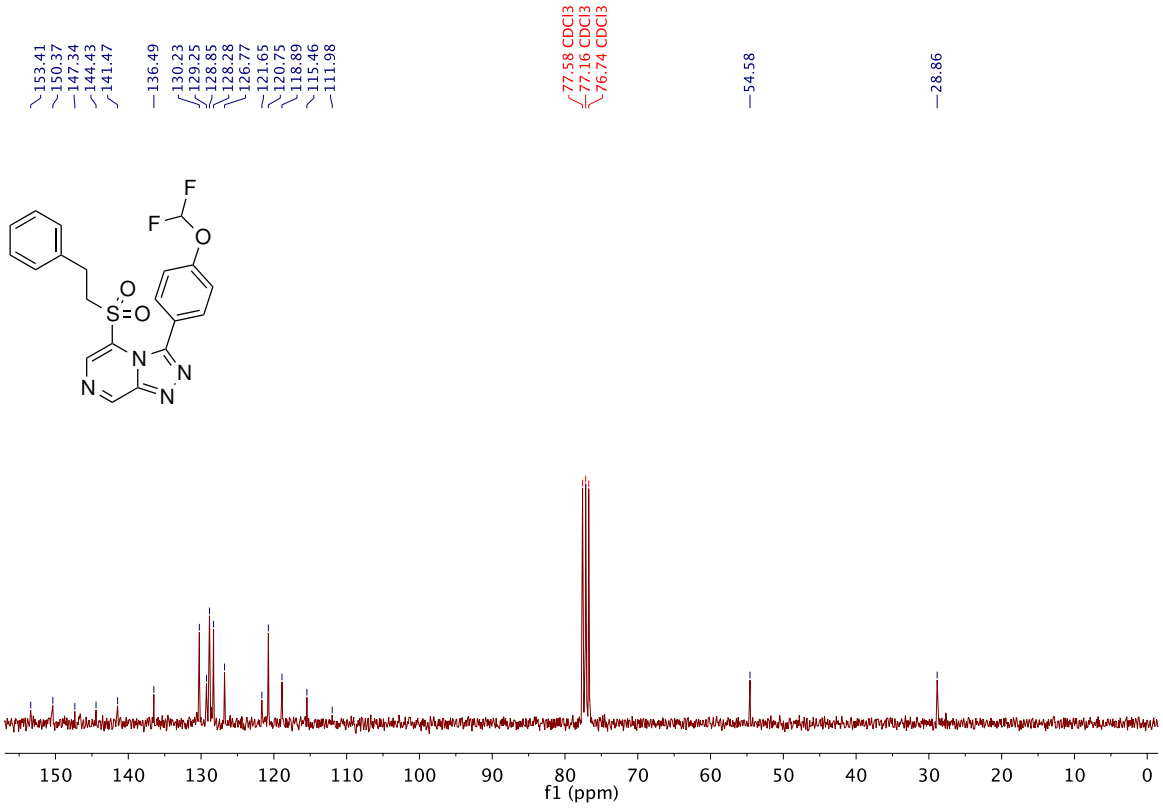

A.16 8-(Benzylthio)-3-(4-(difluoromethoxy)phenyl)-[1,2,4]triazolo[4,3-*a*] pyrazine 75

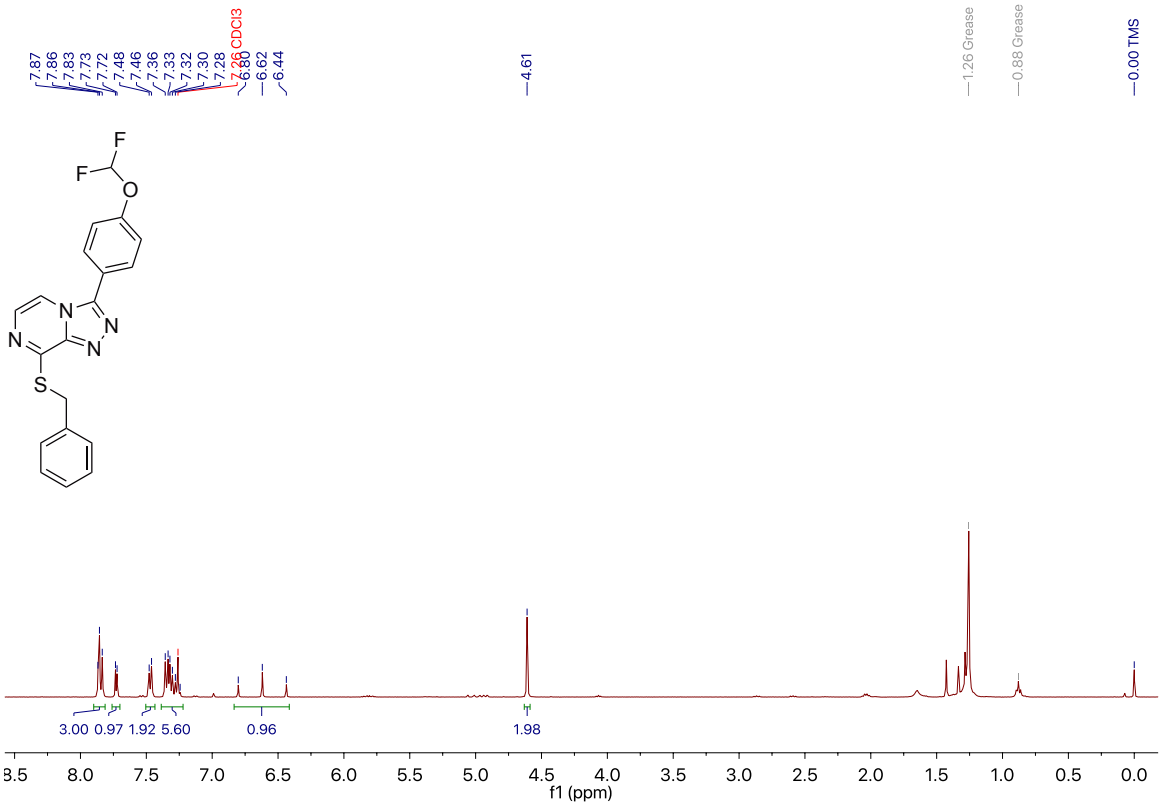

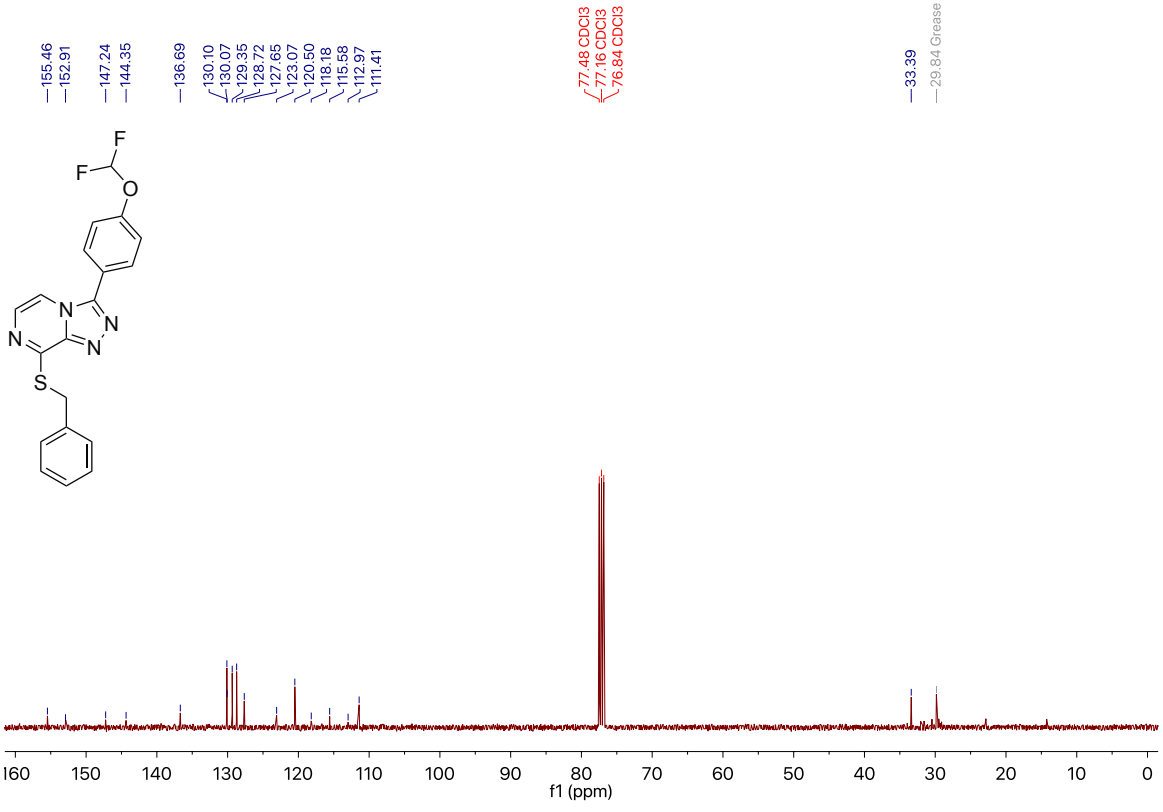

A.17 3-(4-(Difluoromethoxy)phenyl)-8-(phenethylthio)-[1,2,4]triazolo[4,3-*a*] pyrazine 76

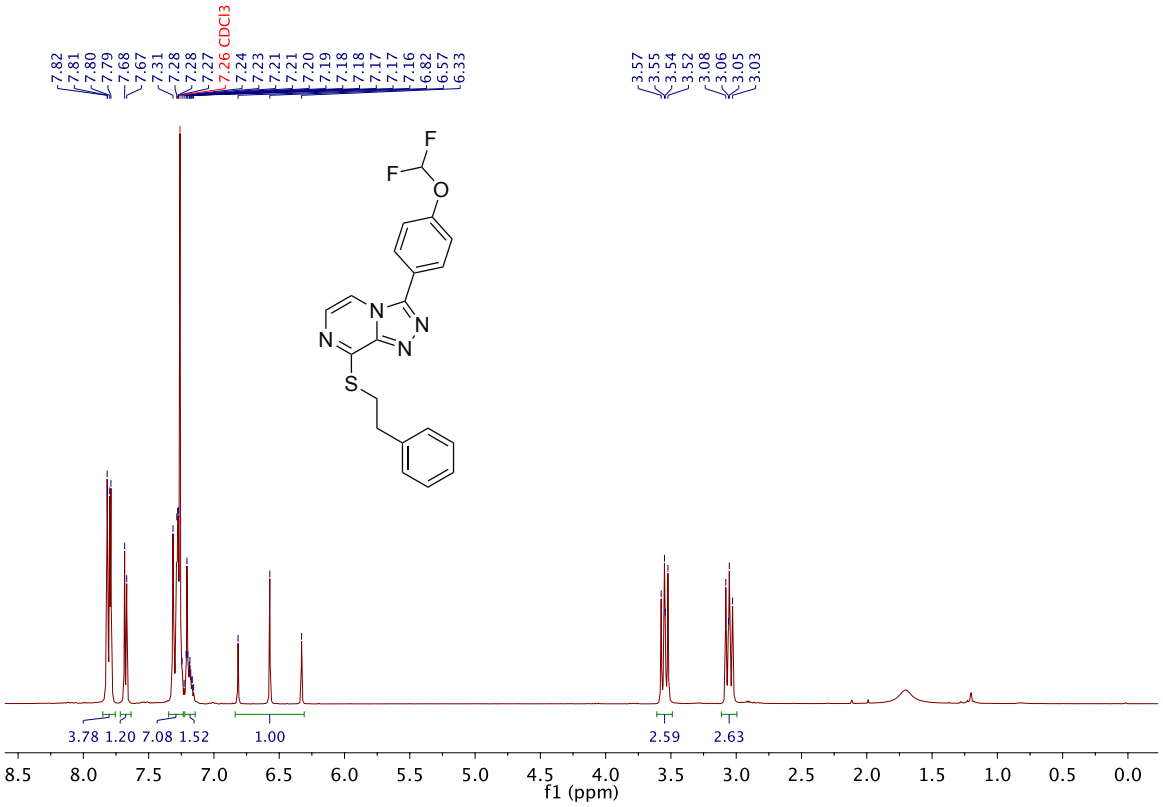

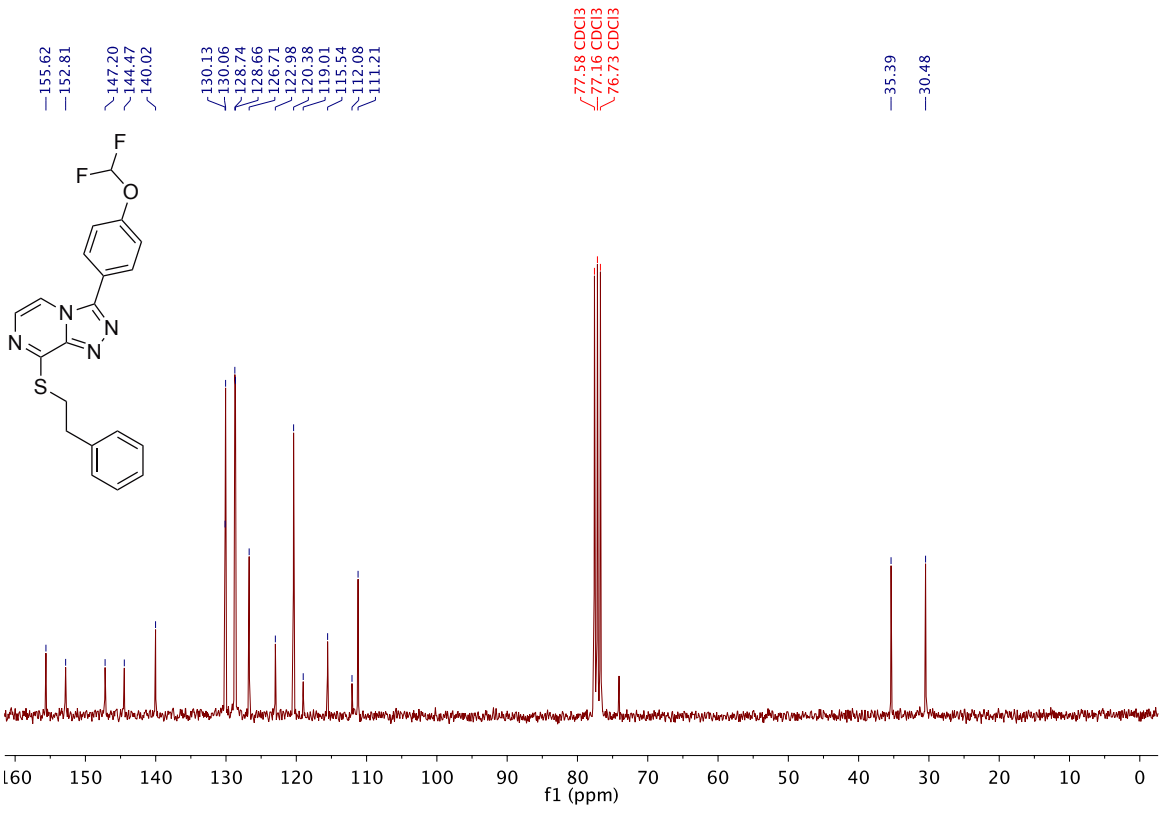

A.18 5-(Benzylsulfonyl)-3-(4-(difluoromethoxy)phenyl)-[1,2,4]triazolo[4,3-*a*] pyrazine 73

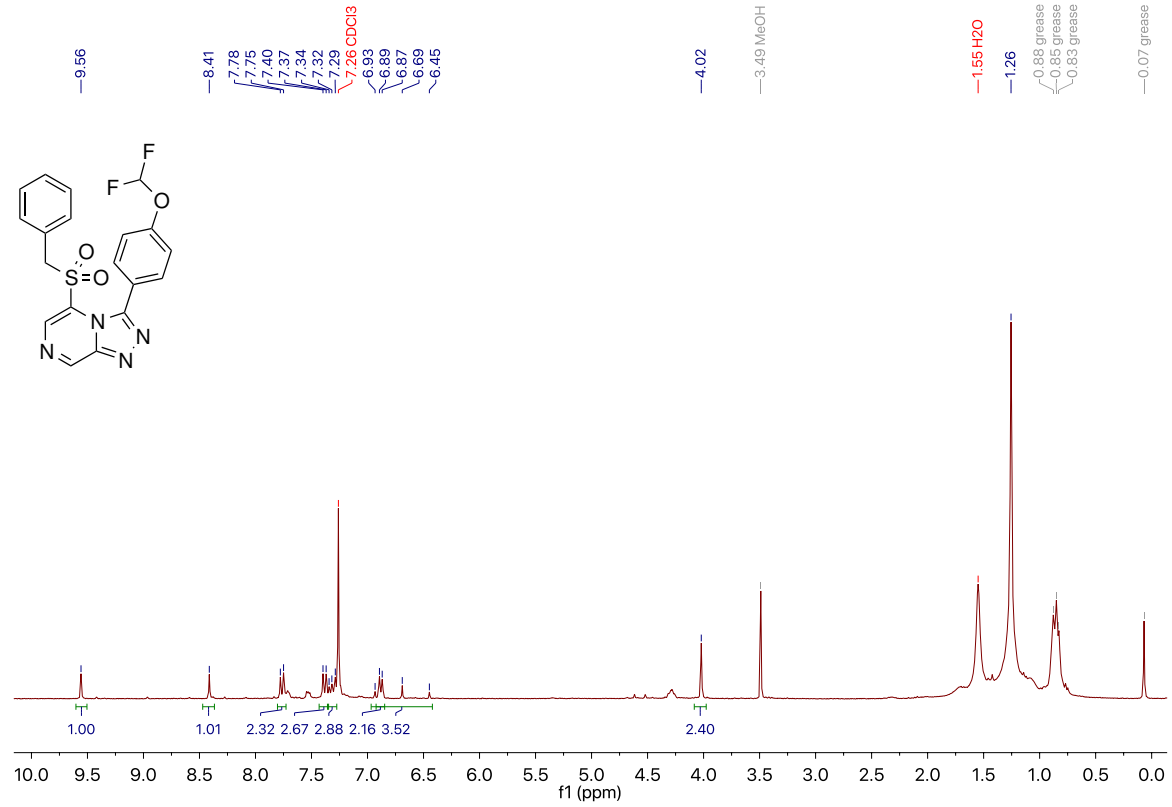

A.19 5-(4-Phenyl-1*H*-1,2,3-triazol-1-yl)-3-(4-(difluoromethoxy)phenyl)-[1,2,4] triazolo[4,3-*a*]pyrazine 78

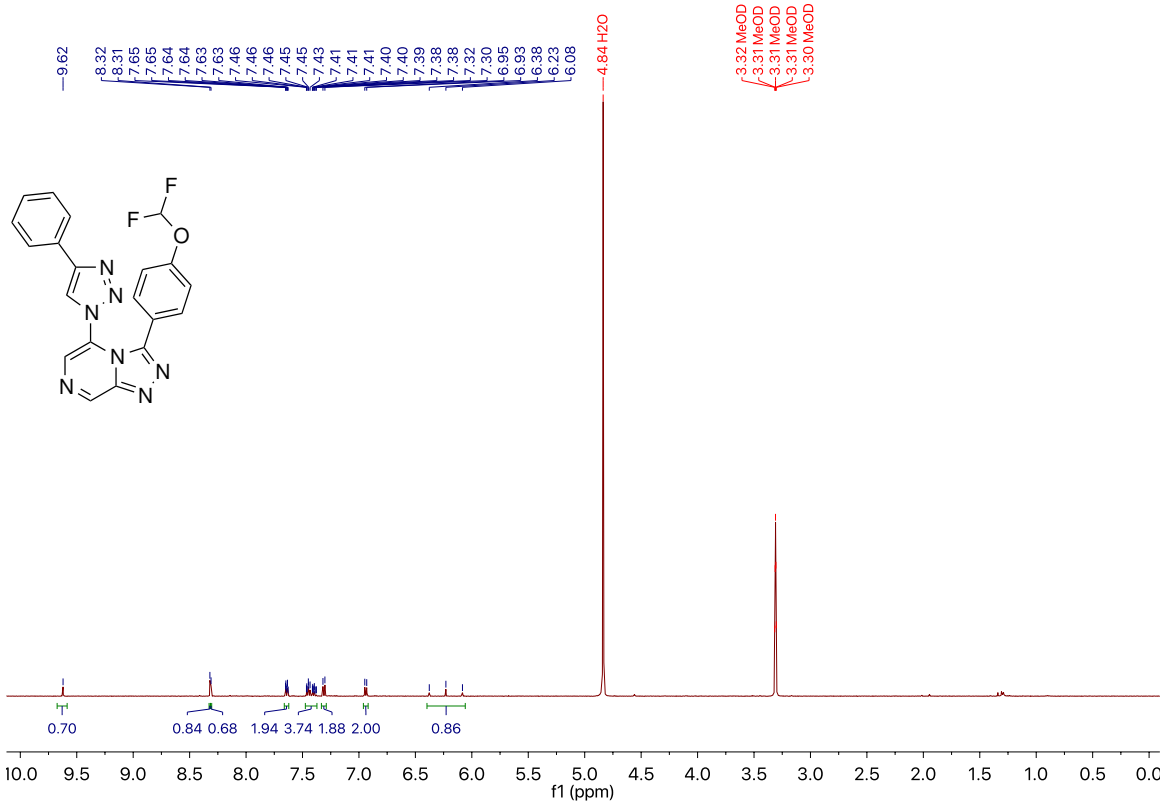

A.20 3-(4-(Difluoromethoxy)phenyl)-5-((1-phenyl-1*H*-1,2,3-triazol-4-yl) methoxy)-[1,2,4]triazolo[4,3-*a*]pyrazine 83

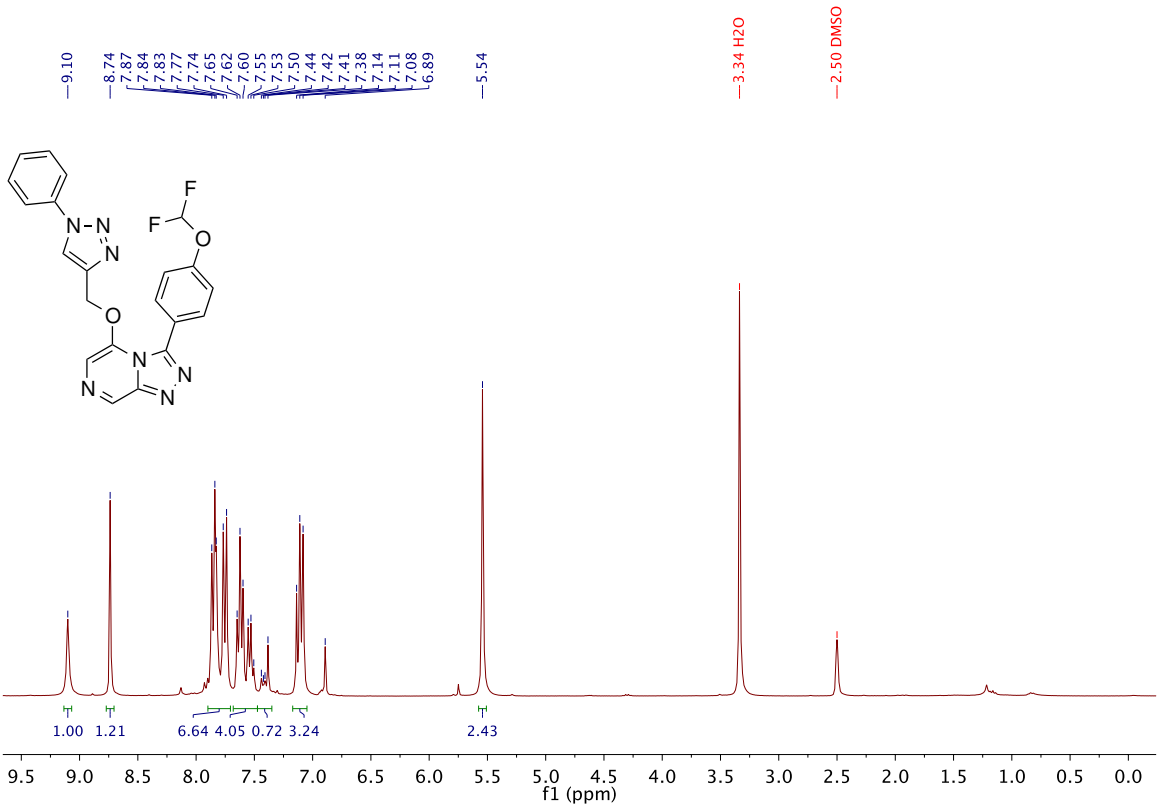

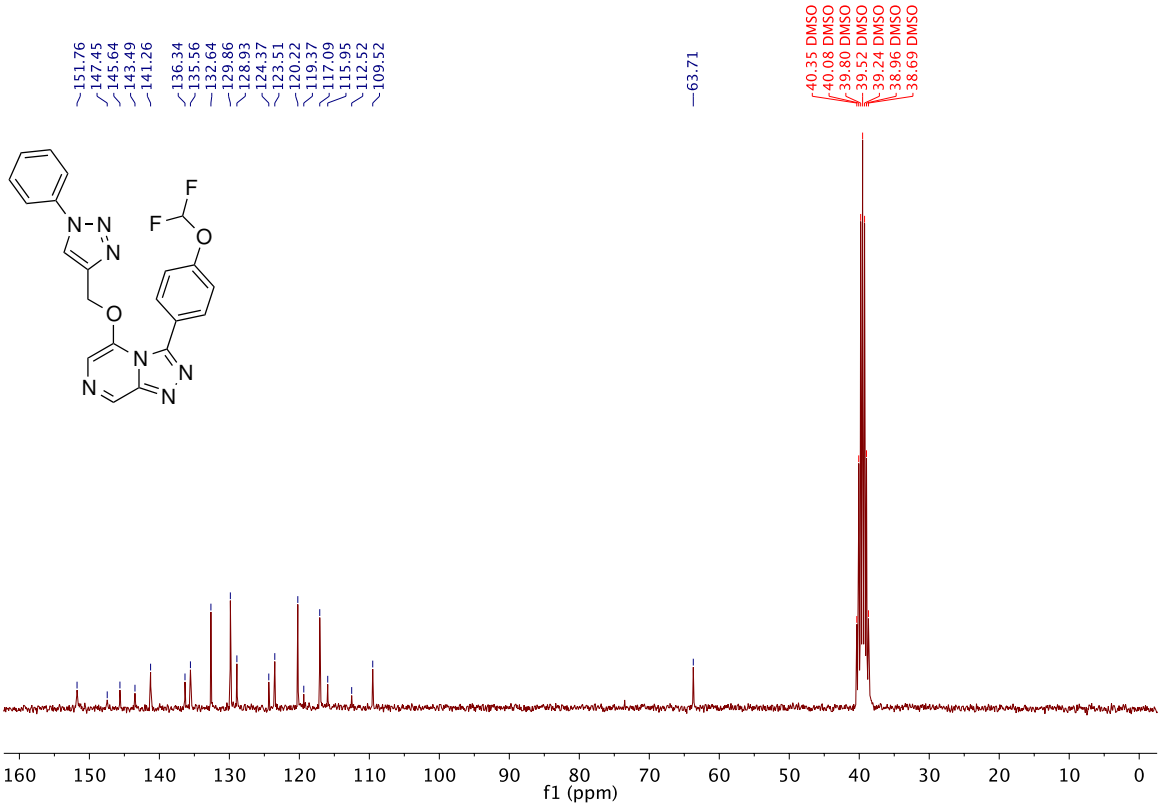

A.21 5-((1-Benzyl-1*H*-1,2,3-triazol-4-yl)methoxy)-3-(4-(difluoromethoxy) phenyl)-[1,2,4]triazolo[4,3-*a*]pyrazine 84

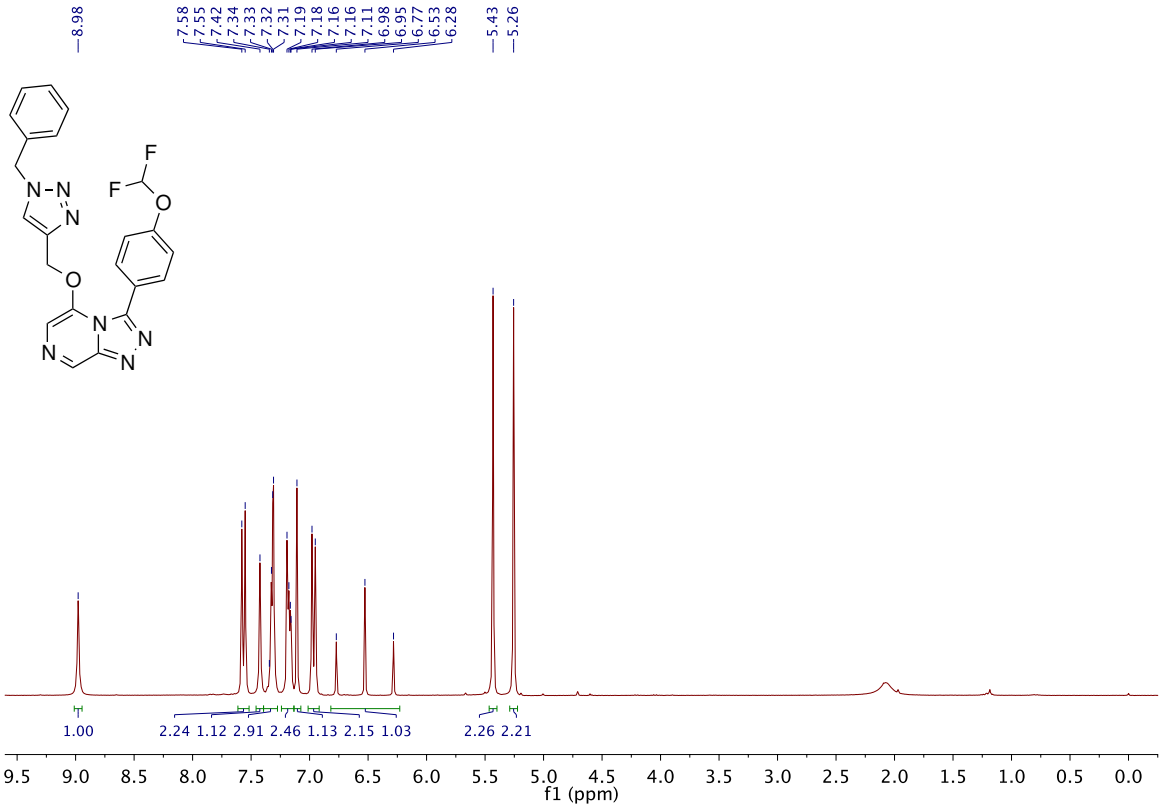

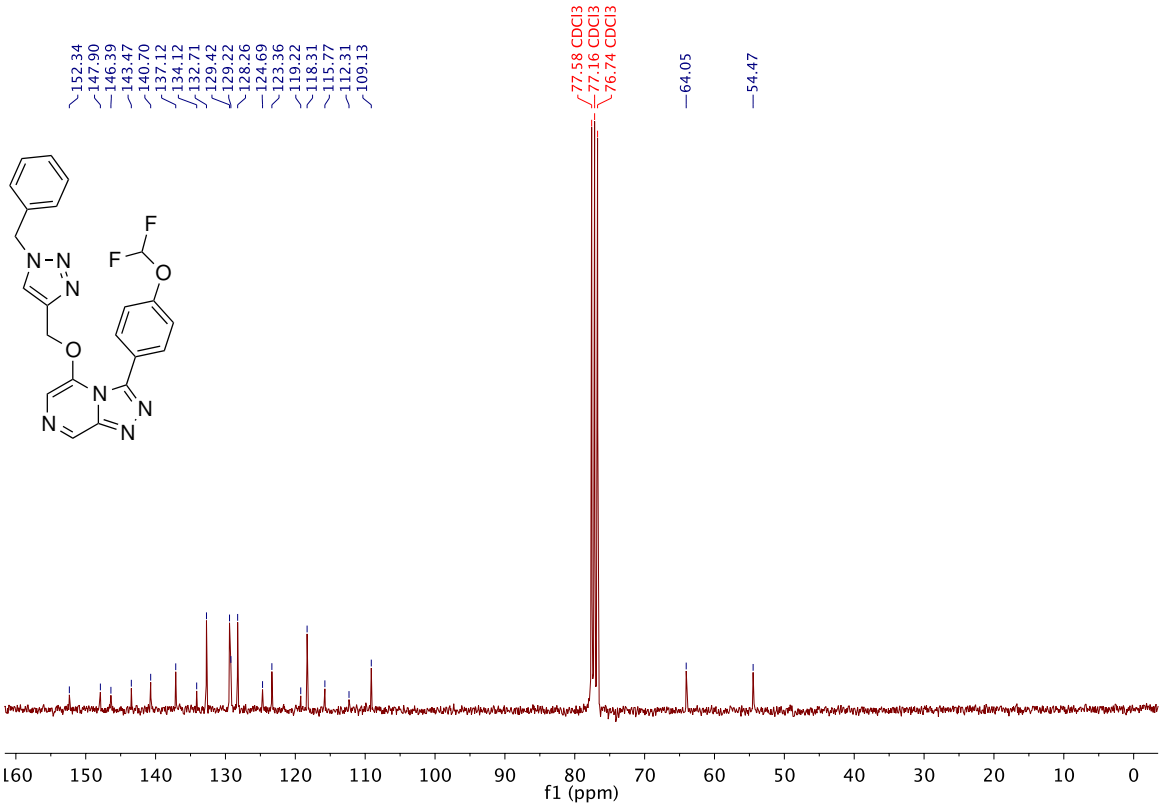

A.22 2-((3-(4-(Difluoromethoxy)phenyl)-[1,2,4]triazolo[4,3-*a*]pyrazin-5-yl) oxy)-1-(3,4-difluorophenyl)ethan-1-one 97

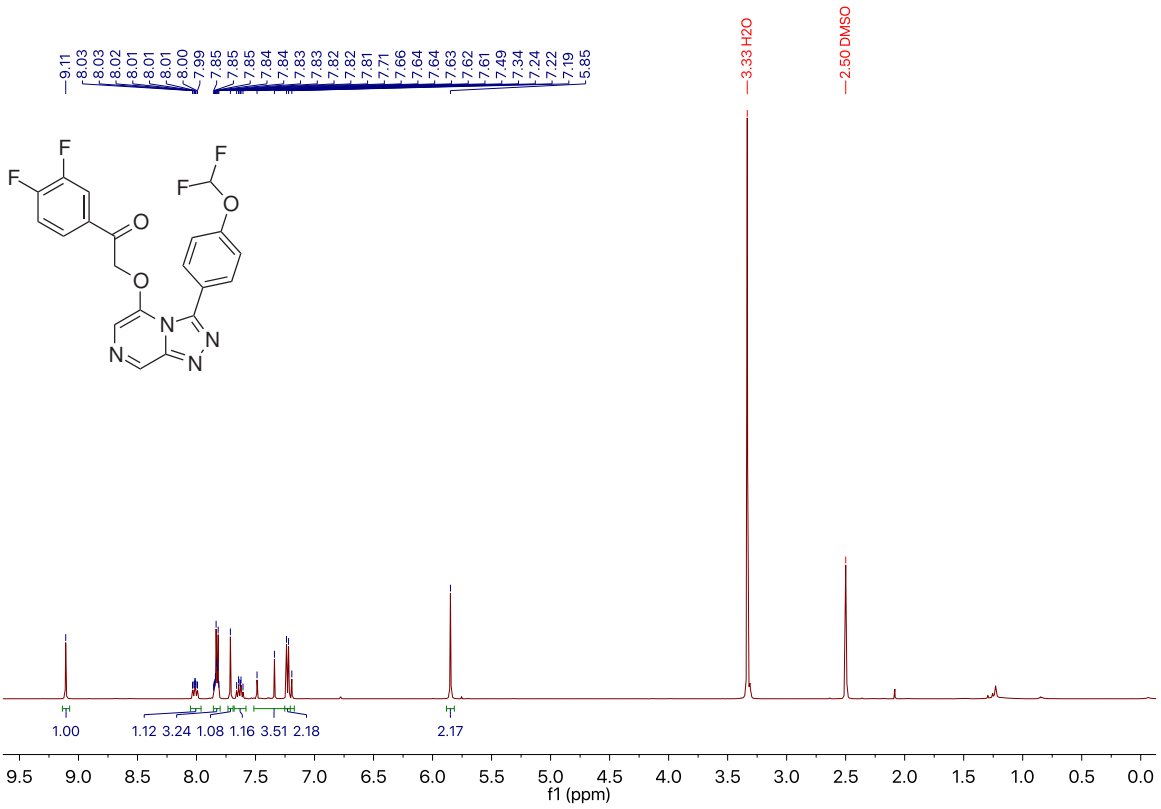

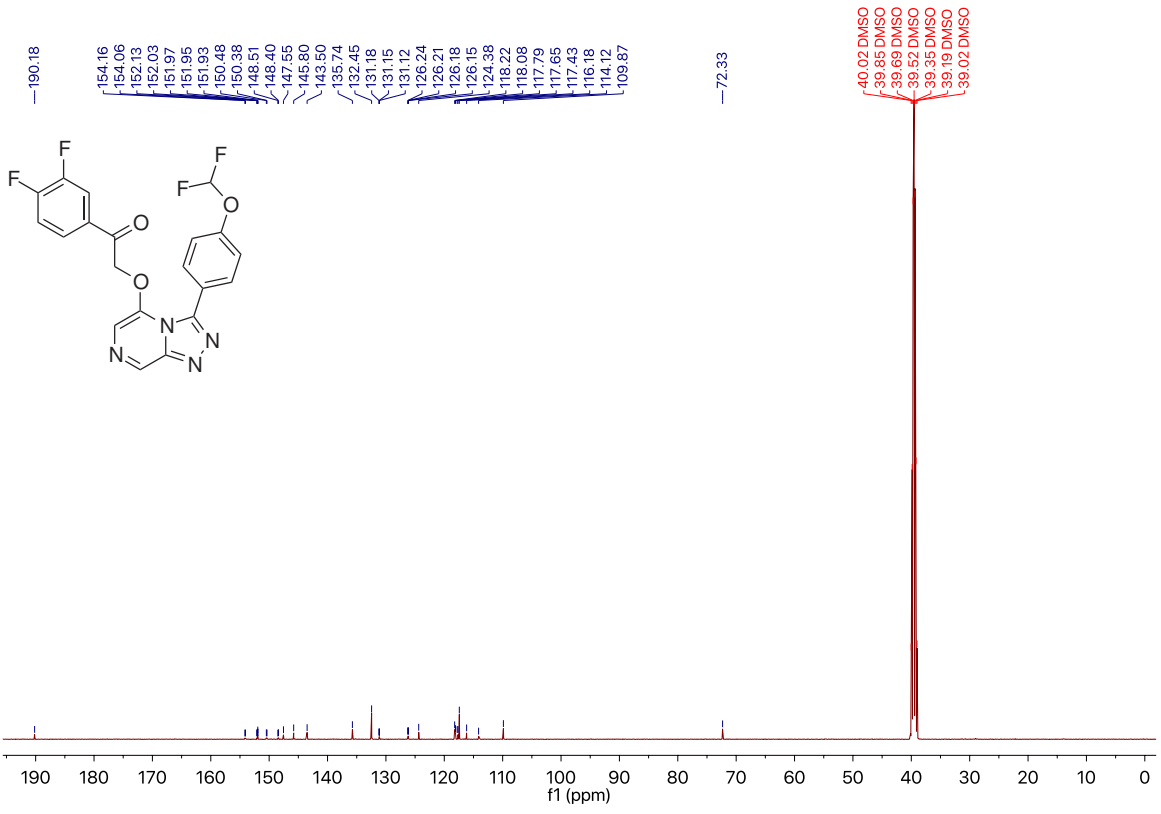

A.23 3-(4-(Difluoromethoxy)phenyl)-5-(2-(3,4-difluorophenyl)-2,2-dimethoxyethoxy)-[1,2,4]triazolo[4,3-*a*]pyrazine 98

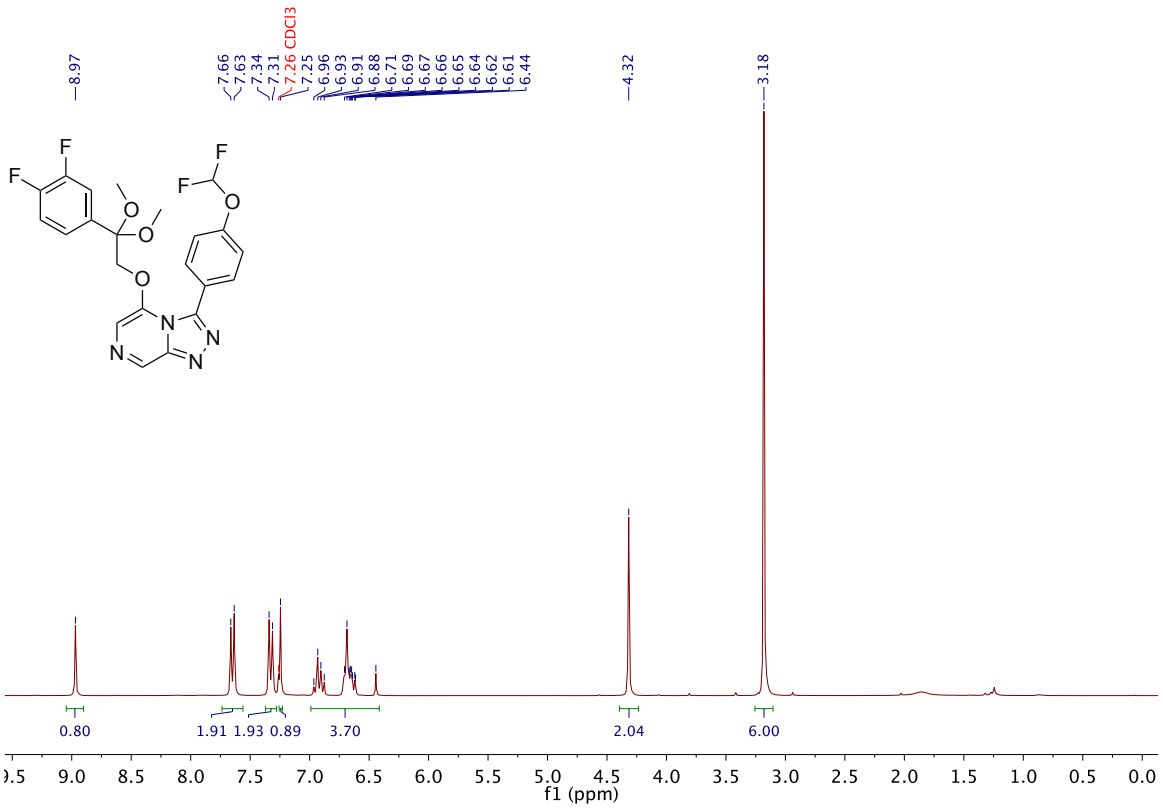

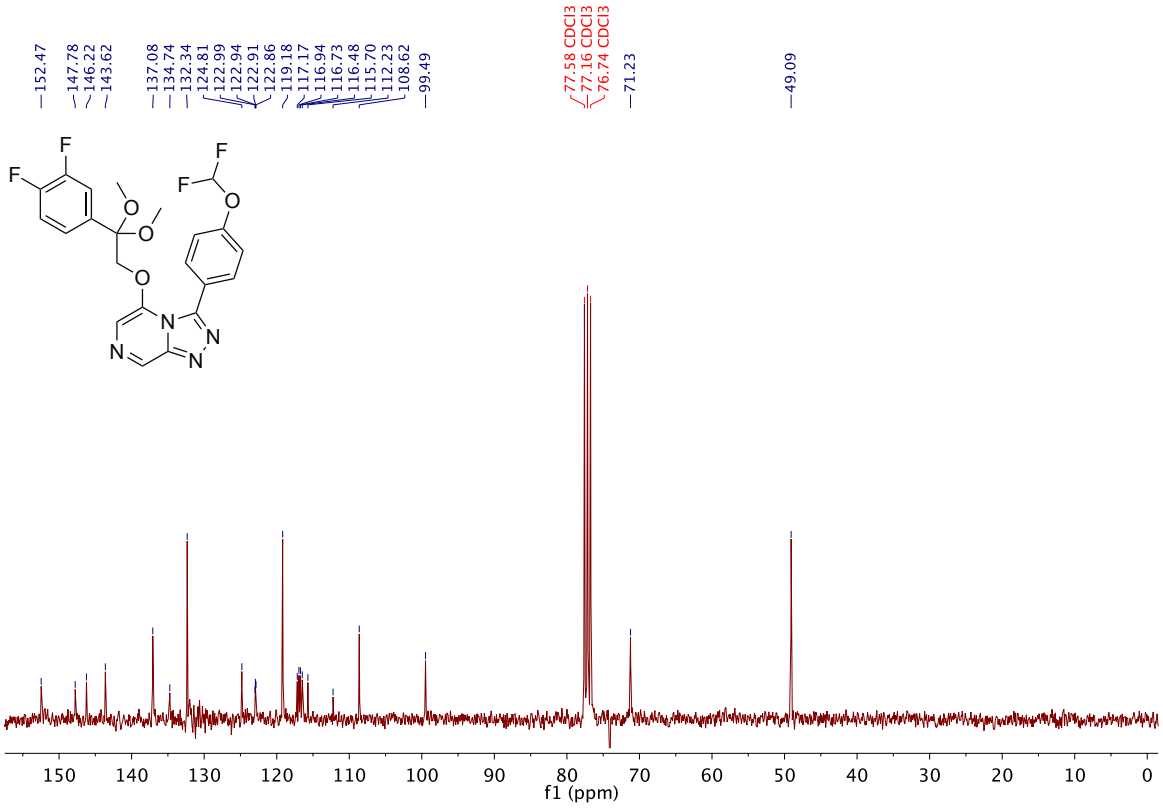

A.24 3-(4-(Difluoromethoxy)phenyl)-5-((2-(3,4-difluorophenyl)-1,3-dioxolan -2-yl)methoxy)-[1,2,4]triazolo[4,3-*a*]pyrazine 100

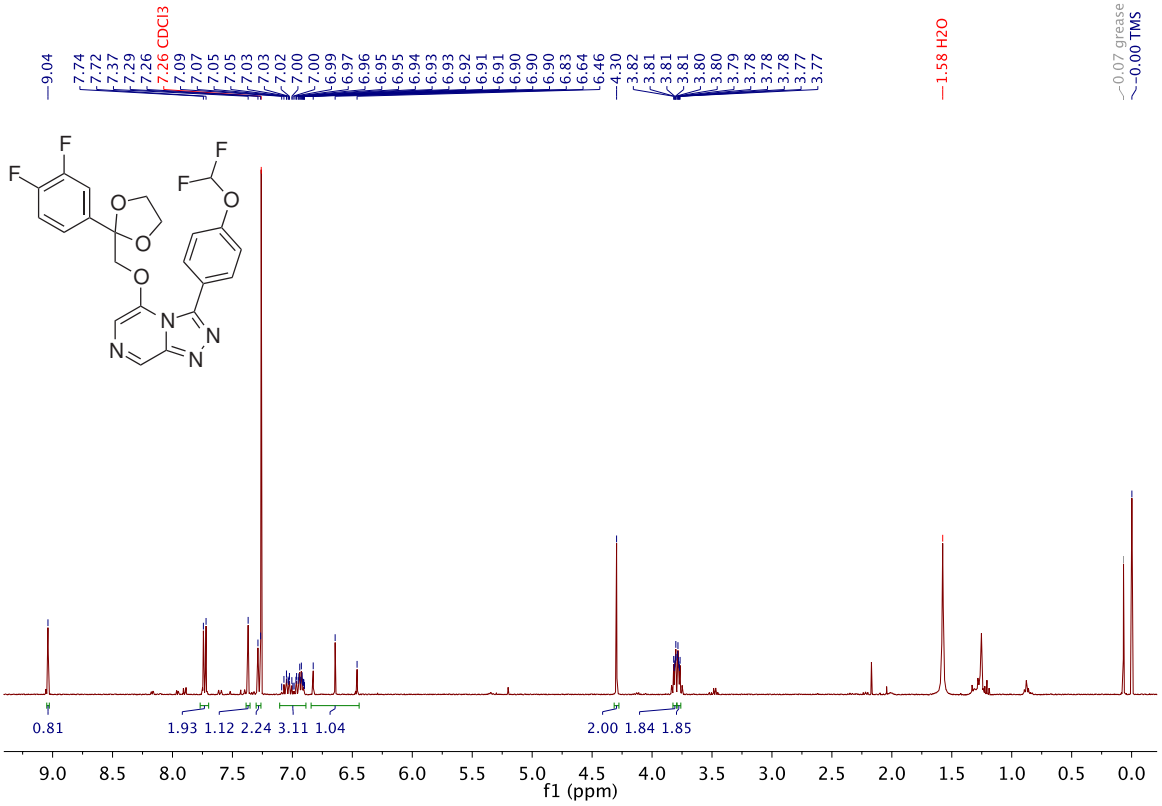

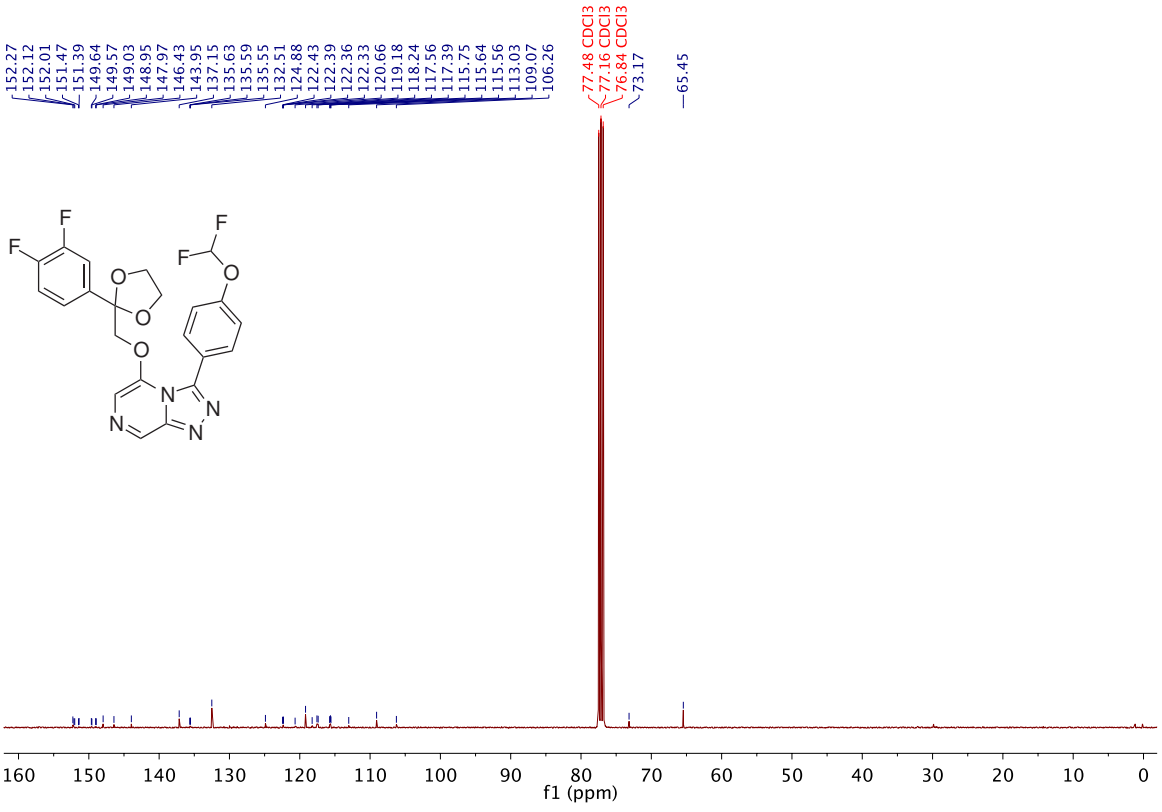

A.25 2-((3-(4-(Difluoromethoxy)phenyl)-[1,2,4]triazolo[4,3-*a*]pyrazin-5-yl)oxy)-1-phenylethan-1-ol 16

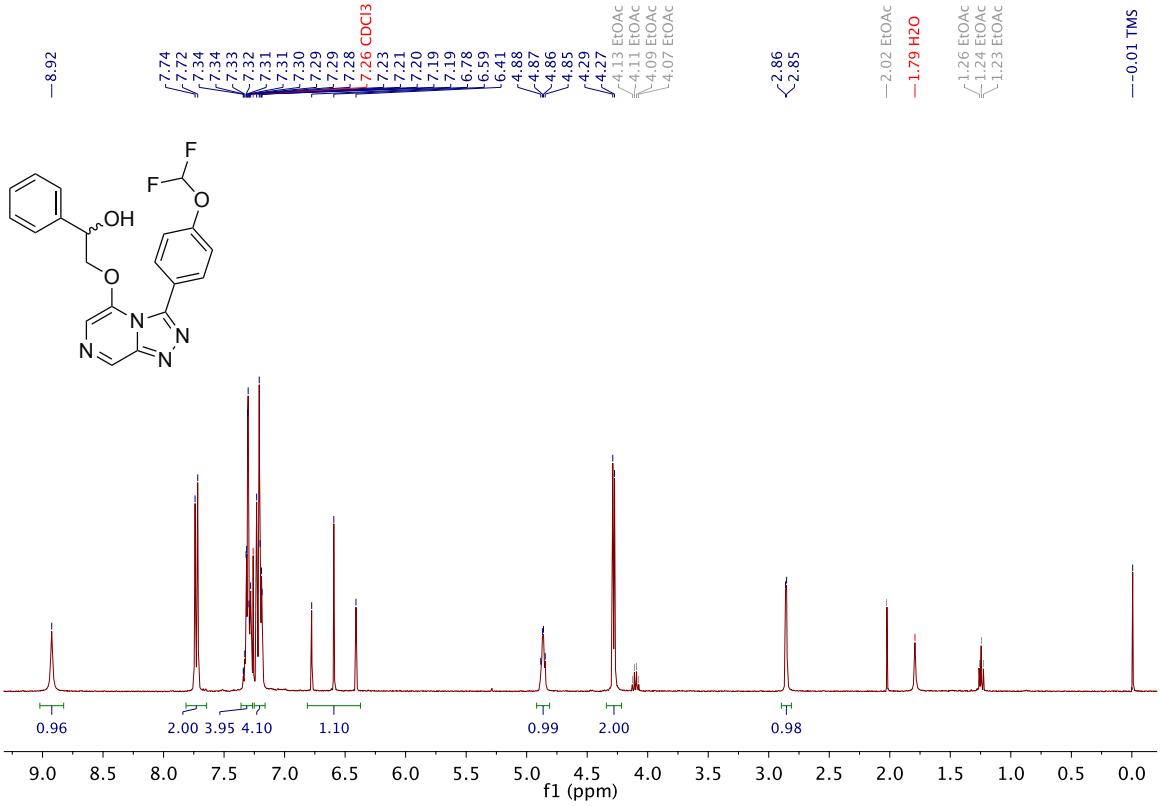

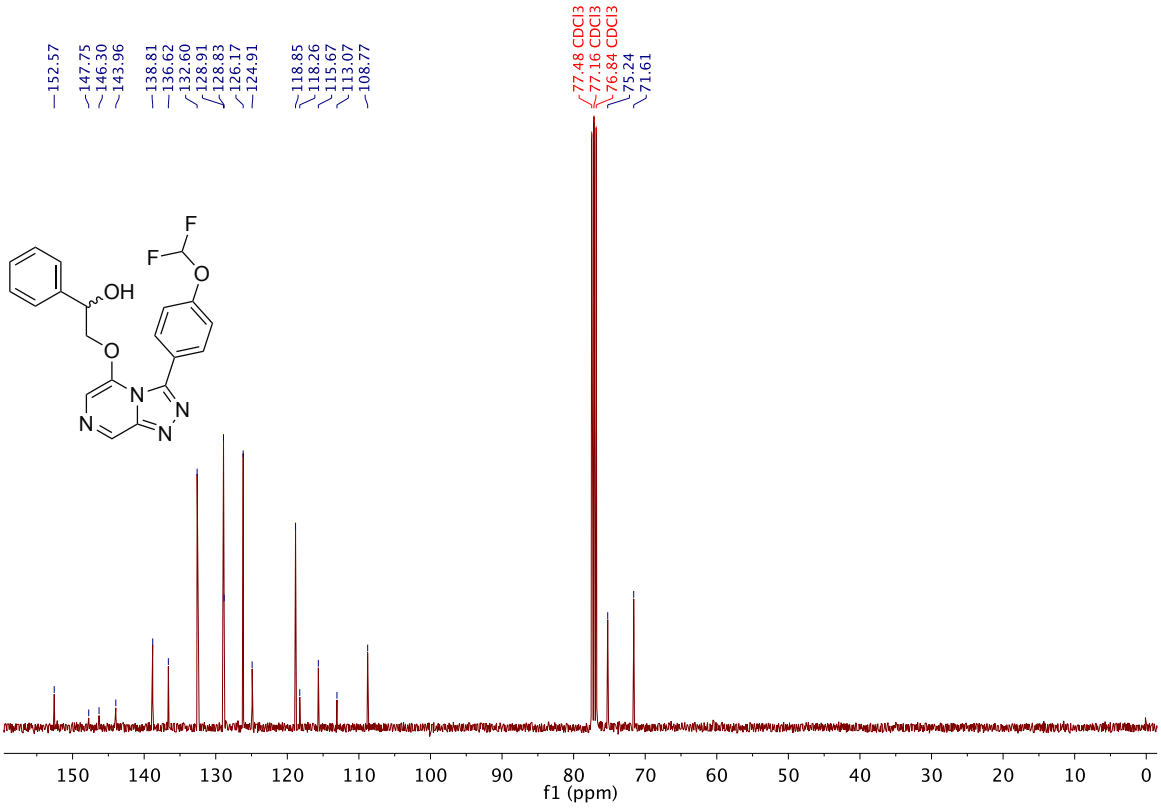

A.26 2-((3-(4-(Difluoromethoxy)phenyl)-[1,2,4]triazolo[4,3-*a*]pyrazin-5-yl) oxy)-1-phenylethan-1-one 105

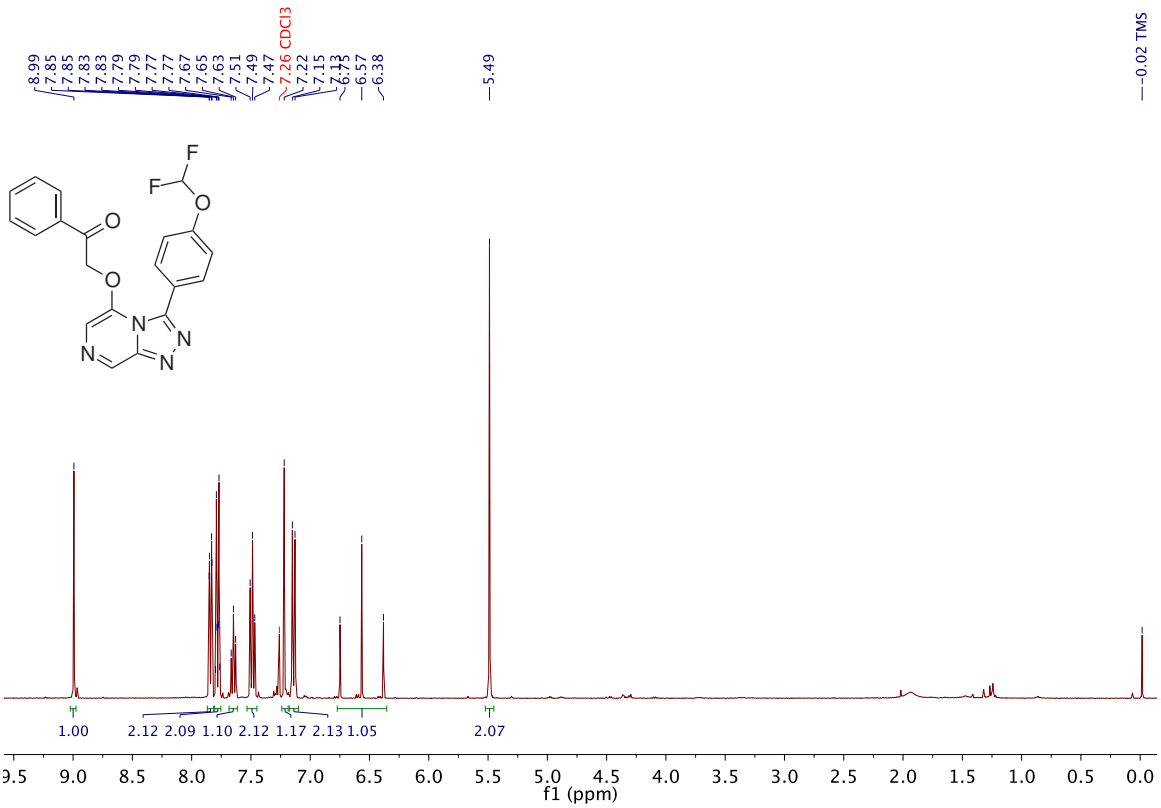

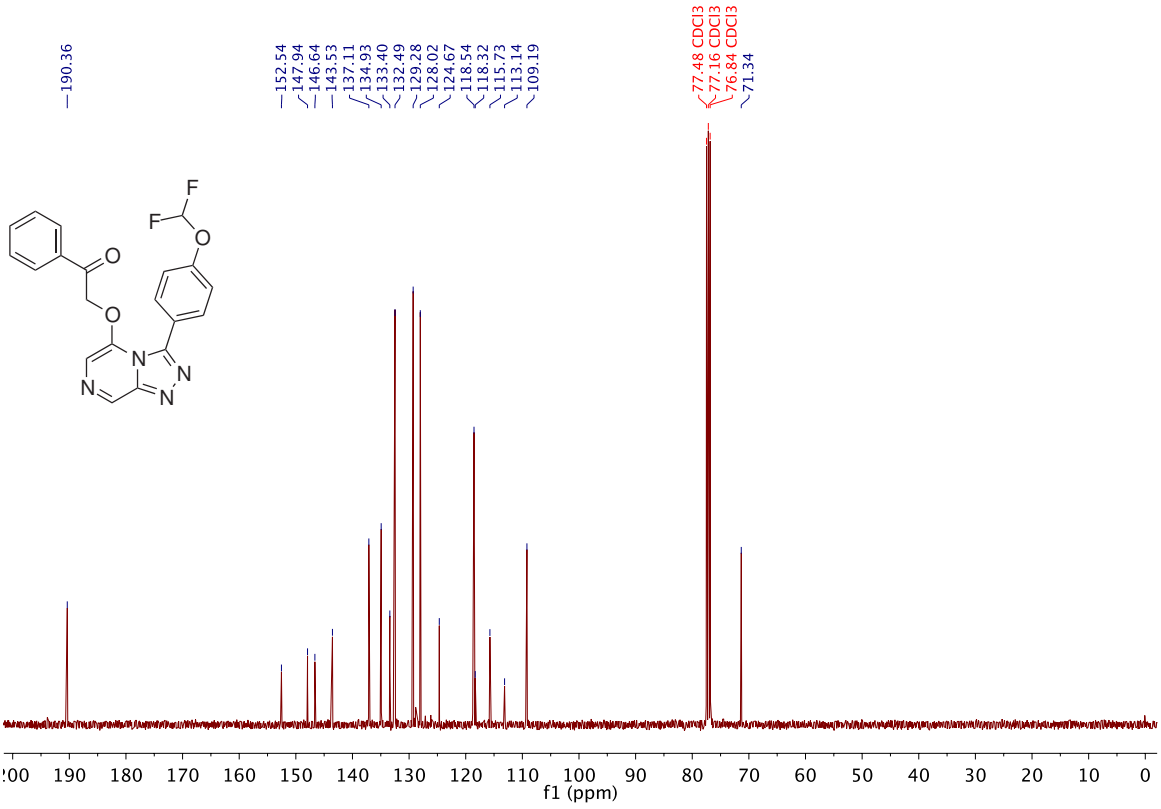

A.27 1-Phenyl-2-((3-(6-(trifluoromethyl)pyridin-3-yl)-[1,2,4]triazolo[4,3-*a*]pyrazin-5-yl)oxy)ethan-1-ol 25

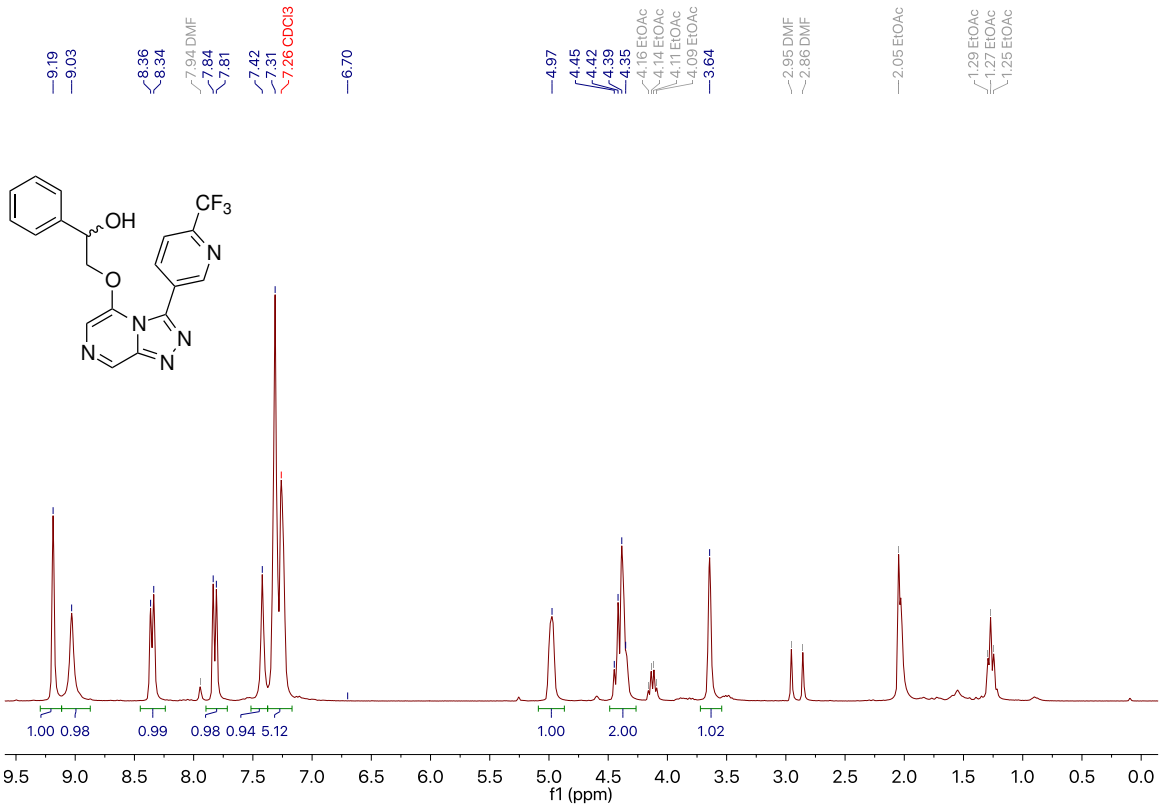

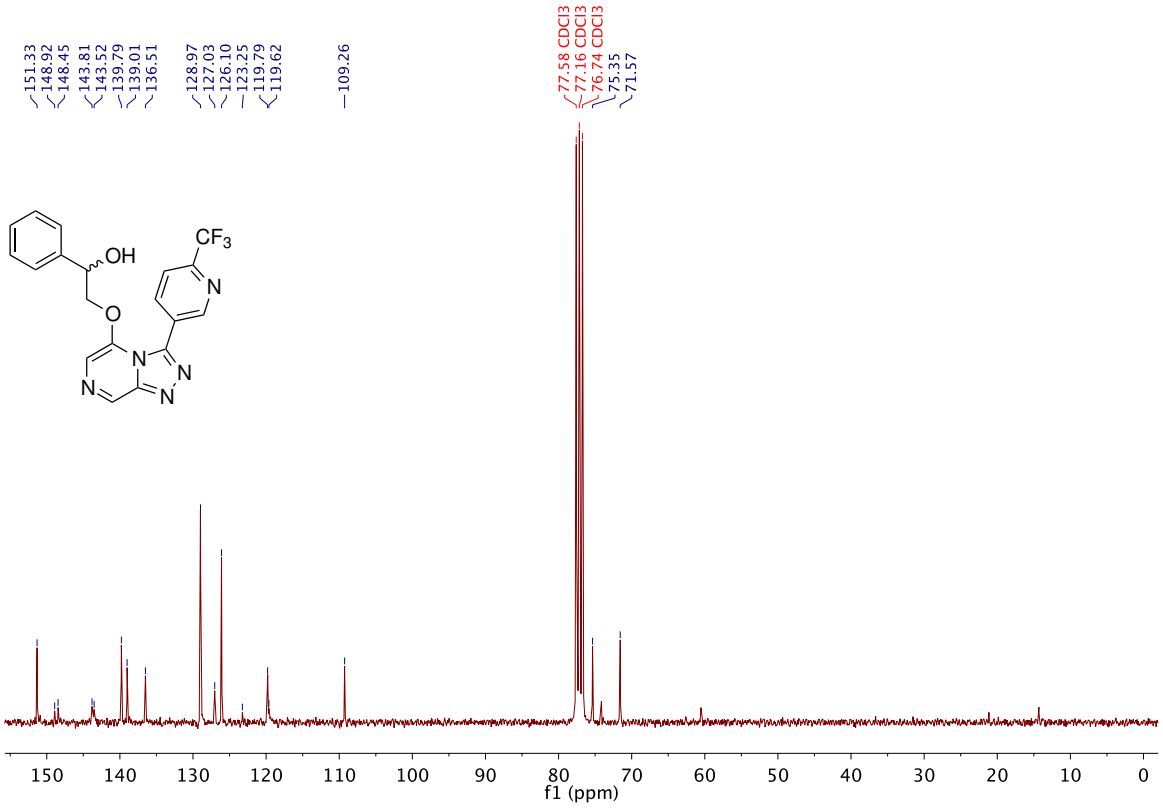

A.28 4-(2-((3-(4-(Difluoromethoxy)phenyl)-[1,2,4]triazolo[4,3-*a*]pyrazin-5-yl) oxy)-1-phenylethyl)morpholine 108

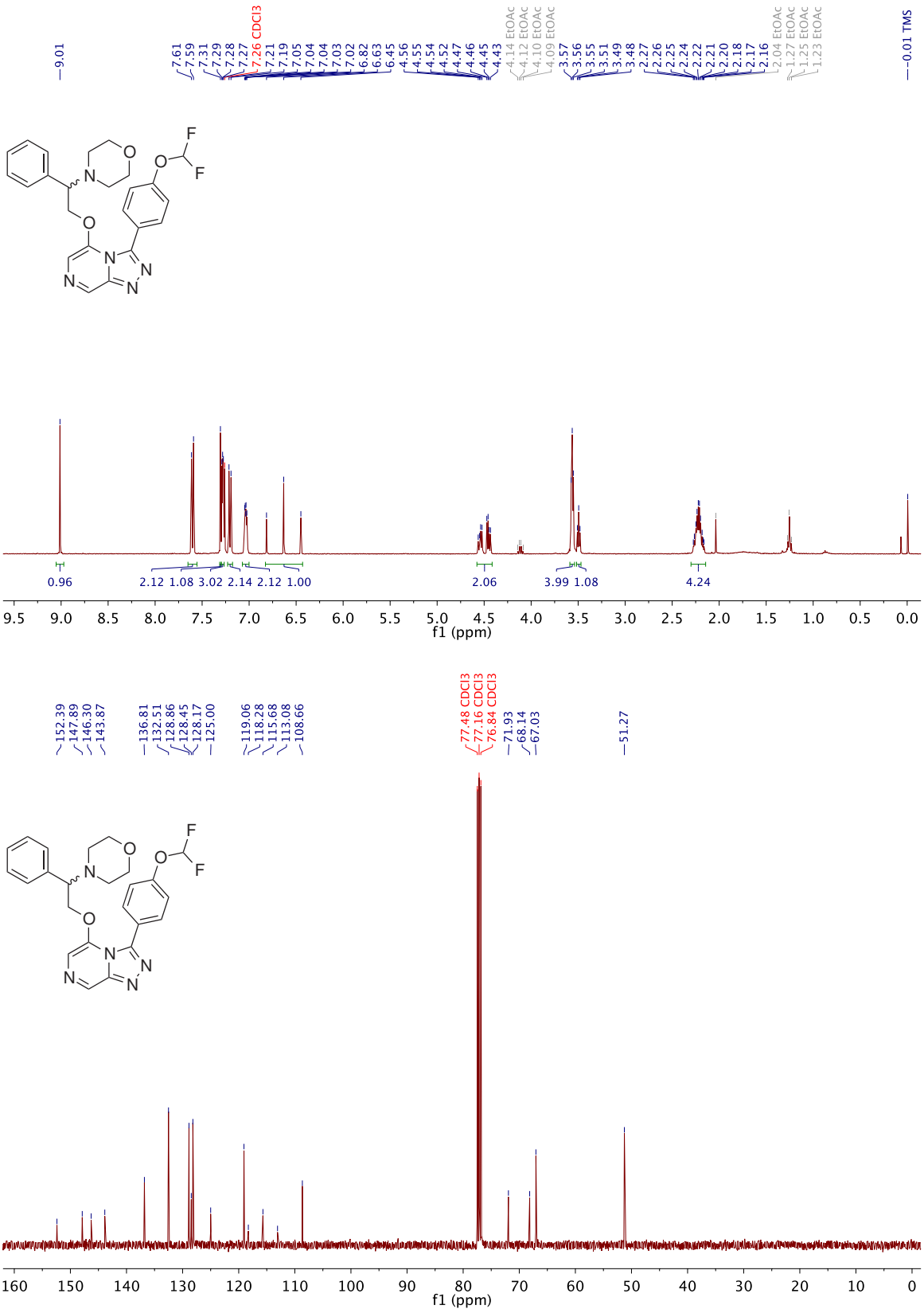

A.29 2-((3-(4-(Difluoromethoxy)phenyl)-[1,2,4]triazolo[4,3-*a*]pyrazin-5-yl) oxy)-1-(3,4-difluorophenyl)-*N*-ethyl-*N*-methylethan-1-amine 113

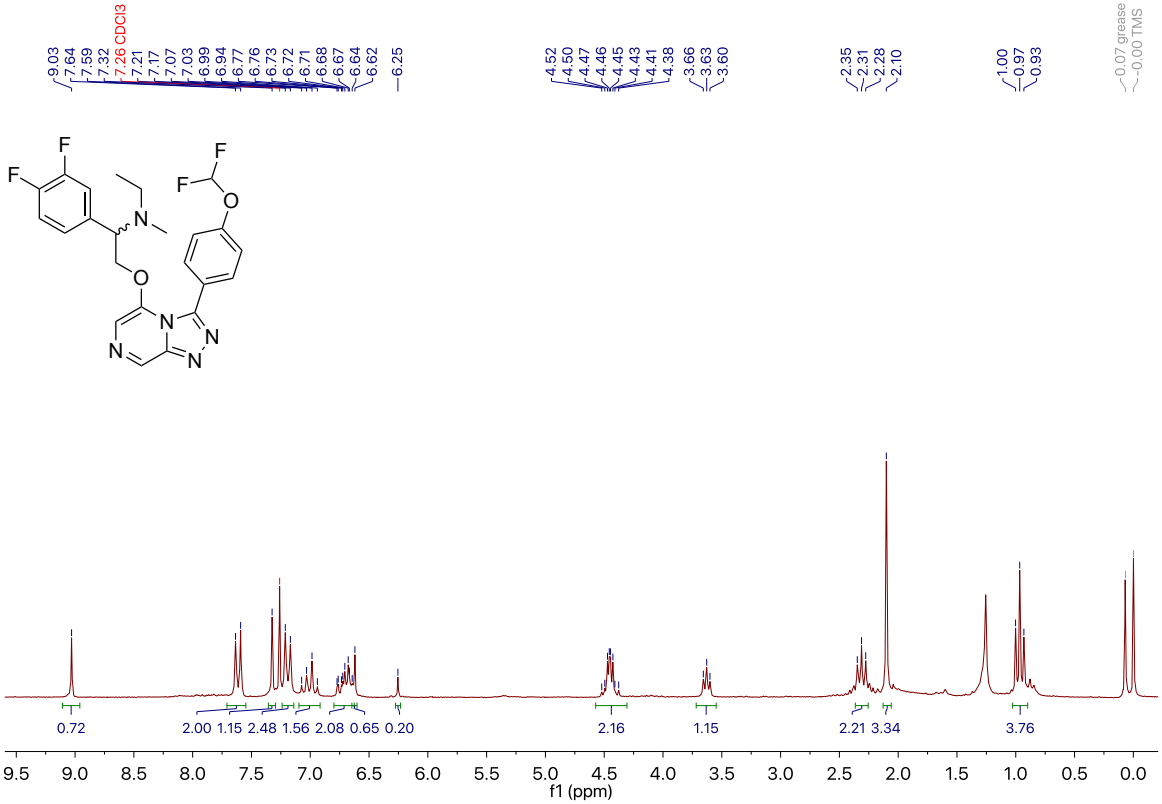

A.30 2-((3-(4-(Difluoromethoxy)phenyl)-[1,2,4]triazolo[4,3-*a*]pyrazin-5-yl) oxy)-1-(3,4-difluorophenyl)-*N*,*N*-diethylethan-1-amine 114

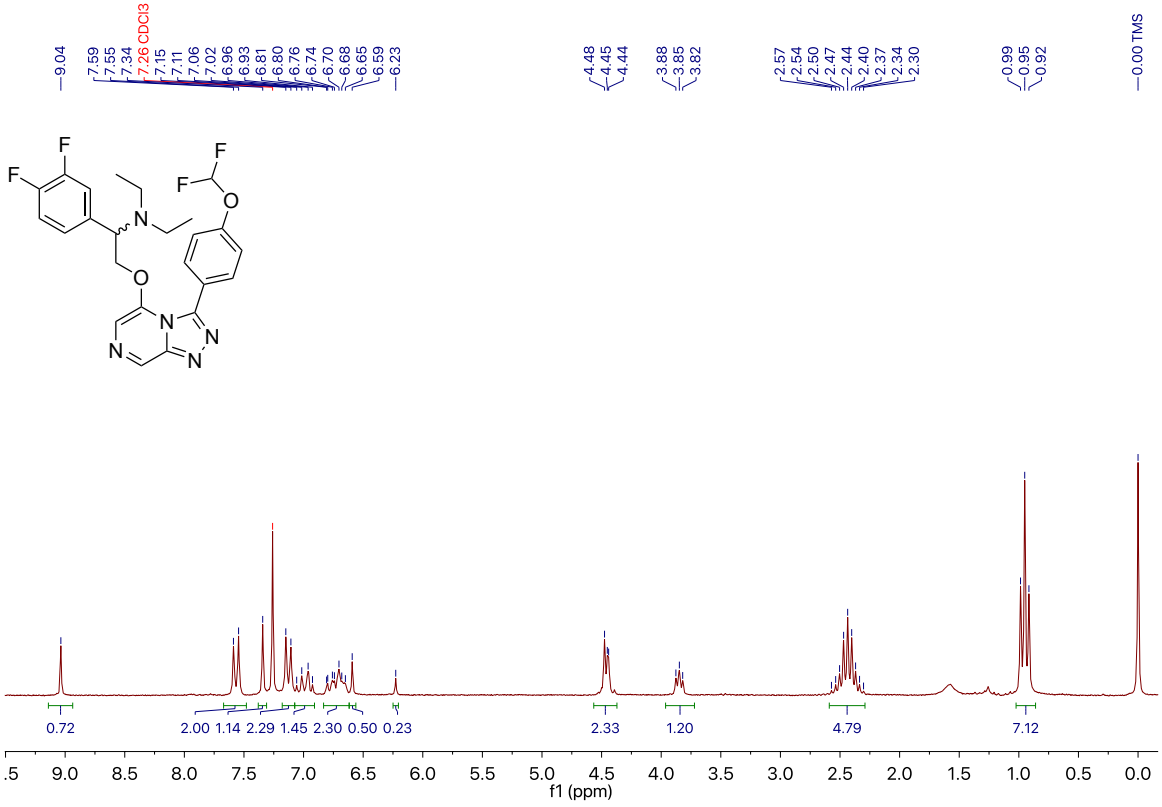

A.31 *tert*-Butyl (*R*)-(1-((3-(4-(difluoromethoxy)phenyl)-[1,2,4]triazolo[4,3-*a*]pyrazin-5-yl)oxy)-3-phenylpropan-2-yl)carbamate 117

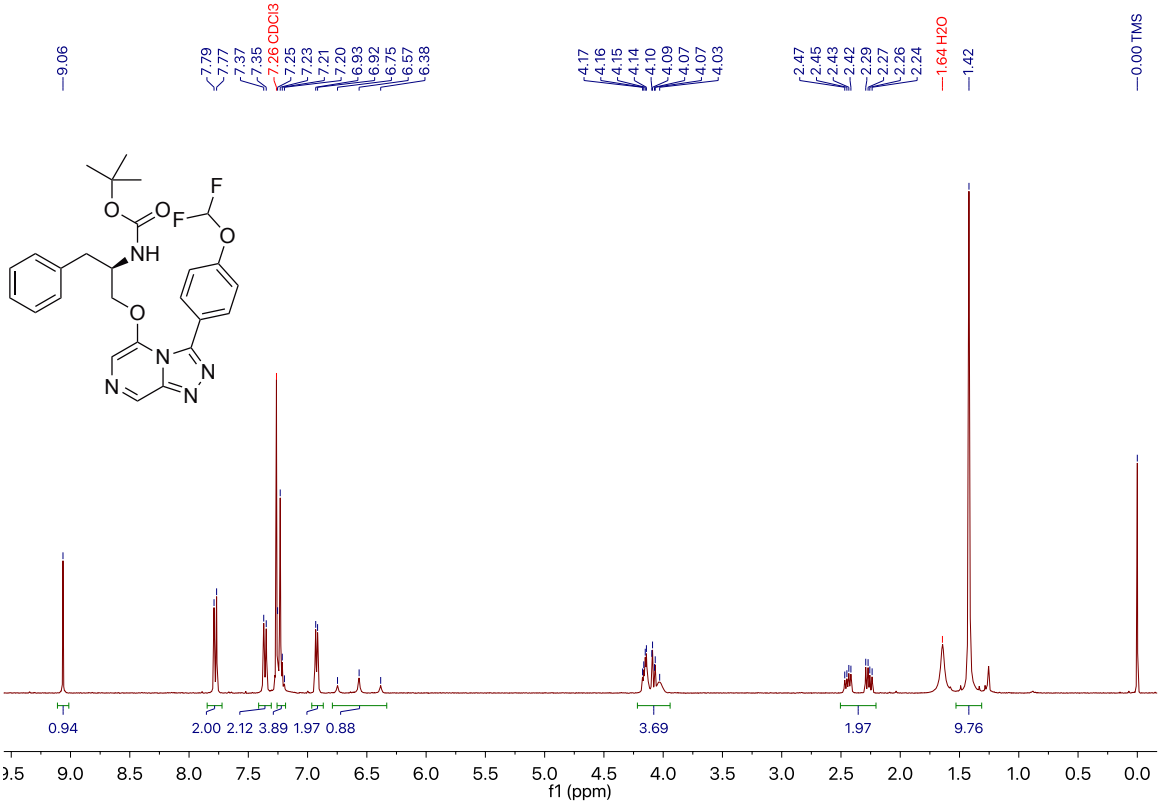

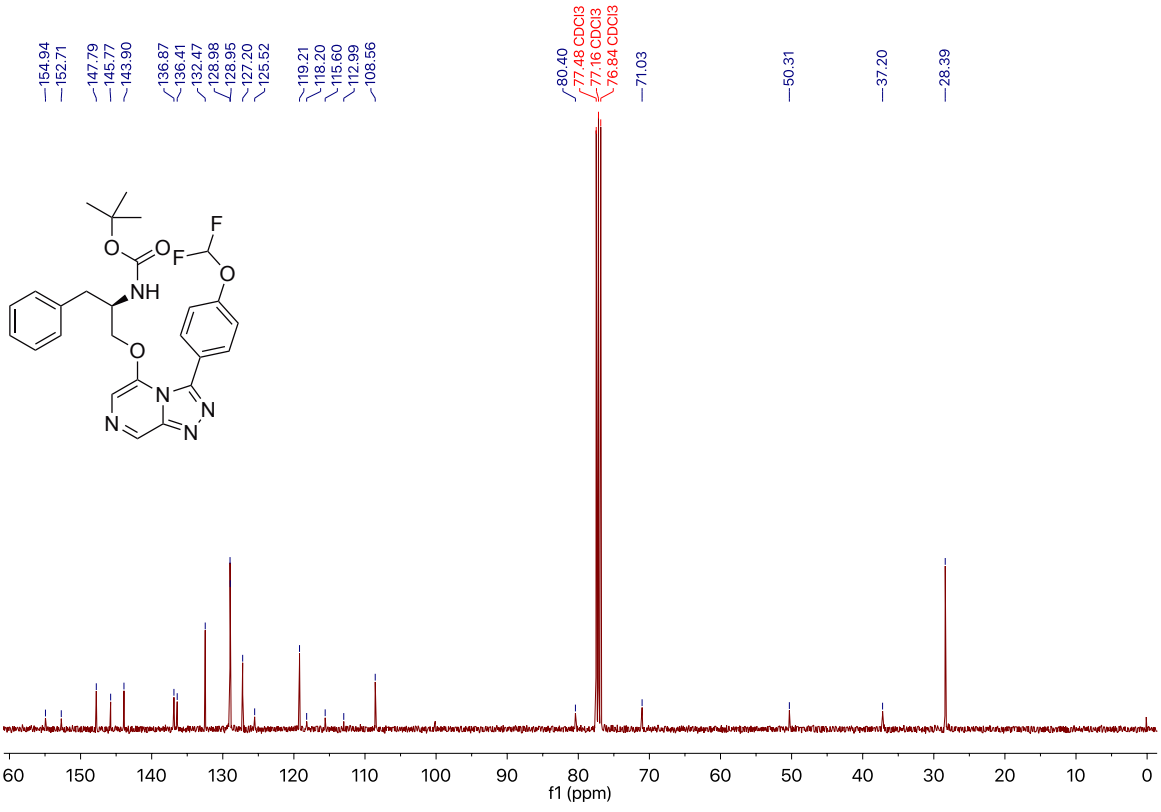

A.32 *tert*-Butyl (*S*)-(1-((3-(4-(difluoromethoxy)phenyl)-[1,2,4]triazolo[4,3-*a*]pyrazin-5-yl)oxy)-3-phenylpropan-2-yl)carbamate 118

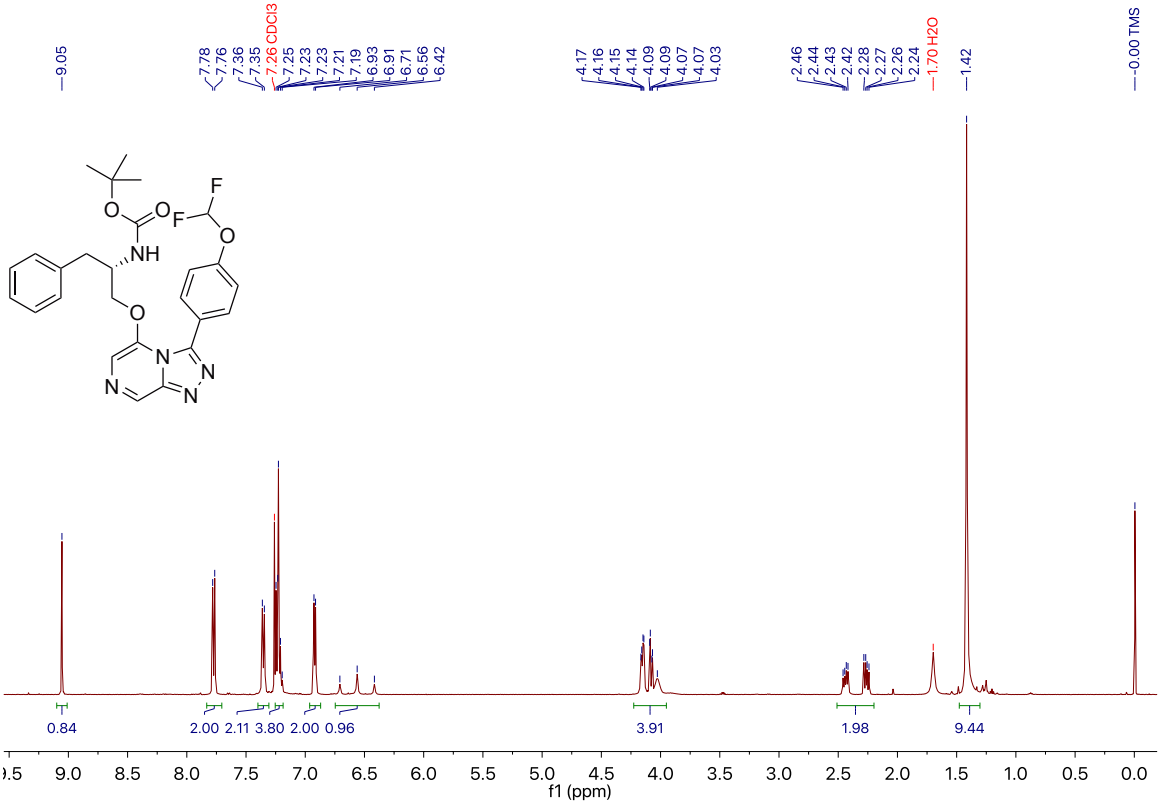

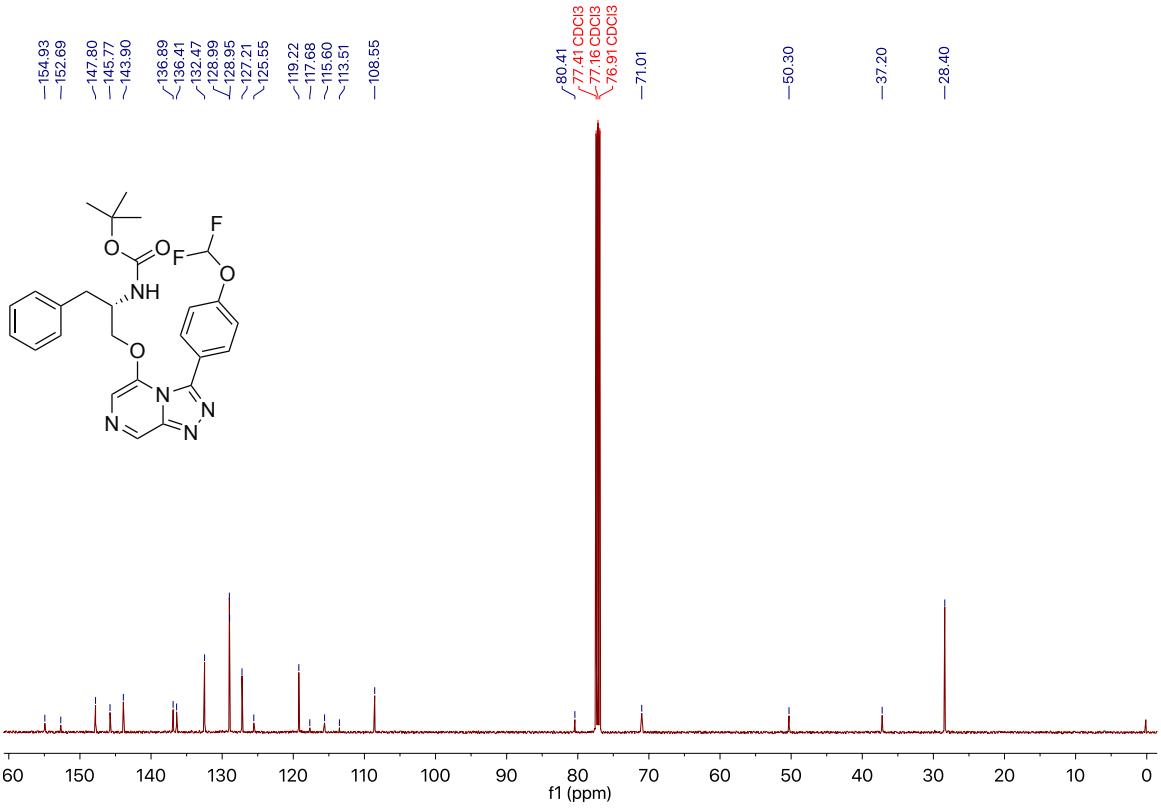

A.33 (*R*)-1-((3-(4-(Difluoromethoxy)phenyl)-[1,2,4]triazolo[4,3-*a*]pyrazin-5-yl)oxy)-3-phenylpropan-2-amine 119

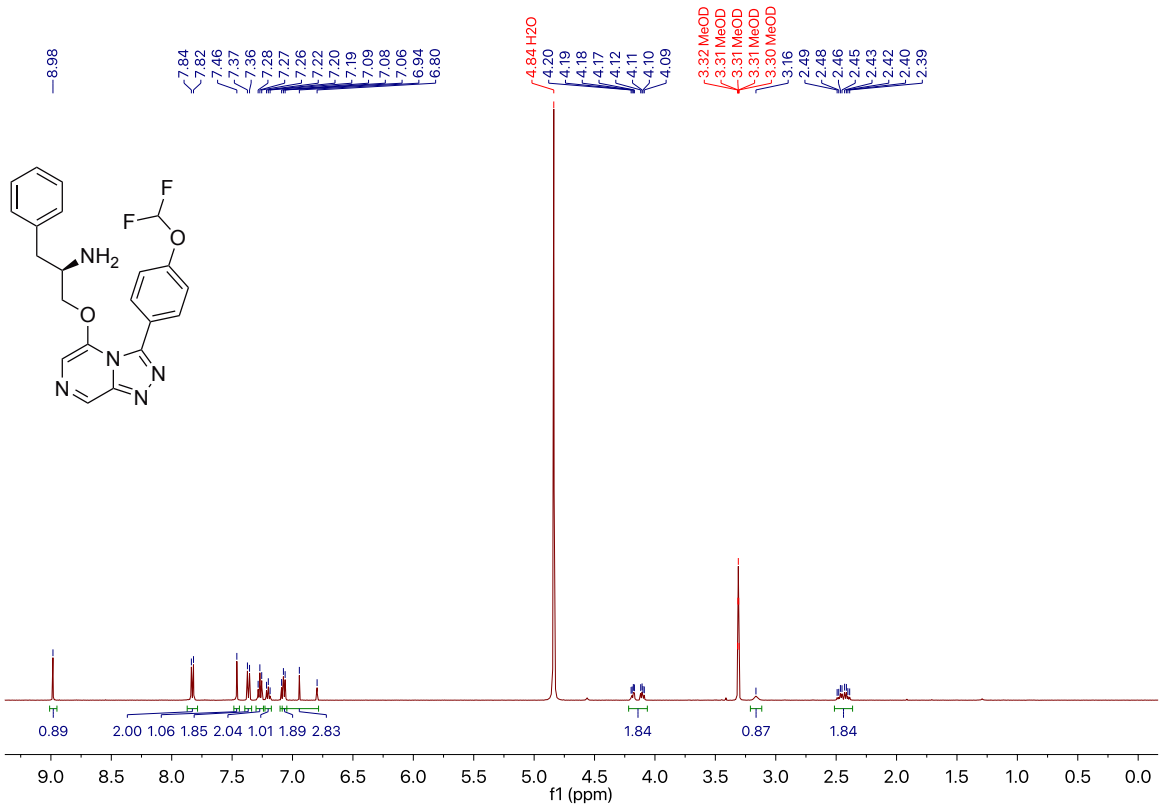

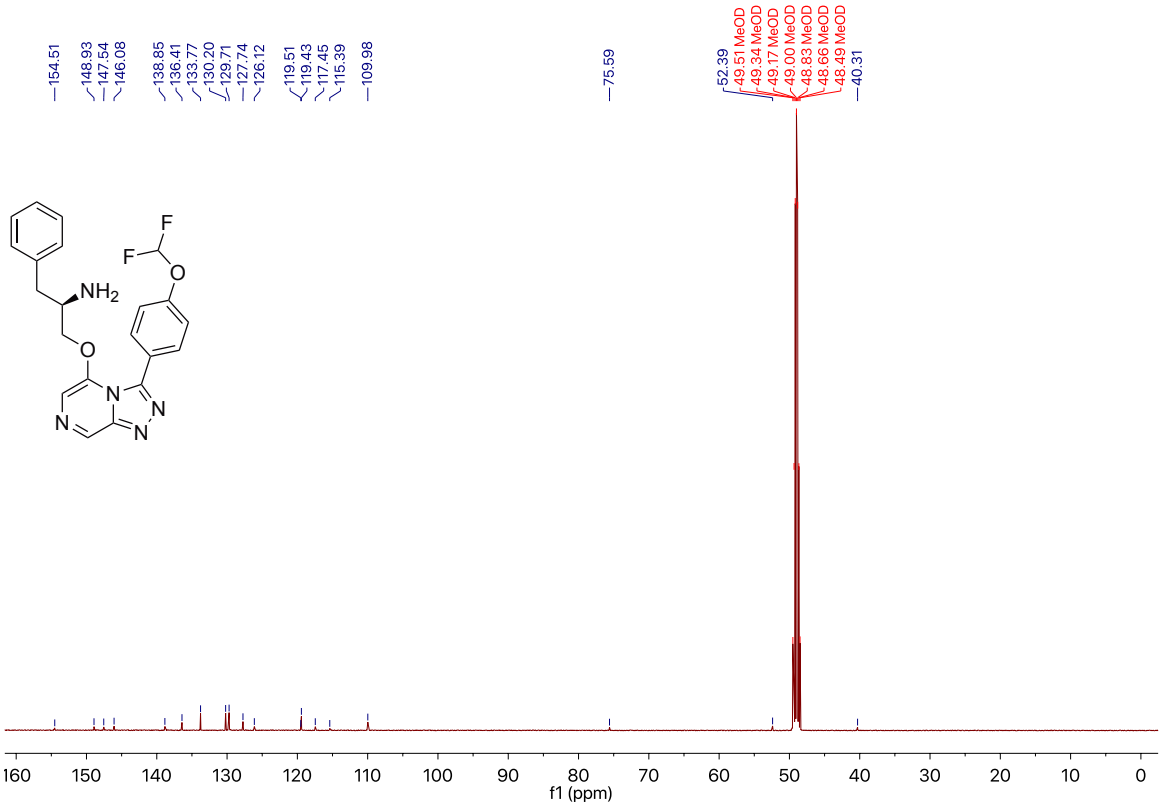

A.34 (*S*)-1-((3-(4-(Difluoromethoxy)phenyl)-[1,2,4]triazolo[4,3-*a*]pyrazin-5-yl)oxy)-3-phenylpropan-2-amine 120

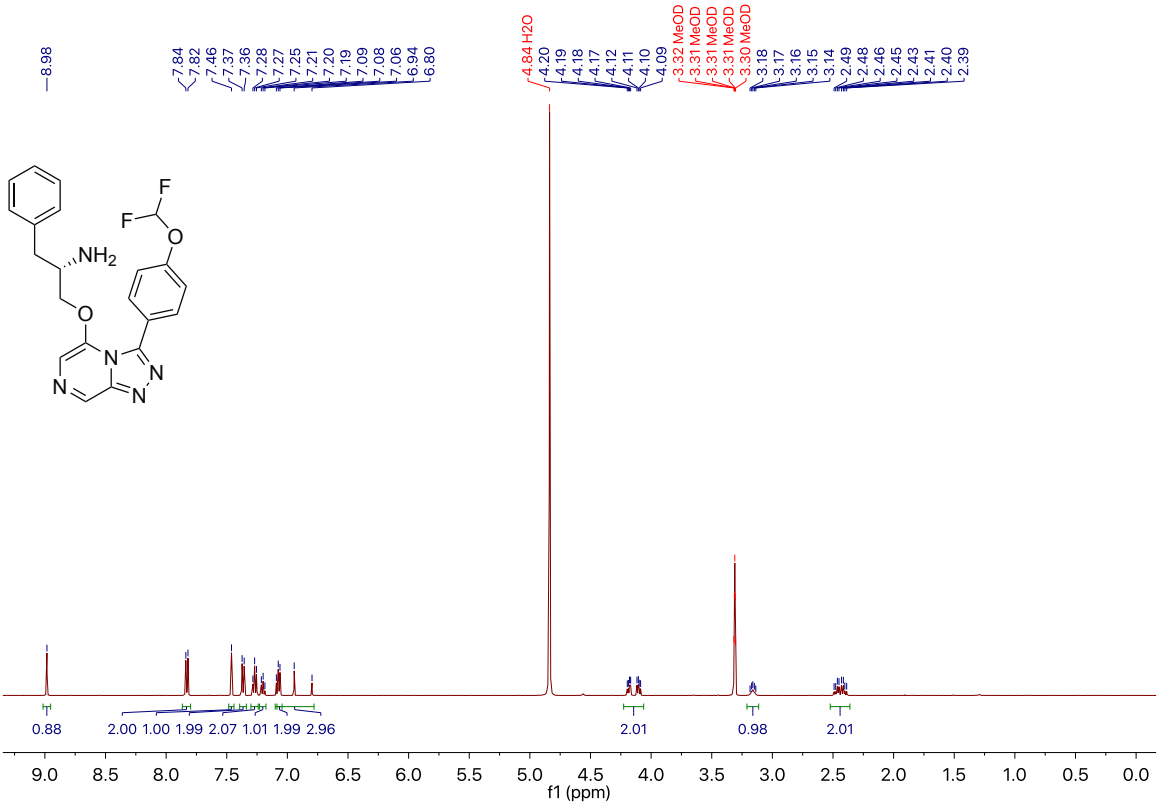

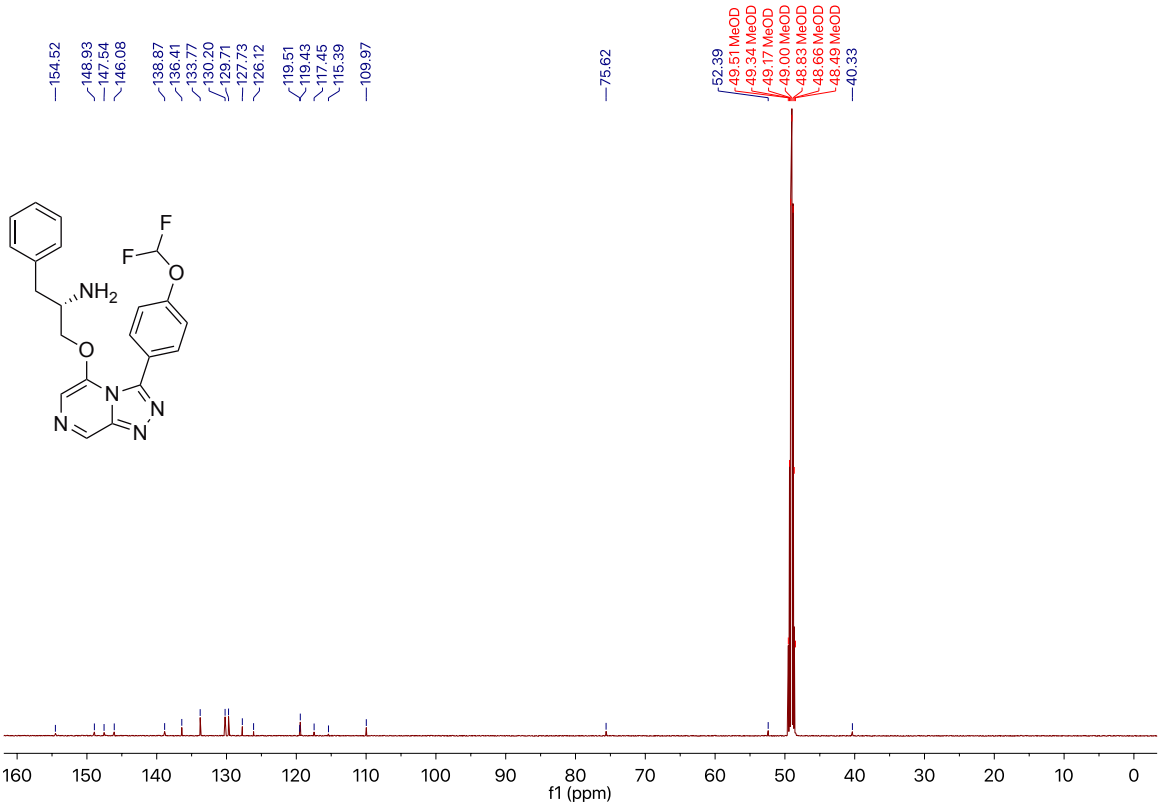

A.35 5-(3,4-Difluorophenethoxy)-[1,2,4]triazolo[4,3-*a*]pyrazine 122

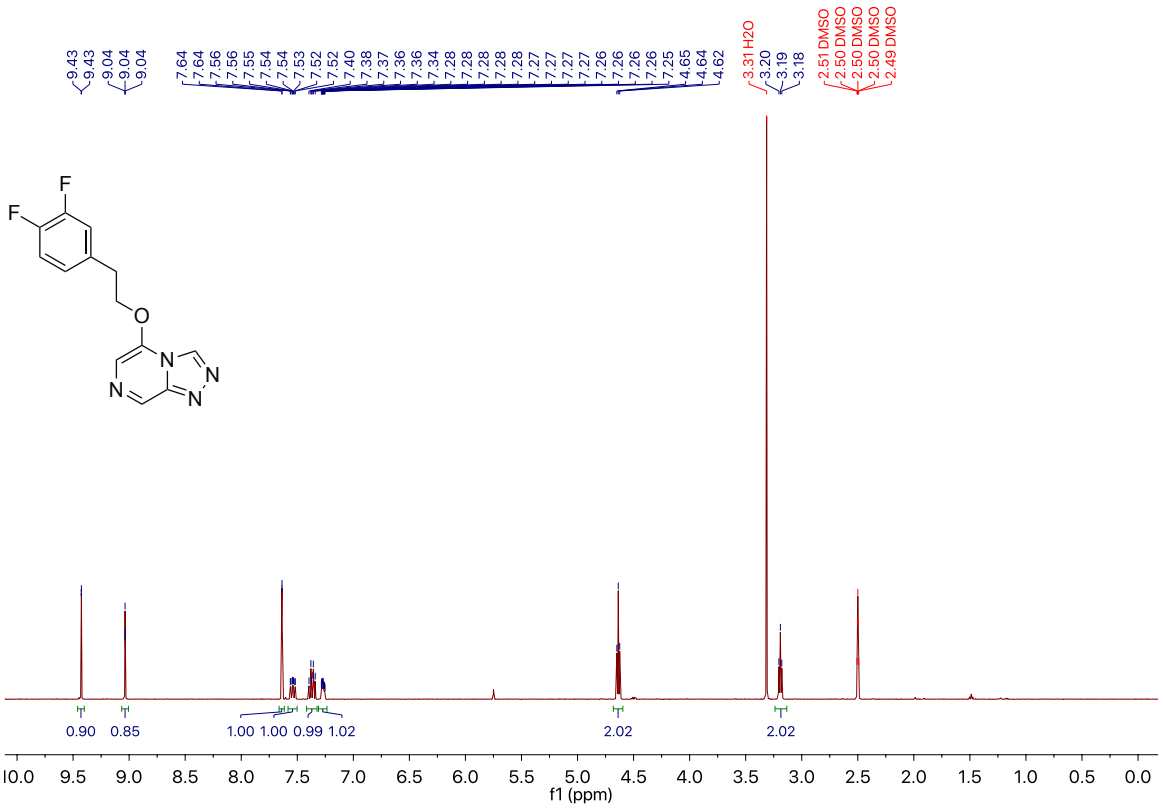

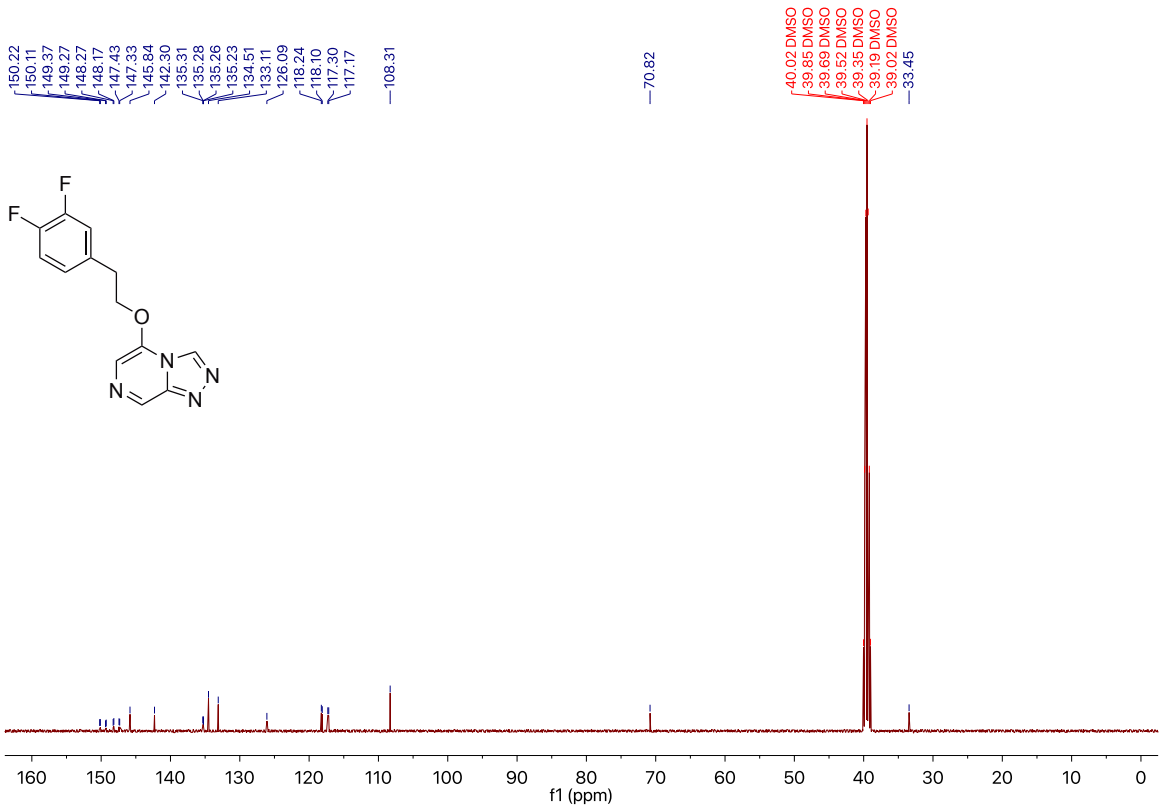

A.36 5-(3,4-Difluorophenethoxy)-3-phenyl-[1,2,4]triazolo[4,3-*a*]pyrazine 125

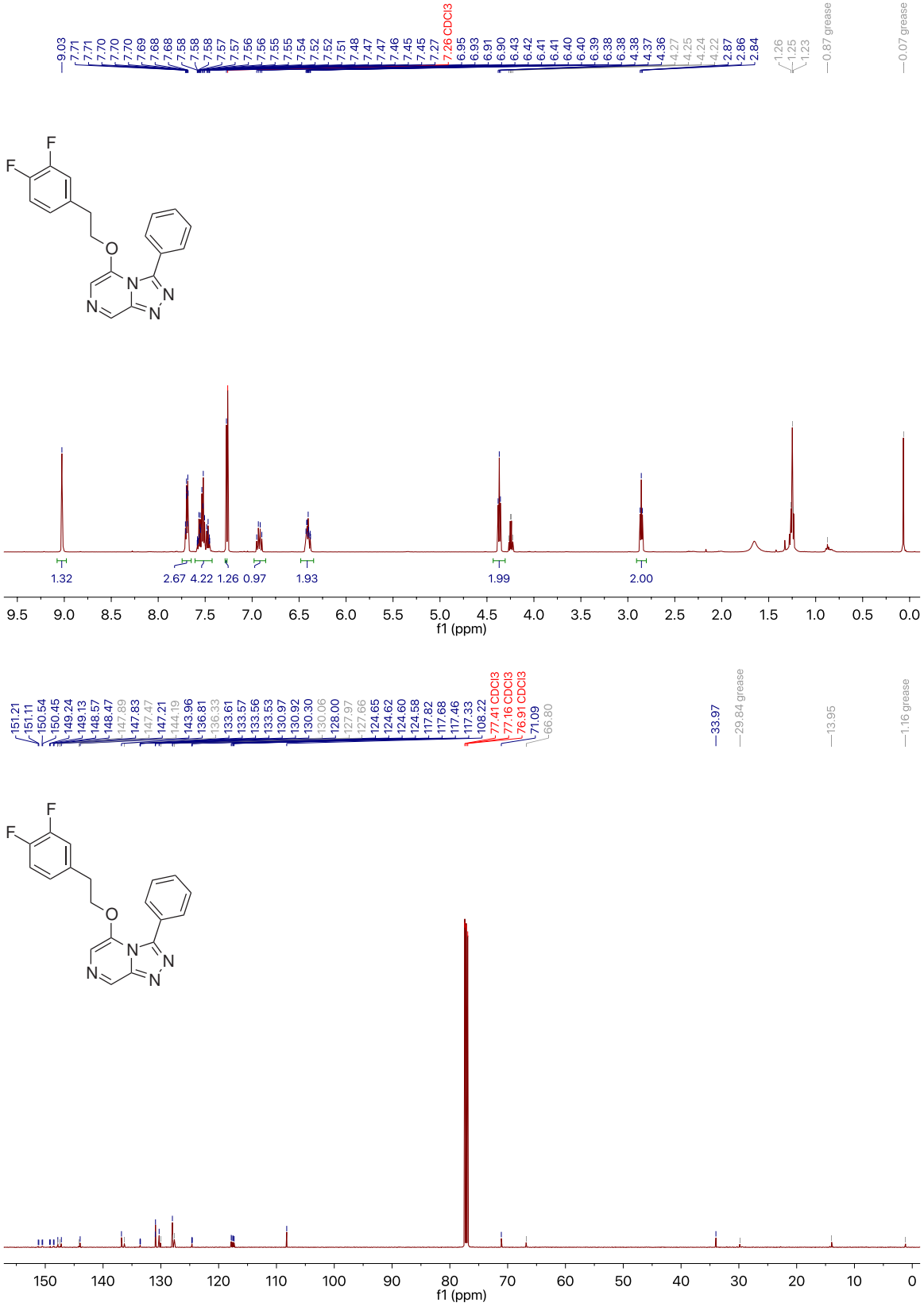

A.37 3-(4-(Pentafluoro-λ6-sulfaneyl)phenyl)-5-phenethoxy-[1,2,4]triazolo [4,3-*a*]pyrazine 128

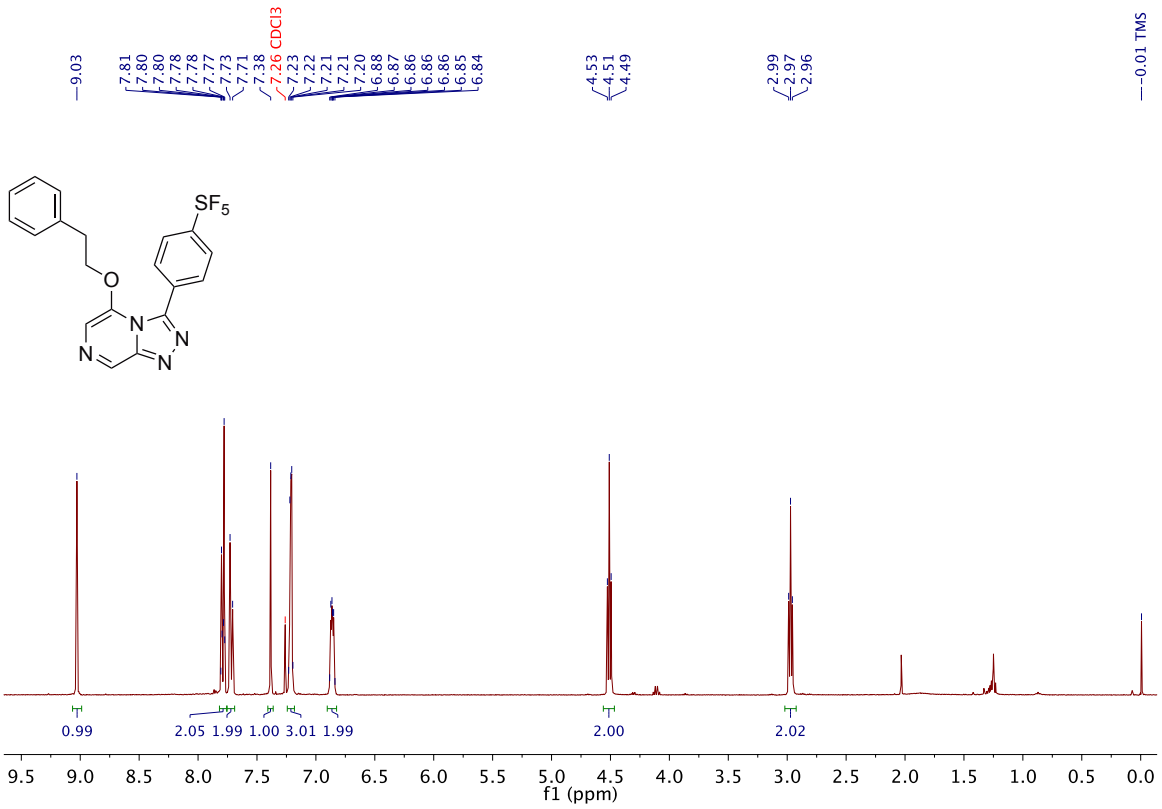

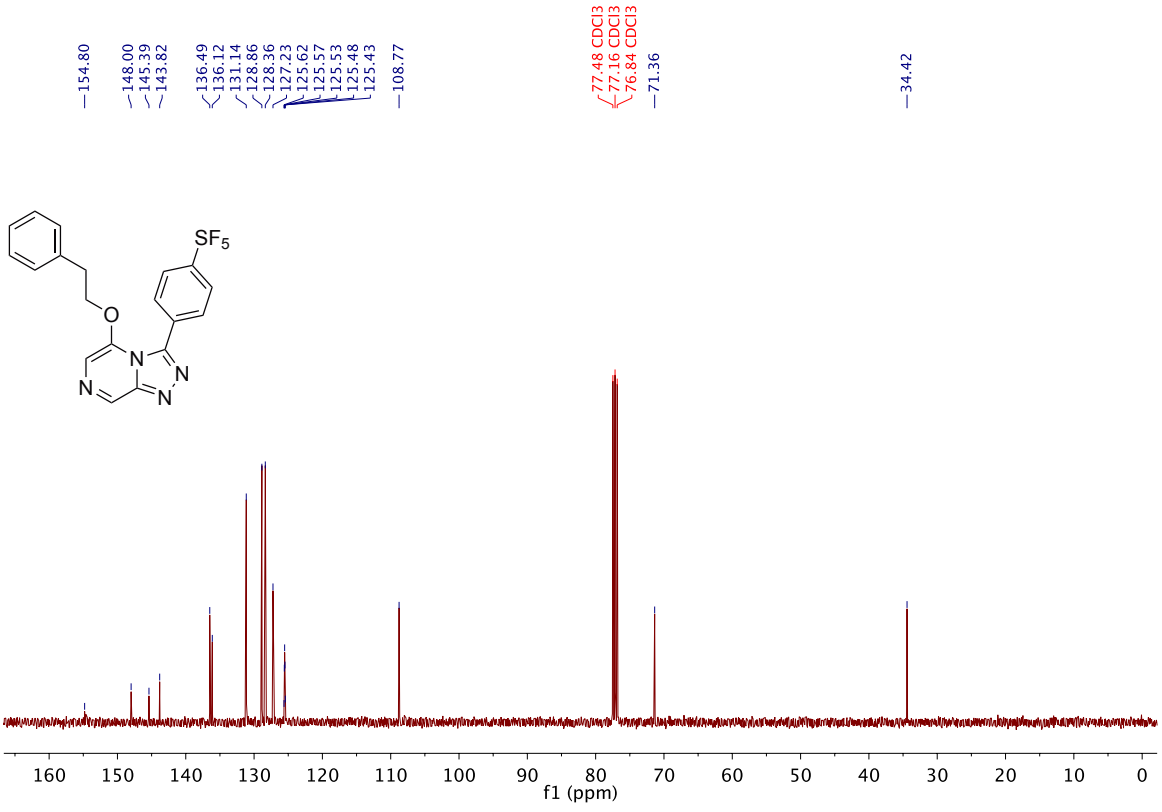

A.38 3-(4-(Difluoromethoxy)phenyl)-5-(3-methoxyphenethoxy)-[1,2,4] triazolo[4,3-*a*]pyrazine 129

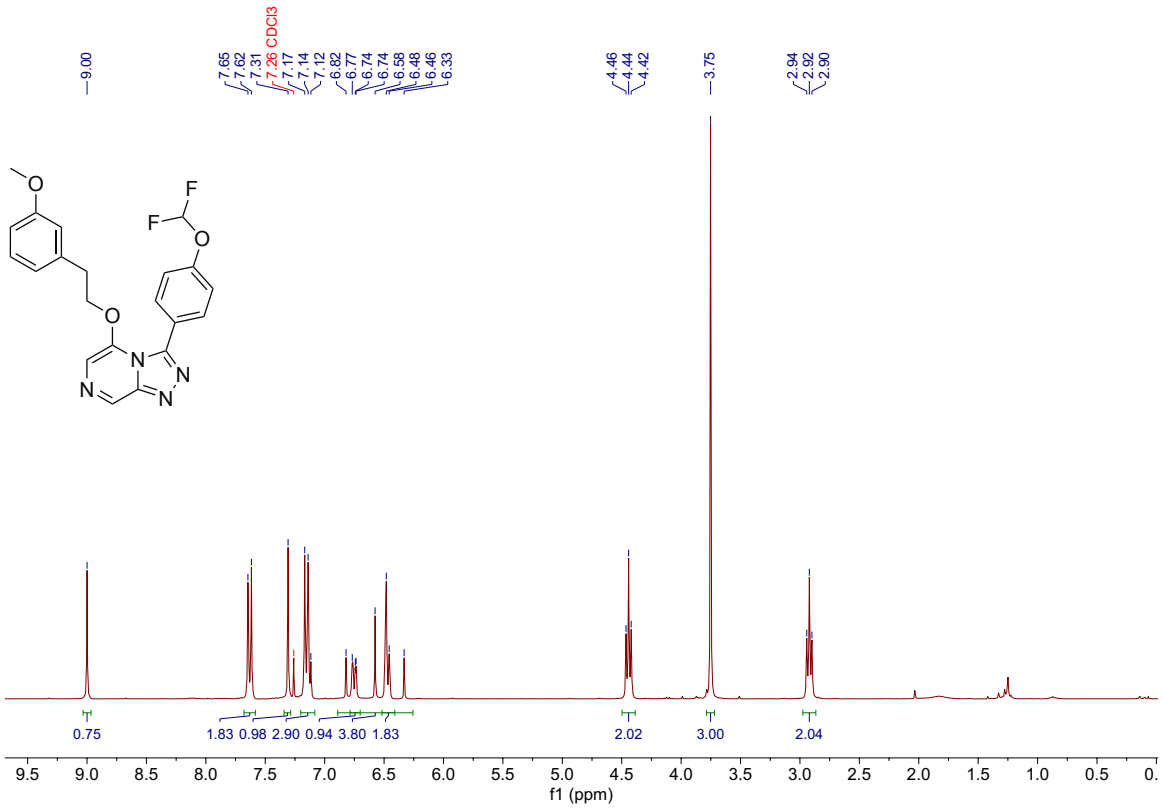

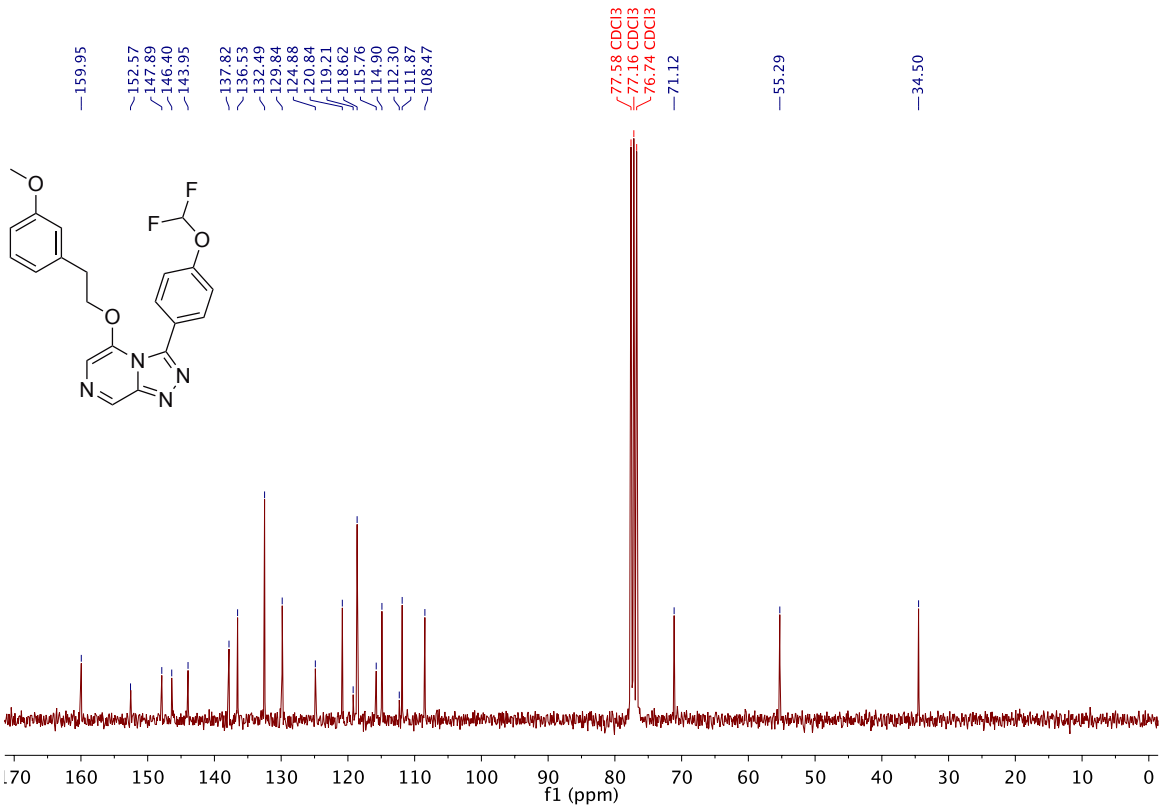

A.39 3-(4-(Difluoromethoxy)phenyl)-5-(4-methoxyphenethoxy)-[1,2,4]triazolo[4,3-*a*]pyrazine 130

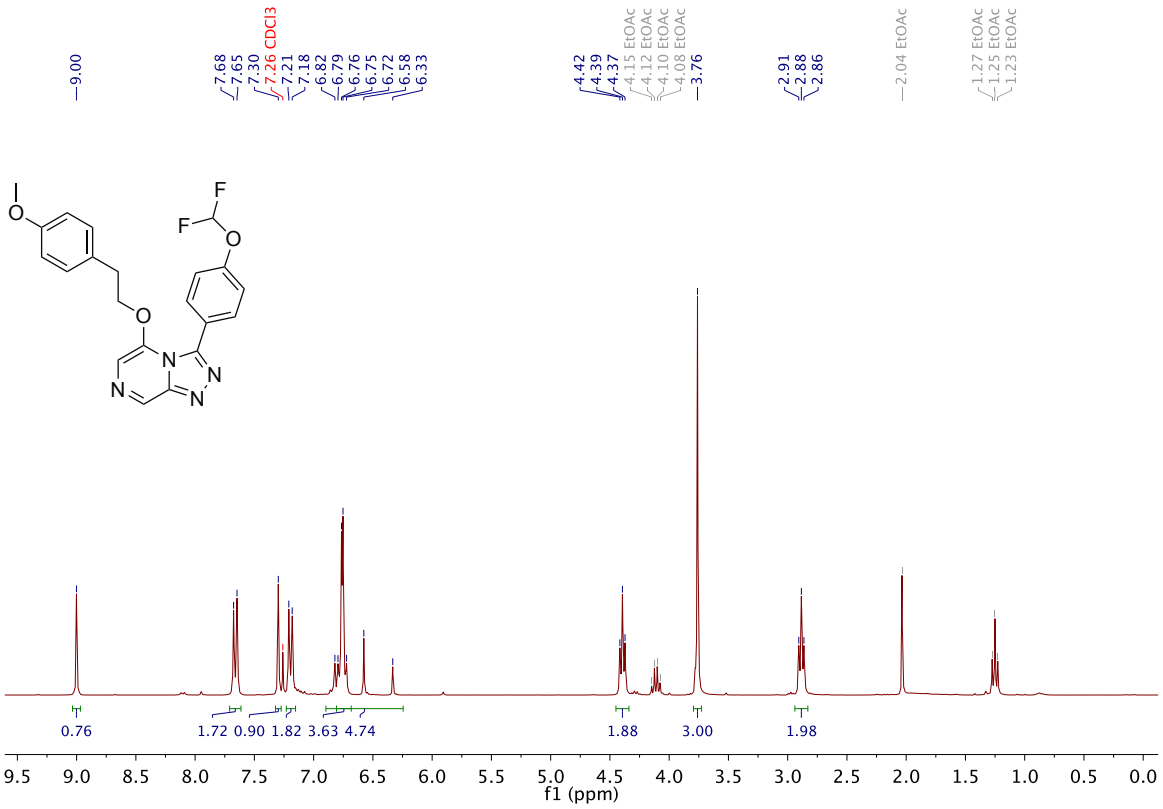

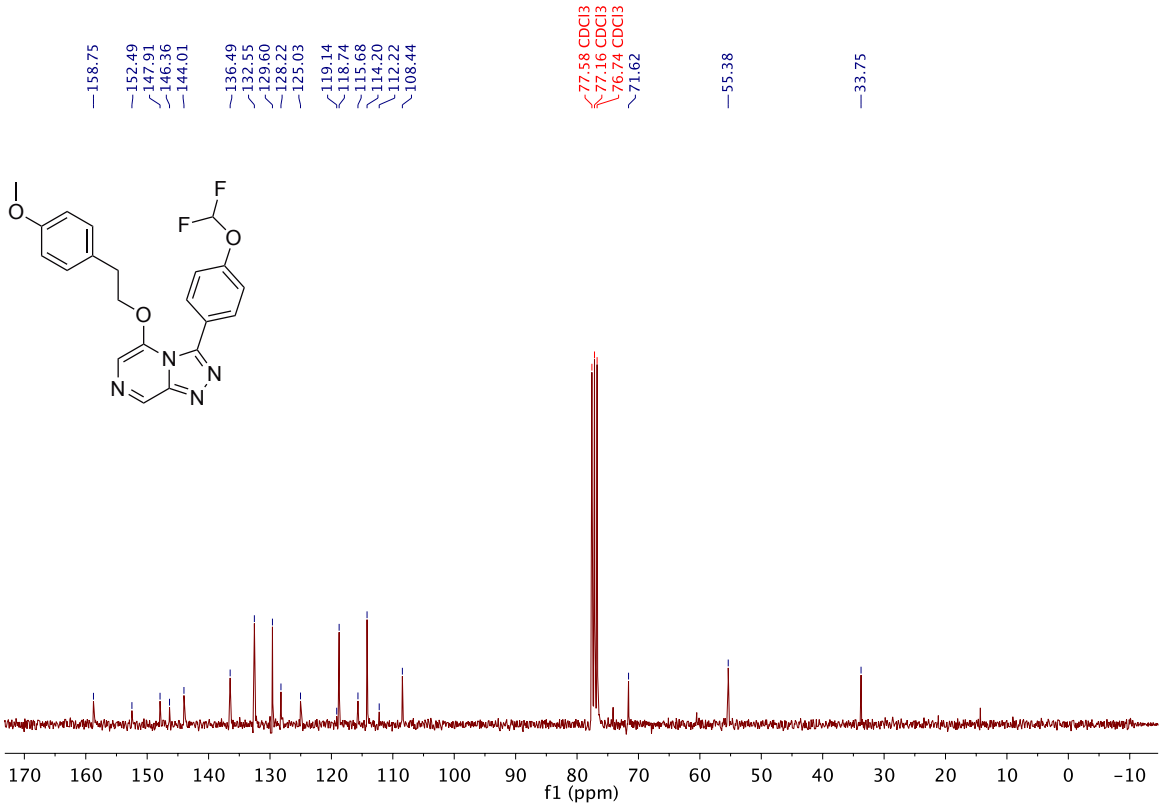

A.40 (4-(((3-(4-(Difluoromethoxy)phenyl)-[1,2,4]triazolo[4,3-*a*]pyrazin-5-yl) oxy)methyl)phenyl)methanol 132

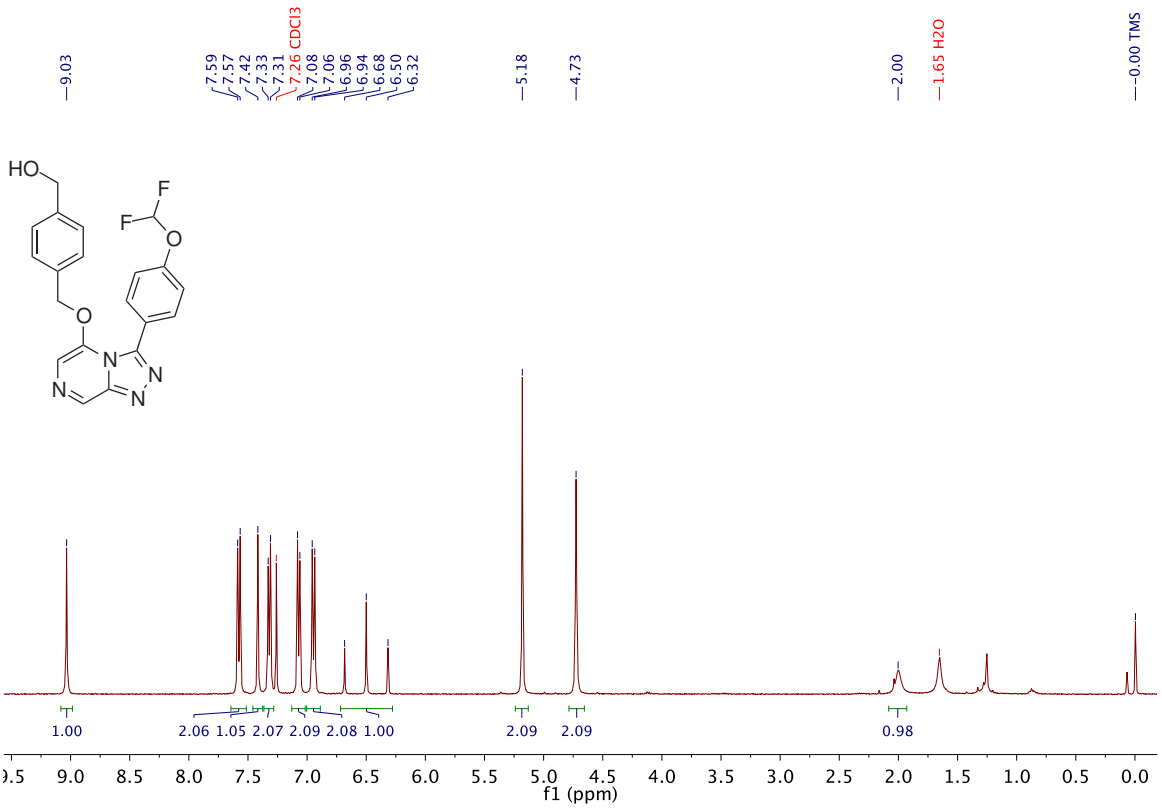

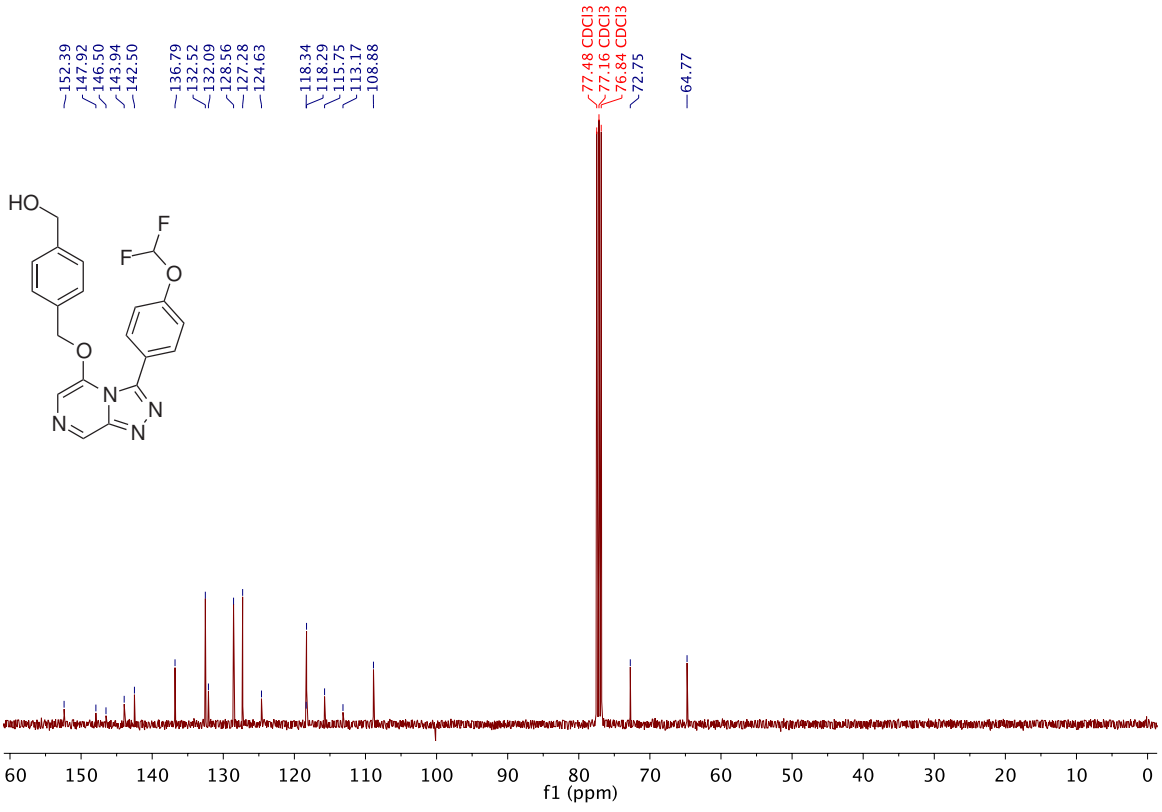

A.41 5-(2-Cyclopropylethoxy)-3-(4-(difluoromethoxy)phenyl)-[1,2,4]triazolo [4,3-*a*]pyrazine 133

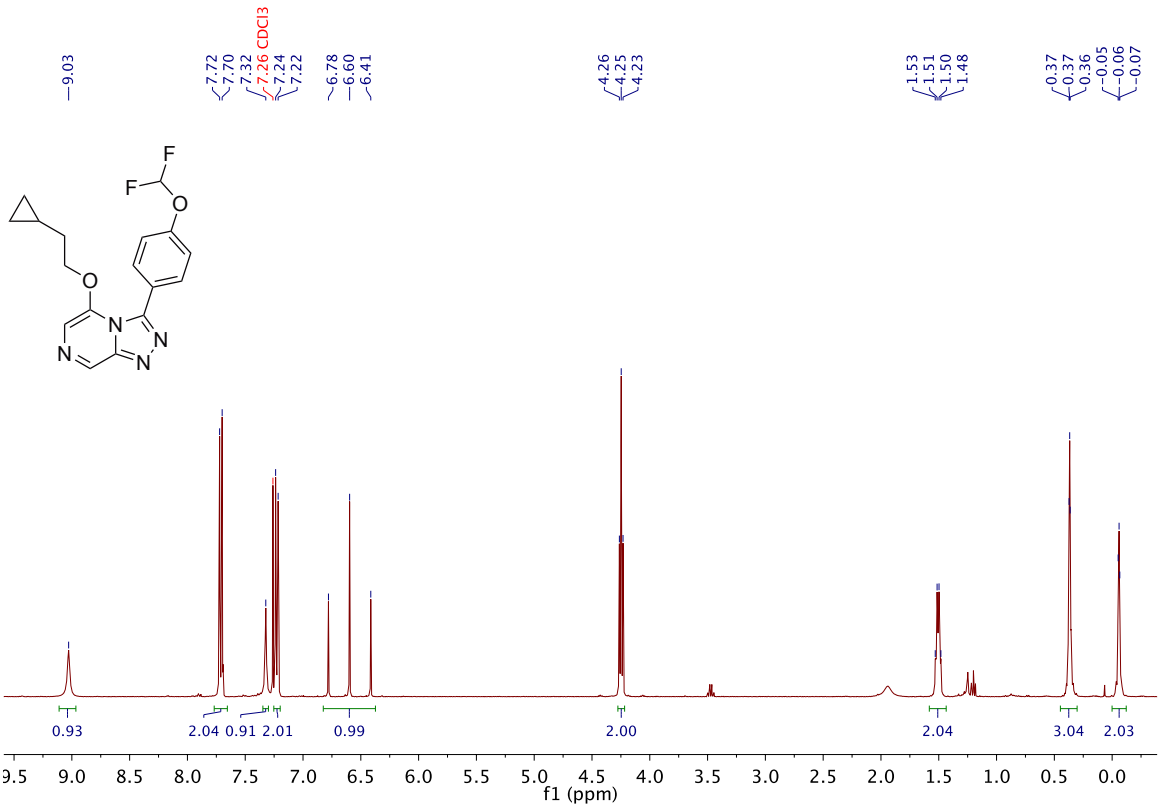

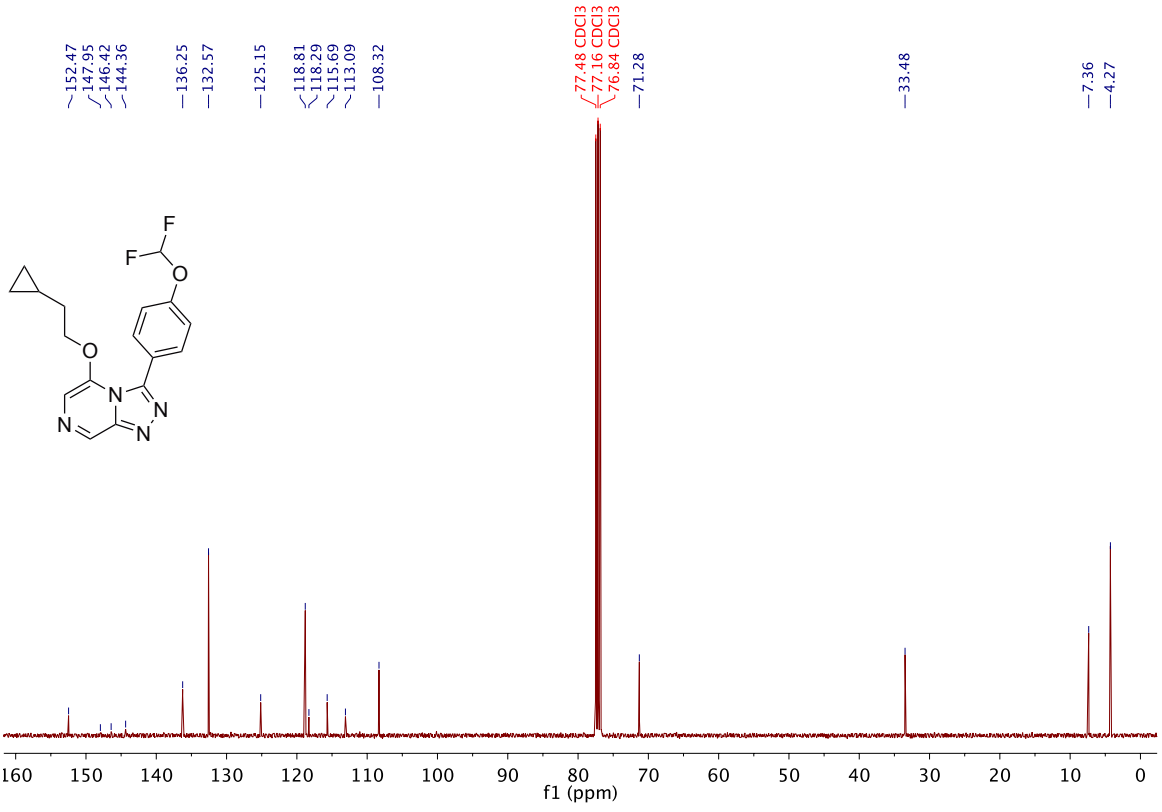

A.42 3-(4-(Difluoromethoxy)phenyl)-5-(2-(oxetan-3-yl)ethoxy)-[1,2,4]triazolo [4,3-*a*]pyrazine 134

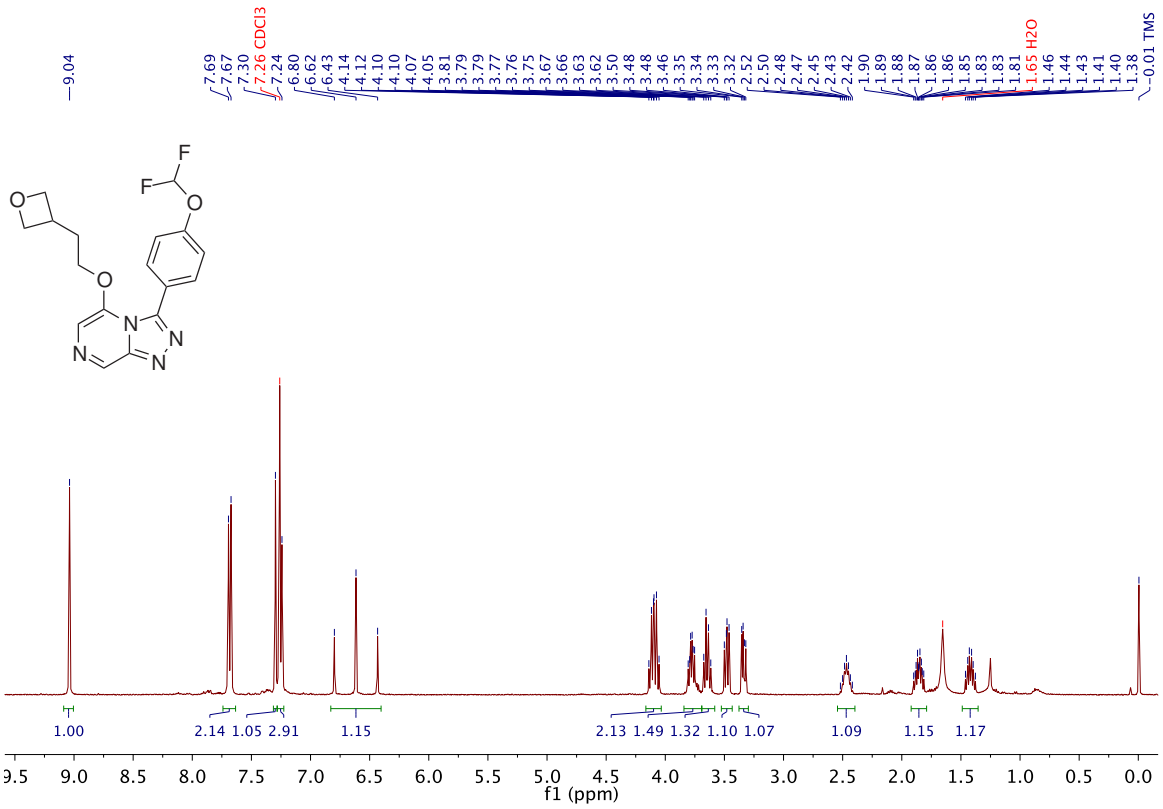

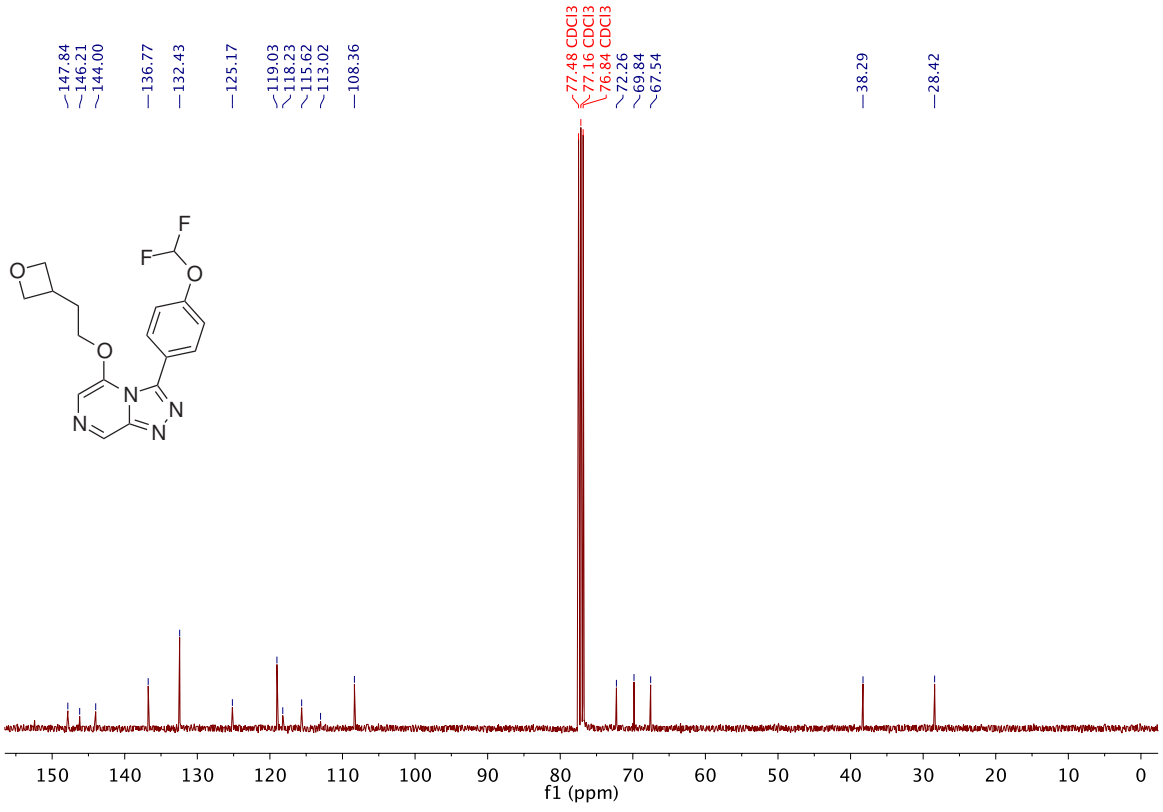

A.43 6-(2-((3-(4-(Difluoromethoxy)phenyl)-[1,2,4]triazolo[4,3-*a*]pyrazin-5-yl) oxy)ethyl)-2-oxa-6-azaspiro[3.3]heptane 135

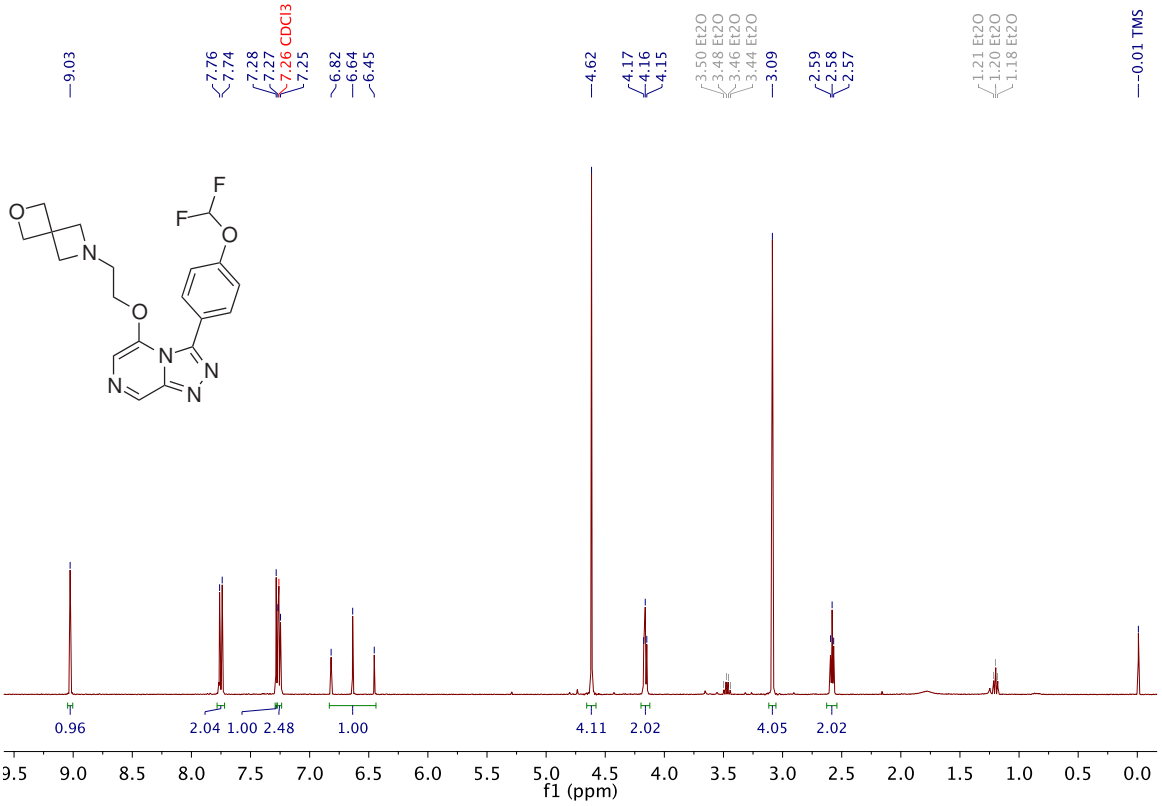

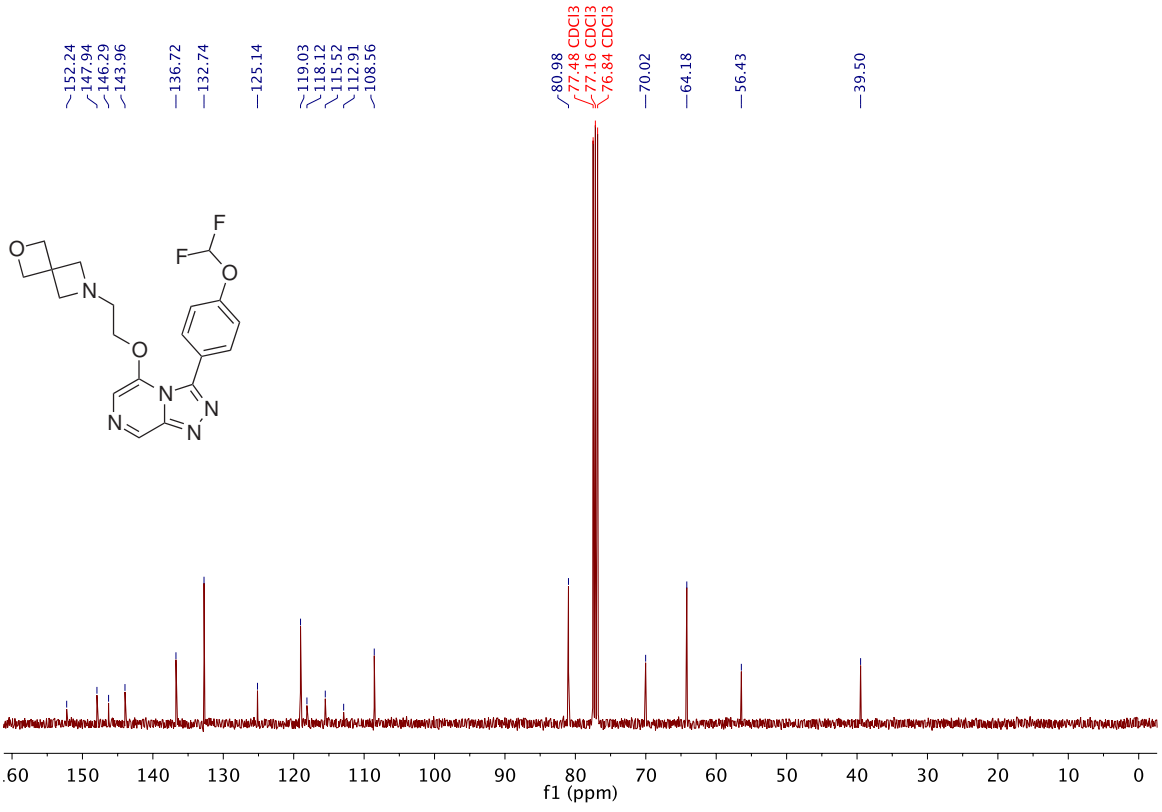

A.44 3-(4-(Difluoromethoxy)phenyl)-5-(2-(pyrrolidin-1-yl)ethoxy)-[1,2,4]triazolo[4,3-*a*]pyrazine 136

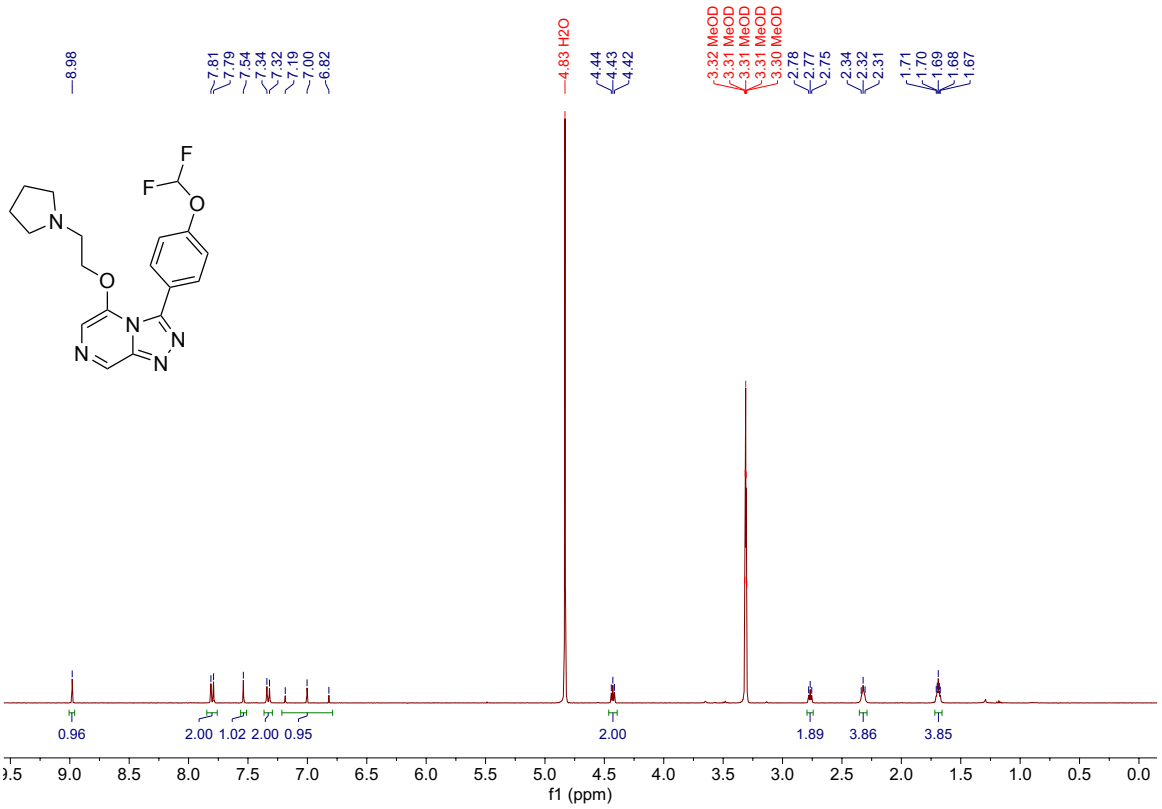

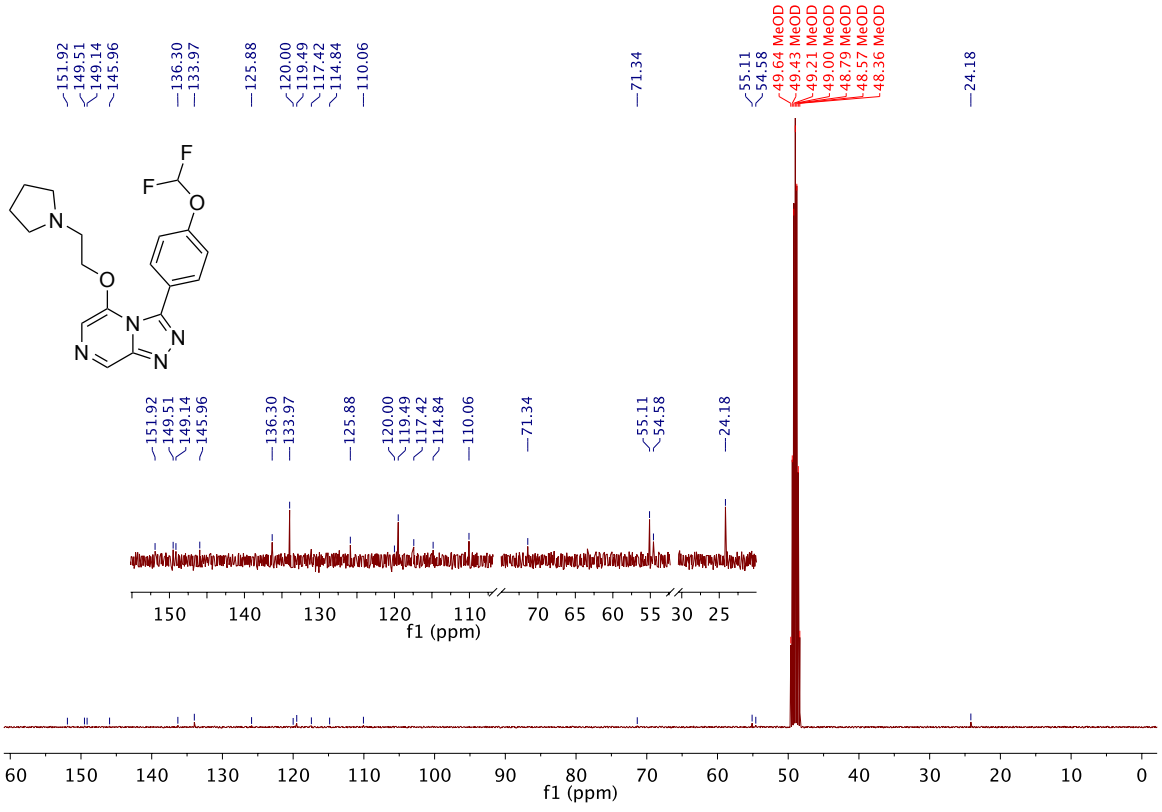

A.45 3-(4-(Difluoromethoxy)phenyl)-5-(2-(piperidin-1-yl)ethoxy)-[1,2,4]triazolo[4,3-*a*]pyrazine 137

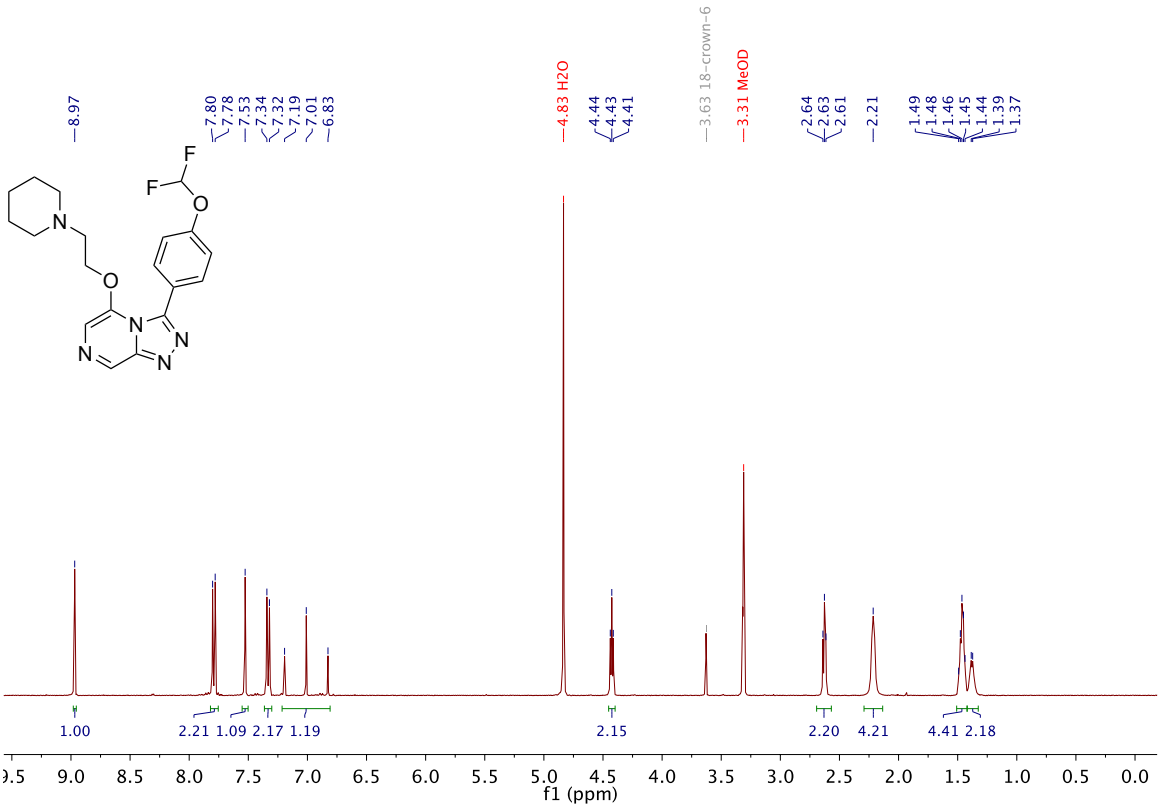

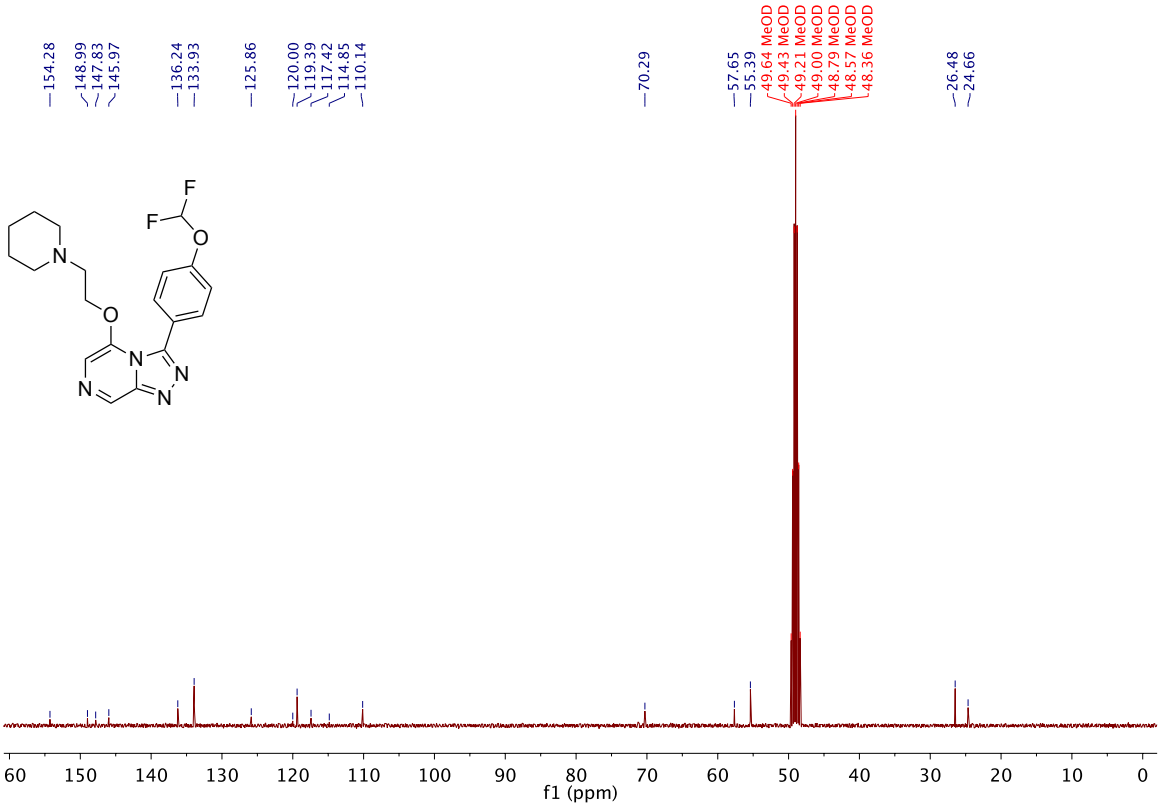

A.46 4-(2-((3-(4-(Difluoromethoxy)phenyl)-[1,2,4]triazolo[4,3-*a*]pyrazin-5-yl) oxy)ethyl)morpholine 138

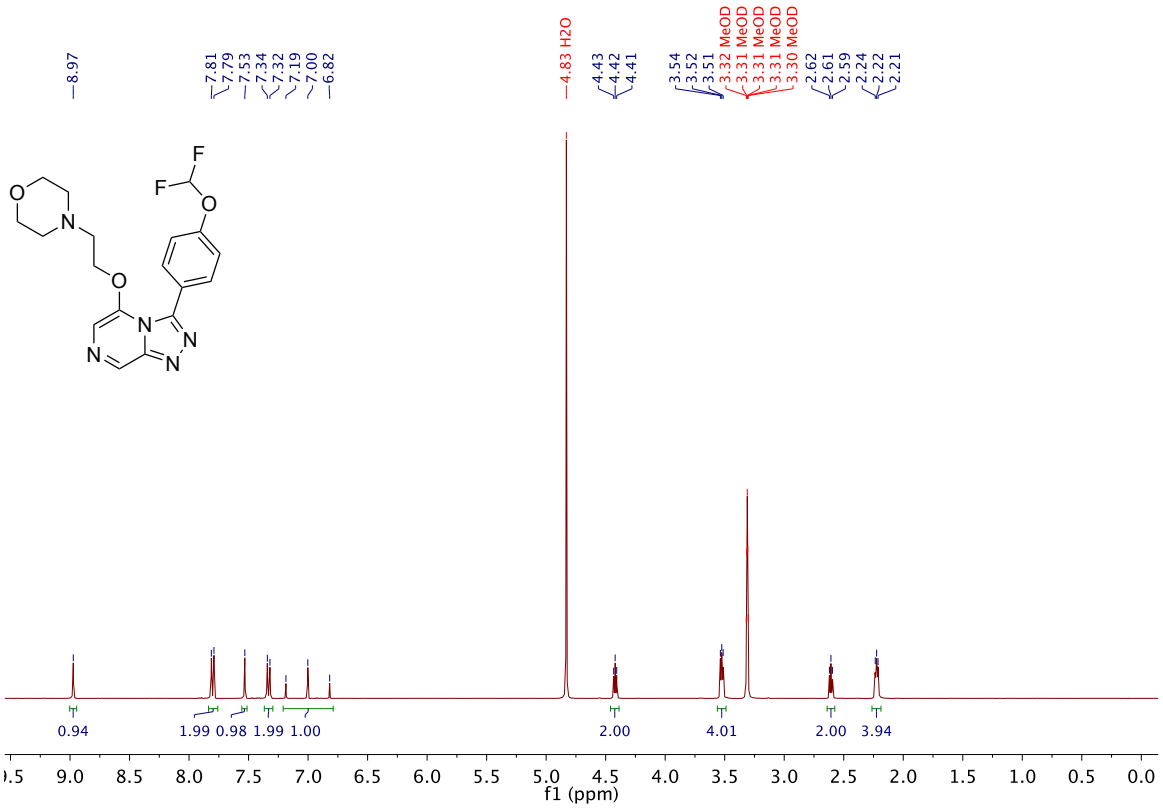

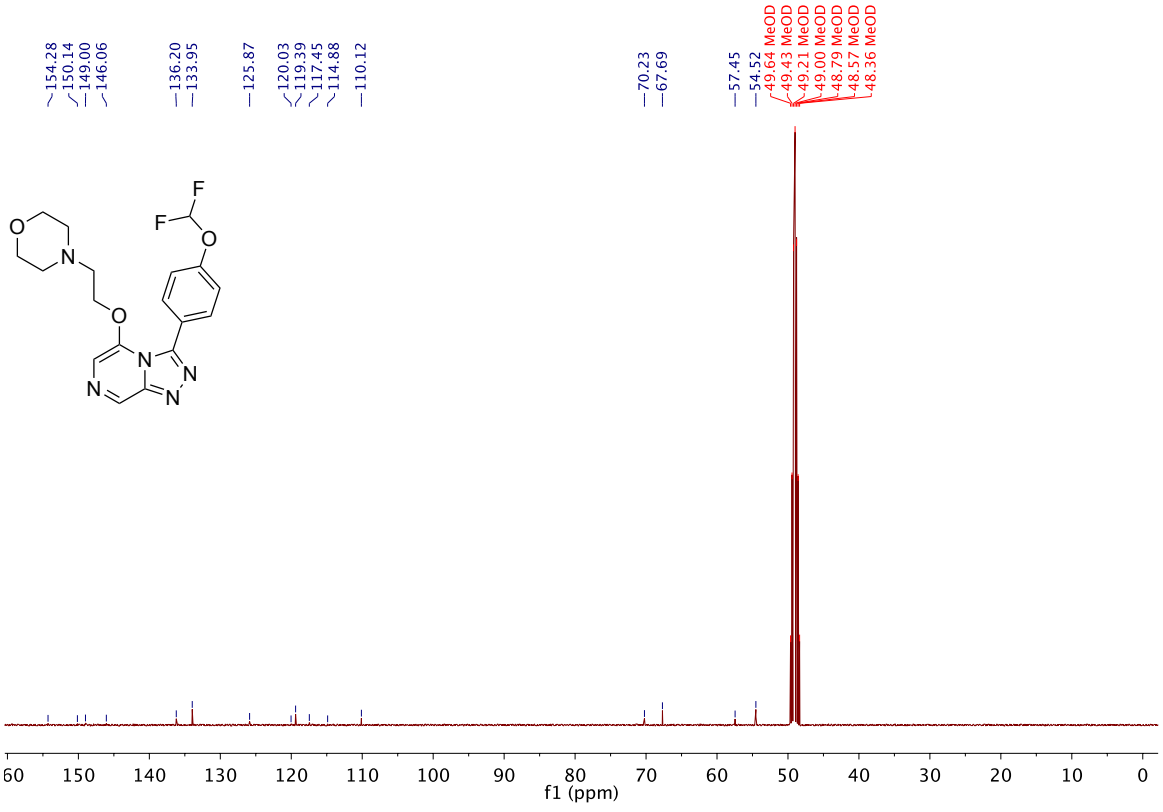

A.47 *tert*-Butyl 4-(2-((3-(4-(difluoromethoxy)phenyl)-[1,2,4]triazolo[4,3-*a*]pyrazin-5-yl)oxy)ethyl)piperazine-1-carboxylate 140

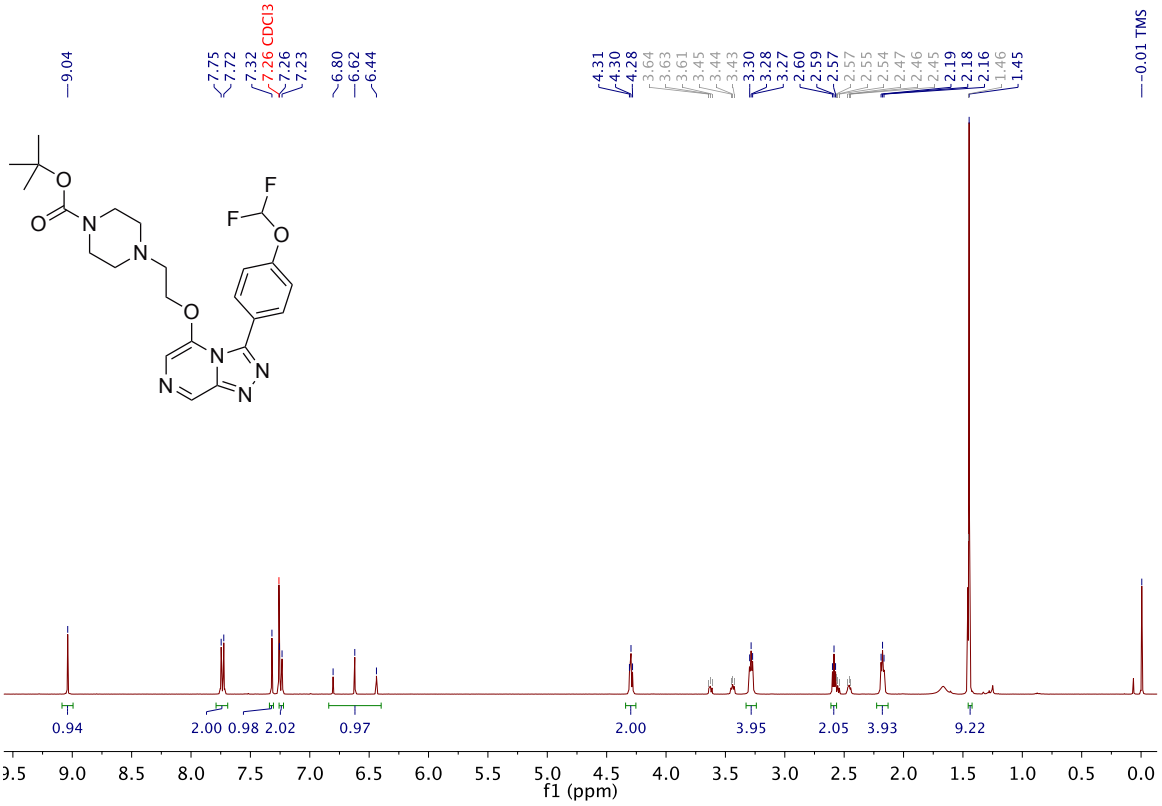

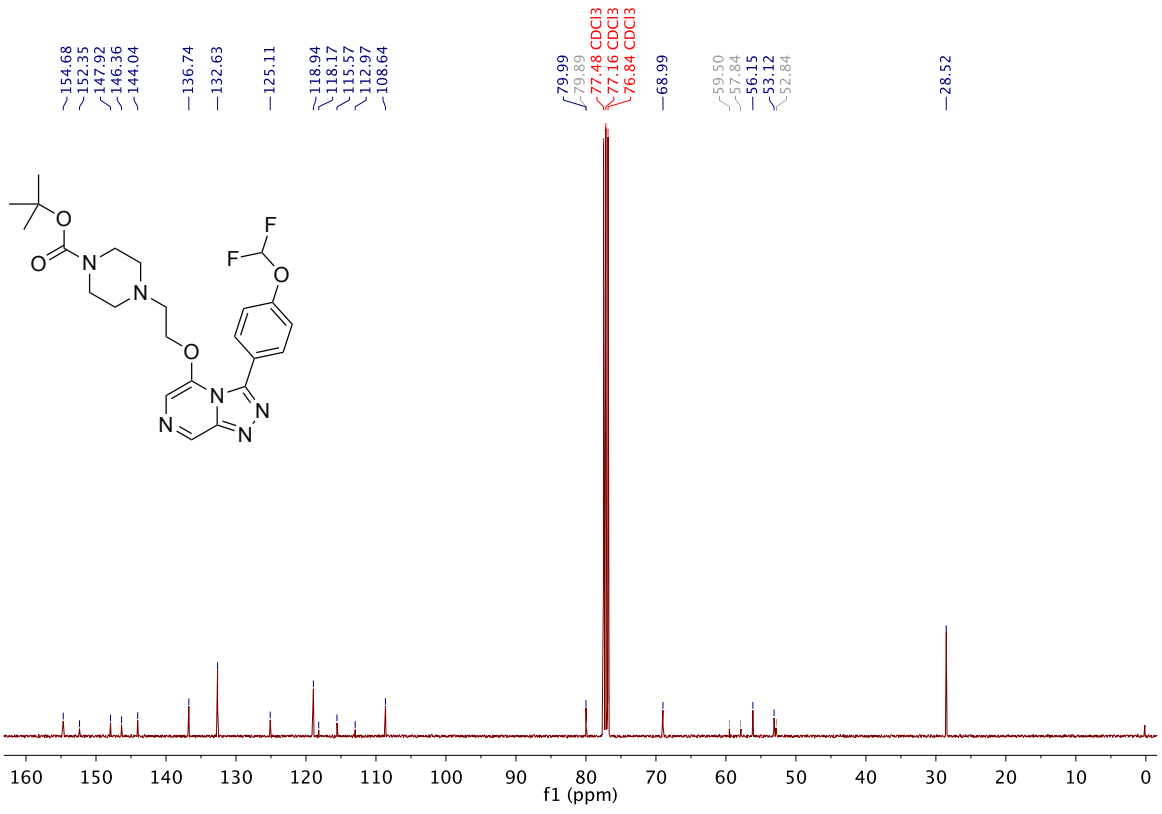

A.48 3-(4-(Difluoromethoxy)phenyl)-5-(2-(piperazin-1-yl)ethoxy)-[1,2,4]triazolo[4,3-*a*]pyrazine 141

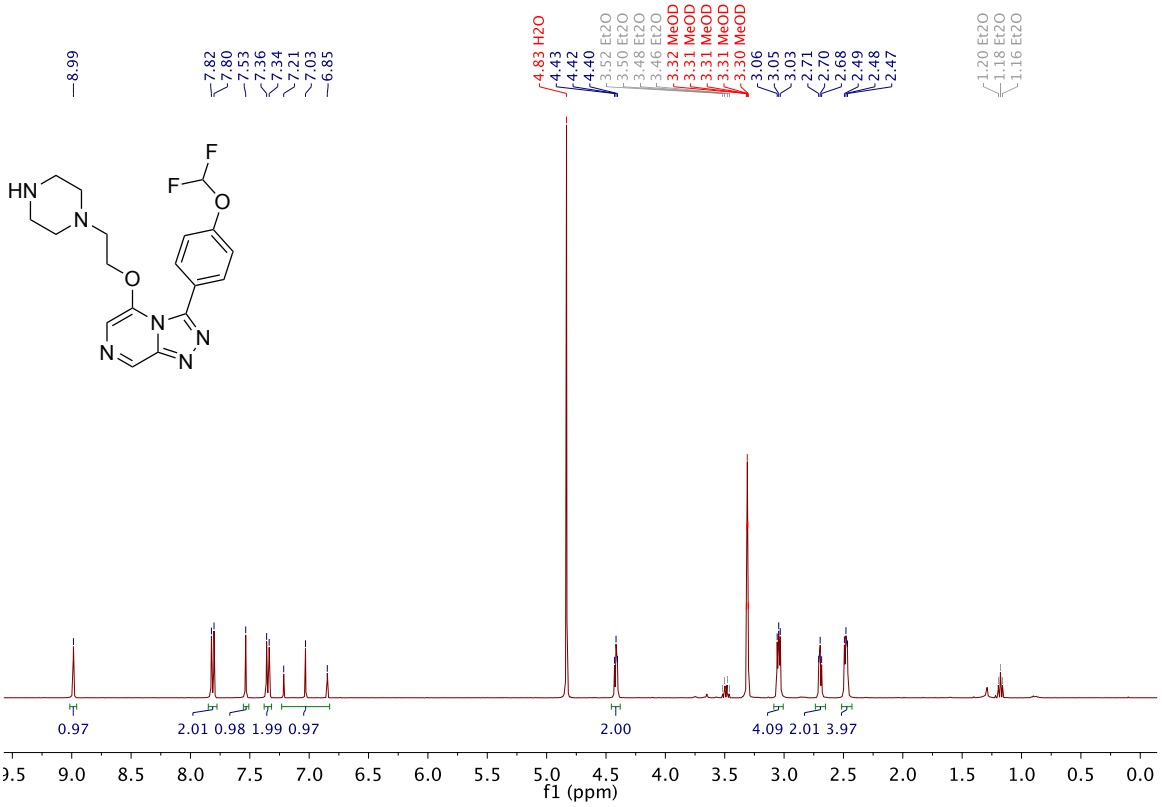

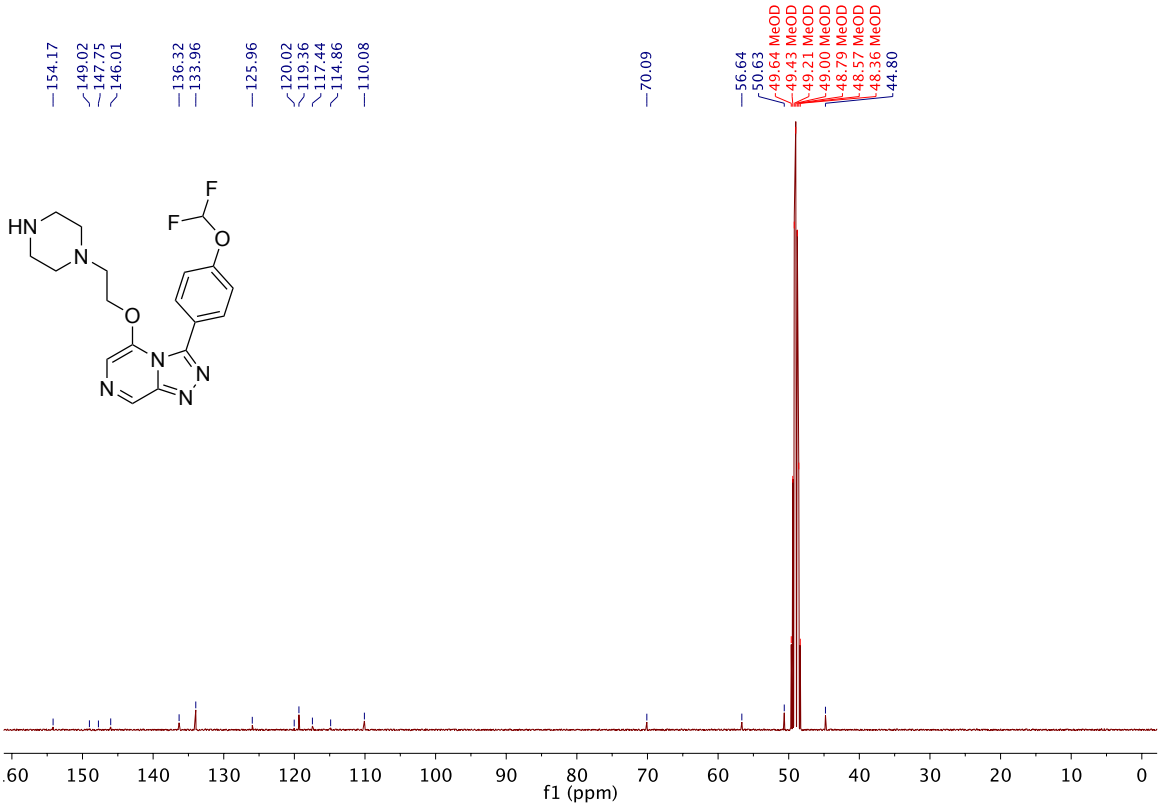

A.49 1-Phenyl-2-((3-(piperidin-3-yl)-[1,2,4]triazolo[4,3-*a*]pyrazin-5-yl)oxy) ethan-1-ol 145

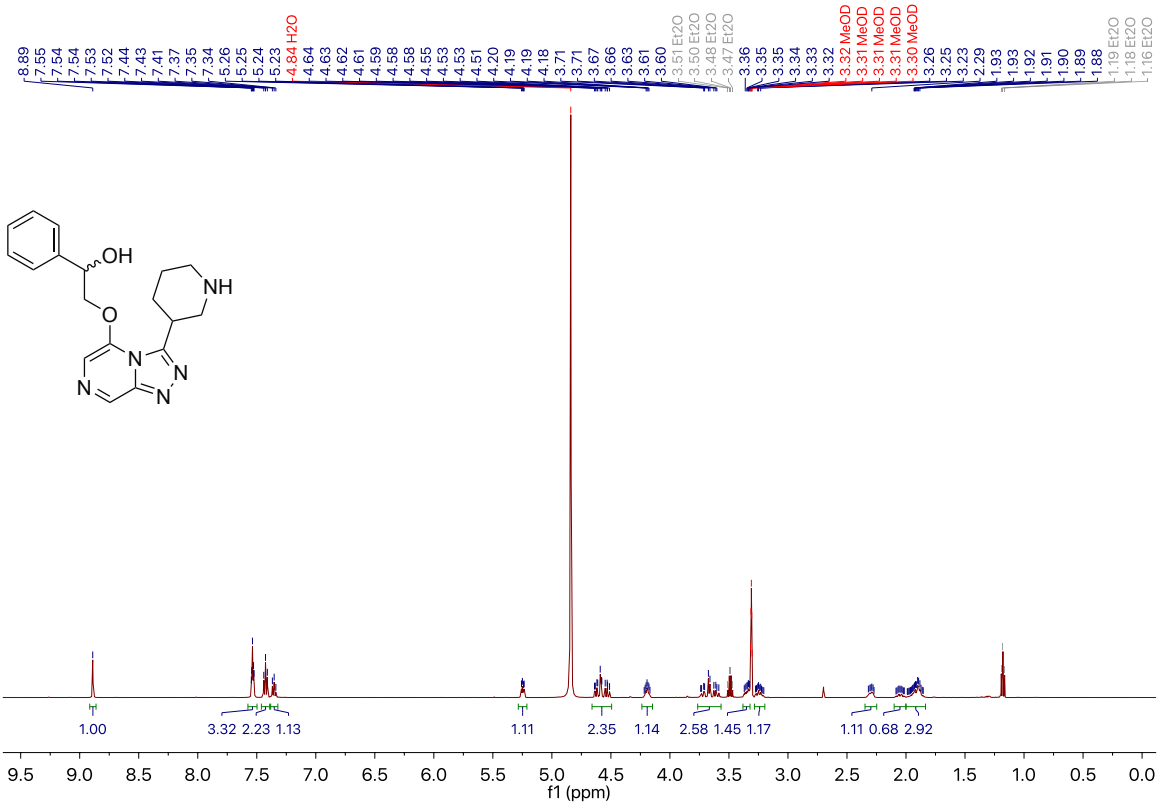

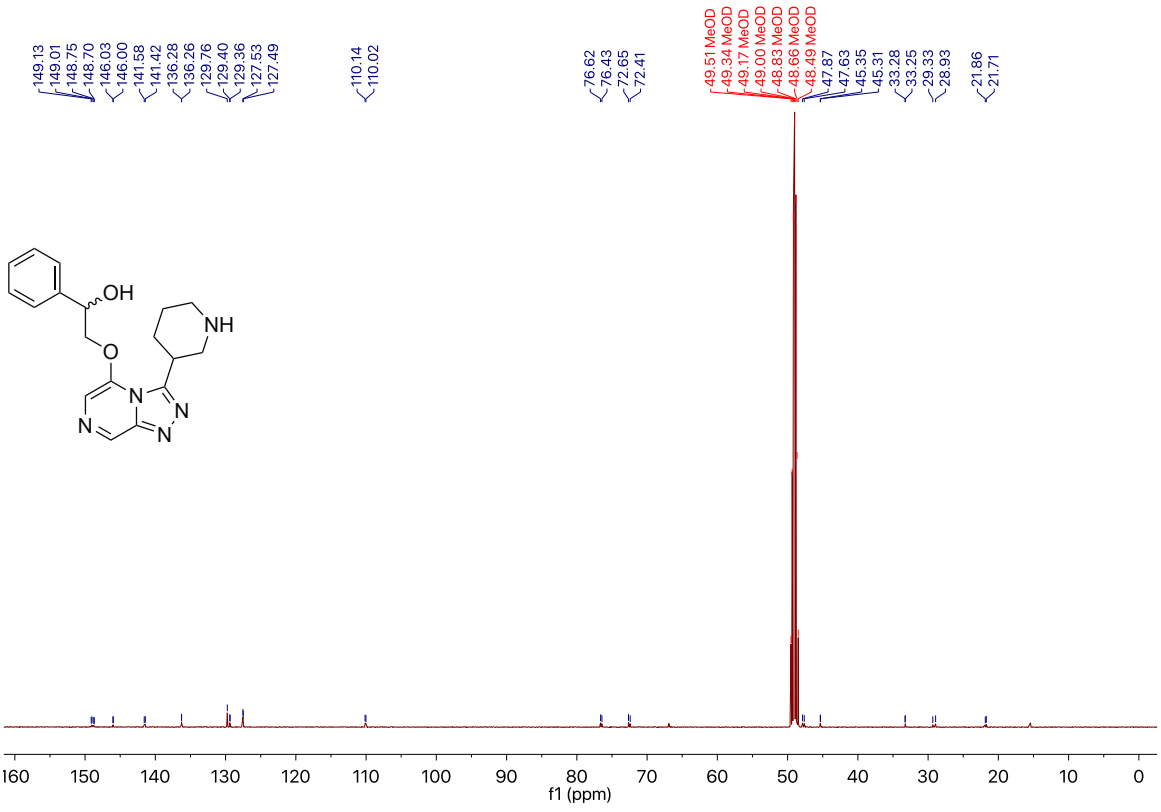

A.50 5-(3,4-Difluorophenethoxy)-3-(piperidin-3-yl)-[1,2,4]triazolo[4,3-*a*] pyrazine 147

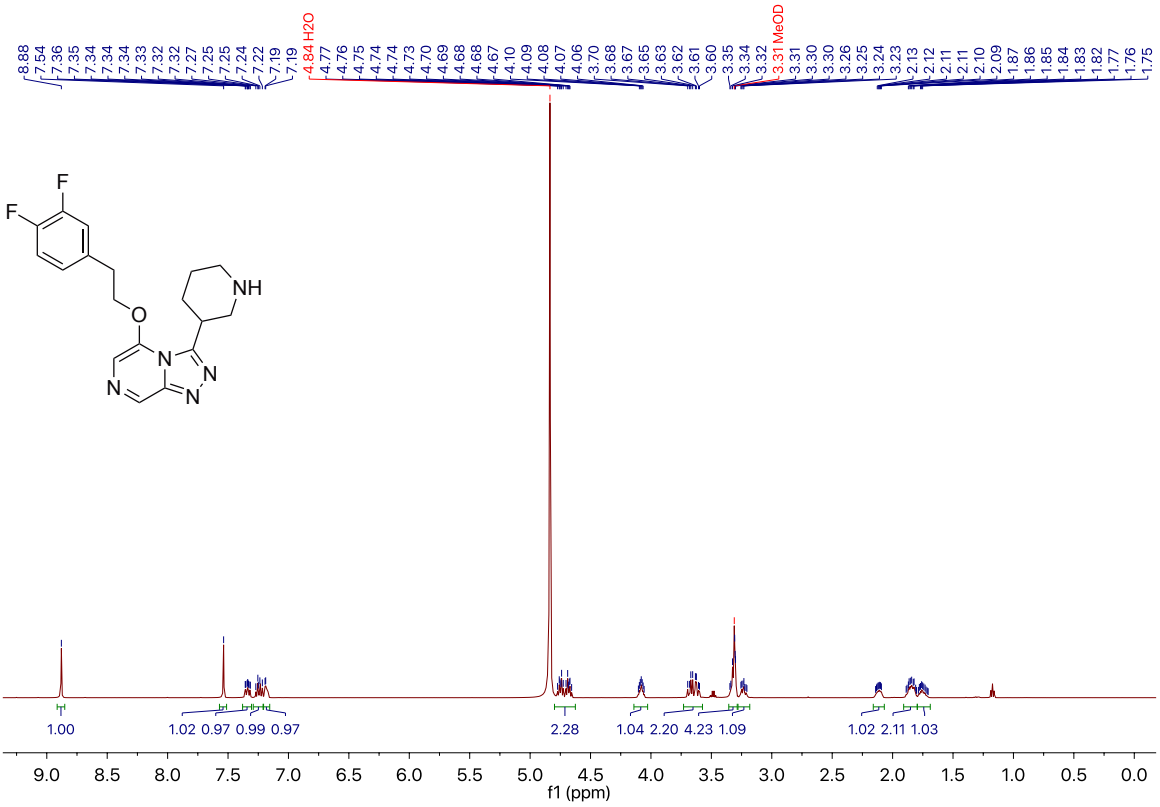

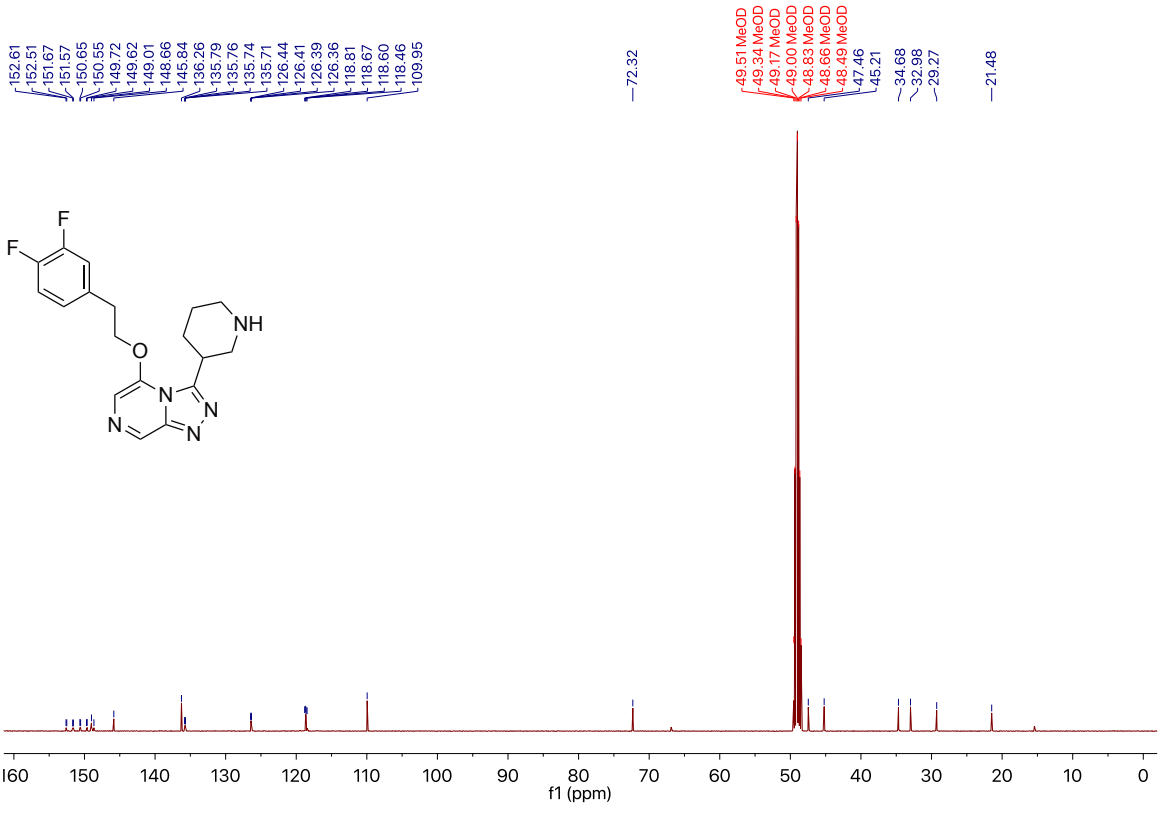

A.51 5-Phenethoxy-3-(tetrahydrofuran-3-yl)-[1,2,4]triazolo[4,3-*a*]pyrazine 148

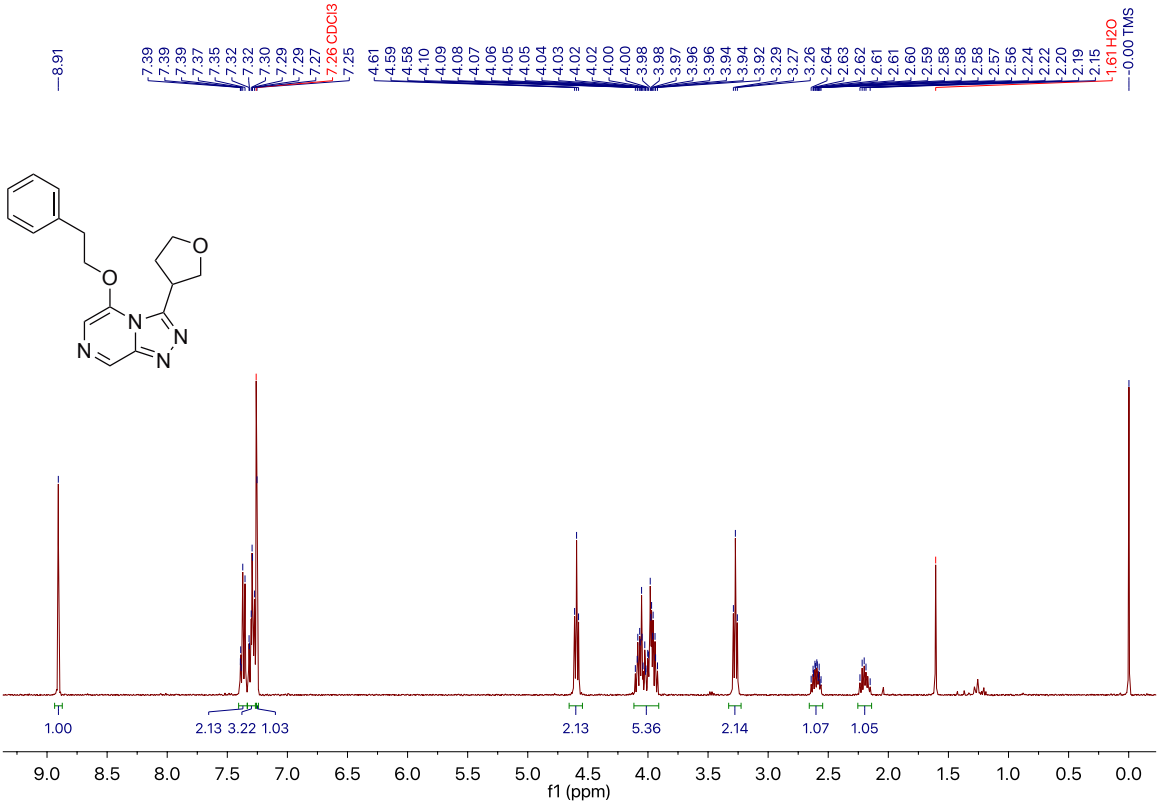

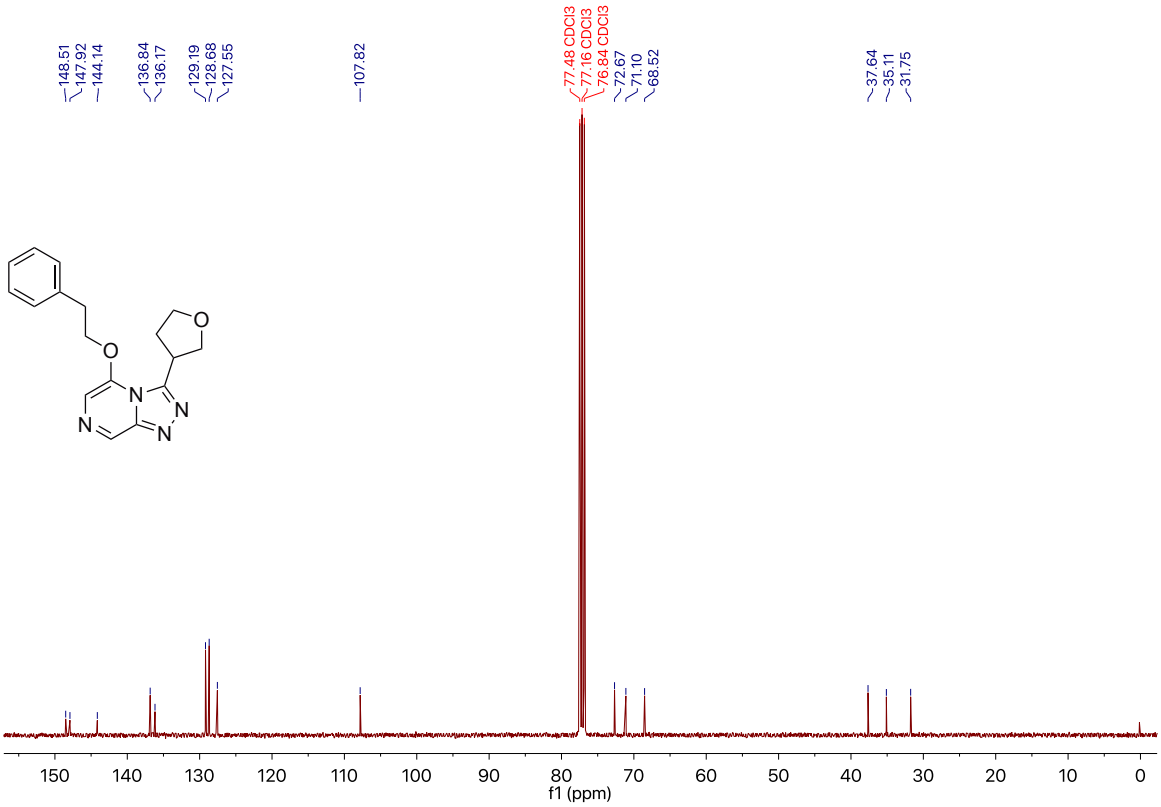

A.52 5-Phenethoxy-3-(tetrahydro-2*H*-pyran-4-yl)-[1,2,4]triazolo[4,3-*a*] pyrazine 149

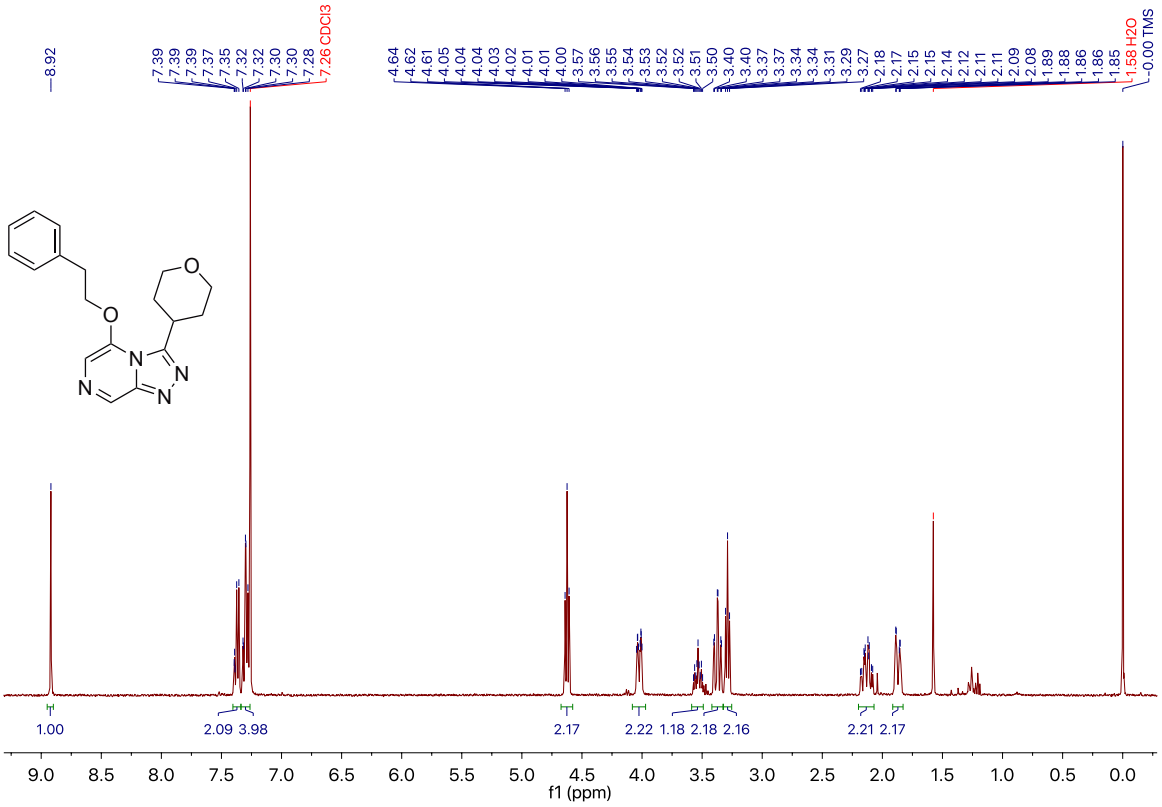

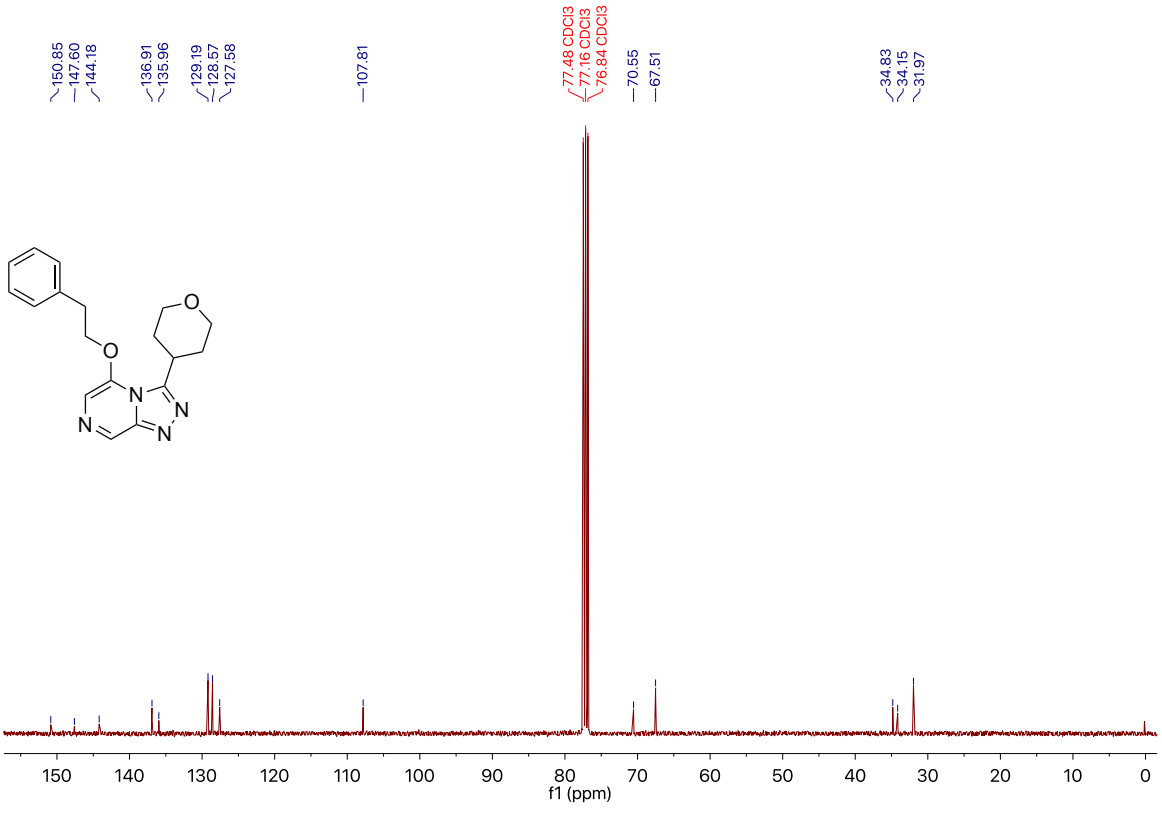

A.53 *tert*-Butyl 3-(5-phenethoxy-[1,2,4]triazolo[4,3-*a*]pyrazin-3-yl) pyrrolidine-1-carboxylate 150

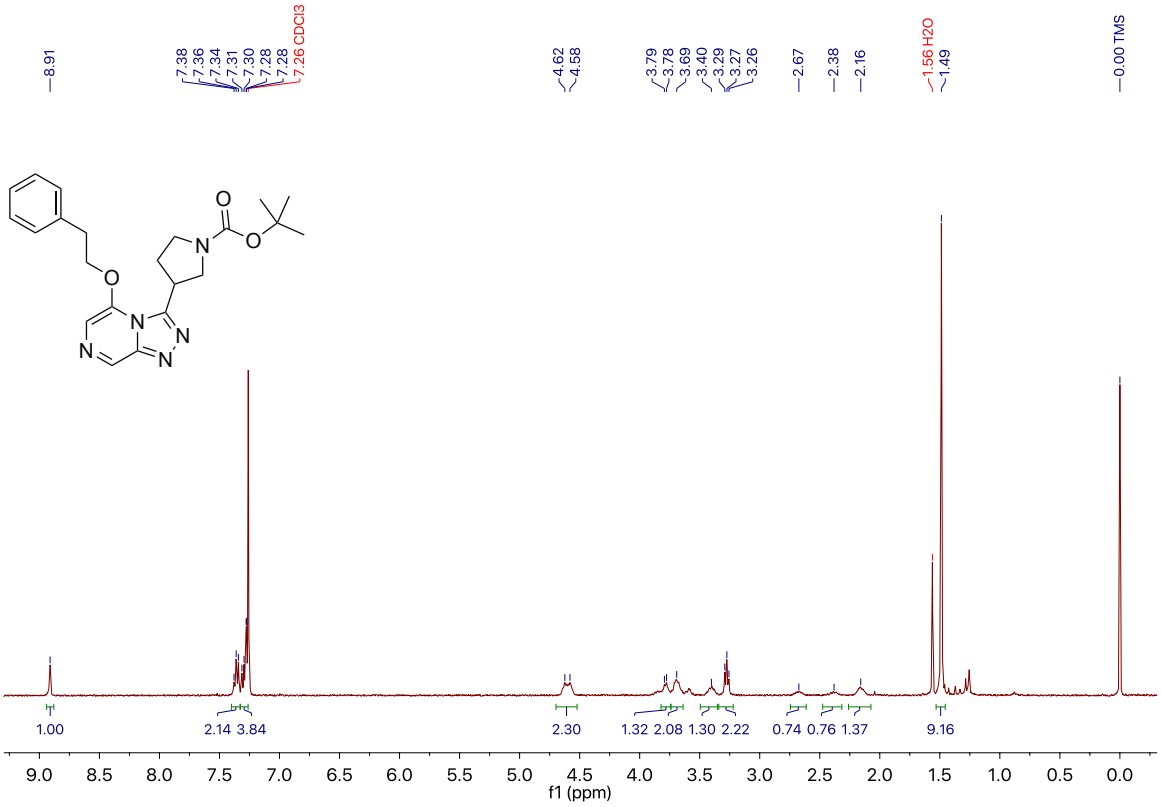

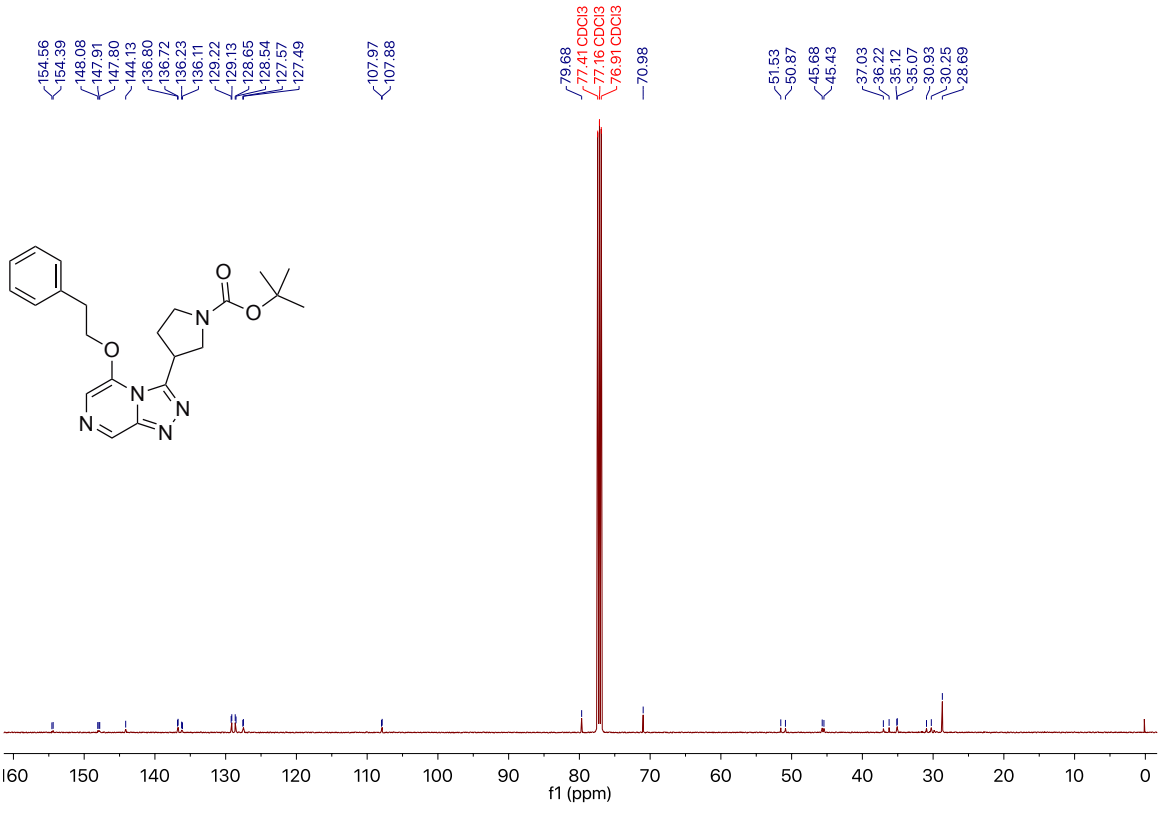

A.54 *tert*-Butyl 4-(5-phenethoxy-[1,2,4]triazolo[4,3-*a*]pyrazin-3-yl)piperidine-1-carboxylate 151

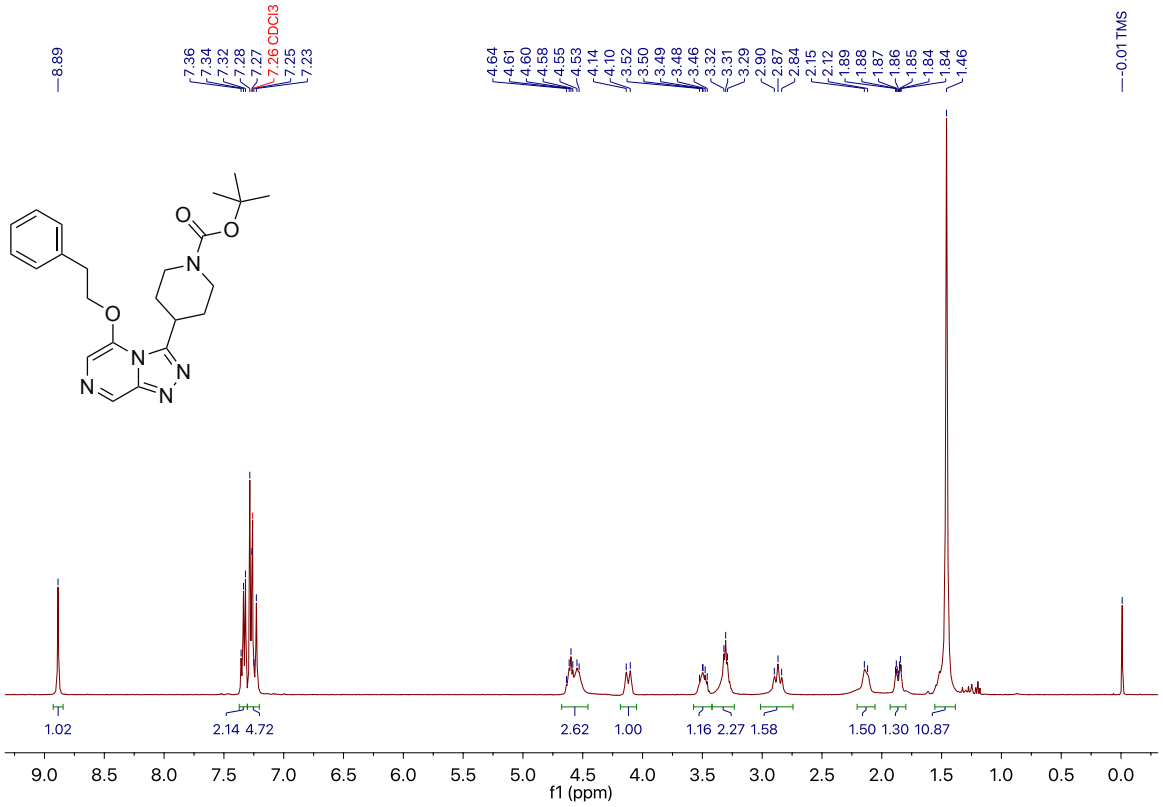

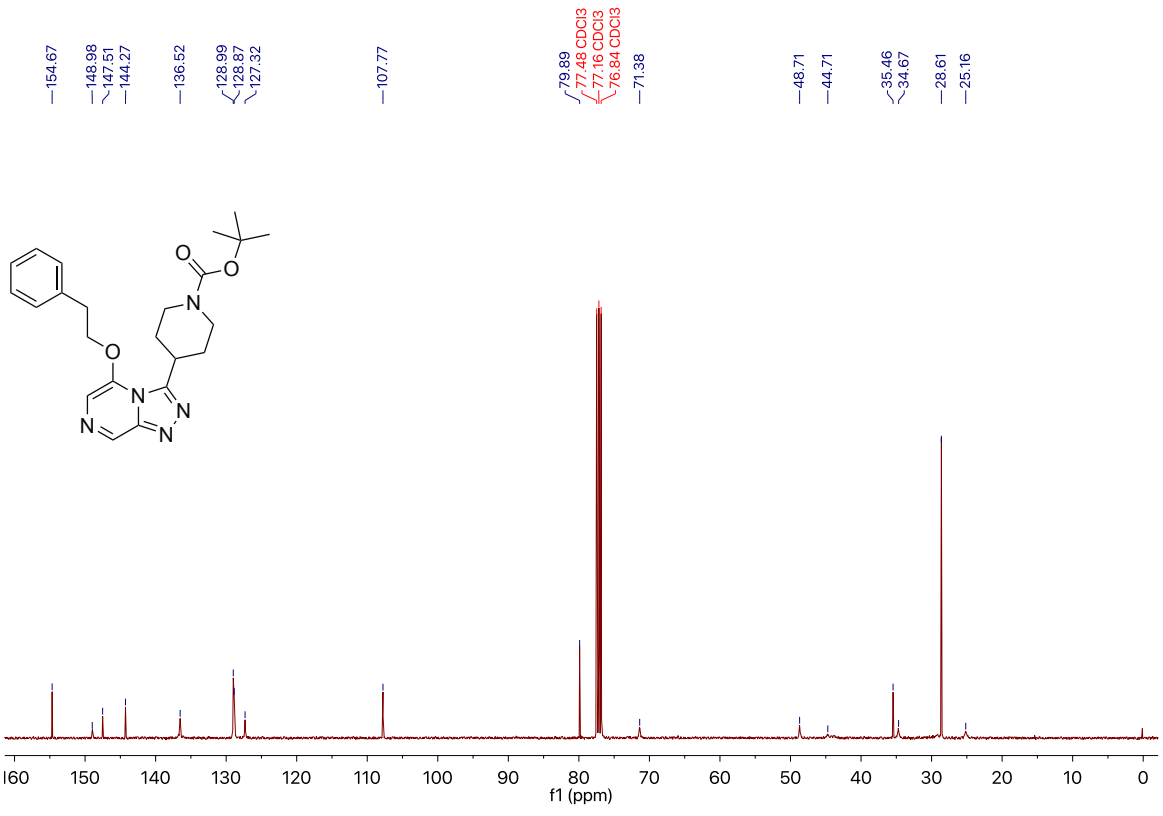

A.55 5-Phenethoxy-3-(pyrrolidin-3-yl)-[1,2,4]triazolo[4,3-*a*]pyrazine 152

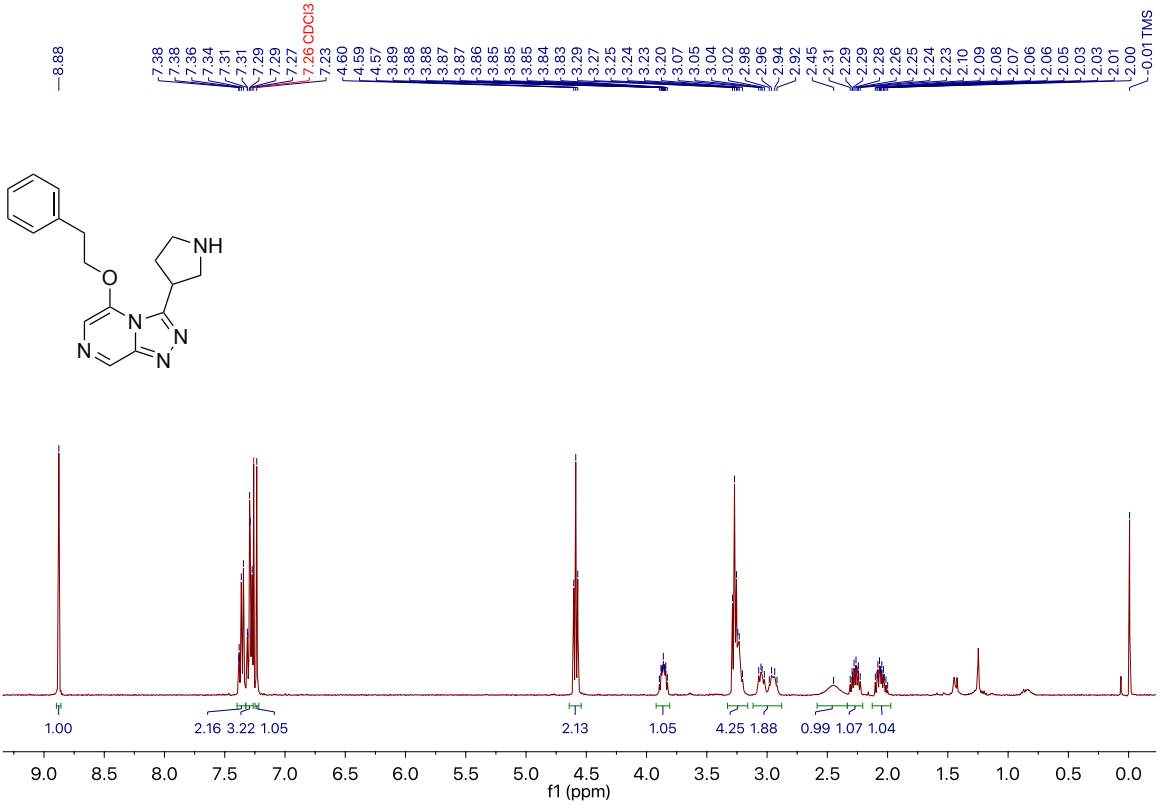

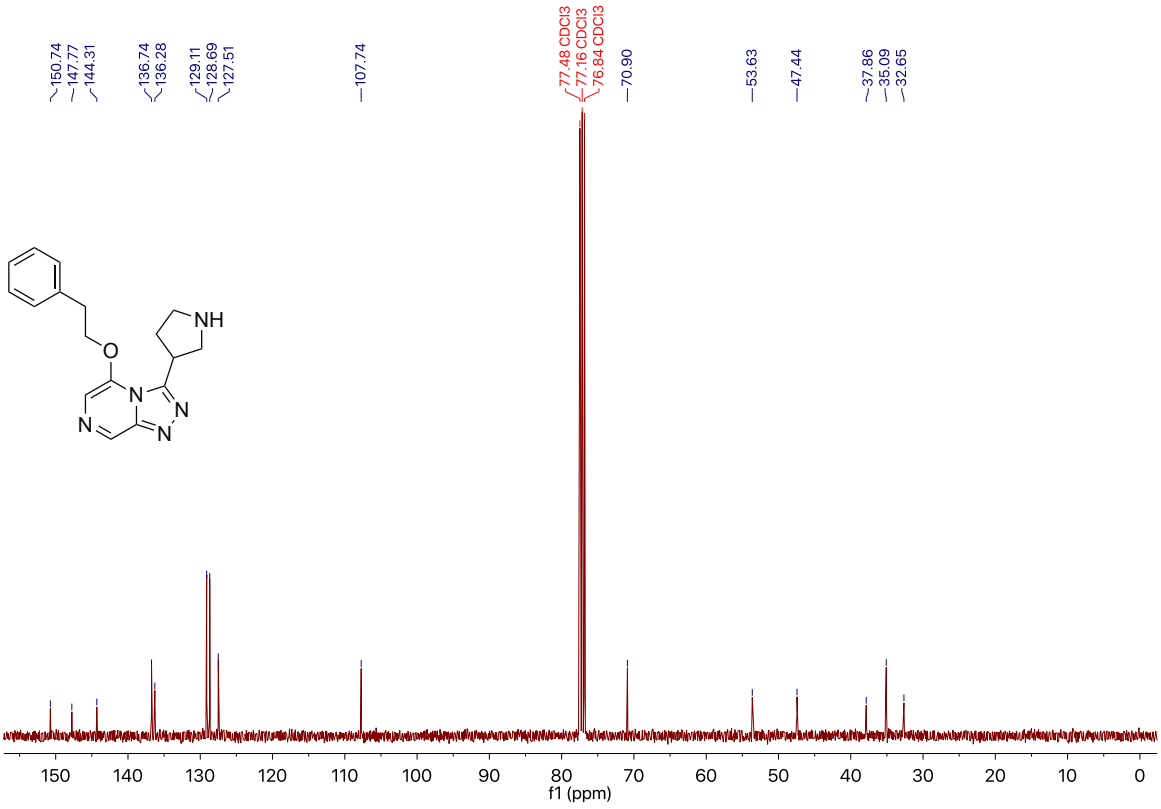

A.56 5-Phenethoxy-3-(piperidin-4-yl)-[1,2,4]triazolo[4,3-*a*]pyrazine 153

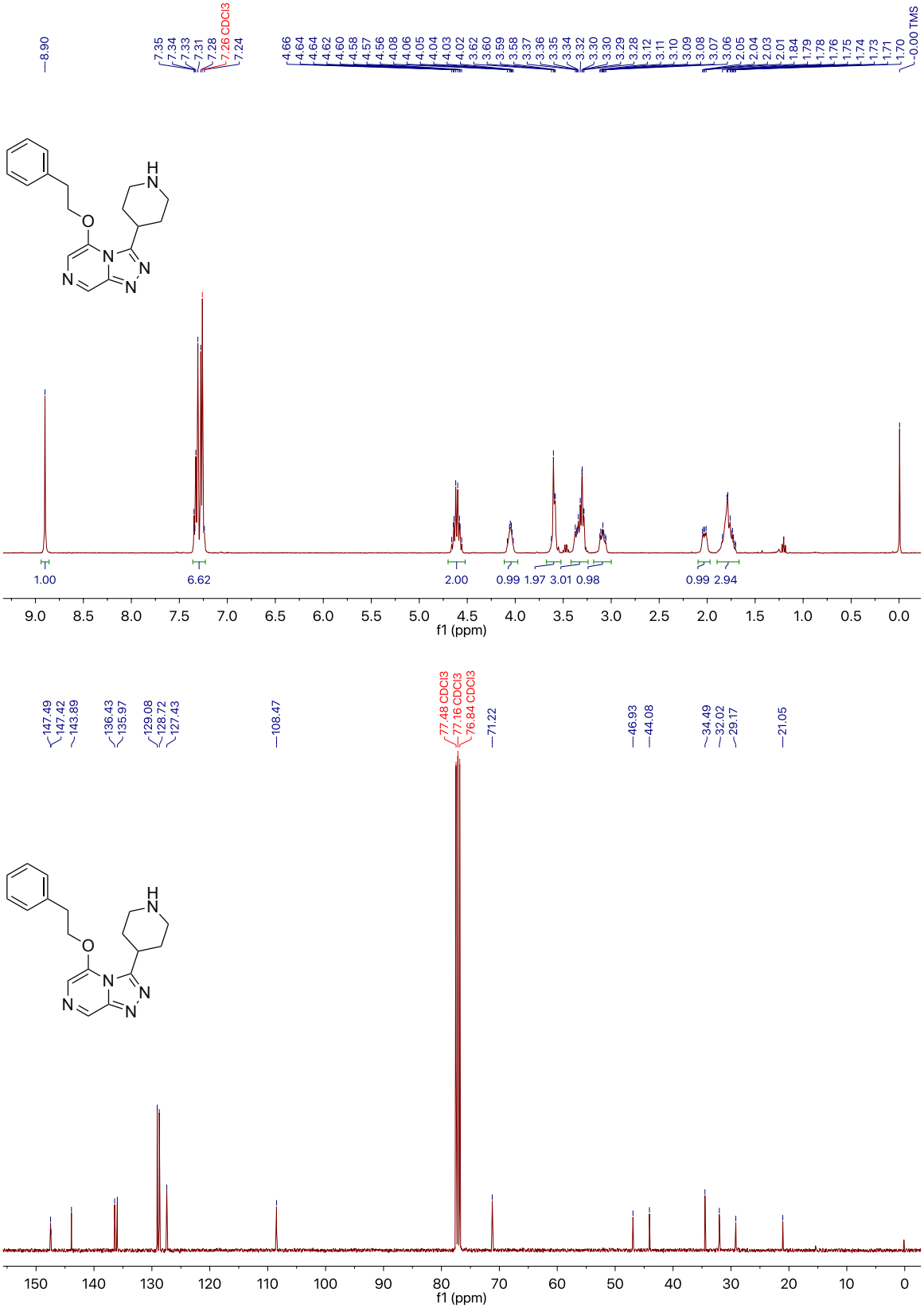

A.57 5-(2-(Cuban-1-yl)ethoxy)-3-(4-(difluoromethoxy)phenyl)-[1,2,4]triazolo [4,3-*a*]pyrazine 154

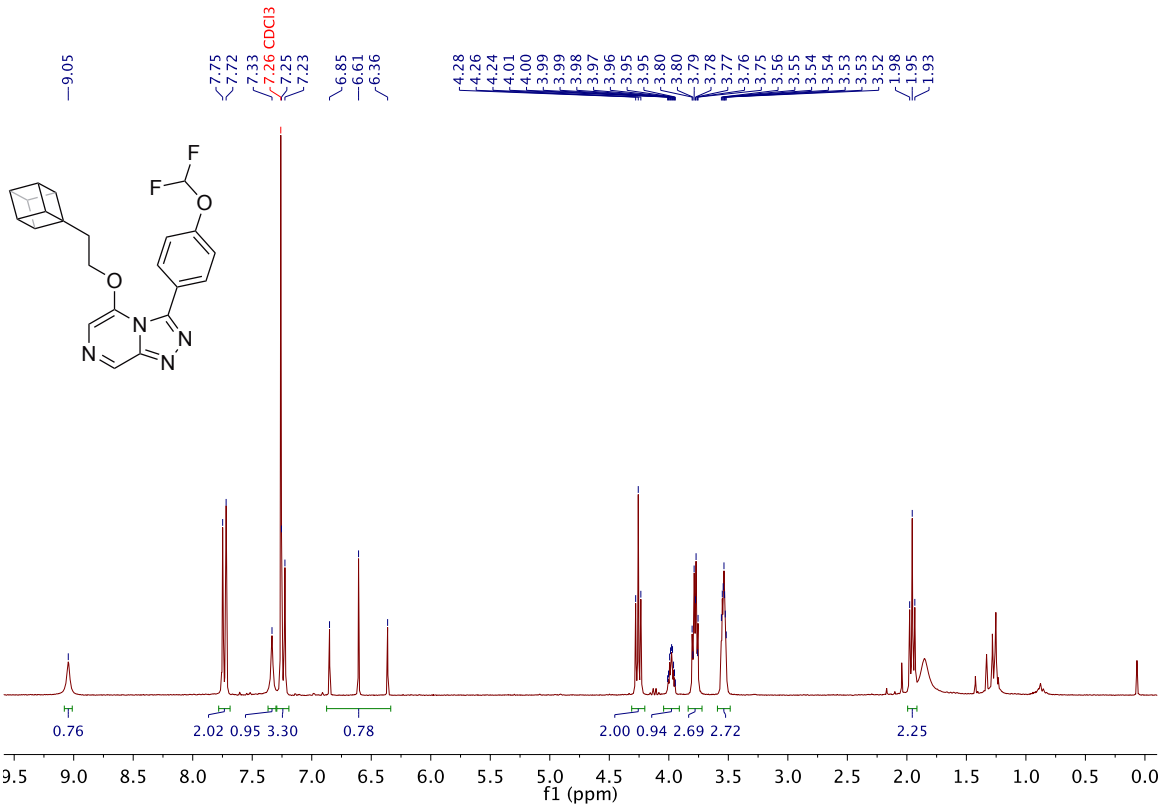

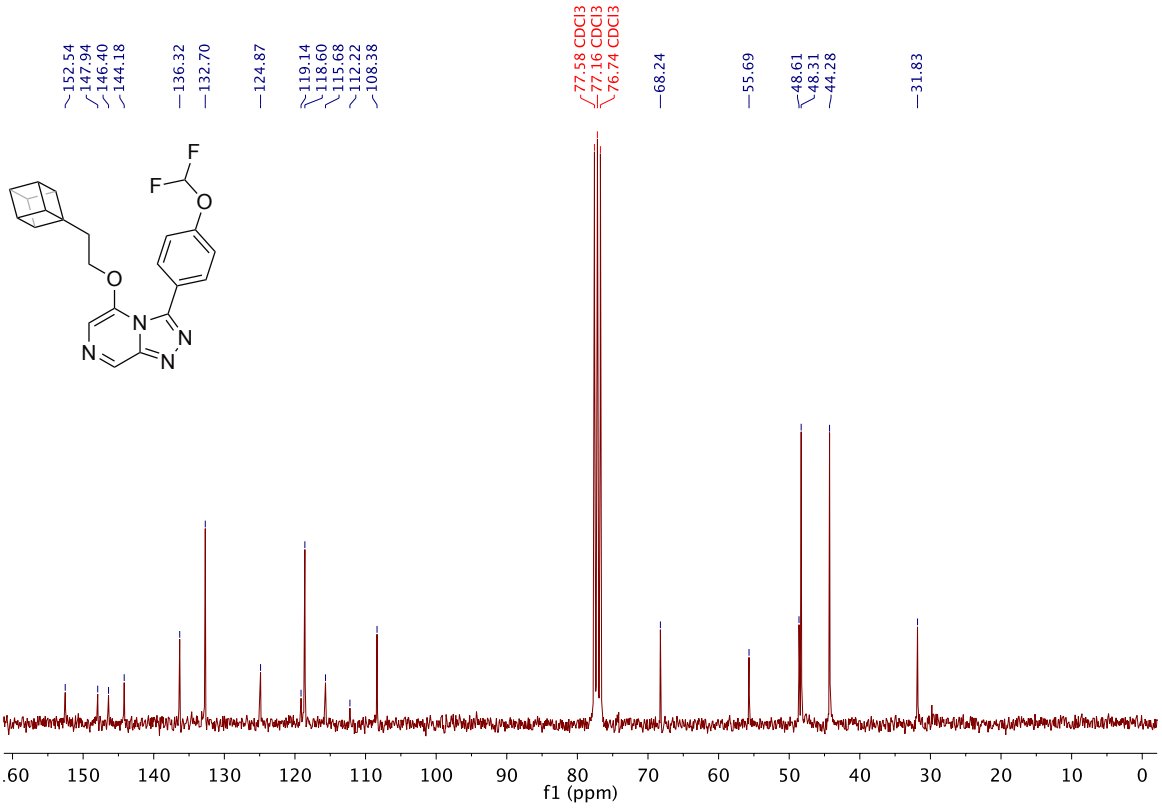

A.58 5-(3-(Cuban-1-yl)propoxy)-3-(4-(difluoromethoxy)phenyl)-[1,2,4]triazolo[4,3-*a*]pyrazine 155

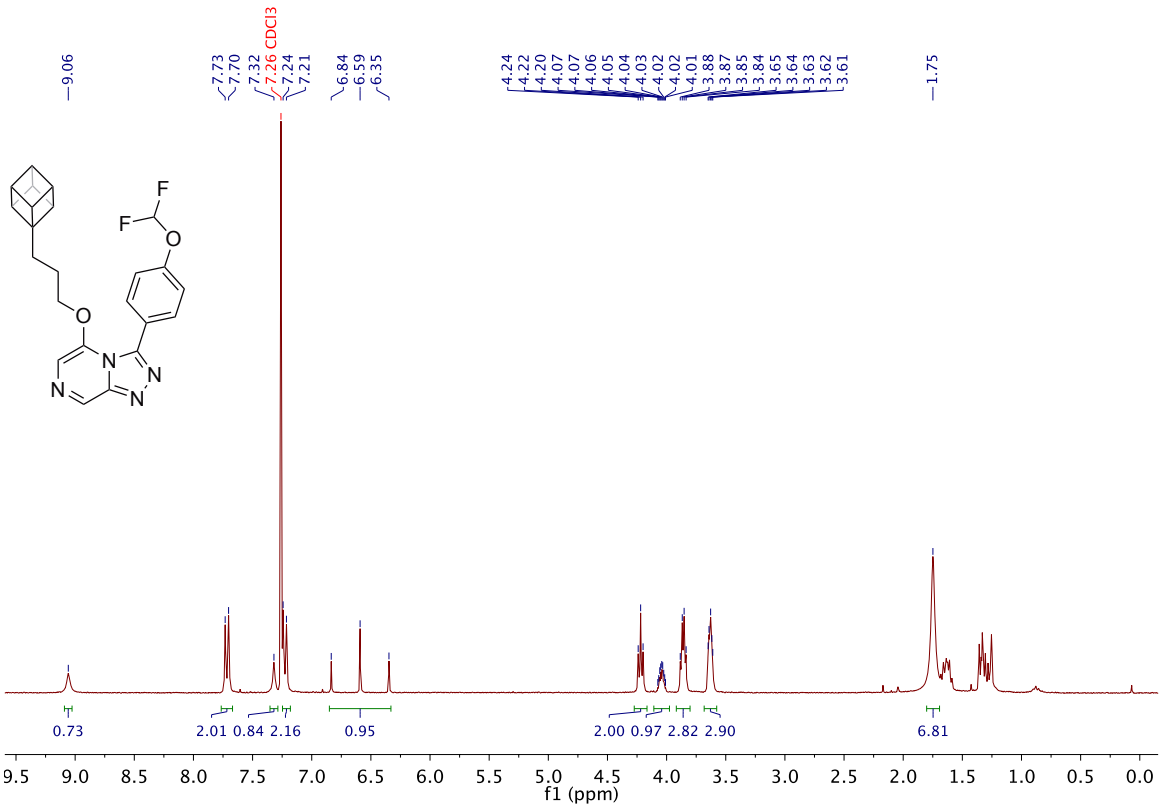

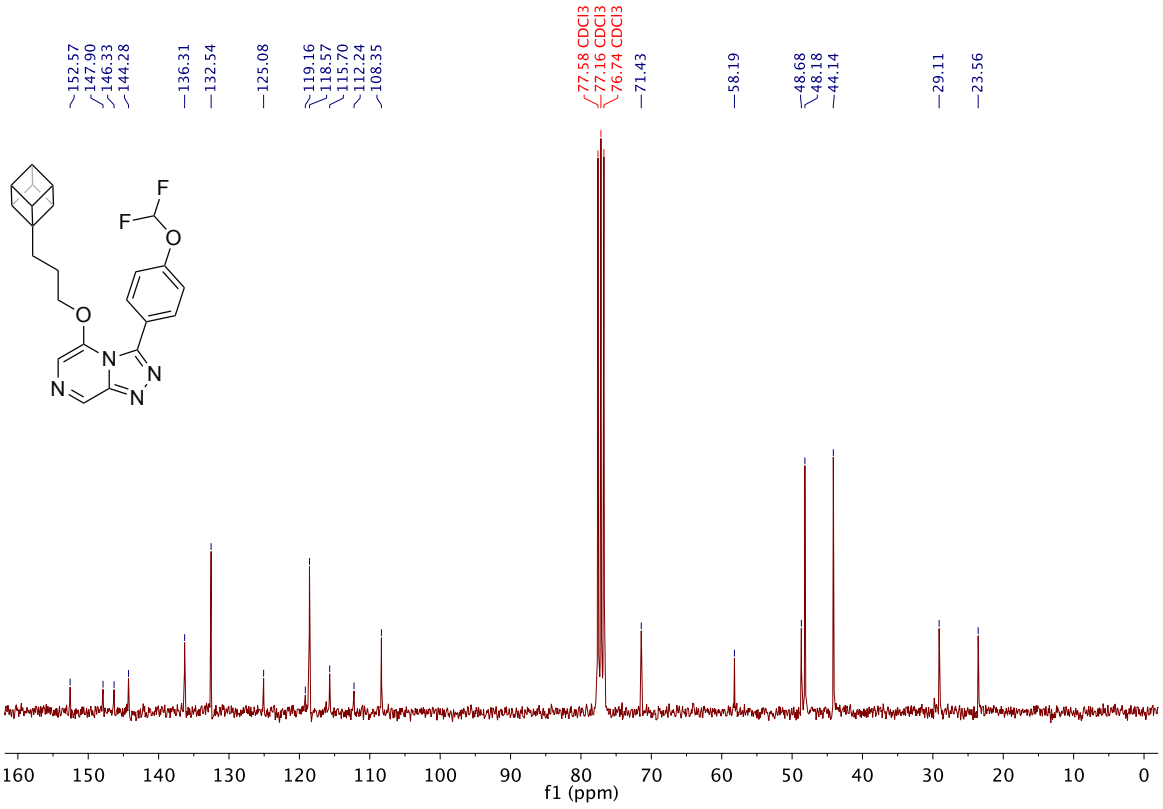

A.59 5-(3,4-Difluorophenethoxy)-3-(4-iodocuban-1-yl)-[1,2,4]triazolo[4,3-*a*] pyrazine 160

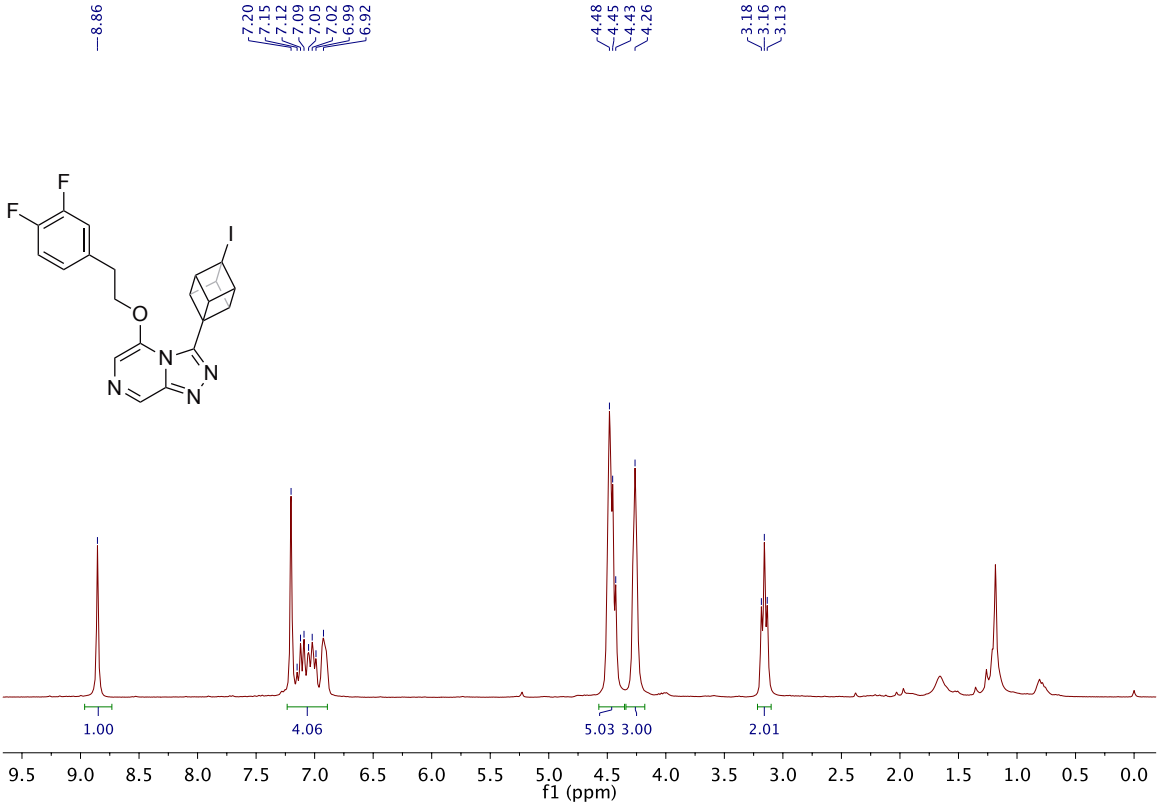

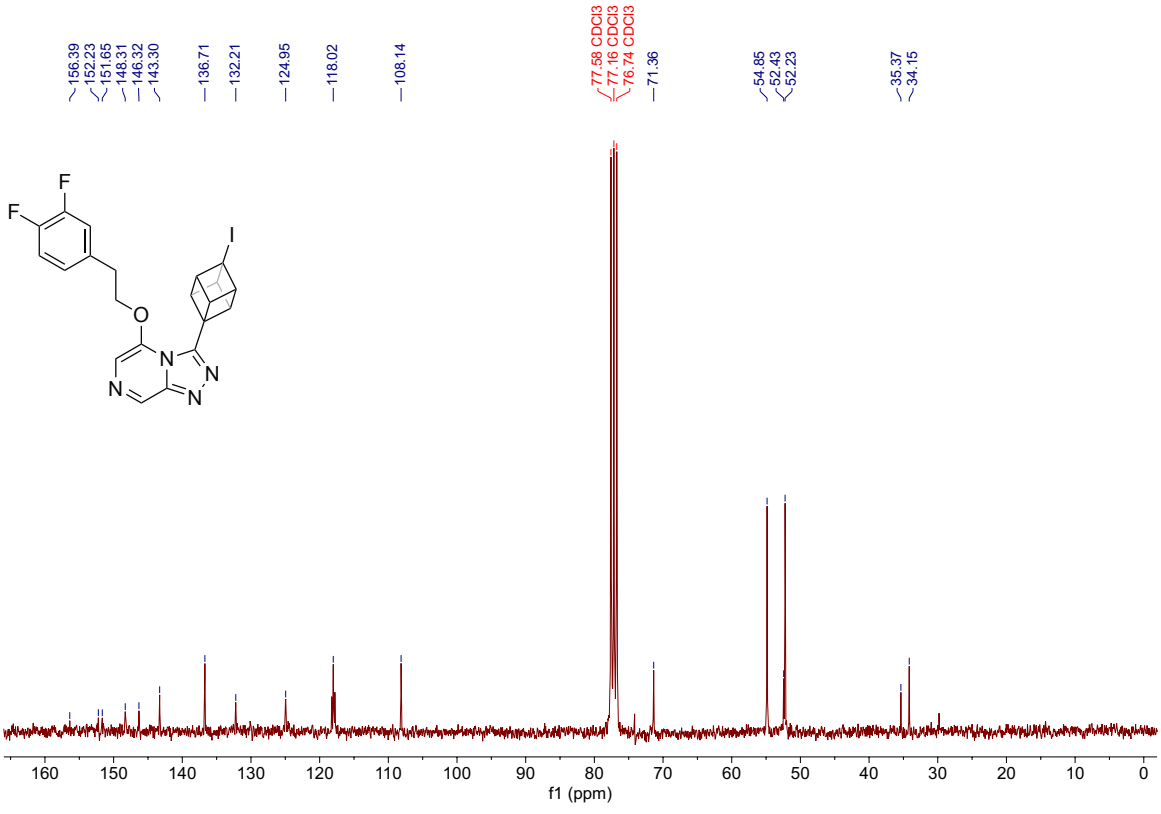

A.60 3-(4-Iodocuban-1-yl)-*N*-(2-(trifluoromethyl)pyridin-4-yl)-[1,2,4]triazolo [4,3-*a*]pyrazine-5-carboxamide 162

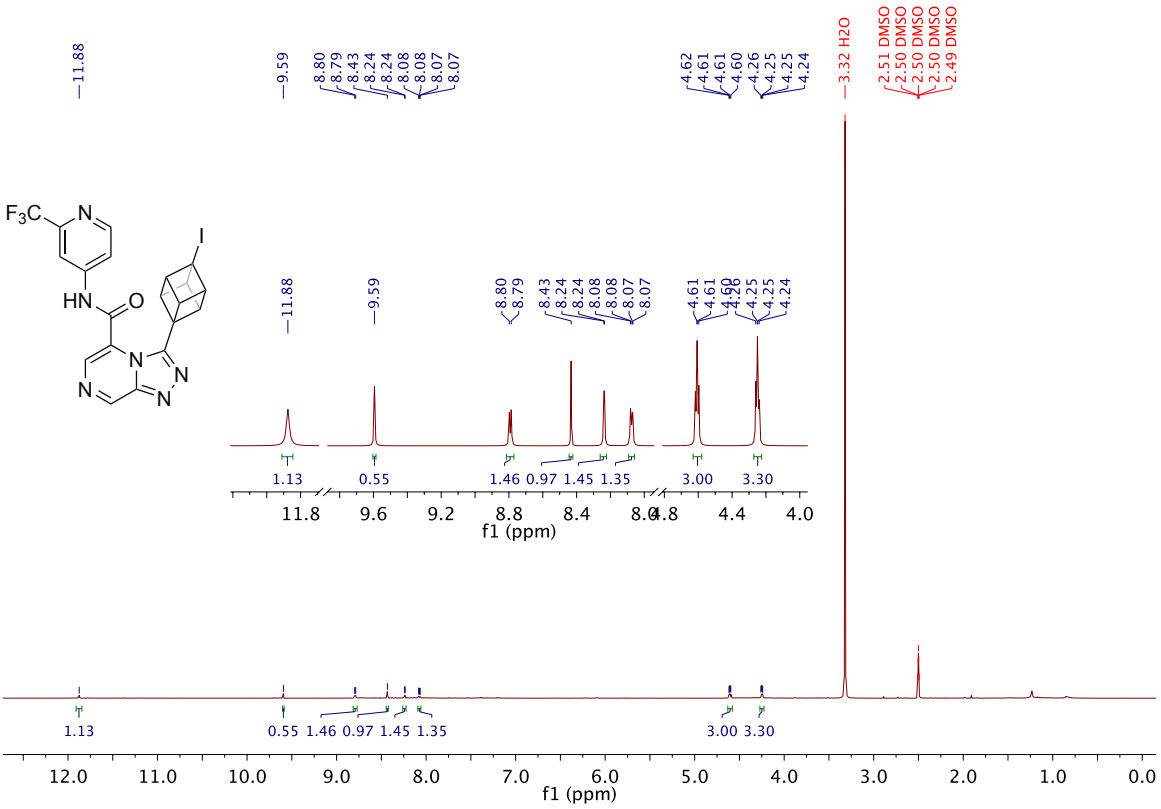

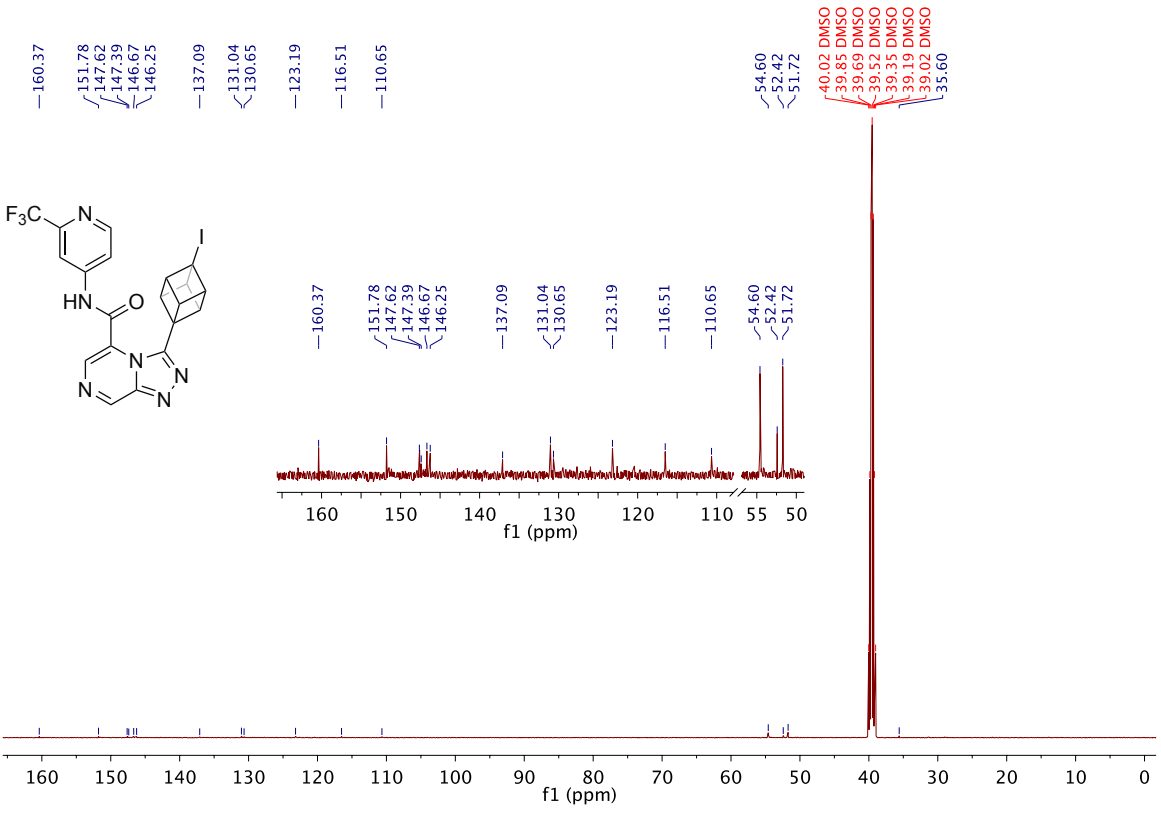

A.61 5-(3,4-Difluorophenethoxy)-3-(4-iodophenyl)-[1,2,4]triazolo[4,3-*a*] pyrazine 165

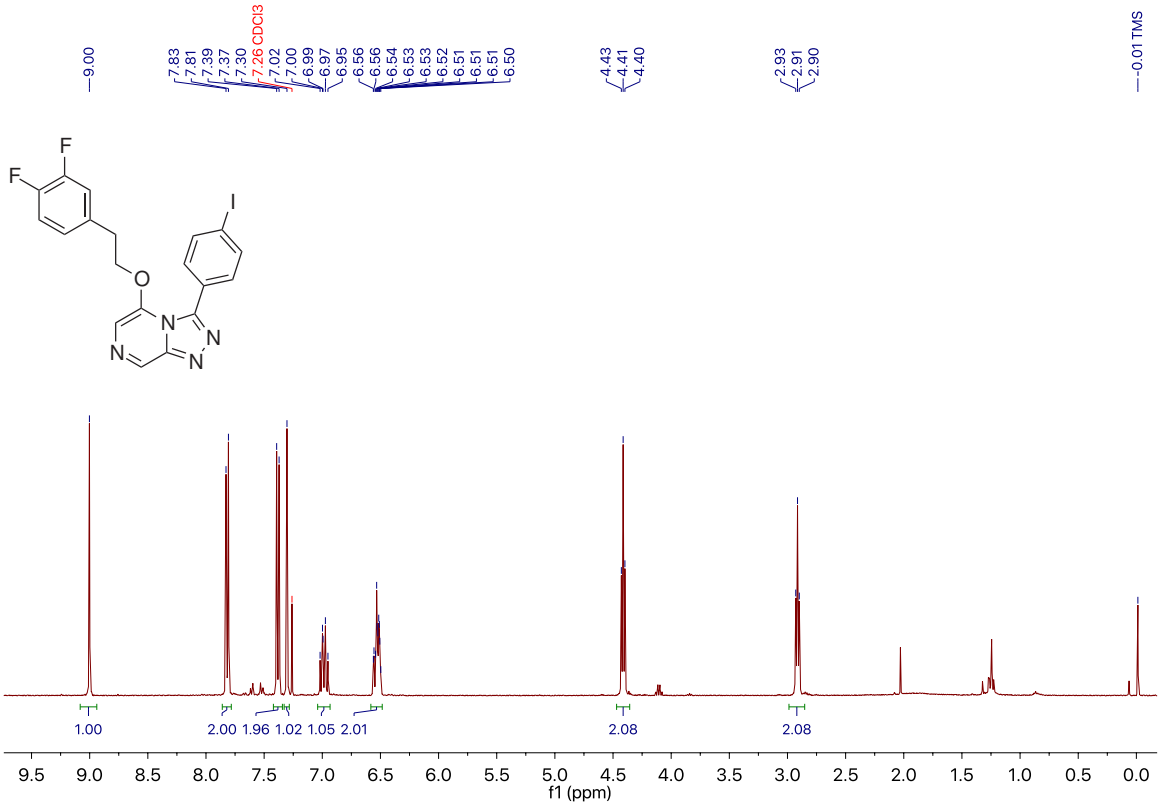

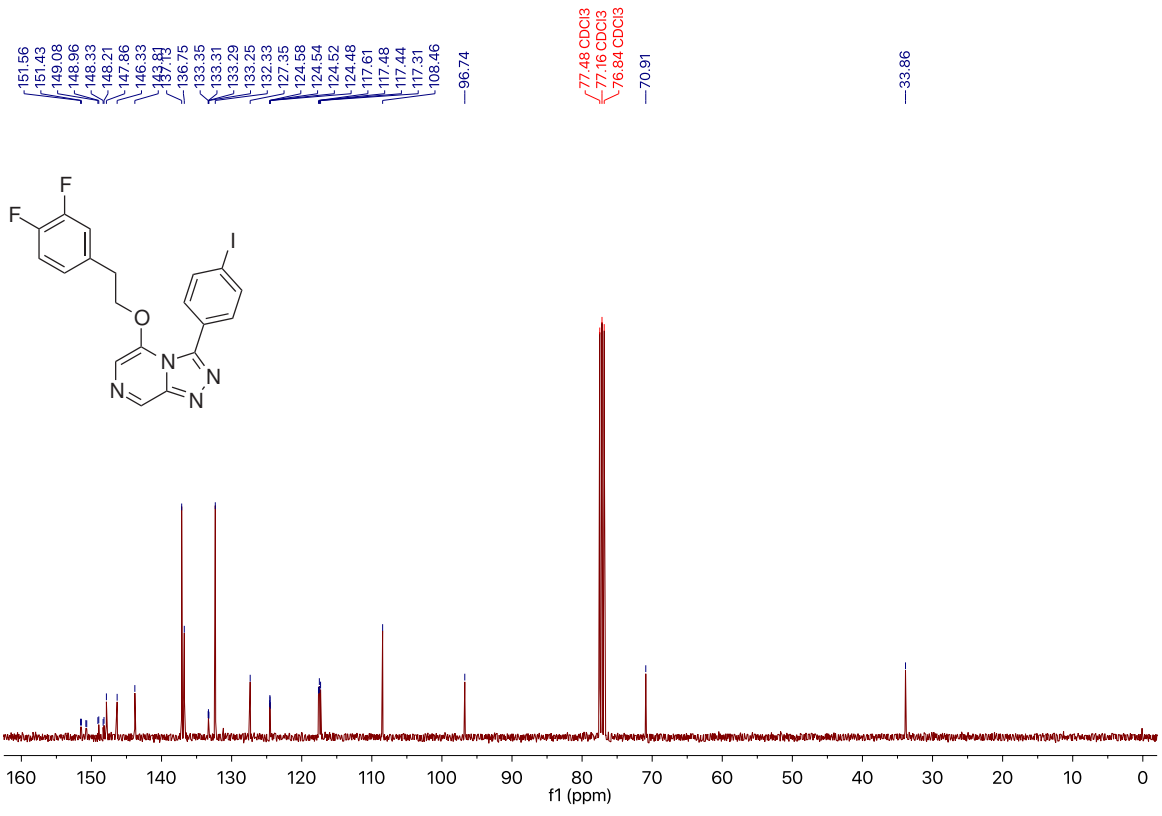

A.62 5-(((3*r*,5*r*,7*r*)-Adamantan-1-yl)methoxy)-3-(4-(difluoromethoxy) phenyl)-[1,2,4]triazolo[4,3-*a*]pyrazine 167

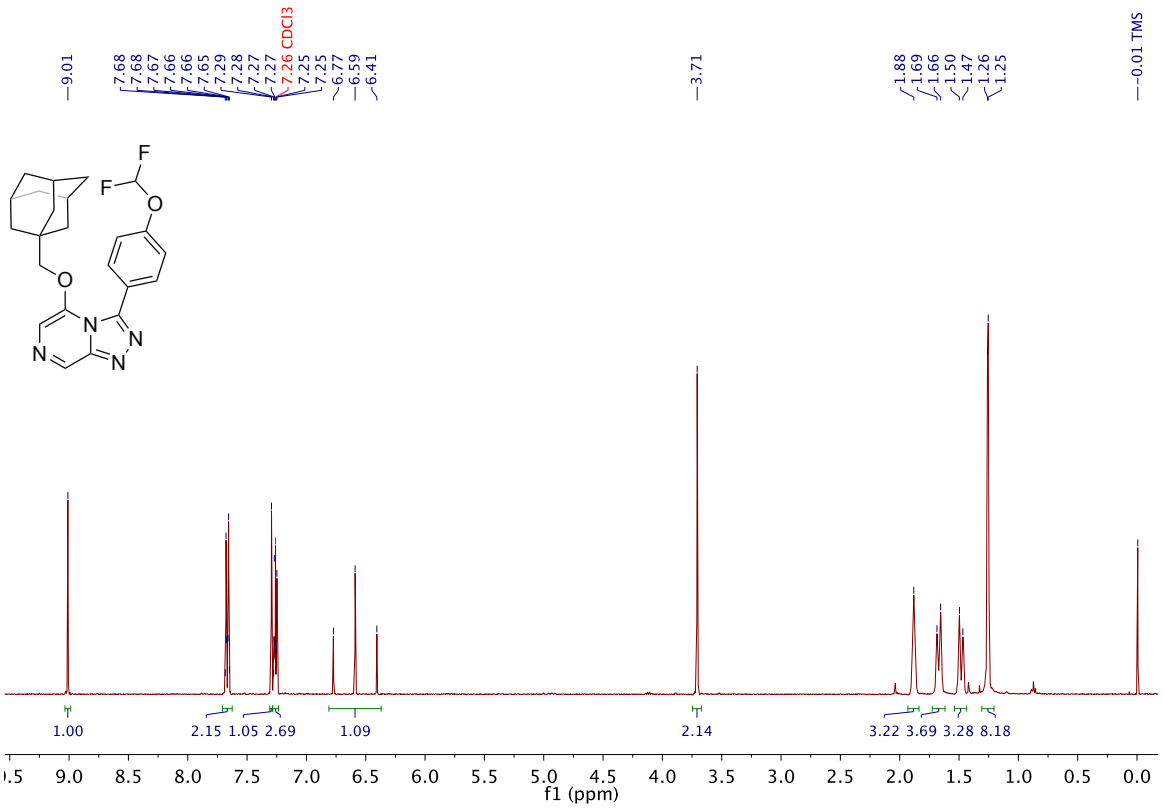

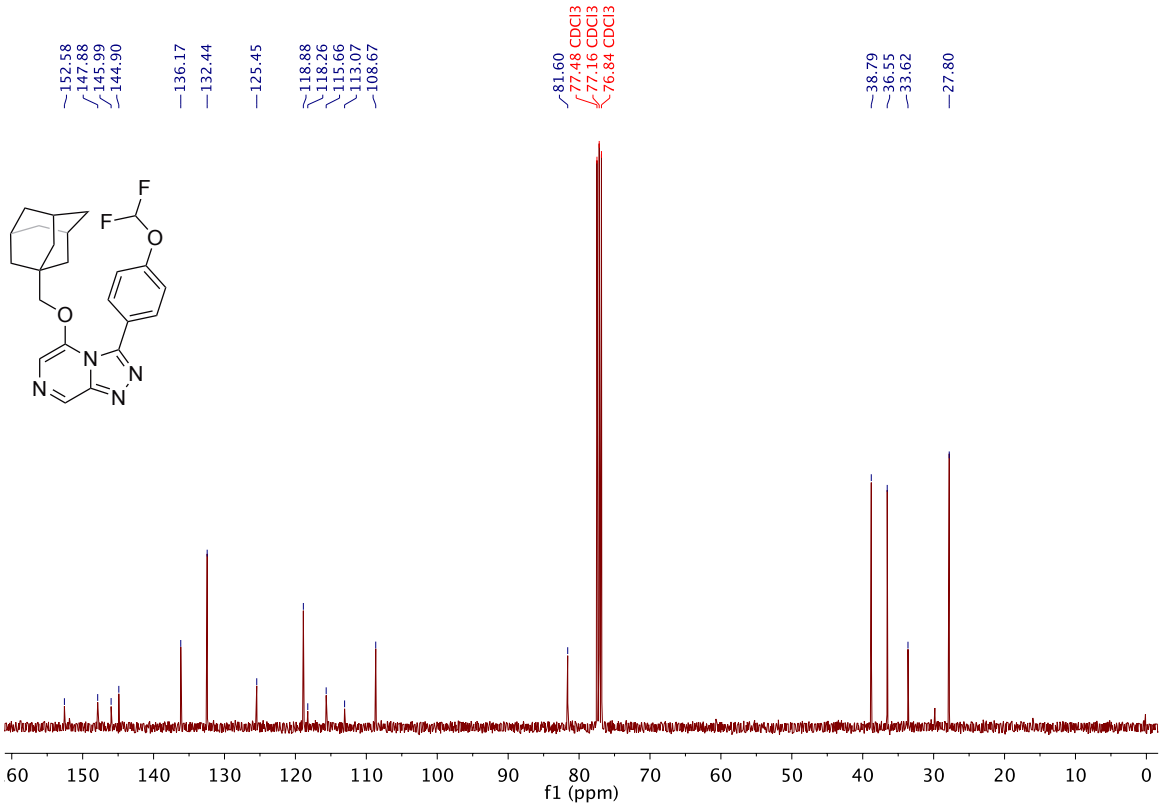

A.63 5-(2-((1*s*,3*s*)-Adamantan-1-yl)ethoxy)-3-(4-(difluoromethoxy)phenyl)-[1,2,4]triazolo[4,3-*a*]pyrazine 168

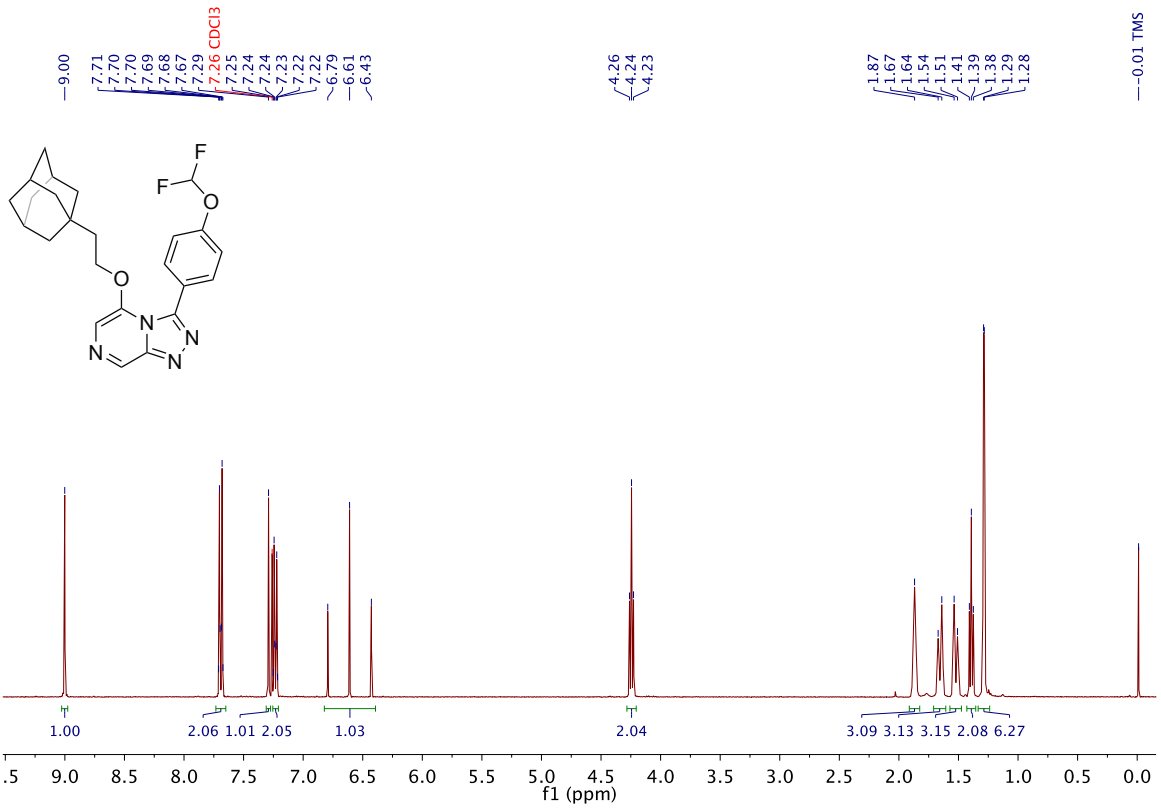

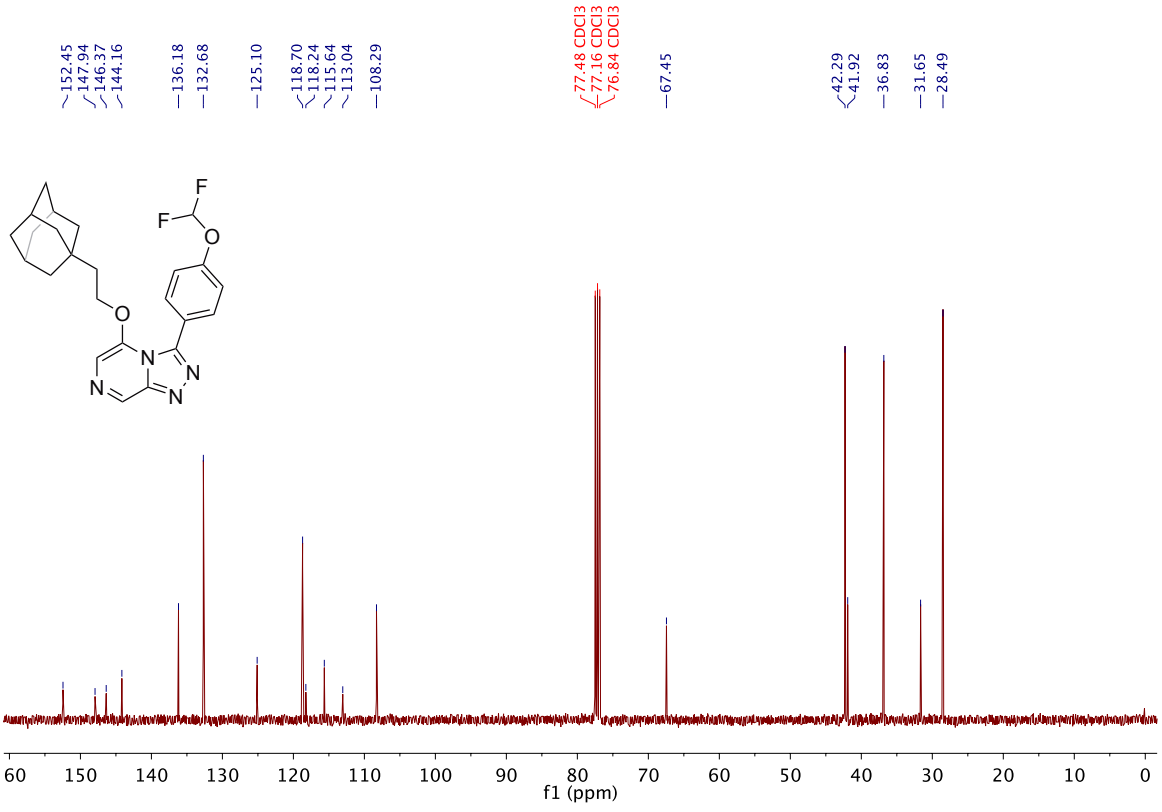

A.64 3-(4-(Difluoromethoxy)phenyl)-5-((3-(difluoromethyl)bicyclo[1.1.1]pentan-1-yl)methoxy)-[1,2,4]triazolo[4,3-*a*]pyrazine 178

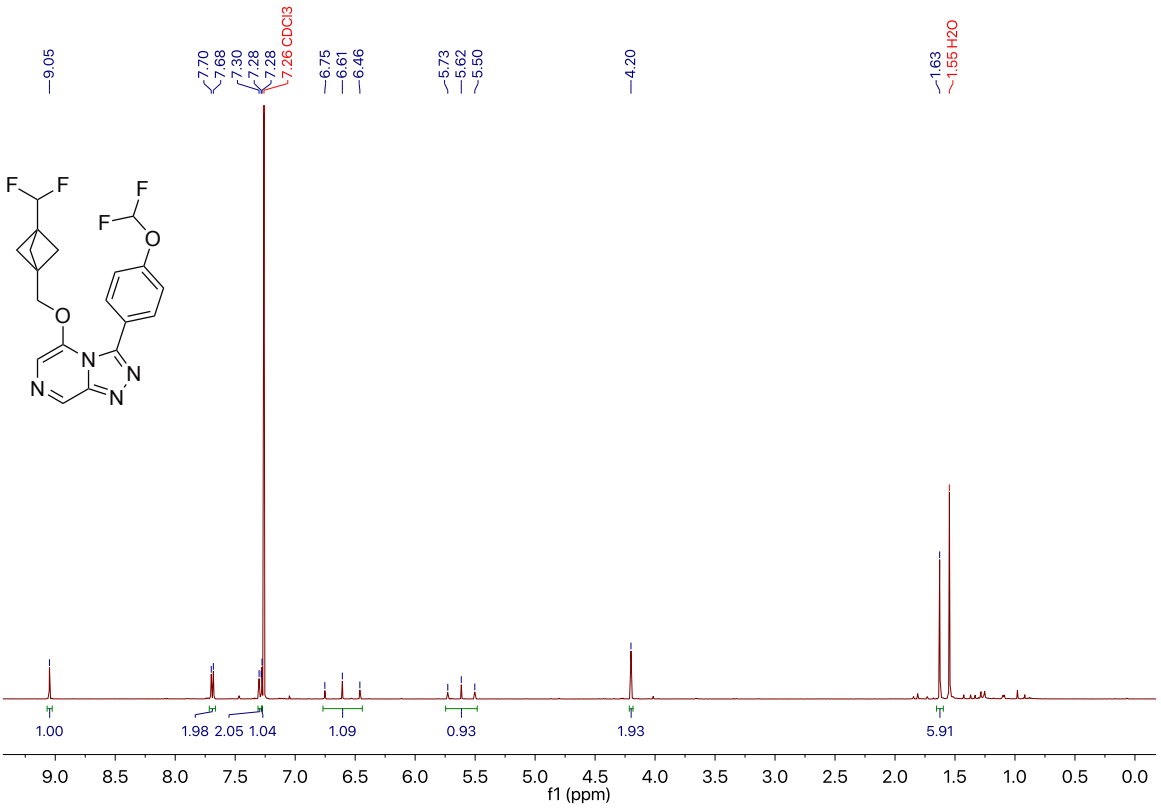

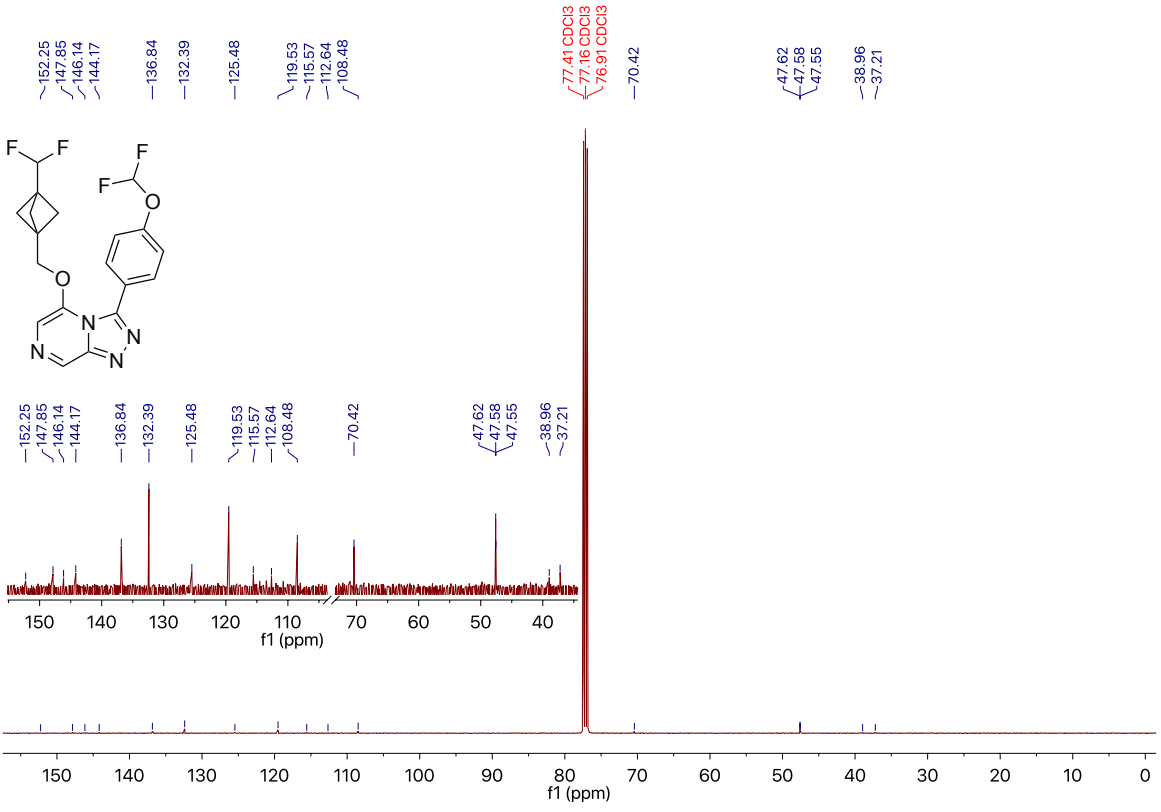

A.65 3-(4-(Difluoromethoxy)phenyl)-5-(2-((1*R*,5*S*)-6,6-dimethylbicyclo[3.1.1]hept-2-en-2-yl)ethoxy)-[1,2,4]triazolo[4,3-*a*]pyrazine 179

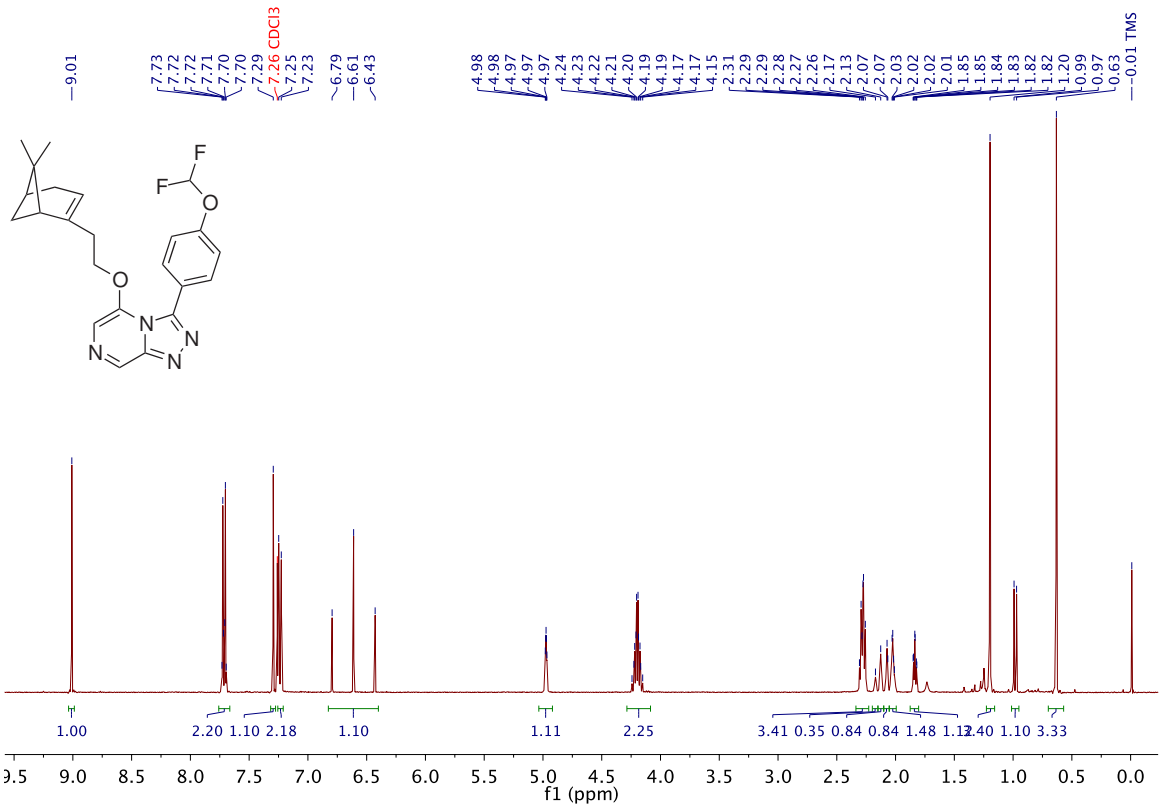

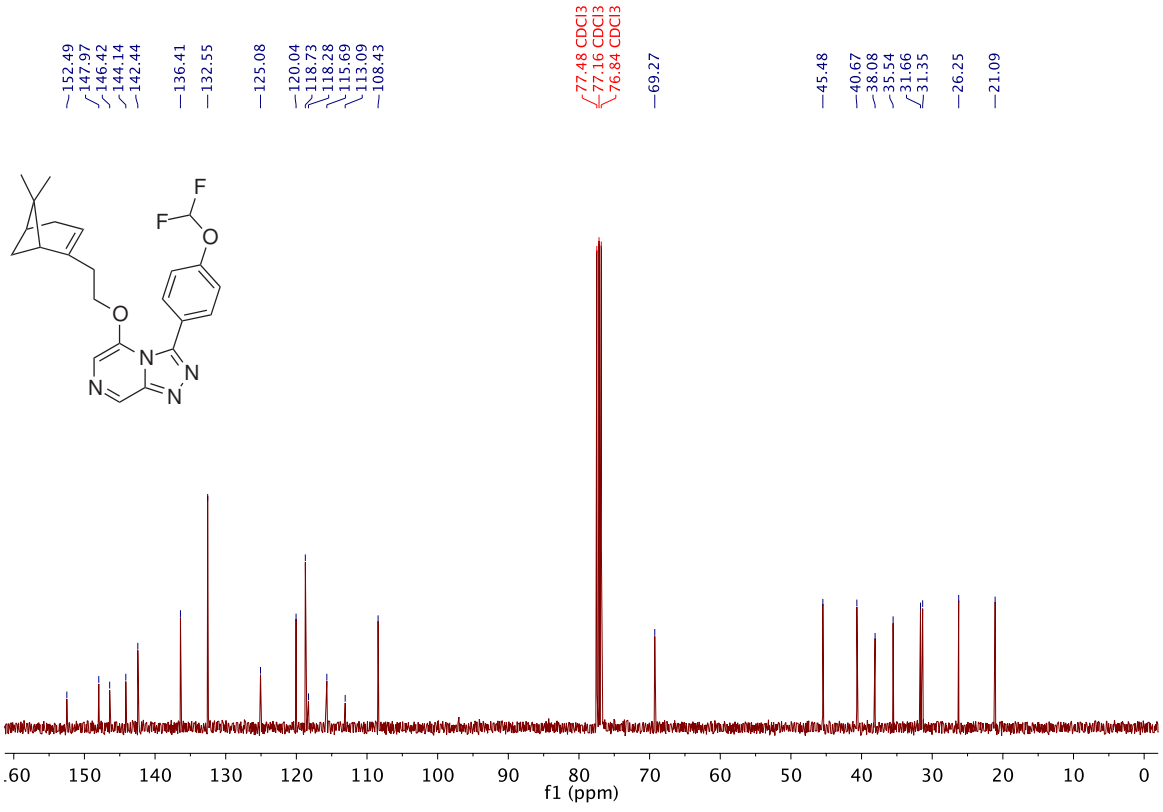

A.66 5-(((1*S*,2*S*,4*S*)-Bicyclo[2.2.1]hept-5-en-2-yl)methoxy)-3-(4-(difluoromethoxy)phenyl)-[1,2,4]triazolo[4,3-*a*]pyrazine 180

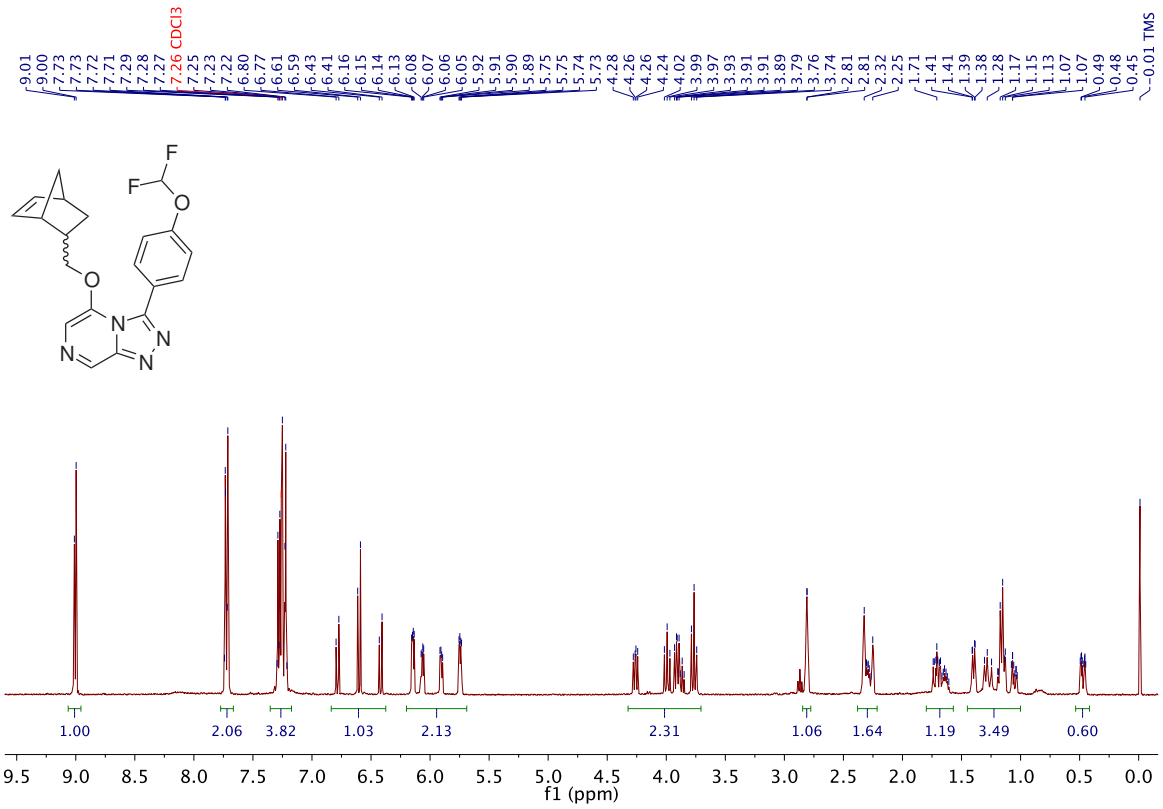

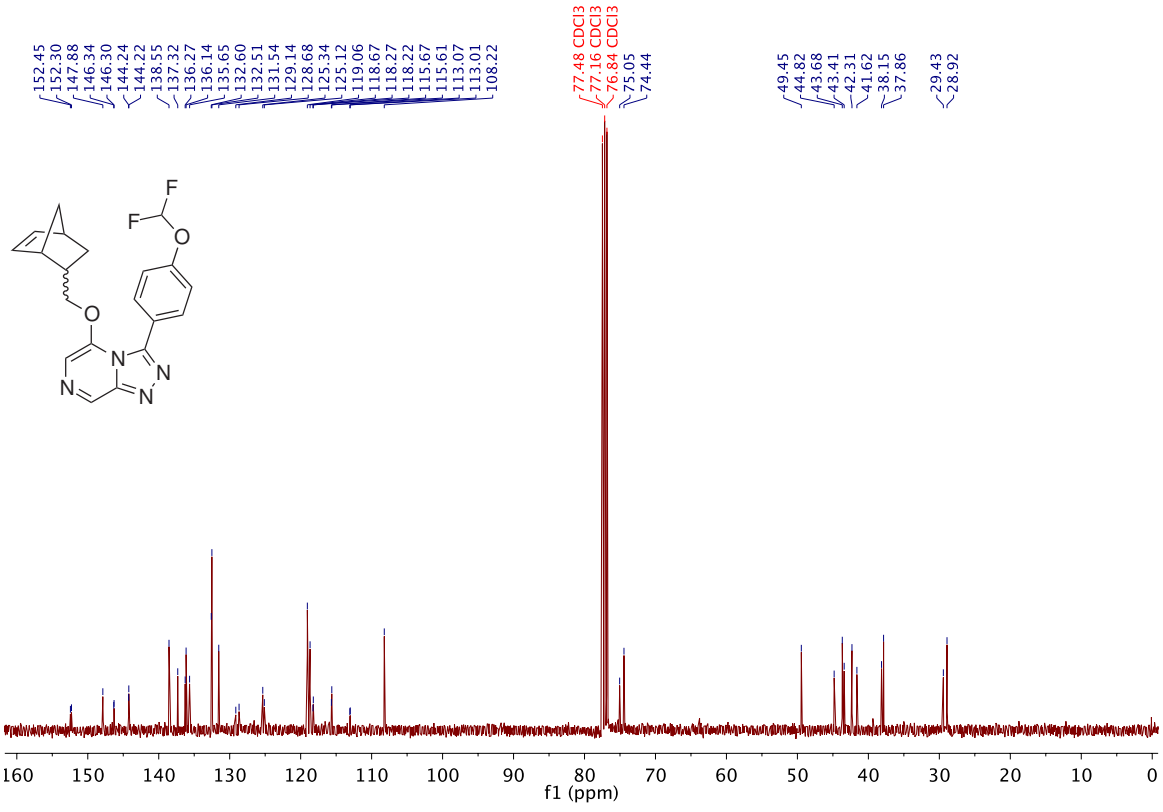

A.67 3-(4-(Difluoromethoxy)phenyl)-5-(2-(octahydro-1*H*-2,4,1-(epiethane[1,1,2]triyl)cyclobuta[*cd*]pentalen-7-yl)ethoxy)-[1,2,4]triazolo[4,3-*a*]pyrazine 187

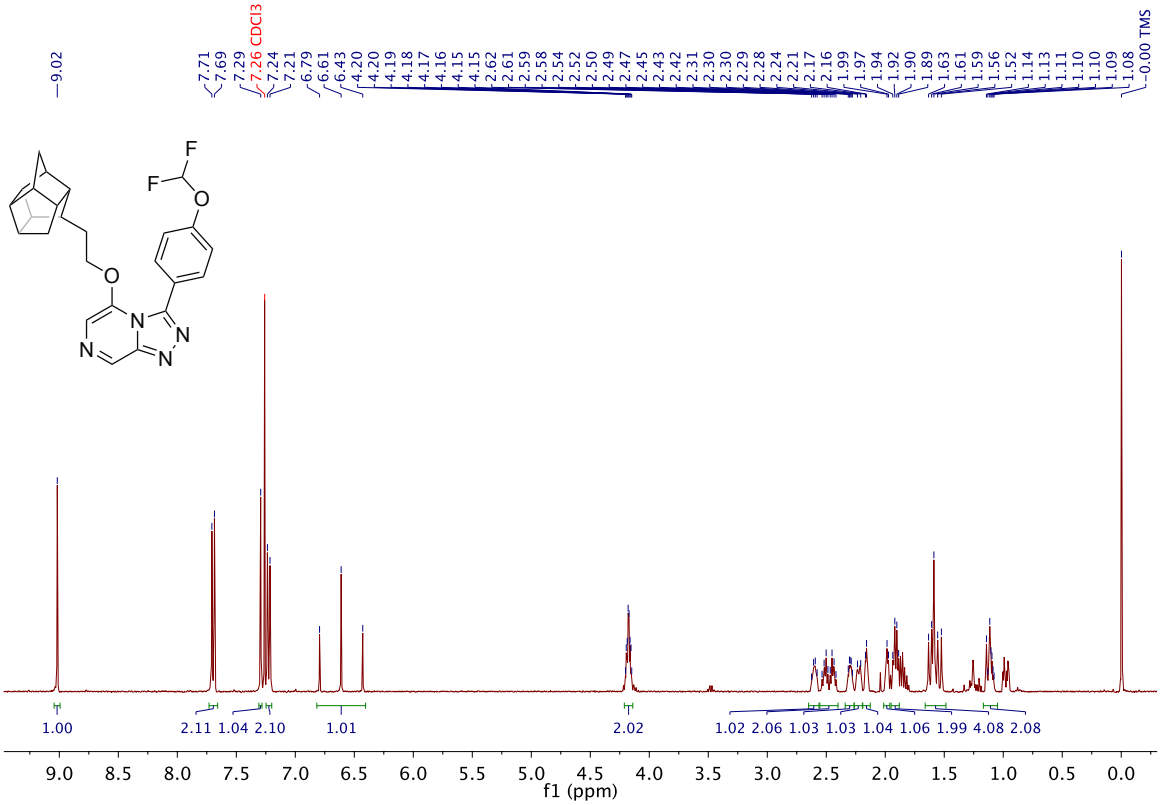

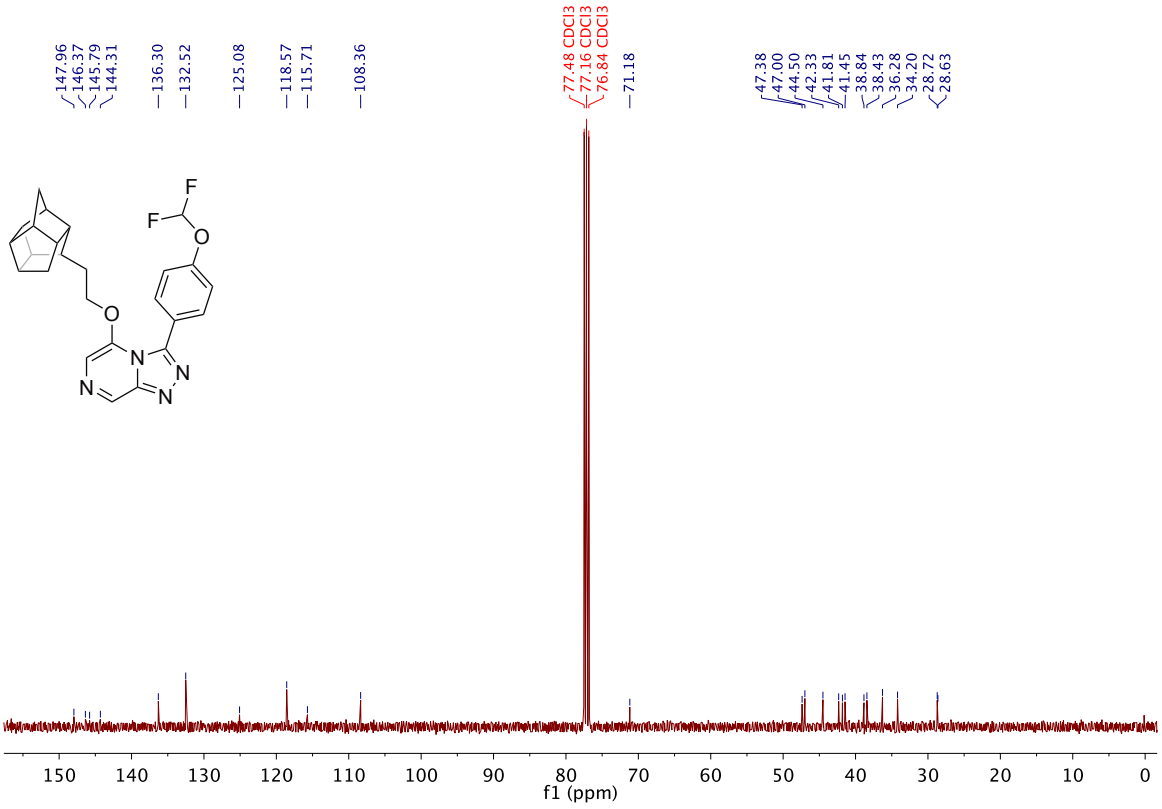

A.68 5-((1,2-Dicarba-closo-decaborane-1-yl)ethoxy)-3-(4-(difluoromethoxy) phenyl)-[1,2,4]triazolo[4,3-*a*]pyrazine 192

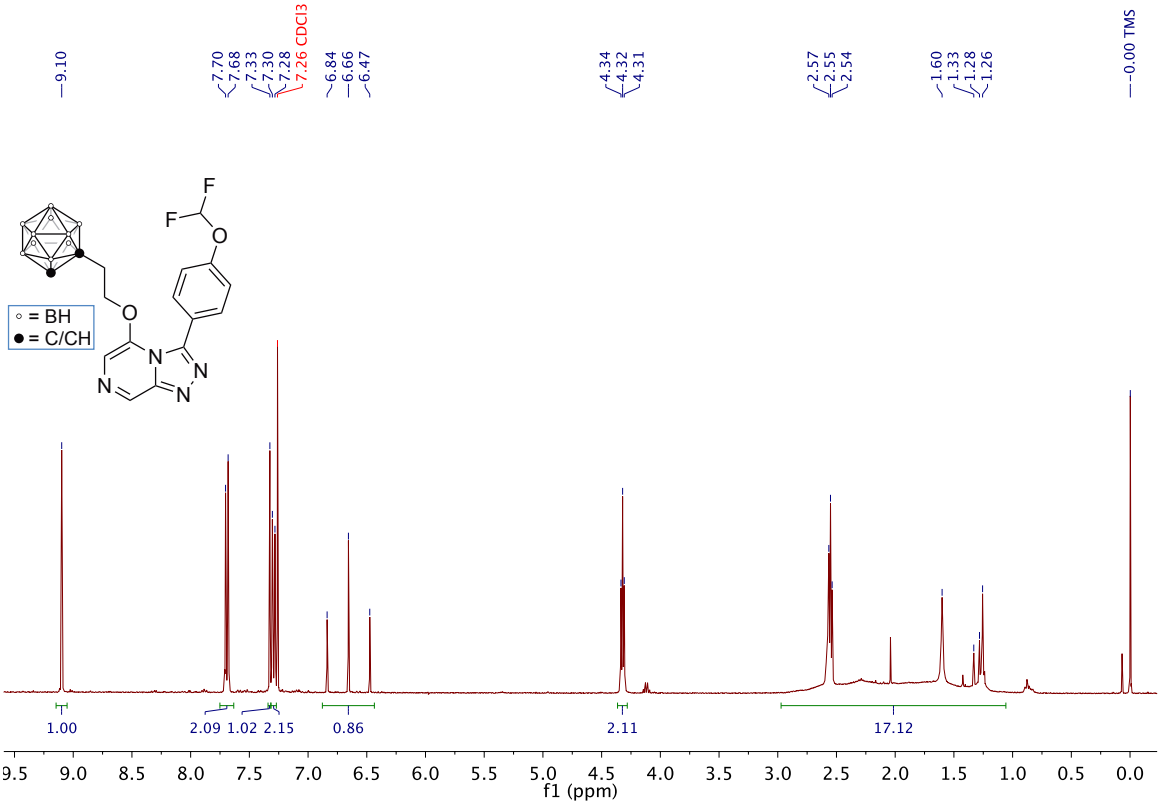

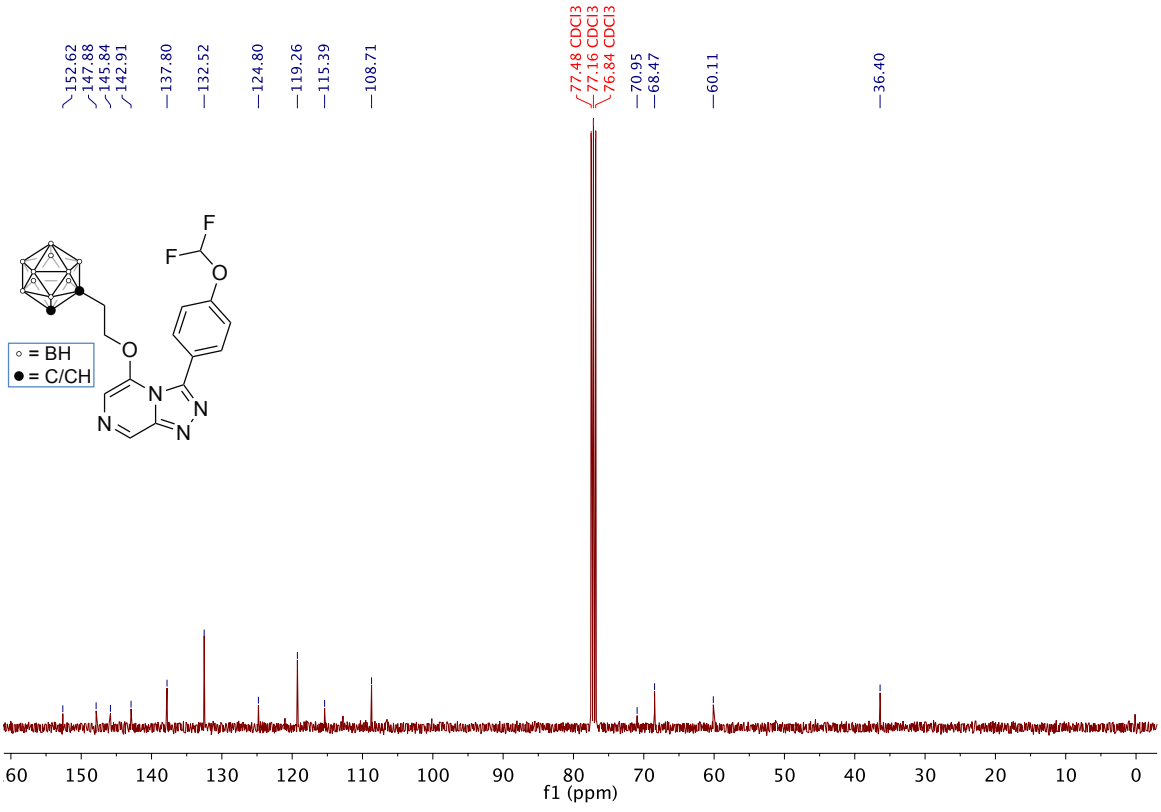

A.69 5-((1,7-Dicarba-closo-decaborane-1-yl)ethoxy)-3-(4-(difluoromethoxy) phenyl)-[1,2,4]triazolo[4,3-*a*]pyrazine 193

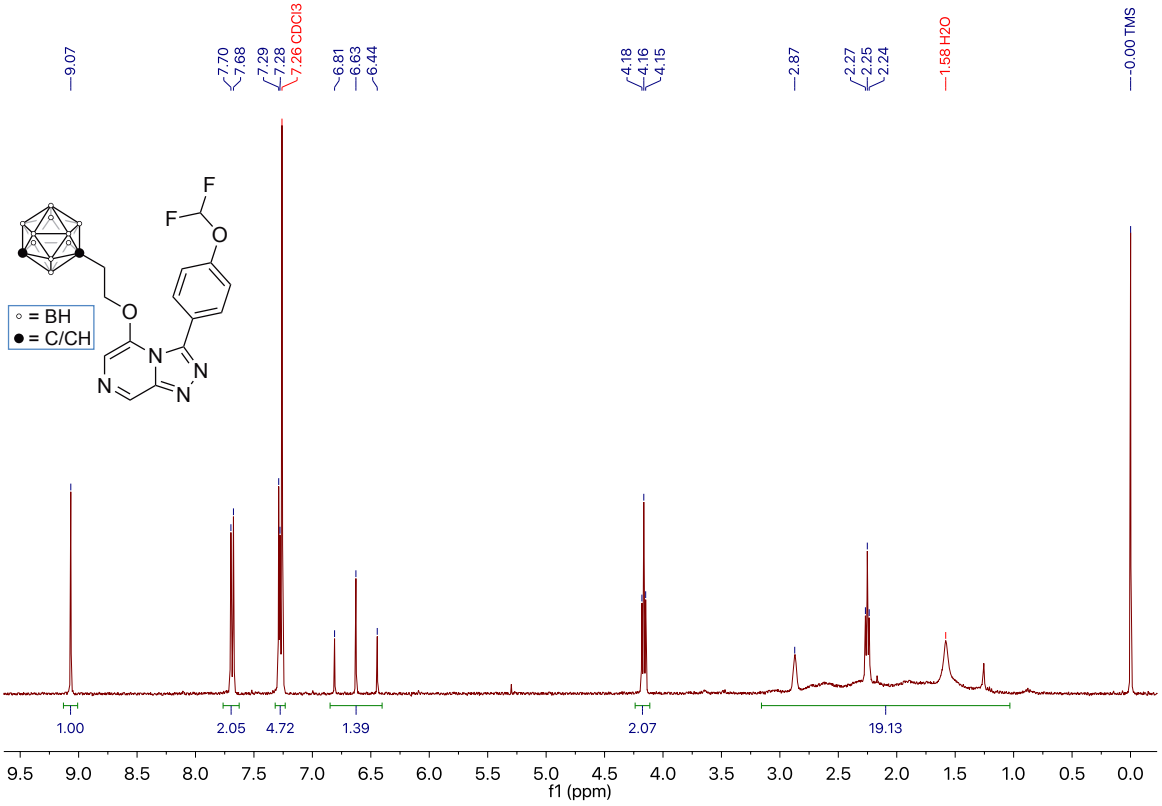

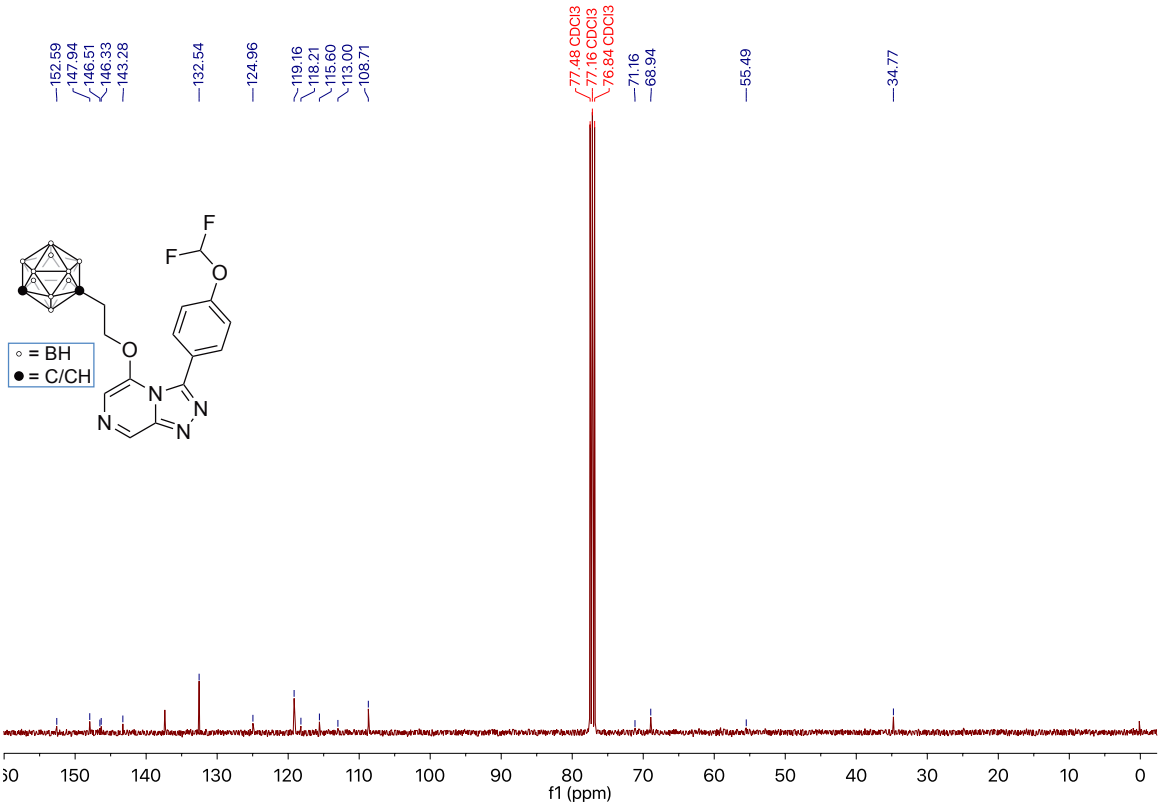

A.70 5-((1,12-Dicarba-closo-decaborane-1-yl)ethoxy)-3-(4-(difluoromethoxy) phenyl)-[1,2,4]triazolo[4,3-*a*]pyrazine 194

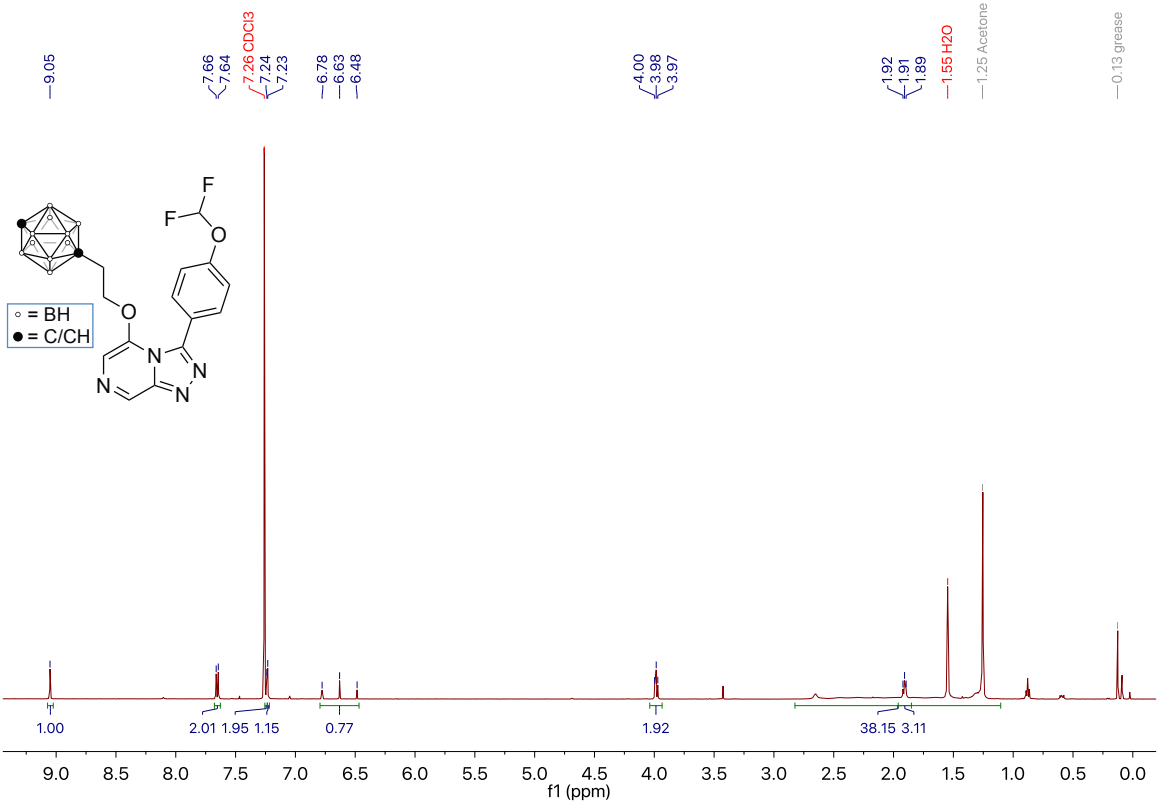

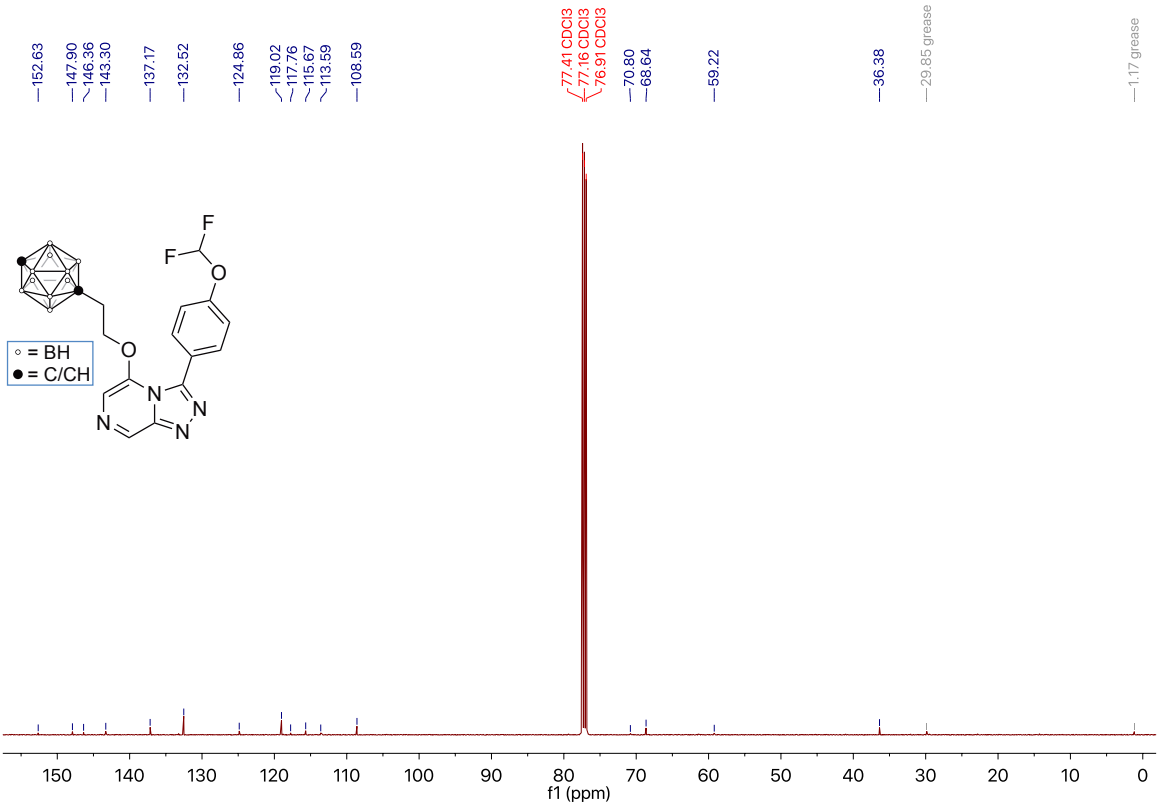

A.71 5-((7,8-Dicarba-nido-undecaborane-7-yl)ethoxy)-3-(4-(difluoromethoxy) phenyl)-[1,2,4]triazolo[4,3-*a*]pyrazine 195

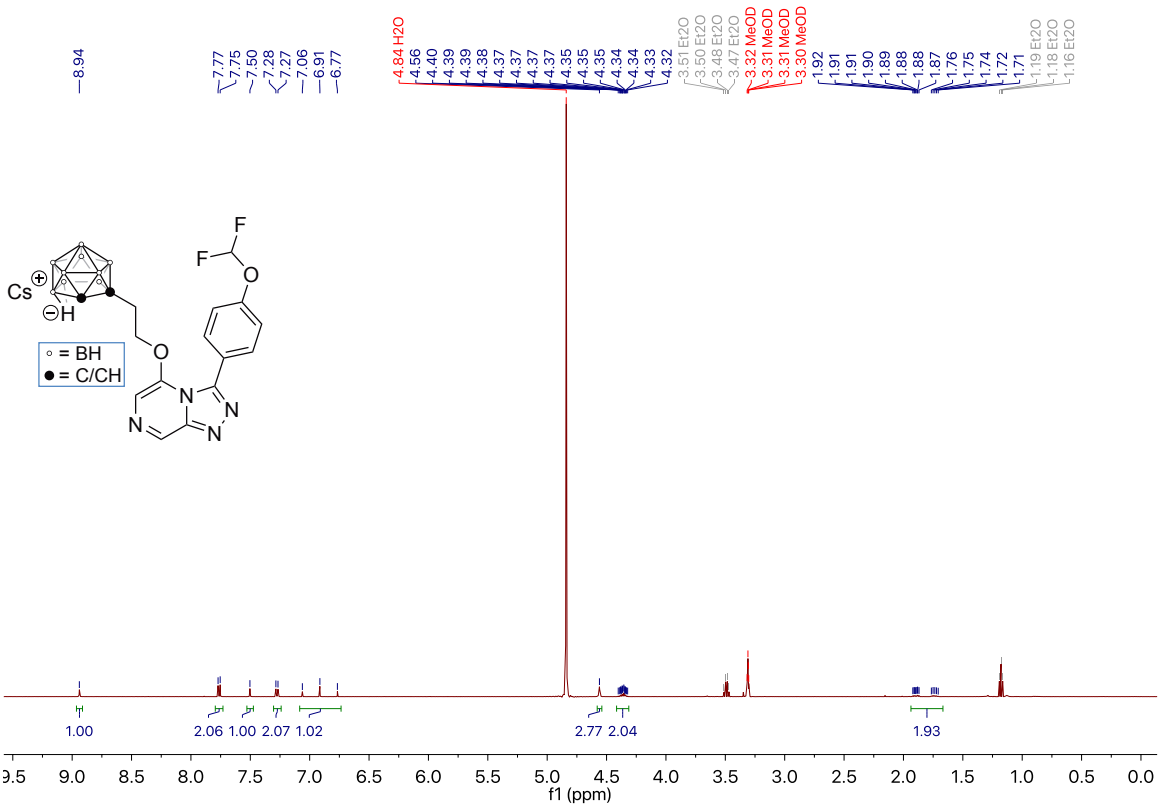

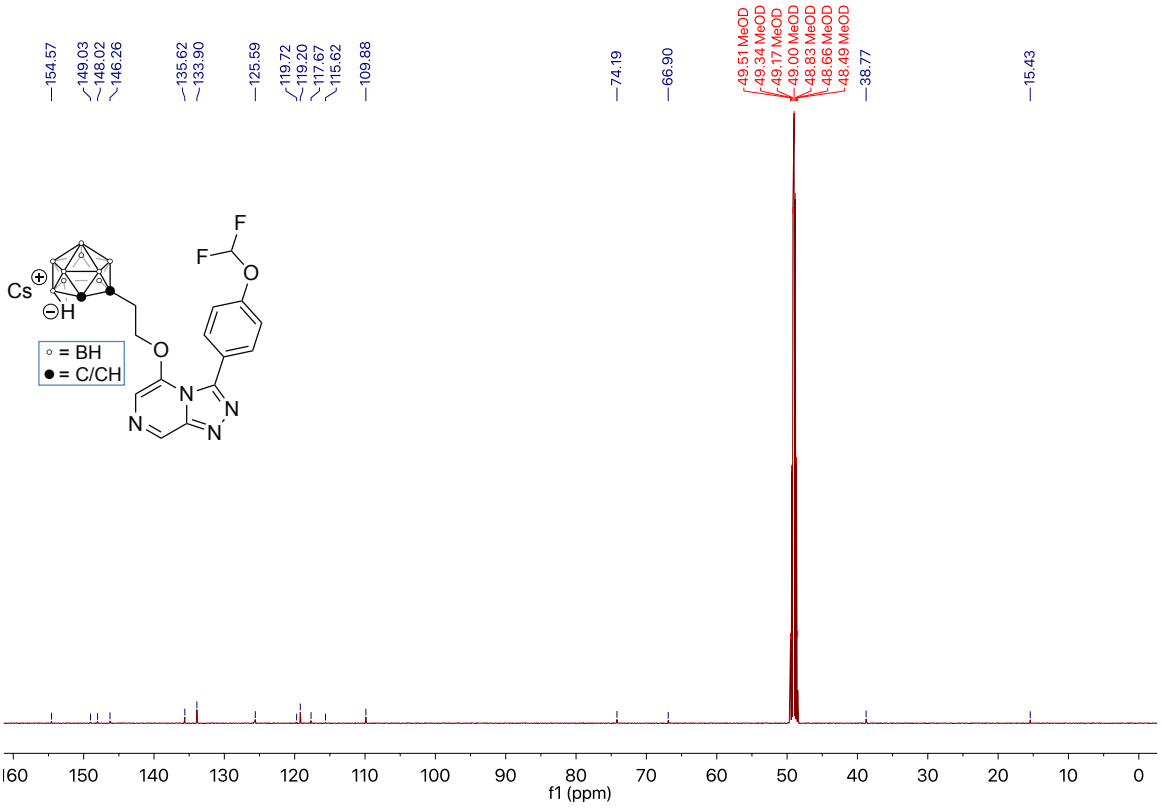

A.72 3-(4-(Difluoromethoxy)phenyl)-5-methoxy-[1,2,4]triazolo[4,3-*a*]pyrazine 211

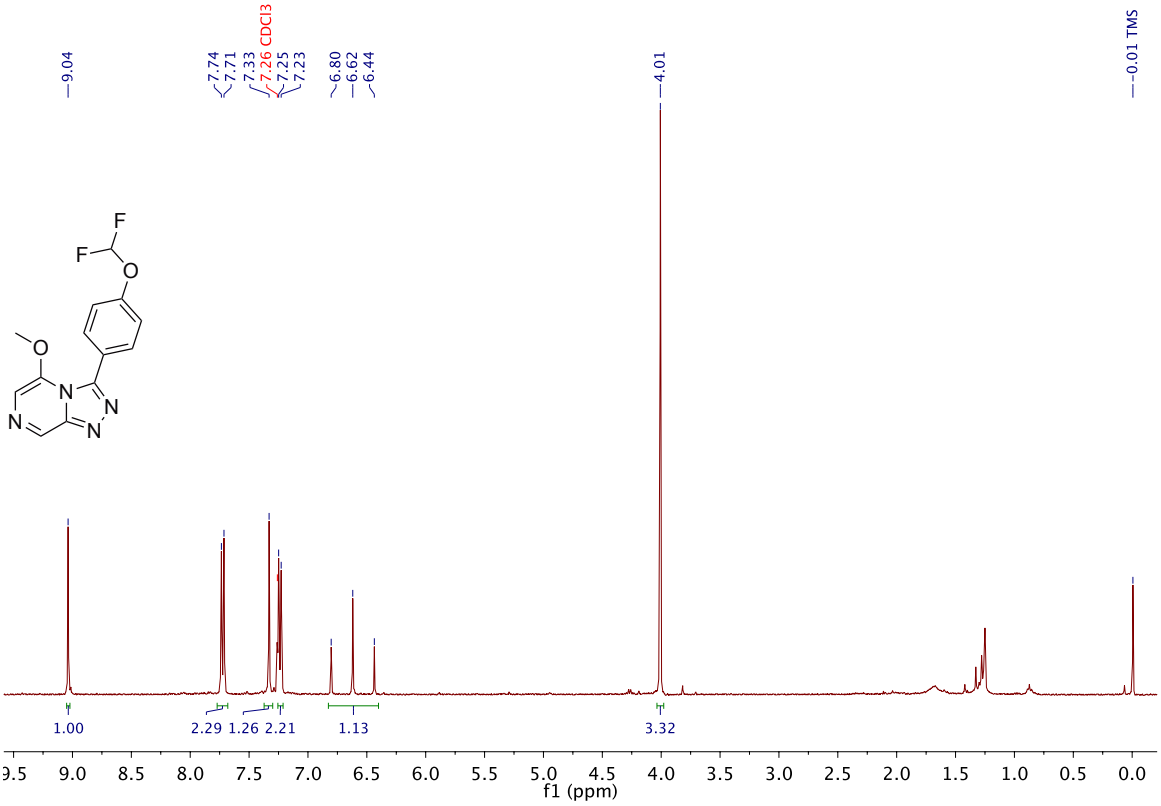

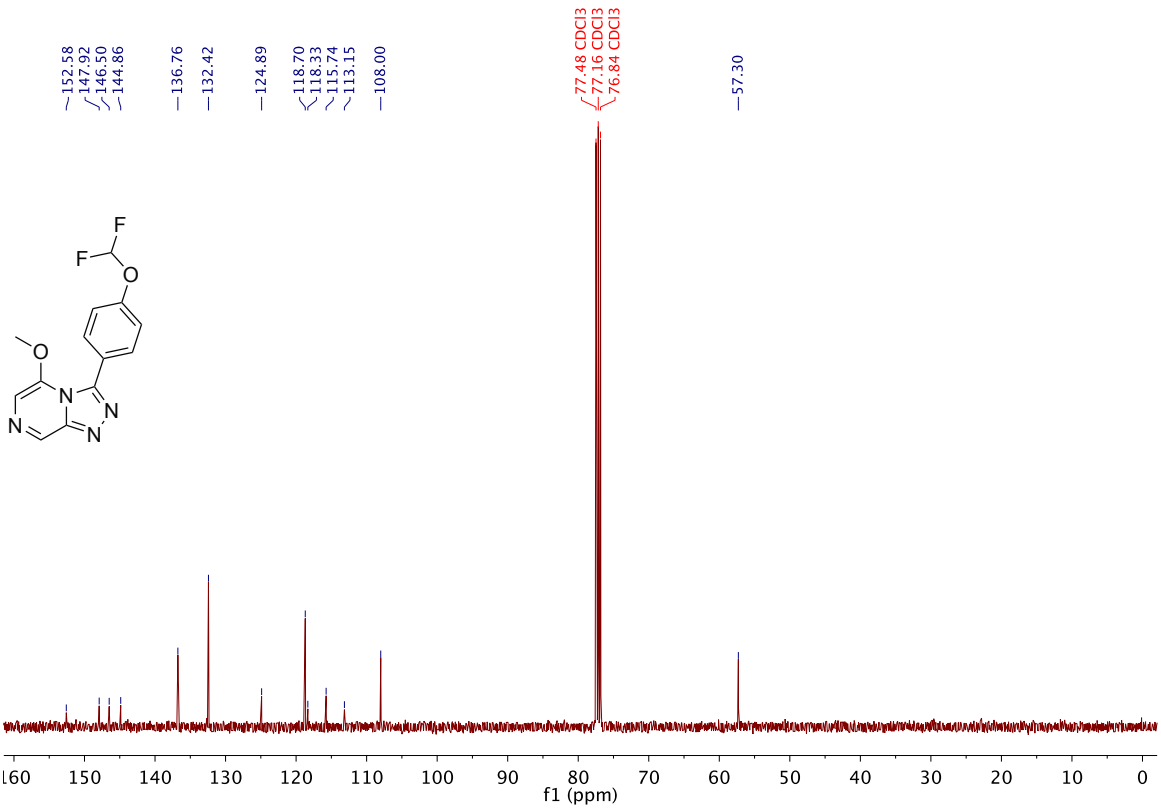

A.73 3-((3-(4-(Difluoromethoxy)phenyl)-[1,2,4]triazolo[4,3-*a*]pyrazin-5-yl) oxy)-2-phenylpropan-1-ol 24

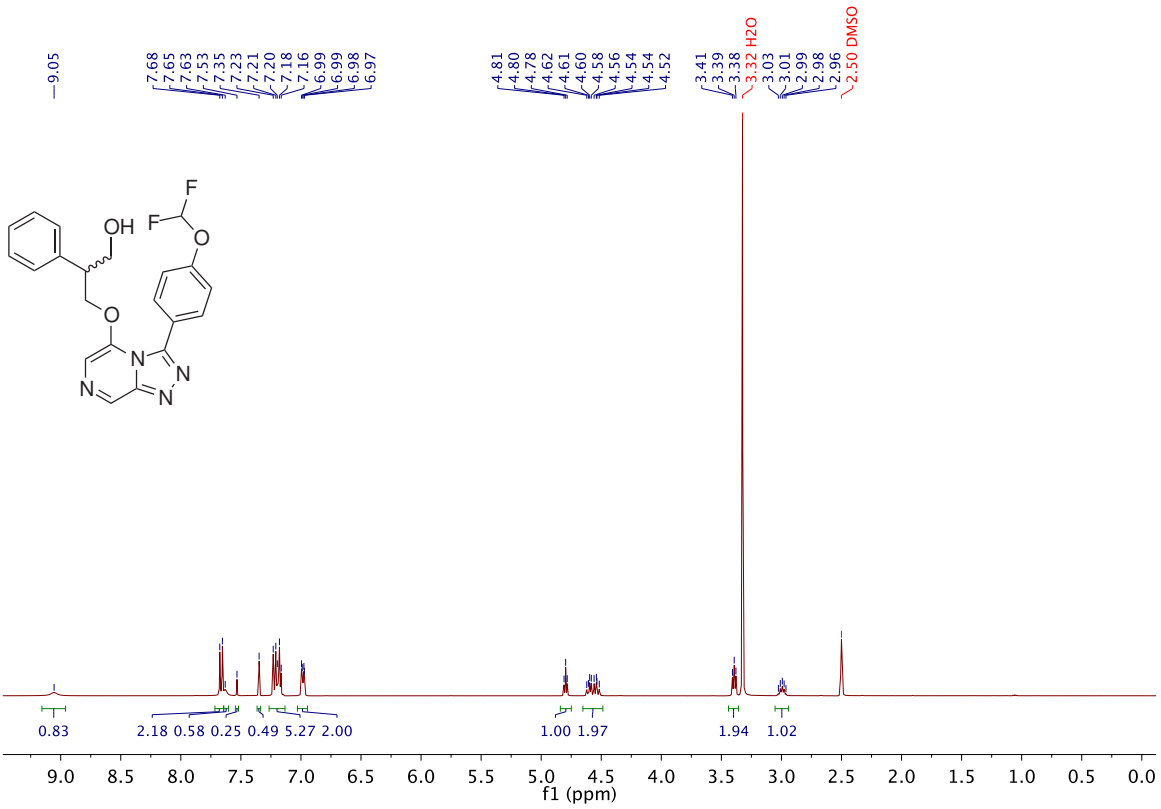

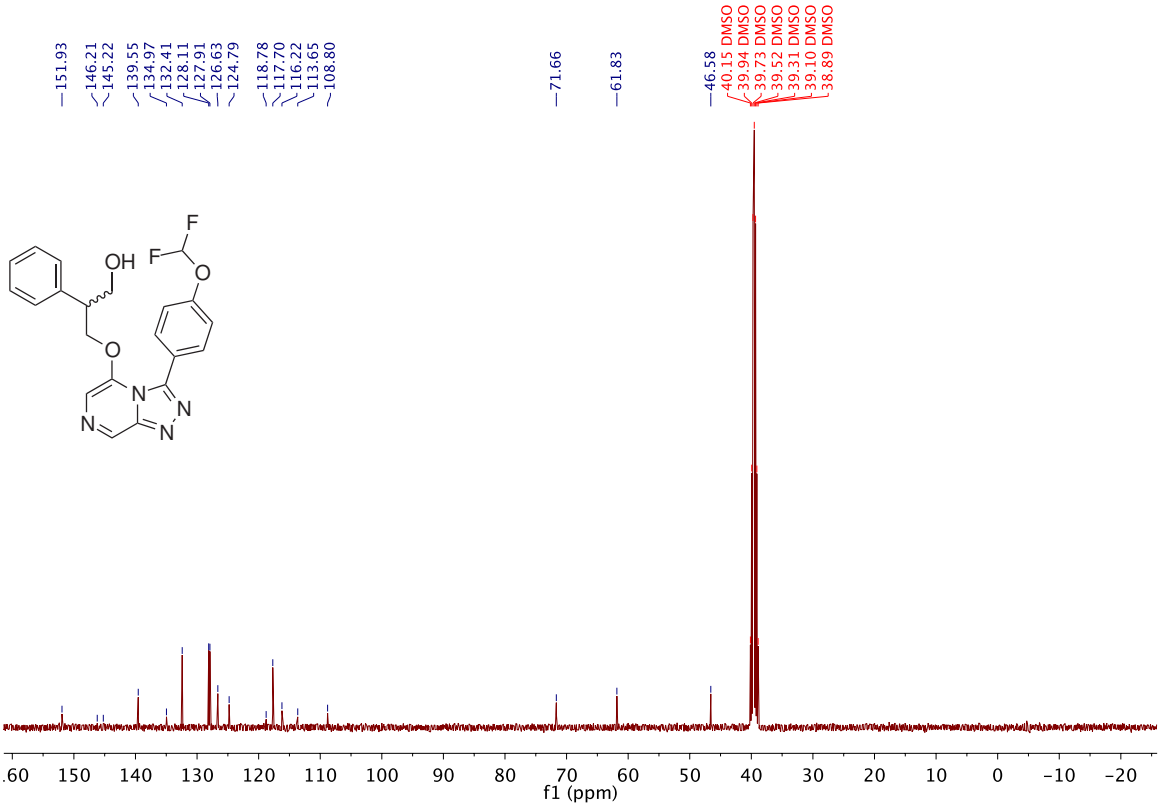

A.74 3-((3-(4-(Difluoromethoxy)phenyl)-[1,2,4]triazolo[4,3-*a*]pyrazin-5-yl) oxy)-2-phenylpropanoic acid 208

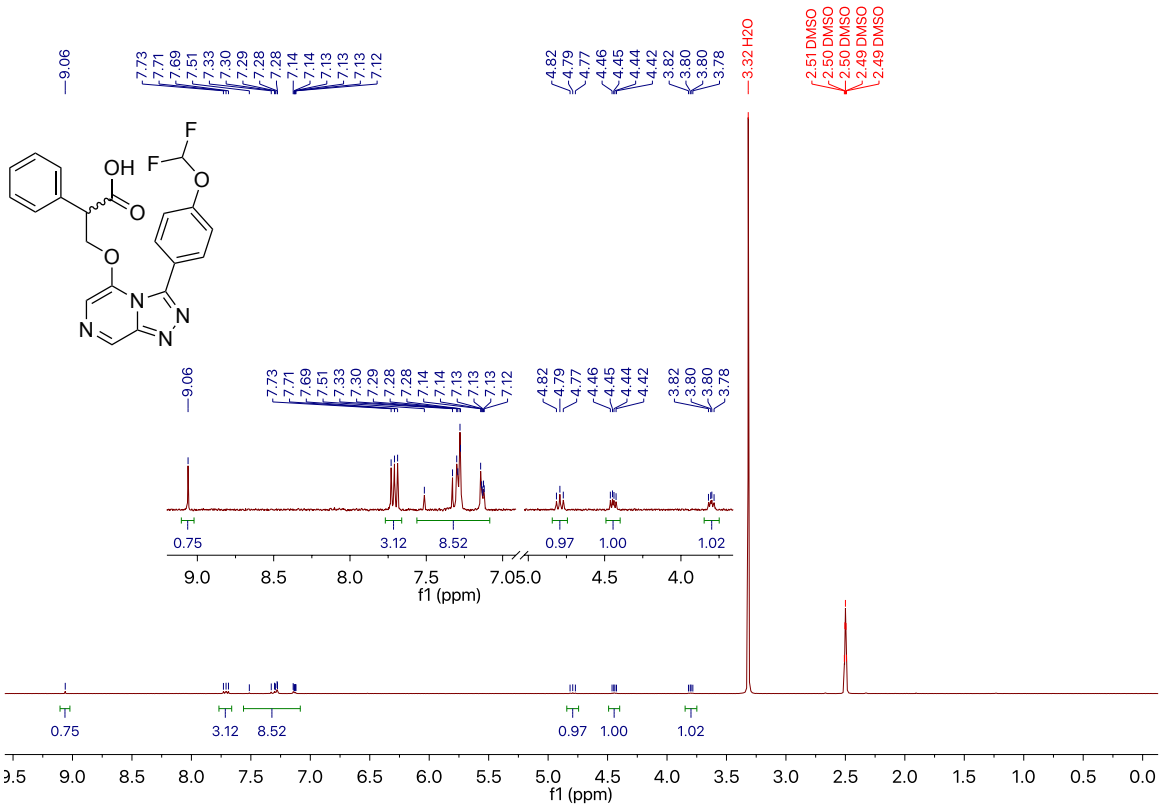

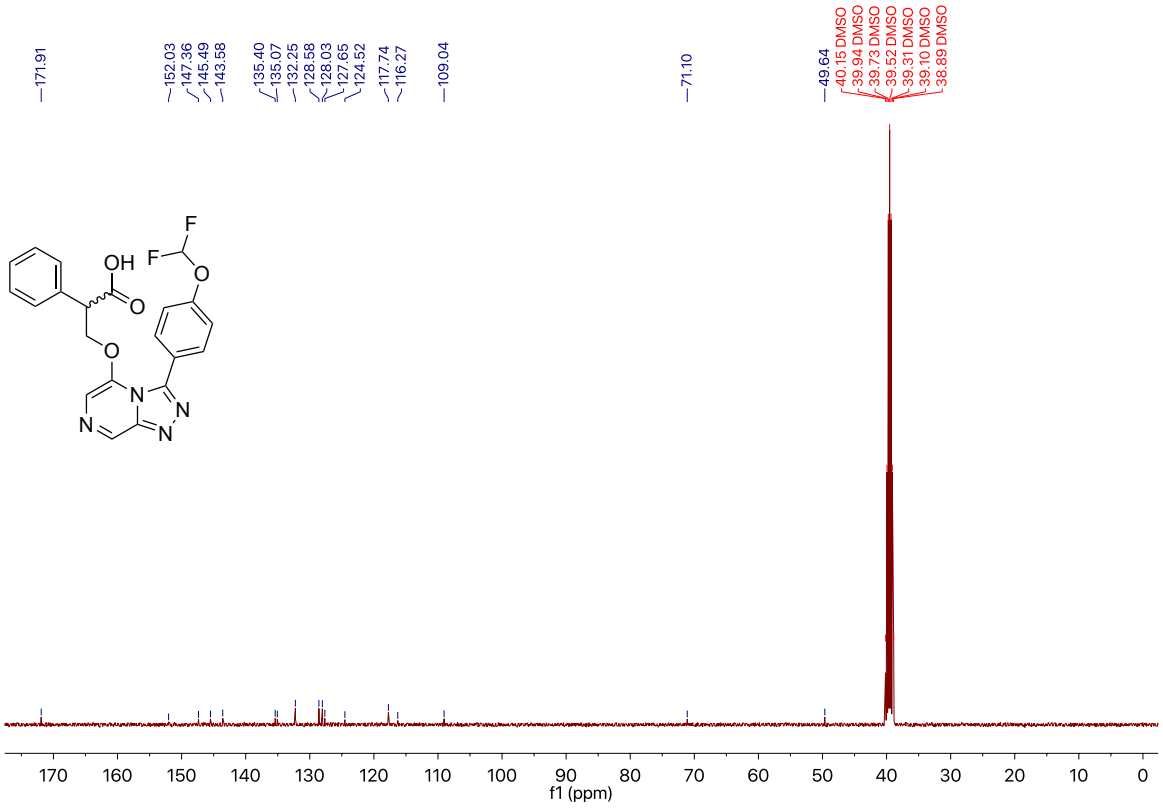

A.75 3-((3-(4-(Difluoromethoxy)phenyl)-[1,2,4]triazolo[4,3-*a*]pyrazin-5-yl) oxy)-2-(2-fluorophenyl)propan-1-ol 219

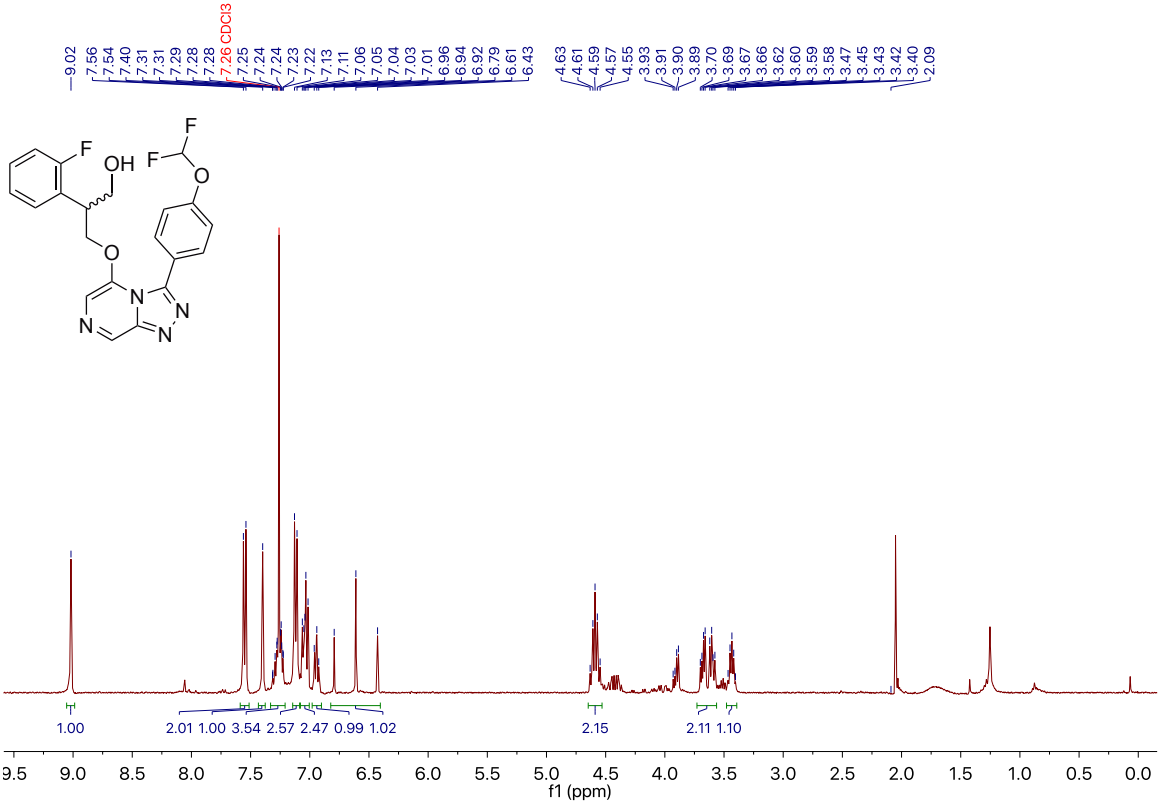

A.76 3-((3-(4-(Difluoromethoxy)phenyl)-[1,2,4]triazolo[4,3-*a*]pyrazin-5-yl) oxy)-2-(2,4,6-trifluorophenyl)propan-1-ol 221

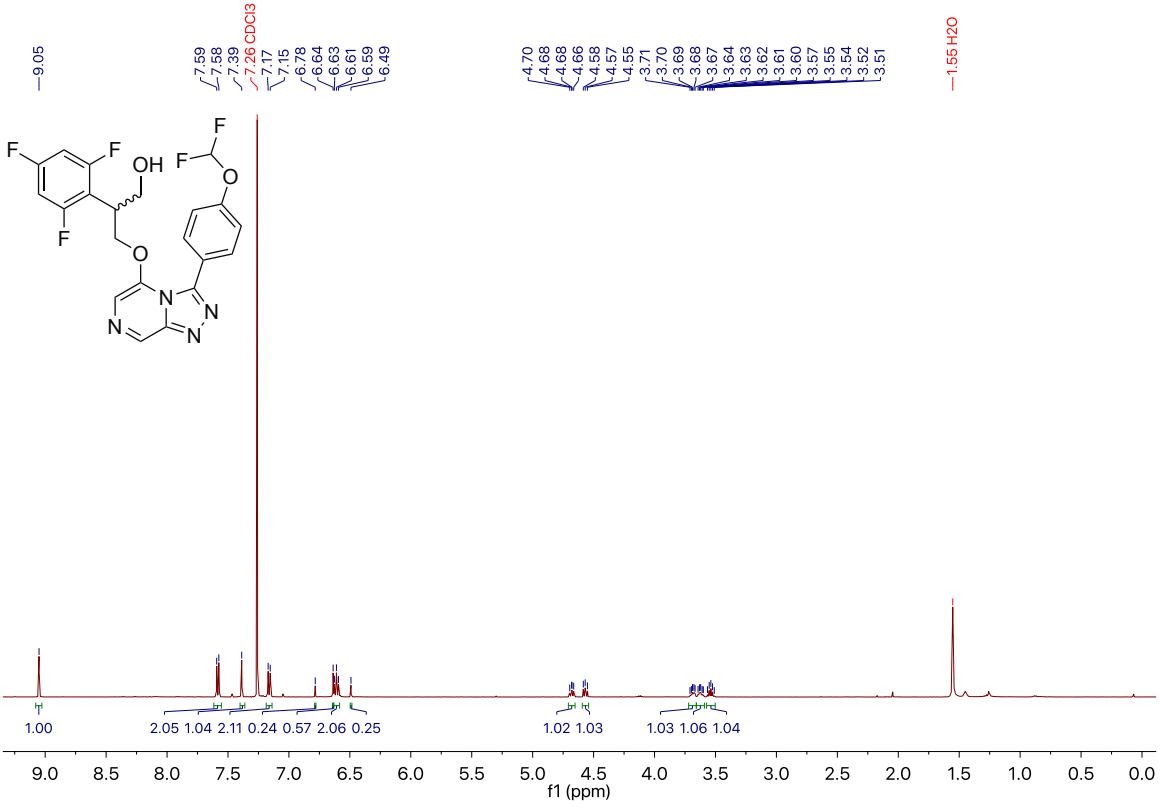

A.77 3-((3-(4-(Difluoromethoxy)phenyl)-[1,2,4]triazolo[4,3-*a*]pyrazin-5-yl) oxy)-2-(2,4,5-trifluorophenyl)propan-1-ol 222

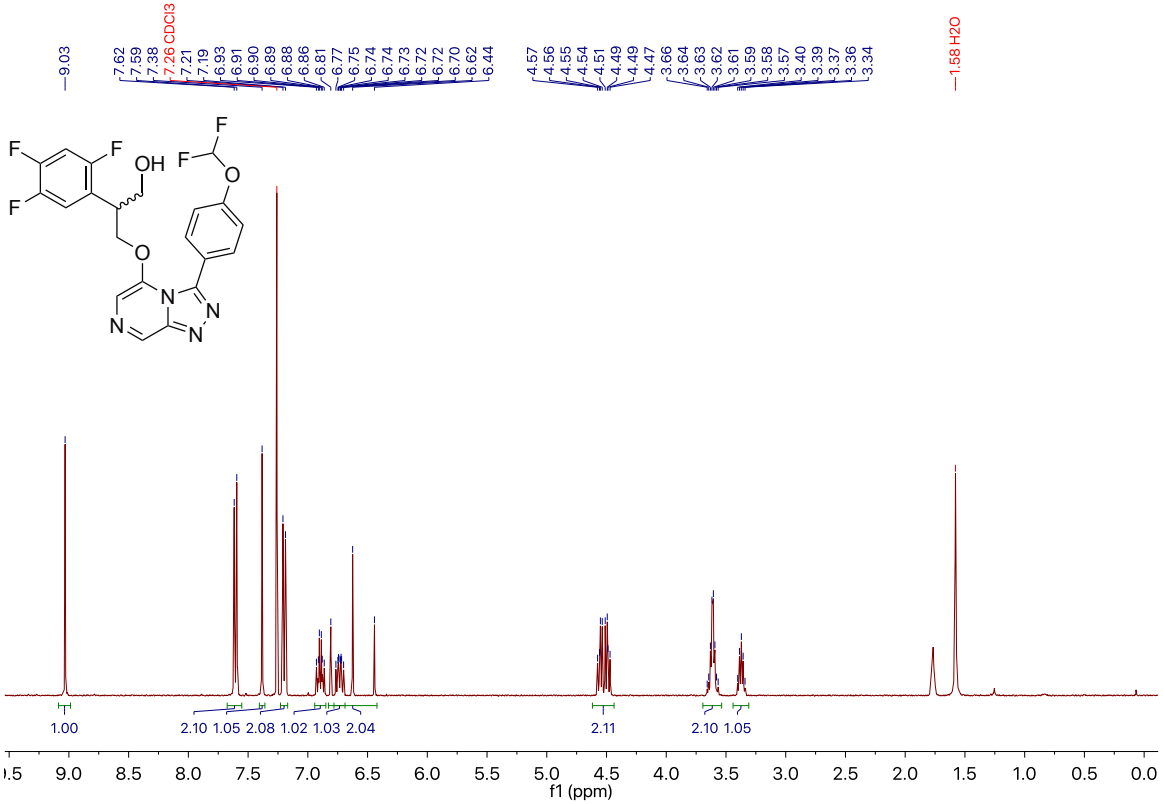

A.78 3-((3-(4-(Difluoromethoxy)phenyl)-[1,2,4]triazolo[4,3-*a*]pyrazin-5-yl) oxy)-2-(3-(trifluoromethyl)phenyl)propan-1-ol 224

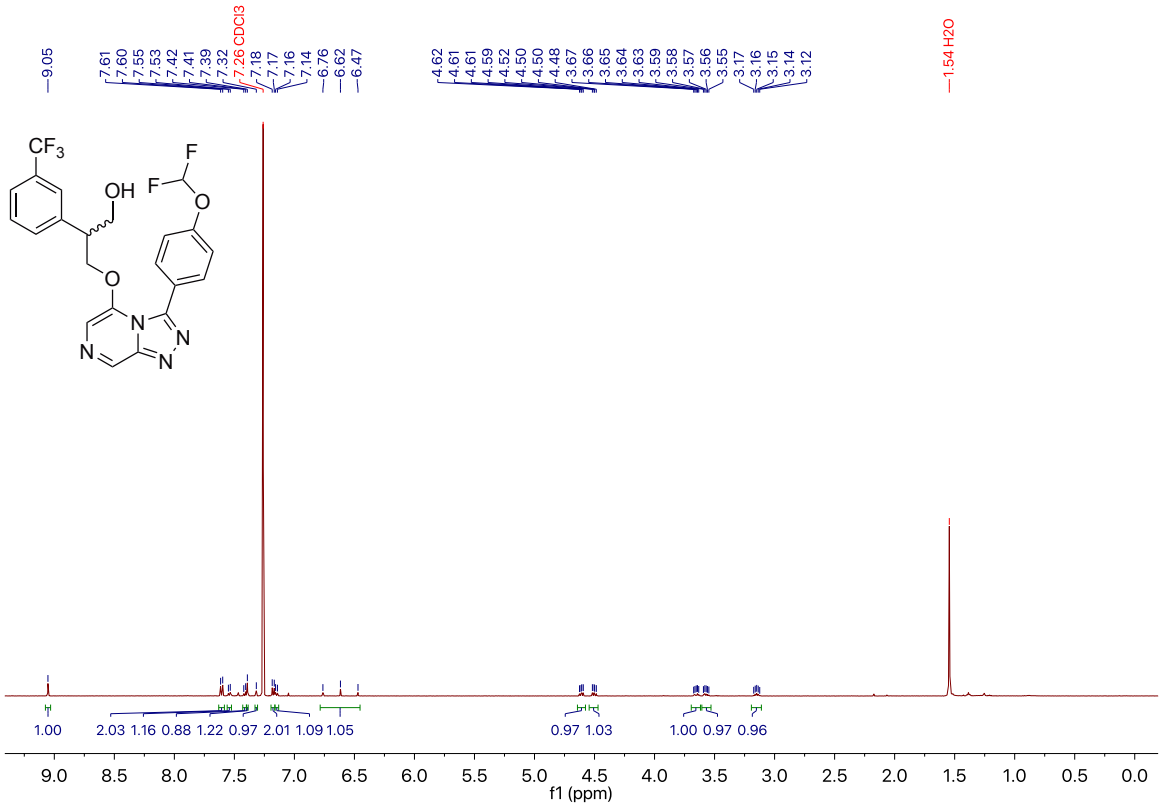

A.79 3-((3-(4-(Difluoromethoxy)phenyl)-[1,2,4]triazolo[4,3-*a*]pyrazin-5-yl) oxy)-2-(2-methoxyphenyl)propan-1-ol 226

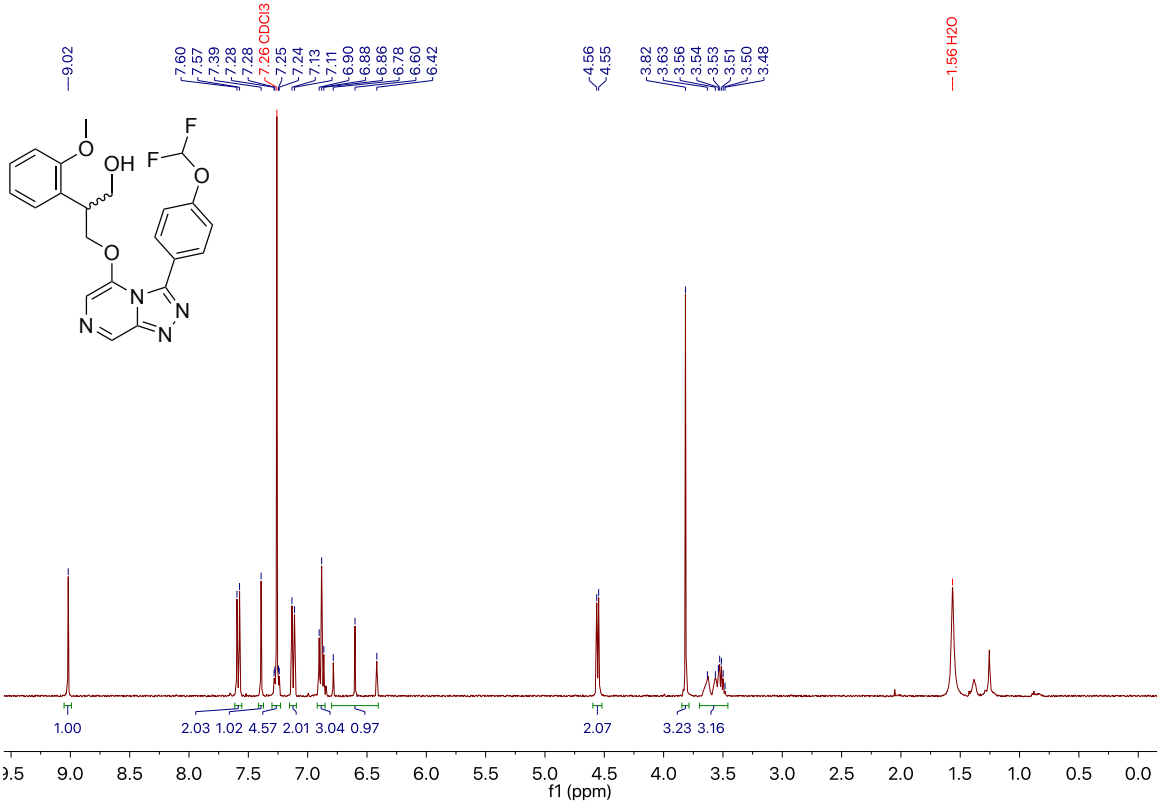

A.80 3-((3-(4-(Difluoromethoxy)phenyl)-[1,2,4]triazolo[4,3-*a*]pyrazin-5-yl) oxy)-2-(3-methoxyphenyl)propan-1-ol 227

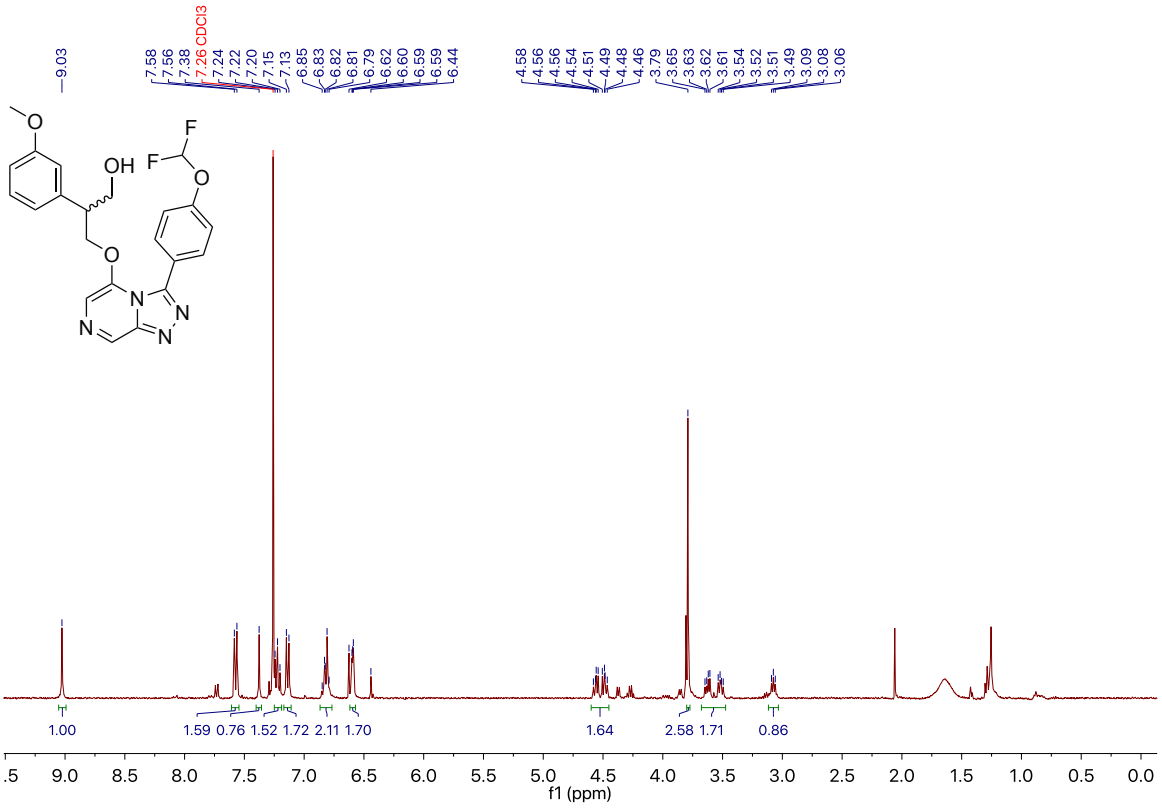

A.81 3-((3-(4-(Difluoromethoxy)phenyl)-[1,2,4]triazolo[4,3-*a*]pyrazin-8-yl) oxy)-2-(3-fluorophenyl)propan-1-ol 229

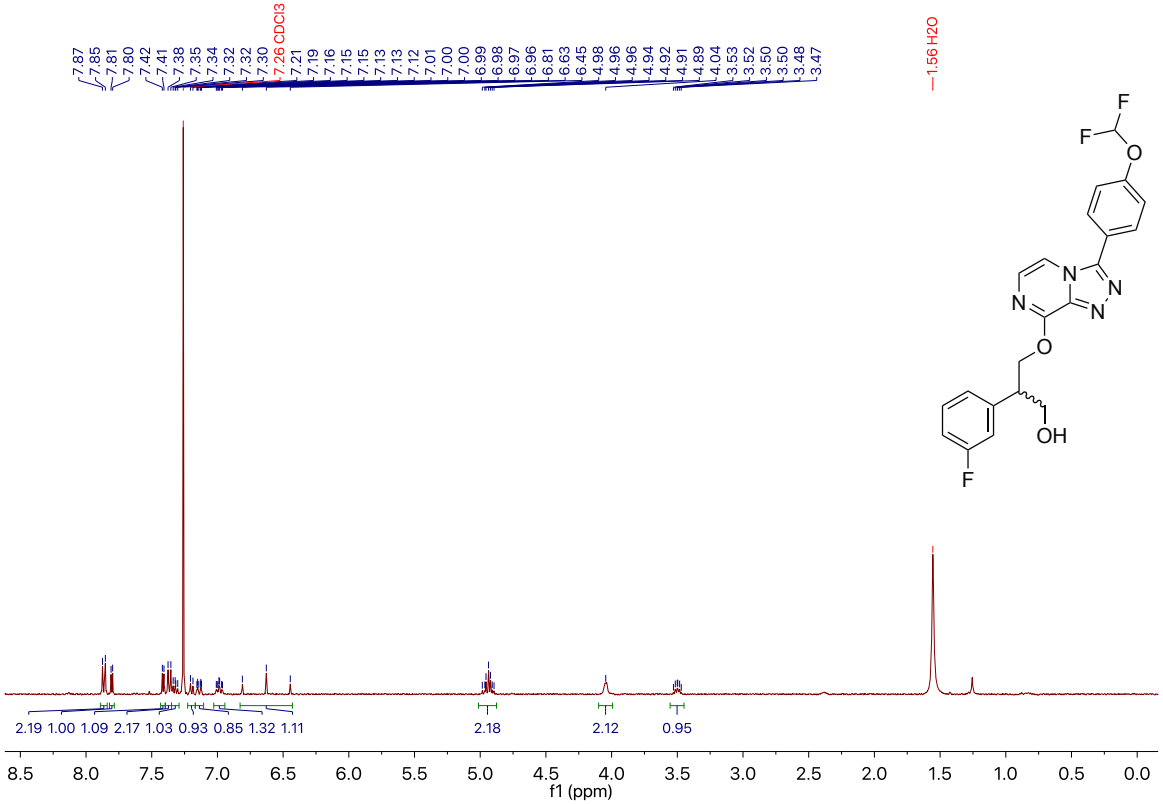

A.82 3-((3-(4-(Difluoromethoxy)phenyl)-[1,2,4]triazolo[4,3-*a*]pyrazin-8-yl) oxy)-2-(2,4,5-trifluorophenyl)propan-1-ol 230

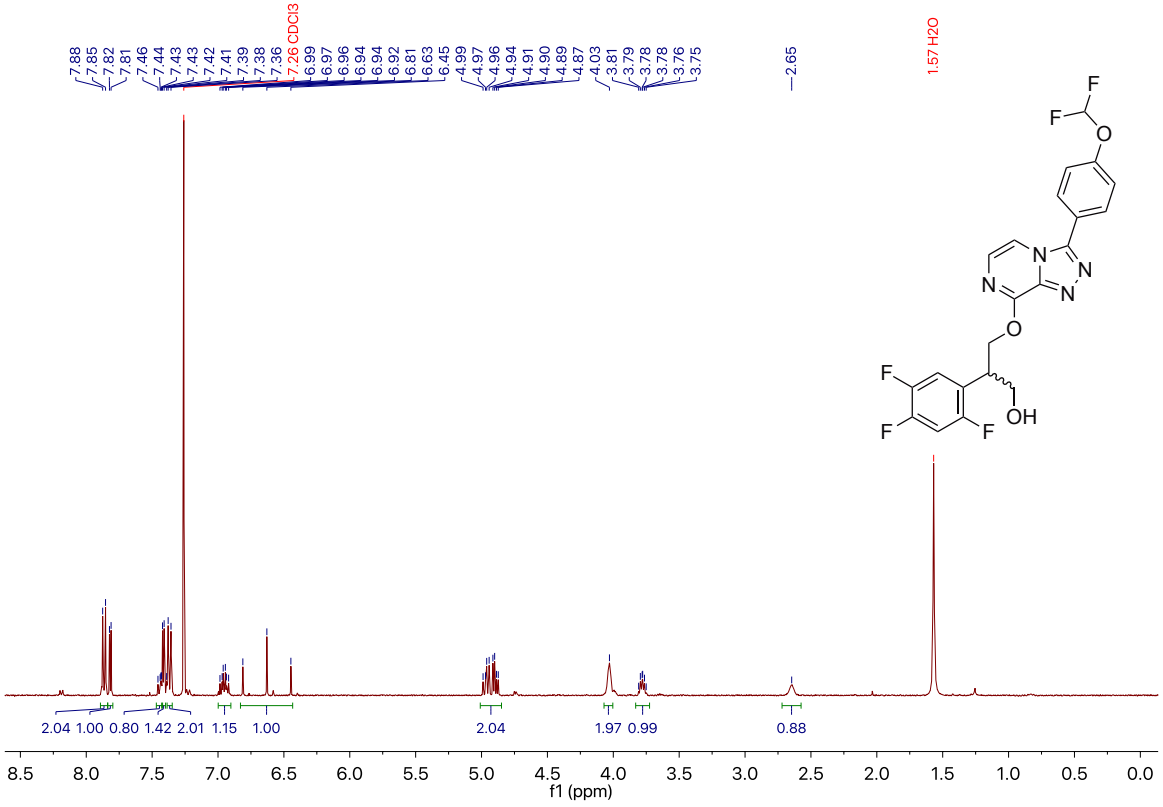

A.83 3-((3-(4-(Difluoromethoxy)phenyl)-[1,2,4]triazolo[4,3-*a*]pyrazin-5-yl) oxy)-2-(4-methoxyphenyl)propan-1-ol 233

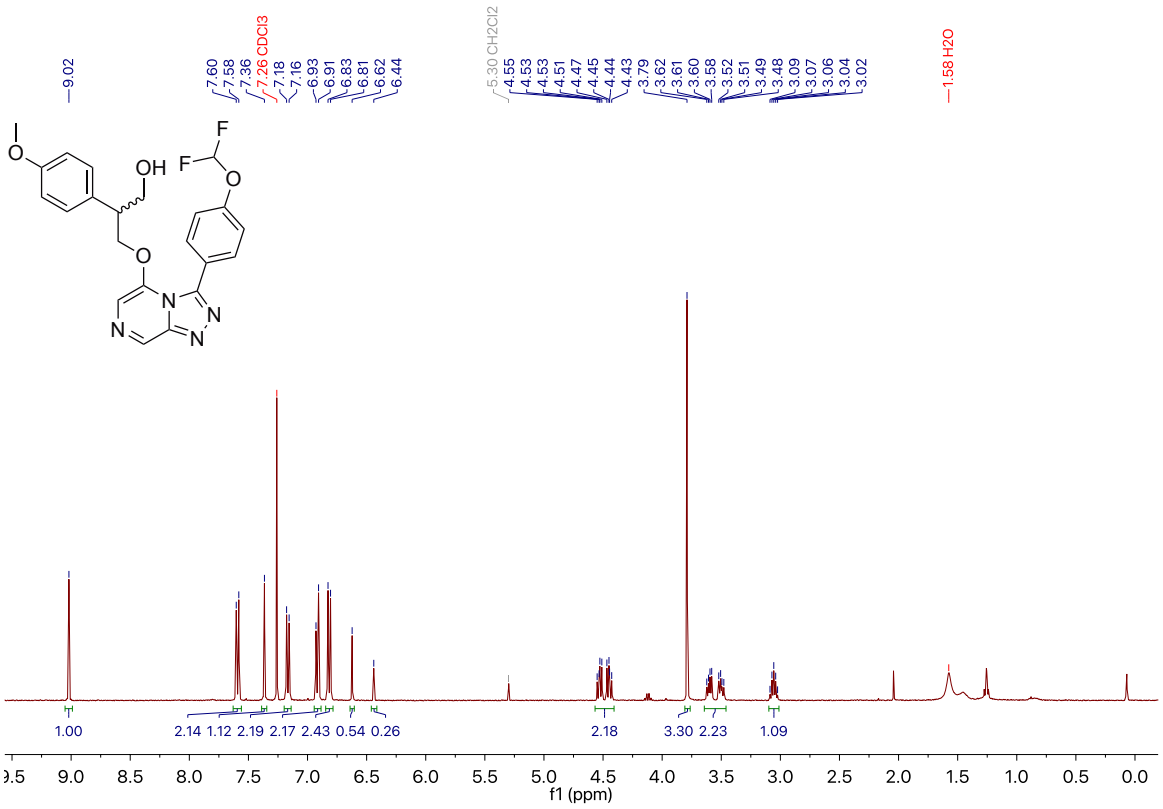

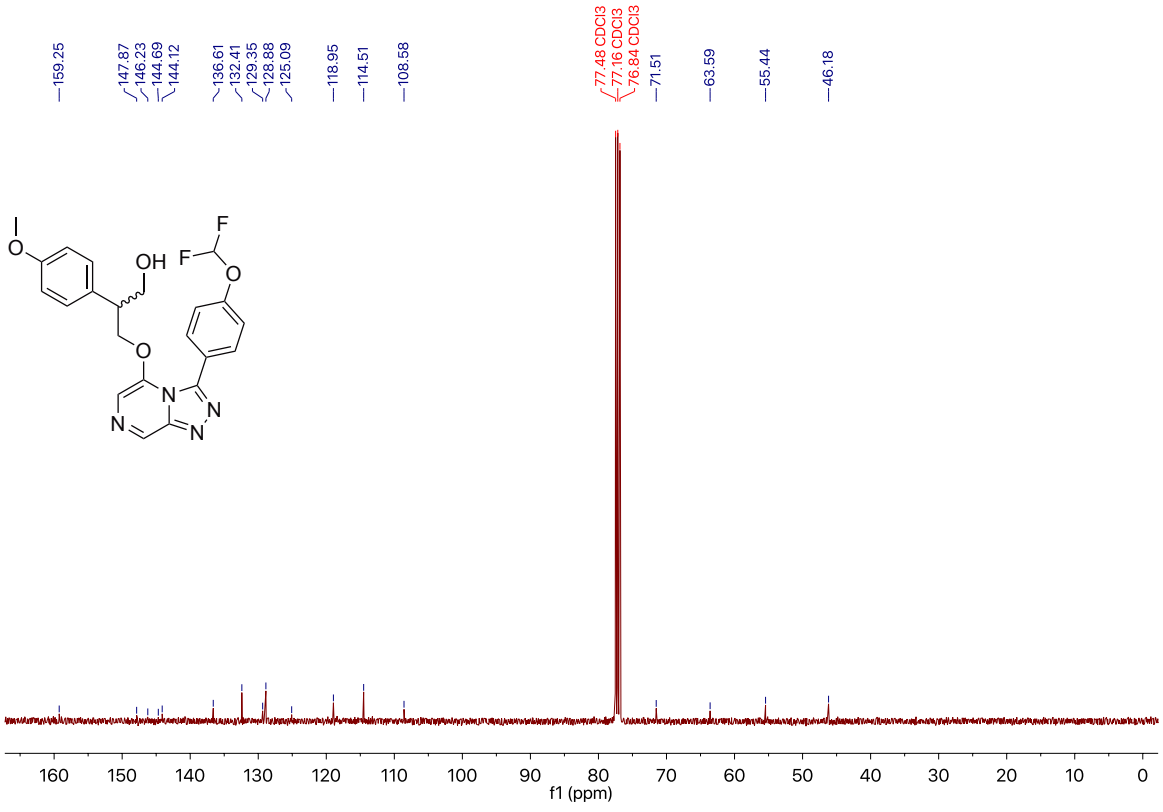

A.84 3-((3-(4-(Difluoromethoxy)phenyl)-[1,2,4]triazolo[4,3-*a*]pyrazin-5-yl) oxy)-2-(2,4,6-trifluorophenyl)propanoic acid 231

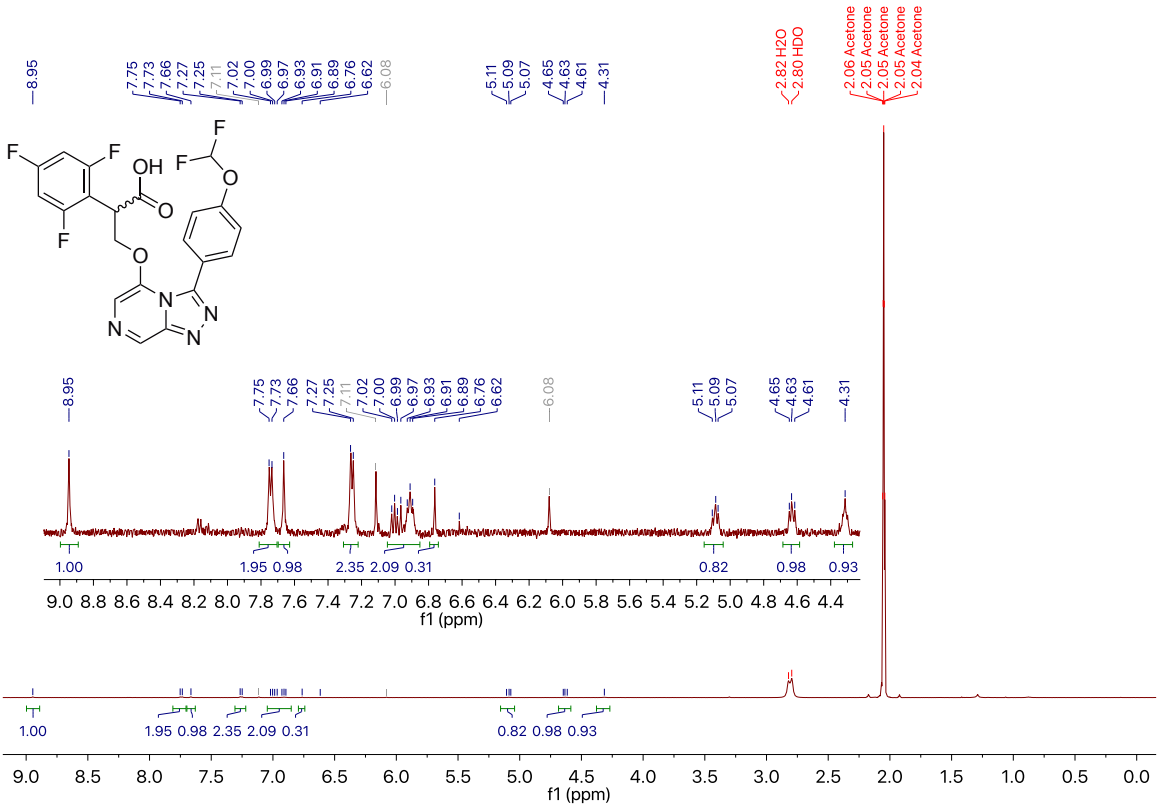

A.85 3-((3-(4-(Difluoromethoxy)phenyl)-[1,2,4]triazolo[4,3-*a*]pyrazin-5-yl) oxy)-2-(4-methoxyphenyl)propanoic acid 234

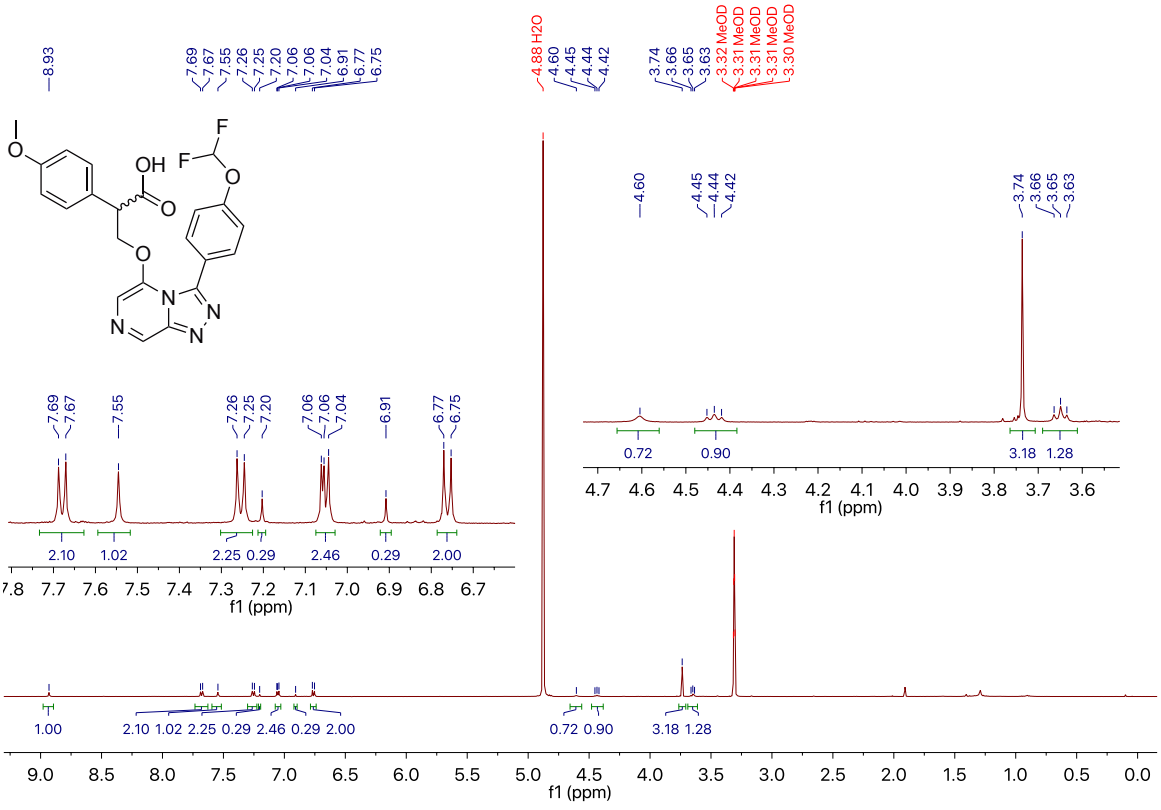

B. Experimental Biological Procedures

B.1 *In Vitro* Antiplasmodial Activity (Drug Discovery Unit, University of Dundee)

Cultures of the widely-used malaria reference strain of chloroquinine-sensitive *P. falciparum* strain 3D7 were maintained in a 5% suspension of human red blood cells cultured in RPMI 1640 medium supplemented with 0.5% Albumax II (available from Gibco Life Technologies, San Diego, CA, cat. no. 11021-037), 12 mM sodium bicarbonate, 0.2 mM hypoxanthine, (pH 7.3), and 20 mg/L gentamicin at 37 °C, in a humified atmosphere of 1% O_2, 3% CO_2 with a gas balance of nitrogen.

Growth inhibition of the *P. falciparum* cultures was quantified in a 10-point dose response curve with a 1 in 3 dilution series from a top assay concentration of 50 μM. This 384 well plate based fluorescence assay utilises the binding of SYBRgreen I (Thermo Fisher Scientific/Invitrogen cat. no. S7585) to double stranded DNA, which greatly increases the fluorescent signal at 528 nm after excitation at 485 nm. Mefloquine was used as a drug control to monitor the quality of the assay ($Z' = 0.6$ to 0.8, where Z' is a measure of the discrimination between the positive and negative controls on a screen plate). Dose-response curves were determined from a minimum of 3 independent experiments. Compound bioactivity was expressed as IC_{50}, the concentration of compound causing 50% inhibition. IC_{50} values were determined from a minimum of 3 independent experiments.

All data was processed using IDBS ActivityBase® raw data was converted into per cent inhibition through linear regression by setting the high inhibition control as 100% and the no inhibition control as 0%. Quality control criteria for passing plates were as follows: $Z' > 0.5$, S:B >3, $\%CV_{(\text{no inhibition control})} < 15$. The formula used to calculate $Z' = 1 - \frac{3\times(StDev_{high}+StDev_{low})}{ABS(Mean_{high}-Mean_{low})}$

All IC_{50} Curve fitting was undertaken using XLFit version 4.2 using Model 205 with the following 4 parametric equation: $y = A + \frac{B-A}{1+(C/x)^D}$, where A = % inhibition at bottom, B = % inhibition at top, C = IC_{50}, D = slope, x = inhibitor concentration and y = % inhibition. If curve did not reach 100% of inhibition, B was fixed to 100 only when at least 50% of inhibition was reached.

B.2 Cytotoxicity Studies (Drug Discovery Unit, University of Dundee)

In vitro cytotoxicity studies were carried out using HepG2 (Human Caucasian hepatocyte carcinoma, ECACC cat. no. 85011430) used as indicators for general mammalian cell toxicity. HepG2 *in vitro* cytotoxicity can be assessed using the assay procedure as described.[409]

B.3 Physicochemical and Metabolic Parameters (Centre for Drug Candidate Optimisation, Monash Institute of Pharmaceutical Sciences)

B.3.1 Kinetic Solubility Estimation using Nephelometry

Compound in DMSO was spiked into either pH 6.5 phosphate buffer or 0.01 M HCl (approx pH 2.0) with the final DMSO concentration being 1%. After 30 minutes had elapsed, samples were then analysed *via* Nephelometry to determine a solubility range.[410]

B.3.2 Distribution Coefficient Estimation using Chromatography

Partition coefficient values (LogD) of the test compounds were estimated at pH 7.4 by correlation of their chromatographic retention properties against the characteristics of a series of standard compounds with known partition coefficient values. The method employed is a gradient HPLC based derivation of the method developed by Lombardo.[411]

B.3.3 *In Vitro* Metabolic Stability

The metabolic stability assay was performed by incubating each test compound in liver microsomes at 37 °C and a protein concentration of 0.4 mg/mL. The metabolic reaction was initiated by the addition of an NADPH-regenerating system and quenched at various time points over a 60 minute incubation period by the addition of acetonitrile containing diazepam as internal standard. Control samples (containing no NADPH) were included (and quenched at 2, 30 and 60 minutes) to monitor for potential degradation in the absence of cofactor.

The human liver microsomes used in this experiment were supplied by XenoTech, lot # 1410230. The mouse liver microsomes used in this experiment were supplied by XenoTech, lot # 1510256. The rat liver microsomes used in this experiment were supplied by XenoTech, lot # 1510115. Microsomal incubations were performed at a substrate concentration of 1 μM.

Species scaling factors from Ring *et al.*[412] were used to convert the *in vitro* CL_{int} (μL/min/mg) to an *in vivo* CL_{int} (mL/min/kg). Hepatic blood clearance and the corresponding hepatic extraction ratio (E_H) were calculated using the well stirred model of hepatic extraction in each species, according to the "*in vitro* $T_{1/2}$" approach.[413] The E_H was then used to classify compounds as low (<0.3), intermediate (0.3–0.7), high (0.7–0.95) or very high (>0.95) extraction compounds.

B.4 Late-Stage Biofunctionalisation of Compounds 154 and 180 (Obach Lab, Pfizer)

Compound **154** (40 μM) was incubated with dog liver microsomes (1 mg/mL) in a total volume of 40 mL potassium phosphate buffer (0.1 M; pH 7.4) containing $MgCl_2$ (3.3 mM) and NADPH

(1.3 mM). The incubation was done in a 500 mL Erlenmeyer flask in a shaking water bath maintained at 37 °C open to the air. After 1 h, the incubation was terminated by addition of MeCN (40 mL) and the precipitated protein was removed by spinning at 1700 × g for 5 min. The supernatant was partially evaporated in a vacuum centrifuge for 1.5 h and to the remaining liquid was added formic acid (0.5 mL), MeCN (0.5 mL) and H_2O to a final volume of 50 mL. This mixture was spun in a centrifuge at 40000 × g for 30 min. The clarified supernatant was applied to a Varian Polaris C18 column (4.6 × 250 mm; 5 μm) at 0.8 mL/min through a Jasco HPLC pump. After the entire solution was applied and another 5 mL of 0.1% formic acid in H_2O was washed through the system, the column was moved to an HPLC-UV-MS (Thermo Velos LTQ mass spectrometer, equipped with a Waters Acquity HPLC-UV system) in line with a fraction collector (Leap Analytics). A mobile phase gradient was applied at 0.8 mL/min beginning with 2% MeCN in 0.1% aqueous formic acid, raised to 20% MeCN at 1 min, held until 5 min, then increased linearly to 55% MeCN at 80 min, followed by a 10 min wash at 95% MeCN and 10 min re-equilibration to initial conditions. Fractions were collected every 20 sec. Fractions predicted to contain products of interest eluted around 39.5 and 42.0 min and were individually analysed on a Thermo Orbitrap Elite UHPLC-UV-HRMS system to ascertain identity and purity for pooling and qNMR analysis. Pooled fractions were evaporated in a vacuum centrifuge and the residue was taken up in DMSO-d_6 (0.05 mL). Compound **180** was subjected to a similar procedure except that rabbit liver microsomes were used as the source of enzyme, the substrate concentration was 25 μM, and the incubation time was 45 min. The fractionation was carried out similarly, except that the MeCN composition was raised to 70% instead of 55%.

B.5 *P. falciparum* ATP4 Assay (Kirk Lab, Australian National University)

B.5.1 Na^+ Regulation

Each compound was initially tested at a concentration of 1 μM, then subsequently at 5 μM. For each compound, a 50 mM stock solution in DMSO was made, with an aliquot taken and diluted to form a 1 mM stock solution of the compound in DMSO. A further 1 μL aliquot of this 1 mM stock was then added to 24 μL of malaria saline (MS) solution. In a 96 well plate, the first column of wells (B2-E2) were loaded with 5 μL of a 0.1% v/v DMSO in MS negative control solution and the second column of wells (B3-E3) loaded with 5 μL of a 50 nM KAE609 in MS positive control solution. Subsequent wells (B-E; 4-8) were loaded with 5 μL of the compound in MS solution prepared above.

Immediately prior to performing the assay, a 195 μL suspension of trophozoite-stage *P. falciparum* parasites (isolated by saponin-permeabilisation of the erythrocyte membrane and loaded with

SBFI dye) was added to each well. The fluorescence was measured using a PerkinElmer LS 50B fluorescence spectrometer with a dual excitation fast filter accessory using excitation wavelengths of 340 nm and 380 nm. The emission was measured at 515 nm. After an arbitrary amount of time, the raw data was obtained and the fluorescence ratio was plotted against time to give a representation of the change in intracellular Na^+ concentration ($[Na^+]_i$) over time.

B.5.2 H^+ Regulation

The relationship between the fluorescence ration and the pH_i was calibrated by following literature procedures.[307] The calibration curve was constructed with solutions at pH 6.8, 7.1, 7.4 and 7.8 to give the equation: y = 4.738x - 27.275; R^2 = 0.9958.

Each compound was initially tested at a concentration of 1 μM. Select compounds were tested at 5 μM instead. A 1.5 mL suspension of BCECF-loaded trophozoite-stage *P. falciparum* parasites was placed in a centrifuge and the supernatant removed. The cells were re-suspended in 1 mL of MS solution and transferred to a cuvette. The fluorescence was measured using a PerkinElmer LS 50B fluorescence spectrometer with a dual excitation fast filter accessory using excitation wavelengths of 490 nm and 440-450 nm. The emission was measured at 520 nm. The fluorescence ratio was monitored until no change was observed. A 1 μL aliquot of compound (solution prepared above) was quickly added and mixed in the cuvette and the change in fluorescence monitored. When the fluorescence change plateaued, a 1 μL aliquot of concanamycin A (100 nM) was quickly added and mixed, leading to a rapid decrease in fluorescence. Between runs of 4-5 compounds, either a positive (50 nM KAE609) or negative control (DMSO) was run to ensure the assay was generating the correct fluorescence ratios. The raw data was obtained and the fluorescence ratio was plotted against time to give a representation of the change in cytosolic pH (pH_i) over time.

B.6 hERG Patch Clamp Assay (Victor Chang Cardiac Research Institute)

Chinese Hamster Ovary (CHO) cells were used for electrophysiological patch clamp recordings due to their low levels of endogenous K^+ current, which allows for more accurate characterisation of Kv11.1 channel current. Cells were cultured in Ham's F12 Nutrient Mixture (Thermo Fisher Scientific Australia) supplemented with 5% foetal bovine serum (FBS), at 37 °C and 5% CO_2. CHO cells stably expressing WT Kv11.1 were passaged using TrypLE^{TM} Express (Thermo Fisher Scientific Australia). Cells were incubated for 48 hours at 37 °C before patch clamp experiments were performed.

B.6.1 Automated Patch Clamp

CHO cells stably expressing WT Kv11.1 were detached from the culture flask using Accumax (Sigma-Aldrich, USA), spun at 300 g for 5 mins, then resuspended in divalent free solution (in mM: NaCl 140, KCl 5, HEPES 10, D-Glucose 5; adjusted to pH 7.4 with NaOH), supplemented with 10% DMEM media. Cells were allowed to recover for 30 minutes at 10 °C while shaking on a rotating platform at 500 rpm before recording.

Automated patch clamp recordings were performed using the Syncropatch 384 PE platform (Nanion Technologies, Munich, Germany) at room temperature (∼25 °C). Single-hole 384-well recording chips with medium resistance (4–4.5 MΩ) were used and recordings were performed in the whole cell voltage clamp configuration. External recording solution contained (in mM): NaCl 140, KCl 5, $CaCl_2$ 2, $MgCl_2$ 1, HEPES 10, D-Glucose 5; adjusted to pH 7.4 with NaOH. Cell sealing was aided using a modified external solution containing 10 mM $CaCl_2$. The internal solution contained the following (in mM): KF 110, KCl 10, NaCl 10, HEPES 10, EGTA 10; adjusted to pH 7.2 with KOH. Automated patch clamp workflows were performed using Biomek software v4.1 (Beckman Coulter) and data were acquired at a sampling rate of 5 to 10 kHz, depending on the protocol, using PatchControl384 v1.5.6 software (Nanion Technologies).

Data analysis was performed using DataControl384 v1.5.2 software (Nanion Technologies, Munich, Germany). Stringent quality control criteria were used to determine the individual cell recordings to be included for final data analysis: Seal resistance $\geq$0.5 GΩ; series resistance $\leq$20 MΩ; and cell capacitance between 5 to 50 pF. Results are expressed as mean ± SEM.

C. Calculated Surfaces from UCSF Chimera

Images of the molecular surfaces from crystal structure files of phenyl bioisosteres that were used to calculate the surface areas and volumes. Mesh surfaces are shown around each structure. Centre structure is benzene. Structures clockwise from top are cubane, adamantane, BCP, norbornene, *o*-carborane, *m*-carborane and *p*-carborane.

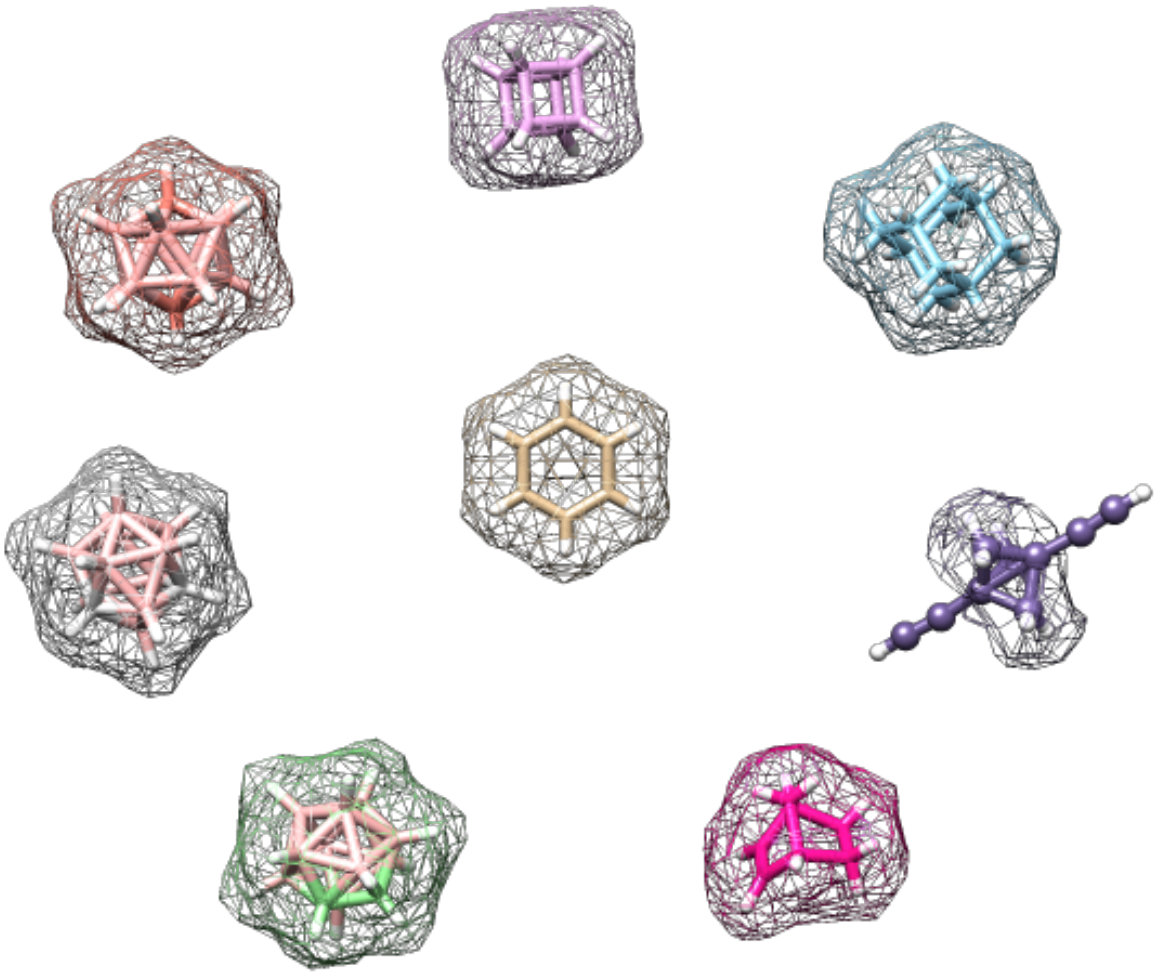

D. Screenshots of Posts from Labtrove

Screenshots of referenced posts from the original OSM ELN (Labtrove).

D.1 Screenshot for Reference[170]

Appeal for assistance on methods for difluoromethylation of AEW 103

7th January 2014 @ 08:18

The OSM team are currently trying to synthesise some triazalopyrazines (series 4) that were found to be promising antimalarial starting points by big pharma.

I (Alice in Mat Todd's group at the University of Sydney) am currently attempting to resynthesise MMV670652 in order to confirm the activity of the racemate and subsequently determine the activity of each enantiomer following resolution.

I have been following a procedure provided by the CRO who had worked on these compounds. (The synthetic route and target are described in more detail here and preparative data found within:

FINAL REPORT MMV670652.doc

The CRO used Freon gas to difluoromethylate AEW 103 (alcohol SM shown below) but unfortunately, due to limitations on the availability of Freon-22 in Australia, the team need to find an alternative method for this transformation:

A review by Jinbo Hu, Wei Zhang and Fei Wang (DOI: 10.1039/b916463d) revealed a variety of methods for selective difluoromethylation and included a chapter on electrophilic difluoromethylation.

'The most widely used method for the incorporation of a CF_2H group into nucleophiles (such as oxygen-, nitrogen-, sulfur-, phosphorus-, and carbon-nucleophiles) is the reaction of the corresponding nucleophile with a proper difluorocarbene reagent.'

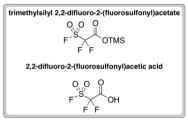

One paper referenced (DOI 10.1021/jm900716v) used trimethylsilyl 2,2-difluoro-2-(fluorosulfonyl)acetate or 2,2-difluoro-2-(fluorosulfonyl)acetic acid (shown above) to enable difluoromethylation of 3,6-dimethyl-5-nitropyridin-2-ol (shown below):

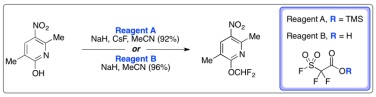

The review focused on methods for phenolic difluoromethylation and when surveying the literature, examples of difluoromethylation of aliphatic alcohols were found to be scarce and use free radical methods for the introduction of the group. In September's online meeting, Joie Garfunkel (MMV) suggested the use of trimethylsilyl 2,2-difluoro-2-(fluorosulfonyl)acetate in combination with a copper catalyst in MeCN at elevated temperatures and pressures (Joie's colleagues had used this method at Merck).

The methods I have attempted so far involved the use of the difluorocarbene generating reagent trimethylsilyl 2,2-difluoro-2-(fluorosulfonyl)acetate. I followed the prep. outlined in the paper and began to explore the reaction with copper at room temperature and then in a sealed tube. So far, I haven't had great success with this reaction.

Representative Reactions	
CsF, NaH, rt, 30 mins	- *Possible trace - methyl ester not present*
CsF, NaH, rt, 1h	- *SM isolated and separate 'grease' spot*
CuI, NaH, rt, 30 mins	- *no reaction*
CuI, NaH, 100 °C (sealed tube), 30 mins	- *no reaction*
CuI, rt, 30 mins	- *no reaction*
CuI, 100 °C (sealed tube), 30 mins	- *decomposition*

I'm going to try some more conditions and also the use of the more toxic 2,2-difluoro-2-(fluorosulfonyl)acetic acid but would be most grateful for any ideas or assistance in how to get this reaction to work.

Additionally, prefered methods for the trifluoromethylation of the same substrate would be greatly appreciated.

D.2 Screenshot for Reference[199]

Synthesis of (R)-1-((3-(4-chlorophenyl)-[1,2,4]triazolo[4,3-a]pyrazin-5-yl)oxy)-3-phenylpropan-2-amine (JU 23-1)

21st August 2014 @ 00:39

Synthesis of an ether with a 4 atom chain to further explore the effect of chain length on the ether series.

GitHub Issue: #254

Literature ref: 10.1021/jo901707x

Reaction Scheme

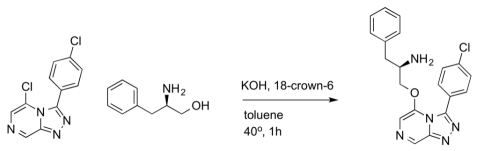

Procedure

Started 3:20pm

(*R*)-2-amino-3-phenylpropan-1-ol (100 mg, 0.66 mmol, 1.1 equiv) was added to 1.5 mL toluene along with JU 8 (157 mg, 0.59 mmol, 1 equiv), potassium hydroxide (110 mg, 1.96 mmol, 3.3 equiv) and 18-crown-6 (9 mg, 0.03 mmol, 0.05 equiv). The reaction was stirred at 40°C (bath temperature) for 1 h. Analysis by TLC showed the reaction was complete.

TLC JU 23-1 50:50 EtOAc:Hex 1 h.jpg

The reaction was stopped and cooled before diluting with water (6 mL). The aqueous layer was extracted with EtOAc (4 x 5 mL). The combined organic layers were washed with water (3 x 6 mL) until pH 9, then with brine (5 mL). The organic layers were dried over Na_2SO_4 and the solvent removed by rotary evaporation. The crude product (129 mg, 58%) was dried in vacuo and analysed by 1H NMR.

1H NMR, crude, DMSO, 200 MHz

JU 23-1 crude 200 MHz.pdf

JU 23-1 crude.zip

The crude material was purified using the biotage isolera, see run details below.

1H NMR, green frac, DMSO, 200 MHz

JU 23-1 green frac 200 MHz.pdf

JU 23-1 green frac pure.zip

1H NMR, yellow frac, DMSO, 200 MHz

JU 23-1 yellow frac 200 MHz.pdf

JU 23-1 yellow frac pure.zip

From the NMRs, it appears that this reaction was unsuccessful, neither SM or product can be seen. This needs to be attempted again, this time by protecting the free amine first before coupling to the triazolopyrazine.

D.3 Screenshot for Reference [308]

Evaluation of Series 4 Compounds vs ATP4-Resistant Mutants

22nd January 2015 @ 23:47

Melanie Ridgeway in Kiaran Kirk's laboratory completed some cross-resistance studies, looking at growth-inhibition by several of the OSM Series 4 compounds of several Kirk ATP4 mutant strains (generated by long-term exposure to increasing concentrations of three Malaria Box hits, as documented in their recent paper).

The data are attached to this post. Each graph is averaged from three independent experiments. **Upshot: Data are supportive of Series 4 targeting ATP4.**

Series 4 growth assays[1].pdf

Each of the six panels shows the response of four strains (the Dd2 parent and three different PfATP4 mutants) to a different compound. Panels A-C show growth inhibition by three different Series 4 compounds. Panel D shows growth inhibition by NITD/KAE 609. Panels E and F show growth inhibition by chloroquine and artemisinin.

The three mutant PfATP4 strains show resistance to all three of the Series 4 compounds (Panels A-C) and to NITD609 (Panel D), providing further evidence of a common mechanism of action.

(Note: For two of the three mutant strains there is no significant shift of the chloroquine or artemisinin dose-response curves. But for one of the three mutants there is what appears to be small shifts in the artemisinin and chloroquine dose-response curves, with the artemisinin and chloroquine curves shifted in opposite directions. The meaning of this is currently unclear.)

Attribution for these data: Kiaran Kirk, Adele Lehane, Melanie Ridgeway. Received by email to Mat Todd, 20th October 2014.

Compound Structures:

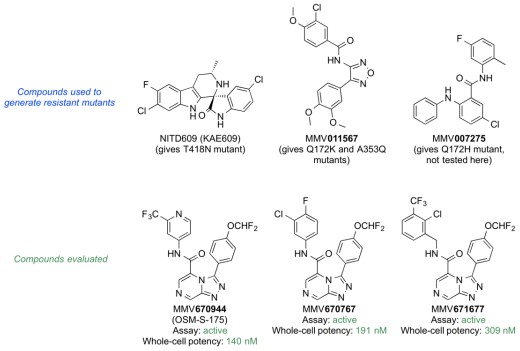

D.4 Screenshot for Reference [309]

Pharmacophore Modelling of the Malaria Box PfATP4 Active Compounds.

16th June 2015 @ 13:05

The following 28 Malaria Box compounds, found to cause disruption against Na+ regulation in PfATP4 were used to search for common pharmacophore features.

Accerlys Discovery Studio was used running the Common Feature Pharmacophore Generation protocol.

Input Files

Protocol Parameter File

Protocol.pr_xml

Input SD file

Malaria_Box_active_cl

Input SMILES and InChI codes

input_smiles.txt

The protocol produced 10 four-feature models, upon inspection of poses and score the following model was selected to be taken forward.

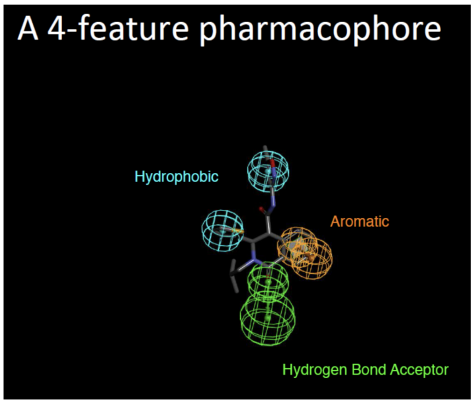

Fine tuning the model

The 28 active compounds aligned to the pharmacophore were used to create a shape feature that could be used to manually predict the shape of the active site. 10 exclusion features were then added in areas where high scoring, inactive ligands penetrated out of this shape. The shape feature itself was never used as a query feature and was never intended to be used as such.

D.5 Screenshot for Reference [310]

Using the Pharmacophore Model to search Commercial Compounds for new leads

16th June 2015 @ 14:07

The pharmacophore model produced in Pharmacophore Modelling of the Malaria Box PfATP4 Active Compounds. was used to screen the Maybridge library to select a small and diverse selection of molecules to test in the PfATP4 assay.

Using Accelrys Discovery Studio, the search 3D database protocol was ran.

Input Files

Protocol.pr_xml

exclusion10_01.chm

The results were then manually filtered based on fit value, pose, shape, fit with "cavity feature" and diversity.

The final selection included 18 compounds with fitValues ranging between 3.88 and 3.66.

selected_and_ordered

round01_18ordered.sd

D.6 Screenshot for Reference[348]

hERG Data for MMV669844 and MMV670944

4th April 2014 @ 04:26

hERG data were obtained by MMV from Essen Bioscences. Report attached.

Summary:

MMV669844 and MMV670944 were both active in this assay with pIC50 values of 5.2 and 5.6.

And solubility issues were observed for compound MMV669844 at 33 uM in the final assay plate.

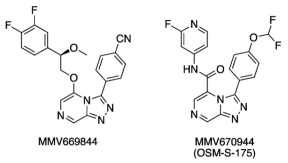

Preparation of OSM-S-175

Series 4 wiki

Data discussed briefly during OSM Online Project Meeting 7 (27th March 2014)

D.7 Screenshot for Reference[349]

Compounds sent for evaluation against the hERG ion channel at AstraZeneca

22nd September 2014 @ 05:02

Background

A selection of Series 4 compounds were sent for evaluation again the hERG ion channel using a "*medium-throughput electrophysiology-based hERG assay using IonWorks™ HT*" at AstraZeneca.

The compounds were selected from compounds synthesised at The University of Sydney (biological data here) and also those inherited from MMV following online discussion (see GitHub Issue #211).

Results

(updated by Mat, original file still attached below. Reason for update: units provided in AZ assay were micromolar, as an IC50. These have been converted into the more standard pIC50, which is -log of the IC50 when expressed in Molar and is unitless)

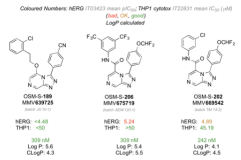

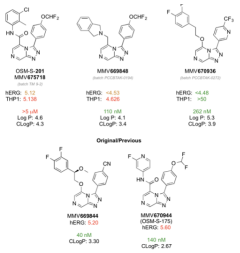

Graphical Representation of ClogP vs -p(IC50) and LogP vs -log10(IC50)

(updated by Mat, original file still attached below)

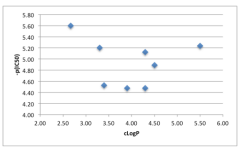

Preliminary Conclusions

Initial examination of the new data suggests that amides/amines show problematic hERG activity whereas ethers are tolerated. However, it is also possible that the Para $OCHF_2$ ether is the problem.

One of the original two data points (for MMV669844) shows that a compound lacking both is still active in the assay, so the answer is more subtle. There is little correlation between CLogP and hERG activity, but clogp is an approximation to actual solubility.

Future Work

The team need to synthesise some amides containing the para-nitrile aromatic group (or pyridyl) on the 'right-hand-side' in order to determine whether amides containing different aryl groups show hERG activity. Despite these data, *only* compounds possessing lower LogP values should be synthesised in the next round to aid solubility, and this will provide more data for the hERG/logP correlation. Following the next two rounds of synthesis and evaluation, more compounds will be evaluated in this assay.

General Assay Principle

"The hERG-expressing Chinese hamster ovary K1 (CHO) cells described by Persson, Carlsson, Duker, and Jacobson (2005) were grown to semi-confluence at 37 °C in a humidified environment (5% CO2) in F-12 Ham medium containing L-glutamine, 10% foetal calf serum (FCS) and 0.6 mg/ml hygromycin (all Sigma- Aldrich). Prior to use, the monolayer was washed using a pre- warmed (37 °C) 3 ml aliquot of Versene 1:5000 (Invitrogen). After aspiration of this solution the flask was incubated at 37 °C in an incubator with a further 2 ml of Versene 1:5000 for a period of 6 min. Cells were then detached from the bottom of the flask by gentle tapping and 10 ml of Dulbecco's phosphate-buffered saline containing calcium (0.9 mM) and magnesium (0.5 mM) (PBS; Invitrogen) was then added to the flask and aspirated into a 15 ml centrifuge tube prior to centrifugation (50xg, for 4 min). The resulting supernatant was discarded and the pellet gently re- suspended in 3 ml of PBS. A 0.5 ml aliquot of cell suspension was removed and the number of viable cells (based on trypan blue exclusion) was determined in an automated reader (Cedex; Innovatis) so that the cell re-suspension volume could be adjusted with PBS to give the desired final cell concentration. It is the cell concentration at this point in the assay that is quoted when referring to this parameter. CHO-Kv1.5 cells, which were used to adjust the voltage offset on IonWorksTM HT, were maintained and prepared for use in the same way."

Reference

Bridgland-Taylor MH, Hargreaves AC, Easter A, Orme A, Henthorn DC, Ding M, Davis AM, Small BG, Heapy CG, Abi-Gerges N, Persson F, Jacobson I, Sullivan M, Albertson N, Hammond TG, Sullivan E, Valentin J-P, Pollard CE (2006) Optimisation and validation of a medium-throughput electrophysiology-based hERG assay using IonWorks™HT. Journal of Pharmacological and Toxicological Methods 54: 189-199 (10.1016/j.vascn.2006.02.003)

Post originally authored by Alice E Williamson

E. Alternative Codes for Final Compounds

Alternative codes for the final compounds synthesised and discussed throughout this thesis. Internal codes refer to the persons initials who synthesised the compound. OSM codes are assigned as part of the OSM project. MMV codes are assigned as part of the MMV registration process.

Chapter 2 Compounds

Compound	Internal	OSM	MMV
11	EGT 90-1	OSM-S-293	MMV663915
12	AEW 302-1	OSM-S-272	MMV639565
13	AEW 296-1	OSM-S-366	MMV670936
14	INHERITED	OSM-S-218	MMV669844
15	EGT 171-1	OSM-S-390	MMV672687
16	EGT 119-3	OSM-S-279	MMV688896
17	INHERITED	OSM-S-377	MMV670652
18	INHERITED	OSM-X-002	MMV670437
22	PCCBTAK-0194	OSM-S-380	MMV669848
23	INHERITED	OSM-S-381	MMV670947
19	EGT 95-3	OSM-S-367	MMV670246
20	EGT 141-1	OSM-S-379	MMV670767
21	AEW 300-1	OSM-S-175	MMV670944
24	EGT 198-1	OSM-S-353	MMV693155
25	EGT 137-1	OSM-S-278	MMV688895
26	TM 9-2	OSM-S-201	MMV675718
27	TM 19-2	OSM-S-204	MMV675946
28	TM 26-1	OSM-S-254	MMV675947
29	AEW 313-1	OSM-S-218	MMV897709
30	EGT 169-1	OSM-S-389	MMV897763
31	EGT 111-1	OSM-S-177	MMV669000

Chapter 3 Compounds

Compound	Internal	OSM	MMV
56	EGT 354-1	OSM-S-579	MMV1581345
57	EGT 96-1	OSM-S-368	MMV897697
58	EGT 92-1	OSM-S-369	MMV897698
59	EGT 353-1	OSM-S-578	MMV1581344
60	EGT 355-1	OSM-S-580	MMV1581346
61	JU 9-1	OSM-S-188	N.A.
62	JU 6-3	OSM-S-187	N.A.
63	EGT 48-2 (f10-20)	OSM-S-359	MMV693161
64	EGT 52-1 (f6-10)	OSM-S-571	MMV1581336
71	EGT 45-1	OSM-S-360	MMV693162

72	EGT 63-1	OSM-S-364	MMV693167
73	EGT 39-1	OSM-S-361	MMV693163
74	EGT 60-1	OSM-S-365	MMV693166
75	EGT 48-2 (f5-7)	OSM-S-570	MMV1581335
76	EGT 52-2 (f2-5)	OSM-S-363	MMV693164
78	EGT 51-4	OSM-S-362	MMV693165
83	EGT 101-1	OSM-S-373	MMV897702
84	EGT 82-1	OSM-S-372	MMV897701
85	N.A.	OSM-S-283	MMV688899
86	AEW 214-1	OSM-S-281	MMV688898
87	INHERITED	OSM-X-010	MMV671651
88	INHERITED	OSM-X-067	MMV670763
89	INHERITED	OSM-X-030	MMV671647
90	INHERITED	OSM-X-003	MMV672936
91	INHERITED	OSM-X-006	MMV672727
92	INHERITED	OSM-X-004	MMV672723
93	INHERITED	OSM-X-022	MMV670438
97	EGT 190-3	OSM-S-392	MMV1557932
98	EGT 191-1	OSM-S-393	MMV1557933
100	EGT 273-1	OSM-S-423	MMV1576789
105	EGT 225-1	OSM-S-400	MMV1557940
108	EGT 236-2	OSM-S-419	MMV1576785
113	EGT 182-3	OSM-S-431	MMV1576792
114	EGT 181-3	OSM-S-430	MMV1576791
117	EGT 306-1	OSM-S-535	MMV1580423
118	EGT 308-1	OSM-S-537	MMV1580425
119	EGT 307-1	OSM-S-536	MMV1580424
120	EGT 311-1	OSM-S-538	MMV1580426
122	EGT 151-2	OSM-S-387	MMV897706
125	EGT 249-1	OSM-S-415	MMV1557949
128	EGT 212-1	OSM-S-394	MMV1557934
129	EGT 147-1	OSM-S-383	MMV897711
130	EGT 148-1	OSM-S-384	MMV897712
132	EGT 262-1	OSM-S-420	MMV1576787

Chapter 4 Compounds

Compound	Internal	OSM	MMV
133	EGT 295-1	OSM-S-442	MMV1577581
134	EGT 265-1	OSM-S-422	MMV1576788
135	EGT 263-1	OSM-S-421	MMV1576786
136	EGT 284-2	OSM-S-500	MMV1577577
137	EGT 283-1	OSM-S-499	MMV1577576
138	EGT 282-1	OSM-S-498	MMV1577575
140	EGT 290-1	OSM-S-501	MMV1577578
141	EGT 281-2	OSM-S-497	MMV1577574
145	EGT 324-1	OSM-S-554	MMV1580441
147	EGT 325-1	OSM-S-555	MMV1580442

148	EGT 350-1	OSM-S-575	MMV1581340
149	EGT 348-1	OSM-S-573	MMV1581338
150	EGT 349-1	OSM-S-574	MMV1581339
151	EGT 347-1	OSM-S-572	MMV1581337
152	EGT 352-1	OSM-S-577	MMV1581342
153	EGT 351-1	OSM-S-576	MMV1581341
154	EGT 65-1	OSM-S-371	MMV897700
155	EGT 64-1	OSM-S-370	MMV897699
160	EGT 117-1	OSM-S-375	MMV897704
162	EGT 123-1	OSM-S-382	MMV897710
165	EGT 176-1	OSM-S-391	MMV1557931
167	EGT 220-1	OSM-S-397	MMV1557937
168	EGT 213-1	OSM-S-395	MMV1557935
178	EGT 363-1	OSM-S-690	MMV1794642
179	EGT 224-1	OSM-S-399	MMV1557939
180	EGT 222-1	OSM-S-398	MMV1557938
187	EGT 286-1	OSM-S-433	MMV1577573
192	EGT 257-1	OSM-S-418	MMV1576784
193	EGT 338-1	OSM-S-564	MMV1581343
194	EGT 411-1	OSM-LO-1	MMV1794644
195	EGT 274-1	OSM-S-424	MMV1576790
196	PF-7091175	OSM-S-513	MMV1577924
197	PF-7091176	OSM-S-514	MMV1577925
198	PF-7091172	OSM-S-511	MMV1577922
199	PF-7091173	OSM-S-512	MMV1577923

Chapter 6 Compounds

Compound	Internal	OSM	MMV
208	EGT 199-5	OSM-S-515	MMV1579336
211	EGT 255-1	OSM-S-280	MMV688897
219	EGT 412-1	OSM-LO-2	MMV1794631
221	EGT 415-1	OSM-LO-7	MMV1794636
222	EGT 416-1 (prod1)	OSM-LO-8	MMV1794637
224	EGT 419-1	OSM-LO-6	MMV1794635
226	EGT 421-1	OSM-LO-4	MMV1794633
227	EGT 420-1	OSM-LO-5	MMV1794634
229	EGT 417-1 (prod2)	OSM-LO-3	MMV1794632
230	EGT 416-1 (prod2)	OSM-LO-9	MMV1794638
231	EGT 422-1	OSM-LO-11	MMV1794640
233	EGT 424-1	OSM-LO-10	MMV1794639
234	EGT 425-1	OSM-LO-12	MMV1794641

Chapter 7 Compounds

Compound	Internal	OSM	MMV
236	SSP2015a	OSM-S-294	MMV689970

237	SSP2015b	OSM-S-291	MMV689968
238	SSP2015c	OSM-S-292	MMV689969
239	SSP2015d	OSM-S-293	MMV663915
240	SSP2016a	OSM-S-351	MMV693153
241	SSP2016b	OSM-S-350	MMV693152
242	SSP2016c	OSM-S-352	MMV693154
243	SSP2016d	OSM-S-349	MMV693151
244	SSP2017a1	OSM-S-402	MMV1557942
245	SSP2017a2	OSM-S-401	MMV1557941
248	SSP2017c1	OSM-S-404	MMV1557944
249	SSP2017c2	OSM-S-403	MMV1557943
250	SSP2017d1	OSM-S-406	MMV1557946
251	SSP2017d2	OSM-S-405	MMV1557945